

Department of Molecular and Clinical Cancer Medicine
Institute of Systems, Molecular and Integrative Biology

**Strategies on the use of Nucleolar Function Inhibitors in cancer
therapy**

Thesis submitted in accordance with the requirements of the University of
Liverpool for the degree of Doctor in Philosophy

by

Lucía Moreno Laporta

January 2023

I wish to dedicate this thesis to my mother:

Lucía Laporta López

Unable to perceive the shape of you,
I find you all around me.
Your presence fills my eyes with your love.
It humbles my heart,
for you are everywhere.

The Shape of Water

Table of contents

I.	Abstract.....	6
II.	Acknowledgements.....	8
III.	Declarations.....	9
IV.	List of Figures.....	10
V.	List of tables.....	14
VI.	Abbreviations	15
1.	Introduction.....	21
1.1	Cancer biology	22
1.1.1	Hallmarks of cancer	25
1.1.2	Kidney cancer and renal cell carcinoma	29
1.2	Cancer: therapeutic strategies.....	32
1.2.1	Chemotherapy	32
1.2.2	Targeted therapy	34
1.2.3	Therapeutic landscape of renal cell carcinoma	36
1.2.4	Drug resistance.....	37
1.2.5	Drug combinations: a strategy against resistance	39
1.2.6	A perspective on the drug discovery and relevance of drug repurposing	40
1.3	The nucleolus: the factory creating ribosomes and a critical stress sensor	42
1.3.1	Interdependence of nucleolar structure and function	46
1.3.2	Diversity of nucleolar function	48
1.3.3	Regulation of nucleolar function.....	51
1.3.4	The nucleolus and cancer.....	53
1.3.5	The nucleolus and cancer therapy	56
1.4	mTOR, the master regulator of cell growth.....	60
1.4.1	mTOR complex 1	61
1.4.2	mTOR complex 2	74
1.4.3	mTOR and cancer.....	78
1.4.4	mTOR inhibitors as targeted cancer therapy	81
1.5	Aims.....	84
2.	Materials and methods	85
2.1	List of reagents.....	85
2.1.1	General reagents.....	85

2.1.2 Tissue culture reagents	87
2.1.3 Drugs.....	87
2.1.4 Antibodies for Western Blotting.....	88
2.1.5 Solutions	90
2.2 Cell culture.....	91
2.2.1 Cell lines and cell culture	92
2.2.2 Cell subculture technique.....	94
2.2.3 Cryopreservation and recovery of cryopreserved cell stocks.....	94
2.2.4 Mycoplasma testing	95
2.2.5 STR profiling	97
2.3 Cell viability assays	97
2.3.1 MTT assay.....	98
2.3.2 Rezasurin assay	99
2.3.3 Data analysis.....	100
2.4 Cell cycle analysis by flow cytometry	100
2.4.1 General principles of flow cytometry	100
2.4.2 General principles of Click-chemistry reaction.....	101
2.4.3 Optimization of the DNA labelling with click chemistry reaction for detection of cell proliferation of RCC cell lines using flow cytometry.....	102
2.4.4 Assessment of the cell proliferation profiles obtained with the DNA labelling with click chemistry reaction protocol.....	103
2.4.5 DNA labelling with click chemistry reaction for detection of cell proliferation of RCC cell lines using flow cytometry	104
2.4.6 Analysis of the data obtained with the Attune NxT flow cytometer.....	105
2.5 Analysis of rRNA synthesis.....	107
2.5.1 5-EU labelling of rRNA with click chemistry reaction for microscopy analysis	108
2.5.2 Image acquisition using an automated microscope and Micromanager Software	109
2.5.3 Image analysis using CellProfiler Software.....	110
2.6 siRNA transfection.....	111
2.6.1 General principles of siRNA transfection.....	112
2.6.2 <i>RRN3</i> siRNA transfection.....	112
2.7 Western Blot.....	113
2.7.1 General principles of Western Blotting.....	113
2.7.2 Protein extraction and preparation of the sample	114
2.7.3 DC Protein assay for protein quantification.....	114
2.7.4 Polyacrylamide gel electrophoresis.....	115

2.7.5	Transfer of proteins to a membrane	115
2.7.6	Protein detection.....	115
2.7.7	Imaging and densitometry analysis	115
2.8	Statistical analysis	117
2.8.1	Dose-response curves analysis	117
2.8.2	Characterisation of nucleolar changes.....	118
2.8.3	Flow cytometry data analysis	118
3.	Results.....	120
3.1	Investigating the effects of mTOR inhibitors on RCC cells	120
3.1.1	Effect of mTOR inhibitors on the phosphorylation of mTORC1 substrates S6K and 4EBP1	120
3.1.2	Modulation of nucleolar function by mTOR inhibitors	132
3.1.3	Inhibition of phosphorylation of the mTORC1 downstream target TIF-IA is a predictor of the activity of mTOR inhibitors on rRNA synthesis	143
3.1.4	Inhibition of mTOR reduces cell viability of RCC cells	150
3.1.5	ActD and Torin 1 cause different cell cycle changes associated with loss of cell viability	163
3.1.6	Conclusion.....	179
3.2	Sensitising RCC cells to nucleolar function inhibitors.....	180
3.2.1	ATP-competitive inhibition of mTOR enhances the inhibition of rRNA synthesis by ActD.....	180
3.2.2	ATP-competitive inhibition of mTOR enhances the suppression of cell viability induced by ActD	183
3.2.3	Effect additivity analysis of the mixture of drugs in the suppression of cell viability	186
3.2.4	Rapamycin also enhances the rRNA synthesis and cell viability suppression activity of ActD	192
3.2.5	Cytostatic and cytotoxic components of the inhibition of cell viability with drug combinations	194
3.2.6	Conclusion.....	200
4.	Discussion	202
5.	Conclusions.....	214
6.	Future Work.....	216
7.	Appendix.....	218
7.1	Certificates of cell line authenticity for RCC cells.....	218
7.2	Analysis protocol for 5-ethynyl uridine-labelled nucleolar images.....	223
7.3	Comparison of the percentage of cells gated on the different phases of cell cycle calculated using EdU incorporation vs. histogram deconvolution with 7-AAD staining	226

7.4 Flow cytometry analysis of the effects of mTORis on the cell cycle	228
7.5 Analysis of 5-ethynyl uridine-labelled nucleolar images	239
8. References	252

I. Abstract

Kidney cancer is the 7th most common cancer in the UK with over 13,300 new cases and about 4,709 deaths per annum (1). Renal cell carcinoma (RCC) accounts for 85% of kidney cancers and stage at diagnosis for this type of kidney cancer is strongly associated with patient outcome with barely 12% 5-year survival rate in patients diagnosed with advanced RCC (2). Patients with metastatic RCC are often treated with systemic treatment, including chemotherapy, targeted therapy and immunotherapy, however, narrowed therapeutic indices limit their use as the high toxicity severely affects the patients' quality of life and ability to follow through treatment regimens (3–5).

The present thesis proposes a strategy to sensitise RCC cells to the effects of nucleolar function inhibitors (NFIs), particularly considering that changes in the morphology of the nucleoli are associated with high aggressiveness and poor prognosis of RCC patients (6), and the role that dysregulated nucleolar activity plays on increased proliferation of cancer cells (7). Given the fact that nucleolar function is modulated by cellular pathways for which targeted therapies have already been developed and are currently used to treat RCC, such as the mechanistic target of rapamycin (mTOR) pathway (8,9), the aims of this research are to determine whether mTOR inhibitors effectively modulate nucleolar function of RCC *in vitro*, to identify potential candidates for target-sensitised chemotherapy, and finally, to assess the effect of the drug combinations proposed.

Microplate-based ribosomal RNA (rRNA) synthesis analysis using click chemistry revealed that ATP-competitive inhibitor Torin 1, but not the allosteric mTOR inhibitors Rapamycin, Temsirolimus and Everolimus, inhibits nucleolar function in ACHN and UoK111 cells. This was consistent with inhibition of cell viability and induction of cell cycle arrest achieved only by Torin 1 in the same cell lines, shown with MTT assay and flow cytometry, respectively. While treatment with both allosteric and ATP-competitive inhibitors of mTOR effectively reduced mTOR activity, as exemplified by the inhibition of the phosphorylation of mTOR complex 1 (mTORC1) substrate S6K and the changes in the phosphorylation patterns of 4EBP1 observed using Western Blot, only Torin 1 inhibited the phosphorylation of the RNA Polymerase I (RNA Pol I) transcription factor TIF-IA, which is a downstream target of mTOR, suggesting that

decrease cell viability of RCC cells in the presence of Torin 1 might be mediated by the ability of this compound to modulate the nucleolar function. Subsequent study of the effects of the combination of Actinomycin D (ActD) and ATP-competitive mTOR inhibitors on cell viability and rRNA synthesis performed with MTT assay and microplate-based rRNA synthesis analysis using click chemistry and isobolographic analysis of the drug interactions, suggest that ATP-competitive mTOR inhibitors can sensitise RCC cells to the cytotoxic effects of ActD.

Ultimately, the findings described in this thesis present the opportunity for a novel strategy for the treatment of RCC, targeting the nucleolus, which plays an important role in RCC, while taking advantage of the existing therapeutic agents. Specifically, we propose that combination of ATP-competitive mTOR inhibitors with the NFI ActD sensitises RCC cells to the cytotoxic effects of ActD, a strategy we termed target-sensitised chemotherapy.

II. Acknowledgements

I would like to start by thanking my supervisor Carlos P Rubbi for believing in me and giving me the opportunity to work with him. Even in the toughest of times, he provided his support and encouraged me to finish my research project. I will be forever grateful for his understanding and his support both academically as personally. I am grateful for his invaluable comments and suggestions, for sharing his knowledge and his passion for science with me and for providing motivation without which I would not have been able to finish this thesis.

I would also like to thank Nikolina Vlatkovic and Mark Boyd for welcoming me into their research group, guiding me and supporting for the last five years. I appreciate their feedback, their guidance and their friendship. As well, I thank the members of the p53 lab group with whom I shared many days in the lab for making the PhD path less lonely, for your friendship and your insights, including Emad Anaam, Moneerah Alshammari, and Neil Farquhar.

I will be forever grateful to my dad, Francisco Moreno, my sister, Fernanda Moreno and my family (los Laporchett) who supported me every step of the way even through the distance. They believed in me, cheered me up and they convinced me that I could do this. Their love and support were the light that kept me going, and their example was my motivation to accomplish this. I also thank Roberto Cruz, Lee Sullivan, Rodrigo Magana, Sofía Huante, Xavier Badia and Mariana Esteva the friends that became family with whom I have shared this road of the PhD and my life in the UK.

To my partner in crime, the love of my life, my husband Gilberto Parra, thank you for pursuing my dreams with me. Thanks for your love, for your sacrifice and believing in me always.

Last, I thank my mother. The woman who taught me that I could do anything. The woman who inspires me to become a better version of myself every day and to pursue my dreams. This would not have happened without her.

III. Declarations

This thesis is a result of my own work performed during the course of my PhD studies in the Department of Molecular and Clinical Cancer Medicine, Institute of Systems, Molecular and Integrative Biology, University of Liverpool, between October 2017 and January 2023.

All the experiments described in this thesis were performed by me unless clearly stated, as was the case for the STR profiling and the monthly mycoplasma testing. This thesis was wholly written by me under the valued guidance of my supervisors Carlos P Rubbi, Nikolina Vlatkovic and Mark Boyd. The Figures were entirely created by me using BioRender.com unless clearly stated in the Figure legend.

Lucía Moreno Laporta

January 2023

IV. List of Figures

1. Introduction

- Figure 1.1. Role of oncogenes and tumour suppressor genes in cancer.
- Figure 1.2. The hallmarks of cancer.
- Figure 1.3. Cell growth and proliferation within the cell cycle.
- Figure 1.4. Staging of RCC and relevant therapeutic approaches.
- Figure 1.5. Summary of the types of chemotherapeutic agents and their mechanism of action.
- Figure 1.6. Mechanisms mediating drug resistance.
- Figure 1.7. Drug discovery and development timeline.
- Figure 1.8. Pre-rRNA and promoter region.
- Figure 1.9. Assembly of RNA Pol I initiation complex.
- Figure 1.10. Ribosomal biogenesis in the nucleolus.
- Figure 1.11. An electron micrograph of the nucleolus of a HeLa cell.
- Figure 1.12. Nucleolar regulation of cell survival functions.
- Figure 1.13. Regulation of nucleolar function in response to availability of nutrients.
- Figure 1.14. Role of the oncogenic pathways on the transcriptional and post-transcriptional regulation of rRNA synthesis.
- Figure 1.15. Chemical structure of Actinomycin D.
- Figure 1.16. Intercalation of Actinomycin D in DNA.
- Figure 1.17. The mTOR pathway is a sensor of extra- and intra-cellular stimuli that controls cell functions that promote growth, proliferation, and cell survival.
- Figure 1.18. Components of the mTORC1.
- Figure 1.19. The role of the TSC1/2 complex as stimuli sensor and mTOR regulator.
- Figure 1.20. Model for role of Rag GTPases in signalling amino acid availability to mTORC1.
- Figure 1.21. mTORC1 amino acid sensing pathway.
- Figure 1.22. Overview of the mTOR pathway.
- Figure 1.23. Regulation of protein synthesis by mTORC1.
- Figure 1.24. Regulation of rDNA transcription by the mTORC1 pathway.
- Figure 1.25. Components of the mTORC2.
- Figure 1.26. Regulation of mTORC2 by mSIN.
- Figure 1.27. Chemical structure of rapamycin and other allosteric inhibitors of mTORC1.

2. Materials and methods

- Figure 2.1. Plate layout showing the distribution of drug treatments, control and blanks using 96 well microplate.
- Figure 2.2. Diagram of the substrate resazurin and its reduced product resorufin.
- Figure 2.3. Representation of the Cu alkyne-azide cycloaddition reaction.

- Figure 2.4. Labelling of nucleic acids using EdU and 5-EU incorporation followed by click chemistry reaction.
- Figure 2.5. Diagram showing the main steps of the established protocol for detection of nascent DNA labelled with click chemistry using flow cytometry.
- Figure 2.6. Dot plot showing how the region selection (R0) to exclude doublets from cell proliferation analysis was carried out.
- Figure 2.7. Density plot showing how the gates were created to calculate the percentage of single cells in the different phases of cell cycle.
- Figure 2.8. Histogram showing the overlays of the populations identified by 7-AAD and 6-FAM staining using flow cytometry.
- Figure 2.9. Histogram with overlays of the different drug concentrations used in a specific experiment to allow direct comparison among treatments.
- Figure 2.10. Methodology used to label RNA using click reaction and detection of resultant fluorescent nucleoli through microscopy.
- Figure 2.11. View of an analysis pipeline in CellProfiler (showing the metadata extraction section).
- Figure 2.12. Methodology used for transfection of RCC with siRNA.

3. Results

- Figure 3.1. Western Blot analyses of relative levels of S6K and the phosphorylated form of S6K in threonine 389 (ph-S6K) in ACHN cells.
- Figure 3.2. Densitometry analysis of Western Blots probing for the phosphorylated form of S6K at threonine 389 using lysates obtained from ACHN treated with different concentrations of A) rapamycin, B) temsirolimus, C) everolimus and D) Torin 1.
- Figure 3.3. Western Blot analyses of relative levels of S6K and the phosphorylated form of S6K in threonine 389 (ph-S6K) in UoK111 cells.
- Figure 3.4. Densitometry analysis of Western Blots probing for the phosphorylated form of S6K at threonine 389 using lysates obtained from UoK111 treated with different concentrations of A) rapamycin, B) temsirolimus, C) everolimus and D) Torin 1.
- Figure 3.5. Western Blot analyses of relative levels of 4EBP1 in ACHN cells.
- Figure 3.6. Densitometry analysis of Western Blots probing for 4EBP1 using lysates obtained from ACHN treated with different concentrations of A) rapamycin, B) temsirolimus, C) everolimus and D) Torin 1.
- Figure 3.7. Western Blot analyses of relative levels of 4EBP1 in UoK111 cells.
- Figure 3.8. Densitometry analysis of Western Blots probing for 4EBP1 using lysates obtained from UoK111 treated with different concentrations of A) rapamycin, B) temsirolimus, C) everolimus and D) Torin 1.
- Figure 3.9. rRNA synthesis staining of U2Os cells.
- Figure 3.10. 5-EU incorporation in U2O cells.
- Figure 3.11. Quantification of newly synthesized rRNA in RCC cells treated with ActD
- Figure 3.12. Assessment of the effect of ActD on nucleolar area and 5-EU incorporation per unit area in RCC cells.
- Figure 3.13. Effect of mTOR inhibitors on the synthesis of rRNA in ACHN cells
- Figure 3.14. Effect of mTOR inhibitors on the synthesis of rRNA in UoK111 cells

- Figure 3.15. Effects of mTOR inhibitors on nucleoli
- Figure 3.16. Western Blot of relative levels of TIF-IA in ACHN cells transfected with siRNA transfection.
- Figure 3.17. Western Blot and densitometry analysis of relative levels of TIF-IA and phosphorylated TIF-IA in ACHN cells treated with 100 nM of Torin 1, Rapamycin, Temsirolimus, and Everolimus.
- Figure 3.18. Western Blot and densitometry analysis of relative levels of TIF-IA and phosphorylated TIF-IA in UoK111 cells treated with 100 nM of Torin 1, Rapamycin, Temsirolimus, and Everolimus.
- Figure 3.19. Western Blot and densitometry analyses of relative levels of TIF-IA and phosphorylated TIF-IA in RCC cells treated with increasing concentrations of Torin 1
- Figure 3.20. Plate effect using successive replicates.
- Figure 3.21. Plate effect using alternated replicates.
- Figure 3.22. Effect of the incubation time with ActD on viability of ACHN cells
- Figure 3.23. Effect of the incubation time with ActD on viability of UoK111 cells
- Figure 3.24. Low concentrations of ActD do not promote DNA damage.
- Figure 3.25. Effect of solvents on cell viability
- Figure 3.26. Effect of ethanol and DMSO on cell viability in comparison with untreated (UT) ACHN cells.
- Figure 3.27. Effect of Rapamycin on cell viability of RCC cell lines.
- Figure 3.28. Effect of Temsirolimus on cell viability of RCC cell lines.
- Figure 3.29. Effect of mTOR inhibitors on cell viability of ACHN cells.
- Figure 3.30. Effect of mTOR inhibitors on cell viability of UoK111 cells.
- Figure 3.31. Inhibition of cell viability and rRNA mediated by Torin 1 in RCC cells.
- Figure 3.32. Testing of different EdU-incubation times for optimal segmentation of cell cycle stages using labelled DNA with Click-chemistry reaction and detection by flow cytometry
- Figure 3.33. Identification of cell cycle changes in ACHN cells treated with ActD by labelling nascent DNA with EdU and detecting using Click and flow cytometry
- Figure 3.34. Identification of cell cycle changes in UoK111 cells treated with ActD by labelling nascent DNA with EdU and detecting using Click and flow cytometry
- Figure 3.35. Identification of cell death and segmentation of cell populations into cell cycle stages in ACHN cultures treated with staurosporine and etoposide for 24 hours.
- Figure 3.36. Percentage of S-phase cells (A) and sub-G1 cells (B) detected by flow cytometry on ACHN and UoK111 cells (indicated) treated either with DMSO (Ctrl) or with different doses of ActD.
- Figure 3.37. Effect of increased concentrations of Torin 1 on the cell cycle of A) ACHN and B) UoK111 cells.
- Figure 3.38. Percentage of S-phase cells (A) and sub-G1 cells (B) detected by flow cytometry on ACHN and UoK111 cells (indicated) treated either with DMSO (Ctrl) or with different doses of Torin 1.
- Figure 3.39. Effect of increased concentrations of allosteric mTORis on the cell cycle of ACHN cells.
- Figure 3.40. Effect of increased concentrations of allosteric mTORis on the cell cycle of UoK111

- Figure 3.41. Percentage of S-phase cells (A) and sub-G1 cells (B) detected by flow cytometry on ACHN and UoK111 cells (indicated) treated either with DMSO (Ctrl) or with different doses of Rapamycin.
- Figure 3.42. rRNA synthesis dose-response curves for ActD and AZD8055 alone and in combination.
- Figure 3.43. Cell viability dose-response curves for ActD and AZD8055 alone and in combination.
- Figure 3.44. Cell viability dose-response curves for ActD and Torin 1 alone and in combination.
- Figure 3.45. Isobologram construction scheme used in this work.
- Figure 3.46. Isobolographic analysis of the cell viability response of a combination of ActD and Torin 1.
- Figure 3.47. rRNA synthesis response curves for ActD and Rapamycin alone and in combination
- Figure 3.48. Cell viability dose-response curves for ActD and Rapamycin alone and in combination.
- Figure 3.49. Effect of ActD and Torin 1 combinations on the cell cycle of RCC cells.
- Figure 3.50. Effect of ActD and AZD8055 combinations on the cell cycle of RCC cells.
- Figure 3.51. Effect of ActD and Rapamycin combinations on the cell cycle of RCC cells

4. Discussion

- Figure 4.1. Model for sensitised nucleolar chemotherapy

7. Appendix

- Figure 7.1. Screenshot of CellProfiler window taken while performing segmentation of nuclear images.
- Figure 7.2. Screenshot of CellProfiler window taken while performing analysis of nucleolar images.
- Figure 7.3. Screenshot of SQLiteStudio window taken while performing data extraction.
- Figure 7.4. Density plot of ACHN cells stained with 7-AAD and 6-FAM.
- Figure 7.5. Histogram showing a comparison of 6-FAM-staining and deconvolution of 7-AAD-staining data for estimation of the percentage of cells in the different phases of cell cycle.
- Figure 7.6. Comparison of the estimation of cell cycle population distribution by labelling with 6-FAM and 7-AAD and by data deconvolution of 7-AAD-stained cells.
- Figure 7.7. Analysis of cell cycle of ACHN cells treated with ActD using click chemistry-labelled DNA detected with flow cytometry.
- Figure 7.8. Analysis of cell cycle of UoK111 cells treated with ActD using click chemistry-labelled DNA detected with flow cytometry.
- Figure 7.9. Analysis of cell cycle of ACHN cells treated with Torin 1 using click chemistry-labelled DNA detected with flow cytometry.
- Figure 7.10. Analysis of cell cycle of UoK111 cells treated with Torin 1 using click chemistry-labelled DNA detected with flow cytometry.

- Figure 7.11. Analysis of cell cycle of ACHN cells treated with Rapamycin using click chemistry-labelled DNA detected with flow cytometry.
- Figure 7.12. Analysis of cell cycle of ACHN cells treated with Temsirolimus using click chemistry-labelled DNA detected with flow cytometry.
- Figure 7.13. Analysis of cell cycle of ACHN cells treated with Everolimus using click chemistry-labelled DNA detected with flow cytometry.
- Figure 7.14. Analysis of cell cycle of UoK11 cells treated with Rapamycin using click chemistry-labelled DNA detected with flow cytometry.
- Figure 7.15. Analysis of cell cycle of UoK11 cells treated with Temsirolimus using click chemistry-labelled DNA detected with flow cytometry.
- Figure 7.16. Analysis of cell cycle of UoK11 cells treated with Everolimus using click chemistry-labelled DNA detected with flow cytometry.
- Figure 7.17. 5-EU incorporation vs. drug dose.
- Figure 7.18. Nucleolar area vs. drug dose.
- Figure 7.19. 5-EU incorporation per unit area vs. drug dose.
- Figure 7.20. Data distribution for the response to a typical treatment of interest.

V. List of tables

1. Introduction

- Table 1.1. Functions of the sub-structures of the nucleolus
- Table 1.2. Hallmarks of cancer enabled by oncogenic activation of the mTOR pathway

2. Materials and Methods

- Table 2.1. General reagents
- Table 2.2. Tissue culture reagents
- Table 2.3. Antibodies for Western Blotting
- Table 2.4. Solutions
- Table 2.5. RCC cell lines used in this study.
- Table 2.6. PCR conditions for Mycoplasma test
- Table 2.7. Flow cytometer set up information

3. Results

- Table 3.1. IC₅₀ values of mTOR inhibitors for inhibition of phosphorylation of S6K at threonine 389 in ACHN and UoK111 cells.
- Table 3.2. Multifactorial analysis of the cell cycle fractions shown in Figure 3.36 A and B.
- Table 3.3. Multifactorial analysis of the cell cycle fractions shown in Figure 3.38 A and B.
- Table 3.4. Multifactorial analysis of the cell cycle fractions shown in Figure 3.41 A and B

7. Appendix

- Table 7.1. Segmentation of nuclear images
- Table 7.2. Analysis of nucleolar images

Table 7.3. Estimated distribution of cells through the cell cycle by labelling with 6-FAM and 7-AAD and by data deconvolution of 7-AAD-stained cells.

VI. Abbreviations

µg	Microgram
µl	Microlitre
µm	Micrometer
µM	Micromolar
4E-BP1	eIF-4E-binding protein 1
5'TOP	5' transcriptional start site
5-EU	5-ethynyl uridine
5-FU	5-fluorouracil
6-FAM	6-Carboxyfluorescein
7-AAD	7-Aminoactinomycin D
ABC	ATP-binding cassette
ACC	Acetyl-CoA carboxylase
ActD	Actinomycin D
Akt	RAC-alpha serine/threonine-protein kinase
AMPK	AMP-activated protein kinase
ANOVA	Analysis of Variance
APS	Ammonium persulfate
ATP	Adenosine triphosphate
AUC	Area under the curve
BSA	Albumin from bovine serum
BrU	5-bromouridine
ccRCC	Clear cell RCC
CE	Core element
chRCC	Chromophobe RCC
CKII	Casein kinase II
Cmax	Maximum concentration
Cmin	Minimum concentration
CML	Chronic myeloid leukaemia
CO ₂	Carbon dioxide
cryo-EM	Cryo-electron microscopy
Cy-3	Cyanine-3
DDR	DNA damage response
DEPDC5	DEP domain-containing protein 5; GATOR complex protein DEPDC5
Deptor	DEP-domain-containing mTOR-interacting protein
DEPTOR	DEP-domain containing mTOR-interacting protein
DFC	Dense fibrillar component
dH ₂ O	Distilled water
DIC	Differential Interference Contrast
DMEM	Dulbecco's modified Eagle's medium
DMSO	Dimethyl sulphoxide

DNA	Deoxyribonucleic acid
DNAse	Deoxyribonuclease
dNTP	Deoxynucleotide
DRB	5,6-Dichloro-1- β -d-ribofuranosylbenzimidazole
DTT	Dithiothreitol
ECL	Enhanced chemiluminescent
EDTA	Ethylenediaminetetraacetic acid
EdU	5-ethynyl-2'-deoxyuridine
eEF2K	Eukaryotic elongation factor 2 kinase
EF3	Elongation factor 3
EGF	Epidermal growth factor
EGFR	Epidermal growth factor receptor
eIF2	Eukaryotic initiation factor 2
eIF4A	Eukaryotic initiation factors 4A
eIF4B	Eukaryotic translation initiation factor 4B
eIF4E	Eukaryotic translation initiation factor 4E
eIF4F	Eukaryotic translation initiation factor 4F
eIF4G	Eukaryotic translation initiation factor 4G
EJC	Exon junction complex
EPO	Erythropoietin
ER	Endoplasmic reticulum
FASN	Fatty acid synthase
FBS	Foetal bovine serum
FC	Fibrillar centre
FCS	Flow Cytometry Standard
FKBP	FK506-binding protein
FKBP12	12-kDa FK506-binding protein
FLK1	Receptor protein-tyrosine kinase
FLT1	Fms Related Receptor Tyrosine Kinase 1
FOXO1	Forkhead box protein O1
FOXO3 α	Forkhead box protein O3 α
FRAP	FKBP-rapamycin-associated protein
FRB	FKBP12-rapamycin binding domain
GAP	GTPase activating protein
GATOR	GAP activity toward Rags complexes
GC	Granular component
GSK3 β	Glycogen synthase kinase 3 β
H ₂ O	Water
HIF	Hypoxia inducible factor
HIF-1 α	Hypoxia inducible factor 1 alpha
HRP	Horseradish peroxidase
Hsp90	Heat shock protein HSP 90
IC50	Half maximal inhibitory concentration
ICI	Immune checkpoint inhibitors
IGF-IA	Insulin-like growth factor IA
IRS1	Insulin receptor substrate 1

ITGA5	Integrin α -5
JNK2	c-Jun N-terminal protein kinase
k-Ras	GTPase KRas
Leu	Leucine
Lipin1	Phosphatidate phosphatase LPIN1
LOXL2	Lysyl oxidase homologue 2
LSU	Large ribosomal subunit
M	Molar
MAPK	Mitogen-activated protein kinase
MDM2	Murine double minute 2
Mek	Dual specificity mitogen-activated protein kinase kinase 1; MAPK/ERK kinase 1
MIOS	Missing oocyte meiosis regulator homolog; GATOR complex protein MIOS
mLST8	Mammalian lethal with Sec13 protein 8
MP1	MAPK binding partner 1
mRNA	Messenger ribonucleic acid
mSin1	Mammalian stress-activated protein kinase interacting protein
mTOR	Mechanistic target of rapamycin
mTORC1	mTOR complex 1
mTORC2	mTOR complex 2
mTORi	mTOR inhibitor
MTT	N,N-dimethylformamide 3-(4,5-dimethylthiazol-2-yl)-2,5-diphenyl tetrasodium bromide
NET	Neuroendocrine tumour
NFI	Nucleolar function inhibitor
nM	Nanomolar
NORs	Nucleolar organising regions
NPRL2	Nitrogen permease regulator 2-like protein; GATOR complex protein NPRL2
NPRL3	Nitrogen permease regulator 3-like protein; GATOR complex protein NPRL3
O ₂	Oxygen
PAGE	Polyacrylamide gel electrophoresis
PBS	Phosphate buffered saline
PCR	Polymerase chain reaction
PDCD4	Programmed cell death 4
PDK1	3-phosphoinositide-dependent protein kinase-1
Pen strep	Penicillin streptomycin
PH	Pleckstrin homology
PI3K	Phosphoinositide 3-kinases
PI3K	Phosphatidylinositol-4,5-bisphosphate 3-kinase
PI3K-AKT	Phosphatidylinositol 3-kinase/protein kinase-B
PIKK	PI3K-related kinase
PIP2	Phosphatidylinositol (4,5)-bisphosphate
PIP3	Phosphatidylinositol (3,4,5)-trisphosphate
PKC α	Protein kinase C α

PMA	phorbol 12-myristate,13-acetate
PPAR-γ	Proliferator-activated receptor-γ
PRAS40	Proline-rich Akt substrate 40kDa
pRCC	Papillary RCC
pre-rRNA	Precursor rRNA
Protor1/2	Protein observed with Rictor-1 or 2
PtdIns(3,4,5)P3	Phosphatidylinositol 3,4,5-trisphosphate
PTEN	Phosphatase and tensin homolog
PTEN	Phosphatase and tensin homologue
R&D	Research and development
Raf	RAF proto-oncogene serine/threonine-protein kinase
Rag	Ras-related small GTPase
Raptor	Regulatory-associated protein of mTOR
Rb	Retinoblastoma
RCC	Renal cell carcinoma
RE	Response element
Rheb	Ras homolog enriched in brain
Rictor	Rapamycin-insensitive companion of mTOR
RISC	RNA-induced silencing complex
RNA	Ribonucleic acid
RNase	Ribonuclease
ROS	Reactive oxygen species
RP	Ribosomal protein
RPA	Replication protein A
rpS6	Ribosomal protein S6
rRNA	Ribosomal RNA
RSK	p90 ribosomal S6 kinase
RTK	Receptor tyrosine kinases
S6K1	p70S6 Kinase 1
SCD-1	Stearoyl-CoA desaturase 1
SD	Standard deviation
SDS	Sodium dodecyl sulphate
SDS	Sodium dodecyl sulfate
SDS-PAGE	SDS-polyacrylamide gel electrophoresis
SEC13	Protein SEC13 homolog; GATOR complex protein SEC13
SEGA	Subependymal giant cell astrocytoma
SEH1L	Nucleoporin SEH1; GATOR complex protein SEH1
SEM	Standard error of the mean
Ser	Serine
SGK1	Serine/threonine-protein kinase Sgk1
siRNA	Small interference RNA
SKAR	S6K1 Aly/REF-like target; Polymerase delta-interacting protein 3
SL1	Selectivity factor 1
snoRNPs	Small nucleolar ribonucleoproteins
SREBP	Sterol regulatory element-binding protein 1
SSU	Small ribosomal subunit

STR	Short tandem repeat
TBC1D7	TBC1 domain family member 7
TEMED	N, N, N', N'-tetramethylenediamine
TGFB111	transforming growth factor beta-1-induced transcript 1 protein
Thr	Threonine
TIF-IA	Transcription initiation factor IA
TKD	Tyrosine kinase domain
TKI	Tyrosine kinase inhibitor
TNF	Tumour necrosis factor
TOS	TOR signalling
TSC	Tuberous sclerosis complex
TSC	Tuberous sclerosis complex
TSC2	Tuberous sclerosis protein 2
UBF	Upstream binding factor
UCE	Upstream control element
UK	United Kingdom
ULK1	Unc-51 like kinase 1
US	United States
UTR	Untranslated region
UV	Ultraviolet
VEGF	Vascular endothelial growth factor
VHL	Von Hippel-Lindau
VPS34	Vacuolar protein sorting-34
WDR24	WD repeat-containing protein 24; GATOR complex protein WDR24
WDR59	WD repeat-containing protein 59; GATOR complex protein WDR59
YY1	Transcription factor yin-yang 1

1. Introduction

Cancer has affected humankind for thousands of years. The earliest descriptions of cancer date from 3000 BC, and today, more than 5000 years later, cancer is still a major concern (10). Advances in technology and the investment in cancer research has led to diagnostic techniques that allow earlier detection, and to the development of cancer therapies that, together, have improved the patient outcomes and the survival rate of many cancer patients.

Nevertheless, cancer is still the leading cause of death in 57 countries, and there were almost 10 million cancer deaths in 2020 (11,12). Late detection, associated with poor prognosis, accounts for 45.4% of new cases of all types of cancer in England (13). In these cases, systemic approaches such as chemotherapy are recommended to treat the patients. However, remission or disease-free survival are rarely achieved by these drugs, and their secondary effects have a severe impact on the quality of life of the patients.

Development of new drugs is expensive, time consuming, and sometimes not viable for the pharmaceutical industry, especially when drug responses can vary depending on the genetic profiles of the patients. Thus, the implementation of strategies for the use of existing and approved drugs including repurposing and novel drug combinations may provide good alternative strategies to improve patient outcomes treated with chemotherapy. The rationale behind these strategies should take into consideration the molecular biology of cancer and clinical observations, since the former can provide relevant information regarding potential targets depending the type of cancer and the genetic signature of the tumours, while the clinical trials and the evidence of the effects of the treatments on patients are necessary to verify safety, efficacy and efficiency of the therapeutic strategies.

The present research study explores the effects *in vitro* of one such drug combination on renal cell carcinoma cell lines. The combination proposed includes nucleolar function inhibitors (NFIs), which as their name suggests, target nucleolar function, that has been demonstrated to be enhanced in several types of cancer (14). The mechanism of action of these drugs relies on the stress-sensor function of the nucleolus through which cell cycle arrest and apoptosis can be promoted upon cellular distress. Nevertheless, existing NFIs such as Actinomycin D (ActD) have the

disadvantage, as other chemotherapeutics do, of targeting a cellular function rather than an oncogenic pathway, thus, having secondary effects by targeting healthy cells irrespective of their proliferation rates.

Interestingly, nucleolar function is modulated by oncogenic signalling pathways, such as the mTOR pathway, a signalling pathway that is dysregulated in many types of cancer, and for which clinically effective inhibitors exist. Therefore, the hypothesis of this research is that mTOR inhibitors (mTORis) may inhibit the nucleolar function and sensitise cancer cells specifically to the cytotoxic effects of the NFIs, a strategy we termed target-sensitised chemotherapy.

Accordingly, an overview of cancer, and specifically, renal cell carcinoma, its relevance as a public health issue and the state-of-the-art treatments for this disease are described in the introduction to highlight the importance of this project. The biology of the nucleolus and the mTOR pathway are also explained in order to establish a clear rationale for the combination of drugs proposed in this research study.

1.1 Cancer biology

Cancer is a group of diseases that occur because of the accumulation of genomic faults that dysregulate the cellular functions, promoting uncontrolled growth and proliferation that disrupt tissue homeostasis. This group of diseases are a main health issue worldwide. In 2018 there were 19.3 million new cancer cases in the world (12) and it is the leading cause of death in 57 countries (11). In the UK alone there are 375,000 new cancer cases per year (15).

Although distinct types of cancers have different outcomes, many of them have a bad prognosis. This is the case especially for cancers that are diagnosed in the later stages, once the tumours have invaded adjacent tissue or metastasised to other organs. This is particularly true of renal cancers, which are often diagnosed as an incidental finding whilst performing other clinical investigations. In the UK, there are approximately 375,400 new diagnoses of cancer each year, and there are over 167,000 cancer deaths per annum (15,16). Globally, there are almost 19.3 million newly diagnosed cancers and 10 million cancer deaths worldwide in 2020 (12).

One may ask, what is the origin of cancer? Why does it happen and why are 1 in 2 people in the UK expected to develop cancer during their lifetime? (17). Cancer arises

because of an accumulation of mutations in critical genes that leads to phenotypic adaptations that have been called the “hallmarks of cancer” as discussed in detail in section 1.1.1. (18,19). These hallmarks include a loss of control of cell proliferation, reduced cell death, the acquisition of cellular immortality amongst others, and when these are combined with the frequently acquired ability to spread to different anatomical sites and establish novel tumours (metastases) this is linked with the observed poor outcomes and often sadly to the death of affected individuals.

Since the disease results from genetic alterations, factors that influence the probability of DNA mutations influence the incidence of cancer developing, a process known as carcinogenesis. This includes both patient intrinsic factors such as the efficiency of DNA repair and also environmental factors such as exposure to mutagenic agents. The chance of a mutation occurring in a critical gene or genes is a largely stochastic event and thus it increases with age (the exception being the impact of certain oncogenic viruses including hepatitis B and hepatitis C viruses, Epstein–Barr virus human papillomaviruses (HPVs), and human herpesvirus type 8) (20). As the life expectancy of global populations increase, the likelihood that individuals within the population may develop cancer also increases.

In normal cells, growth and proliferation are tightly regulated through signalling pathways that recognise availability of resources and respond to certain stimuli in order to maintain homeostasis. Transmembrane receptors recognise nutrients, ATP, and mitogens and initiate downstream transduction of signals that regulate cellular functions that drive cell growth and proliferation, such as biosynthesis of proteins and lipids. In cancer cells, these signalling pathways are often found to be dysregulated or over-activated, due to alterations in genes that confer a growth advantage to the cell, known as oncogenes (21) (Figure 1.1). Dysregulation of the mechanisms that modulate cell growth and proliferation in cancer cells is also associated with alterations in genes that inhibit replication in normal cells or in those required for the conservation of genome integrity, known as tumour-suppressor genes (22) (Figure 1.1).

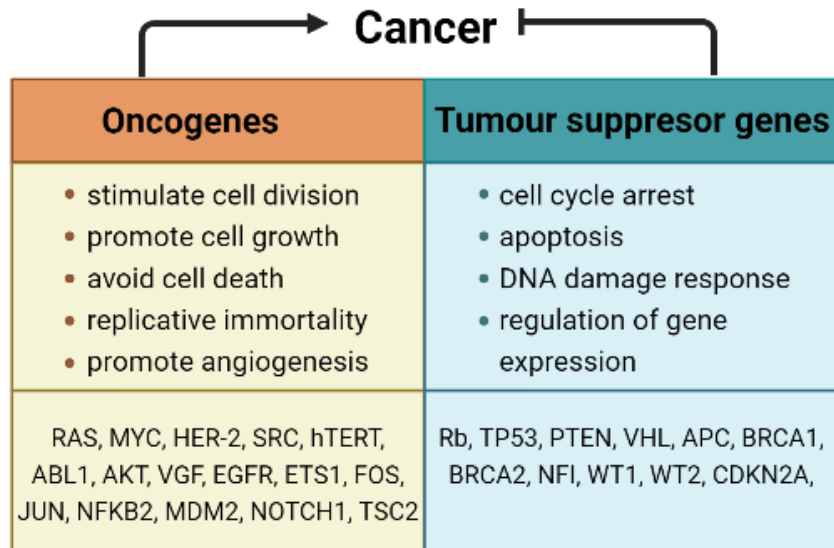


Figure 1.1. Role of oncogenes and tumour suppressor genes in cancer. Oncogenes regulate cell functions that promote carcinogenesis, while tumour suppressor genes are involved in cell functions that prevent it as shown in the middle row. Examples of frequently mutated oncogenes and tumour suppressor genes are mentioned in the bottom row.

Normal cells have various mechanisms to preserve cellular function and prevent carcinogenesis. Amongst these mechanisms, cells can repair DNA damage through at least five different DNA repair pathways including base excision repair, nucleotide excision repair, mismatch repair, homologous recombination and non-homologous recombination (23). Furthermore, cells also have a contingency protocol for instances when the damage is too extensive that cannot be repaired. This process called apoptosis, also known as cellular suicide, is tightly controlled and initiated by the cleavage of caspase-3, which leads to DNA fragmentation, degradation of the cytoskeleton and nucleus, formation of the apoptotic bodies, and finally, uptake by phagocytic cells (24). Tumour suppressor genes play key roles in both DNA repair and apoptosis.

Tumour suppressor genes oppose carcinogenesis. Thus, genetic alterations that render cells without functional tumour suppressor genes prevent inhibition of the pathways promoting cell growth and proliferation, therefore stimulating uncontrolled growth and continuous cell division that promote the development of tumours. That is the case of retinoblastoma (*Rb*), a tumour suppressor that plays a key role as a regulator of the G1 checkpoint, blocking the entry to the S-phase and cell growth (25). The *Rb* gene was the first tumour suppressor identified and loss of its function is associated with cell cycle dysregulation and tumorigenesis (26). Additionally, loss of function of tumour suppressor genes such as *TP53*, the most frequently mutated gene

in human cancers, allows cells to avoid programmed cell death and accumulate faults in the DNA that have not been repaired properly (27).

Contrary to tumour suppressor genes, oncogenes promote carcinogenesis. Mutations, gene amplification, and chromosome rearrangement are associated with activation of oncogenes, thus subsequent over activation of signalling pathways that promote cell growth and/or proliferation (19,21). These genes encode the proteins involved in the promotion of cell growth, proliferation and other hallmark traits such as angiogenesis and anti-apoptotic signalling. They include membrane receptors that receive the signals, the growth factors themselves, and the different proteins that participate in the transduction of the signalling pathways, generally kinases. The products of oncogenes can also be transcription factors and chromatin remodelers that modulate the expression of other genes. Finally, oncogenes can code for proteins involved in the regulation of apoptosis (28).

Some oncogenes will promote the secretion of factors to the extracellular matrix that, in turn, will promote secretion of specific growth factors by the surrounding cells, thus activating the signalling pathways. Alternatively, mutations in oncogenes can affect the structure of the translated product generating an always-active protein, even in the absence of the signal. Mutations can also lead to over-expression of membrane receptors or kinases, enabling the signalling pathways even when the presence of the activating factors is low.

Identification of cancer driver genes, including both tumour suppressor genes and oncogenes, and their association to different types of cancer and cell origin is relevant to predict prognosis and response to treatments.

1.1.1 Hallmarks of cancer

The list of critical phenotypes that cancer cells typically acquire that contribute to the process of carcinogenesis are known as hallmarks of cancer. This set of characteristics was first discussed by Hanahan and Weinberg in 2000, who proposed that most types of cancer display a multi-step transformation of cell functions involving self-sufficiency in growth signals, insensitivity to growth-inhibitory signals, evasion of apoptosis, limitless replicative potential, sustained angiogenesis, and tissue invasion and metastasis (29).

As cancer research advanced and thousands of papers published provided a better understanding of the disease, an updated list of the hallmarks of cancer was published in 2011, which included two additional hallmarks: reprogramming of cellular energy metabolism and avoiding of immune destruction. Furthermore, genomic instability and tumour promoting inflammation were introduced as enabling characteristics that play a key role promoting the acquisition of the carcinogenic traits (Figure 1.2.) (30).

After 11 years, the hallmarks of cancer have been reviewed and unlocking phenotypic plasticity and senescent cells have been proposed as new emerging hallmarks. Additionally, non-mutational epigenetic reprogramming and polymorphic microbiomes have been added as enabling characteristics (31).

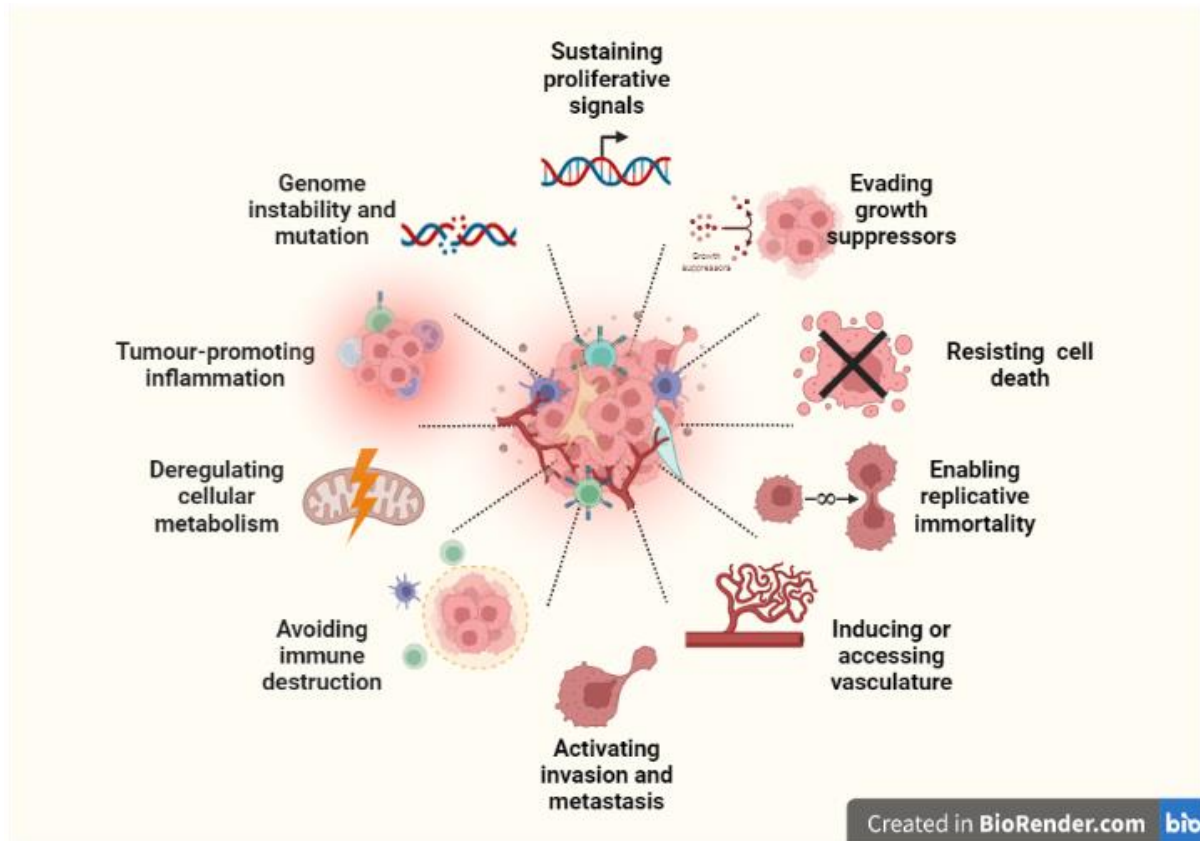


Figure 1.2. The hallmarks of cancer. A diagrammatic representation of the hallmarks of cancer. Adaptation from Hanahan and Weinberg, 2011.

Since they were first proposed, the hallmarks of cancer were a summary of the main changes that cells go throughout the carcinogenic process. It was a way to make simple a very complex process, but also the means to illustrate the variables involved in the development of cancer and the manner in which they are interconnected (29).

As new hallmarks and enabling characteristics have been proposed, one can realise that even the simplified overview of cancer is quite complex.

The following sub-section describes how acquisition of self-sufficiency in growth signals and insensitivity to growth-inhibitory signals promote carcinogenesis.

1.1.1.1 Evading growth suppressors & sustaining proliferative signals

As mentioned in section 1.1.1, uncontrolled cell growth and proliferation are two significant hallmarks that give cancer cells the ability to grow more and divide faster than normal cells. These two features disrupt tissue homeostasis since larger and more numerous cells require more space, thus promoting tumour growth. Sometimes these two terms are confused or used interchangeably. Although these cellular functions are extremely intertwined and both are essential for cellular and tissue homeostasis, they have different roles.

Cell growth refers to the ability of the cell to produce the biomass required to increase its volume (32). This involves the activation of numerous signalling pathways that coordinate the synthesis of nucleic acids, proteins, and lipids, and ribosome biogenesis. Cell growth is strictly regulated in normal cells in response to availability of nutrients, oxygen, internal and external signalling, such as growth factors and extracellular matrix molecules (33).

Conversely, cell proliferation involves increase of the number of cells achieved by cell division (34). For cell division to occur, the cell needs to attain a certain size so DNA replication can take place, which is then followed by mitosis. Together, these processes integrate the cell cycle (Figure 1.3). In mammalian cells, cell growth occurs during the G1 phase of the cell cycle. For the cell to be able to progress into the S-phase, it must comply with a set of requisites known as the G1 checkpoint, that include size, availability of resources, appropriate signalling, and DNA integrity. If a cell has not produced enough biomolecules or there are not enough resources for the cell to divide, the cell might exit the cell cycle into G0 or rest phase.

Once in S-phase, the cell replicates its DNA, creating two identical copies of its genetic code for the two daughter cells. Similar to the G1-check point, the S-check point halts progression of the cell into the G2-phase of the cell cycle when problems with DNA replication arise. The presence of long strands of ssDNA coated by the replication

protein A (RPA), stalled forks, and double-stranded breaks are amongst the main issues related to DNA replication (35,36).

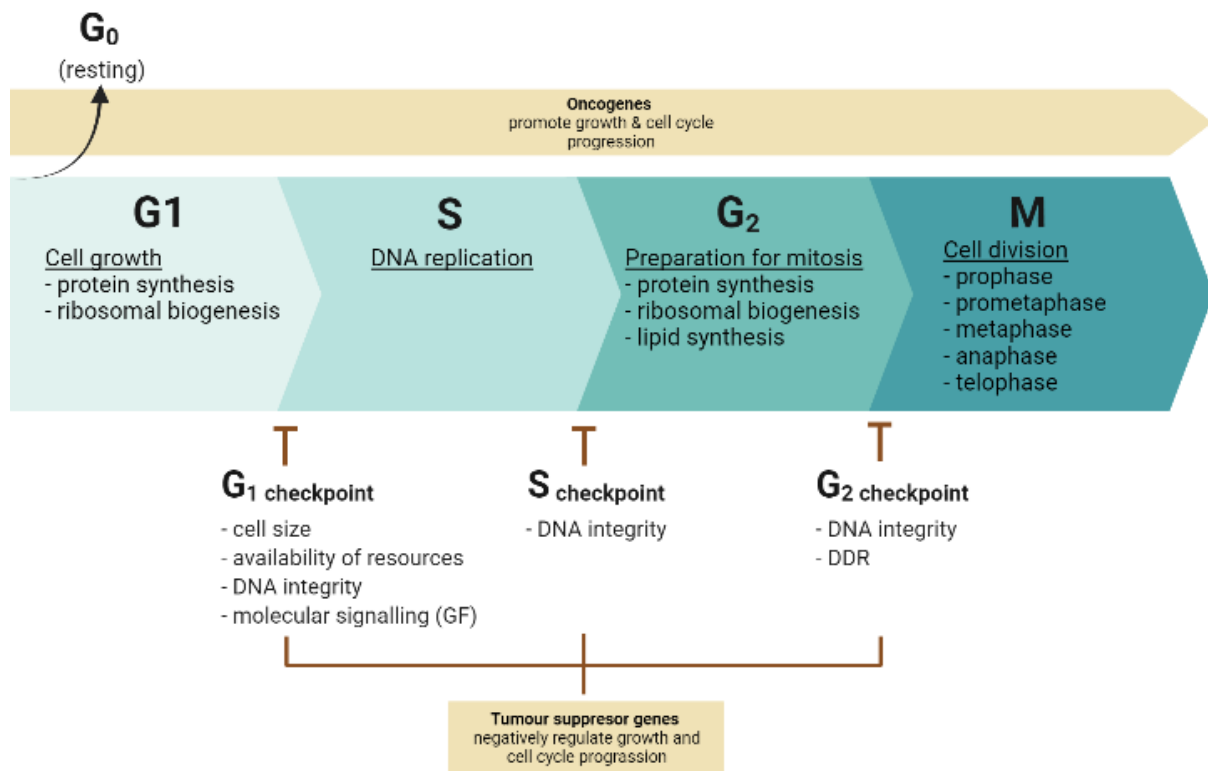


Figure 1.3. Cell growth and proliferation within the cell cycle. Relationship of oncogenes and tumour suppressor genes with cell cycle progression is described.

During the G₂ interphase, the cell prepares for mitosis so a high production of proteins and lipids is needed for the formation of the two new daughter cells to take place. Of special relevance is the G₂/M checkpoint, the last opportunity of the cell to check for genomic integrity and to activate DNA damage response (DDR) mechanisms when DNA lesions are detected before cell division. Mitosis is the last phase in the cell cycle and consists in the division of a single cell that has a copy of its genetic material into two new cells. This phase is subdivided into prophase, prometaphase, metaphase, anaphase, and telophase.

In cancer, these two processes become dysregulated and take place even in the absence of cues such as nutrients or molecular signalling. There are two ways in which cells can overcome the restrictions for cell growth and proliferation. Activation of oncogenes enable cells to grow and proliferate even upon deficiency of nutrients, mitogens, and oxygen as is frequently the case in tumour environments (37). An example of this mechanism is the mutation of Ras GTPases. These proteins function

as molecular controls that regulate cell proliferation and cell survival pathways in response to extracellular signals. When activated, Ras proteins activate effectors that stimulate specific signalling pathways (38). Ras mutations are found in about 19% of cancer cases, and they promote overexpression or constitutive-activation of RAS proteins (39).

Alternatively, cells that have lost function of tumour suppressor genes can bypass the cell cycle check points and proceed to cell division despite DNA damage or absence of molecular signalling (40). This is the case of TP53 that has a key role in both G1 and G2/M checkpoints by regulating the expression of proteins that promote cell cycle arrest and apoptosis upon DNA damage and other types of stressors (41).

1.1.2 Kidney cancer and renal cell carcinoma

As mentioned before, cancer is a group of diseases characterised by cells that grow and divide uncontrollably, leading to the formation of tumours that as the disease progresses, invade adjacent tissues and other organs in a process called metastasis. Thus, kidney cancers include a group of diseases in which the growth of neoplasms in the kidneys occur. In 2015, kidney cancer represented the 9th most common cancer in men and 14th most common cancer in women worldwide (42). Kidney cancer was also among the 10 cancer with highest incidence in the UK in 2015, and it is projected to follow this trend until 2035 (43).

About 85% of kidney cancers are renal cell carcinoma (RCC), 8% are transitional cell carcinoma, between 5% and 6% are Wilms' tumour, and less than 1% include collecting duct tumours, renal sarcomas and renal medullary carcinomas (44). Renal cell carcinoma, the most common type of kidney cancer, often develops from renal tubular epithelial cells in the kidney cortex. Although its incidence has doubled in developed countries over the last 50 years, death rates have remained stable (45). This might be related to the high percentage of new cases discovered serendipitously during imaging, where smaller and localised tumours are detected (2).

1.1.2.1 Renal cell carcinoma

Renal cell carcinoma has a higher incidence in males between 60-80 years old, and has been associated with a number of risks factors, such as active and passive smoking, obesity and hypertension (44,46). Additionally, multiple hereditary disorders

increase the risk of developing RCC, including Von Hippel–Lindau syndrome, tuberous sclerosis, hereditary papillary renal carcinoma, syndrome of hereditary leiomyomatosis and renal-cell cancer, and Birt–Hogg–Dubé syndrome (47,48)

The prognosis of patient with RCC is tightly related to the stage of the disease upon diagnosis, as happens with most types of cancer (Figure 1.4). RCC tumours are staged according to the size, location, involving of the lymph nodes and presence of metastatic disease. Stages I and II of RCC, which have a 5-year survival rate of 95% and 88% respectively, present a single tumour within the kidney (46). In contrast, stage III tumours can spread out into major veins or adrenal glands within the Gerota fascia, or can involve a regional lymph node (49). Once the tumour invades beyond the Gerota fascia or presents metastasis, it is considered a stage IV tumour.

According to the histology and genetic features of the tumours, RCC is sub-classified in clear cell RCC (ccRCC), papillary RCC (pRCC) and chromophobe RCC (chRCC) (46,50). Clear cell RCC accounts for 75% of renal cell carcinoma. Mutations and silencing of VHL are a characteristic feature of ccRCC. The product of tumour suppressor VHL (Von Hippel–Lindau) gene negatively regulates the hypoxia-inducible factor (HIF) through polyubiquitilation that leads to proteosomal degradation in normoxic conditions (51). Inactivation of VHL causes accumulation of HIF, and as consequence, upregulation of genes involved in angiogenesis and metabolic reprogramming, including erythropoietin (EPO), vascular endothelial growth factor (VEGF), vascular endothelial growth factor receptors FLT1 and FLK1 and several glycolytic enzymes (52).

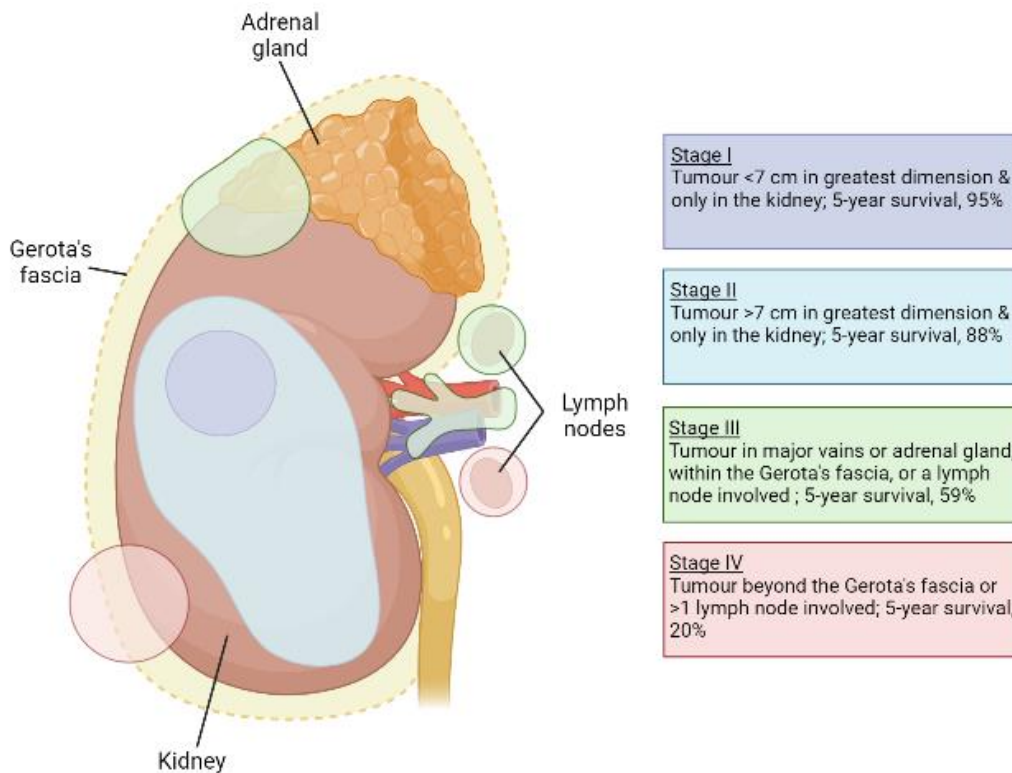


Figure 1.4. Staging of RCC and relevant therapeutic approaches. The staging of RCC depends on the size of the tumour, its locations and the involvement of lymph nodes. Staging of the disease determines the therapeutic approach selected to treat the patients and their outcome. Adaptation from (49).

Papillary RCC represents about 15% of RCC and is a heterogeneous disease further divided into sub-type 1 and sub-type 2, based on histological and genetic features. Sub-type 1 is characterised by papillae covered by a layer of small cells with basophilic cytoplasm and small nuclei (53,54). Also, papillary RCC sub-type 1 tumours often display hereditary and somatic mutations of the MET oncogene (55). In contrast, sub-type 2 tumours present papillae covered by cells with eosinophilic cytoplasm and large nucleoli, organised in a pseudostratified manner (53,54). These tumours show over-activation of the NRF2–antioxidant response element (NRF2-ARE) pathway, and are associated with a poor prognosis (53,55).

Chromophobe RCC accounts for 5% of RCC cases, generally of a more indolent nature than ccRCC (56,57). This sub-type of RCC often presents as a solid mass composed of eosinophilic cells and pale cells from the collecting duct (58). The most distinctive molecular feature of chRCC is the loss of chromosomes 1,2,6,10,13 and 17 displayed in most cases and 3,5,8,9,11,18 and 21 observed in a significant number of cases (59). Additionally, mutations in *TP53* and *PTEN*, as well as genomic rearrangement of the *TERT* gene promoter have been observed in chRCC (58).

1.2 Cancer: therapeutic strategies

Strategies to treat cancer have evolved according to the technology and knowledge of the disease available since the discovery of the disease. Selection of the therapeutic strategy depends on the type of cancer, the stage upon diagnosis and the localization of primary and metastatic tumours. When detected at early stage and the site of the tumour allows complete removal of the tumour, surgery is the goal standard as a curative approach. Radiotherapy can also be used to treat localised tumours alone as curative radiotherapy or combined with surgery and other therapies as adjuvant treatment.

Unfortunately, numerous patients are diagnosed once the cancer has invaded adjacent tissue or has even spread to other organs. For these cases, surgery or radiotherapy are not sufficient to maintain the patients in remission and systemic treatment is needed such as chemotherapy, hormone therapy, immunotherapy, and targeted therapy. Existing guidelines are used by clinicians to determine the most effective therapy to be used for each patient depending on the type of cancer, the stage of the disease, involvement of lymph nodes, hormone receptivity and genetic signatures of the tumour.

The upcoming sub-sections 1.2.1 and 1.2.2 contain a brief description about chemotherapy and targeted therapy, as they are both relevant for this research study.

1.2.1 Chemotherapy

Chemotherapeutic agents, as the name suggest are chemical compounds used as therapy in the battle against cancer. This therapeutic approach was born in the 20th century with the discovery of the alkylating agent nitrogen mustard that prevents DNA replication by triggering crosslinking lesions in the DNA that lead to cell death (60,61). As years have gone by, additional chemical compounds that inhibit cell functions related to growth and proliferation through different mechanisms have been discovered and have been used in the treatment of different types of cancer.

There is a broad range of chemotherapeutic drugs, including alkylating agents, DNA intercalating agents, topoisomerase inhibitors, and radiomimetic agents (Figure 1.5) (62). Alkylating agents react with DNA linking both strands. This cross-linking avoids DNA replication and when the lesion is not repaired, it induces apoptosis (63).

Procarbazine, melphalan and cyclophosphamide are currently used in the treatment of Hodgkin's lymphoma, multiple myeloma and breast cancer, respectively (60). DNA intercalating agents such as ActD, inhibit DNA replication and transcription and promote cell death by inserting between adjacent DNA bases and damaging the chromatin structure (64). ActD is used as therapy against rhabdomyosarcoma, gestational trophoblastic neoplasia, and Wilms' tumour (65). Topoisomerase inhibitors, as the name suggest are compounds than disrupt the activity of topoisomerases, enzymes that promote unwinding of DNA to enable its replication (66). Drugs as camptothecin and etoposide impair topoisomerases I and II, respectively, and have cytotoxic effect in lung cancer, cervical cancer, and ovarian cancer, among others (67). Lastly, the radiomimetic compound bleomycin reacts with the sugar moiety of nucleotides and leads to DNA strand breaks that impair DNA replication. Additionally, the reaction generates oxygen radicals that further attack DNA in a similar manner to ionizing radiation (68,69). Even though bleomycin displays high toxicity, it is used in the treatment of lymphomas and squamous cell cancers (70).

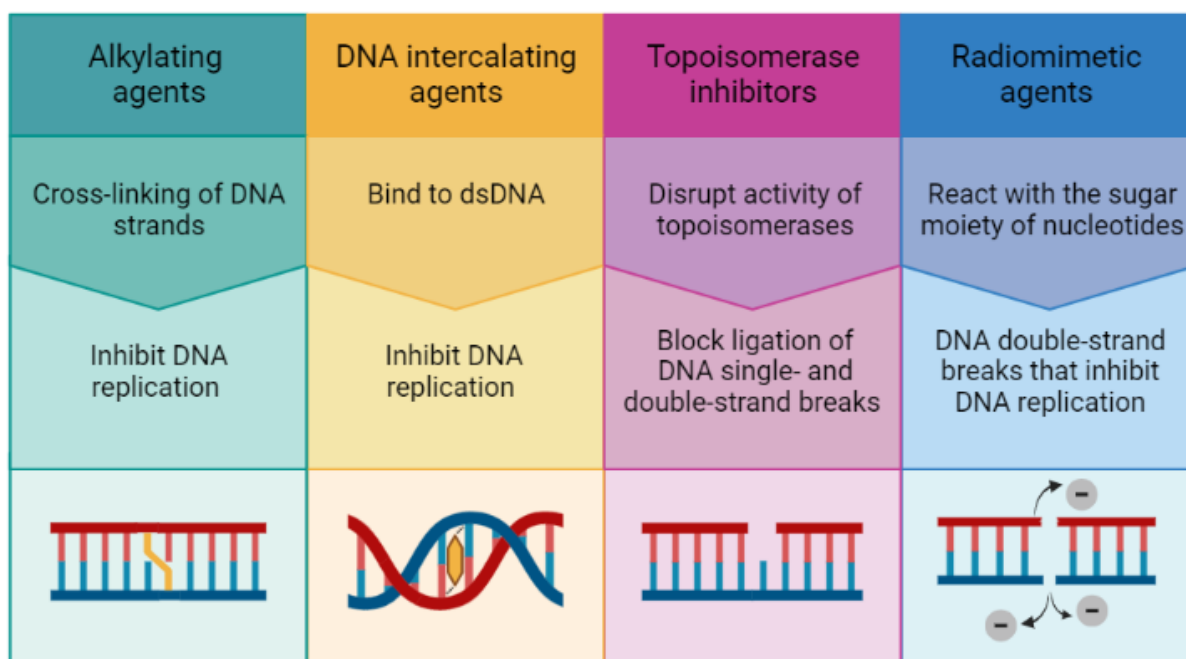


Figure 1.5. Summary of the types of chemotherapeutic agents and their mechanism of action. The four types of chemotherapeutic agents inhibit DNA replication through different mechanisms of action. The (-) icons represent oxygen radicals generated by the reaction of radiomimetic compounds with the sugar moiety of nucleotides.

Even though the mechanisms of actions vary, these cytotoxic drugs promote cell death by blocking fundamental cellular processes such as DNA transcription and replication that are needed by a cell to grow and divide, respectively. Such processes are not

exclusive to cancer cells, but they are enhanced in cancer cells that incur faster division rates and dysregulated growth. However, there are different types of somatic cells including hematopoietic cells and epithelial cells that also display high rates of mitosis. The secondary effects caused by chemotherapy happen as consequence of the non-specific activity of the compounds on rapidly dividing cells found in the bone marrow, hair follicles and mucosa, among other tissues.

1.2.2 Targeted therapy

Considering the latter and supported by advances in the field of molecular biology of cancer, research has focused on discovering new targets found specifically in cancer cells, and on developing compounds that could aim for those targets. This approach initiated with the discovery of the Bcr-Abl1 onco-protein resultant of the truncated chromosome 22, known as Philadelphia chromosome, characteristic in chronic myeloid leukaemia (CML). This feature is produced by a reciprocal translocation between the chromosomes 9 and 22, which produces a constitutively active tyrosine kinase that promotes oncogenic behaviours such as enhanced proliferation rates, inhibition of cell differentiation and resistance to cell death (71,72). Identification of this unique characteristic, led to the development of imatinib (Gleevec), a tyrosine kinase inhibitor that targets the chimeric onco-protein and as consequence inhibits proliferation and induces apoptosis only in Bcr-Abl1-expressing cells (73). Patients with CML treated with this drug had better responses, prognosis and overall survival than patients that received previous treatments (74).

Unregulated growth and proliferation are known hallmarks of cancer, thus, the mechanisms involved in these cellular functions have been deeply explored for the development of targeted therapy. As it would be expected, these processes are tightly regulated in normal cells through different signalling pathways that, depending on external and internal conditions, allow or restrain growth and proliferation. In cancer, dysregulation of growth and proliferation results from enhancement of the signalling pathways by overexpressed or truncated proteins that are encoded by oncogenes, or by loss of function of proteins that negatively control these signalling pathways, encoded in tumour suppressor genes. Hence, targeted therapy has focused on some of the proteins that play a role in the hyper-activation of these signalling pathways.

Growth factor receptors and kinases are amongst the proteins that upregulate growth and proliferation in cancer. Consequently, many of them have been used as targets of the new therapeutic approach. For example, truncated or overexpressed receptor tyrosine kinases of the EGFR family promote cancer by constitutively activating the signalling cascade, sending growth signals even in the absence of its ligand. Compounds as the small molecule kinase inhibitors Gefitinib and Erlotinib used for the treatment of lung cancer, target tyrosine kinase activity of this family of receptors (75). Additionally, the monoclonal antibody Trastuzumab binds specifically to the ErbB2 receptor and promotes its degradation (76).

The Src family of kinases that promote cell proliferation and survival are often hyperactivated in cancer (77). Thus, drugs such as Bosutinib and Dasatinib that inhibit their kinase activity have been developed and are used in the treatment of breast cancer (78). Similarly, activity of mTOR, a serine/threonine kinase that works as a central hub in the regulation of cell growth, is frequently enhanced in cancer through different mechanisms, including the loss of function of the tumour suppressor *PTEN*. As this kinase plays an essential role transducing signals to promote growth, different types of inhibitors to suppress its activity such as Everolimus and Temsirolimus are used in the treatment of different types of cancer such as breast cancer, kidney cancer, and colon cancer (79–81). Compounds targeting KRAS, which is product of an important oncogene and driver of many types of cancer, are still unavailable. A strategy that aims to inhibit the enhanced signalling of KRAS, is to target its downstream effector RAF. Vemurafenib and dabrafenib are drugs that bind and inhibit RAF, which have been used for treatment of melanoma (82).

A different approach of targeted therapy consists in compounds that promote reactivation or reconstitution of the negative controls of the signalling pathways encoded by tumour suppressor genes. *TP53* is mutated in about 50% of all human cancers and it is downregulated by genetic amplification of its negative regulator *MDM2* in a large percentage of different types of cancer (83,84). It is known as the guardian of the genome because the expressed protein plays an essential role in DNA damage repair mechanisms. Additionally, p53 controls cell cycle and growth, it induces apoptosis in the presence of certain stressors and modulates cellular metabolism (85). Thus, it is not surprising that its absence or loss of function promotes carcinogenesis. Since this protein is involved in several key functions of cell survival, under normal

circumstances, it is tightly regulated and low levels of p53 are maintained by MDM2-mediated proteosomal degradation. In the presence of stress, p53 stabilises and modulates cell cycle arrest and apoptosis. However, overexpression of MDM2 in cancer cells blocks accumulation of p53 even in the presence of stressors, allowing growth, proliferation and resistance to apoptosis. Considering this, the inhibition of MDM2 by the compound Nutlin-3A represents another strategy of targeted therapy (86–88). This small molecule binds to MDM2 in the p53-binding pocket, impairing p53-MDM2 interaction, stabilising p53, which in turn leads to cell cycle arrest and apoptosis (89).

Targeted therapy has also focused on angiogenesis, an important hallmark of cancer through which the tumour promotes the formation of new blood vessels to get access to oxygen and nutrients. Cancer cells stimulate angiogenesis through secretion of pro-angiogenic factors like VEGFs, TNF- α , angiogenin, interleukin 8, and others (90). Hence, compounds such as Sorafenib and Sunitinib that inhibit VEGF receptors and the monoclonal antibody bevacizumab that neutralizes secreted VEGF have been developed as anti-cancer therapies (91,92).

1.2.3 Therapeutic landscape of renal cell carcinoma

The therapeutic approaches with RCC vary greatly depending on the stage of the disease. Surgical excision of the tumour is the gold-standard treatment and can lead to cure of the disease when the tumour is solely localised in the kidney. Partial nephrectomy rather than radical nephrectomy is preferred to salvage renal function, but selection of the approach depends on the size, location, stage of the tumour, and the experience of the surgeon. For elderly patients or those unable to undergo a surgical procedure, alternatives such as cryoablation and radiofrequency are available (93,94).

Unfortunately, around 43% of the new kidney cancer cases that were staged when detected in England in 2019 were stage III and IV (13). Patients with invasive and metastatic RCC require a systemic approach such as chemotherapy or immunotherapy. Nevertheless, metastatic RCC generally shows poor response to conventional chemotherapy, and has a 5-year survival rate of only 12% (2,95).

An improved understanding of the genetic signatures of RCC has allowed implementation of better-tailored therapies. Such is the case for patients with loss of

function of *VHL*. The tumour suppressor gene *VHL* is the most frequently mutated gene in clear cell renal cell carcinoma. Loss of functional *VHL* leads to upregulation of hypoxia-inducible factors (HIFs), and consequently, increased expression of HIF targets involved in angiogenesis, apoptosis, and glycolysis (49). Accordingly, targeted therapies that inhibit the HIF pathway including VEGF inhibitors sunitinib and cabozantinib, are now the standard therapy for ccRCC (96).

Other genes associated with higher risk of kidney cancer include *PTEN*, *TSC1* and *TSC2*, tumour suppressor genes that regulate the mTOR pathways (97). Inhibitors that target the mTORC1 such as temsirolimus and everolimus are used to treat RCC and have been proved to be more successful in patients whose tumours harbour mutations in *TSC1*, *TSC2* or loss of expression in *PTEN* (98).

In the last decade, immunotherapy has also become an important strategy for RCC treatment. Monoclonal antibodies that block PD-1, PD-L1, or CTLA-4 to re-activate T-cell antitumour activity called immune checkpoint inhibitors (ICI) have been developed and shown promising results (99,100). The use of ICI such as nivolumab, ipilimumab, Pembrolizumab, and axitinib, alone and in combination with tyrosine kinase inhibitor (TKI), has been approved by the FDA to be used as RCC first-line treatments based on the benefits observed in Phase III trials (100).

1.2.4 Drug resistance

As mentioned before, the discovery of Bcr-Abl1 and the positive response of patients with CML to Gleevec led the way to targeted therapy. In the last two decades, identification of the differences between cancer and normal cells has become a priority, and the list of compounds that have been developed and tested in clinical trials keeps growing. Nevertheless, many of these compounds have not achieved the expected results, and one of the main reasons is the development of drug resistance.

Resistance to targeted therapy can be either innate or acquired. The former exists due to the heterogeneity of tumours, and it means that some cancer cells within the tumour are already resistant to the drug before exposure. Acquired-resistance is promoted by genetic instability and by the activation of alternative signalling pathways. In both cases, the administration of the drugs acts as a selective pressure that eliminates drug-sensitive cells and thus, promotes thriving of the resistant clones (101,102). Additionally, there are different mechanisms that mediate drug resistance that consist

in 1) alteration of the driver gene; 2) activation of parallel or downstream signalling pathways; 3) activation of different pro-survival pathways; 4) morpho-phenotypic evolution (Figure 1.6.) (103,104). Alteration of the driver gene generally involves mutations that modify the composition or structure of the target protein and consequently, prevents the binding of the inhibitor. In the case of kinase inhibitors, which mainly bind to the ATP-pocket of the kinase domain, the mutations block binding of the drug whereas allow interaction with the substrate (103). Drug resistance through activation of parallel signalling pathway occur by overexpression of an alternative protein that feeds the same signalling pathway. An example of this mechanism is the amplification of MET oncogene in gefitinib-resistant non-small cell lung carcinoma (NSCLC) cell lines. The trans-membrane tyrosine kinase receptor encoded by MET activates the ERBB3/Akt signalling independently from genfitinib-inhibited EGFR (105). Similarly, activation of downstream signalling pathway requires upregulation of a signal transducer that acts downstream the blockage caused by the inhibitor. As can be observed in FLT3 TKI-resistant cell lines, exposure to TKIs, abrogate the activity of FLT3 receptor but not that of the substrates downstream of the signalling pathway such as Akt and/or MAPK (106). Drug resistance can be achieved through activation of different pathways that promote cell survival, such as inhibition of apoptosis. Activation of the anti-apoptotic NF- κ B pathway has been associated with development of drug resistance in a variety of cancers (107,108). Last, morpho-phenotypic transformation has been associated to drug resistance. Although a causal relationship between the phenotypic changes and acquisition of drug resistance has not been demonstrated, epithelial-to-mesenchymal transition has been connected to acquired-resistance versus targeted therapy. Similarly, transformation of non-small cell lung adenocarcinoma to small cell carcinoma has been observed in targeted therapy-resistant tumours (103).

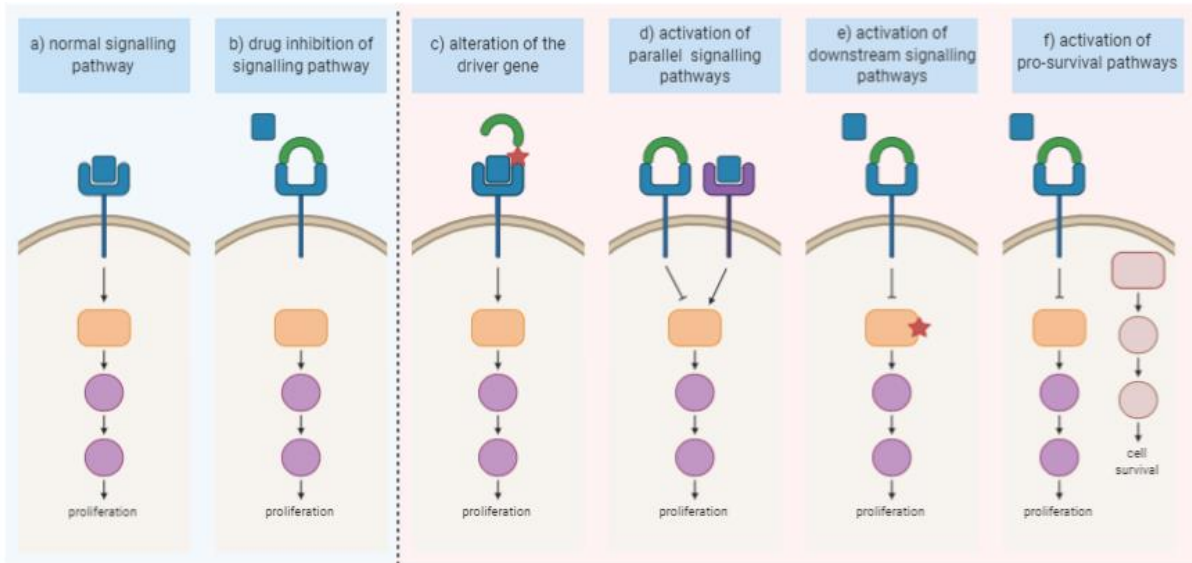


Figure 1.6. Mechanisms mediating drug resistance. Representation of the flow of a signalling pathway a) and its inhibition by targeted therapy b). Alteration of the driver gene causes conformational/composition changes on the target protein that prevent the binding of the inhibiting compound c). Activation of parallel d) or downstream e) signalling pathways allows propagation of the signal even if the inhibitor is properly suppressing the activity of its target. Activation of different pro-survival pathways prevent cell death caused by the inhibitor through heightening of anti-apoptotic pathways f). Figure adapted from (103).

1.2.5 Drug combinations: a strategy against resistance

As stated before, chemotherapy acts as a selective pressure for the resistant clones, and this effect is enhanced when the therapy is cytostatic rather than cytotoxic, as most of the targeted therapies are. When cells are arrested but not killed, they can survive long enough to acquire resistance. Thus, strategies to tackle development of resistance include combinatorial therapies that aim at different mechanisms simultaneously to promote cell death. Combination of chemotherapeutic agents started with the use of VAMP regimen which integrates the use of four agents in a treatment against acute lymphocytic leukaemia in children. The administration of multiple drugs yielded better results, decreasing tumour burden and prolonging disease-free survival (109). Nowadays, the use of combinatorial therapy is still widely implemented in the clinic. In particular, the use of targeted therapy in combinatorial regimens has overcome the low responses and high rates of drug resistance attained when these drugs are administered as single agents (110).

Drug combinations vary and the way they are administered to the patients depend greatly on the strategy they follow to achieve apoptosis in cancer cells. Some strategies focus on the use of agents that target different mechanisms simultaneously

in order to promote apoptosis while avoiding development of drug resistance (110). Other combinations take advantage of the effect of one to enhance the effect of the other. The use of inhibitors that cause cell cycle arrest, plus a cytotoxic drug that targets arrested cells, follow this strategy (111). Similarly, the use of carbonic anhydrase inhibitors enhances the toxicity of the chemotherapeutic agent doxorubicin by increasing drug intake in cancer cells (112). Additionally, some strategies take advantage of the resistance mechanisms in cancer cells to certain drugs, to protect the normal cells and kill cancer cells in a more selective manner (113). An example of this is the cyclotherapy. This regimen consists in providing an inhibitor of cell cycle to which the cancer cells are resistant, followed by a cytotoxic drug that targets proliferating cells. Thus, the normal cells are arrested as an effect of the inhibitor of cell cycle and are protected from the effects of the second drug, while cancer cells bypass the cell cycle arrest and are induced into apoptosis by the cytotoxic agent (114).

Importantly, combinatorial therapy has also re-purposed drugs as anti-cancer therapies (115). Re-purposing of drugs is a cost-effective strategy that allows implementing previously approved drugs, for which proper dosages and toxicity are known, in the treatment of a different disease from the original intended (116). The compound rapamycin, an mTOR inhibitor that was originally used to treat patients with organ transplants, was discovered to inhibit proliferation of cancerous cells, and has been used in combinatorial regimens as cancer therapy (117).

The strategy presented in this project proposes that targeting the synthesis of rRNA, a highly activated process in cancer cells, through two different mechanisms, might promote cell death in cancer cells. The hypothesis proposes that the used of mTOR inhibitors, a targeted therapy, can sensitise cancer cells to the cytotoxic effect of ActD.

1.2.6 A perspective on the drug discovery and relevance of drug repurposing

The process of drug discovery is long, expensive, and frequently unsuccessful. It requires not only discovery and development of a compound, but also pharmacological and toxicity studies using *in vitro* and *in vivo* models, and ultimately clinical studies to assess safety, determine dosage, evaluate efficacy, and identify secondary effects and adverse reactions in patients (Figure 1.7.) (118,119).

New technologies that enable high-throughput drug screening can be used to test thousands of compounds per day, aiding identification of potential effective drugs

(120). Nevertheless, the rest of the process has not changed much since 1960's, while the costs to get a drug out to the market have increased to over \$2 billion USD and the average time for clinical development and regulatory approval exceeds 10 years (119,121,122). This, in addition to a registration success rate of only 8% for cancer drugs that entered Phase I clinical trials, are the main obstacles for the development of cancer therapies (123).

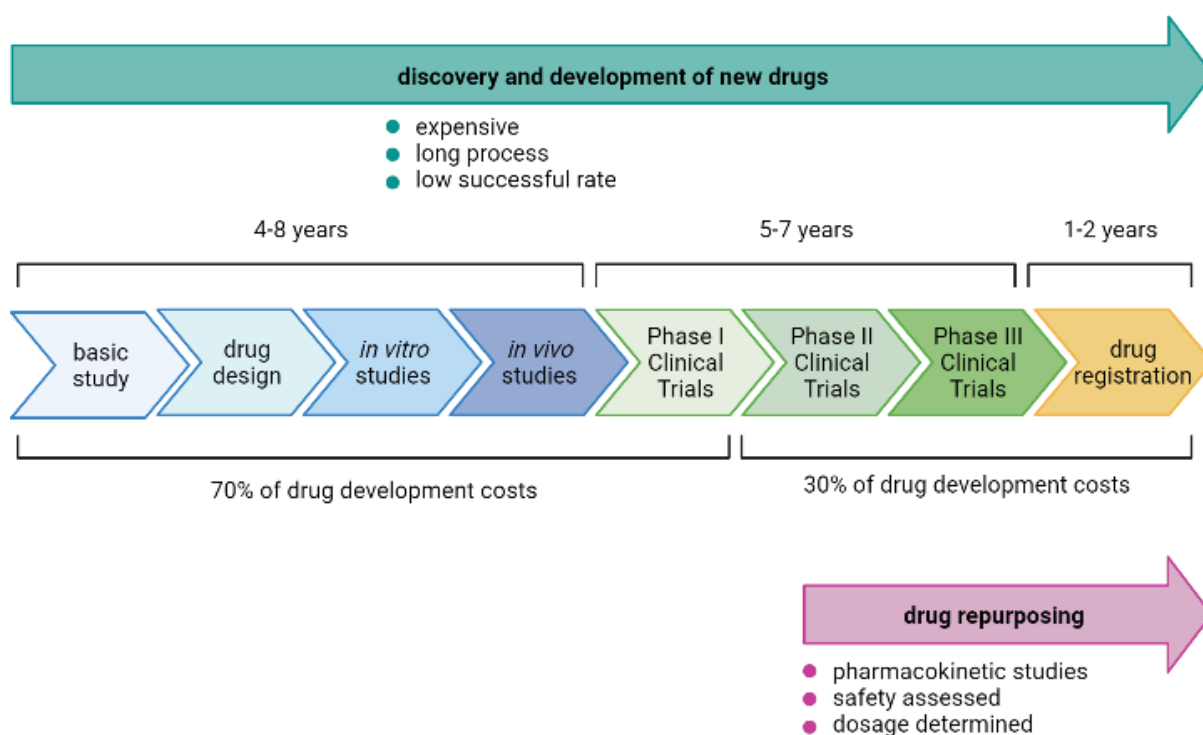


Figure 1.7. Drug discovery and development timeline. The process takes in average 13 years from drug discovery to successful registration. Time and costs are drastically reduced with repurposed drugs as pharmacokinetic, pharmacodynamic, and toxicity studies have already been carried out for these drugs. Illustration adapted from (119).

Drug repurposing is an attractive strategy that aims to reduce the time and economic burden of research and development (R&D) of new drugs (Figure 1.7) (124). This is achieved because pharmacokinetics and pharmacodynamics have been previously assessed for repurposed drugs. In addition, phase I clinical trials that assess safety and dosage can also be bypassed (119).

Additionally, the success of drug repurposing can be increased when using the compound in combinations that produce a synergistic effect (125). Different rationales for drug combination have been discussed. Some argue that for cancers that depend on a single oncogene, a phenomenon known as oncogene addiction, the use of

multiple drugs that target the same kinase is the preferred approach (126). Others propose that since several pathways are dysregulated in cancer and interconnection of signaling pathways through feedback loops is a main concern for development of drug resistance, combination of drugs that target multiple mechanisms are more appropriate (127).

Moreover, maintaining a balance between targeting multiple signaling pathways and preserving treatment specificity for cancer cells needs to be taken into consideration when proposing a drug combination. The proposal described in the present study considers targeting a cellular function enhanced in cancer cells, in this case nucleolar function, through different mechanisms simultaneously, using kinase inhibitors that modulate ribosomal biogenesis to sensitize cancer cells specifically to the cytotoxic effects of the NFI ActD. This strategy aims to take the best of both drugs: enhance the promotion of apoptosis caused by traditional chemotherapy while increasing treatment specificity granted by targeted therapy.

1.3 The nucleolus: the factory creating ribosomes and a critical stress sensor

The nucleolus is a complex and dynamic subunit of the nucleus that has become an important target for research in recent decades. It is now known to be more than just the locus where the biogenesis of ribosomes takes place; the role of the nucleolus as a regulator of cell cycle progression and cell proliferation has also become well established (128).

The nucleolus assembles around sections of the DNA with a high content of GC bases, where ribosomal RNA (rRNA) genes are present in tandemly repeated clusters called nucleolar organising regions (NORs). The promoters of pre-ribosomal RNA genes have two transcription control regions (Figure 1.8). The first one, located around -100bp from the start site is known as the upstream control element (UCE). And the second one, the core element (CE) contains the transcriptional initiation site including bases -31 to +6 is required for transcription of the 47S precursor rRNA (pre-rRNA).

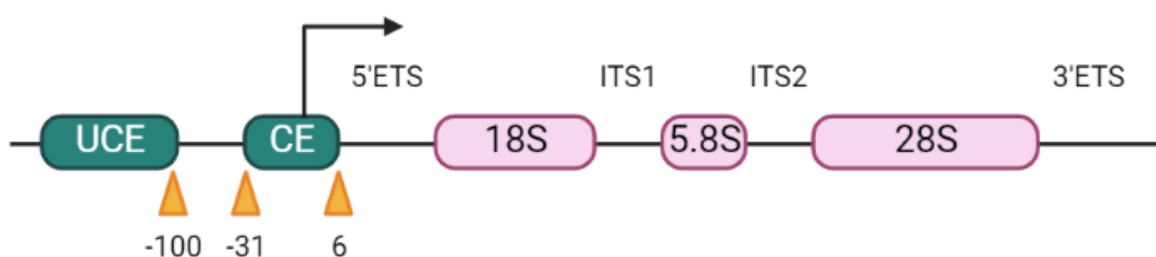


Figure 1.8. Pre-rRNA and promoter region. The promoter region of the rRNA includes an upstream control element (UCE) and a core element (CE). rDNA contains two introns that separate the coding regions for 18S, 5.8S and 28S. The information displayed in the diagram was obtained from (129).

As illustrated in Figure 1.9, both transcriptional control regions are recognized by the upstream binding factor (UBF), a HMG-box protein, which binds to them and generates a loop in the DNA between the two sections (129,130). Following UBF binding, selectivity factor 1 (SL1) binds to the UBF-DNA complex and stabilises it, facilitating incorporation of RNA Pol I and initiation of rDNA transcription. RNA Pol I requires prior activation by the transcription initiation factor TIF-IA. Interaction of TIF-IA with RNA Pol I promotes stabilisation of the RNA Pol I monomer and induces structural changes required for DNA loading into the DNA template-binding site of RNA Pol I and transcription initiation (131,132). The TIF-IA-RNA Pol I complex then binds to the transcription complex formed by UBF, SL1 and the rDNA promoter (133), and this complex then initiates rRNA transcription.

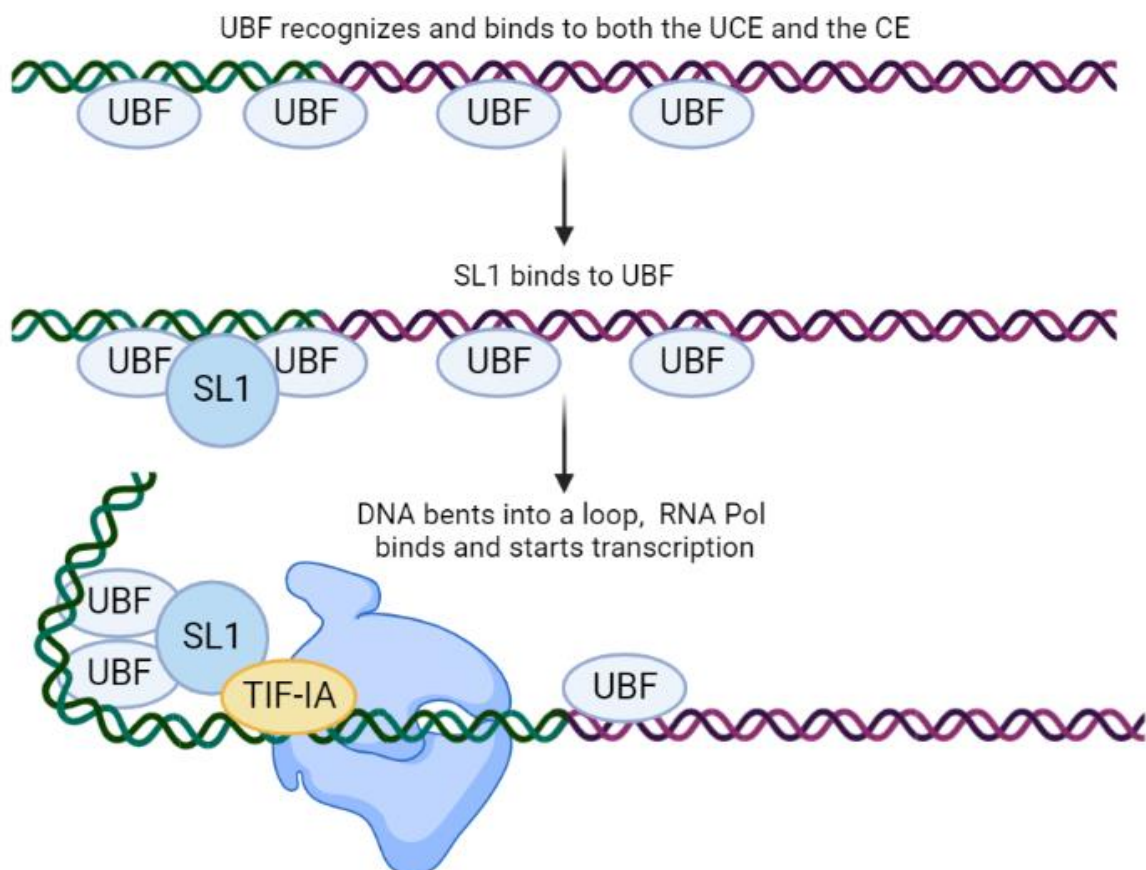


Figure 1.9. Assembly of RNA Pol I initiation complex. Assembly of the RNA Pol I initiation complex requires UBF binding to the UCE and CE, followed by binding of SL1 to UBF. This interaction enables bending of DNA required by a TIF-IA-activated-RNA Pol I to recognise the promoter region and initiate rDNA transcription.

The transcriptional initiation and elongation of the 47S pre-rRNA take place in the fibrillar centre (FC), the inner component of the nucleolus (see Figure 1.10). The processing of pre-rRNA consists of post-transcriptional modifications including nucleoside modification and cleavage reactions that occur in the dense fibrillary component (DFC) of the nucleolus. Among the chemical modifications, methylation is carried out by a group of small nucleolar ribonucleoproteins (snoRNPs) called C/D snoRNPs (134,135). In the same way, H/ACA snoRNPs are involved in the pseudouridylation of pre-rRNA (134,135). Ribonucleases mediate cleavage of pre-rRNA that lead to the formation of 18S, 5.8S and 28S pre-rRNA segments (136).

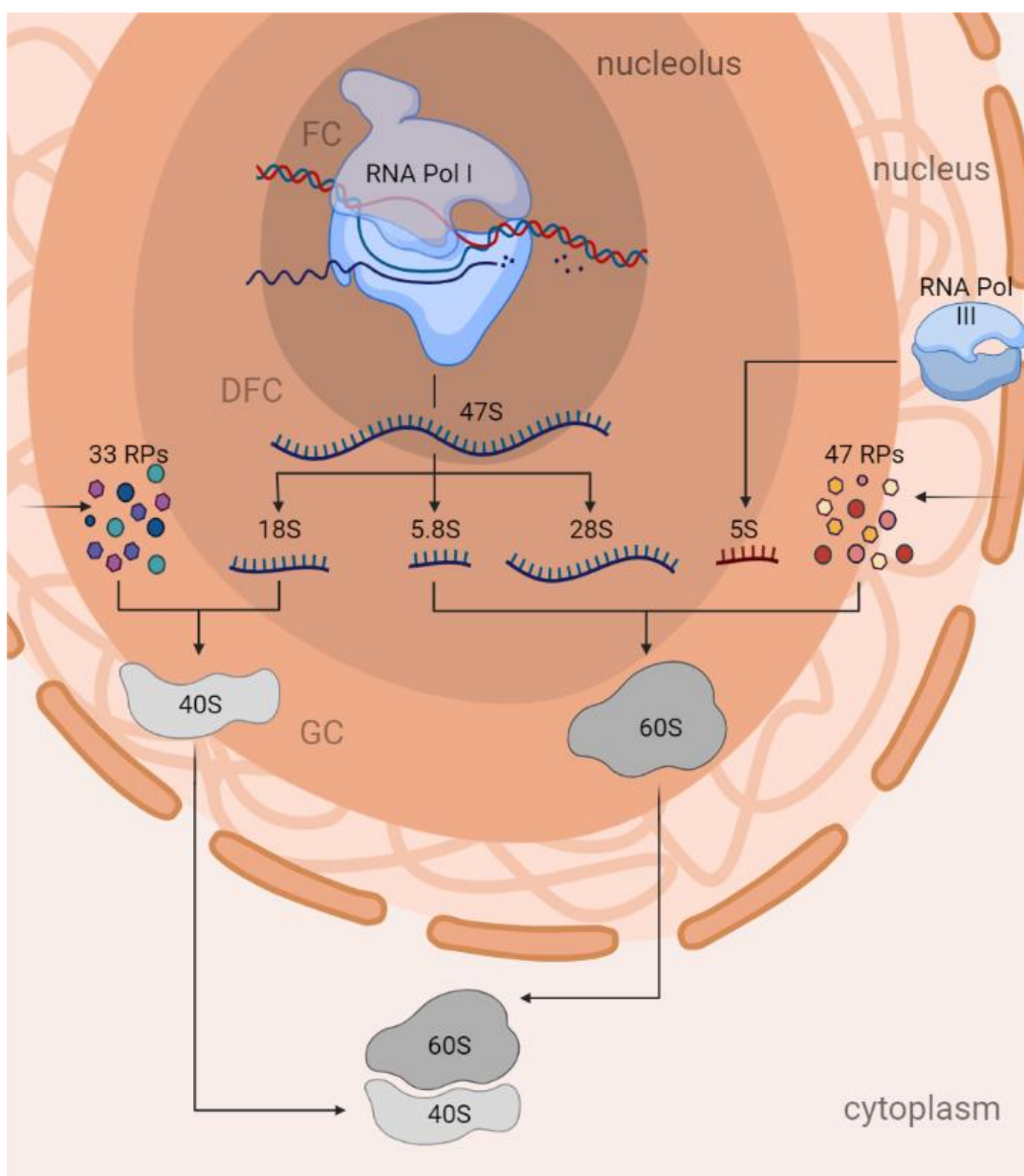


Figure 1.10. Ribosomal biogenesis in the nucleolus. The process is initiated in the fibrillar centre with the transcription of the 47S pre-rRNA. The transcript is then processed and cleaved to produce

18S, 28S and 5.8S transcriptional segments in the dense fibrillary component of the nucleolus. The resulting segments are combined with ribosomal proteins (RPs) to assemble the small and large ribosomal subunits in the granular component, and then transported to the cytoplasm to build up the ribosomes. Diagram adapted from (14)

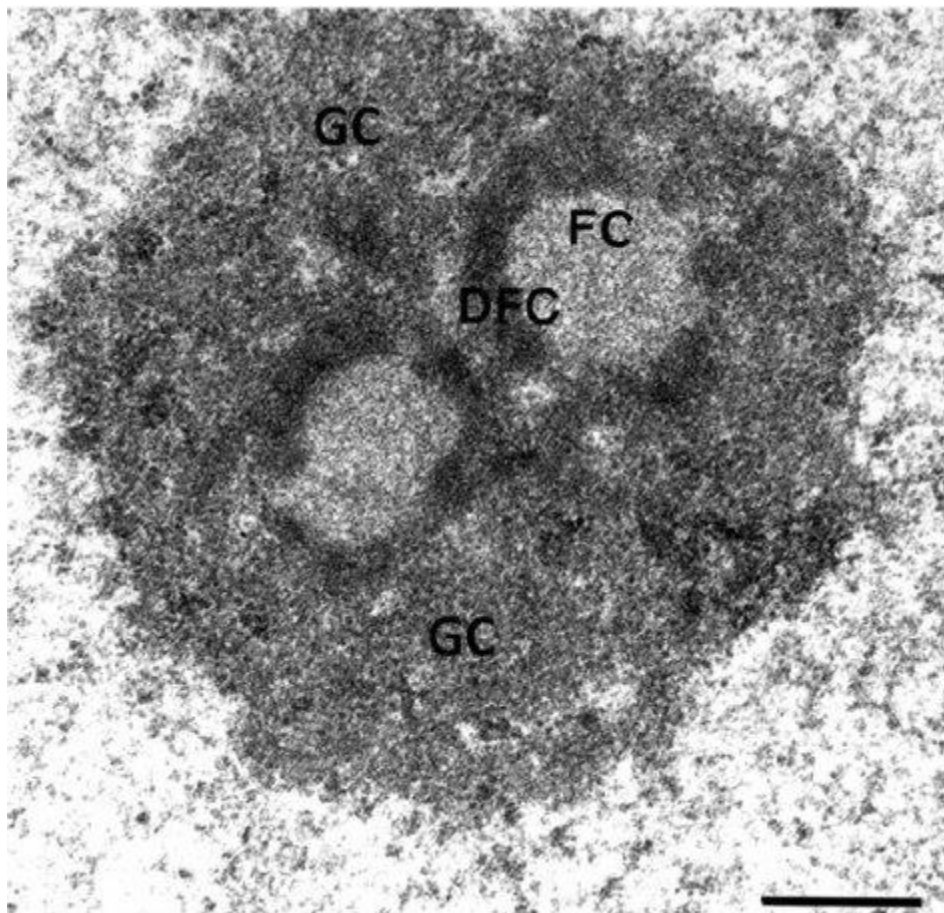


Figure 1.11. An electron micrograph of the nucleolus of a HeLa cell. The three sub-structures comprising the nucleolus are the fibrillar centre (FC), the dense fibrillar component (DFC), and the granular component (GC). Bar 0.5 μm . Figure reproduced from (137)

Once the rRNA segments have been processed, ribosome assembly factors or trans-acting factors promote the formation of a complex containing rRNA segments and ribosomal proteins to assemble the ribosomal subunits in the outer layer of the nucleolus, known as the granular component (GC) (138,139). The 18S transcript along with 33 ribosomal proteins are assembled into the small ribosomal subunit (SSU). The 5.8S and the 28S segments, together with the 5S transcription product of RNA Pol III and 47 ribosomal proteins are assembled to create the large ribosomal subunit (LSU) (135,140). Both subunits are transported to the cytoplasm, where they are combined into a functional ribosome.

Table 1.1. Functions of the sub-structures of the nucleolus. Information obtained from (129,135).

Fibrillar centre	Dense fibrillar component	Granular centre
<ul style="list-style-type: none"> • rRNA transcription initiation (rDNA, UBF, SL1, TIF-IA, RNA Pol I) • rRNA transcription elongation (rDNA, RNA Pol I) 	<ul style="list-style-type: none"> • post-transcriptional modifications of 47S pre-rRNA segment (methylation & pseudouridylation by snoRNPs) • cleavage of 47S pre-rRNA (ribonucleases) 	<ul style="list-style-type: none"> • Assembly of the small ribosomal subunit (18S and 33 ribosomal proteins) • Assembly of the large ribosomal subunit (5.8S, 28S, 5S, and 47 ribosomal proteins)

1.3.1 Interdependence of nucleolar structure and function

The nucleolar structure and its function are intimately linked in such a way that disruption of one promotes the disruption of the other and vice versa (141). The nucleolus, as previously mentioned has three main structures: the fibrillar centre, the dense fibrillar component and the granular component, and it is in each of these sites that different processes required for ribosome biogenesis take place (Figure 1.11). It is generally believed that the formation of said structures is promoted by the concentrations, conformation and interactions of the components that play a role for ribosome biogenesis, such as proteins, RNA and DNA, through a physical phenomenon known as liquid-liquid phase separation (LLPS) (142,143). The fibrillar centre, the site where rDNA transcription initiation takes place (see Figure 1.10), contains rDNA and topoisomerase I, along with key components of the RNA Pol I machinery including RNA Pol I, UBF and TIF-IA (143). The dense fibrillar component displays high concentration of fibrillarin, an RNA-binding protein involved in the post-transcriptional processing of pre-rRNA, along with snoRNAs and snoRNPs which are also pre-rRNA processing factors (144,145). Last, the granular component is rich in nucleophosmin (NPM1), which has been shown to mediate the translocation of the 40S and 60S ribosomal subunits from the nucleolus to the nucleus and cytoplasm (146). The interaction of fibrillarin and NPM1 in vitro has been shown to simulate the organisation of the dense fibrillar component and the granular component within the

nucleolus (147), supporting the idea that LLPS contributes to the formation and conservation of the nucleolar structure.

The formation of nucleolar structure is also coordinated with the cell cycle. Assembly of the nucleolus occurs at the beginning of telophase and requires both activation of rDNA transcription and the recruitment and activation of the RNA processing complexes that form the sub-nucleolar structures (148). RNA Pol I activation at the end of mitosis is mediated by repression of the CDK1-cyclin B kinase activity by phosphatases PP1 and PP2A (149), while the recruitment and activation of the RNA processing complexes occurs through the formation of foci known as prenucleolar bodies (PNBs) constituted by nucleolar processing proteins, snoRNAs, ribosomal proteins and pre-rRNAs, and the migration of these components to the rDNA transcription sites (148). In contrast, nucleolar disassembly takes place at the beginning of mitosis with the translocation of nucleolar proteins, ribosomal proteins, snoRNAs and pre-rRNAs from the GC and DFC to the perichromosomal compartment. This is followed by inactivation of the rDNA transcription mediated by Cdk1-cyclin B phosphorylation of the components of the RNA Pol I transcription machinery (148). A strict coordination of the processes involved in the assembly and disassembly of nucleoli is required for adequate formation and maintenance of the nucleolar structure and function.

Considering that the composition, concentration and interactions among nucleolar components influence the structure and function of nucleoli through LLPS, it is no surprise that changes in the expression, localisation and degradation of nucleolar components including proteins, pre-rRNAs, snoRNAs, and snoRNPs are associated with nucleolar morphological changes and impairment of nucleolar function (145). Generally denoted as nucleolar disruption, nucleolar morphological alterations include segregation and fragmentation (141,145,150). Nucleolar segregation is characterised by the condensation and separation of the nucleolar sub-components, along with the translocation of nucleolar proteins such as NPM1, fibrillarin, UBF, and other proteins related to the RNA pol I transcriptional machinery from the sub-nucleolar compartments to the nucleolar periphery, forming the 'nucleolar caps' (145,151). Nucleolar segregation is caused by DNA damage and/or transcriptional inhibition and accordingly, it is observed following UV irradiation, inhibition of topoisomerase II by drugs such as etoposide, and exposure to low concentrations of ActD (141,145).

Nucleolar fragmentation occurs following inhibition of RNA Pol II or protein kinases, and leads to unravelling of the FC (145,150). Other nucleolar changes such as increased size and number of nucleoli are associated with different pathologies including viral infection and cancer where RNA Pol I activity is enhanced through activation of oncogenes or loss of function of tumour suppressor genes (145,150,152–154). In addition, nucleolar disruption has been associated with aging and neurodegenerative diseases (155–159).

1.3.2 Diversity of nucleolar function

For decades, the nucleolus was essentially recognized as the ribosomal factory of the cell. However, with the arrival of proteomics and improvements in the technology underpinning this, the composition of the nucleolus has been studied and this has revealed that only a small percentage of the nucleolar proteome is involved directly in ribosomal synthesis (160). Among the 350 different proteins identified in the nucleolus by different research groups, only ~30% have been linked to ribosome biogenesis either as active players or as chaperones involved in rRNA processing (161,162). The rest of the nucleolar proteome is related to other cellular processes, including cell growth and cell proliferation (163).

Several of these proteins are only transiently located in the nucleolus, whilst their known function is performed outside of the nucleolus. Such behaviour suggested that the nucleolus might be involved in a broader range of cellular pathways than was initially thought, perhaps through the sequestration and re-location of proteins. Indeed, further studies confirmed this, and there is evidence that the activity of proteins such as MDM2, p53, VHL, Hsp70, and H2B is regulated by such a nucleolar mechanism (164,165). Through regulating the activities of these nucleolus-associated proteins, the nucleolus is involved in a broad range of cellular functions including regulation of cell cycle progression, modulation of oncogenic pathways, DNA damage repair and stress signalling (166).

One of the most critical functions of the nucleolus is its role as a stress sensor for the cell. Different types of stressors impair nucleolar function, which is followed by disruption of the nucleolar structure (167,168). This in turn, leads to stabilisation of p53 and, as a consequence, induces cell cycle arrest or apoptosis (141). Nucleolar stressors include DNA-damaging agents such as UV irradiation, chemicals that impair

rDNA transcription like ActD and 5,6-Dichloro-1- β -d-ribofuranosylbenzimidazole (DRB), compounds that inhibit RNA processing such as 5-fluorouracil (5-FU), or depletion of nucleotides that prevents synthesis of RNA amongst others (141). Additionally nucleolar function is modulated by stress-activated c-Jun N-terminal protein kinase (JNK2) through phosphorylation of TIF-IA at position Thr200, which leads to inhibition of rRNA transcription (169). In a similar manner, under conditions of low energy availability, AMP-activated protein kinase (AMPK) phosphorylates TIF-IA at Serine 635, and prevents it from binding to the transcription initiation complex, inhibiting rRNA transcription (170)

The response of p53 to stress is modulated by the nucleolus through different mechanisms (150). Following exposure to various stress factors that impair nucleolar function, the nucleolus is disrupted and interactions between proteins are altered. In this scenario, increased binding of nucleolar proteins RPL5, RPL11, RPL23 and ARF to MDM2 occurs, and this prevents MDM2-mediated degradation of p53, followed by stabilisation of p53 (167,171,172). Furthermore, nucleolar disruption decreases the export of ribosomal subunits to the cytoplasm, and thus prevents the translocation of MDM2 and p53 to the cytoplasm which is facilitated by their interaction with ribosomal subunits, a mechanism known as “riding the ribosome” (141,150,173). Thus, disrupting nucleolar structure leads to an increase in the pool of nuclear p53 and enhances transcription of p53 targets (150,174). Moreover, the disruption of 40S biogenesis promotes the release of RPL11 mRNA from the nucleolus. This mRNA contains a 5-TOP motif, which promotes its translation and leads to excess production of RPL11 which then increasingly binds to MDM2, preventing MDM2-mediated ubiquitination of p53 (175). Similarly, RPL26 is released upon disruption of 60S biogenesis, and it then enhances translation of p53 by binding to the 5'-untranslated region (UTR) of p53 mRNA, promoting its association with heavy polysomes (176,177).

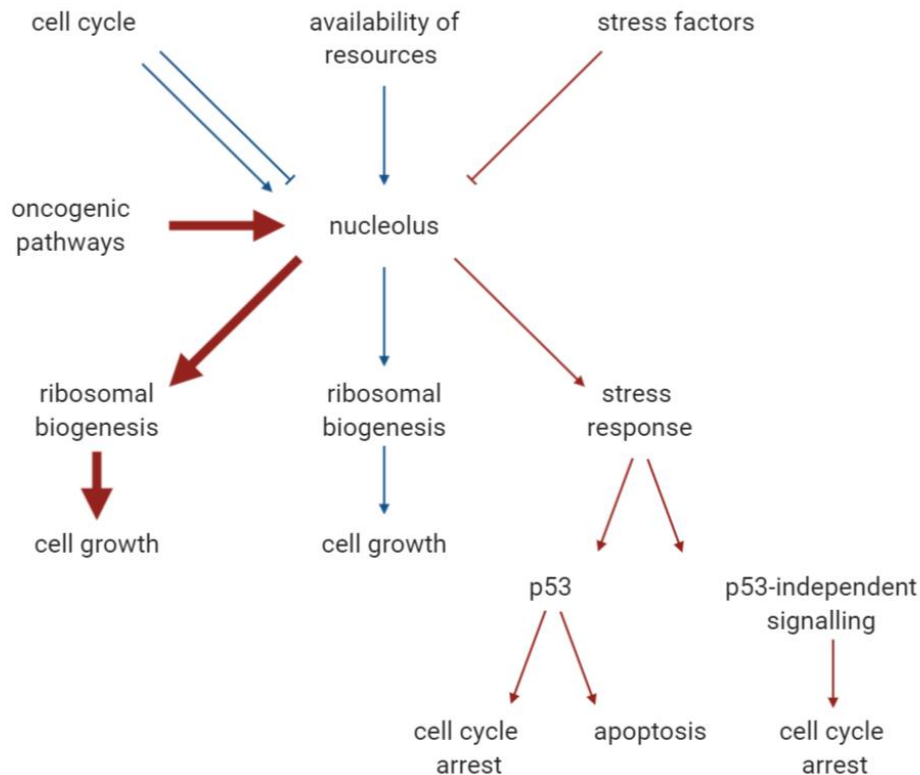


Figure 1.12. Nucleolar regulation of cell survival functions. The nucleolus has long been recognised as the locus of ribosomal biogenesis, a key regulator of cell growth. However, the more recent realisation that it has a role as a stress sensor has unveiled its importance as a modulator of cell survival. Nucleolar function is modulated by different stimuli, for example, under normal conditions (blue lines), ribosomal biogenesis depends on the availability of biomolecules needed to synthesize the ribosomes and is influenced by progression of the cell cycle. In response to the presence of different stressors (thin red arrows), the nucleolus promotes cell cycle arrest and/or apoptosis in a p53-dependent and independent manner. Oncogenic pathways such as those regulated by Ras and mTOR hyper-activate ribosomal biogenesis (thick red arrows), thus promoting increased cell growth.

Nucleolar function also regulates cell cycle progression through p53-independent mechanisms. c-Myc regulates ribosome biogenesis by binding to rDNA promoters, recruiting the SL1 pre-initiation complex, which promotes binding of RNA Pol I to rDNA, and in so doing activates rDNA transcription (178,179). Moreover, c-Myc promotes expression of RPL11, and an excess of RPL11 prevents the interaction of c-Myc and its co-activator TRRAP and so inhibits transcription of c-Myc targets required for cell proliferation (180). Another p53-independent connection with cell cycle regulation has been proposed to involve the nucleolar protein pescadillo, which is essential for ribosomal biogenesis (181). Knockdown of pescadillo leads to up-regulation of p27, protein encoded by the *CDKN1B* gene, decreased expression of cell cycle protein cyclin D1, and inhibits proliferation of breast cancer cells (182), and thus it can be speculated that pescadillo contributes to the promotion of normal cell cycle progression. Furthermore, nucleolar dysfunction has been shown to downregulate

E2F-1, and to decrease E2F-1-mediated expression of genes that promote cell cycle progression (183). Activation of the NF- κ B pathway in response to degradation of the transcription factor TIF-1A has also been shown promote the nucleolar stress response pathway independently of p53 (168). Together, these findings suggest that there might be several nucleolar mechanisms that mediate the stress response, both dependent and independent of p53.

1.3.3 Regulation of nucleolar function

As discussed in section 1.3.1, the nucleolus plays a fundamental role in cell survival (Figure 1.12.). Firstly, through the biogenesis of ribosomes, which is one of the most energy-consuming processes in the cell and a required step for the production of proteins needed to sustain cell viability and growth. Secondly, through the modulation of cell proliferation and apoptosis. Therefore, tight regulation of the nucleolus is needed to maintain cellular homeostasis. Various pathways have been identified as regulators of nucleolar function via mechanisms such as post-translational modifications of transcription initiation factors.

Growth-dependent stimulation of nucleolar function has been attributed to TIF-1A, which promotes transcriptional initiation of rRNA genes in response to growth signals transduced by ERK and mTOR pathways (Figure 1.13). Mitogen-dependent activation of the ERK pathway, activates TIF-1A through phosphorylation at serines S633 and S649 by ERK and RSK respectively (184). Similarly, activation of the mTOR pathway by amino acids, glucose and growth factors, promotes RNA Pol I transcription through increased phosphorylation of TIF-1A at serine S44 and decreased phosphorylation at serine S199 (185,186). Additionally, the mTOR pathway modulates rRNA transcription through the S6K-dependent activation of UBF (8) (Figure 1.13). Furthermore, evidence suggests that mTOR and its downstream target S6K also influence formation of rRNA transcription initiation complexes, since PTEN-dependent inhibition of these kinases triggers disruption of the SL1 pre-initiation complex, which leads to decreased rRNA transcription (187). Casein kinase II (CKII) also activates UBF through phosphorylation upon serum stimulation (188,189).

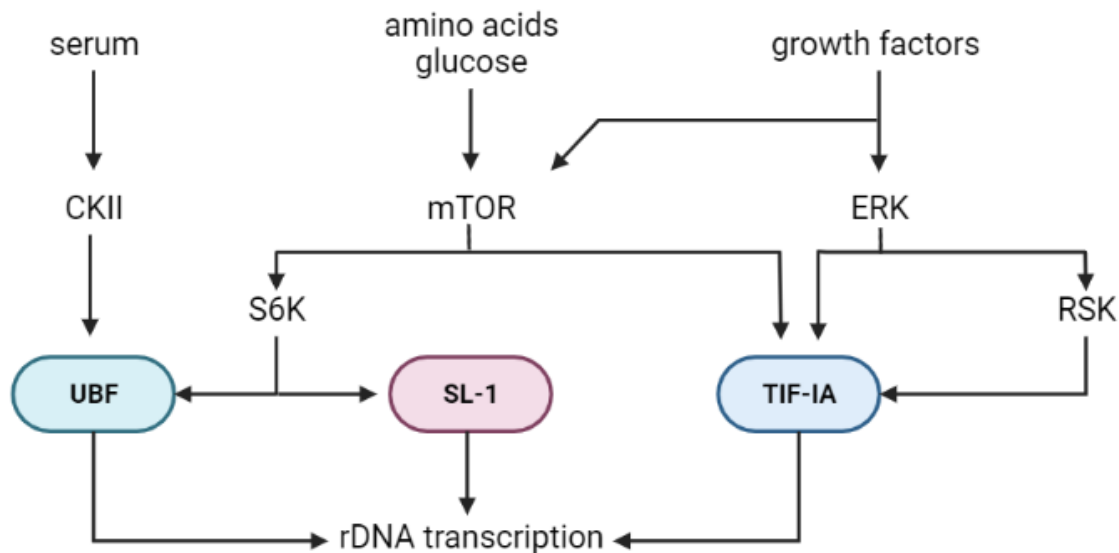


Figure 1.13. Regulation of nucleolar function in response to availability of nutrients. The mTOR and the ERK pathways, modulate ribosomal biogenesis through the activation of key transcription factors TIF-1A, SL-1 and UBF in the presence of nutrients. Information displayed on the diagram was obtained from (8,184–187,189).

Importantly, rDNA transcription is also controlled in a cell cycle-dependent manner. Both UBF and SL1 are inactivated by mitotic-specific kinases such as cdk2/cyclin B thus suppressing ribosomal biogenesis during late G2 and throughout M phase (190,191). Reactivation of UBF upon entering G1 phase requires dephosphorylation of UBF by PP2A and phosphorylation at S484 by cdk-cyclin complexes cdk4/cyclin D1 and cdk2/cyclin E (192,193). Additionally, the transactivating function of UBF is enabled by phosphorylation at Ser388 by cdk2/cyclin A and cdk2/cyclin E during late G1/ early-S phase (191). This is consistent with observations of the structural changes of the nucleolus throughout the cell cycle. The nucleolus assembles during telophase and early G1 phase around the NORs, activating rRNA transcription (148,194). The nucleolus then remains active during the course of the cell cycle, with increased activity during S and G2 phases. During mitosis, rRNA transcription is abrogated and the nucleolus is disassembled (148).

Thus, changes in either cell growth or cell cycle affect rRNA transcription. Interestingly, this connection between ribosomal biogenesis and cell cycle acts in both directions. Ribosomal biogenesis is essential for cell growth and proliferation and defective ribosomal biogenesis exerts control over cell cycle progression by triggering stabilisation of p53 that leads to cell cycle arrest or apoptosis (181). Alternately, rDNA transcription is modulated in a cell-cycle dependent manner through the

phosphorylation of transcription factors by cyclin complexes, as described above. Accordingly, the nucleolus acts as a central regulation hub in the cell that integrates information about cell status, including growth, proliferation, and stress, and translates this information into signalling cascades that lead to different cellular outcomes.

1.3.4 The nucleolus and cancer

Considering that cell growth and proliferation are significantly heightened in cancer cells, it is no surprise that nucleolar activity is also enhanced in these cells (152,195). This translates into an increase in the number of nucleoli that can be observed by pathologists in cancerous tissues and indeed, these have been used as a biomarker for tumour aggressiveness and prognosis for certain cancers (196). Higher rates of rRNA transcription have also been reported in several types of cancer, including breast cancer (197), colon cancer (198), and prostate cancer (199).

As mentioned in section 1.3.3, transcription of rDNA is strongly dependent on post-translational modifications of the core components of the RNA Pol I transcription machinery: UBF, TIF-IA and SL1. Importantly, oncogenic signalling pathways such as those regulated by c-Myc, Ras-Raf-MEK-ERK and the PI3K/Akt/mTOR pathways orchestrate many of these modifications (179,184,186,200). Thus, nucleolar activity is frequently upregulated in cancers driven by the enhanced activity of oncogenic proteins, or by the absence of the repression exerted by mutated tumour suppressor proteins (Figure 1.14).

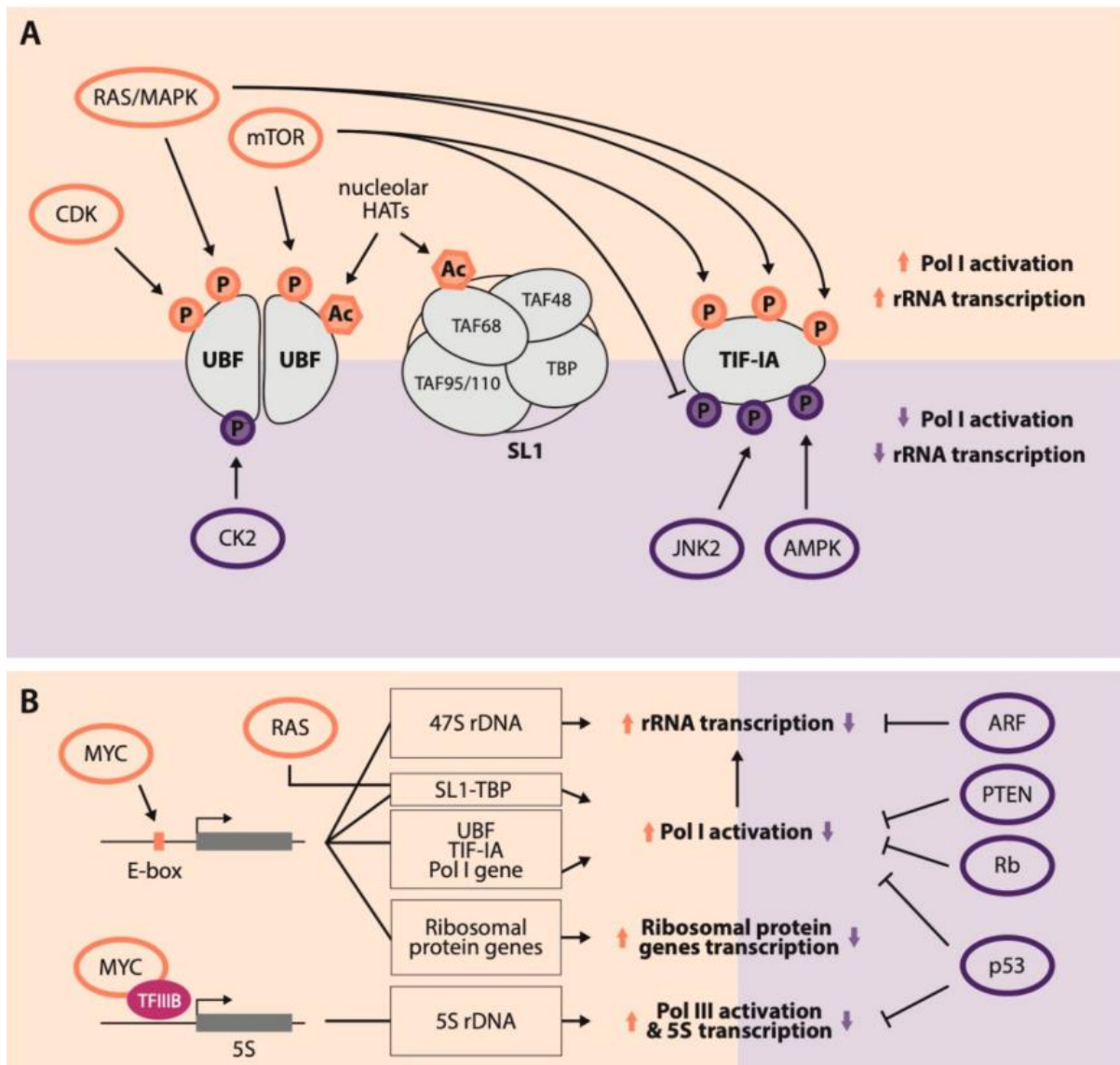


Figure 1.14. Role of the oncogenic pathways on the transcriptional and post-transcriptional regulation of rRNA synthesis. A) Diagram showing the components of the RNA Pol I machinery and the main up-regulating (orange) and down-regulating (purple) post-transcriptional modifications induced by oncogenes and tumour suppressor genes, respectively as well as by histone acetyltransferases (HATs) found in the nucleolus. B) Diagram displaying the signalling pathways that upregulate rRNA transcription upon oncogene activation (orange) or inhibit it via tumour suppressor genes (purple). Figure retrieved from (201).

The product of the c-Myc oncogene, which has been found to be elevated in 70% of human cancers, plays an important role in different stages of ribosomal biogenesis, including rDNA transcription and pre-rRNA processing (202). It upregulates expression of UBF and TIF-IA, increasing rDNA transcription as a consequence (203,204). In addition, it stabilises the formation of transcription initiation complexes by binding to the rDNA promoter and interacting with SL1 (178). Moreover, c-Myc

promotes the transcription of ribosomal proteins by RNA Pol II, 5S rRNA by RNA Pol III and coordinates pre-rRNA processing (166,205–207).

Increased mTOR activity, which modulates rDNA transcription initiation by regulating S6K-dependent phosphorylation of TIF-IA and UBF, often occurs in cancer (8,186). Constitutive activation of Ras drives elevated activation of the mTOR pathway, thus hyper stimulating ribosomal biogenesis (208). Additionally, the Ras pathway modulates nucleolar activity through ERK. Oncogenic activation of the Ras pathway enhances phosphorylation-dependent activation of TIF-IA by ERK and RSK, heightening RNA Pol I-dependent rDNA transcription (184,209,210). In colon cancer, activated Ras pathway has been shown to upregulate expression of TBP, required for formation of the RNA Pol I pre-initiation complex, promoting enhanced rRNA transcription (211).

Loss of function of tumour suppressor genes are also involved in enhanced ribosomal biogenesis. For example, the loss of function of *PTEN*, a negative regulator of mTOR that disrupts the integrity of the SL1 complex, leads to increased rDNA transcription (187). Alterations in *Rb* and *TP53* have also been associated with enhanced ribosomal biogenesis in cancer cells, since the loss of function of these tumour suppressor genes enables upregulation of rRNA transcription (212). The absence of a functional ARF occurs in many types of cancer (213). Apart of the role of this tumour suppressor gene in the stabilisation of p53, it represses ribosomal biogenesis by inhibiting the nucleolar import of TTF-I, a RNA Pol I transcription termination factor (214).

Tumour suppressor genes also control rRNA transcription through the post-transcriptional modifications of the components of the RNA Pol I transcription machinery. That is the case of JNK2, a kinase that phosphorylates TIF-IA at Thr200 and prevents the interaction of TIF-IA with RNA Pol I and SL-1, inhibiting rRNA transcription initiation (169). Reduced expression of JNK2 has been shown to promote tumorigenesis and cancer cell migration (215,216). AMPK, whose function as a tumour suppressor has been demonstrated in lung, colorectal, liver, and prostate cancer, also impairs the interaction of TIF-IA with SL-1 and inhibits the formation of RNA Pol I initiation complex by phosphorylating TIF-IA on Ser635 (217,218). Phosphorylation by kinase CKII promotes rRNA transcription through the phosphorylation of UBF, as mentioned in section 1.3.3, but it also represses the ability of SL-1 to bind to the rDNA

promoter, functioning as both positive and negative regulator of rRNA transcription initiation (219).

As described in section 1.3.3, cdk/cyclin complexes regulate UBF in a cell-cycle-dependent manner. Oncogenic upregulation of proliferation by cdk4/cyclin D and cdk2/cyclin A/E is followed by enhanced synthesis of rRNA (192,193,220). In addition, these cdk/cyclin complexes inhibit the tumour suppressor protein Rb that inhibits transcription by RNA Pol I by binding to UBF and preventing the formation of the transcription initiation complex (221,222). Importantly, p53 which plays a central role in the nucleolar-mediated stress response, is mutated in over 50% of all human cancers, thus impairing stress-induced cell cycle arrest and apoptosis (141).

1.3.5 The nucleolus and cancer therapy

Empirical evidence has accumulated over many years showing a correlation between nucleolar disruption and the cytotoxic activity of anti-tumour drugs such as daunomycin, Actinomycin D (ActD), toyocamycin, mycophenolic acid, camptothecin, doxorubicin and deferoxamine (223,224). In fact, the magnitude of translocation of the nucleolar protein nucleophosmin/B23 from the nucleolus to the nucleoplasm, which occurs following drug-induced nucleolar stress, has been proposed as an indicator of cytotoxicity for many drugs (225,226). This correlation between nucleolar disruption and cytotoxicity may in some cases reflect a major mechanism of action for several well-known cancer chemotherapeutics. For some chemotherapeutic agents a major role for nucleolar disruption in their mechanisms of action has been established (227–229). A number of DNA-intercalating antibiotics that target transcription, consequently, also target nucleolar function, the best known of these being ActD, which has a well-established high specificity for inhibition of rRNA production at low concentrations (230). This specificity was often overlooked when considering the function of ActD as a chemotherapeutic agent. Increasingly though, the therapeutic utility of NFIs is being recognised and with that recognition there comes a greater interest in the exact mechanism of action of these agents. While the assumption generally is that inhibition of RNA polymerisation depends on intercalation with the transcript and template (with varying degree of sequence specificity), at least in the case of BMH-21, the mechanism appears to be more complicated and to involve the specific degradation of components of the nucleolar RNA Polymerase (Pol I) machinery (229,231). The

small molecule inhibitor CX-5461 raised significant interest in recent years due to its reported capacity to inhibit nucleolar function (160,227). However, it was later reported that its primary target is actually Topoisomerase II (232,233).

Nucleolar disruption, however, may be a more common component of the mechanisms of actions of chemotherapeutic agents than realised. Below are three examples of widely used anti-cancer drugs whose mechanism of action, generally assumed to be mediated by disruption of DNA replication, may in some instances be better explained through nucleolar disruption.

Actinomycin D

Actinomycin D (ActD) also known as dactinomycin is an antibiotic produced by *Streptomyces* with antibacterial and antitumoral activity that has been used in cancer therapy since 1954. A member of the actinomycin family, this compound is formed from a chromophoric phenoxazinone dicarboxylic acid which is bound to two cyclic nonribosomal peptides (Figure 1.15). The chromophore intercalates into the DNA, preferentially at guanine-cytosine pairs, and the resulting structure is stabilised via hydrogen bonds and hydrophobic interactions of the pentapeptides with the DNA minor groove (Figure 1.16) (234).

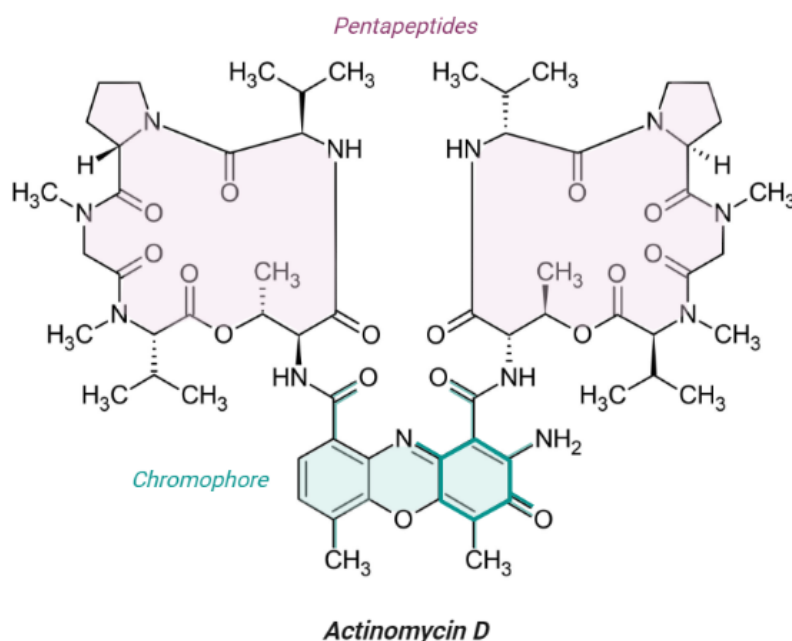


Figure 1.15. Chemical structure of Actinomycin D. Image adapted from (234).

The ActD-DNA complex prevents unwinding of the dsDNA, inhibiting transcription elongation by RNA polymerase (234,235). It has been suggested that the higher

sensitivity of rRNA synthesis to ActD is the result of the close-presence of multiple RNA Pol I complexes along the DNA, where interference in the movement of one RNA Pol I complex caused by the intercalation of ActD, would affect the movement of the rest of the RNA Pol I complexes, thus, their activity (236).

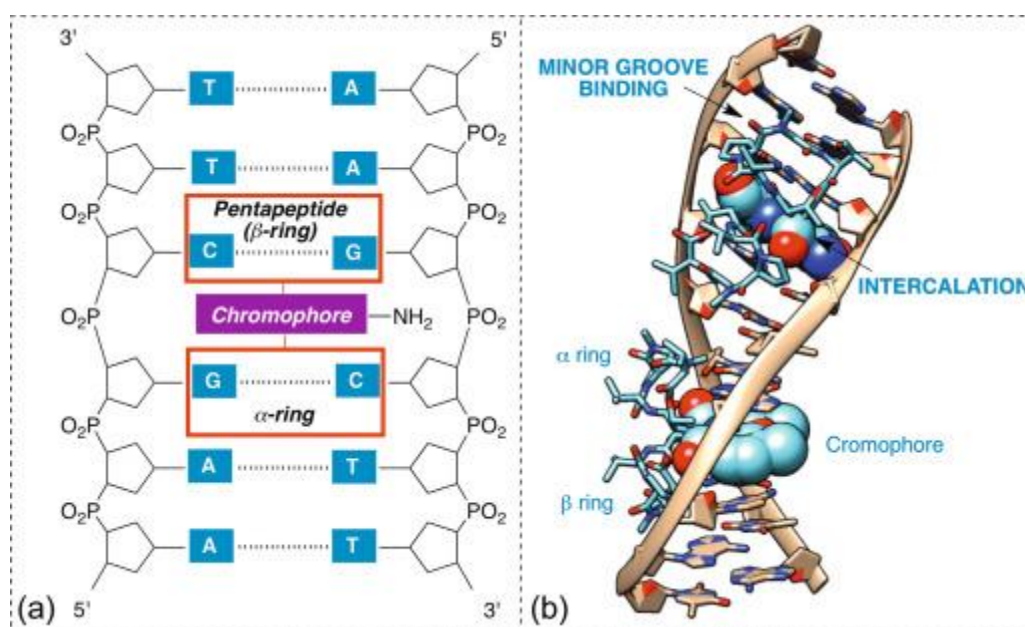


Figure 1.16. Intercalation of Actinomycin D into DNA. The chromophore of the actinomycin D molecule intercalates in CpG double stranded DNA and the structure is stabilised by the interactions of the α - and β -rings with the DNA minor groove. Image retrieved from (234).

Dactinomycin has been used for over 50 years to treat different types of cancer including Wilms' tumour, Ewing sarcoma, embryonal rhabdomyosarcoma, choriocarcinoma, testicular tumours, and gestational trophoblastic neoplasia (237). Its cytotoxicity has been attributed to its ability to prevent DNA transcription and activation of the nucleolar stress pathway, in addition to its capacity to inhibit topoisomerase II and production of free radicals (238,239). Unfortunately, the therapeutic index of this drug is limited by adverse effects including mucositis, pulmonary toxicity, hepatotoxicity, and cutaneous lesions (240).

5-Fluorouracil

The widely used anti-cancer drug 5-Fluorouracil (5-FU) is a well-known inhibitor of the enzyme thymidylate synthase (TS) that participates in the *de novo* synthesis of 2'-deoxythymidine-5'-monophosphate (dTMP) (241). Its inhibition by 5-FU impairs DNA synthesis and S-phase progression, as it deprives S-phase cells of dTTP, causing stalling of DNA replication ("thymineless death"). Highly proliferating tumour cells

which also express higher levels of thymidylate synthase (TS) (241). However, Pritchard and colleagues have shown that bypassing TS inhibition with exogenous thymidine could not prevent p53-dependent apoptosis induced by 5-FU in intestinal cells (242). Apoptosis induced by the specific TS inhibitor Tomudex, on the other hand, could be prevented by exogenous thymidine (242). These observations imply that at least in some cells 5-FU may induce apoptosis through a mechanism of action different from thymineless death. Although 5-FU has practically no effect on mRNA or rRNA synthesis or on mRNA splicing, it inhibits rRNA maturation and ribosomal assembly and Ghoshal and colleagues have proposed that it is precisely this activity rather than TS inhibition that is responsible for the anti-cancer properties of 5-FU(243).

Cis-Platin

Cis-Platin (cis-Pt) is one of the most commonly used anti-cancer drugs. As it severely bends DNA 32-34° towards the major groove – (244) it is generally assumed that it causes cell death through DNA damage. However, cis-Pt-mediated DNA damage has several interesting features that put this mechanism into doubt. Some cell lines become resistant to cis-Pt and can remove cis-Pt-DNA adducts (245) instead of undergoing apoptosis. High mobility group (HMG) proteins, due to their capacity to bind cis-Pt-DNA with high affinity (see (244) for the structural details of the interaction), were initially proposed to be responsible for the recognition of cis-Pt-DNA adducts for repair, which would offer an explanation for the onset of cis-Pt resistance. However, this proposition is contradicted by the fact that cells underexpressing HMG proteins can remove the adducts and that binding of HMG proteins to cis-Pt adducts can actually block nucleotide excision repair *in vitro* (246). Furthermore, cells overexpressing HMG proteins are frequently resistant to cis-Pt and do not undergo apoptosis (247). However, one alternative explanation for the critical role of HMG proteins in the outcome of cis-Pt therapy is that cell death occurs when cis-Pt-DNA adducts hijack the HMG protein UBF away from its rRNA synthesis sites, inhibiting rRNA synthesis (248–250). This view is strongly supported by the fact that DNA adducts of the clinically ineffective trans-isomer of cis-Pt platin, trans-Platin (251), does not bind HMG proteins (252). The abundant evidence of the nucleolar disrupting activity of cis-Pt therefore offers an alternative, realistic mechanism for the antitumour mechanism of action of cis-Pt (141,248,253).

Camptothecin

The anti-cancer agent Camptothecin (CPT) induces apoptosis by stabilising DNA breaks introduced by Topoisomerase I, which subsequently stall replication and cause DNA damage (254). However, CPT can also kill non-replicating cells such as neurons, raising questions about the model of replication stalling (255). Topoisomerase I is essential for rRNA synthesis and is concentrated in the nucleolus (256,257). When CPT blocks Topoisomerase I it also blocks rRNA synthesis and causes nucleolar disruption (258). Thus, nucleolar disruption is a possible component of the mechanism of action of the Topoisomerase I inhibitor CPT, which may explain why it can still be active in cells of low proliferation rates. Therefore, not only NFIs are emerging drugs of which we know very little in terms of their therapeutic behaviour, but also nucleolar function inhibition must be better understood therapeutically as it may be a major component of the mechanisms of action of other established anti-cancer agents.

1.4 mTOR, the master regulator of cell growth

The mTOR signalling pathway is the master controller of cell growth and is involved in the regulation of cell functions that promote proliferation and cell survival. This pathway receives information from extra and intra-cellular stimuli and initiates the transduction of signals that activate various mechanisms to promote the synthesis of proteins and lipids required for sustaining growth (Figure 1.17). The mTOR pathway is also a regulator of the biogenesis of organelles such as ribosomes and lysosomes, and of cytoskeleton organization. Additionally, it plays a role in cell survival through inhibition of autophagy and blocking the expression of pro-apoptotic factors.

The pathway is named after a serine-threonine kinase that functions as the signalling hub called mTOR discussed below. The mTOR kinase is the fundamental component of two multi-protein complexes, mTOR complex 1 (mTORC1) and mTOR complex 2 (mTORC2), which differ in structure, effector activation, roles within the mTOR pathway, and regulation of cell processes (Figure 1.17).

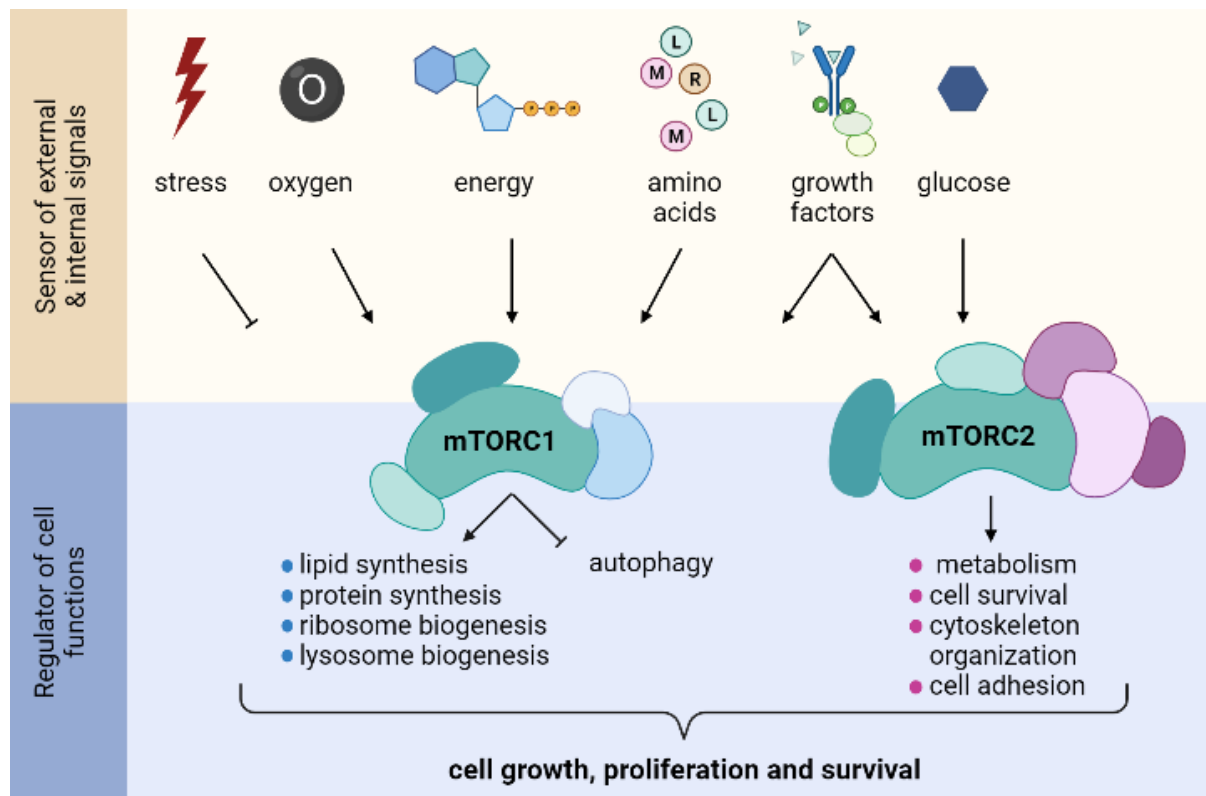


Figure 1.17. The mTOR pathway is a sensor of extra- and intra-cellular stimuli that controls cell functions that promote growth, proliferation, and cell survival. mTOR is a component of two protein complexes called mTOR complex 1 (mTORC1) and mTOR complex 2 (mTORC2) that regulate a wide array of signalling responses associated with cell growth, proliferation and survival (lower panel) in response to different external and internal signals (upper panel).

1.4.1 mTOR complex 1

The mTOR was first discovered in 1994 by David M. Sabatini, Robert T. Abraham, and Stuart L. Schreiber independently, while studying the mechanism of action of rapamycin, a macrolide produced by *Streptomyces* with immunosuppressant properties. Originally, it was named the mammalian Target of Rapamycin (hence mTOR) after its homology to the yeast TOR gene, although currently it is also known as the mechanistic Target of Rapamycin. This complex is formed by mTOR, regulatory-associated protein of mTOR (Raptor), DEP-domain containing mTOR-interacting protein (DEPTOR), mammalian lethal with SEC13 protein 8 (mLST8) and proline-rich AKT substrate of 40 kDa (PRAS40) (Figure 1.18). The mTOR subunit acts as a scaffold and the rest of the components assemble around it, each playing a role in the regulation of the kinase activity of mTORC1.

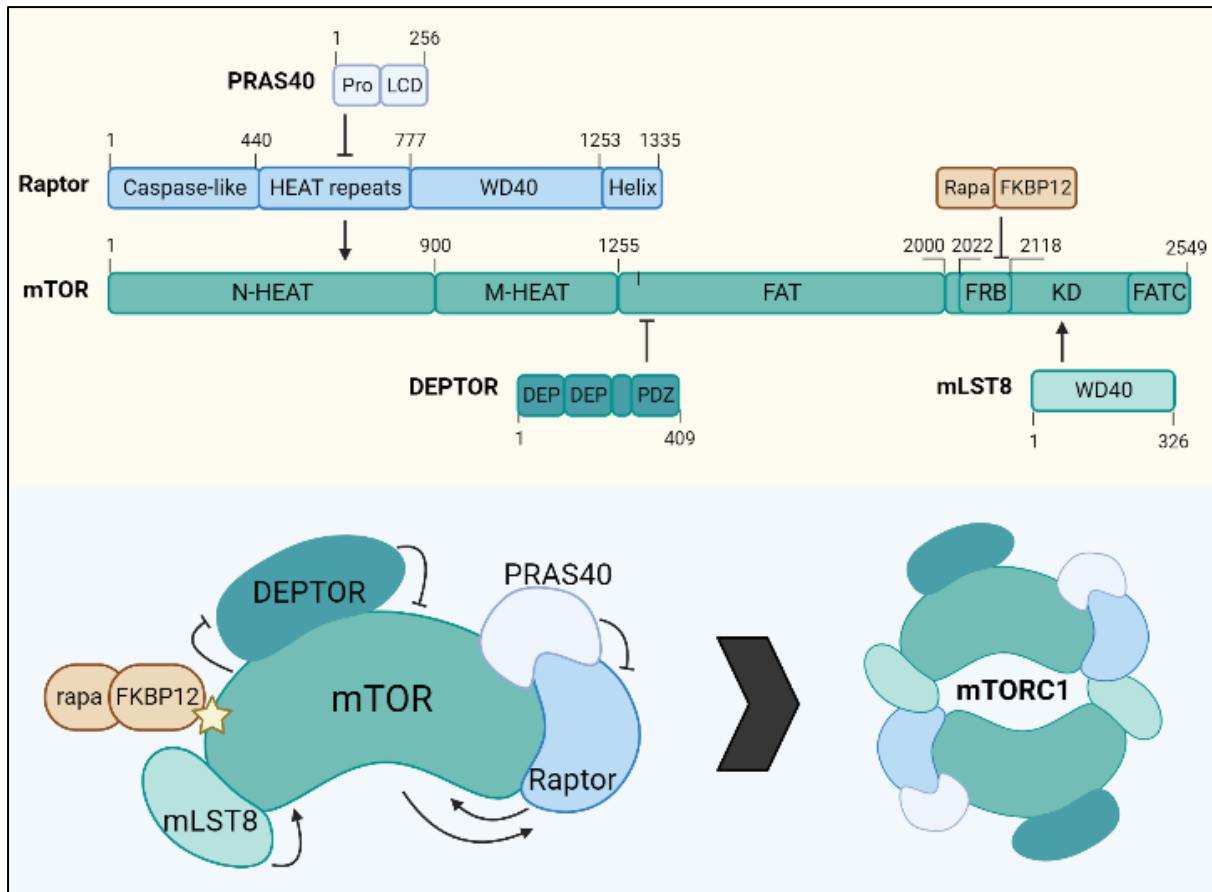


Figure 1.18. Components of the mTORC1. The mTORC1 is an obligate homo-dimeric complex formed by mTOR, Raptor, DEPTOR, mLST8 and PRAS40. A linear representation of the different components of mTORC1 shows the relative positions of the structural motifs along the polypeptide chain for each component, and the relative sites where the mTORC1 components interact with each other. mTOR contains tandemly repeat arrays of α -helices known as HEAT domains in the amino-terminus (N-HEAT) and the middle section (M-HEAT) (259). The M-HEAT domain of mTOR is followed by a FRAP, ATM, TRRAP (FAT) domain, which plays a role as structural scaffold or as a protein-binding domain (260). The kinase domain (KD) of mTOR is located between the FKBP12-Rapamycin binding domain (FRB), the site where the complex formed by rapamycin and the FKBP12 protein (Rapa-FKBP12) binds mTORC1 (261), and a C-terminal FAT domain (FATC). Regulatory-associated protein of mTOR (Raptor) is a key component of mTORC1 and contains a caspase-like domain in the N-terminus, also known as the raptor N-terminal conserved (RNC) domain, a HEAT domain, seven WD40 repeats that act as a scaffold that mediate the interaction of different proteins within multiprotein complexes (262), and a Helix domain. Raptor binds and activates mTOR by binding to the N-HEAT domain of mTOR, and it is inhibited by interaction with PRAS40. mTOR is bound and inhibited by DEPTOR a protein formed by two globular protein domains of about 80 residues of length present in proteins such as Dishevelled, EGL-10, and Pleckstrin, known as DEP domains (Ponting and Bork, 1996), and a PDZ domain, characterised by a length of 80-100 amino acid that usually display 6 β -strands, a short α -helix, and a long α -helix (263). mTOR is also activated by mLST8, which displays a WD40 domain. The cartoon representation displayed in the lower left panel shows the negative and positive regulation exerted by the components of the mTORC1 complex, and the FKBP12-rapamycin complex. The cartoon representation on the lower right shows dimerization of the mTORC1.

The serine/threonine kinase mTOR is the catalytic subunit of both mTOR protein complexes. mTOR belongs to the family of phosphatidylinositol 3-kinase related

protein kinases (PIKKs), whose members participate in the signalling of multiple pathways. Accordingly, the kinase domain of mTOR is flanked by a FRAP, ATM, TRRAP (FAT) domain on the amino-terminal end, and by a FATC domain on the carboxy-terminal end, both domains characteristic of PIKK (264). In addition, mTOR contains up to 20 tandem HEAT repeats on the N-terminus (265). Importantly, mTOR presents an FRB domain between the FAT domain and the kinase domain (266), where the FKBP12-rapamycin complex binds, inhibiting mTORC1 activity by restricting access of the substrates to the catalytic site and promoting dissociation of Raptor from the complex.

Analyses by cryo-electron microscopy (cryo-EM) have shown that functional mTORC1 is a dimer, which is stabilised by the interaction of mTOR and Raptor (267,268). In addition to its role in the stabilisation of mTORC1 complex, Raptor contains a substrate-binding site that modulates the interaction of mTORC1 with the different substrates and regulates substrate specificity (268). Moreover, Raptor plays an essential role in the nutrient-dependent activation of mTORC1 by interacting with Rag proteins and mediating the translocation of mTORC1 to the lysosome, where Rheb, an mTORC1 activator, localises (269).

PRAS40 is a negative regulator of mTORC1 that binds to Raptor in response to deprivation of insulin and prevents substrate binding (270). Importantly, PRAS40 itself is a substrate of mTORC1. Thus, when nutrients and mitogens are available, mTORC1 phosphorylates PRAS40, and the latter dissociates from Raptor and releases its inhibitory effect from mTORC1 (271,272). This regulatory relationship between PRAS40 and mTOR highlights the role of the mTOR complex as sensor of different types of nutrients, not only amino acids. Another negative regulator of mTOR is DEPTOR, which affects both mTOR complexes by binding to the carboxy-terminal region of mTOR and inhibiting the catalytic activity of mTOR (273). Interestingly, DEPTOR is also a substrate of mTORC1 and mTORC2. Nutrient-activated mTOR complexes phosphorylate DEPTOR and promote its degradation (274). mLST8 is another component of both mTOR complexes which appears to be required for the formation of the complex, but its role in mTORC1 function remains elusive (275,276). It is important to note that most components of the mTOR complexes play a role in the regulation of mTORC1 and mTORC2 activity linked to the availability of nutrients. This

explains how the mTOR pathway is sensitive to multiple stimuli, but also underlines the importance of the negative regulation of the mTOR pathway in response to nutrient deprivation to maintain homeostasis.

1.4.1.1 Regulation of mTORC1

As a direct target of rapamycin, the mTORC1 has been extensively studied and various inputs that modulate its activity have been discovered. mTORC1 acts as a sensor of nutrient that enables the cell to synthesize the biomolecules it needs to sustain growth when essential nutrients such as amino acids, glucose, insulin and growth factors are available. But this raises the question, how do mTORC1 sense the availability or levels of these nutrients?

mTORC1 is activated by Rheb, a small GTPase localised on the lysosomal outer surface. Rheb, in turn, is negatively regulated by tuberous sclerosis complex (TSC), composed of TSC1, TSC2, and TBC1 domain family member 7 (TBC1D7) (277). Mutations in TSC1 and TSC2 give rise to the tuberous sclerosis syndrome, a rare, multi-system genetic disease characterised by the growth of non-cancerous tumours in the brain and other organs. The TSC1/2 complex inhibits Rheb through its GAP activity by switching it from its GTP-bound active state to its GDP-bound inactive state. Interestingly, the TSC1/2 complex is regulated through phosphorylation by kinases involved in various signalling pathways, including PI3K and RAS pathways, among others, as described below (Figure 1.19) (278).

1.4.1.1.1 TSC1/2 complex: the switch for mTORC1

A number of growth factors activate the PI3K pathway and its effector AKT. AKT-dependent phosphorylation of TSC2 on serine residues 939, 981, and threonine 1462, blocks the negative regulation of TSC1/2 complex on mTORC1 (279,280). AKT promotes mTORC1 activity by phosphorylating PRAS40 on Thr246, which enables subsequent phosphorylation of PRAS40 at Ser183 and Ser221 by mTORC1, resulting in dissociation from mTORC1 (272,281). Activation of the RAS-ERK pathway by phorbol 12-myristate,13-acetate (PMA) prevents TSC1/2 inhibition of mTORC1 via TSC2 phosphorylation by ERK and ERK's substrate RSK (282,283). Importantly, both ERK and RSK also modulate mTORC1 activity through phosphorylation of Raptor at serine residues 8, 696, and 863, and 719, 721, and 722, respectively (284,285).

Cellular energy levels are also sensed by TSC1/2 via AMPK-dependent phosphorylation of TSC2. Under conditions of reduced cellular energy availability, the ratio of AMP:ATP increases, resulting in increased binding of AMP to AMPK, which activates it, and this in turn activates the TSC1/2 complex via phosphorylation of TSC2 on threonine 1271 and serine 1387 (286). Furthermore, phosphorylation of TSC2 on serine 1387 by AMPK is needed for subsequent phosphorylation of TSC2 on serine residues Ser1371, Ser1375, Ser1379, and Ser1383 by glycogen synthase kinase 3 β (GSK3 β), facilitating TSC1/2 activation. Thus, repression of GSK3 β by Wnt signalling, leads to activation of mTORC1 (287,288).

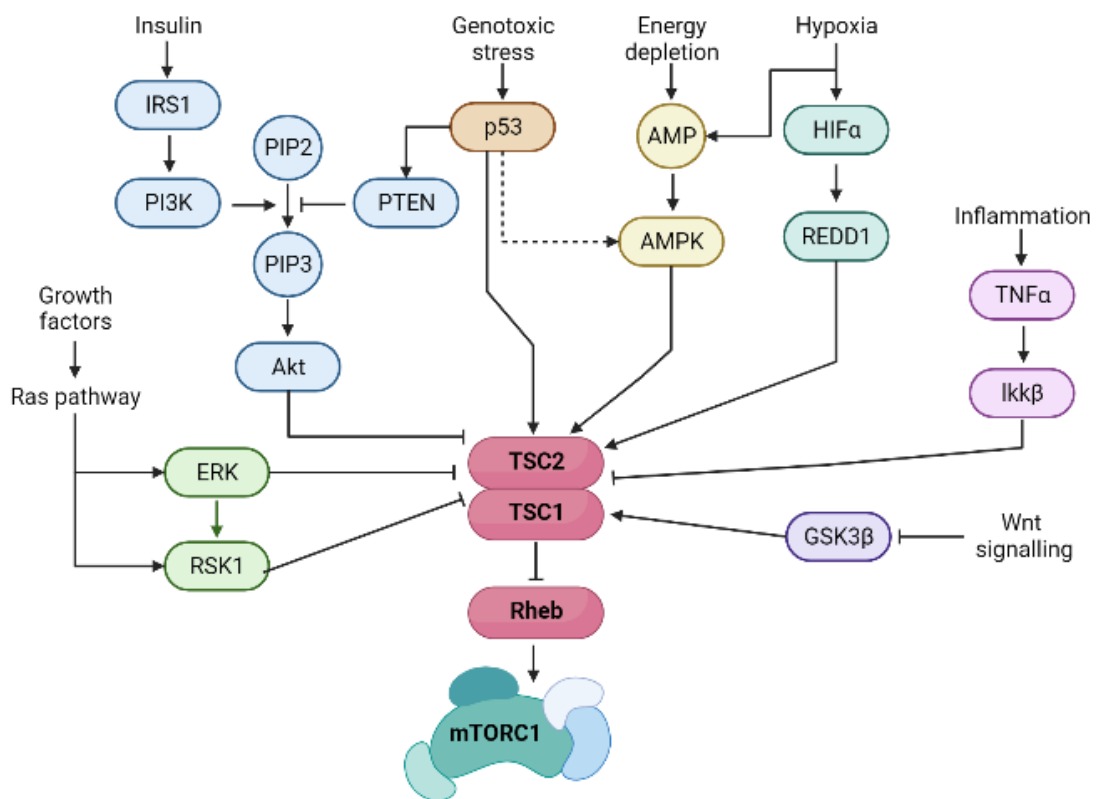


Figure 1.19. The role of the TSC1/2 complex as stimuli sensor and mTOR regulator. The TSC complex works as a switch that regulates mTOR activity in response to availability of resources and certain stressors through signalling pathways such as RAS, PI3K/AKT, and Wnt.

The TSC1/2 complex also functions as an effector of responses to oxygen levels through inhibition of the mTORC1 pathway. Since oxygen is required for oxidative phosphorylation, the main pathway used by cells to produce energy, hypoxic conditions lead to low levels of ATP and subsequent AMPK-dependent activation of TSC1/2, described above (278). Hypoxia promotes TSC1/2-dependent inactivation of mTORC1 through an additional mechanism. Hypoxic conditions enhances expression

of *REDD1*, whose product promotes binding of the TSC1/2 complex to mTORC1, and subsequent inhibition of mTORC1 activity (289).

As illustrated in Figure 1.19, various types of stress have been shown to regulate the mTOR pathway via the TSC1/2 complex. Inflammation for example has been demonstrated to positively regulate mTORC1 through phosphorylation-dependent inhibition of the TSC1/2 complex by IKK β (290). Genotoxic stress also downregulates mTORC1 through the stabilisation of p53 in response to DNA damage, which induces transcription of TSC2 and of the tumour suppressor gene PTEN, a negative regulator of AKT (291). Additionally, there is evidence that p53 upregulates mTORC1 by activating AMPK (292). Osmotic stress promotes AKT-mediated translocation of TSC2 to the lysosomes, and enables inhibition of Rheb (293), resulting in decreased mTORC1 activity. Relocation of TSC2 to the lysosome is a mechanism observed in response to pH stress, hypoxia, and energy stress, in addition to osmotic stress, that leads to inhibition of mTORC1 (294).

1.4.1.1.2 The role of amino acids in regulating mTOR localisation and activation

Regulation of the localisation of mTOR plays a vital role in determining the activity of the mTOR pathway, and this is primarily modulated by the activity of Rag GTPases (Figure 1.20). In the presence of amino acids, heterodimeric complexes formed by RagA/RagB and RagC/RagD are activated and bind to Raptor. This binding mediates relocation of mTORC1 to the lysosomal membrane, where Ragulator acts as a docking station for Rag-bound-mTORC1. Once in the lysosome, it is activated by Rheb (295,296).

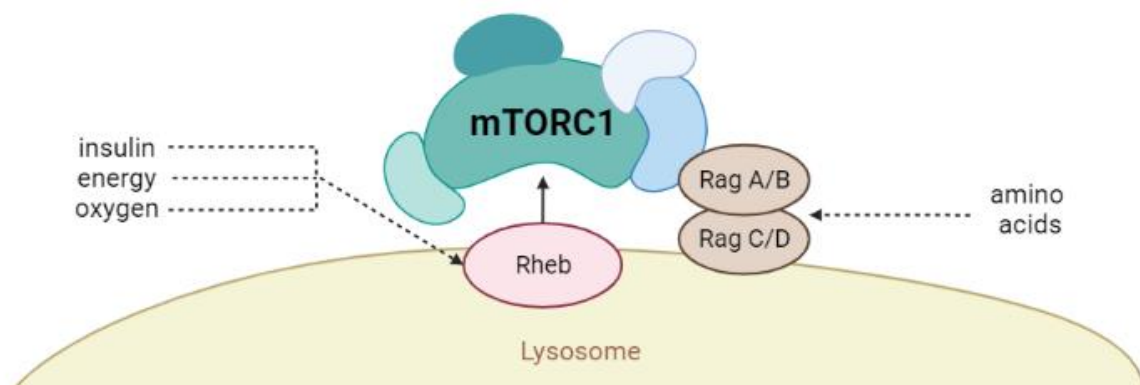


Figure 1.20. Model for role of Rag GTPases in signalling amino acid availability to mTORC1. Upon availability of amino acids, the Rag heterodimers are activated and bound to Raptor, mediating

translocation of mTORC1 to lysosomes, where its activator Rheb is also localised. Figure adapted from (296)

1.4.1.1.3 Activation of Rag monomers and their role in sensing amino acids

As mentioned before, Rag heterodimers are activated in response to availability of amino acids and mediate mTOR translocation to the lysosomal membrane (Figure 1.21). Activation of the Rag heterodimer requires a GTP-bound RagA/B and a GDP-bound RagC/D. Ragulator, a pentameric complex that acts as a docking station for the Rag heterodimer on the lysosomal membrane, tethers the Rag heterodimer to the lysosome and mediates its activation by catalysing the release of GTP RagC (297,298). Also found in the lysosome, the human member 9 of the solute carrier family 38 (SLC38A9) is a transmembrane protein that acts as a lysosomal arginine sensor that activates Rag heterodimer (299,300). When bound to arginine, SCL38A9 activates the Rag heterodimer by transforming RagA from GDP-bound to GTP-bound state (298)

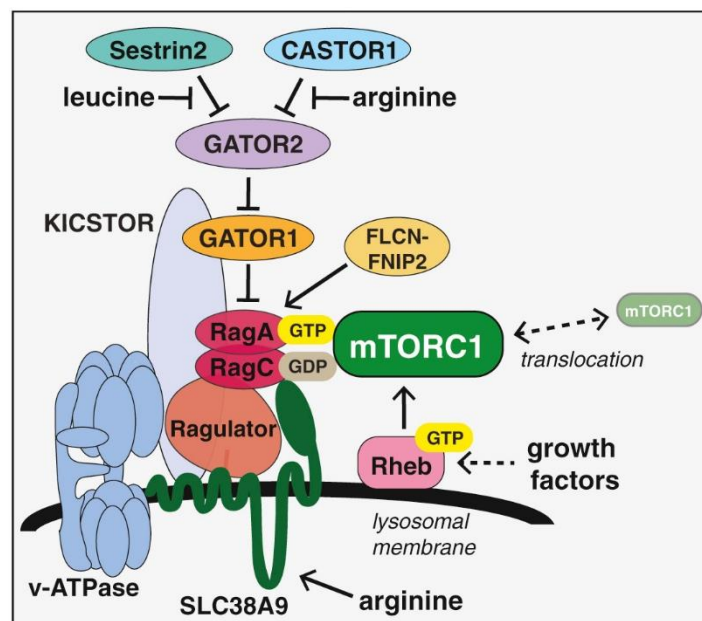


Figure 1.21. mTORC1 amino acid sensing pathway. In the presence of arginine and leucine, the negative regulation on Gator2 is released, leading to activation of the Rag heterodimer. This enables Rag-dependent translocation of mTORC1 to the lysosomal membrane, and subsequent activation of mTORC1 by Rheb. Arginine also promotes activation of the Rag heterodimer via SLC38A9. Figure obtained from (301).

Additionally, the Rag heterodimer is regulated by the Gator proteins. Gator1 a multi-protein complex composed of DEPDC5, NPRL2 and NPRL3, and negatively regulates mTOR by inhibiting the activity of Rag heterodimer through its GTPase activity towards RagA and Rag B in response to amino acid deprivation (302). In turn, the activity of Gator1 is inhibited by Gator2, a complex formed by MIOS, WDR24, WDR59, SEH1L,

and SEC13. Gator2 activates the mTOR pathway in the presence of amino acids. Specifically, leucine and arginine play an important role in the activation of Gator2. In the presence of leucine, Sestrin2 dissociates from Gator2 releasing it so that it can inhibit Gator1 (303,304). Similarly, arginine blocks repression of Gator2 by Castor (305,306).

1.4.1.2 mTORC1 and its role in cell growth and survival

As described in section 1.4.1, the mTOR pathway regulates cell growth by sensing nutrients, amino acids, growth factors, oxygen and energy levels, in addition to some types of stressors, and transducing this information into signals that activate numerous mechanisms involved in the synthesis of biomass required to sustain growth. Accordingly, the mTOR pathway activates, through mTORC1 and its effectors, anabolic processes such as protein synthesis, lipid synthesis, and ribosome biogenesis as well as repressing autophagy to promote cell survival (Figure 1.22).

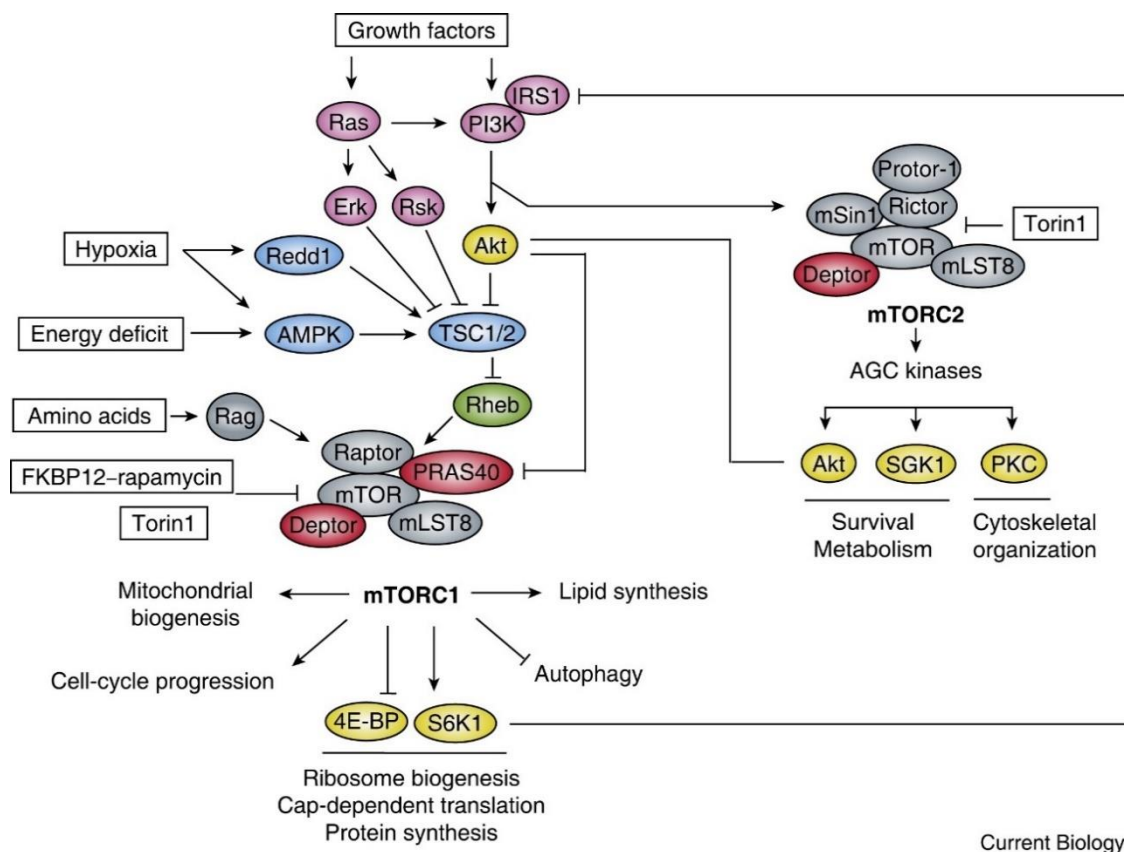


Figure 1.22. Overview of the mTOR pathway. Activation of mTORC1 depends on availability of growth factors, amino acids, energy and oxygen levels. mTORC1 regulates several cellular processes including protein and lipid synthesis, ribosome biogenesis, mitochondrial biogenesis, cell cycle progression, cap-dependent mRNA translation, and autophagy. mTORC2 is activated by insulin through the PI3K pathway and regulates survival metabolism and cytoskeletal organisation through the activation of various kinases belonging to the AGC family. Interestingly, mTORC1 and mTORC2 repress

each other through a negative feedback loop involving AKT, a downstream substrate of mTORC2 that inhibits mTORC1 activation. In turn, phosphorylation of IRS1 by mTORC1 effector S6K, represses activation of the PI3K pathway, inhibiting activation of mTORC2. Colour code: yellow indicates that the proteins are substrates of the mTOR complexes. Grey indicates that the proteins are components of the multiprotein complexes mTORC1 and mTORC2. Red indicates that the proteins are components of mTOR1/2 complexes that repress mTOR kinase activity. Blue indicates that the proteins inhibit mTORC1. Pink indicates that the proteins activate mTORC1/C2. Green indicates that the protein is an activator of mTORC1. Figure reproduced from (307).

1.4.1.2.1 mTORC1 regulation of protein synthesis

One of the first functions of the mTORC1 pathways to be identified was its role as a positive regulator of cell growth through the activation of anabolic processes such as protein and lipid synthesis, and ribosomal biogenesis. Regulation of these various processes is achieved through the phosphorylation of mTORC1 effectors S6K and 4EBP1 (Figure 1.23). These substrates of mTORC1 contain a conserved sequence of five amino acids recognised by Raptor, termed the TOR signalling (TOS) motif (308).

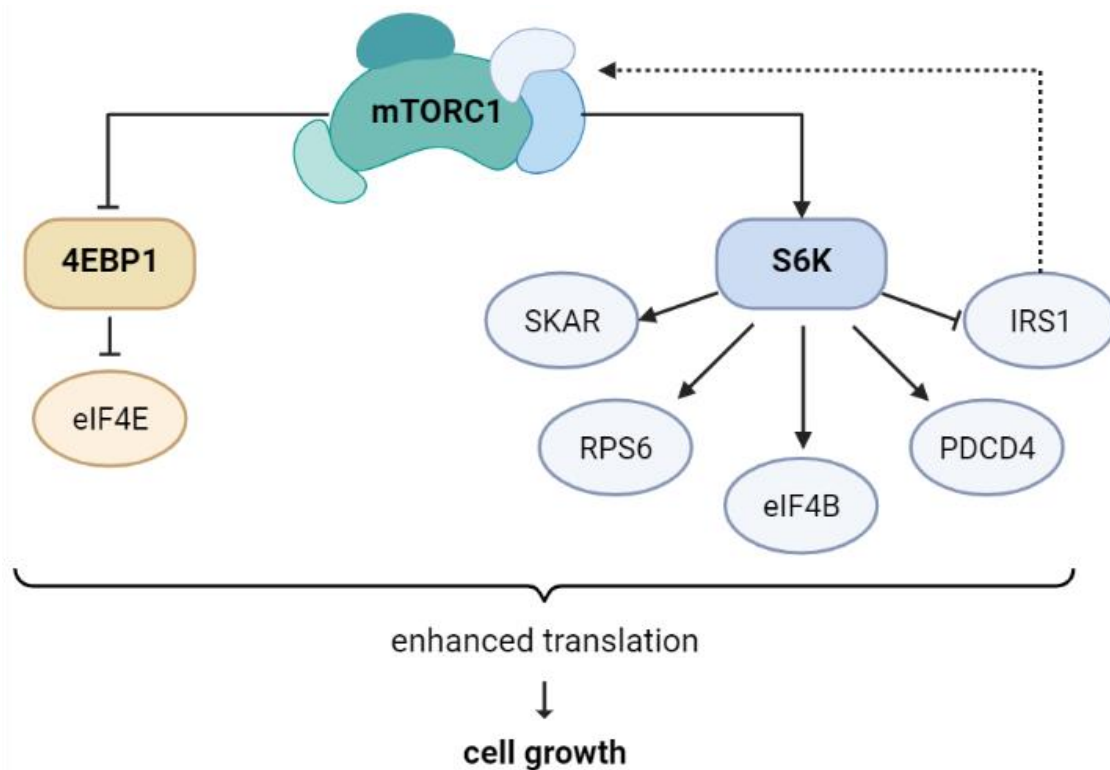


Figure 1.23. Regulation of protein synthesis by mTORC1. mTORC1 phosphorylates and inhibits 4EBP1, relieving its repression on eIF4E factor, thus allowing translation of mRNA (yellow). Phosphorylation-dependent activation of S6K by mTORC1, enables phosphorylation of S6K substrates, which promote translation of proteins needed to sustain cell growth. Additionally, S6K regulates mTORC1 by inhibiting mTOR1 activator IRS.

Activation of S6K requires multi-site phosphorylation, but Thr339 and Thr389 have been identified as two key phosphorylation sites. It has been shown that upon Raptor binding to the TOS motif, mTORC1 phosphorylates S6K Thr389, which then enables

subsequent phosphorylation of S6K Thr339 by phosphoinositide-dependent kinase 1 (PDK1) which fully activates S6K (309,310).

Once activated, S6K phosphorylates downstream effectors required for translation of mRNA and ribosomal biogenesis. The ribosomal protein S6 (rpS6) was the first known substrate of S6K. Multi-site phosphorylation by S6K is required for rpS6-mediated translation of a group of mRNAs characterized by an oligopyrimidine motif at their 5' transcriptional start site (5'TOP), which allows cells to rapidly adjust regulation of the expression of proteins involved in ribosome biogenesis and protein synthesis (311–313).

eIF4B phosphorylation by S6K or by ribosomal S6 kinase (RSK), promotes recruitment of eIF4B to the translation pre-initiation complex of mRNAs that display 5' untranslated region sequences, and enhances the RNA helicase activity of eukaryotic translation initiation factor 4A (eIF4A), thus, enabling unwinding of the RNA required for the initiation of translation by 40S ribosomal subunit (310). Additionally, phosphorylation by S6K on Ser 67 of the tumour suppressor Programmed cell death 4 (PDCD4), promotes degradation of PDCD4, releasing inhibition of RNA helicase activity of eIF4A (314).

Another downstream target of S6K, SKAR plays a role in protein synthesis by up-modulating translation of spliced mRNAs and mRNA export. SKAR localises at the exon junction complex (EJC), which assembles at the junction of two exons of newly spliced mRNA (315). Once activated, S6K binds to SKAR and this promotes translation of spliced mRNA (316). Importantly, IRS1 has been identified as a direct substrate of S6K. Phosphorylation of IRS1 at serine residues 270, 307, 636, and 1101 leads to inhibition of insulin signalling and consequently, represents a negative feedback loop in the mTORC1 pathway, which is activated by insulin (317).

Yet another important substrate of mTORC1 is the eukaryotic translation initiation factor 4E)-binding protein 1 (4E-BP1). Initiation of translation requires recruitment of the 40S ribosomal subunit to mRNA. This process is mediated by the eukaryotic translation initiation factor 4F (eIF4F) complex, composed of eIF4E, eIF4G and eIF4A. eIF4E binds to the 5' cap structure of mRNA and both eIF4G and eIF4A attach, assembling the eIF4F complex. In response to nutrient deprivation, 4E-binding protein 1 (4E-BP1) inhibits assembly of the eIF4F complex by blocking eIF4G binding to eIF4E

(318). Activation of mTORC1 pathway enables mTORC1-mediated phosphorylation of 4E-BP1 first on threonine residues 37 and 47, and subsequently on Ser65, Thr70 and Ser83, which results in structural modification of 4E-BP1 and its release from eIF4E (319). Free eIF4E allows recruitment of eIF4G and formation of the eIF4F complex, promoting cap-dependent translation.

1.4.1.2.2 mTORC1 and ribosomal biogenesis

Considering that ribosomal biogenesis is one of the cellular processes with highest energy requirements and that rRNA accounts for 50% of all synthesized RNA, it is to be expected that it must be a tightly regulated process that responds to energetic cues and the availability of resources (320). Accordingly, mTORC1 has been shown to modulate ribosomal biogenesis, contributing to its role in the regulation of cell growth.

In addition to upregulation of translation of 5'TOP mRNA encoding ribosomal proteins (described in section 1.4.1.2.1), mTOR has also been shown to promote rRNA synthesis through direct association with the promoter of 45S rDNA (321). Interestingly, it has also been reported that mTORC1 phosphorylates and activates two essential transcription factors of the RNA Pol I machinery, TIF-IA and UBF, which might explain the mechanism by which chromatin-bound mTOR stimulates rDNA transcription (Figure 1.24.) (8,186). TIF-IA activation requires phosphorylation at Ser44, while phosphorylation at serine 199 represses its activity. Inactivation of mTORC1 leads to dephosphorylation of both residues which prevents TIF-IA from binding to rDNA promoters and to RNA Pol I, abrogating assembly of the transcription initiation complex (186). Importantly, mTOR, S6K or recombinant TIF-IA are able to rescue rRNA impaired synthesis in cell extracts treated with rapamycin (185). Together, these studies suggest that mTORC1 and modulation of downstream kinases and phosphatases modulate TIF-IA activity (320). Additionally, the mTOR pathway appears to control the nucleolar localisation of TIF-IA, since inactivation of mTORC1 by rapamycin leads to cytoplasmic translocation (320).

Another member of the RNA Pol I machinery regulated by the mTORC1 pathway is UBF. Multi-site phosphorylation of UBF at the carboxy-terminal acidic tail region, and at serine residues Ser388 and Ser389 have been observed to be essential for UBF activation and interaction with SL1 (8,191,322). Interestingly, activated S6K has been shown to phosphorylate the carboxy-terminal region of UBF, promoting its interaction

with SL1 (8). Moreover, phosphorylation appears to play a role in determining UBF localisation, since nutrient-mediated phosphorylation of UBF relocates it to the nucleolus whereas it disperses to the nucleus in response to starvation (322).

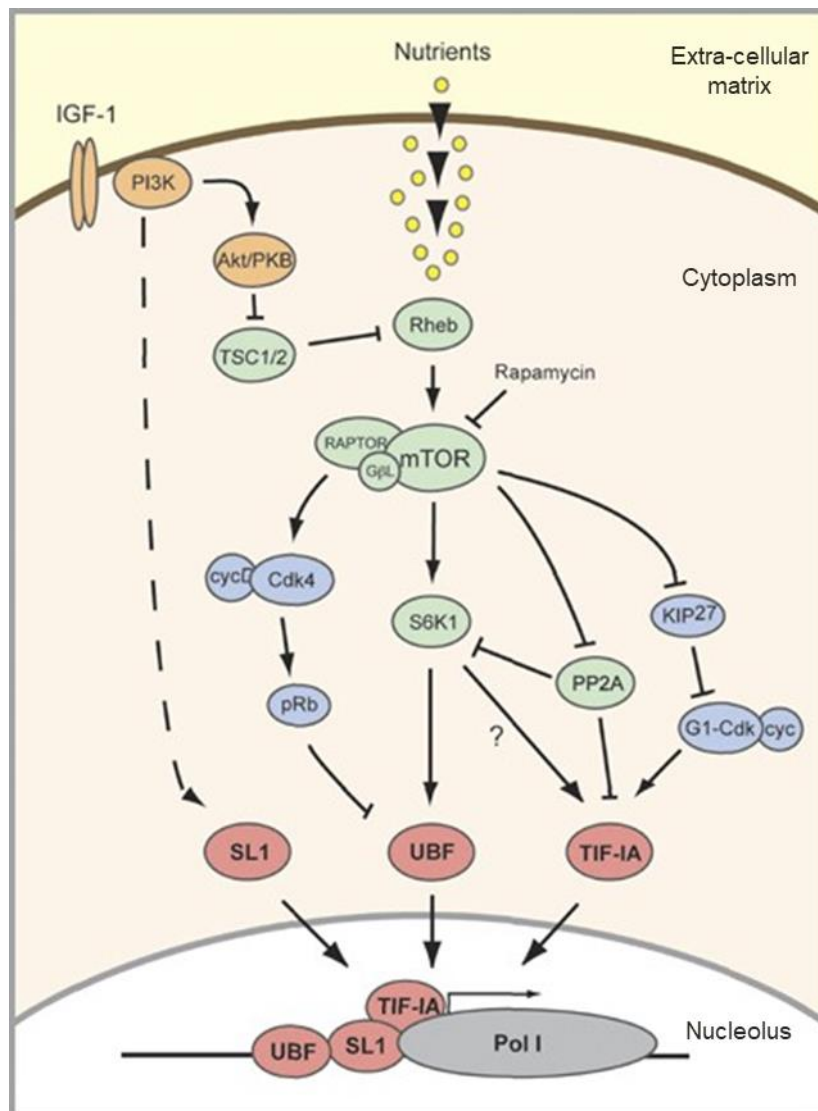


Figure 1.24. Regulation of rDNA transcription by the mTORC1 pathway. In the presence of nutrients, the mTORC1 pathway promotes transcription of rDNA through the phosphorylation-mediated activation of TIF-IA and UBF, essential elements of the RNA Pol I machinery required for rDNA transcription initiation. Figure obtained from (320).

1.4.1.2.3 mTORC1 regulation of lipid synthesis

The role of mTORC1 in lipogenesis has been established through the identification of effectors that regulate the synthesis of lipids. Among these downstream targets, Lipin1 is an enzyme that catalyses the dephosphorylation of phosphatidic acid to yield diacylglycerol during triglyceride synthesis. Additionally, the activity of Lipin1 as a transcriptional co-factor regulates the expression of genes involved in lipid metabolism

(323). Multi-site phosphorylation of Lipin1 by mTOR relocates it to the cytoplasm, whereas the hypo-phosphorylated Lipin1 localises in the nucleolus and reduces nuclear levels of sterol regulatory element-binding protein 1 (SREBP-1), impairing SREBP-1-dependent gene transcription of acetyl-CoA carboxylase (ACC), fatty acid synthase (FASN), and stearoyl-CoA desaturase 1 (SCD-1) (307,324).

mTORC1 also regulates adipogenesis through modulation of both expression and activation of the peroxisome proliferator-activated receptor- γ (PPAR- γ). It has been reported that activation of mTORC1 and subsequent inhibition of 4EBP1 promotes expression of PPAR- γ and induces adipocyte differentiation of mouse embryonic fibroblasts (325). Moreover, the transcriptional activity of PPAR- γ is enhanced by Lipin1, a downstream target of mTORC1 (307). The role of mTOR on the regulation of lipogenesis and adipogenesis described in this section suggests implication of dysregulation of mTOR as a critical factor in the development of obesity related cancers, such as gastrointestinal cancer (326).

1.4.1.2.4 mTORC1 and its role in autophagy

Autophagy is a catabolic process characterised by degradation of cytoplasmic components that provides the cell with energy and biomolecules that can be used for cell growth, particularly under conditions of nutrient deprivation. In response to starvation, activation of autophagy is a mechanism to preserve energy and resources, promoting cell survival. Initiation of autophagy requires participation of the kinases unc-51 like kinase 1 (ULK1) and vacuolar protein sorting-34 (VPS34). Following nutrient deprivation, activation of ULK1 mediates subsequent activation of VPS34, which promotes maturation of the autophagosome (327).

ULK1 is negatively regulated by mTOR through phosphorylation at Ser758 (328,329). Additionally, mTORC1 inhibits ULK1 by phosphorylation-dependent inactivation of Autophagy/Beclin-1 regulator 1 (AMBRA1), which promotes stabilisation and enhancement of the kinase activity of ULK1 through Lys-63-linked ubiquitination (327). ULK1 is also activated by AMPK-mediated phosphorylation in response to energetic stress (329). AMPK-activated ULK1 binds to Raptor and deactivates it through phosphorylation (330). Additionally, mTORC1 inhibits the activity of VPS34 complex by phosphorylating ATG14 (331).

1.4.1.2.5 Regulation of mitochondrial metabolism and biogenesis by mTORC1

mTORC1 has been linked with the regulation of mitochondrial metabolism and biogenesis. For example, upregulation of mitochondrial genes involved in oxidative phosphorylation, increased copies of mitochondrial DNA and enhanced production of reactive oxygen species have been observed in hematopoietic stem cells with TSC1 deletion (332). Additionally, mTORC1 has been reported to interact with and inhibit the transcription factor yin-yang 1 (YY1), which regulates mitochondrial gene expression and oxygen consumption (333).

1.4.2 mTOR complex 2

Although extensive research has been conducted on mTORC1, there is less information on mTORC2. This might be a consequence of the lack of an mTORC2 inhibitor, in contrast to mTORC1. Nevertheless, the structure of mTORC2 has been revealed together with the components that form the protein complex. Comparable to mTORC1, the main component of mTORC2 is the serine/threonine kinase mTOR (Figure 1.25). Likewise, the negative regulator DEPTOR and mLST8 are also part of mTORC2, although it has been shown that mLST8 plays an essential role in the assembly and function of mTORC2 that is not observed in mTORC1 (334).

Instead of Raptor being a component of mTORC1, mTORC2 requires the presence of rapamycin-insensitive companion of TOR (RICTOR), which is fundamental for stabilisation and activity of the complex (335). In addition to RICTOR, mTORC2 has other specific components, including the mammalian stress-activated protein kinase interacting protein (mSIN1) and protein observed with Rictor-1/2 (Protor-1/2) (Figure 1.25) (275). The interaction between Rictor and mSIN1 plays a key role in the complex structure and the regulation of the enzymatic activity of mTORC2 (336). Additionally, mSIN1 is necessary for specific mTORC2 kinase activities including recruiting and enabling phosphorylation of the substrates AKT and SGK1 (337).

In addition to the components already listed, Protor-1 and Protor-2 have been observed to bind to Rictor but not Raptor in HEK-293 cells, which suggests that these proteins are likely to be specific components of mTORC2. It has also been reported that the expression of Protor-1 is regulated by Rictor, however a role for Protor-1/2 in complex formation nor mTORC2 activity has not been identified (338). However, in

Protor-1 knockout mice, a reduction of the phosphorylation of SGK1, an mTORC2 substrate has been detected, and this suggests that Protor-1 might contribute to the activity of mTORC2 (339).

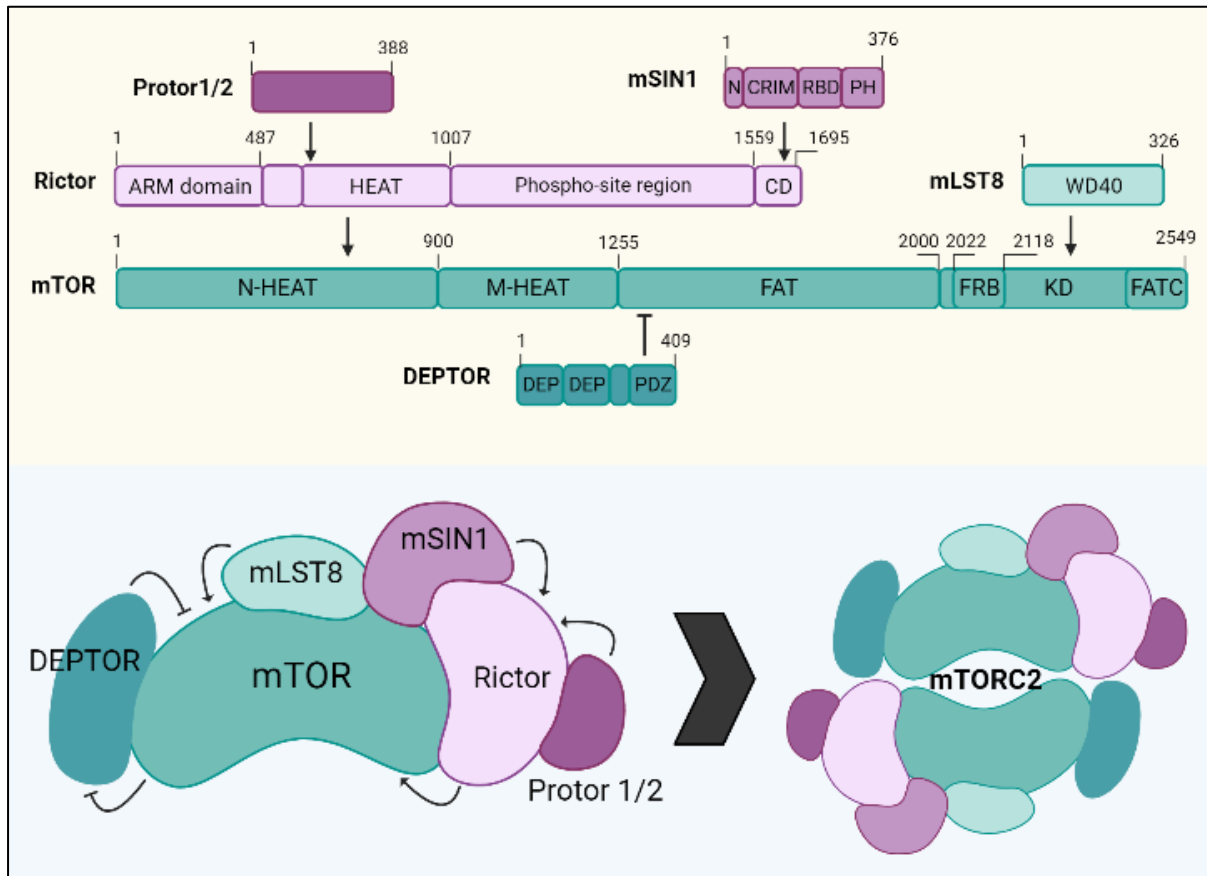


Figure 1.25. Components of the mTORC2. The mTORC2 is an obligate dimeric complex formed by mTOR, Rictor, DEPTOR, mLST8, mSIN1, and Protor-1/2. A linear representation of the different components of mTORC2 shows the relative positions of the structural motifs along the polypeptide chain for each component, and the relative sites where the mTORC2 components interact with each other. mTOR contains tandemly repeat arrays of α -helices known as HEAT domains in the amino-terminus (N-HEAT) and the middle section (M-HEAT) (259). The M-HEAT domain of mTOR is followed by a FRAP, ATM, TRRAP (FAT) domain, which plays a role as structural scaffold or as a protein-binding domain (260). The kinase domain (KD) of mTOR is located between the FKBP12-Rapamycin binding domain (FRB) (261), and a C-terminal FAT domain (FATC). Rictor binds to mTOR through the interaction of its HEAT domain with the N-HEAT domain of mTOR. Additionally, Rictor contains three sets of α -helices known as ARM domain and a C-terminal domain (CD) (340). Rictor is bound and activated by Protor-1/2 and mSIN1, composed of a conserved region in the middle (CRIM) domain that plays an important role in the substrate recognition of mTORC2, a pleckstrin homology (PH) domain, and a RAF-like RAS-binding domain (RBD), involved in the binding of SIN1 to lipid and membrane, and inhibition of the RAS pathway, respectively (341,342). Apart from Rictor, mTOR is bound and activated by mLST8 that contains a WD40 domain (334). Similarly to mTORC1, mTORC2 is also repressed by DEPTOR (343). The cartoon representation displayed in the lower left panel shows the negative and positive regulation exerted by the components of the mTORC2 complex. The cartoon representation on the lower right shows dimerization of the mTORC2.

1.4.2.1 Activation of mTORC2

Although the mechanisms that regulate activation of mTORC2 remain poorly understood, it has been reported that the mTORC2 subunit mSIN1 suppresses the enzymatic activity of mTORC2 through the interaction of its phospholipid-binding pleckstrin homology (PH) domain with the kinase domain of mTOR (Figure 1.26) (344). Additionally, it has been shown that the PH domain of mSIN1 might mediate the localization of mTORC2 in the plasma membranes, and that interaction of PtdIns(3,4,5)P₃ (PIP₃) with the PH domain of mSIN1, releases inhibition of the mTORC2 kinase domain and enables AKT activity, linking the PI3K pathway to mTORC2-dependent activation of AKT (344). Moreover, it has been reported that in the presence of growth factors, phosphorylation of mSIN1 by either S6K or AKT at the threonine residues 86 and 398 leads to dissociation of mSIN1 from mTOR and thus, mTORC2 activation (345), revealing a complex regulation network of the mTOR pathway, involving a negative feedback loop between mTORC1 and mTORC2, and a positive feedback loop between mTORC2 and AKT.

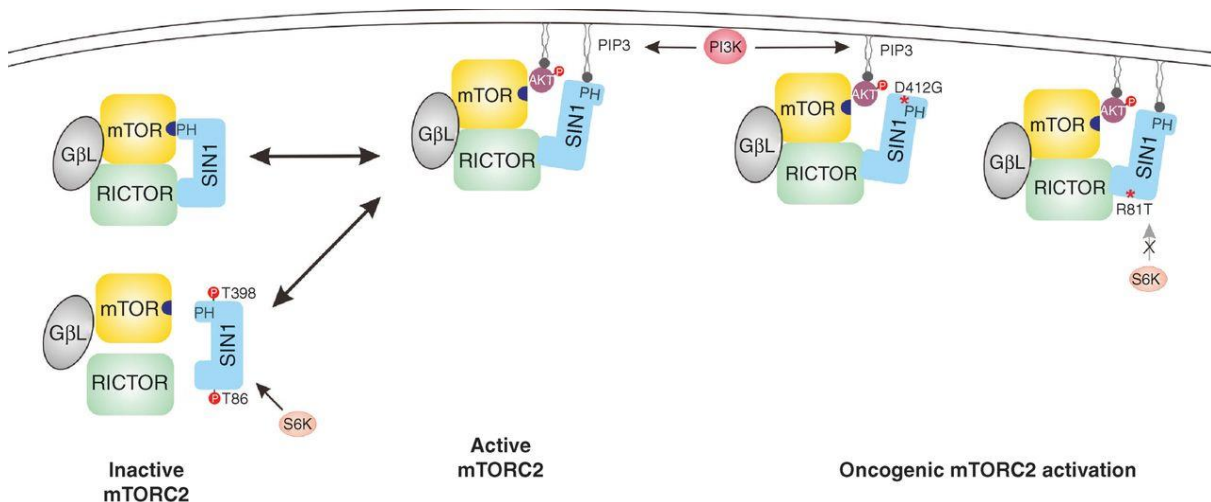


Figure 1.26. Regulation of mTORC2 by mSIN1. On the left, two mechanisms that render mTORC2 inactive are shown. First, phosphorylation of mSIN1 by AKT or S6K promotes dissociation of the mTORC2 and abolishes mTORC2 activity. Alternatively, interaction of the PH domain of mSIN1 with mTORC2 kinase domain inhibit mTORC2 activity. In the presence of insulin, mTORC2 re-localises to the membrane and PIP₃ binds to the PH domain of mSIN1, releasing inhibition over mTORC2 and enabling activation of AKT. The D412G mutant that displays a mutation on the PH domain of mSIN1 that prevents binding to mTORC2 kinase domain and enhances AKT activation (Liu et al., 2015). Additionally, R81T mutation of mSIN1 prevents S6K-dependent phosphorylation and leads to enhanced mTORC2 activity (346). Figure obtained from (345).

1.4.2.2 Regulation of biological functions by mTORC2

Protein kinase b (PKB), also known as AKT, is one of the key targets regulated by phosphorylation by mTORC2 (at Ser477 and T479 in the hydrophobic motif (338,347)). AKT has a critical role in the upregulation of proliferation, metabolism, and cell survival acting as a kinase for a range of substrates. AKT substrates include the transcription factors forkhead box protein O1 (FOXO1) and FOXO3 α , two tumour suppressors that upregulate genes involved in stress resistance, metabolism, cell cycle arrest and apoptosis (348).

AKT also phosphorylates and inactivates glycogen synthase (GSK3 β), a serine/threonine protein kinase with over 100 known substrates, implicated in the regulation of DNA repair, cell cycle control, proliferation and cell metabolism (349). NF- κ B, mTORC1 and the components of the WNT/ β -catenin complex are some of the better studied GSK3 β downstream targets (350). Dysregulation of GSK3 β in particular has been implicated in carcinogenesis and not surprisingly, the use of GSK3 β inhibitors has been shown to sensitise cancer cells to the effects of chemo- and radiotherapy (350,351).

In renal cancer cells, mTORC2 has also been observed to play a role in the regulation of the cell adhesion and migration proteome through AKT-dependent regulation of the expression of cell adhesion factors such as integrin α -5 (ITGA5), transforming growth factor beta-1-induced transcript 1 protein (TGFB111), and lysyl oxidase homologue 2 (LOXL2) (352), implicating oncogenic activation of the mTORC2 pathway in the process of metastasis in renal cancer cells. Importantly, AKT activates mTORC2 through phosphorylation of mSIN1 at its threonine 86 in a positive feedback loop, while AKT activation is repressed in a negative feedback loop by the mTORC1 substrate S6K (345). The complex regulatory mechanisms of the mTOR pathway, comprising positive and negative feedback loops, might be partly responsible for the lack of efficacy of the mTOR inhibitors, and so a better understanding of the mTOR signalling is needed to identify biomarkers to stratify patients that could have a better response.

mTORC2 also activates serum- and glucocorticoid-induced protein kinase 1 (SGK1) by phosphorylating Ser422 on its C-terminal hydrophobic residue (353). Importantly, SGK1 regulates proteins involved in ion transport, growth, and cell survival. Through phosphorylation, SGK1 inactivates FOXO3 α , a tumour suppressor gene and

transcription factor that regulates expression of proteins that promote protein degradation and modulate cellular processes such as metabolism, cell survival and apoptosis (354–356). SGK1 also promotes cell survival by phosphorylating and activating MDM2, a ubiquitin-protein ligase known for the degradation of tumour suppressor p53 (355,357). Accordingly, over-expression of SGK1 has been associated with cancer and is even considered a prognostic factor for some types of cancer (358).

Another effector of mTORC2 is protein kinase C α (PKC α), a kinase that deactivates various transmembrane receptors including EFGR, HER2, and G-protein coupled receptors (359). Furthermore, PKC α has been reported to regulate the activity of ATP-binding cassette (ABC) transporters and solute-like carriers, and to inhibit the activity of oncoproteins KRAS, PI3K and AKT (359). Interestingly, mTORC2 phosphorylation of PKC α has been associated with regulation of the actin cytoskeleton (360).

1.4.3 mTOR and cancer

As described in sections 1.4.1 and 1.4.2 the mTOR pathway plays a key role in the regulation of cellular growth, proliferation, metabolism and survival. The activity of both mTOR complexes depend on the availability of resources, in addition to intra- and extra-cellular signalling, and together, they control synthesis of biomolecules, organelles, metabolism, proliferation, cell survival, and cytoskeleton organisation. Accordingly, dysregulation of the mTOR pathway is associated with the development of pathologies such as cancer, diabetes, and neurodegenerative diseases (361). Importantly, oncogenic activation of the mTOR pathway is associated with various hallmarks of cancer including promoting proliferative signalling, angiogenesis, invasion and metastasis, as well as escaping programmed cell death and changing cellular energetics (362–366) (see table 1.2).

Table 1.2. Hallmarks of cancer enabled by oncogenic activation of the mTOR pathway

Cellular process modulated by the mTOR pathway	Hallmark of cancer associated to oncogenic activation of mTOR pathway	References
Growth and proliferation	Proliferative signals	(307,367–369)
Survival	Escaping programmed death	(362,363)
Metabolism	Change of cellular energetics	(370,371)
Migration and cell adhesion	Invasion and metastasis	(364)
Homeostatic response to hypoxia	Angiogenesis	(366,371)

Enhanced activity of the mTOR pathway is observed across different types of cancer. Such over-activation can derive from mutations in the mTOR kinase that promote constitutive activation of the mTOR pathway. For example, Sato and colleagues identified that the point mutation R2505P in the human cancer genome database enhances the activity of the mTOR pathway, even in response to nutrient starvation, and promotes cell growth in renal cell carcinoma (372). Additionally, a study that identified 33 mutations in mTOR, reported that the identified mutations either enhanced the activity of mTORC1 or mTORC2, and also rendered the cells more sensitive to rapamycin (373).

Mutations in the components of the mTOR complexes that regulate the kinase activity, can also lead to carcinogenesis. Such is the case of DEPTOR, a negative regulator of both complexes, which can act as both a tumour suppressor and an oncogene (273,374,375). While decreased expression of DEPTOR is observed in multiple types of cancer, a group of multiple myelomas that display translocations of cyclin D1/D3 or c-MAF/MAFB show overexpression of DEPTOR (273). Xiaoyu Chen and colleagues recently showed that DEPTOR depletion promotes cell proliferation, survival, migration, and invasion in human prostate cancer cells (374). Additionally, they demonstrated that *DEPTOR* knockout promotes tumorigenesis prompted by the activation of the mTOR signalling and subsequent loss of *PTEN in vivo* (374). Deletion of DEPTOR also enhanced *KRAS*-driven lung tumorigenesis in a mouse model, increasing tumour burden and shortening the lifespan of *KRAS^{G12D}; p53^{fl/fl}; Sftpc-CreERT²* mice while enhancing mTOR signalling (376).

Amplification of *Rictor* has been observed in different types of cancer including gliomas, breast cancer, and lung cancer, and is associated with poor prognosis and short-term

survival (377). Higher levels of Rictor protein and mRNA were found to increase the activity of mTORC2 in glioma cell lines and tumour cells, and xenograph models using these cell lines suggested that enhanced mTORC2 activity has a role in tumorigenesis and heightened tumour growth (378). Overexpression of Rictor was observed in *HER2*-amplified breast tumours, and *Rictor* knockout *in vivo* was associated with decreased cell survival and tumour burden (379). Rictor was also found to be overexpressed in colorectal cancer tissues and was associated with worsening prognosis of patients with colorectal cancer (380).

Mutations of upstream regulators of mTOR including oncogenic activation of *KRAS*, *PIK3CA*, or *AKT* or loss of function of tumour suppressors *PTEN*, *TSC1/2*, or *VHL* can all result in upregulation of the mTOR pathway (377). Interestingly, these mutations can be used as biomarkers for prognosis and for therapeutic response for example, genetic alterations in *PTEN*, including deletions and mutations that lead to loss of function, which occur in 4% of kidney cancer cases, are associated with poor prognosis of patients with ccRCC (381,382). Besides being a biomarker for prognosis, expression of *PTEN* might be a relevant predictive biomarker for therapy response, since low expression of *PTEN* has been associated with better response to mTORC1 inhibitors in patients with advanced renal cell carcinoma (383).

The PI3K/AKT pathway is frequently over-activated in cancer and its dysregulation is associated with carcinogenesis, cell proliferation, cell migration and metastasis, and development of drug resistance. Mutations of PI3K that render constitutive activation of the kinase and amplification of genomic regions that contain *AKT*, *PDPK1*, or *PIK3CA* genes are found in various types of cancer (384).

Enhanced mTOR signalling in *KRAS*-mutant lung cancer appears to mediate therapy resistance, and the use of rapamycin has been shown to sensitise cells to the effects of cisplatin when used in combination (385). Similarly, targeting an over-active mTOR pathway in mutant *KRAS* colorectal cancer with an ATP-competitive inhibitor of mTOR in combination with BCL-2/BCL-XL inhibitors was shown to promote tumour regression (386). Similarly, the use of rapamycin to target an enhanced mTOR pathway in lung cancer cells that harbour mutant *KRAS* in combination with cisplatin, suppressed proliferation and tumour growth in preclinical mouse models (385).

1.4.4 mTOR inhibitors as targeted cancer therapy

Rapamycin, also known as sirolimus, originally discovered in soil samples from Easter Island, is a natural compound produced by *Streptomyces hygroscopicus* that possesses antifungal, immunosuppressive and anti-proliferative properties. The ability of rapamycin to block cytokine signalling and thus prevent lymphocyte growth and differentiation, results in the potent immunosuppressant activity used to prevent rejection of grafts and organ transplantation, while preserving nephron function (387,388). Importantly, the anti-proliferative properties of rapamycin are relevant for its use in the treatment of cancer, especially in cancers where the mTOR pathway is dysregulated.

Rapamycin acts by binding to the 12-kDa FK506-binding protein (FKBP12). The rapamycin-FKBP12 complex interacts with the FKBP12-rapamycin binding domain (FRB) of mTORC1, which is situated upstream of the kinase domain between residues 2022 and 2118 (Figure 1.18) (389,390). This interaction blocks the recruitment of substrates and prevents substrate access to the catalytic site of mTORC1 (391). Even though mTORC2 is not rapamycin sensitive, long exposure to rapamycin has been shown to reduce activity of mTORC2 by inhibiting the complex formation in some cell lines (392).

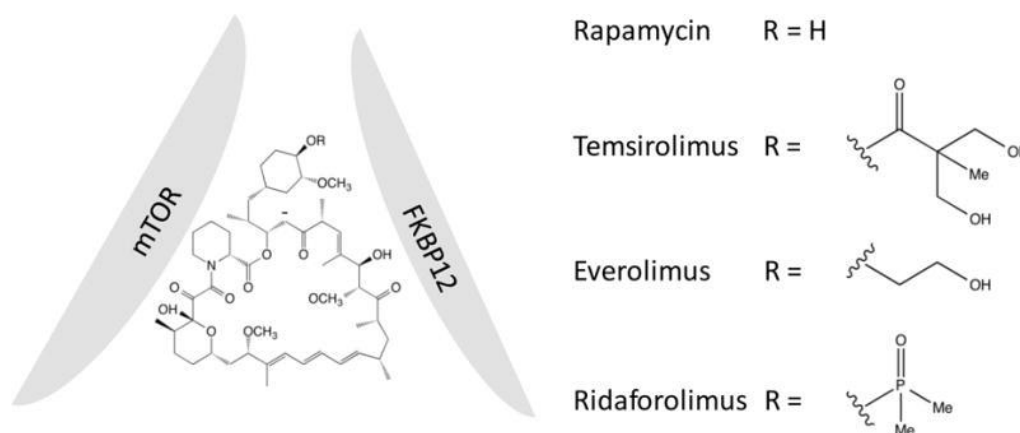


Figure 1.27. Chemical structure of rapamycin and other allosteric inhibitors of mTORC1. Rapamycin and its analogues inhibit mTORC1 activity by binding to FKBP12 and subsequent interaction of the rapamycin-FKBP12 complex with the FRB domain of mTORC1. Figure obtained from (393).

Although rapamycin displays properties that suggest it could be suitable for a range of clinical uses, its therapeutic use is limited by low oral bioavailability. Thus, various compounds with similar structure but increased bioavailability and solubility were

developed. This group of rapamycin analogues, also known as rapalogs, include compounds such as Everolimus, Temsirolimus, and Ridaforolimus (Figure 1.27) (393).

Like rapamycin, Everolimus and Temsirolimus inhibit mTORC1 allosterically by forming a complex with FKBP12 that binds to the FRB region of mTOR1 preventing the interaction of substrates with the kinase domain. Both drugs inhibit activation of mTORC1 downstream substrates, inhibiting cell growth and promoting cell cycle arrest in tumour cells (394). Temsirolimus was approved by the FDA as a Targeted first-in-class mTOR inhibitor for the treatment of advanced RCC in 2007 (395). The recommended dose is 25 mg infused over a 30-60 minute period once a week. Following the recommended dosage, the maximum concentration (C_{max}) in blood was 585 ng/mL and the area under the concentration-time curve (AUC) in blood was 1627 ng·h/mL (CV=26%) (396). Everolimus has been approved to treat advanced kidney cancer, pancreatic neuroendocrine tumours (NET), advanced breast cancer, gastrointestinal and lung NET, and subependymal giant cell astrocytoma (SEGA), a rare type of paediatric brain tumour (397). The recommended dose for Everolimus is 10 mg orally once daily, which has been shown to provide a C_{max} of 61.5 ng/ml, minimum concentration (C_{min}) of 9.6 ng/ml, and AUC of 435 ng h/ml (398).

Even though there were great expectations for success with these mTOR inhibitors for cancer treatment, clinical results have shown only limited efficacy of these drugs. Lack of sensitivity of some types of cancer to the mTOR inhibitors, toxicity and drug resistance are the main limitations of mTOR inhibitors. It has been suggested that resistance to mTOR inhibitors is mediated by the over-activation of mTORC2 in response to mTORC1 inhibition and subsequent release of the negative feedback loop induced by S6K-phosphorylation-dependent inactivation of IRS1 (399). Additionally, rapamycin inactivation of S6K prevents it from phosphorylating of Rictor at threonine 1135 by S6K, which hinders formation of mTORC2 by promoting binding of Rictor with 14-3-3 proteins (400).

Additionally, resistance to mTOR inhibitors can be a consequence of the differential inhibition of phosphorylation of mTORC1 downstream targets. While phosphorylation of S6K in threonine 389 is completely abrogated in response to rapamycin treatment, rapamycin prevents mTORC1-mediated phosphorylation of 4EBP1 only temporarily, recovering cap-dependent translation even under S6K continued inhibition (401).

In an attempt to circumvent the negative regulation loops of the mTOR complexes that might promote drug resistance, mTOR inhibitors are currently being used in combination with IGF-IR, PI3K, Hsp90, Raf or Mek modulators (García-Echeverría, 2010). Additionally, dual mTORC1-mTORC2 inhibitors have also been developed. These new drugs are small molecules that selectively bind to the kinase active site of mTOR and inhibit phosphorylation of mTORC1 and mTORC2 substrates (402).

These pan mTOR inhibitors include AZD-8055, OSI-027, INK128, WYE-132, Torin 1, and Torin2, and have been shown to prevent the phosphorylation of the mTORC1 substrate 4EBP1 more effectively than rapamycin and have also achieved significantly better inhibition of tumour growth in xenograft mouse models than rapamycin or its analogues (403–405). However, patients with advanced solid tumours or lymphoma treated with AZD8055 showed no complete or partial response (406,407).

In summary, the mTOR pathway is a key regulator of cell growth and proliferation, and its dysregulation is associated with diverse pathologies, among them cancer. Over-activation of the mTOR pathway can be driven by oncogenic *KRAS*, *PI3K* and *AKT*, as well as loss of function of tumour suppressors such as *PTEN*, *TSC1/2*, or *VHL*, and so, targeting mTOR became an interesting strategy for cancer therapy, and several mTOR inhibitors have been developed. Two main types of mTOR inhibitors exist, the allosteric inhibitors, which bind and prevent mTORC1 activity, and ATP-competitive inhibitors that bind to the kinase domain of mTOR and prevent phosphorylation of mTORC1 and mTORC2 downstream targets. Although allosteric mTOR inhibitors have been approved and are used for the treatment of certain types of cancer, including renal cell carcinoma, patients treated with these drugs struggle with low response rates and development of resistance, attributed to the complex network of feedback loops that have been discovered over the last two decades. This situation highlights the importance of understanding better the mTOR pathway and the downstream substrates that are targeted by mTOR inhibitors.

1.5 Aims

As outlined in the section 1.1.2.1, RCC remains to have a bad prognosis, especially in patients who are diagnosed when the disease has progressed and the tumour has invaded adjacent tissue or other organs. These patients are treated with systemic therapies, including chemotherapy, immunotherapy and targeted therapy, to which the tumours have partial or no response, and frequently develop drug resistance.

NFIs have been proposed as potential cancer therapy because nucleolar functions such as ribosome biogenesis, regulation of cell cycle and stress response are dysregulated in cancer. However, these drugs, similarly to other chemotherapeutics, target a cellular function rather than an oncogenic pathway, and thus, their therapeutic index is narrow. Interestingly, the nucleolar function is also modulated by oncogenic pathways for which targeted inhibitors have been developed, as is the case of the mTOR pathway.

The aims of the present study are to assess if mTOR inhibitors effectively modulate nucleolar function in RCC cell lines, and if they can be used to sensitise cancer cells to the effects of NFIs.

2. Materials and methods

2.1 List of reagents

2.1.1 General reagents

Table 2.1 General reagents

Reagent or product	Manufacturer
1,4-diazabicyclo[2.2.2]octane (DABCO)	Sigma-Aldrich
1,4-dithiothreitol (DTT)	Sigma-Aldrich
10% Mini-PROTEAN® TGX™ Precast Protein Gels, 10-well, 50 µl #4561034	Bio-Rad
2'-Deoxy-5-ethynyluridine (EdU)	Carbosynth
3-(4,5-dimethylthiazol-2-yl)-2,5-diphenyl tetrasodium bromide (MTT)	Molekula
4–15% Mini-PROTEAN® TGX™ Precast Protein Gels, 10-well, 30 µl with Dual Color Standards #4561083DC	Bio-Rad
5-Ethynyluridine (EU)	Carbosynth
FAM azide, 6-isomer	Lumiprobe
7-aminoactinomycin D (7-AAD)	Biotium
Acrylamide/Bis-acrylamide	VWR
Ammonium persulphate (APS)	Sigma-Aldrich
Blotting grade blocker, non-fat dry milk	Bio-Rad
Blue Prestained Protein Standard, Broad range (11-190 kDa)	New England's Biolabs
Bovine Serum Albumin (BSA)	Sigma-Aldrich
Bromophenol blue	Sigma-Aldrich
Chloroform	Sigma-Aldrich
CuSO ₄ ·5H ₂ O	Sigma-Aldrich
DAPI	Sigma-Aldrich
DC protein assay reagent A	Bio-Rad
DC protein assay reagent B	Bio-Rad
Dimethyl Sulphoxide (DMSO)	Sigma-Aldrich
DNA ladder (100bp)	New England Biolabs
ECL Clarity	Bio-Rad

ECL Clarity Max	Bio-Rad
Ethanol, absolute	Sigma-Aldrich
EveryBlot Blocking Buffer	Bio-Rad
Formaldehyde solution 37%	Merck
Glycerol	Sigma-Aldrich
Glycine	Thermo Fisher Scientific
Hydrochloric acid (HCl)	Sigma-Aldrich
L-ascorbic acid	Sigma-Aldrich
Methanol, analytical grade	Thermo Fisher Scientific
N, N, N', N'-tetramethylethylenediamine (TEMED)	VWR
Nitrocellulose membrane 0.45 µm	Thermo Fisher Scientific
Phosphate-buffered saline 10x	Fisher Scientific
Ponceau S	Sigma-Aldrich
Proteinase K	Sigma-Aldrich
RNase A	Qiagen
Sodium acetate	Sigma-Aldrich
Sodium chloride	VWR
Sodium dodecyl sulphate (SDS)	Thermo Fisher Scientific
Sodium pyruvate solution (100mM)	Sigma-Aldrich
Sulfo-Cyanine3 azide	Lumiprobe
Tetramethylethylenediamine (TEMED)	VWR
Tris base	Calbiochem
Tris base (2-Amino-2-(hydroxymethyl)-1,3-propanediol)	Sigma-Aldrich
Tris EDTA buffer (20x)	Invitrogen
Tris HCl	Fisher Scientific
Triton X-100	GE Healthcare
Tween-20	Sigma-Aldrich

2.1.2 Tissue culture reagents

Table 2.2 Tissue culture reagents

Reagent or product	Manufacturer
Dulbecco's modified Eagle's medium (DMEM) #D6171	Sigma-Aldrich
Eagle's Minimum essential medium	Sigma-Aldrich
Fetal bovine serum (FBS)	Sigma-Aldrich
L-glutamine solution 200mM	Sigma-Aldrich
McCoy's 5A Medium	Sigma-Aldrich
MEM non-essential amino acid solution (100x)	Sigma-Aldrich
Opti-MEM Reduced Serum Medium	Gibco
PBS, PH 7.2	Invitrogen
Penicillin-streptomycin	Sigma-Aldrich
RPMI-1640	Sigma-Aldrich
Sodium pyruvate	Sigma-Aldrich
Trypsin-EDTA solution (1x)	Sigma-Aldrich
ON-TARGET plus Human RRN3 (54700) SMARTpool siRNA	Dharmacon
Lipofectamine2000	Invitrogen

2.1.3 Drugs

Actinomycin D (dactinomycin): DNA intercalator that binds to ribosomal DNA and inhibits RNA polymerase I (Pol I) transcription. Stock solution prepared by dissolving 1 mM in DMSO. Supplied by LC Laboratories. Stored at -20°C.

AZD8055: mTOR kinase inhibitor/ATP-competitive inhibitor that targets mTORC1 & mTORC2. Stock solution prepared by dissolving 10 mM in DMSO. Supplied by Selleckchem. Stored at -20°C for 4 weeks.

BMH-21: DNA intercalator that binds to ribosomal DNA and inhibits RNA polymerase I (Pol I) transcription. Stock solution prepared by dissolving 10 mM in DMSO. Supplied by Selleckchem. Stored at -20°C for 4 weeks.

Etoposide: Topoisomerase II inhibitor. Stock solution prepared by dissolving 100 mM in DMSO. Supplied by Sigma. Stored at -20°C.

Everolimus: mTOR allosteric inhibitor that targets mTORC1. Stock solution prepared by dissolving 10 mM in DMSO. Supplied by LC Laboratories. Stored at -20°C.

Rapamycin (sirolimus): mTOR allosteric inhibitor that targets mTORC1. Stock solution prepared by dissolving 0.5 mM in DMSO. Supplied by LC Laboratories. Stored at -20°C.

Staurosporine: a broad spectrum Protein kinase (PK) inhibitor. Stock solution prepared by dissolving 10 mM in DMSO. Supplied by LC Laboratories. Long-term storage was at 4°C.

Temsirolimus: mTOR allosteric inhibitor that targets mTORC1. Stock solution prepared by dissolving 5 mM in DMSO. Supplied by LC Laboratories. Stored at -20°C.

Torin 1: mTOR kinase inhibitor/ATP-competitive inhibitor that targets mTORC1 & mTORC2. Stock solution prepared by dissolving 3 mM in DMSO. Supplied by LC Laboratories. Stored at -20°C.

2.1.4 Antibodies for Western Blotting

Table 2.3 Antibodies for Western Blotting

Antibody	Manufacturer	Final Conc.	Diluent
p70 S6 Kinase Antibody #9202	Cell Signaling Technology	1:1000	5% Blotting grade blocker
Phospho-p70 S6 Kinase (Thr389) Antibody #9205	Cell Signaling Technology	1:1000	EveryBlot Blocking Buffer
Phospho-p70 S6 Kinase (Ser371) Antibody #9208	Cell Signaling Technology	1:1000	EveryBlot Blocking Buffer
4E-BP1 antibody #9452	Cell Signaling Technology	1:1000	5% Blotting grade blocker
Phospho-4E-BP1 (Thr37/46) (236B4) Rabbit mAb #2855	Cell Signaling Technology	1:1000	EveryBlot Blocking Buffer
Rrn3 (D-9): sc-390464	Santa Cruz Biotechnology	1:100	EveryBlot Blocking Buffer

Anti-phospho-TIF-IA (pSer649) SAB4504731	Sigma-Aldrich	1:1000	EveryBlot Blocking Buffer
UBF (F-9): sc-13125	Santa Cruz Biotechnology	1:200	5% Blotting grade blocker
UBF (phospho-Ser484) antibody orb128892	Biorbyt	1:1000	EveryBlot Blocking Buffer
Anti- β -actin antibody AC15 (A1978)	Sigma-Aldrich	1:80,000	5% Blotting grade blocker
Monoclonal Anti-Vinculin antibody produced in mouse (V9131)	Sigma-Aldrich	1:10,000	5% Blotting grade blocker
Sheep α -mouse antibody (RPN4201)	GE Healthcare	1:5000	5% Blotting grade blocker
AffiniPure Donkey Anti- Mouse IgG (715-655-150)	Jackson ImmunoResearch	1:5000	5% Blotting grade blocker
Donkey α -rabbit antibody (NA934)	GE Healthcare	1:5000	5% Blotting grade blocker
P70 S6 Kinase MCF7 Control Cell Extracts (#34499)	Cell Signaling Technology	10 μ l per well	N/A

2.1.5 Solutions

Table 2.4 Solutions

Solution	Components
PBS 10x	[NaCl]: 1.37 M [KCl]: 27 mM [Na ₂ HPO ₄]: 100 mM
	[KH ₂ PO ₄]: 18 mM
PBS 1x	[PBS 10x]: 10% v/v in distilled H ₂ O
PBST	PBS 1x [Tween20]: 0.05% v/v
TBS 10x	Tris base: 24 g NaCl: 88 g distilled H ₂ O to final volume 1 L Adjust pH to 7.6 with NaOH or HCl
TBS 1x	[TBS 10x]: 10% v/v in distilled H ₂ O
TBST	TBS 1x [Tween20]: 0.05% v/v
TBS 0.5% Triton X-100	TBS 1x [Triton X-100]: 0.5% v/v
Click solution – 5-EU (labelling of rRNA)	1. [Tris HCl]: 0.1 M 2. [CuSO ₄ ·5H ₂ O]: 1 mM 3. [L-ascorbic acid]: 0.1 M 4. [Sulfo-Cy3 azide]: 10 μM
Click solution – EdU (flow cytometry)	1. [Tris HCl]: 0.1 M 2. [CuSO ₄ ·5H ₂ O]: 1 mM 3. [L-ascorbic acid]: 0.1 M 4. [6-FAM azide]: 10 μM
Imaging Solution	[Tris HCl pH 8.5]: 0.1 M [Glycerol]: 25% (w/v) [DABCO]:1% (10 mg/ml) [DAPI]: 0.1 mg/ml
1.5 M Tris pH 8.8	Tris base: 18.17 g

	distilled H ₂ O up to 100 ml
1 M Tris pH 6.8	Tris base: 7.88 g Tris HCl: 6.06 g distilled H ₂ O up to 100 ml
Lysis buffer	10% SDS: 2.8 ml 1 M Tris pH 6.8: 1.75 ml Glycerol: 1.4 g distilled H ₂ O up to 14 ml
6x loading buffer	1.0 M Tris pH 6.8: 563 µl 3 M DTT: 120 µl Glycerol: 900 mg distilled H ₂ O up to 1.5 ml
Electrophoresis running buffer 10x	Tris base: 60.6 g Glycine: 288.4 g SDS: 20 g distilled H ₂ O up to 2000 ml
Bio-Rad Transfer Buffer 5x	Bio-Rad
Bio-rad transfer buffer 1x	Bio-Rad Transfer Buffer 5x: 200 ml Ethanol: 200 ml distilled H ₂ O 600 ml
MTT solution	[MTT]: 5 mg/ml in PBS
Sorenson's glycine buffer pH 10.5	[Glycine]: 0.1 M [NaCl]: 0.1 M

2.2 Cell culture

All cell culture protocols were carried out inside a laminar flow cabinet. The laminar flow cabinet was sterilised with UV light before working with each cell line to prevent cross-contamination. All the cell lines were authenticated by STR profiling and tested for mycoplasma regularly.

2.2.1 Cell lines and cell culture

Cell lines are a relevant *in vitro* model used for cancer research. Their ability to survive long-term storage and to continuously provide biomass are strong advantages for this model. Additionally, cancer cell lines have been shown to preserve the genetic identity of their parental tumours (95). Thus, they can be used to understand the molecular mechanisms behind carcinogenesis and to identify the main traits and pathways altered in different types of cancer. Even though they are not able to reproduce the effects of the drugs in the body, they can also be useful to assess drug sensitivity and to identify biomarkers that might predict treatment response (408,409).

The first RCC cell lines were established in the 1970's and many of them continue to be used today. Although originally classified as RCC, advances in genomics have allowed to sub-classify the existing RCC cell lines according to their phenotypic and genomic signatures (410). The Genomics of Drug Sensitivity in Cancer database presents information of a large-scale drug screen performed in collaboration by the Wellcome Sanger Institute and the Centre for Molecular Therapeutics, Massachusetts General Hospital Cancer Centre. In this database, 34 kidney cancer cell lines have been screened to assess sensitivity to mTOR inhibitors.

For this study, four cell lines mentioned in the database were selected. Three of the cell lines selected displayed an $IC_{50} < 50$ nM for Rapamycin or Temsirolimus (786-O, ACHN, and Caki-1 cells) and one cell line displayed an $IC_{50} > 100$ nM to both drugs (A704 cells). These cell lines were chosen to observe different types of responses to the mTOR inhibitors, to compare the results obtained in this study with those reported, and to decide which of them could be better candidates for the combination of mTOR inhibitors with the NFIs. Additionally, the ccRCC cell line UoK111, which is not included in the database was used to provide new information on the sensitivity of this cell line to these drugs.

The following RCC cell lines were used in the present research project:

- ACHN is a RCC cell line established from metastatic kidney cancer. It has been sub-classified as papillary renal cell cancer (PRCC) because of the mutations and chromosomal aberrations that it displays (Brodaczewska et al., 2016). This cell line was split every 3-4 days at a 1:10 ratio.

- UoK111 is a cell line representative of clear cell renal cell carcinoma (ccRCC) and was established in the National Cancer Institute in Bethesda in 1989 (411). This cell line was split every 3-4 days at a 1:10 ratio.
- Caki-1 is a cell line derived from metastatic renal cell carcinoma. Even though Caki-1 does not harbour the typical mutations in VHL, this cell line promotes the growth of clear cell tumours (410). Additionally, sub-classification as ccRCC subtype ccb, has been assigned to this cell line because of its aggressive phenotype (412). This cell line was split every 3-4 days at a 1:5 ratio.
- 786-O is one of the first RCC cell lines established (413). It displays typical ccRCC features such as VHL mutations and copy number alterations of key kidney cancer genes. It is considered to be a more aggressive subtype of ccRCC ccb (412). This cell line was split every 3-4 days at a 1:6 ratio.
- A704 was established in 1973 and is classified as renal cell carcinoma (414). This cell line was split every 3-4 days at a 1:2 ratio.

Cells were grown in Nunc™ T75 flasks and kept in incubation at 37°C with 5%CO₂. The cells were grown in medium described on table 2.5., supplemented with 10% Foetal Bovine Serum (FBS), 1% penicillin/streptomycin, 1% L-glutamine, 1% non-essential amino acids (NEAA), and 1% sodium pyruvate.

Table 2.5. RCC cell lines used in this study.

Cell line	ATCC designation	RCC type	Stage	p53 status	VHL status	Medium
786-O	ATCC® CRL-1932	Clear cell renal cell carcinoma	Primary tumour	TP53 – HGNC: 11998; c.560-2A>G; p.Pro278Ala	VHL – HGNC: 12687; p.Gly104Alafs*55 (c.311delG)	RPMI 1640
A704	ATCC® HTB-45	Renal cell carcinoma	Primary tumour	TP53 – HGNC: 11998; p.Tyr126Asp (c.376T>G); p.Cys135Arg (c.403T>C); p.Glu258Ter (c.772G>T)	WT	Minimum Essential Medium (MEM)

ACHN	ATCC® CRL-1611	Papillary renal cell carcinoma	Metastatic	WT	WT	Dulbecco's Modified Eagle's Medium (DMEM) – high glucose
Caki-1	ATCC® HTB-46	Clear cell renal cell carcinoma	Metastatic	WT	WT	McCoy's 5a
UoK111	NA - National Cancer Institute in Bethesda	Clear cell renal cell carcinoma	NA	TP53 – HGNC: 11998; p.Val173Gly (c.518T>G)	TGG -> AGG; NT 562	Dulbecco's Modified Eagle's Medium (DMEM) – high glucose

2.2.2 Cell subculture technique

Cells were passaged every 3 or 4 days, when they reached 80-90% confluency. To this purpose, the medium was removed and a volume of 15 ml of sterile PBS was used to wash the cells grown in monolayer in the T75 flasks. After removing the PBS, 3 ml of trypsin were added per flask, and the flask were placed back in the incubator for 5 to 10 minutes. Once cells were detached from the flask the cell solution was pipetted up and down a couple of times to get a single cell solution and prevent clump formation. Then, a volume of 7 ml of medium was used to stop trypsinization. Depending on the growth rate for each cell line, the cells were splitted in a 1:5, 1:10, or 1:20 ratio. The volume of cell suspension and media were adjusted accordingly for a final volume of 10 ml per T75 flask.

2.2.3 Cryopreservation and recovery of cryopreserved cell stocks

To minimise the genetic change of cell lines, new stocks of cryopreserved cells were prepared with cell cultures that had only been passed two times. Cryopreservation was also carried out as a safety measure in case of culture contamination.

The stocks were prepared by washing and trypsinising the cells as described in section 2.2.2., and the cell suspension was centrifuged at 100-200 g for 5 minutes. The supernatant was removed without disturbing the pellet and the pellet was resuspended in cold freezing medium (10% DMSO in FBS). The cell suspension was dispensed in 1.5 ml aliquots in Nunc™ cryogenic storage vials (Thermo Fisher Scientific). The vials were placed in styrene foam boxes and stored at -80°C for 48-72 hours to allow slow

freezing of and avoid crystal formation. The frozen vials were then transferred to liquid nitrogen.

To retrieve the cryopreserved cells, the vials were removed from the liquid nitrogen and immediately thawed in a water bath at 37°C for a couple of minutes, until the medium was completely melted. Using a pipette, the contents of the vial were transferred to a 15 ml tube with 10 ml of culture medium to decrease the percentage of DMSO and prevent toxicity to the cells. The tube was centrifuged at 100g for 5 minutes and the supernatant was discarded. The pellet was resuspended in 10 ml of culture medium and transferred to a T75 flask. The flask was then placed in the incubator at 37°C with 5%CO₂.

2.2.4 Mycoplasma testing

Whenever a new stock of cryopreserved cells was thawed, and the cells had reached about 80% confluence, mycoplasma test was carried out to ensure that the cells were free of contamination with mycoplasma.

Confluent cell cultures were washed and trypsinised as described in section 2.2.2. and at least 5x10⁴ cells were transferred to a 1.5 ml Eppendorf tube. The tube was centrifuged at 7,000 rpm for 5 minutes, the medium was removed and the pellet was washed with sterile PBS twice. The pellet was then resuspended in 100 µl of sterile PBS and the sample was heated at 95°C for 10 minutes. After vortexing for 5 seconds, the sample was centrifuged at 13,000 rpm for 2 minutes and then an aliquot of 100 µl of the heated supernatant was transferred into a fresh tube.

Once the sample was ready, a volume of 10 µl of the sample was added to a tube of the e-Myco Mycoplasma PCR detection kit and resuspended in 10 µl of sterile DNase-free water for a final PCR reaction volume of 20 µl. The PCR reaction was carried out with the following the conditions shown in the table 2.6.

Table 2.6. PCR conditions for Mycoplasma test

PCR Condition		Temp	Time
Initial denaturation		94°C	1 min
35 cycles	Denaturation	94°C	30 sec
	Annealing	60°C	20 sec
	Extension	72°C	1 min
Final extension		72°C	5 min

The agarose gel electrophoresis protocol was adapted from (415). The agarose gel was prepared while the PCR was running. A mass of 2 g of agarose was dissolved in 100 ml TAE buffer. The agarose/buffer /mixture was melted using a microwave. The flask was removed from the microwave at 30-second intervals and swirled the contents to mix thoroughly. This was repeated until the agarose was completely melted. The flask was then placed in a 65°C to cool down. A volume of 60 µl of Syto™60 Red nucleic acid stain was added to 30 ml of agarose and the flask was swirled to ensure proper dilution of the stain in the mix. The gel tray was taped on the open edged to create a mold and the comb was placed to create the wells. A volume of 30 ml of molten agarose were poured into the mold and the gel was allowed to set at room temperature. Once the gel was solidified, the comb was removed and the gel was placed in the gel box. TAE Running buffer was poured into the chamber covering the gel.

Once the PCR was through, the concentration of DNA was measured using a nanodrop at 260 nm. A volume of 4 µl of loading dye 6x (30% glycerol, 0.25% bromophenol blue) were added per 20 µl of DNA sample and to the DNA ladder. The samples were gently mixed and loaded into the gel. Electrophoresis ran at 100V for 40 minutes. Post-electrophoretic staining was performed by diluting Syto™60 Red nucleic acid dye 1:5000 in distilled water and staining the gel for 45 minutes at room temperature. The gel was rinsed briefly with distilled water and imaged using the ChemiDoc MP Imaging System at 700 nm channel.

In order to ensure that the cell lines were healthy and free of contamination with mycoplasma, the technical staff of the Institute of Systems, Molecular & Integrative Biology, carried out monthly mycoplasma tests. Samples were prepared as described and stored at -20°C.

2.2.5 STR profiling

As mentioned before, cell lines are a relevant *in vitro* model used in broadly in life sciences research. Nevertheless, lack of adherence to good laboratory practices summed to the existence of very aggressive and fast growing cell lines such as HeLa, enable cross-contamination of cell lines in culture. This problem has scientific and economic repercussions, since results from studies that used cross-contaminated cultures cannot be concluded (416).

Short tandem repeat (STR) analysis is a molecular technique used to correctly identify the cell lines. It consists in the simultaneous amplification of 17 polymorphic markers and the amelogenin gene using multiplex polymerase chain reaction (PCR). A specific STR identity profile is assigned to each cell line depending on the length of the amplicons (417).

STR analysis for all the cell lines used in this study was carried out by the Cell Line Authentication Facility of the Institute of Translational Medicine of the University of Liverpool (see appendix [sections 7.1]).

2.3 Cell viability assays

Assessment of cellular viability plays a relevant role in drug discovery, as it provides information about the toxicity of certain compound(s) on a specific type of cell. Assays that measure the metabolic activity can be used to provide information of the viability of a cell population. An advantage of this type of assays is that they can be carried out on 96-well microplates with adherent cells, making them useful for high-throughput screenings where several compounds are tested.

Metabolic activity can be determined by measuring the reduction tetrazolium salts, because the reaction requires NADH and NADPH, which are sub-products of nucleotide metabolism, as co-substrate. The reduction of these reagents produces

coloured or fluorescent compounds that can be detected using a microplate reader (418).

2.3.1 MTT assay

The first and one of the most popular metabolic activity assays is the MTT (3-(4,5-dimethylthiazol-2-yl)-2,5-diphenyltetrazolium bromide) tetrazolium reduction assay. For this study, an adapted version of the protocol published by Terry Riss and colleagues was used (419).

About 5,000 cells were seeded per well in a 96-Well CytoOne® Plate, TC-Treated, and grown overnight. No cells were seeded in wells marked as blank, but a volume of 100 μ l of the same media used in the cell cultures was added to these wells in order to use them as a control for background. The media was aspirated from two rows of wells each time to prevent cells from drying and then, 100 μ l of the media with treatment were added per well using triplicates. A volume of 100 μ l 0.1% v/v of the drug stock diluent (DMSO or ethanol) in culture medium were added to the wells labelled as control. Each plate was divided in two sections, each containing a different drug treatment. Each section had its own control and blank, as shown in Figure 2.1. The replicates were distributed throughout the plate to prevent “edge effect”. In addition, 12 ml of distilled sterile water were added to the plate to prevent evaporation of the medium. Plates were incubated for 72 hours at 37°C 5%CO₂. A volume of 20 μ l of MTT solution (5 mg/ml) was added per well and plates were incubated at 37°C. After 3-hour incubation, the media was carefully aspirated using a gel loading tip, without touching the bottom of the wells. A volume of 100 μ l of DMSO was added to each well. Then, a volume of 12 μ l of Sorenson’s glycine buffer pH 10.5 was added per well, and the plate was incubated for 15 minutes at room temperature on the shaker. Complete solubilisation of the formazan crystals was assessed and the plate was placed in the SpectraMax Plus 384 Microplate Reader to measure the absorbance. The wavelength used to measure absorbance of the formazan product was 570 nm and the reference wavelength used was 630nm.

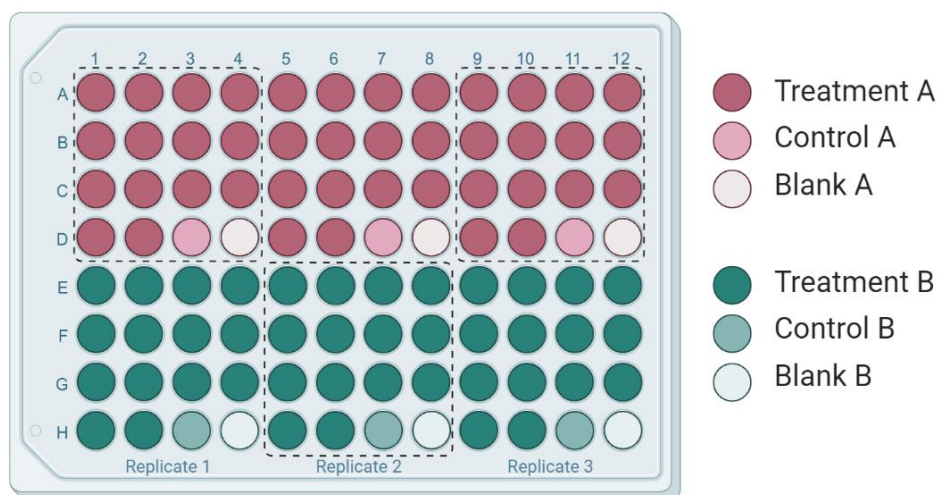


Figure 2.1. Plate layout showing the distribution of drug treatments, control and blanks using 96 well microplate.

2.3.2 Resazurin assay

Similar to the MTT assay, the resazurin assay measures metabolic activity through the detection of the reduced product of resazurin called resorufin (Figure 2.2). This product can be measured with a microplate reader equipped to read fluorescence with a 560nm excitation / 590 nm emission filter set. For this study an adapted version of resazurin assay protocol published by Terry Riss and colleagues was used (419).

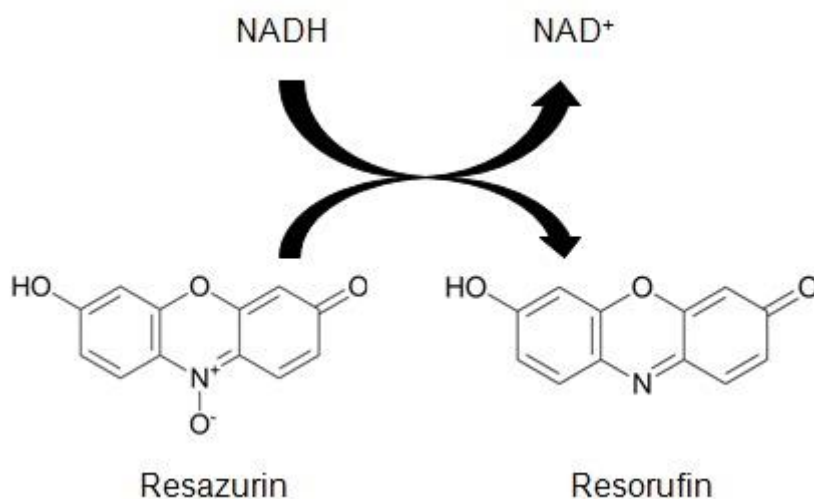


Figure 2.2. Diagram of the substrate resazurin and its reduced product resorufin. Figure obtained from (419).

Around 5,000 cells were seeded in Corning® 96 Well Black Polystyrene Microplate and grown overnight. The media was aspirated from two rows each time then, 100 µl of the media with treatment were added per well using triplicates. The same treatment

layout as the one described for MTT assay was used. Plates were incubated for 72 hours at 37°C 5%CO₂. A volume of 20µl of resazurin (0.15 mg/ml in PBS) was added per well and plates were incubated 2 hours at 37°C. Fluorescence was recorded using TECAN Spark reader using 560nm excitation / 590nm emission filter set. Data was analysed as described in the section 2.3.3.

2.3.3 Data analysis

Data obtained from the plate reader was saved as Excel files and analysis of the absorbance readings was also performed using Excel. First, the mean and the standard error of the mean (SEM) were calculated for each set of triplicates. The mean of three blank wells (medium but no cells) was subtracted from the mean for each treatment and the resulting data was divided by the control.

2.4 Cell cycle analysis by flow cytometry

The applications of flow cytometry are diverse, and for this study we used it to analyze cell proliferation to understand better the effects that the drugs had on the cell cycle and to identify if decrease in cell viability was caused by a cytostatic or a cytotoxic effect of the drugs. To do so, treated cells were pulsed with ethynyl deoxyuridine (EdU) and then, click chemistry reaction was used to detect the newly synthesized DNA containing EdU. Counterstaining with 7-aminoactinomycin D (7-AAD) was also used for detection of apoptotic cells, as described by Zembruski, 2012 (420).

We used the protocols of Suzanne B. Buck et al. (2008) and Darzynkiewicz et al. (2006) as a reference for the development of our protocol using RCC cell lines (421,422).

2.4.1 General principles of flow cytometry

Flow cytometry is a molecular biology technique that performs qualitative and quantitative measurements of several characteristics of single cells. Not only shape and size of the cells can be measured, but also the presence and concentration of biomolecules such as DNA, RNA, proteins, and other factors that work as indicators of certain cell functions, or biomarkers. The flow cytometer detects the scattered light and/or the fluorescent signals emitted by single cells suspended in a buffered-solution that passes through a laser beam at high speed. Then, it transforms that information into parameters associated with cellular structure and function (423).

2.4.2 General principles of Click-chemistry reaction

The term click chemistry encompasses a group of versatile and fast reactions that produce compounds that are easily purified at a high yield (424). The 1,3-dipolar cycloaddition between azides and alkynes catalysed by copper(I) salts complies with the mentioned characteristics and has become the representative click chemistry reaction (425). Apart from being an inexpensive reaction, the ability to incorporate azide and alkyne functional groups to a broad range of compounds permits the application of the Cu alkyne-azide cycloaddition (CuAAC) in many fields. Additionally, the harmless nature of the reagents involved in the reaction and the ability of the reaction to be carried out in aqueous environments pinpoints its use in biological systems (424,426).

The Huisgen 1,3-dipolar cycloaddition is a reaction of an organic azide and terminal alkyne that produces a basic aromatic heterocycle that was first described by Huisgen in 1960. In 2002, Sharpless and colleagues showed that in the presence of copper, the reaction is accelerated and produces the 1,4-isomer of triazole rather than the mix of 1,4 and 1,5-isomers (Figure 2.3) (427,428). Since then, the click chemistry reaction has gained much popularity.

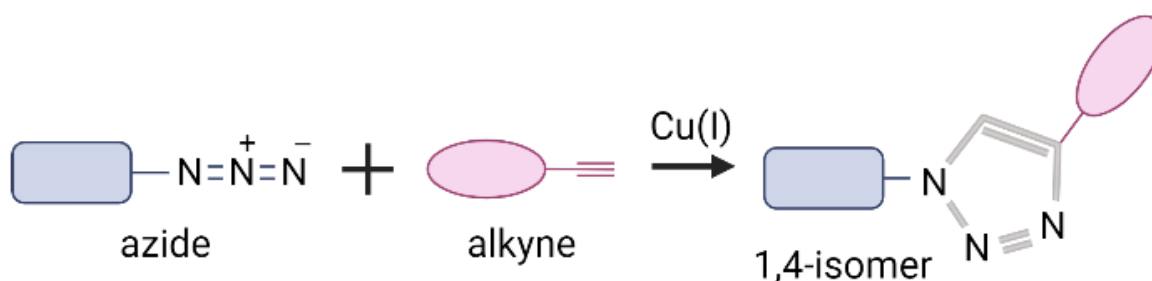


Figure 2.3. Representation of the Cu alkyne-azide cycloaddition reaction. Figure adapted from (425).

Click chemistry has been used to label DNA and RNA with fluorophores by conjugating alkyne-labelled oligonucleotides to fluorescently-tagged azides (429,430). The application of click reactions after the incorporation of 5-ethynyl-2'-deoxyuridine (5-EdU) and 5-ethynyluridine (5-EU) into newly synthesized DNA and RNA respectively, allows quantification of the biomolecules using flow cytometry and microscopy, among other molecular biology techniques (Figure 2.4).

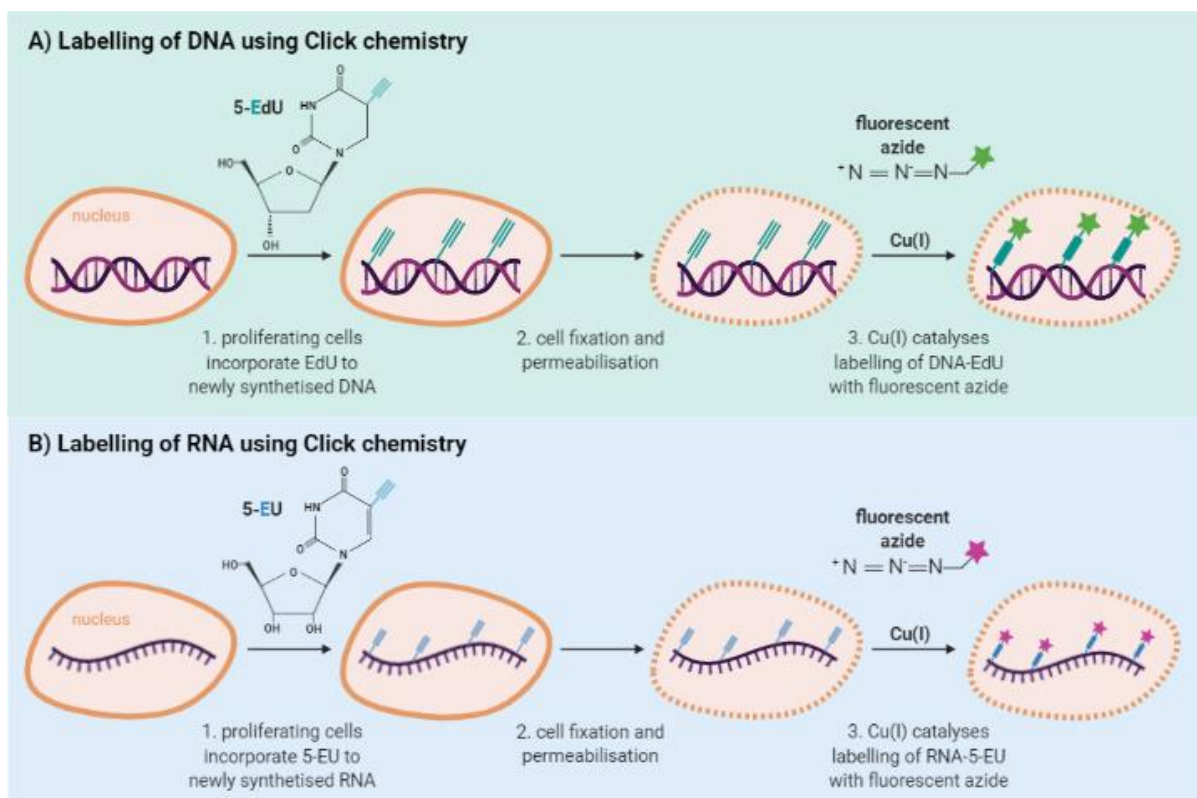


Figure 2.4. Labelling of nucleic acids using EdU and 5-EU incorporation followed by click chemistry reaction. A) The upper panel shows a diagram DNA labelling using Click-chemistry, where proliferating cells incorporate 5-EdU into newly synthesised DNA, and after fixation and permeabilization, a cyclo-addition reaction occurs between the 5-EdU and a fluorescent azide in presence of copper. B) The lower panel displays the process for labelling RNA using click chemistry, which requires incorporation of 5-EU to nascent RNA in proliferating cells, followed by fixation and permeabilization of the cells. This is followed by a cyclo-addition reaction between the 5-EU-labelled RNA and a fluorescent azide in the presence of copper.

2.4.3 Optimization of the DNA labelling with click chemistry reaction for detection of cell proliferation of RCC cell lines using flow cytometry

To determine the optimum incubation time for incorporation of EdU, three 30 mm TC-treated dishes were seeded with 3×10^5 cells each, which were incubated overnight at 37°C , $5\% \text{CO}_2$. Next morning, a dilution of EdU in DMEM was added to each well with a final concentration of $10 \mu\text{M}$. The dishes were incubated for 15, 30 and 60 minutes at 37°C , $5\% \text{CO}_2$. The culture medium was retrieved in 15 ml falcon tubes, and the adherent cells were trypsinised as described previously described. The cell suspension was transferred to the falcon tubes. Dishes were washed with PBS to retrieve remaining cells and the washing solution was transferred to the tubes as well. The tubes were centrifuged at 100 g for 7 minutes at 4°C and the pellet was washed twice with cold PBS. After the last washing, most of the PBS was removed and the pellet was resuspended as much as possible by flicking the tube with a finger.

Immediately, 5 ml of 70% ethanol kept at -20°C were added to the tube while vortexing at slow speed to fix the cells. The tubes were kept at -20°C overnight.

After at least 12 hours at -20°, the tubes were centrifuged at 200-300 g for 4 minutes and ethanol was discarded without disrupting the pellet. The pellet was washed once with 5 ml of TBS+0.05%Tween20 and the tube was vortexed to rinse the walls thoroughly. Cells were counted using a Neubauer chamber and 5×10^5 cells were transferred to a 1.5 ml Eppendorf tube. After centrifuging at 200-300 g, the pellet was resuspended in 500 µl of click-chemistry solution (final 10 µM 6-FAM azide) and incubated at room temperature protected from light for 30 minutes. The tubes were centrifuged and the pellet was washed with TBS+0.05%Tween20 twice. The pellet was resuspended in TBS+0.05% Tween20 with 10 µg/ml 7-AAD and 0.1 mg/ml RNaseA, and incubated at room temperature for 1 hour. The tubes were transferred to ice and taken to the flow cytometer. An Attune NxT flow cytometer was used and the parameters were set as shown in table 2.7.

Table 2.7. Flow cytometer set up information

Channel	Staining	Parameter	Voltage	Scale
BL-1	6-FAM	New DNA (EdU incorporation)	350	Logarithmic
BL-3	7-AAD	DNA	400	Linear

Samples were vortexed before being used. Sample input rates of 100 µL/minute and 200 µL/minute were used along sample volumes of 450 µl to avoid introduction of bubbles into the flow cytometer.

2.4.4 Assessment of the cell proliferation profiles obtained with the DNA labelling with click chemistry reaction protocol

Staurosporine, etoposide and an untreated control were used to assess the results obtained with the established protocol as the effect of these compounds on cell proliferation have been reported and could be taken as reference (431,432). As in section 2.4.3, three 30 mm TC-treated dishes were seeded with 3×10^5 cells each,

which were incubated overnight at 37°C, 5% CO₂. A staurosporine dilution of 1 μM and an etoposide dilution of 10 μM in culture medium were prepared. A 0.01% v/v DMSO dilution was used as a control. The medium was removed from the dishes and 10 ml of drug dilution or control was added. The cells were incubated at 37°C, 5% CO₂ for 24 hours. Pulsing with 10 mM final EdU was performed for an hour and the rest of the protocol was carried out as described in section 2.4.3.

2.4.5 DNA labelling with click chemistry reaction for detection of cell proliferation of RCC cell lines using flow cytometry

To be consistent with time of drug exposure used in the cell viability assay, RCC cells were treated with the compounds of interest for 72 hours. To prevent the effects of cell confluency from affecting assessment of the effects of the drugs on the cell cycle, low seeding density was used in 100 mm TC-treated dishes. After overnight incubation, medium was removed and drug dilutions (mTOR inhibitors, ActD or drug combinations diluted in culture medium) were added to the plates. After 72-hour exposure to the treatment at 37°C, 5% CO₂, cells were pulsed with EdU (final 10 mM) for 1 hour and the rest of the protocol was carried out as described in section 2.4.3 (Figure 2.5).

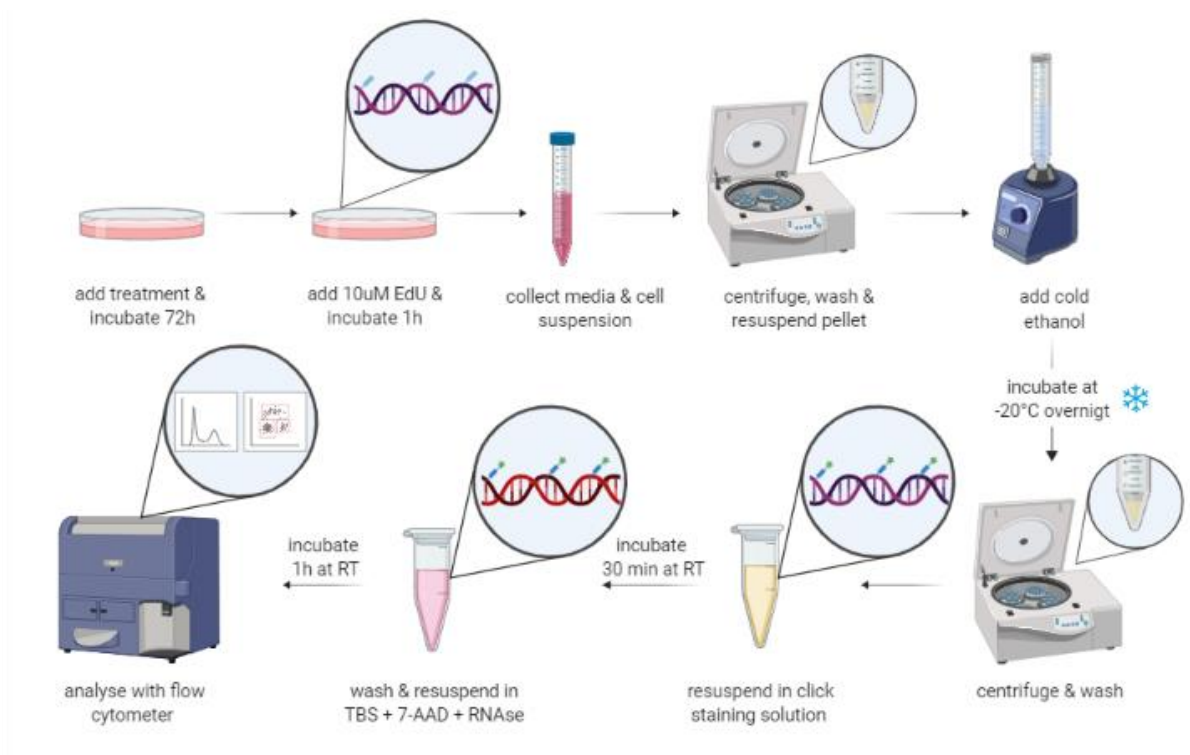


Figure 2.5. Diagram showing the main steps of the established protocol for detection of nascent DNA labelled with click chemistry using flow cytometry.

2.4.6 Analysis of the data obtained with the Attune NxT flow cytometer

Data obtained from the flow cytometer was saved as FCS files, which were analysed using the free software FCSalyzer by Dr. Sven Mostböck available at: <https://sourceforge.net/projects/fcsalyzer/>. Doublet exclusion was performed by plotting the height against the area for the scatter of BL-3 channel. A region that included only single cells was created and used as the total population for further analyses (Figure 2.6).

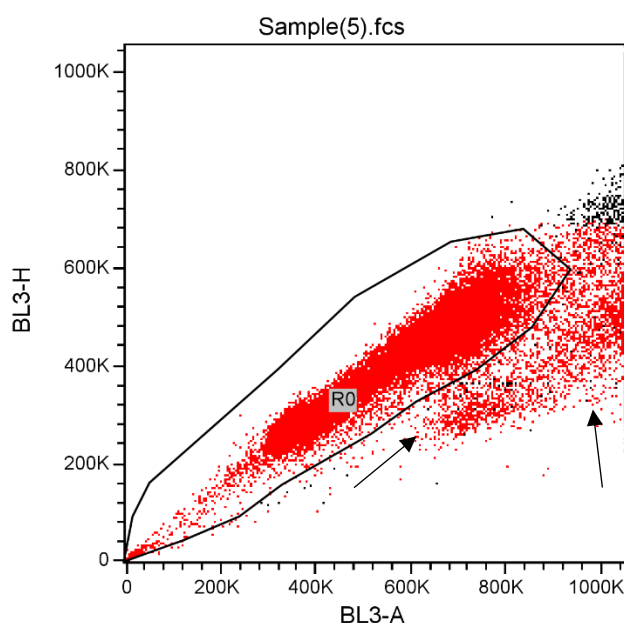


Figure 2.6. Dot plot showing how the region selection (R0) to exclude doublets from cell proliferation analysis was carried out. The selection of the region allows discriminating doublets indicated with the arrows.

The data from BL-3 and BL-1 were plotted as axes x and y, respectively, of density plots to identify cell populations in the different phases of cell cycle, including G1, S, G2, and also cell death. Populations were gated and percentage of the cells in the different phases of the cell cycle and cell death was calculated (Figure 2.7). Both the interest region (single cells) and the gates were created using the control of each experiment and then, applied to the different samples of the same experiment.

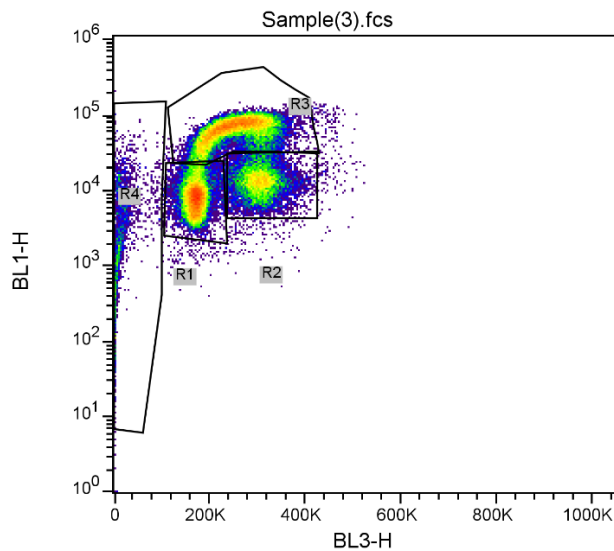


Figure 2.7. Density plot showing how the gates were created to calculate the percentage of single cells in the different phases of cell cycle. R1 is equivalent to G1 phase, R2 to G2, R3 to S and R4 to apoptosis.

Additionally, histograms using the data of BL-3 channel were created and the sub-populations gated in the density plots were overlaid on the histogram in order to assess appropriate identification of the sub-populations (Figure 2.8). The same colour code was used for all the histograms, where black represents the entire sample, green is G1, blue is G2, pink is S phase and red shows cell death. The calculations of the percentage of cells in the phases of cell cycle were compared to the estimated values obtained by histogram deconvolution, and the results were quite similar (appendix [section 7.3]).

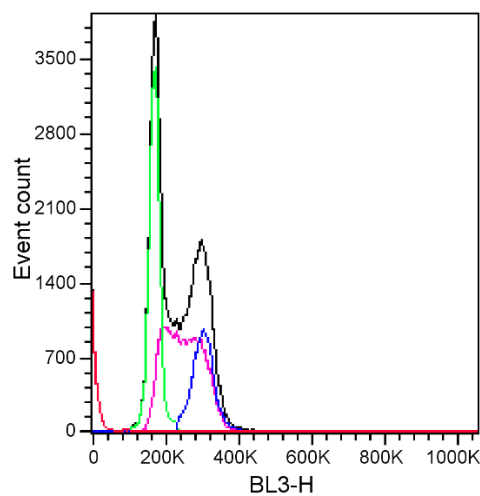


Figure 2.8. Histogram showing the overlays of the populations identified by 7-AAD and 6-FAM staining using flow cytometry. The entire sample is represented in black. The populations gated in

the density plot shown in Figure 2.4.6.2 are shown in green (G1), pink (S), blue (G2), and red (apoptotic cells).

For each experiment, a histogram that showed overlays of the different treatments against the control was used to compare the distribution of treated cells within the cell cycle (Figure 2.9). The colour code used for this type of histograms was: black as control, green as the lowest drug concentration used, blue as the IC50, and red as the highest drug concentration used.

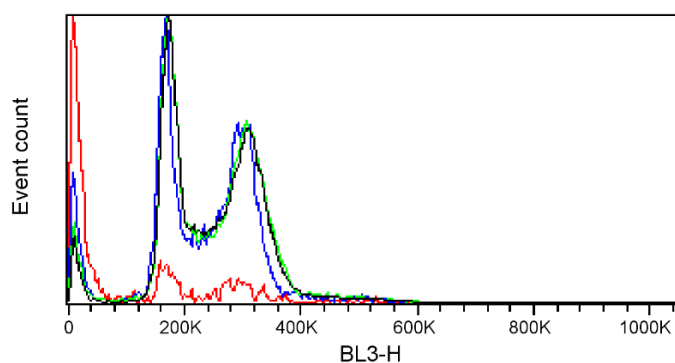


Figure 2.9. Histogram with overlays of the different drug concentrations used in a specific experiment to allow direct comparison among treatments. Each colour represents a sample treated with a different concentration of the same drug, allowing comparing the effects of different treatments on cell cycle. The colour code used for this type of histograms was black representing the control, green as the lowest drug concentration used, blue as the IC50, and red as the highest drug concentration used.

2.5 Analysis of rRNA synthesis

Different techniques used to measure newly synthesized RNA have been described. Autographic visualization of RNA labelled with radioactive nucleosides is a slow and hazardous technique that provides poor resolution visualization of the RNA (430). Immunostaining of RNA labelled with 5-bromouridine (BrU) or 5-bromouridine triphosphate (BrUTP) is limited by the access of the antibodies into the cells, and specifically into the nuclear envelope (433). Imaging of RNA labelled with fluorescently tagged UTP can be restricted by the size of the fluorophore as well (434). However, fluorescent labelling of 5-EU-tagged RNA by click chemistry allows easy, fast and sensitive detection of newly synthesized RNA with high resolution images (430,435).

In this study, assessment of the effect of the drugs of interest in the nucleolar function, was performed by labelling of nascent rRNA with 5-EU and detection using click

chemistry on fixed cells and visualized by microscopy using the assay described by Jao and Salic as reference (Figure 2.10). Image acquisition was performed using an automated microscope and Micromanager Software. CellProfiler Software was used for image analysis.

2.5.1 5-EU labelling of rRNA with click chemistry reaction for microscopy analysis

About 20,000 ACHN cells or 10,000 UoK111 cells were seeded per well in 96-well TC-treated plates for fluorescent applications (VWR #734-1609) and grown overnight. The medium was removed from two rows by two rows each time to prevent wells from drying, and 100 µl of the medium containing the drugs were added per well using triplicates. The plate layout previously described for MTT assay was used (Figure 2.1). After optimisation it was determined that plates were to be incubated for 2 hours at 37°C 5%CO₂ with the treatment.

Subsequently, 20 µl of medium containing 5-EU (0.5mM final) were added per well and plates were incubated 60 minutes at 37°C. Cells were washed with cold PBS pH 7.2 once and 200 µl of methanol at -20°C were carefully added to each well. The plate was stored at -20°C and the methanol was replaced with another 200 µl of cold methanol an hour later. The plates were stored overnight at -20°C. Then, methanol was aspirated carefully using a gel loading tip to avoid disrupting the cells and 200 µl of cold acetone were carefully added per well. After 10 minutes, acetone was removed, the cells were left to dry for 10 minutes and then washed with cold PBS.

A volume of 50 µl per well of TBS+0.5% Triton X-100 was used to permeabilise the cells. After 15-minute incubation at room temperature, cells were washed with TBS once. Washing solution was removed and 50 µl of Click reaction solution (100uM final Sulfo-Cy3 azide, see materials and reagents section) were added per well. The plate was incubated at room temperature for 30 minutes protected from light, as reaction is light sensitive. The cells were washed 4 times with filtered TBS+0.05% Tween-20. Finally, 100 µl of filtered imaging solution (see materials and reagents section) were added per well and the plate was ready to be imaged or stored at 4°C. An illustrated flow diagram of the entire 5-EU labelling of rRNA with click chemistry reaction protocol is shown in Figure 2.10.

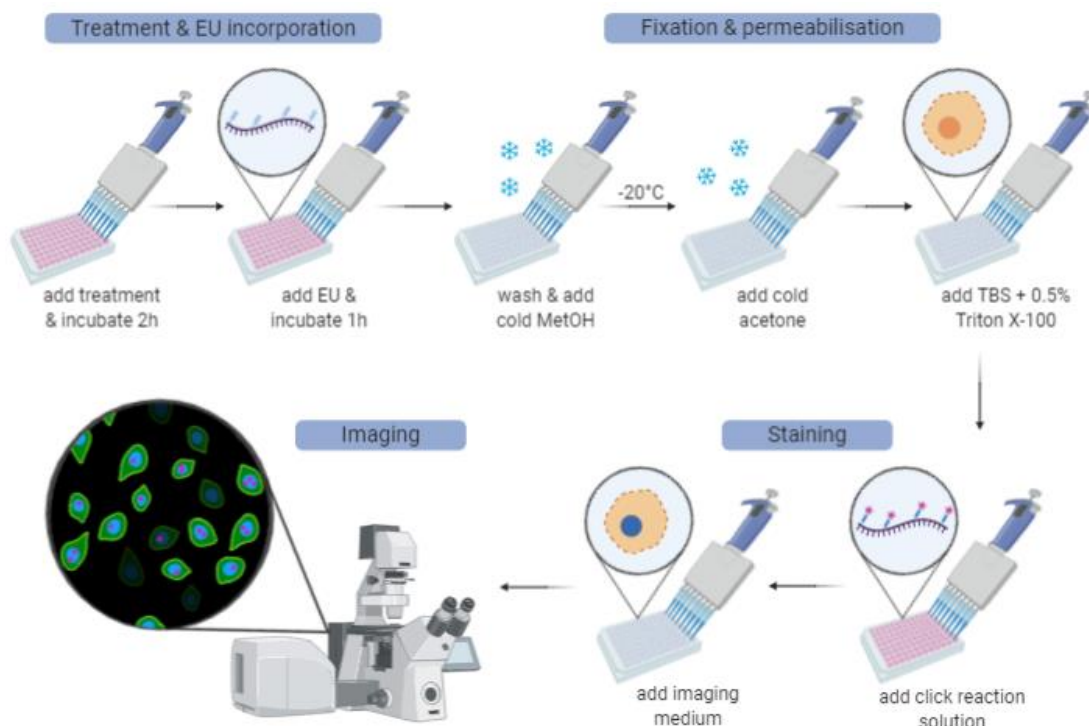


Figure 2.10. Methodology used to label RNA using click reaction and detection of resultant fluorescent nucleoli through microscopy.

2.5.2 Image acquisition using an automated microscope and Micromanager Software

Imaging was performed using a fully motorised Olympus IX-61 inverted microscope with a 40X Plan Apo 0.95NA objective and hardware autofocus (Olympus ZDC). The microscope was equipped with an Applied Scientific Instrumentation MS 2000 motorised stage and illumination was performed using a Sutter Lambda LS Xenon Arc light source and Sutter Lambda L-3 filter wheels with a Chroma 89000 - ET - Sedat Quad filter set in Sedat configuration. The camera was a Hamamatsu Orca Flash 4.0LT PLUS and images were acquired using MicroManager 1.4 (Edelstein et al., 2014) in a PC running Windows 10.

Imaging comprised the following steps:

- 1) The 96-well plate was placed on the microscope stage.
- 2) Cells were located manually and focused optimally and the autofocus offset was determined using the MicroManager Autofocus ZDC driver.
- 3) Camera exposure for the DAPI and Cy3 channels was optimised by observing the brightest labelled sample (usually an untreated well).

- 4) The centre of well A1 was located, and the MicroManager plugin “HCS Site Generator” was run in order to generate the scanning pattern over the 96-well plate. Depending on the cell density achieved, the imaging pattern of each well was set to 3x3, 4x4 or 5x5 frames, in order to achieve a target of approximately 200-300 cell nuclei per well.
- 5) Image acquisition was performed.

2.5.3 Image analysis using CellProfiler Software

Images were analysed using CellProfiler v.2.2.1 (436) running a purpose-written analysis pipeline (see Figure 2.11). Metadata was introduced via a comma-separated value (CSV) file that matched the well codes (A1-H12) with the experiment metadata (cell line, drug, concentration).

First, a pipeline was executed over all the blank fields (no cells – labelled Blank in the metadata CSV file) in order generate and average and smoothed image for each fluorescence channel that would quantitate the background (stray) light over the whole image field. A second pipeline was occasionally run over all images in order to generate an illumination reference image (generated and used with the CellProfiler modules `CorrectIlluminationCalculate` and `CorrectIlluminationApply`, respectively). However, this illumination image was, as expected, reproduced well enough across acquisitions so we decided that it was not necessary to generate a new one after each acquisition.

The pipeline first corrected the illumination of the DAPI and Cy3 images, then segmented the DAPI images in order to create nuclear masks, then segmented the Cy3 within each nuclear mask in order to create masks for nucleolar regions. Cy3 fluorescence (AU) was quantitated within each cell nucleus, both inside the nucleolar masks (nucleolar fluorescence) and outside (nucleoplasmic background).

The quantification data (nucleolar and nucleoplasmic fluorescence) together with the metadata were exported to SQLite databases. These databases were accessed with an in-house written ImageJ (Rasband, 1997-2018) plugin in order to inspect visually the accuracy of the image segmentation. Next, data (mean +/- SEM) was extracted and exported to a CSV file by running queries in SQLite Studio 3.2.1(438).

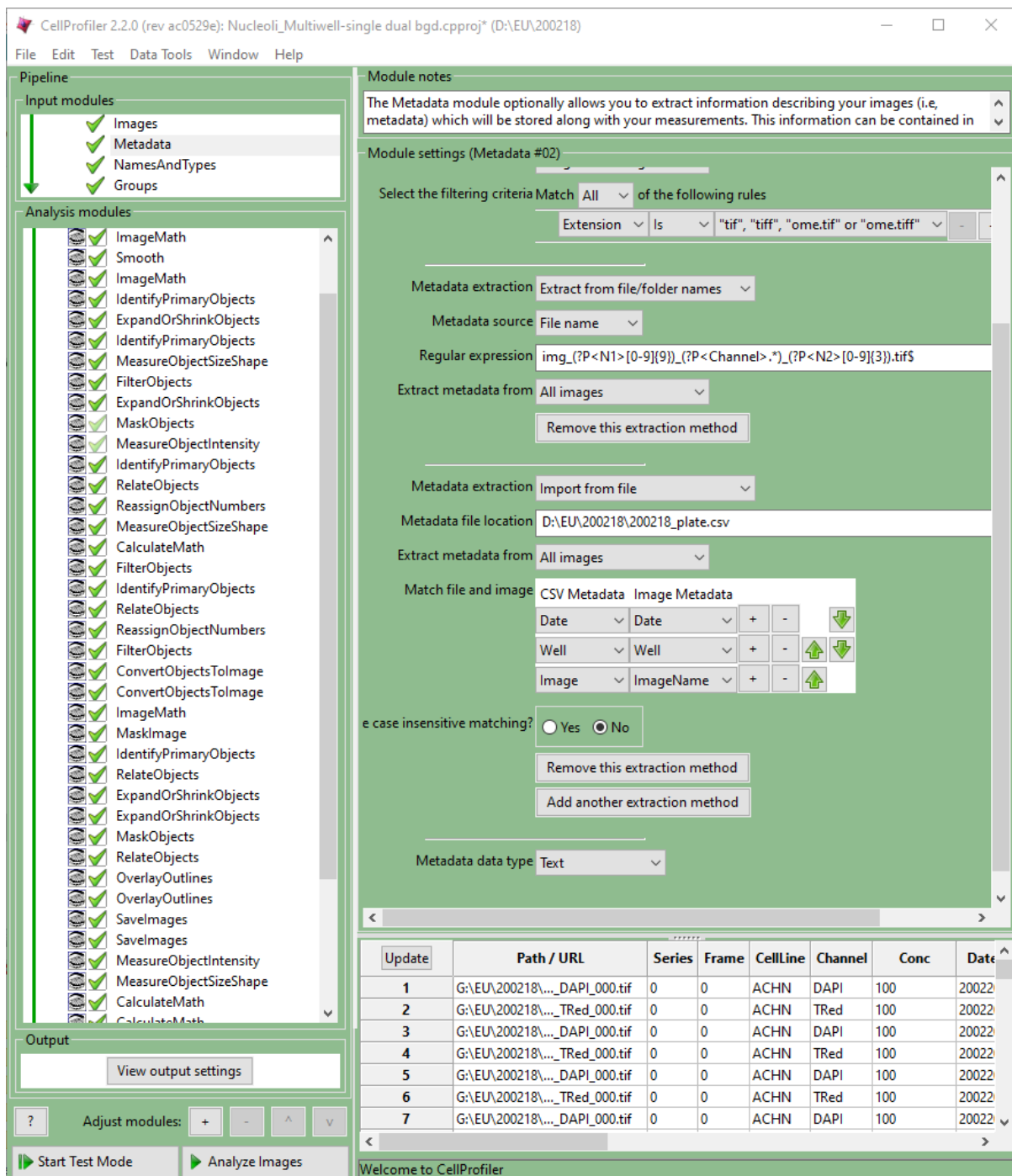


Figure 2.11. View of an analysis pipeline in CellProfiler (showing the metadata extraction section).

See appendix 6.2 for a further description of the processes and management of the data involved in the analysis of 5-ethynyl uridine-labelled nucleolar images.

2.6 siRNA transfection

Antibody validation is crucial to ensure research reproducibility. This is even more relevant in the case of unverified antibodies. Knockdown using siRNA is among the

protocols used to confirm specificity of an antibody (439). The technique relies in decreased expression of the protein of interest in siRNA-treated cells, which can be visualised by Western Blot. For this study, we used siRNA transfection to knockdown the transcription factor TIF-IA in order to validate the antibodies against Rrn3 (D-9) (sc-390464) and phospho-TIF-IA (pSer649) (SAB4504731).

2.6.1 General principles of siRNA transfection

Transfection of cells with siRNA is used to silence expression of a specific gene of interest. This method requires the introduction of dsRNA into the cells, which is then processed by the ribonuclease Dicer into 21-23 base-pair small interfering RNA (siRNA). The resulting siRNAs are then incorporated into the RNA-induced silencing complex (RISC). Once part of the complex, the siRNA is used as a template to target specific mRNA and enable its destruction by RISC (440,441).

2.6.2 *RRN3* siRNA transfection

Enough cells to have 60-80% confluence by the time of the experiment were seeded in 100 mm dishes and then incubated overnight at 37°C 5%CO₂. A dilution of 25 uM final siRNA in 1 ml OptiMEM, and a dilution of 22.5 µl Lipofectamine2000 in 1 ml OptiMEM were prepared for each dish. The siRNA and the Lipofectamine2000 dilutions were incubated separately at room temperature for 5 minutes. The 1 ml of Lipofectamine2000 dilution was transferred to the siRNA dilution and then, mixed thoroughly by pipetting up and down. The mix was incubated at room temperature for 20 minutes. In the meantime, the growth medium was removed from the dishes, they were washed with PBS, and 8 ml of OptiMEM were added per dish. After the 20 minutes incubation, the 2 ml of siRNA-Lipofectamine2000 mix was added to each dish. Following a 6-hour incubation at 37°C 5%CO₂, the transfection medium was removed and replaced with complete culture medium. After 24/48 hour incubation, gene knockdown was assessed by Western Blot. Figure 2.12 shows an illustrated flow diagram of the protocol.

siRNA transfection

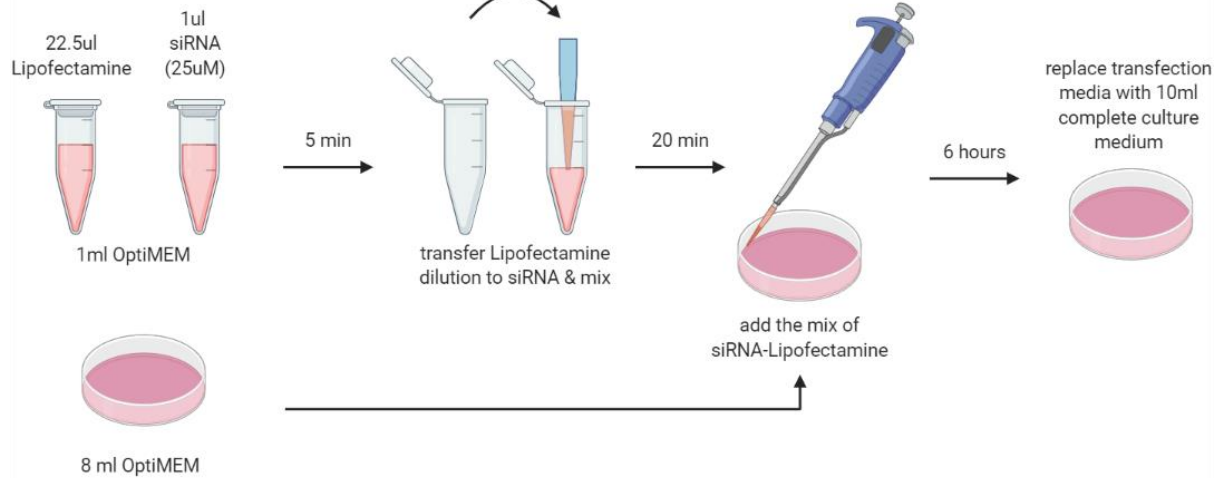


Figure 2.12. Methodology used for transfection of RCC with siRNA.

2.7 Western Blot

Western blotting is a commonly used molecular biology technique that was first described in 1979 by Renart and colleagues (442), although the technique used nowadays is more similar to the ones published by Harry Towbin and colleagues later that year (443) and Burnette and colleagues in 1981 (444). It is used to separate the proteins of a complex sample by their molecular weight and then transferring them into a membranous support for identification and relative-quantitation.

2.7.1 General principles of Western Blotting

The technique involves a series of processes with multiple variables and reagents that can be modified in order to optimise the method according to the proteins of interest of a particular assay. In broad terms, the Western Blotting consists mainly of five parts that involve preparation of the sample, fractionation of the proteins by polyacrylamide gel electrophoresis (PAGE), transfer of the proteins from the gel to the membrane, identification of the protein of interest using antibodies, and last, imaging and analysis of data.

Polyacrylamide gel electrophoresis is used to separate the proteins of a complex sample. The polyacrylamide gel serves as the matrix through which the proteins of a sample migrate in response to an electrical field. The migration rate of the proteins depends on their size, charge and shape. The percentage of acrylamide in the gel

determines the size of the pores, which decreases as acrylamide percentage increases.

The proteins are then transferred to a membrane and the membrane is exposed to a specific antibody to identify the proteins of interest. Detection of the presence and concentration of the desired protein requires the use of an anti-immunoglobulin antibody labelled with fluorophores or enzymes such as horseradish peroxidase that upon exposure to a chemiluminescent substrate can be detected by digital imaging devices.

2.7.2 Protein extraction and preparation of the sample

The first step in the Western Blot is to prepare the sample of proteins that needs to be analysed. Lysates were prepared from cell cultures treated with the drugs of interest. First, cells were seeded in 100 mm dishes and grown overnight. After treatment administration followed by two-hour incubation, the plates were placed on ice to prevent enzymatic activity, the medium was removed, and cells were washed once with cold PBS. Washing solution was removed and cold PBS was added. Cells were scrapped and the cell suspension transferred to tubes. An additional volume of cold PBS was used to retrieve the remaining cells on the dishes. Cells were centrifuged at 1000rpm, 4°C for 5 minutes. Pellet was resuspended in lysis buffer. Lysates were sonicated for 10 seconds to achieve an efficient extraction, homogenisation of the sample and to reduce viscosity by shredding the DNA. The samples were then stored at -20°C or -80°C for long-term storage.

2.7.3 DC Protein assay for protein quantification

Before samples were prepared for Western Blot, protein quantification of the cell lysates was performed to ensure 20 µg of protein were loaded of each sample. The Bio-Rad DC Protein Assay kit was used for protein quantification in 96-well plates as per manufacturer instructions. BSA dilutions in a concentration range from 0.25 µg/µto 2.0µg/µl were used for the standard curve. 5µl of lysate were added per well, using duplicates. Then, 25 µl of Reagent A were added per well, followed by 200µl of Reagent B per well. After 15 minutes of incubation at room temperature, absorbance was read at 750 nm using SpectraMax Plus 384 Microplate Reader. The standard curve and calculation of protein concentration was done using the SoftMax Pro Software.

2.7.4 Polyacrylamide gel electrophoresis

Acrylamide gels (10% and 12.5%) were casted according to the protocol of Laemmli, using an A-Bis ratio of 30:0.8 (445). For low molecular weight proteins such as 4E-BP1, 4–15% precast protein gels were used. Lysates were diluted in lysis buffer to get 20µl samples with a protein concentration of 1µg/µl. A volume of 4µl of 6X loading buffer were added per sample, then vortexed, boiled at 95°C for 5 minutes and centrifuged for 30 seconds. The 24µl per sample were loaded into the gels and electrophoresis was run at 120V for 15 minutes and 150V for 1 hour and 15 minutes.

2.7.5 Transfer of proteins to a membrane

The proteins were then transferred to 0.45µm nitrocellulose membranes (Thermo Fisher Cat 88018) using BioRad TransBlot® Turbo™ system at 2.5A, 25V for 13 minutes. The membranes were retrieved, rinsed with distilled water, and stained with 0.1% Ponceau S solution. They were carefully marked with pencil to be cut later and blocked for an hour at room temperature. Since antibodies against both, phosphorylated and total proteins were used, two different sets of blocking solutions and buffers were utilised depending on the antibody. When using an antibody against a phosphorylated protein, EveryBlot blocking buffer and TBST buffer were used. Alternatively, when using an antibody against a total protein, 5% non-fat dry milk in PBS and PBST buffer were used.

2.7.6 Protein detection

After blocking, the membranes were then cut and incubated with primary antibodies overnight at 4°C. The membranes were washed with TBST/PBST 3 times for 15 minutes and incubated with secondary antibodies (fluorescent-tagged for housekeeping protein and HRP-conjugated for the proteins of interest) for an hour at room temperature. The membranes were washed with TBST/PBST 3 times for 5 minutes and soaked in chemiluminescent reagent for 5 minutes.

2.7.7 Imaging and densitometry analysis

The blots were imaged using the ChemiDoc MP imaging system using chemiluminescent channel to detect the protein of interest and the Alexa790 fluorescent filter set to detect the loading control protein and the molecular weight ladder. The densitometry analysis of the resulting images was performed with the

Image Lab (Bio-Rad v 6.1) software to determine the concentration of the proteins of interest by quantifying the signal intensity of the bands. Molecular weight was determined using the molecular weight tool available in Image Lab software.

The lane and band tools were used since multiple bands were detected for some of the proteins of interest. Definition of the lanes was done manually by overlaying the lane frames on the blot lanes. The bands were detected using the automatic settings and adjusted manually when needed. For background subtraction the rolling disc method was used. The standard disc size used was 70.7 mm to ensure consistent background subtraction between lanes across experiments. Nevertheless, when background was very high, a smaller disc size was used. Quantification of the signal of the proteins was also performed using ImageJ to verify reliability of the automated and manual setting of the Image Lab software and the results were similar.

The band signal, called adjusted volume (Adj. Volume (Int)) by the Image Lab software, was calculated for each protein we could be pan or phospho-protein of interest or a reference house-keeping protein (HKP), which would be either β -actin or vinculin, depending of the MW required for the loading marker. Next, the band signal of the proteins of interest both native proteins and phosphorylated proteins, was normalised using HKP. The normalised signal of phosphorylated proteins was further normalised against the signal of the corresponding total proteins in order to ensure that the calculated value reflected the fraction of phosphorylated protein rather than its absolute abundance. (see section 2.8.1).

First, HKP normalisation was done by identifying the lane with the highest signal for the HKP band, and dividing the HKP signal for each lane by the HKP signal from the lane with the HKP signal to obtain the lane normalisation factor.

$$\text{Lane Normalization Factor} = \frac{\text{HKP Signal for Each Lane}}{\text{HKP Signal from Lane with Highest HKP Signal}}$$

Then, the Normalized Target Signal for each target band was calculated by dividing the target band signal (either native or phospho-protein) by the lane normalisation factor.

$$\text{Normalised signal} = \frac{\text{target band signal}}{\text{lane normalisation factor}}$$

To calculate the effect of the drugs on the phosphorylation of the target proteins, we normalised the signal of phospho-proteins to that of the native proteins, using the HKP-normalised values. As before, the lane normalisation factor for each lane was calculated by identifying the lane with the highest signal for native protein and dividing the native protein signal for each lane by the highest native protein signal. We followed by dividing the phospho-protein signal for each lane by the lane normalisation factor to calculate the normalised phospho-target signal.

2.8 Statistical analysis

The following section describes the different statistical tests applied to the data obtained from the various experiments performed along this research in order to be able to determine the significance of our results.

2.8.1 Dose-response curves analysis

Curve fitting: Dose response data were fitted to the Hill equation, since it is the best semi-empirical dose-response model (see for example Goutelle et al (2008) (446). Calculations were performed using software written in-house in Java v7 using the commons-math3-3.6.1 mathematics library and the statistics for the fitted parameters were calculated from the asymptotic errors produced by the non-linear least square method. Outputs (fitted parameters and their errors) were validated against the same calculations performed with SigmaPlot v13.

Drug combination analyses: The different applicability of Loewe isobolograms and Bliss score is discussed in the relevant results sections (3.2.3). Homodynamic isobolograms (447,448) were fitted from the Hill parameters for single drugs plus the measurements of responses from drug combination, and the combination indices calculated. Error calculation for the estimation of statistical significance was performed using the error propagation equation given by Tallarida (448); however, since this method is asymptotic (delta method) we found that on occasions parameters would have unrealistic errors (e.g. negative or symmetric), therefore we confirmed our statistical analysis using Monte Carlo simulation. For Monte Carlo simulation we took advantage of the fact that replicates at each concentration were generally normally distributed (Shapiro-Wilke). This was particularly useful for the case of 5-EU

incorporation dose-response analyses where single cell microscopy data were analysed using a nested design (449,450) and see Appendix).

In the cases where Bliss score was applicable (cytotoxicity, as in Section 3.2.5) this analysis was performed as described by Geary (2013) and Demidenko and Miller (2019) (447,451).

Statistical analyses. To calculate 95% confidence intervals, errors for fitted parameters (IC50, combination indices, maximum effect, etc.) were assumed to have normal distribution (by Central Limit Theorem). Given the limitations mentioned above on the errors of some fitted parameters, these calculations were validated by Monte Carlo analysis. For statistical comparisons of parameters t-test was used where applicable. Similarly, for the above reasons, statistical differences were confirmed by Monte Carlo analysis.

2.8.2 Characterisation of nucleolar changes

The quantification and analysis of images of 5-EU incorporation is described in section 2.5.3. In addition, we ran further an analyses to characterise the nucleolar changes accompanying the different drug treatments. The data of 20 randomly selected nuclei that included 5-EU incorporation vs drug concentration, nucleolar area vs drug concentration, and 5-EU incorporation per unit area vs drug concentration was exported as CSV files. Data for 5-EU incorporation vs drug concentration and 5-EU incorporation per unit area vs drug concentration was standardised against DMSO-treated controls. Dot plots with the data from single cells were created using Excel for 5-EU incorporation vs drug concentration, nucleolar area vs drug concentration, and 5-EU incorporation per unit area vs drug concentration and are found in annex 7.5.

2.8.3 Flow cytometry data analysis

Flow cytometry data pooled from various independent experiments and analysed for proportions of sub-G₁ and S-phase cells, which were the phases relevant to these studies. From the total population gated for doublets (see Section 2.4.6) the sub-G₁ fraction was identified and quantitated, then, from the remaining interphase cells the proportion of S-phase cells was determined. These proportions were determined for drug concentrations that corresponded to the low and high plateaus of the cell viability dose-response curves and to the region of maximum slope (IC50) in the cases of drugs

that induced a clear Hill-type sigmoidal response (ActD and Torin 1 see section 3.1.4, and the high and low doses tested for drugs that did not induce a Hill-type response (allosteric mTOR inhibitors). However, the statistical distributions of percentages or proportions are not symmetrical and normal, thus precluding the standard ANOVA approach. In order to solve this, we “normalised” the proportions using a logit transform. Additionally, we used the Kruskal-Wallis test which is non-parametric. Multifactorial analysis was performed by ANOVA with *post-hoc* Bonferroni correction. The existence of any correlation between drug dose and proportion of cell cycle phase was determined by using Spearman’s rank test. All calculations were performed in Excel, with the aid of the Real Statistics Resource Pack (<https://real-statistics.com/free-download/real-statistics-resource-pack/>).

3. Results

As stated in the section 1.5, the main purpose of the present research is to investigate if tumour cells can be sensitised to chemotherapy directed against the nucleolus by using targeted therapies against selected metabolic pathways that modulate the nucleolar function, in this case, the mTOR pathway. Accordingly, we assessed a group of mTOR inhibitors to determine if this type of targeted therapy constituted a suitable model to modulate nucleolar function and test the hypothesis, and the results are presented in section 3.1. Having studied the effects of mTOR inhibitors on the nucleolar function and identifying potential candidates to be used in combination with NFIs, in section 3.2 we present the investigation of the effects of combination of selected mTOR inhibitors with ActD on nucleolar function and cell viability to prove the working hypothesis.

3.1 Investigating the effects of mTOR inhibitors on RCC cells

The mTOR pathway is a key regulator of cell growth and proliferation that is frequently over-activated in cancer cells (452), and for which targeted cancer therapeutics have been developed (79,453). Interestingly, the mTOR pathway modulates nucleolar function through the activation of the transcription factor TIF-IA, which along with mTOR that has been shown to be inhibited in cells treated with Rapamycin (186). Given the different types of mTOR inhibitors and the variability of the effects observed *in vitro* across cell lines with these drugs, the aim of this chapter is to examine the effects of allosteric and ATP-competitive inhibitors on mTOR in two RCC cell lines and to determine if these drugs can modulate the nucleolar function. First, we examined the inhibitory effect of these drugs on the activity of mTOR through the inhibition of the phosphorylation of mTORC1 substrates S6K and 4EBP1. Then, we set up an assay that would enable us to label and quantify nascent rRNA to evaluate the effects of mTORis on the nucleolar function. We followed to assess the effect of these drugs on cell viability and investigated whether the mTOR inhibitors display cytotoxic or cytostatic effect.

3.1.1 Effect of mTOR inhibitors on the phosphorylation of mTORC1 substrates S6K and 4EBP1

As discussed in section 1.4.3, the mTOR pathway is a signalling pathway frequently over-activated in cancer cells for which cancer therapeutics exist and are used to treat

different types of cancer, including RCC. In this section, we aim to assess the inhibitory effect of different mTOR inhibitors on the activity of mTOR, through the analysis of the phosphorylation of mTORC1 substrates S6K and 4EBP, the best known and most widely used markers of mTOR activity, to confirm that the inhibitors were active in our system and to estimate the range of concentrations at which they were active.

For this purpose, ACHN and UoK111 cells were treated for 2 hours with Rapamycin, Temsirolimus, Everolimus and Torin 1, harvested and lysed as described in section 2.7.2. Subsequently, Western Blot analyses were performed on cell lysates as described in sections 2.7.4 to 2.7.7, using the applicable antibodies for detection of total and phosphorylated S6K as listed in table 2.3. The resulting Western Blots are displayed in Figures 3.1 and 3.3, and the respective densitometry analyses are presented in Figures 3.2 and 3.4. Table 3.1 presents the IC₅₀ of the mTOR inhibitors for inhibition of the phosphorylation of S6K at Thr389, site phosphorylated by mTORC1.

In Figure 3.1, the labelling for total S6K kinase of ACHN cells treated with Rapamycin, Temsirolimus, Everolimus and Torin 1 displays a double band in untreated controls and that the upper (lower mobility) band disappears as the drug concentration increases. This is consistent with the disappearance of a phosphorylated form of the protein, as lower mobility forms can often be observed in phosphorylated proteins due to large conformational changes (454). The first panel in Figure 3.1 shows that phosphorylation of S6K at Thr389 is completely inhibited in ACHN cells treated with Rapamycin concentrations as low as 1 nM. Densitometry analysis of the Western Blot presented in Figure 3.2 A) produces an estimate of 0.22 nM for the IC₅₀. Increased phosphorylation of S6K in ACHN cells treated with 10 nM Rapamycin displayed in Figure 3.2 A) appears to be an artefactual result due background noise observed in Figure 3.1. In the second panel on Figure 3.1, we can observe that in ACHN cells treated with Temsirolimus, phosphorylation of S6K at Thr389 decreases in a concentration-dependent manner, achieving complete inhibition at 10 nM. The densitometry analysis shown in Figure 3.2 B) confirms inhibition of S6K phosphorylation in ACHN cells treated with Temsirolimus at low nanomolar concentrations, with IC₅₀ of 0.83 nM. ACHN treated with Everolimus, show reduced phosphorylation of S6K at Thr389 with concentrations as low as 0.2 nM compared to control, according to the third panel in Figure 3.1. The densitometry analysis displayed in Figure 3.2 C) confirms inhibition of S6K phosphorylation in ACHN cells treated with

Everolimus with an IC₅₀ of 0.22 nM. The last panel on Figure 3.1 shows inhibition of the phosphorylation of S6K at Thr389 in ACHN cells treated with increasing concentrations of Torin 1, achieving the maximal inhibition at concentrations as low as 10 nM. Accordingly, the densitometry analysis presented in Figure 3.2 D) corroborates inhibition of the phosphorylation of S6K at Thr389 mediated by increasing concentrations of Torin 1, with an IC₅₀ of 0.03 nM.

In UoK111 treated with Rapamycin, phosphorylation of S6K at 389 is inhibited with concentrations as low as 0.2 nM, as shown in the top panel in Figure 3.3. The densitometry analysis of this Western Blot displayed in Figure 3.4 A), confirms abrogation of the phosphorylation of S6K with an IC₅₀ of 0.14 nM. Treatment with increasing concentrations of Temsirolimus also inhibit phosphorylation of S6K at Thr389 in UoK111 cells, as shown both by diminished signal of the phospho-S6K antibody in Figure 3.3 and the densitometry analysis in Figure 3.4 B). The IC₅₀ of Temsirolimus for inhibition of phosphorylation of S6K at Thr389 in Uok111 cells is 0.01 nM. The third panel on Figure 3.3 shows a maximum inhibition of the phosphorylation of S6K in UoK111 treated with 1 nM Everolimus. Additionally, the double band of S6K is only observed in the control and UoK111 cells treated with 0.02 and 0.2 nM Everolimus. The densitometry analysis for signal of the phospho-S6K antibody in UoK111 cells treated with Everolimus presented in Figure 3.4 C) confirms inhibition of the phosphorylation of S6K, even at low concentration (0.2 nM), with an IC₅₀ of 0.1 nM. The last panel on Figure 3.3 shows a concentration-dependent inhibition of S6K phosphorylation in UoK111 cells treated with Torin 1 that is further illustrated by the reduction of the signal of phospho-S6K antibody from the densitometry analysis shown in Figure 3.4 D). The IC₅₀ of Torin 1 for inhibition of phosphorylation of S6K at Thr389 in Uok111 cells is 0.27 nM.

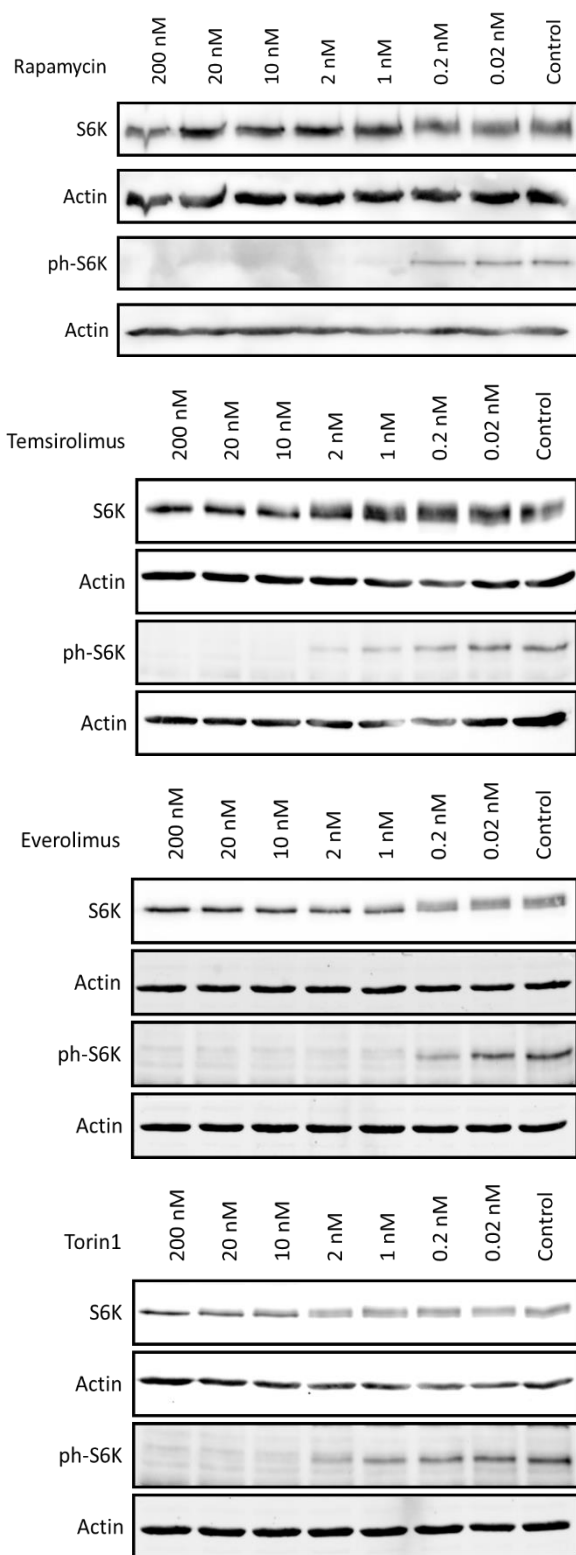


Figure 3.1. Western Blot analyses of relative levels of S6K and the phosphorylated form of S6K in threonine 389 (ph-S6K) in ACHN cells. ACHN cells were treated with allosteric and ATP-competitive mTOR inhibitors for two hours, and subsequently harvested and lysed as described in section 2.7. A total of 20 μ g of protein from lysates obtained from cells treated with different concentration of the respective mTOR inhibitor were analysed in each lane with the antibodies listed in section 2.1.4. Actin was used as loading control. Clear patterns for inhibition of the phosphorylation of S6K at threonine 389 are observed for the four mTOR inhibitors tested.

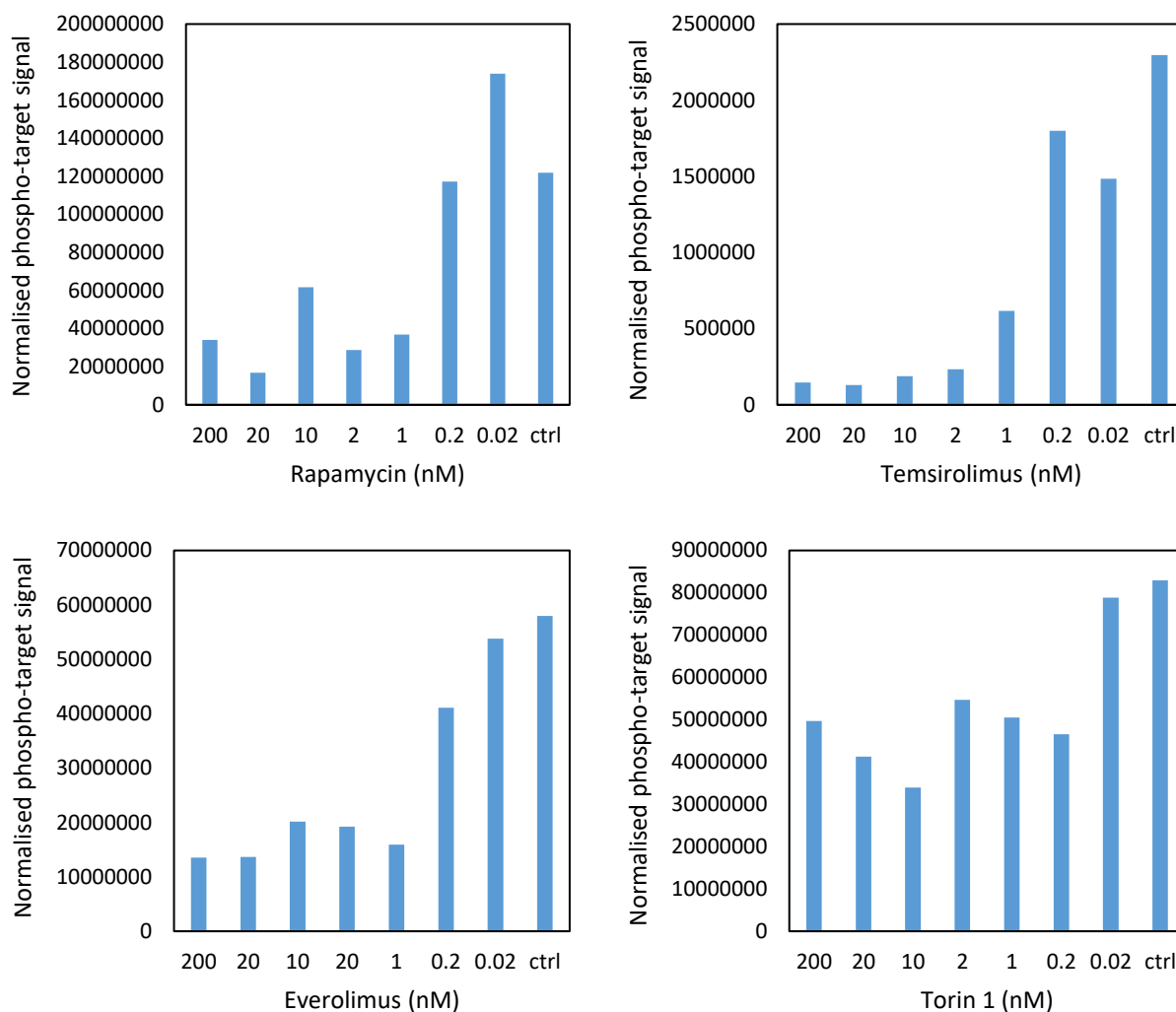


Figure 3.2. Densitometry analysis of Western Blots probing for the phosphorylated form of S6K at threonine 389 using lysates obtained from ACHN treated with different concentrations of A) Rapamycin, B) Temozolomide, C) Everolimus and D) Torin 1. Densitometry analysis demonstrated that the mTOR inhibitors tested, Rapamycin, Temozolomide, Everolimus and Torin 1, inhibit the phosphorylation of S6K at threonine 389 at low nanomolar concentrations. Pan and phospho-protein signals were first normalised using house keeping protein β -actin. The normalised phospho-protein signal was then divided by the normalised pan-protein signal (see detailed method in section 2.7.7). Densitometry analysis was performed on a single set of blots.

As observed in table 3.1, the IC₅₀ of all the mTOR inhibitors tested for inhibition of S6K phosphorylation at S389 were in a similar range and below 1 nM. Together, these results demonstrated that both allosteric and ATP-competitive mTOR inhibitors abrogate the phosphorylation of S6K in threonine 389 at low nanomolar concentrations, indicating that these drugs effectively inhibit the activity of mTORC1 in ACHN and UoK111 cells.

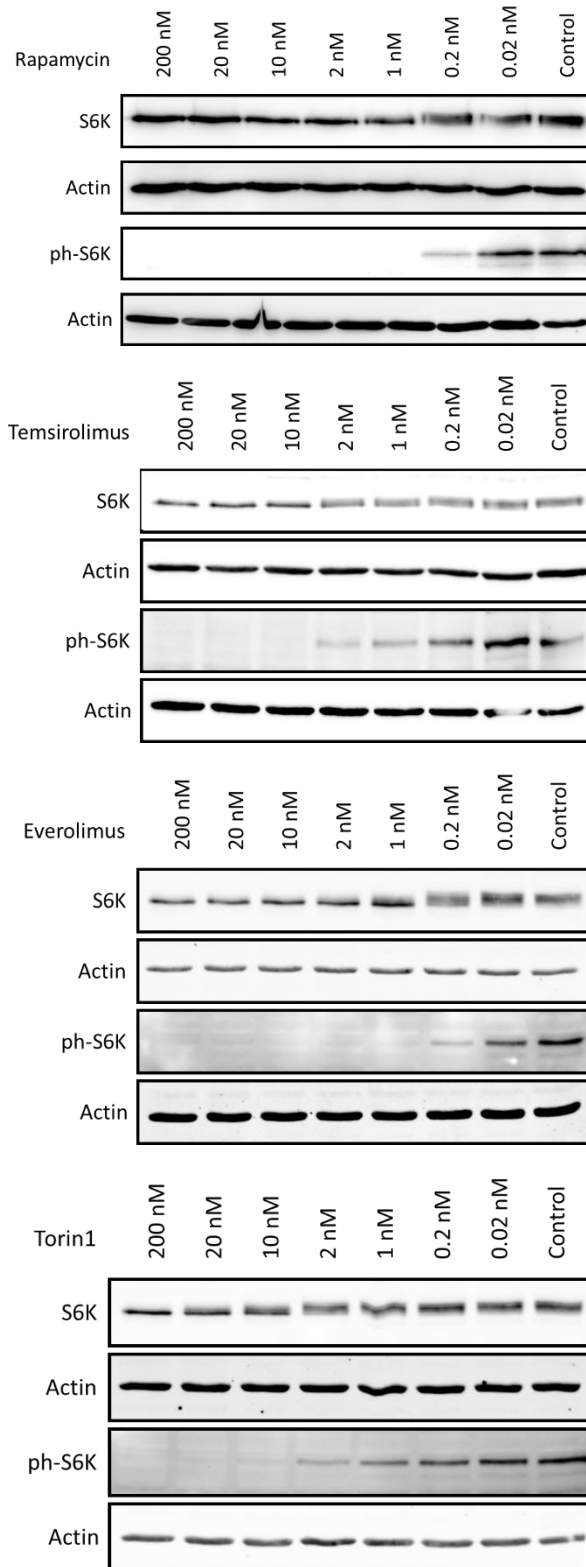


Figure 3.3. Western Blot analyses of relative levels of S6K and the phosphorylated form of S6K in threonine 389 (ph-S6K) in UoK111 cells. UoK111 cells were treated with allosteric and ATP-competitive mTOR inhibitors for two hours, and subsequently harvested and lysed as described in section 2.7. A total of 20 μ g of protein from lysates obtained from cells treated with different concentration of the respective mTOR inhibitor were analysed in each lane with the antibodies listed in section 2.1.4. Actin was used as loading control. Clear patterns for inhibition of the phosphorylation of S6K at threonine 389 are observed for the four mTOR inhibitors tested.

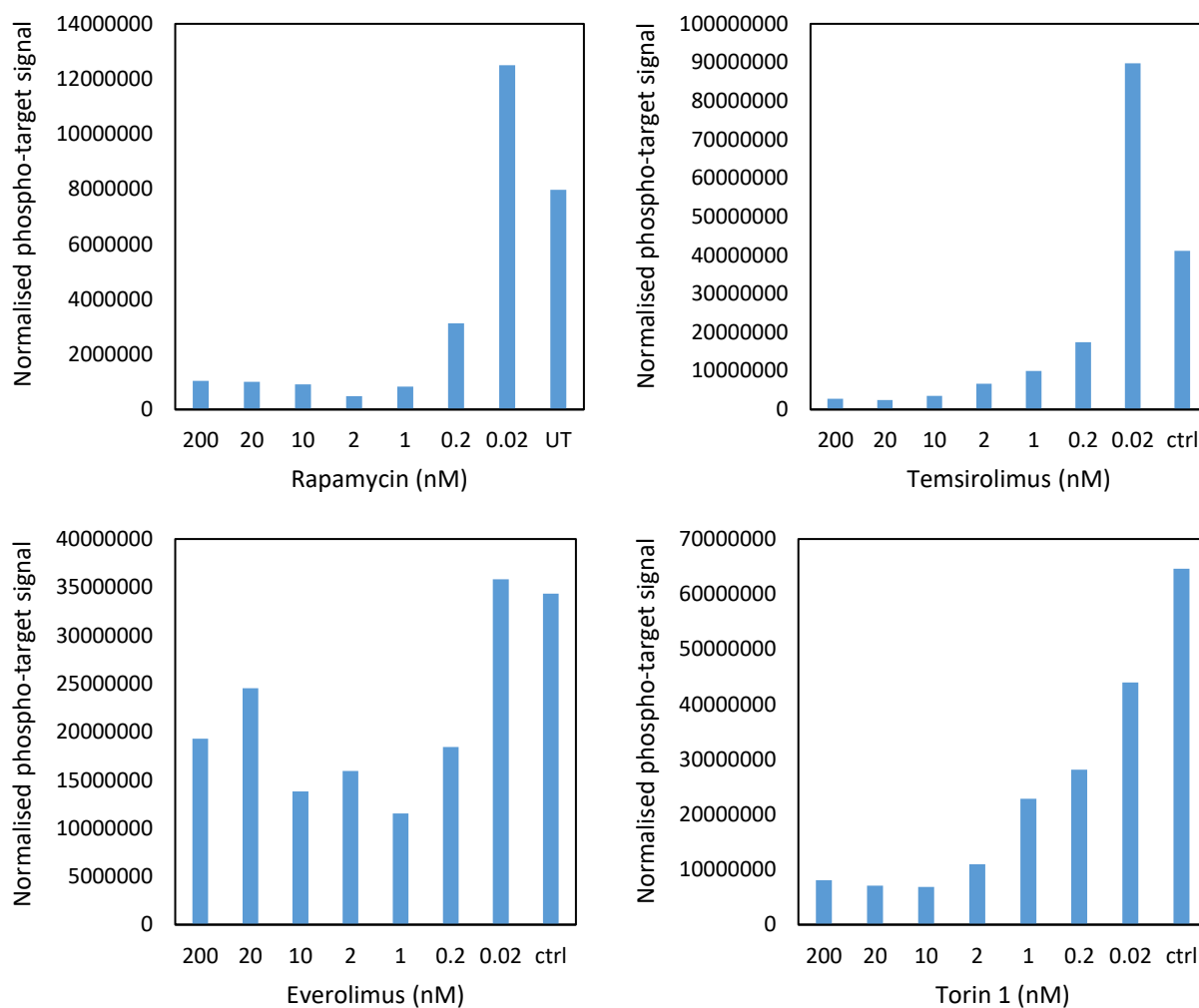


Figure 3.4. Densitometry analysis of Western Blots probing for the phosphorylated form of S6K at threonine 389 using lysates obtained from UoK111 treated with different concentrations of A) Rapamycin, B) Temsirolimus, C) Everolimus and D) Torin 1. Densitometry analysis demonstrated that the mTOR inhibitors tested, Rapamycin, Temsirolimus, Everolimus and Torin 1, inhibit the phosphorylation of S6K at threonine 389 at low nanomolar concentrations. Pan and phospho-protein signals were first normalised using house keeping protein actin. The normalised phospho-protein signal was then divided by the normalised pan-protein signal (see detailed method in section 2.7.7). Densitometry analysis was performed on a single set of blots.

Table 3.1. IC50 values of mTOR inhibitors for inhibition of phosphorylation of S6K at threonine 389 in ACHN and UoK111 cells. The IC50 values were calculated from a single set of blots for each drug.

Drug/Cell line	Rapamycin (nM)	Temsirolimus (nM)	Everolimus (nM)	Torin 1 (nM)
ACHN	0.22	0.83	0.22	0.03
UoK111	0.14	0.01	0.10	0.27

Next, we investigated the effect of mTOR inhibitors on the phosphorylation of the mTORC1 substrate 4EBP1. Again, ACHN and UoK111 cells were treated with Rapamycin, Temsirolimus, Everolimus and Torin 1 for 2 hours, followed by harvesting and lysing, as detailed in section 2.7.2. Thereafter, Western Blot analyses were performed as described on sections 2.7.4 to 2.7.7, using the appropriate antibodies to detect 4EBP1 protein detailed in table 2.3. Antibodies for the phosphorylated form of 4EBP1 were not used because 4EBP1 has seven phosphorylation sites, and at least five of them are phosphorylated by mTORC1 (455,456). Thus, the use of an antibody for the phosphorylated protein in only one site, could lead to inaccurate conclusions. We took advantage of the fact that, immunoblotting using an antibody for total 4EBP1 results in three visible bands of different electrophoretic mobilities that have been identified as α , β , γ , which represent the conformational variations of 4EBP1 as the outcome of hierarchical phosphorylation (455,457). The resulting Western Blots are displayed in Figures 3.5 and 3.7, and the respective densitometry analyses are presented in Figures 3.6 and 3.8. In both sets of Figures, the α , β , γ bands are indicated.

The Western Blots of ACHN cells treated with Rapamycin, Temsirolimus, Everolimus and Torin 1 are displayed in Figure 3.5. The lower mobility β and γ bands, which are attributed to less phosphorylated forms of 4EBP1 (455,457), consistently increase in intensity with higher concentrations of Rapamycin, Everolimus and Torin 1, while α band decreases in intensity in lysates from ACHN cells treated with 20 and 200 nM of Torin 1. The absence of a band in the column containing the sample of ACHN treated with 20 nM Rapamycin is a result of insufficient protein loaded, since the band for the loading control is also missing. The densitometry analysis displayed in Figure 3.6 shows that increase in the concentration of Rapamycin, Everolimus and Torin 1, alter the phosphorylation patterns of 4EBP1, leading to an increase the relative amount of the 4EBP1 β form. The same concentration-dependent increase of the 4EBP1 γ form is also observed for samples of ACHN cells treated with Everolimus and Torin 1. We found no clear patterns of changes in the intensity of α , β , and γ bands that could indicate a difference in the relative amount of the conformational variations of 4EBP1 in ACHN cells treated with Temsirolimus (and see below for the case of UoK11 cells). Clear patterns of increased intensity of bands β and γ are observed in cells treated with increased concentrations of Torin 1, as well as Rapamycin and Everolimus.

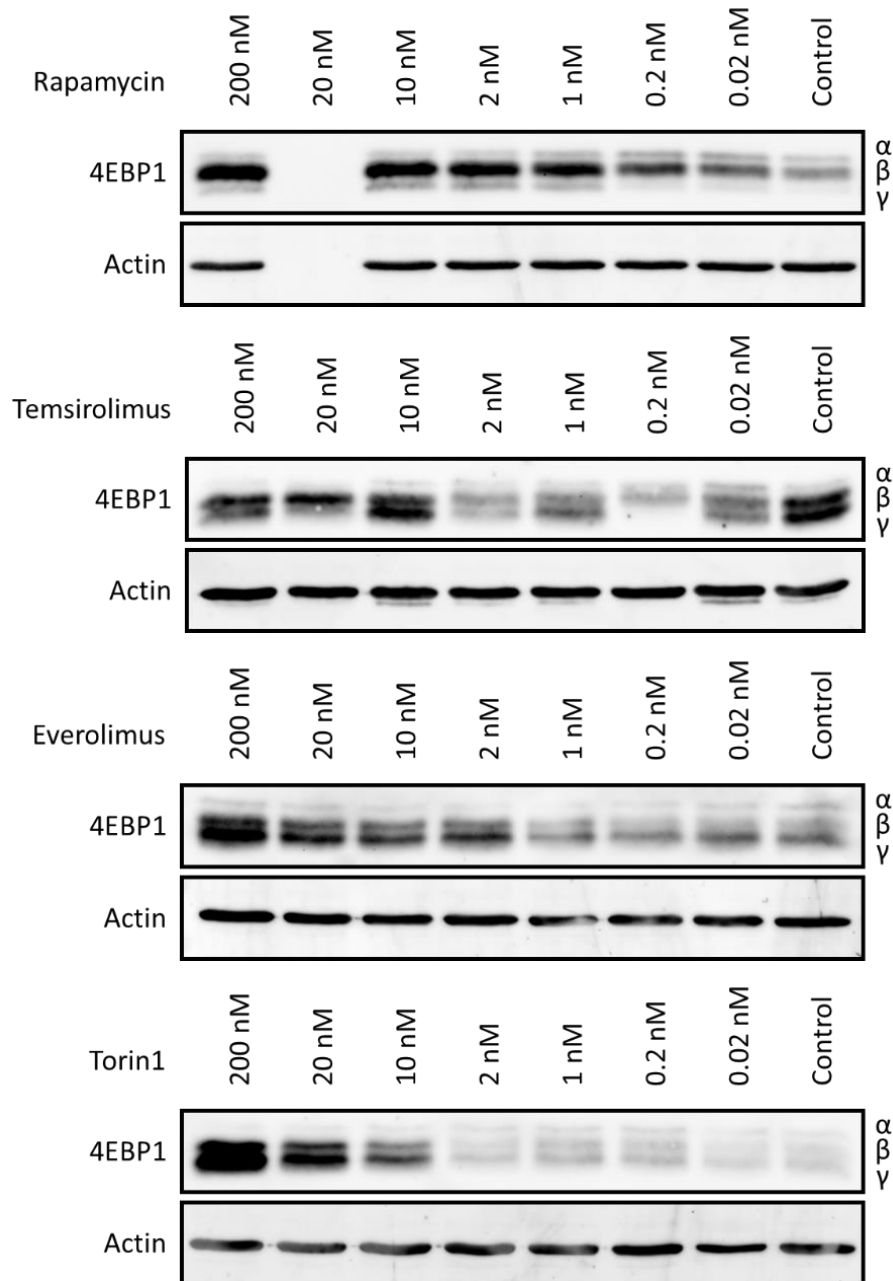


Figure 3.5. Western Blot analyses of relative levels of 4EBP1 in ACHN cells. ACHN cells were treated with allosteric and ATP-competitive mTOR inhibitors for two hours, and subsequently harvested and lysed as described in section 2.7. A total of 20 μ g of protein from lysates obtained from cells treated with different concentration of the respective mTOR inhibitor were analysed in each lane with the antibodies listed in section 2.1.4. Actin was used as loading control.

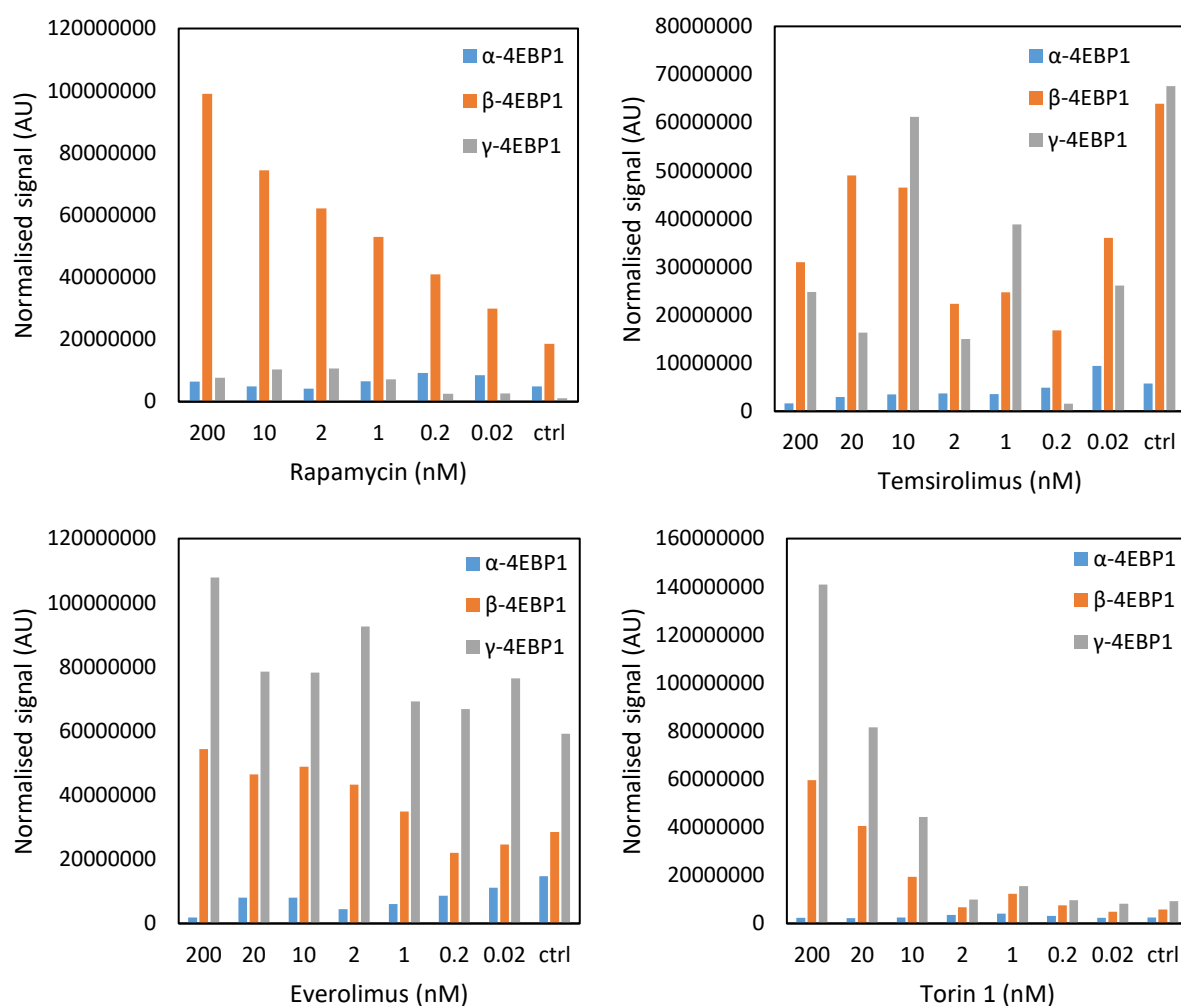


Figure 3.6. Densitometry analysis of Western Blots probing for 4EBP1 using lysates obtained from ACHN treated with different concentrations of A) Rapamycin, B) Temsirolimus, C) Everolimus and D) Torin 1. Densitometry analysis shows that the mTOR inhibitors tested, Rapamycin, Temsirolimus, Everolimus and Torin 1 alter the phosphorylation patterns of 4EBP1. Protein signals were normalised using housekeeping protein β -actin (see detailed method in section 2.7.7). Densitometry analysis was performed on a single set of blots.

Figures 3.7 and 3.8 show the Western Blots using antibody against 4EBP1 and the densitometry analysis, respectively, from lysates obtained from UoK111 cells treated with different concentrations of mTOR inhibitors for 2 hours. As can be observed in Figure 3.7, the intensity of bands β and γ increase consistently with increased concentrations of Rapamycin, Everolimus and Torin 1. These observations can be confirmed with the densitometry analysis shown in Figure 3.8, in which a pattern for increased intensity of bands β and γ consistent with increased concentrations of Rapamycin, Everolimus and Torin 1 can be appreciated. Inspection of the Western

Blot images on Figure 3.7 shows that the transition from an α -rich to β -rich pattern occurs around 1-2 nM for most drugs.

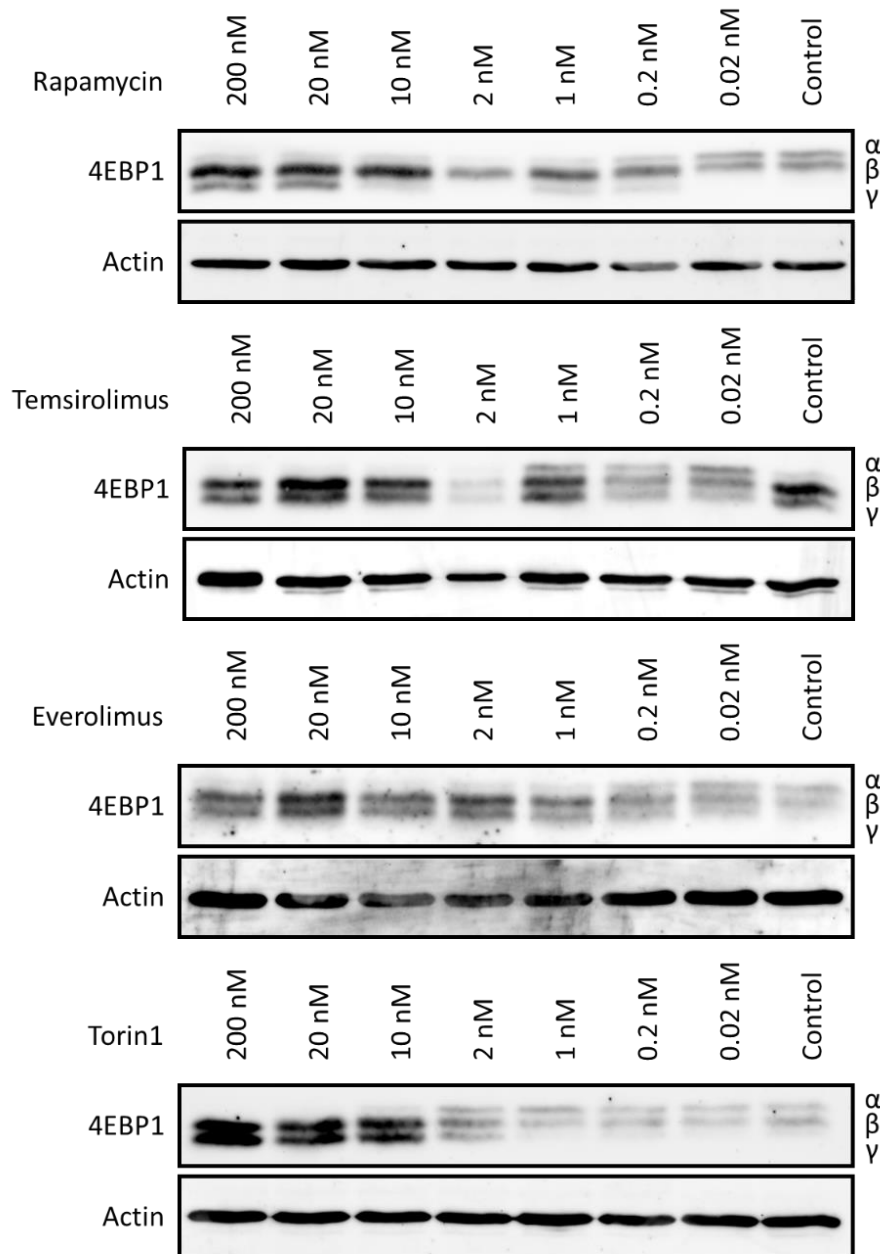


Figure 3.7. Western Blot analyses of relative levels of 4EBP1 in UoK111 cells. UoK111 cells were treated with allosteric and ATP-competitive mTOR inhibitors for two hours, and subsequently harvested and lysed as described in section 2.7. A total of 20 μ g of protein from lysates obtained from cells treated with different concentration of the respective mTOR inhibitor were analysed in each lane with the antibodies listed in section 2.1.4. Actin was used as loading control.

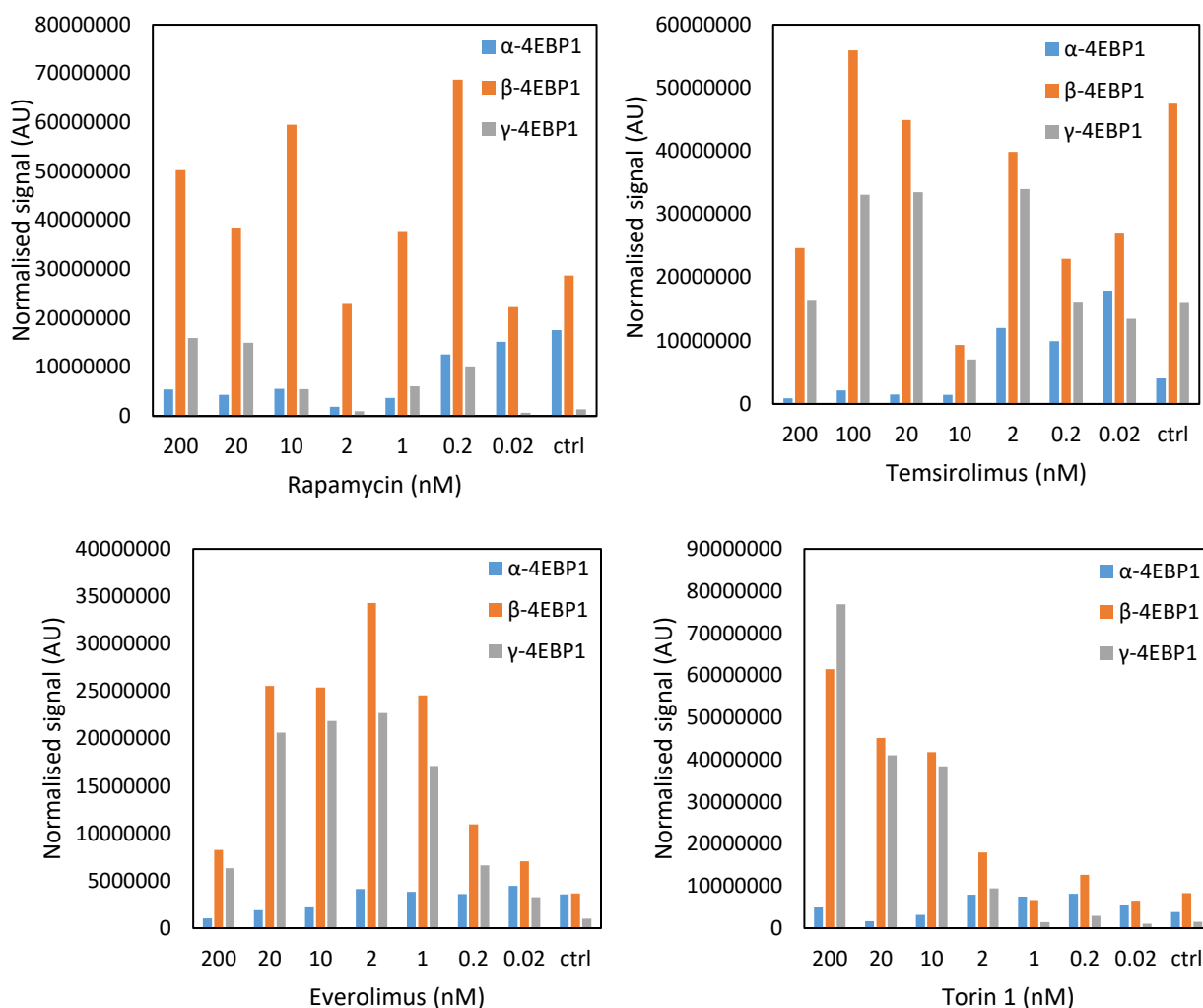


Figure 3.8. Densitometry analysis of Western Blots probing for 4EBP1 using lysates obtained from UoK111 treated with different concentrations of A) Rapamycin, B) Temsirolimus, C) Everolimus and D) Torin 1. Densitometry analysis shows that the mTOR inhibitors tested Rapamycin, Temsirolimus, Everolimus and Torin 1 alter the phosphorylation patterns of 4EBP1. Protein signals were normalised using housekeeping protein β -actin (see detailed method in section 2.7.7). Densitometry analysis was performed on a single set of blots.

The densitometry analysis on Figure 3.8 used to estimate the IC₅₀s shows a lack of pattern for the changes of the α bands. Nevertheless, it should be considered that densitometry depends sequentially on background subtraction and ratio calculation, thus it is prone to artefactual variations due to local staining and background changes. Furthermore, while densitometry is straightforward in the case of S6K phosphorylation, where there is a separate identification of the total and phosphorylate forms of the protein, in the case of 4EBP1 quantification depends on the clear resolution of the different mobility bands, which is difficult and to some extent subjective. Therefore, analysis of the Western Blots of Figure 3.7 suggest that the mTOR inhibitors tested

alter the phosphorylation of 4EBP1 at concentrations around 1-2 nM, causing a conformational change from α to β form. It is also important to mention that the increased signal of 4EBP1 β - and γ -forms observed in ACHN and UoK111 cells treated with allosteric and ATP-competitive mTORis might not only indicate changes in the phosphorylation of 4EBP1, but also an increase in the amount of the protein. Further discussion regarding these results are found in section 4.

Interestingly, the transition from an α -rich to β -rich pattern are observed to happen within a 1-2-fold change in concentration at the expected concentrations, which appear slightly higher than the IC50s for S6K Thr389, except perhaps for Torin 1, where it is similar. Additionally, excluding Everolimus, the IC50s for inhibition of signal of α form and IC50s for enhanced signal of β , and γ forms of mTOR inhibitors do not exceed 40 nM. This is an important guidance for us, as it suggests that effects of mTOR inhibitors on cellular processes such as synthesis of rRNA or viability should be observed within the nanomolar range. The variety of the phosphorylation patterns of 4EBP1 observed in ACHN and UoK111 treated with different mTOR inhibitors suggest that the mechanism by which these drugs repress mTOR activity might be different.

3.1.2 Modulation of nucleolar function by mTOR inhibitors

Having established that the four mTOR inhibitors tested inhibit mTORC1, these observations indicate that the drugs tested can be expected also to modulate the rate of rRNA synthesis, since this is also partially dependent on mTOR activity, through phosphorylation of TIF-IA (see section 1.4.1.2.2). Thus, we proceeded to assess if mTOR inhibitors can modulate the synthesis of rRNA. For this purpose, microscopic analysis of nascent rRNA in RCC cells was performed by labelling newly synthesised rRNA using 5-EU followed by detection using Click-chemistry as described in section 2.5. This approach was chosen because the flexibility of the assay allows for its adaptation to multi-well plates, which permits automation of dose response analysis. Additionally, the minimal number of processing steps of this assay reduces the number of variables affecting the results.

3.1.2.1 rRNA synthesis detected is nucleolar

Quantitation of rRNA synthesis was initially developed using 5-bromouridine (BrU) labelling of nascent RNA, but an approach using 5-EU staining followed by Click-chemistry detection was later adopted because of the various advantages that these

technique presents. Firstly, as a bio-orthogonal reaction, Click-chemistry ensures a negligible non-specific staining, which facilitates the subsequent image analysis by preventing spurious detections. Both the 5-EU pulse-labelling and the Click-chemistry reaction use small compounds, thus eliminating potential problems of antibody accessibility to nucleoli which may occur in BrU staining (458). Additionally, this approach ensures linearity of the response, which immunolabelling does not.

To check whether nascent rRNA staining method detected nucleolar synthesis we cultured U2Os cells in the presence of 1mM FU for 45 minutes. U2Os cells were selected for this purpose because their flat morphology and contact inhibition are desirable characteristics for microscopy and make them ideal for optimising a staining method. The incorporated FU was detected using a cross-reacting anti-BrdU antibody, followed by a Cy3-labelled secondary antibody.

Cy3 fluorescence was imaged alongside Differential Interference Contrast (DIC – see Figure 3.9). As can be seen in Figure 3.9, upper panel, the Cy3 signal is confined to nucleoli. The nucleolar specificity of the labelling method, which efficiently excludes nucleoplasmic nascent RNA, is achieved by the fixation method which consists of sequential cold methanol and acetone (see Materials and Methods section 2.5.1). When cells were fixed with 4% paraformaldehyde (as more commonly used in immunofluorescence) extensive nucleoplasmic staining was observed which prevented efficient segmentation of nucleolar images (data not shown). The drawback of methanol/acetone fixation is that it prevents efficient immunofluorescent staining or retention of fluorescent protein-labelled nucleolar components (e.g. Ribosomal Protein L11-GFP). In any case, these nucleolar markers are often lost when ActD treatment disrupts nucleoli which reduces their marking ability. For these reasons we resorted to DIC, which is one of the most reliable methods of identifying nucleoli (223,459).

In conclusion, the nucleolar localisation of the Cy3 signal, together with the fact that the signal is lost following ActD treatment at low concentration (10nM – Figure 3.9, lower panel), which is well known to specifically inhibit 48S rRNA synthesis (230), confirms that the labelling method specifically detects nucleolar RNA synthesis.

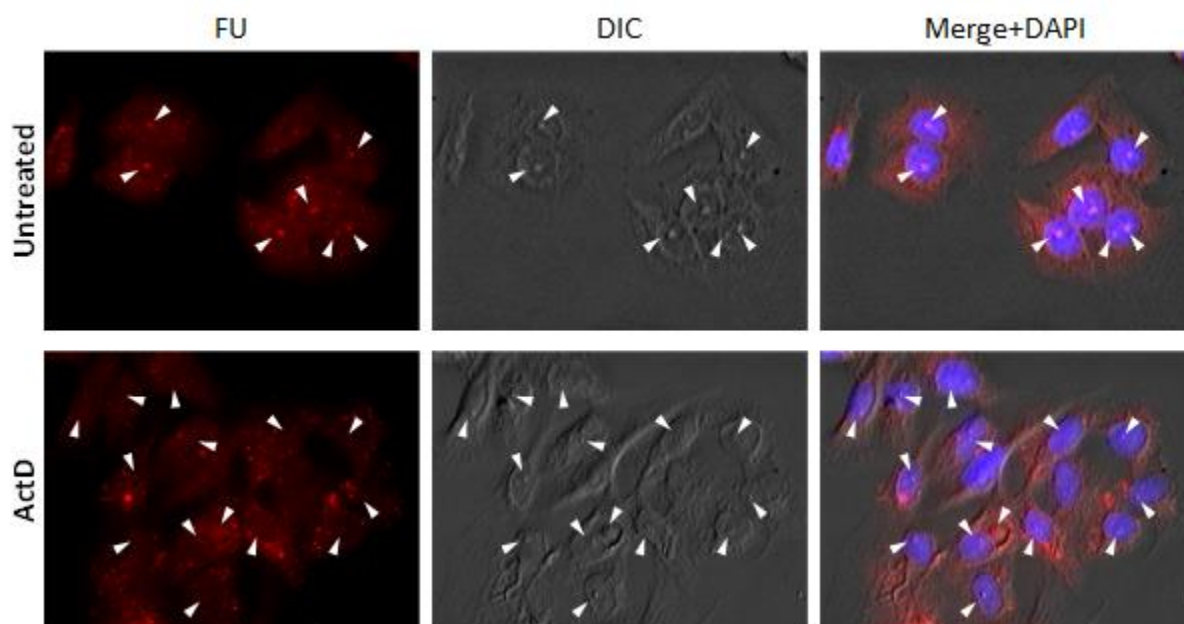


Figure 3.9. rRNA synthesis staining of U2Os cells. Cells were incubated with 1mM FU for 45min, fixed with MetOH/Acetone and labelled with anti-BrdU antibody, detected with an anti-mouse Cy3 labelled secondary antibody. Whole nuclei were stained with DAPI.

To set up the assay using microplates, untreated U2Os cells seeded in 96-well microplates were pulse-labelled with 0.5 mM 5-EU for 30, 45 and 60 minutes. Following methanol/acetone fixation, the labelled rRNA was fluorescently tagged using Click-chemistry, the nuclei were stained with DAPI and cells were imaged using an automated microscope and Micromanager software, and then analysed using CellProfiler Software, as described in section 2.5.2 and 2.5.3. As shown in Figure 3.10, incorporation of 5-EU showed good linearity and pulse-labelling time of 60 minutes was used for all following tests.

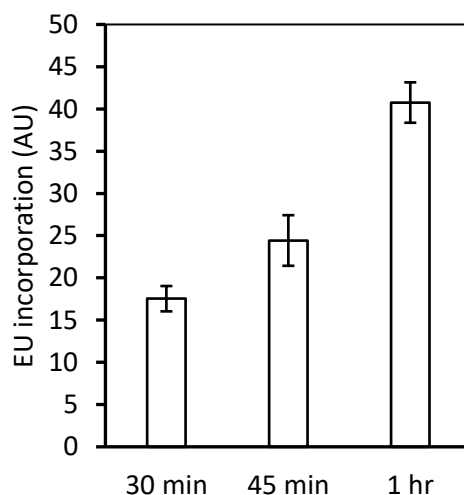


Figure 3.10 5-EU incorporation in U2O cells. U2Os cells were pulse-labelled with 5-EU for 30, 45 and 60 minutes and incorporation of 5-EU proved to be linear.

3.1.2.2 Dose-response curve for rRNA synthesis inhibition by ActD

To establish the concentration range at which ActD would be active in our system we measured full dose-response curves for rRNA synthesis inhibition by ActD. ACHN and UoK111 cells were treated with the NFI ActD for 2 hours, after which the cells were pulsed with 5-EU for 60 minutes, followed by methanol fixation. Figure 3.11 shows the decrease in 5-EU incorporation in A) ACHN and B) UoK111 cells treated with increasing concentrations of ActD, which corresponds to ActD mediated inhibition of rRNA synthesis. The IC₅₀s of ActD for inhibition of rRNA synthesis in ACHN and UoK111 cells were calculated to be 1.25 nM and 1.26 nM, respectively. Figure 3.13 A) below shows an example of labelling of nascent rRNA with 5-EU and of the image segmentation applied in order to quantitate the total Cy3 signal per nucleus.

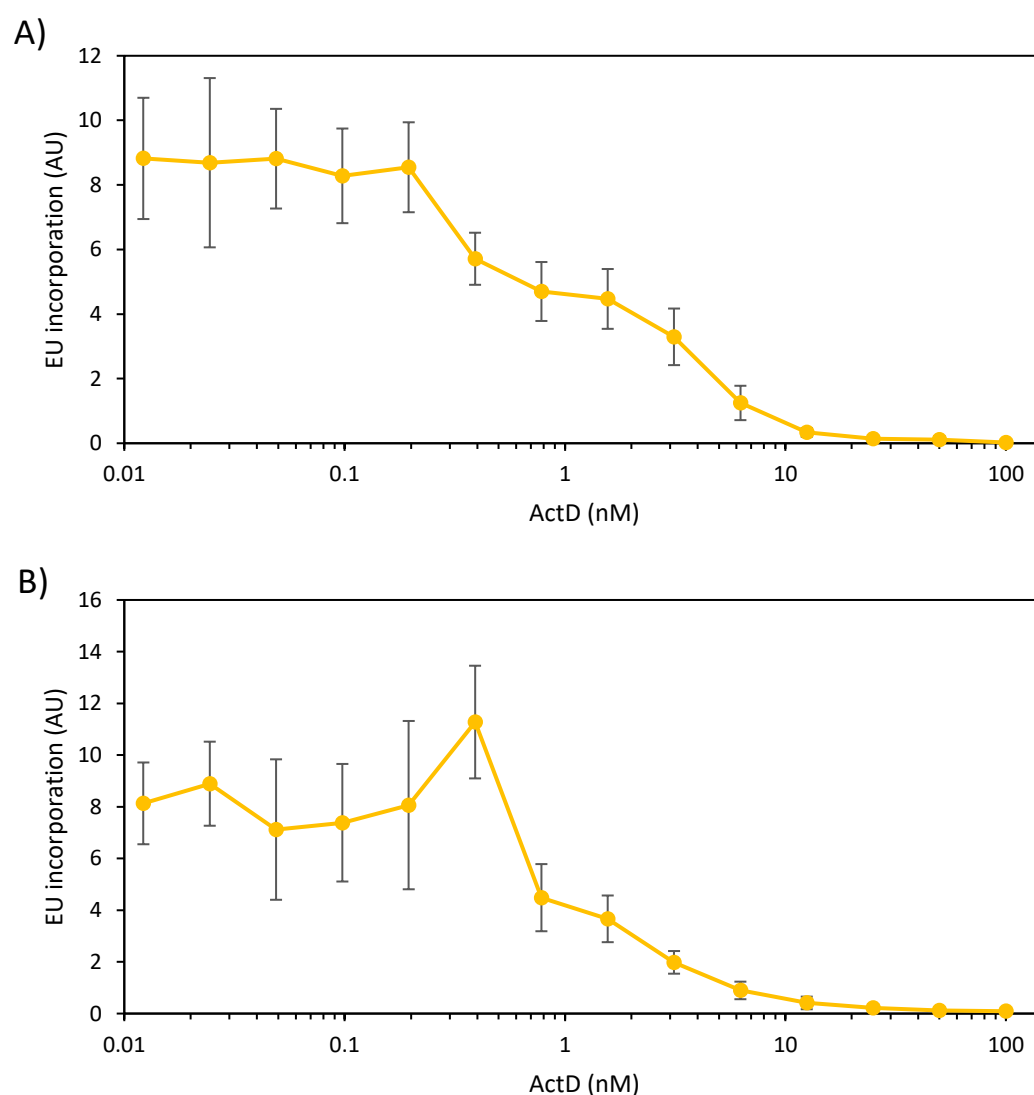
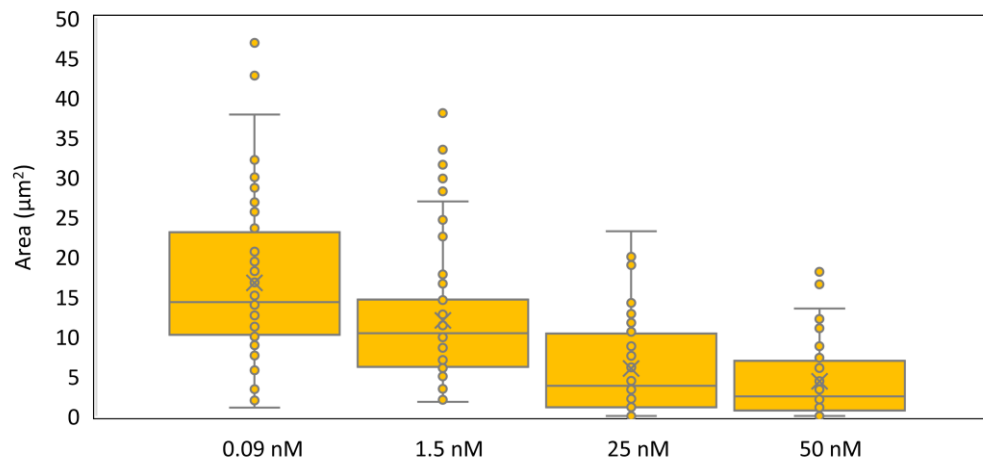


Figure 3.11. Quantification of newly synthesized rRNA in RCC cells treated with ActD. A) ACHN and B) UoK111 cells were treated with ActD (0.01-100 nM) for 2 hours, then pulsed with 5-EU for the last 60 minutes, followed by methanol fixation and labelling using Click-chemistry, as described in section 2.5.1. Inhibition of the nucleolar function by increasing concentrations of ActD is observed for

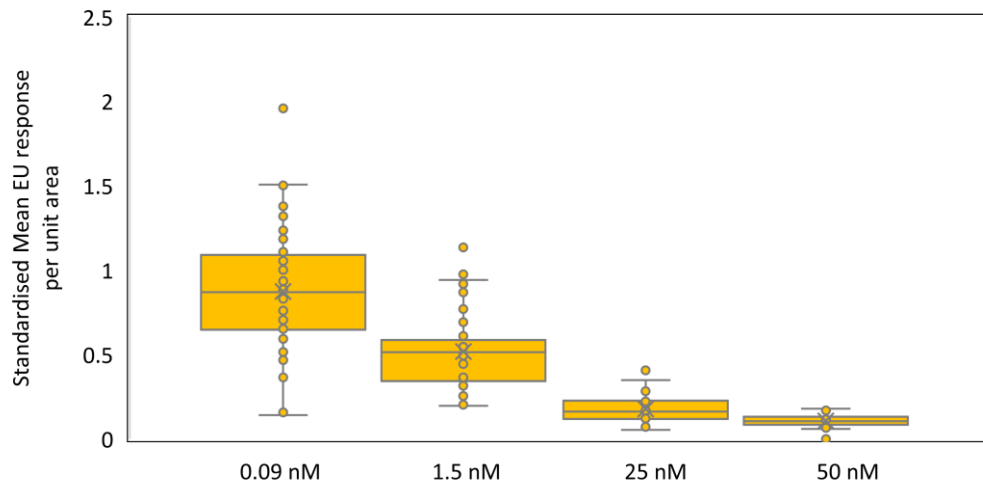
ACHN and UoK111 cells. The error bars indicate Standard Error of the Mean for replicates of 3 wells (50-300 cells imaged per well) of a single experiment.

Since ActD (and potentially other drugs used in this study) causes segregation of nucleoli (460), it could be possible that the overall loss of 5-EU incorporation signal would be due to loss of active nucleolar regions rather than a direct inhibition of RNA Pol I. In an attempt to resolve this, we assessed the changes of nucleolar area and incorporation of 5-EU per unit area in ACHN and UoK111 cells treated with increasing concentrations of ActD. As shown in Figures 3.12 A) and C), increasing concentrations of ActD significantly reduce nucleolar area of ACHN and UoK111, respectively, while decreasing the 5-EU incorporation per unit area in the same cells (Figures 3.12 B) and D)). To assess the statistical significance of these changes, we applied ANOVA with *post-hoc* Bonferroni correction and obtained p-values < 0.01 (significant) for both ACHN and UoK111 cells. We observe the expected reduction in nucleolar area with increasing concentration of ActD; however, the mean 5-EU fluorescence also diminishes with increasing concentrations of ActD, which suggests that there is a reduction in RNA Pol I activity. Nuclear structure and rRNA synthesis are intimately related such that when one changes the other is expected to change as well. Current thinking is that this relationship is explained by the liquid drop/phase transition model, where the RNA type and concentration implicated for the phase transition is maintained by RNA Pol I; conversely the transport and synthesis machinery that supports rRNA synthesis is compartmentalised by the LLPS (461,462). In Appendix 7.5, Figures 7.17 I and J 7.18 I and J, and 7.19 I and J, show the plots for 20 randomly selected nuclei from each treatment well (the total number of nuclei per well generally varied between 100 and 400) where it can be seen that the whole population of nuclei are similarly affected resulting in a unimodal distribution of areas and intensities (see also Figure 7.20). These support the notion that the nucleolar disruption associated with ActD treatment entails impairment of both the nucleolar structure (nucleolar segregation) and rDNA transcription by RNA Pol I.

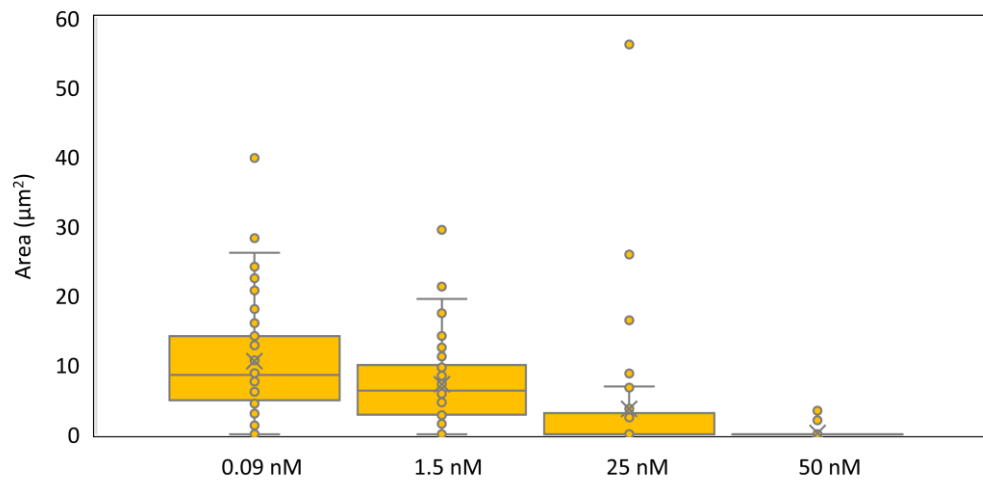
A)



B)



C)



D)

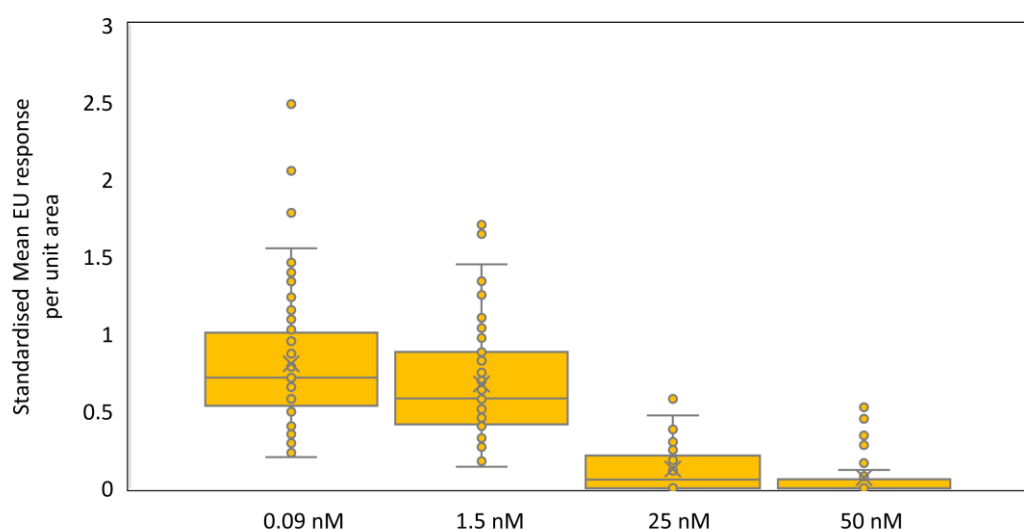


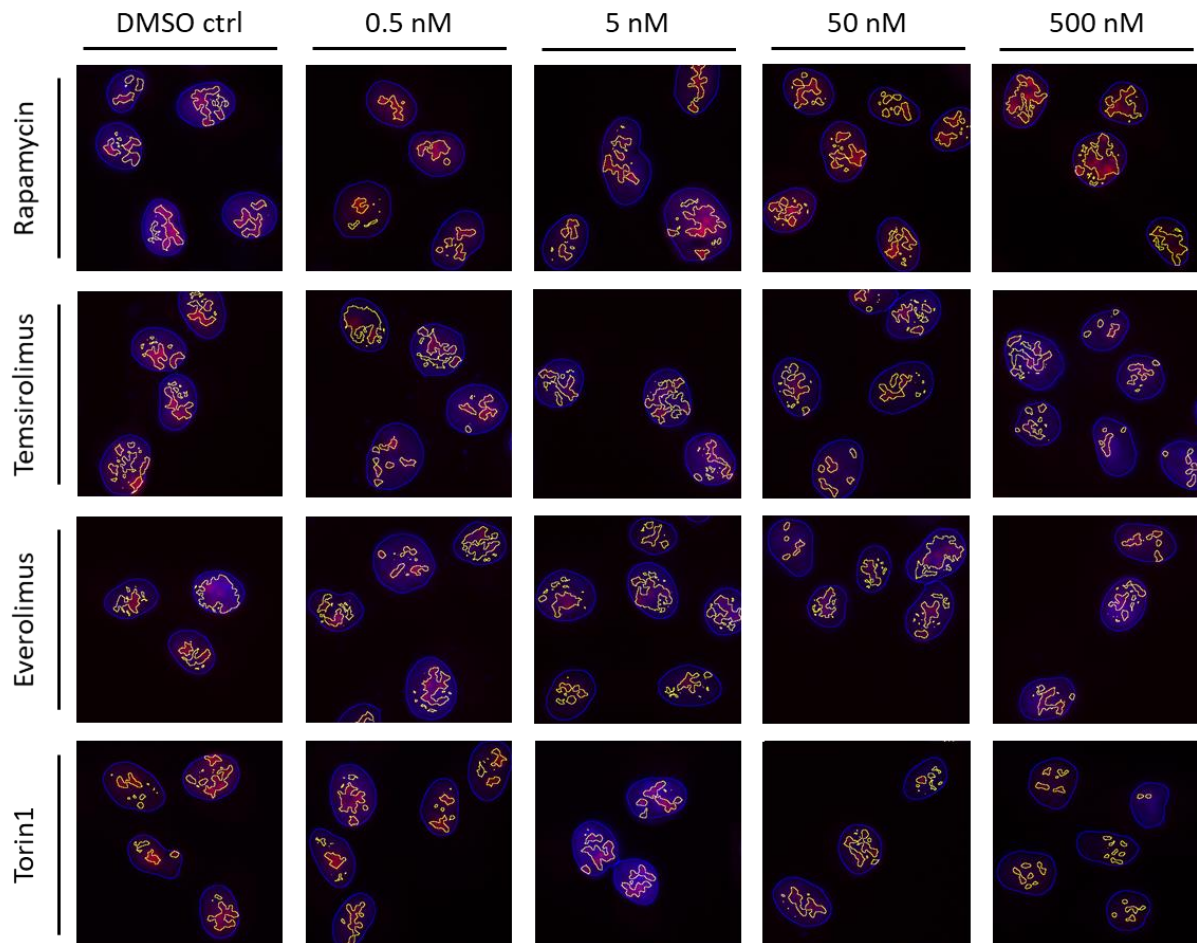
Figure 3.12. Assessment of the effect of ActD on nucleolar area and 5-EU incorporation per unit area in RCC cells. ACHN and UoK111 cells were treated with ActD (0.01-100 nM) for 2 hours, then pulsed with 5-EU for the last 60 minutes, followed by methanol fixation and labelling using Click-chemistry, as described in section 2.5.1. Assessment of the nucleolar area for 20 random cells per well using triplicates of A) ACHN and C) UoK111 cells treated with 0.09 nM, 1.5 nM, 25 nM and 50 nM ActD. Evaluation of the changes in the incorporation of EU per unit area for 20 random cells per well using triplicates of B) ACHN and D) UoK111 treated with the same concentrations of ActD.

3.1.2.3 rRNA synthesis inhibition with mTORis

Having demonstrated in section 3.1.1 that the mTOR inhibitors tested effectively inhibit activity of mTOR in our system, and considering that the mTOR pathway has been shown to activate rRNA synthesis, we examined if these drugs can inhibit nucleolar function. For this purpose, ACHN and UoK111 cells were treated with Rapamycin, Temsirolimus, Everolimus, and Torin 1 with concentrations ranging from 0.06 to 640 nM for 2 hours and then labelling the nascent rRNA with 5-EU as described in section 2.5.1. Figure 3.13 A) shows the images of labelled nascent rRNA (Cy3/red) within each nucleus (DAPI/blue). The image analysis process segments nuclei (blue contours) in a first pass, then segments nucleoli (yellow contours) in a second pass, and finally quantitates the total intensity within the segmented nucleoli, per nucleus. ACHN cells untreated (DMSO) and treated with Rapamycin, Temsirolimus and Everolimus present numerous active nucleoli, as indicated by a high 5-EU incorporation detected at all concentrations tested that represents high amount of nascent rRNA. In contrast, cells treated with Torin 1 display a reduction of 5-EU incorporation at the higher concentrations tested, indicating that this ATP-competitive inhibitor impairs the synthesis of rRNA in ACHN cells. Quantification of the 5-EU incorporation in Figure 3.13 B) shows the concentration-dependent inhibition of rRNA synthesis in ACHN

treated with Torin 1, but the same dose-response curve is not observed in ACHN cells treated with the allosteric mTOR inhibitors, suggesting inhibition on mTORC1 and mTORC2 is required for effective modulation of the nucleolar function.

A)



B)

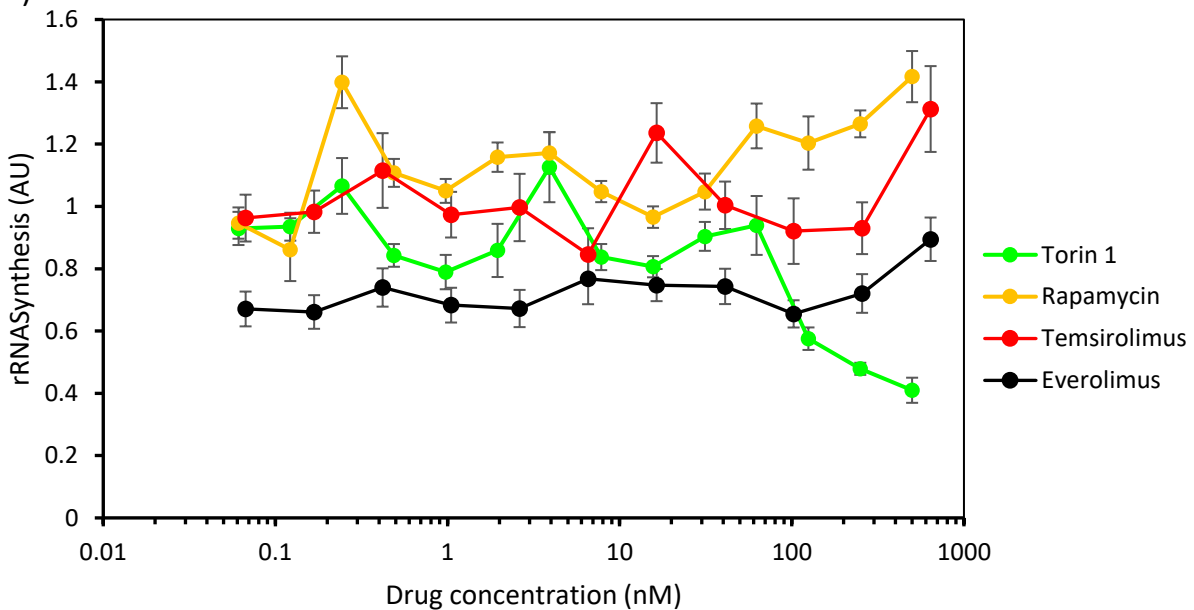
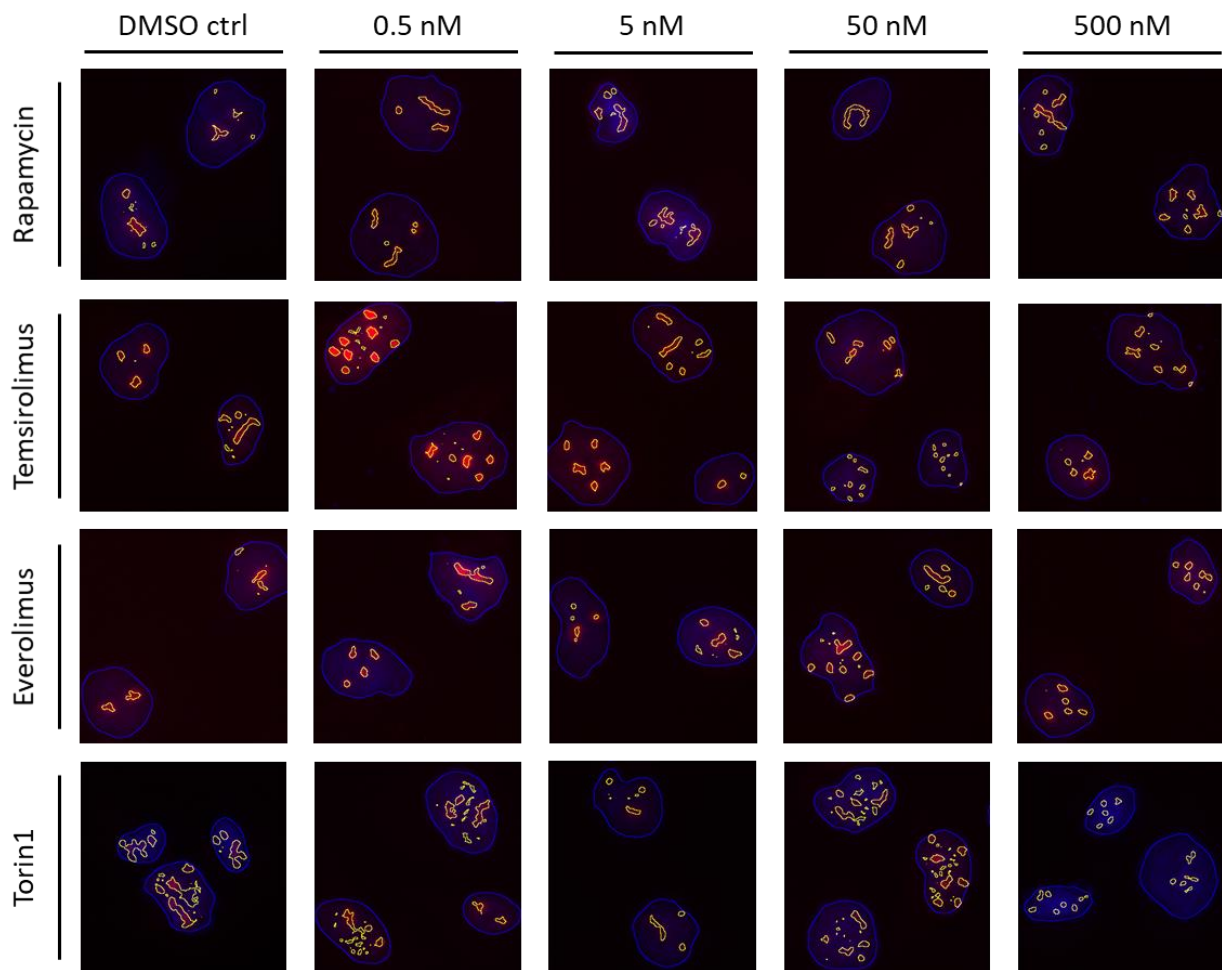


Figure 3.13. Effect of mTOR inhibitors on the synthesis of rRNA in ACHN cells. ACHN cells were treated with different concentrations of mTOR inhibitors for 2 hours and labelled for nascent rRNA with 5-EU. A) Fluorescence images showing nucleolar incorporation of 5-EU (red/Cy3) and nuclear staining (blue/DAPI). Images were subjected to two-stage thresholding, first to segment individual nuclei (blue contours), then to segment individual nucleoli within those nuclei (yellow contours). The segmented regions were subsequently used to quantitate the total 5-EU/Cy3 signal per nucleus (expressed in arbitrary units – AU). B) Quantification of the 5-EU incorporation from microscopy images of ACHN cells treated with Torin 1 (green), Rapamycin (yellow), Temsirolimus (red), and Everolimus (black) for 2 hours and labelled using Click-chemistry. The error bars indicate Standard Error of the Mean for replicates of 3 wells (50-300 cells imaged per well) of a single experiment.

A)



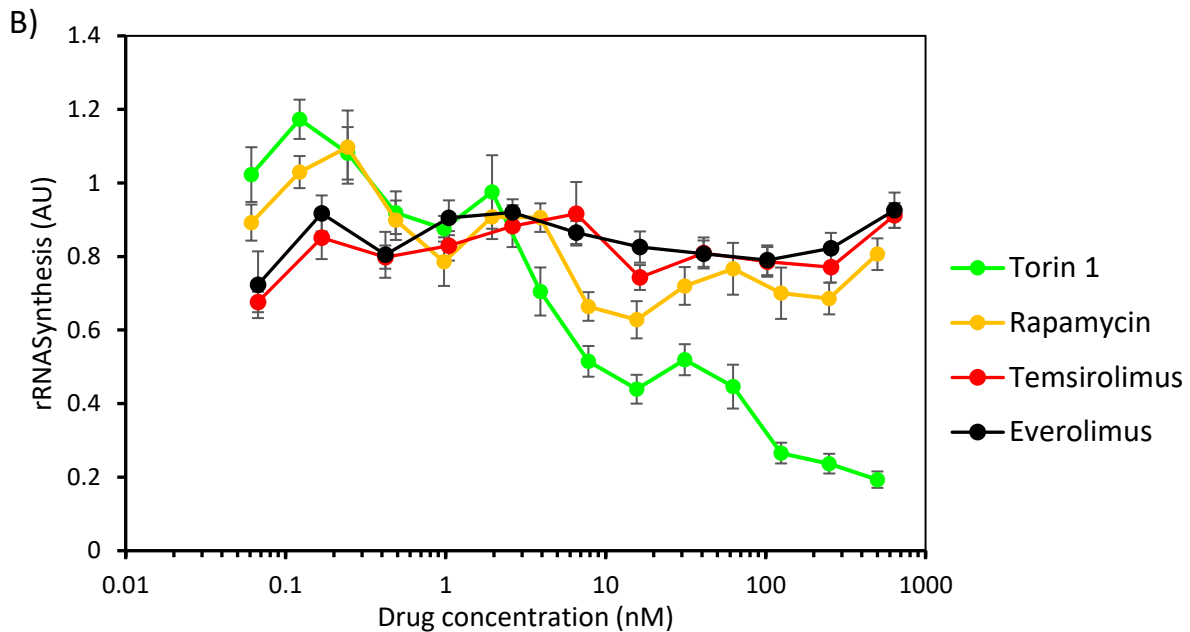


Figure 3.14. Effect of mTOR inhibitors on the synthesis of rRNA in UoK111 cells. UoK111 cells were treated with different concentrations of mTOR inhibitors for 2 hours and labelled for nascent rRNA with 5-EU. A) Fluorescence images showing nucleolar incorporation of 5-EU (red/Cy3) and nuclear staining (blue/DAPI). Images were subjected to two-stage thresholding, first to segment individual nuclei (blue contours), then to segment individual nucleoli within those nuclei (yellow contours). The segmented regions were subsequently used to quantitate the total 5-EU/Cy3 signal per nucleus (expressed in arbitrary units – AU). B) Quantification of the 5-EU incorporation from microscopy images of UoK111 cells treated with Torin 1 (green), Rapamycin (yellow), Temsirolimus (red), and Everolimus (black) for 2 hours and labelled using Click-chemistry. The error bars indicate Standard Error of the Mean for replicates of 3 wells (50-300 cells imaged per well) of a single experiment.

Comparable to ACHN cells, UoK111 cells treated with allosteric inhibitors display similar number of active nucleoli than their corresponding untreated controls, as shown in Figure 3.14 A). Additionally, quantification of the 5-EU incorporation illustrated in Figure 3.14 B) demonstrates that increased concentration of Rapamycin, Temsirolimus and Everolimus do not inhibit rRNA synthesis. On the other hand, UoK111 cells treated with Torin 1 present reduced nucleolar number and activity with concentrations as low as 6.6 nM. UoK111 cells treated with Torin 1 at concentrations higher than 100 nM display over 75% reduction of the synthesis of rRNA compared to the controls. The quantification of the 5-EU incorporation of UoK111 cells treated with Torin 1 presented in Figure 3.14 B) shows that the ATP-competitive inhibitor decreases rRNA synthesis in a concentration–dependent manner with an IC50 of approximately 6 nM. Similarly to ActD, we characterised the nucleolar changes induced by the mTOR inhibitors both with respect to the nucleolar area and the 5-EU incorporation per unit area. Figure 3.15 A and B show box and whisker plots for nucleolar areas and 5-EU incorporation per unit area, respectively. Neither ACHN nor

UoK111 cells show major differences in either parameter, which agrees with our observations that these drugs either do not cause or cause a limited an extensive inhibition of rRNA synthesis. Appendix 7.5, Figures 7.17, 7.18, and 7.19 show in more detailed the distribution of these parameters.

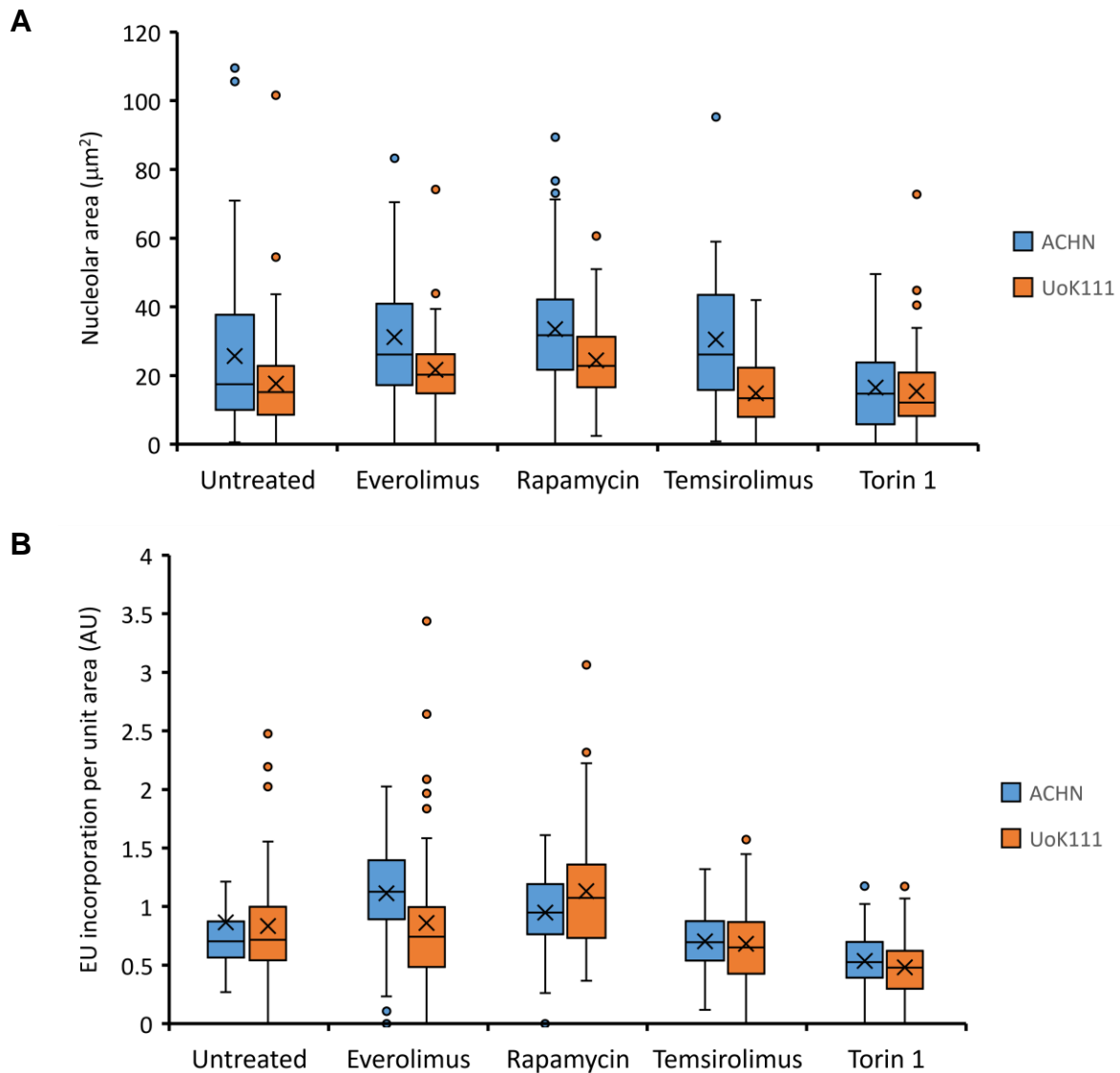


Figure 3.15. Effects of mTOR inhibitors on nucleoli. Plots show the distributions of nucleolar areas (A) and 5-EU incorporation per unit area (B) for ACHN and UoK111 cells (indicated) treated with different drugs at a concentration of 500nM (high end of concentrations used in most experiments) or DMSO (Untreated).

However, while the allosteric inhibitors do not appear to show any dose-dependent reduction in 5-EU incorporation, it is noticeable in some cases that the dose response curves show a level of 5-EU incorporation that is below the controls (<1.0 in the standardised plots). This is unlikely to be a solvent effect since controls include the corresponding solvent.

Together, these results indicate that despite showing similar capacity to inhibit the phosphorylation of the well-known mTOR targets S6K and 4EBP1, only the ATP-competitive mTOR inhibitor Torin 1 was capable of inhibiting rRNA synthesis. Furthermore, the IC50 for rRNA synthesis inhibition by Torin 1 was within 10-fold of the IC50 for inhibition of S6K phosphorylation, suggesting that inhibition of rRNA observed in cells treated with Torin 1 is mediated by the on-target effect of the drug on mTOR.

3.1.3 Inhibition of phosphorylation of the mTORC1 downstream target TIF-IA is a predictor of the activity of mTOR inhibitors on rRNA synthesis

As described in section 3.1, mTOR inhibitors Rapamycin, Temsirolimus, Everolimus, and Torin 1 effectively impair mTORC1 activity in ACHN and UoK111 cells at nanomolar concentrations, as shown by the inhibition of the phosphorylation of S6K in Thr389. In addition to the abrogation of S6K phosphorylation, treatment of ACHN and UoK111 with these mTOR inhibitors also induced phosphorylation changes of mTORC1 substrate 4EBP1 in a concentration-dependent manner at nanomolar concentrations, as shown by decreased intensity of α form and enhanced intensity of β and γ forms using an antibody against 4EBP1 (Table 2.3). However, to our surprise, only ATP-competitive inhibitor Torin 1, and not the allosteric inhibitors, impaired the synthesis of rRNA, as presented in section 3.1.2.3.

Since phosphorylation of S6K and 4EBP1 could not explain the different effect observed in rRNA synthesis by Torin 1 and the allosteric mTOR inhibitors, we decided to assess the phosphorylation of mTOR substrates involved in the modulation of or participating in the synthesis of 48S rRNA. We selected the transcription factor TIF-IA because it is a fundamental component of the RNA Pol I machinery needed to initiate rDNA transcription (185), which has been reported to be a downstream target of mTORC1 (186) (see introduction section 1.4.1.2.2).

Unlike the antibodies against phosphorylated forms of S6K and 4EBP1, antibodies against phosphorylated forms of TIF-IA were not vastly referenced, which meant that we could not rely on existing data to be confident of their specificity. In addition, the signals observed in Western blot were consistently weak. For these reasons, we decided to confirm the specificity of the bands detected with these antibodies by siRNA knockdown of TIF-IA/RRN3 previous to their use to assess the effects of the mTOR

inhibitors. ACHN cells were transfected with TIF-IA siRNA for 24 and 48 hours as described in section 2.6. Scrambled siRNA was used as negative control and, due to the weak TIF-IA signals detected in Western Blot, we also included a knockdown control using p53 siRNA well-known in our laboratory. After transfection, cells were harvested and lysed as detailed in section 2.7.2. Subsequently, Western Blot analyses were performed as described on sections 2.7.4 to 2.7.7, using the appropriate antibodies to detect TIF-IA and phosphorylated TIF-IA at serine 649 detailed in table 2.3. The resulting Western Blots are illustrated in Figure 3.16.

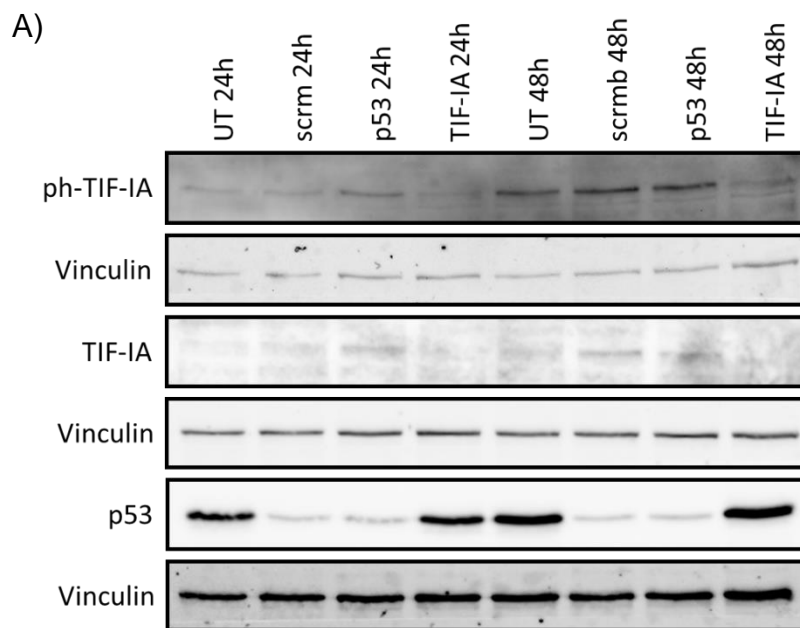
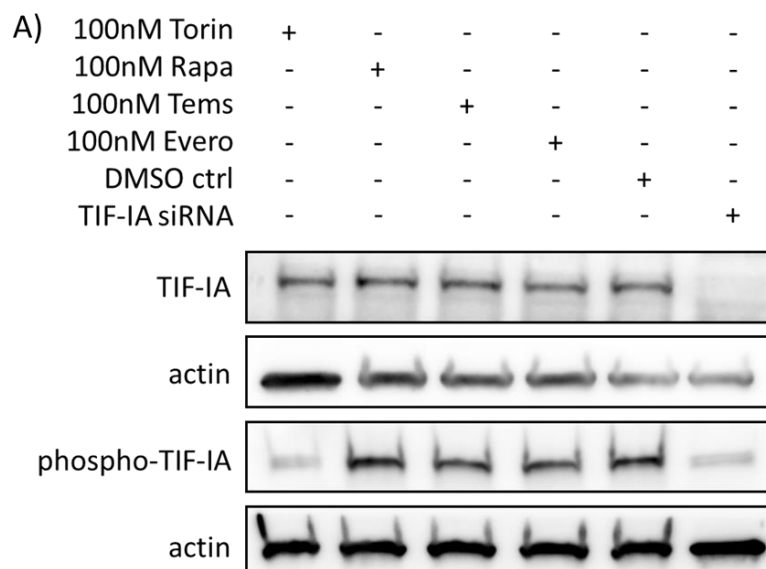


Figure 3.16. Western Blot of relative levels of TIF-IA in ACHN cells transfected with siRNA transfection. A) ACHN cells were transfected with siRRN3 for 24 and 48 hours as described in section 2.6. Subsequently, cells were harvested and lysed as described in section 2.7. A total of 20 µg of protein from lysates obtained from transfected cells were analysed in each lane with the antibodies listed in section 2.1.4. Vinculin was used as loading control.

The expected band of TIF-IA was reduced in cells treated with siRRN3 with respect to the untreated, scrambled siRNA and p53 siRNA-treated cells, especially after 48-hour incubation. The phosphospecific antibody for TIF-IA (S649) detects several bands, with the specific one identifiable by siRNA knockdown at the expected molecular weight of 74 kDa. Although p53 appears to be depleted in cells transfected with p53 siRNA and the negative control, transfection with the scrambled siRNA did not knockdown TIF-IA and was still a valid negative control for TIF-IA siRNA transfection having no effect on the phenotype of interest.

To make an initial assessment of the effects of the different mTOR inhibitors on the phosphorylation of TIF-IA, ACHN and UoK111 cells were treated with 100 nM of Rapamycin, Temsirolimus, Everolimus and Torin 1, a concentration which was in the range of 100-fold higher than the IC50s observed for the inhibition of the mTOR kinase activity against S6K and 4EBP1. Cells were treated for two hours, then harvested and lysed as detailed in section 2.7.2. Subsequently, Western Blot analyses were performed as described on sections 2.7.4 to 2.7.7, using the appropriate antibodies to detect TIF-IA and phosphorylated TIF-IA at Ser649 detailed in table 2.3. The resulting Western Blots and the densitometry analysis of the blot used to detect phosphorylated TIF-IA are shown in Figures 3.17 and 3.18. As can be observed in Figure 3.17 A), ACHN cells treated with 100 nM of Torin 1, Rapamycin, Temsirolimus and Everolimus show constant relative amounts of TIF-IA, indicating that mTOR inhibitors do not affect the availability of TIF-IA. Nevertheless, ACHN cells treated with 100 nM Torin 1 display reduced relative amount of phosphorylated TIF-IA compared to ACHN treated with allosteric inhibitors, the DMSO control and the lysates from transfected ACHN with TIF-IA siRNA, which were used as negative control, indicating that treatment with Torin 1 strongly abrogates the phosphorylation of TIF-IA in ACHN cells. The densitometry analysis shown in Figure 3.17 B) confirms that only Torin 1 reduces phosphorylation of TIF-IA at Ser649.



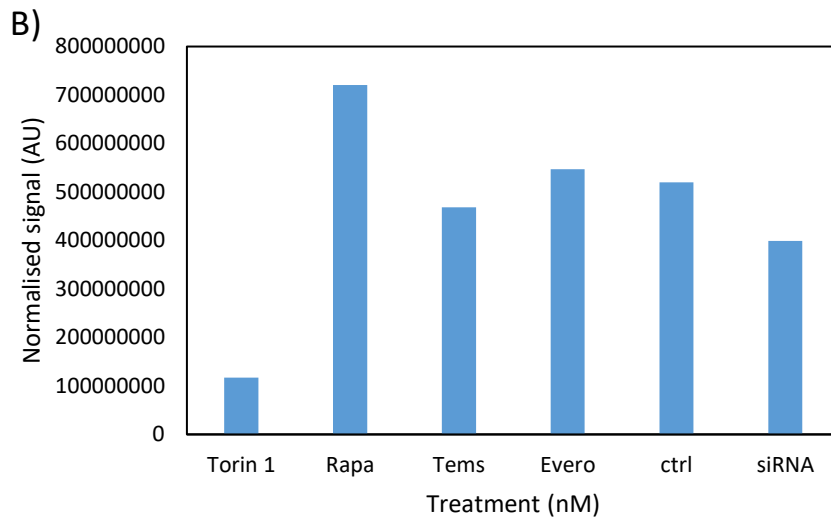


Figure 3.17. Western Blot and densitometry analysis of relative levels of TIF-IA and phosphorylated TIF-IA in ACHN cells treated with 100 nM of Torin 1, Rapamycin, Temozolomide, and Everolimus. A) ACHN cells were treated with 100 nM of Torin 1, Rapamycin, Temozolomide, and Everolimus for 2 hours as described in section 2.7. Subsequently, cells were harvested and lysed as described in section 2.7. A total of 20 µg of protein from lysates obtained from transfected cells were analysed in each lane with the antibodies listed in section 2.1.4. Pan and phospho-protein signals were first normalised using house keeping protein actin. The normalised phospho-protein signal was then divided by the normalised pan-protein signal (see detailed method in section 2.7.7). B) Densitometry analysis of the blot used to detect phosphorylated TIF-IA shows that 100 nM Torin 1 but not the other mTOR inhibitors abrogate the phosphorylation of TIF-IA. Torin= Torin 1; Rapa=Rapamycin; Temo=Temozolomide; Evero=Everolimus; ctrl=DMSO control; siRNA=ACHN transfected with TIF-IA siRNA for 48 hours (negative control). Densitometry analysis was performed on a single set of blots.

Similarly to ACHN cells, the resulting Western Blots from UoK111 treated with 100 nM mTOR inhibitors illustrated in Figure 3.18 show lower amount of phosphorylated TIF-IA in UoK111 cells treated with Torin 1 than that observed with the other mTOR inhibitors, the DMSO and the negative control. Although the amount of total TIF-IA appears to be lower in UoK111 cells treated with Torin 1, the loading control indicates a lower concentration of protein. The densitometry analysis shown in Figure 3.16 B) takes into account the fluctuations on native TIF-IA observed in Figure 3.16 A) and confirms that Torin 1 reduces phosphorylation of TIF-IA at Ser649 further than the allosteric mTORis. These results suggest that in UoK111 cells, the phosphorylation of TIF-IA can also be used as a marker to predict the effect of Torin 1 on cell viability and rRNA synthesis.

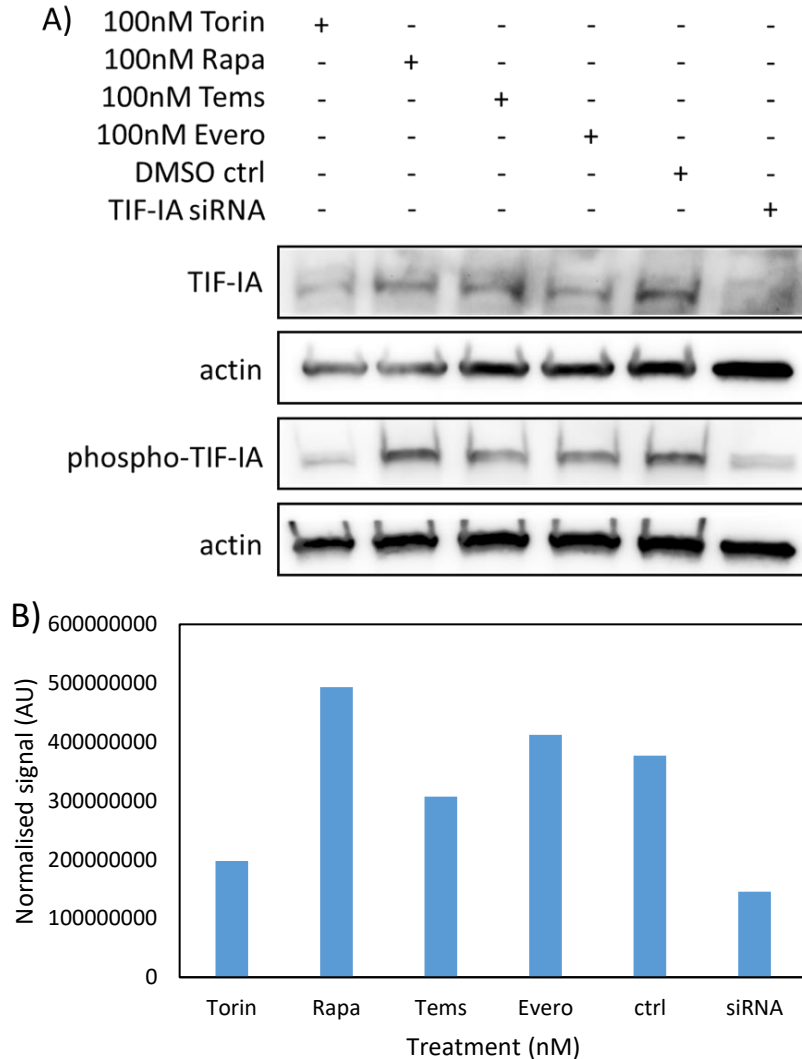


Figure 3.18. Western Blot and densitometry analysis of relative levels of TIF-IA and phosphorylated TIF-IA in UoK111 cells treated with 100 nM of Torin 1, Rapamycin, Temozolomide, and Everolimus. A) UoK111 cells were treated with 100 nM of Torin 1, Rapamycin, Temozolomide, and Everolimus for hours as described in section 2.7. Subsequently, cells were harvested and lysed as described in section 2.7. A total of 20 μ g of protein from lysates obtained from transfected cells were analysed in each lane with the antibodies listed in section 2.1.4. Pan and phospho-protein signals were first normalised using house keeping protein actin. The normalised phospho-protein signal was then divided by the normalised pan-protein signal (see detailed method in section 2.7.7). B) Densitometry analysis of the blot used to detect phosphorylated TIF-IA shows that 100 nM Torin 1 but not the other mTOR inhibitors abrogate the phosphorylation of TIF-IA. Torin= Torin 1; Rapa=Rapamycin; Tems=Temozolomide; Evero=Everolimus; ctrl=DMSO control; siRNA=ACHN transfected with TIF-IA siRNA for 48 hours (negative control). Densitometry analysis was performed on a single set of blots.

These results suggest that inhibition of TIF-IA phosphorylation might predict the ability of an mTOR inhibitor to downregulate rRNA synthesis. If this was the case we would expect the dose-response curve of Torin 1 for inhibition of TIF-IA phosphorylation to be similar to that for S6K and 4EBP1 phosphorylation, particularly to display an IC₅₀ in the low nanomolar range. To analyse in detail the effect of Torin 1 on the

phosphorylation of TIF-IA, ACHN and UoK111 cells were treated with a range of concentrations of Torin 1 from 0.02 to 200 nM for 2 hours, cells were harvested and lysed as described in section 2.7. Western Blot analyses were then performed as described on sections 2.7.4 to 2.7.7, using the antibodies to detect TIF-IA and phosphorylated TIF-IA at Ser649 detailed in table 2.3. The resulting Western Blots and the densitometry analysis are shown in Figure 3.19. In Figure 3.19 A) the amount of TIF-IA appears to be consistent through the samples of ACHN cells treated with increasing concentrations of Torin 1. The ninth lane containing 20 µg of lysate of ACHN cells transfected with siRRN3 was used as a negative control and is the only lane that presents a significant decrease of the amount of TIF-IA. In contrast, the amount of the phosphorylated form of TIF-IA decreases consistently with increased concentrations of Torin 1. These observations can be confirmed by the densitometry analysis of the Western Blot on Figure 3.19 C), which was performed taking into account the reduction of native TIF-IA with Torin 1, and shows that the phosphorylation of TIF-IA at S649 in ACHN cells treated with Torin 1 decreases in a concentration-dependent manner with an IC₅₀ of 0.13 nM calculated using ATT Bioquest IC₅₀ Calculator (463). Figure 3.19 B) shows a slight reduction of the amount of TIF-IA in the samples from UoK111 cells treated with Torin 1 concentrations above 1 nM. Of particular interest is the reduction of the amount of the phosphorylated form of TIF-IA which appears to be consistent with increased concentrations of Torin 1, excluding the sample on the fourth lane obtained from UoK111 treated with 2 nM Torin 1. Densitometry analysis of the phosphorylated form of TIF-IA in relation with native TIF-IA, displayed in Figure 3.19 D), shows a concentration-dependent decrease of the amount of phosphorylated TIF-IA in UoK111 treated with Torin 1 with an IC₅₀ of 1.08 nM according to the ATT Bioquest IC₅₀ Calculator (463).

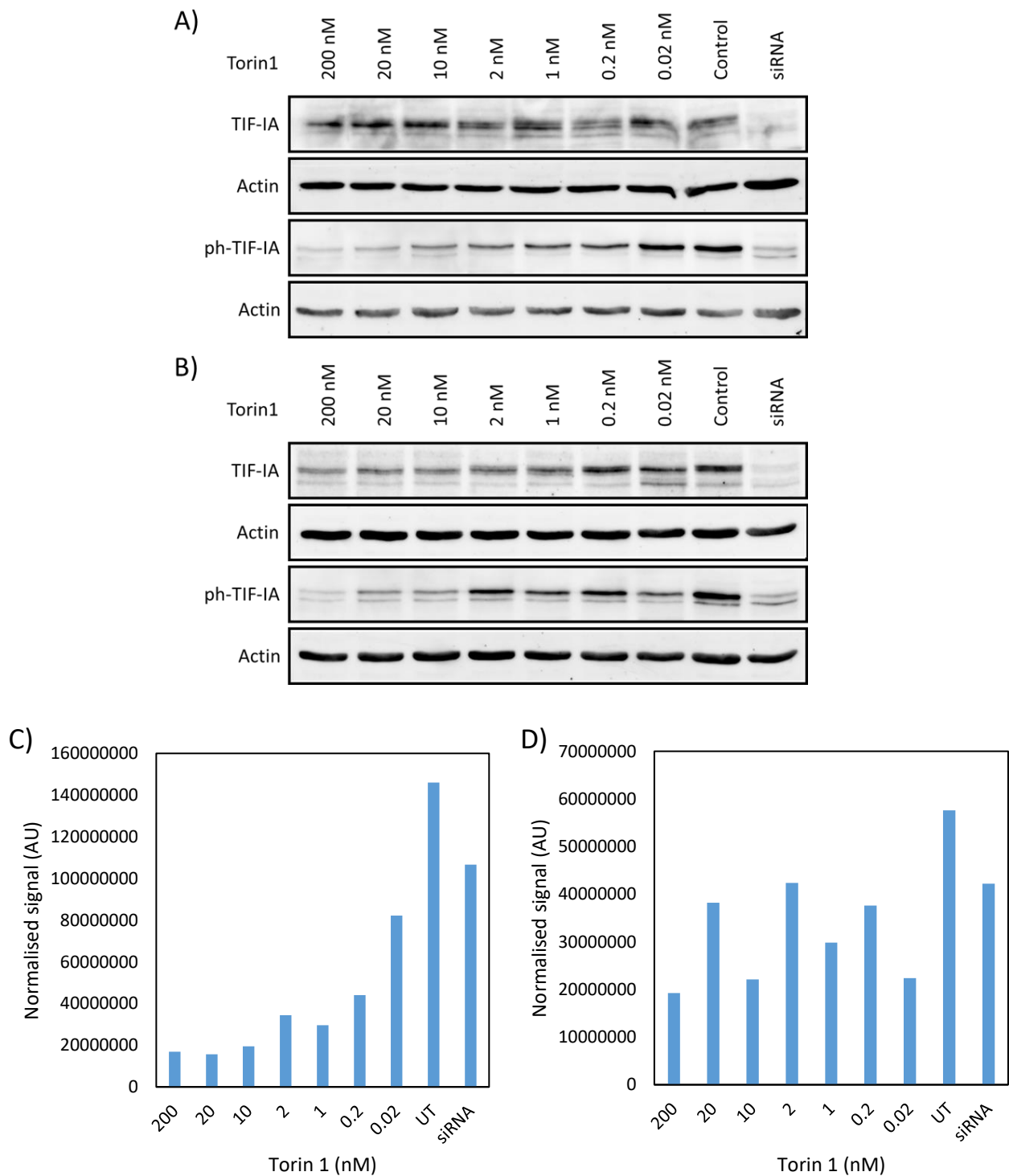


Figure 3.19. Western Blot and densitometry analyses of relative levels of TIF-IA and phosphorylated TIF-IA in RCC cells treated with increasing concentrations of Torin 1. A) ACHN and B) UoK111 cells were treated with different concentrations of Torin 1 for two hours, and subsequently harvested and lysed as described in section 2.7. A total of 20 μ g of protein per sample were detected in each lane with the antibodies listed in section 2.1.4. Pan and phospho-protein signals were first normalised using house keeping protein actin. The normalised phospho-protein signal was then divided by the normalised pan-protein signal (see detailed method in section 2.7.7). Densitometry analyses of the blot used to detect phosphorylated TIF-IA in C) ACHN and D) UoK111 cells show that

Torin 1 reduces the phosphorylation of TIF-IA in a concentration-dependent manner in ACHN and UoK111 cells. Data was standardised as described in section 2.7. ctrl=DMSO control: siRNA=ACHN transfected with siRRN3 for 48 hours (negative control). Densitometry analysis was performed on a single set of blots.

From these results, we conclude that the ATP-competitive Torin 1 inhibits TIF-IA phosphorylation at S649 with dose-response behaviour similar to that for inhibition of S6K and 4EBP1 phosphorylation. Allosteric mTOR inhibitors, on the other hand, fail to inhibit TIF-IA phosphorylation at S649. Although rapamycin has been reported to inactivate TIF-IA by decreasing phosphorylation at S44 and enhancing phosphorylation at S199 (186), our findings suggest that the differential effect of allosteric and ATP-competitive mTOR inhibitors on rRNA synthesis might be mediated by inhibition of another mTOR-mediated phosphorylation site of TIF-IA, which is a fundamental component of the RNA polymerase I machinery.

3.1.4 Inhibition of mTOR reduces cell viability of RCC cells

The results above show that we can use an mTOR inhibitor, the ATP-competitive Torin 1, to induce the mTOR-dependent modulation of rRNA synthesis in RCC cell lines. Hence, Torin 1 offers a system by which we can test our hypothesis of sensitisation of cells to the action of a NFI by means of mTOR-mediated modulation on nucleolar activity. Unexpectedly, we have found that allosteric mTOR inhibitors have no noticeable effect on rRNA synthesis. TIF-IA phosphorylation correlates with this differential effect among mTOR inhibitors and presents a plausible mechanism to explain this difference. The lack of rRNA synthesis inhibitory activity by allosteric mTOR inhibitors offers an extra control for our hypothesis since they inhibit mTOR in a manner that does not affect rRNA synthesis. Thus, we would extend our working hypothesis to predict that allosteric mTOR inhibitors would fail to sensitise cells to the action of a NFI.

Therefore, the next step was therefore to determine whether mTOR inhibitors affect cell viability of RCC cell lines using MTT assay. Of particular interest, we wanted to determine whether the differential effect observed on rRNA synthesis would be recapitulated in cell viability. To study overall changes in cell viability we resorted to using the MTT assay (418,464).

3.1.4.1 Optimisation of MTT assay

Prior to conducting the MTT assay to assess cell viability, it was necessary to optimise the seeding density to ensure that a dynamic range sufficient for all the possible cell densities reached in up to three days in culture was achieved. We also optimised the plate layout to account for any edge effects that might cause uneven cell proliferation or drug response. Firstly, a 96-well plate was seeded with 5×10^4 cells per well, 10×10^4 cells per well and 20×10^4 cells per well using triplicates. Cells were treated with increasing concentrations of Torin 1 to enable observation of cell confluency within a range of growth rates, considering the cytostatic effects of Torin 1. After 72-hour incubation at 37°C it was observed that the wells that were seeded with 10×10^4 and 20×10^4 cells per well reached 90-100% confluence, while those seeded with 5×10^4 cells per well were 85% confluent. Similar results were obtained for all the RCC cell lines tested. The seeding density used for all upcoming MTT assays presented in this thesis was 5×10^4 cells per well, which ensured that growth saturation would not be reached by 72hs.

The edge effect has been documented as a problem affecting cell culture using microplates (465), thus, the next step in optimisation involved the assessment of the impact of the distribution of the replicates on the plate on the assay results. In order to be consistent with the range of cell growth rates that would be tested in the following assays, the effect was tested in the presence of Torin 1 for 72 hours. When triplicates were arranged in consecutive groups of three wells the resulting plot of MTT response vs Torin 1 concentration did not follow the expected smooth curve; rather it displayed periodic "jumps" which largely followed the position along a plate row (Figure 3.20). As can be seen in Figure 3.20, the cell viability response (blue, orange and grey dots) was lower in triplicate groups that contained wells close to the edges of the plate (columns 1 and 12, indicated with black border) than in central regions of the plate (the responses within individual rows are indicated in the Figure). The variability within triplicates was also largest in those groups that contained wells close to the edges of the plate, as can be observed by the distribution of the three replicates for each treatment set (Figure 3.20).

The results shown in Figure 3.20, in addition to changes observed in the colour of the culture medium across the plate during the incubation due to the phenol red indicator,

which suggested differential evaporation, indicated that the problem of response in homogeneity across the multiwell plate had to be addressed. For this purpose, 12 ml of sterilised distilled water were added into the space between the wells to preserve humidity within the plate. Additionally, the plate layout was modified as described in section 2.3.1 to distribute the different treatments evenly throughout the plate. After these changes were implemented, the Torin 1 dose-response curve displayed the expected dependence of cell viability (Figure 3.21), and the standard deviation for each concentration set diminished. Thus, the addition of sterilised distilled water to the plate and distribution of the replicates according to plate layout shown in section 2.3.1 were used in all subsequent multiwell plate assays.

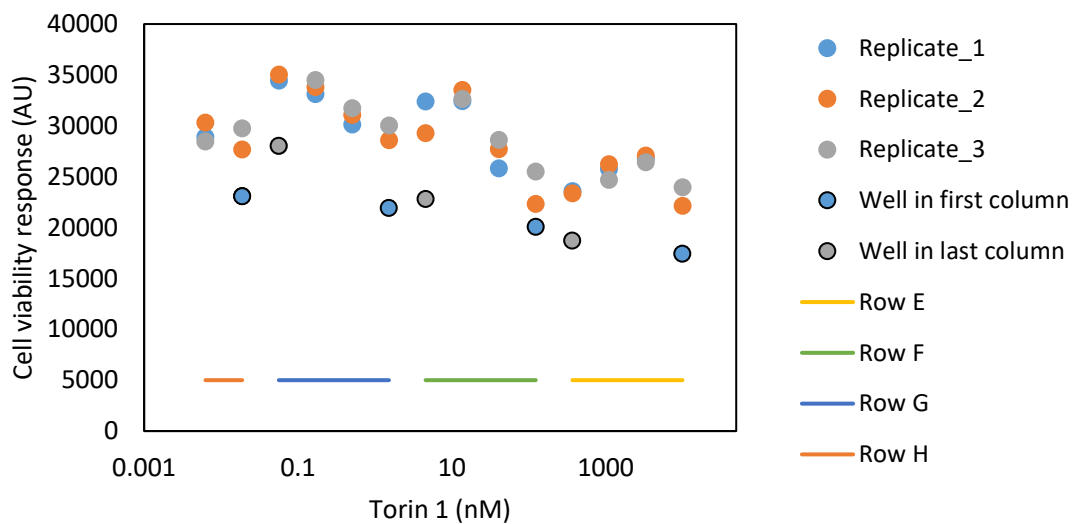


Figure 3.20. Plate effect on cell viability using successive replicates. The blue, orange and grey series represent the cell viability response of the first, second and third replicate, respectively, of ACHN cells treated with increasing concentrations of Torin 1. The black border highlights those wells in the first and last column of the plate, which are the more exposed wells to the evaporation effect. The yellow, green, blue and orange lines represent the distribution of the treatment groups in the different rows of the plate. The plot displays the results of a single experiment.

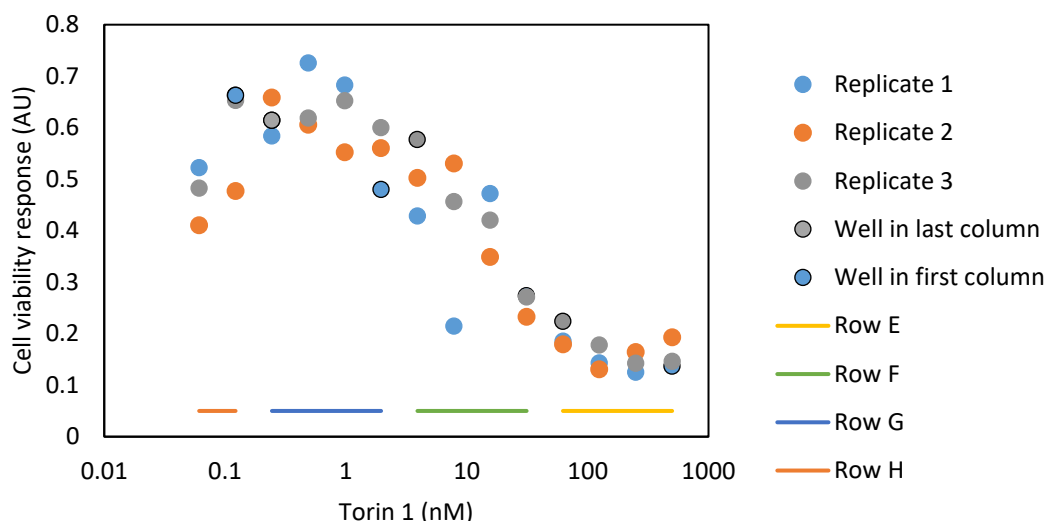


Figure 3.21. Plate effect using alternated replicates. The blue, orange and grey series represent the cell viability response of the first, second and third replicate, respectively, of ACHN cells treated with increasing concentrations of Torin 1. The black border highlights those wells in the first and last column of the plate, which are the more exposed wells to the evaporation effect. The yellow, green, blue and orange lines represent the distribution of the treatment groups in the different rows of the plate. The plot displays the results of a single experiment.

Following optimisation of the plate layout, optimisation of the treatment incubation time for assessment of cell viability with MTT assay was performed on two different RCC cell lines, ACHN and UoK111 cells. Cells were treated with increasing concentrations of ActD for 24, 48 and 72 hours, ensuring a full dynamic range of possible responses to test cell loading that includes cell cycle arrest at low concentrations and cell death at high concentrations. As shown in Figures 3.22 and 3.23, at 24 hours the inhibitory effects of ActD were not as clearly displayed, with a reduction of cell viability of merely 40% and 65% with the highest dose of ActD in ACHN and UoK111 cells, respectively. In comparison, a reduction of 93% and almost 98% of cell viability was achieved with 100 nM of ActD after 72 hours in ACHN and UoK111 cells, respectively. Given that 72 hours was the incubation period that consistently induced a maximal reduction of cell viability in the RCC cell lines, this incubation time was selected for use in all following MTT assays.

Since the maximum screening concentration of ActD used in our assay is 100 nM, we considered that it is unlikely that the effect of ActD on cell viability is mediated by DNA damage, as shown by colleagues in our laboratory (Figure 3.24) (466). This has also been reported by others, see for example (467).

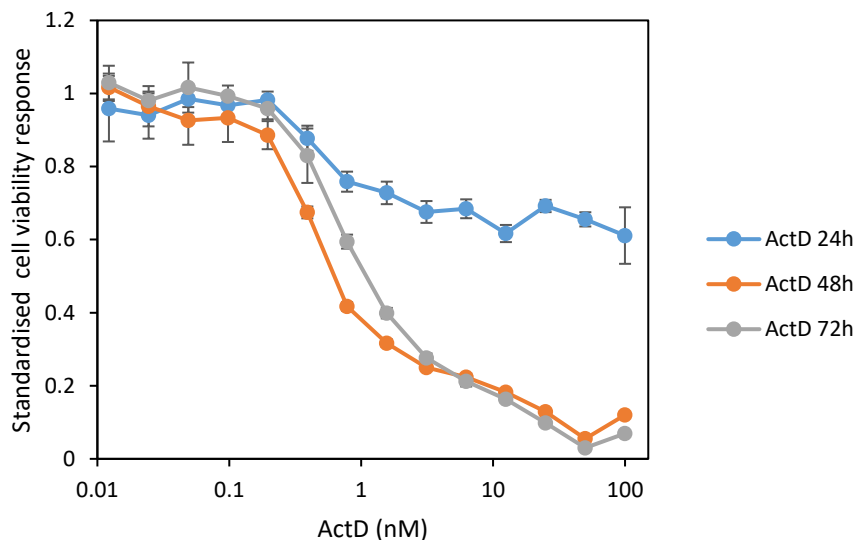


Figure 3.22. Effect of the incubation time with ActD on viability of ACHN cells. The plot shows a decrease of viability in ACHN cells treated with increasing doses of ActD for 24 hours (blue), 48 hours (orange), and 72 hours (grey). The error bars indicate Standard Error of the Mean for replicates of 3 wells of a single experiment.

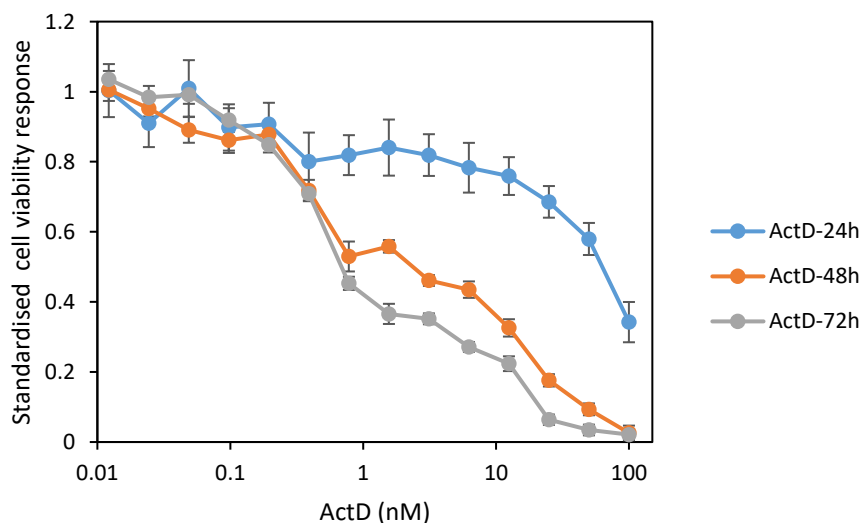


Figure 3.23. Effect of the incubation time with ActD on viability of UoK111 cells. The plot shows a decrease of viability in UoK111 cells treated with increasing doses of ActD for 24 hours (blue), 48 hours (orange), and 72 hours (grey). The error bars indicate Standard Error of the Mean. The error bars indicate Standard Error of the Mean for replicates of 3 wells of a single experiment.

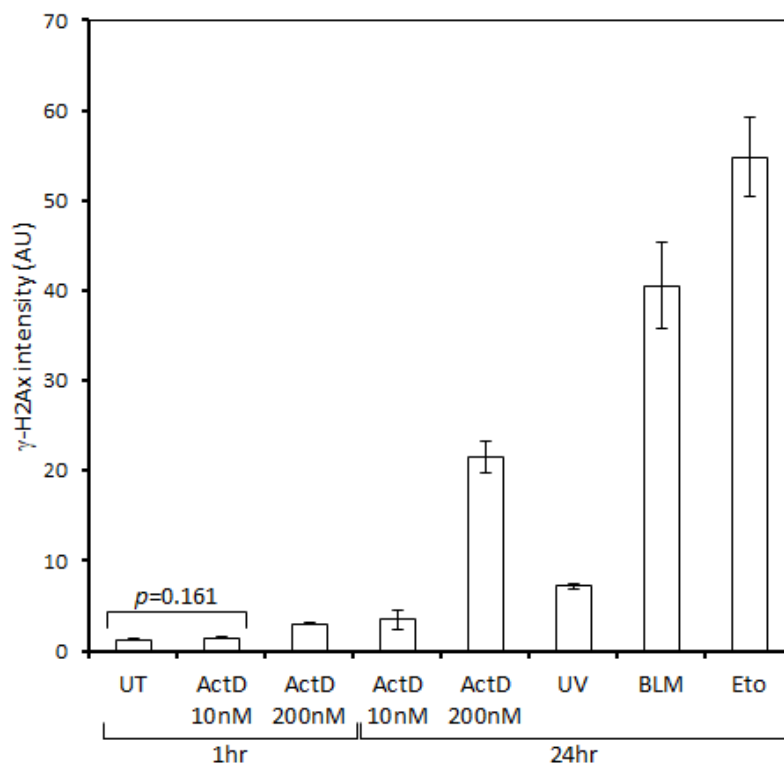


Figure 3.24. Low concentrations of ActD do not promote DNA damage. Detection of γ -H2AX was performed in U2Os cells treated with 10 nM and 200 nM ActD for 1 hour and 10 nM, 200 nM ActD, 10 μ M etoposide, 1 U/ml Bleomycin, and UV 20 J/m² for 24 hours. Figure courtesy of (466).

Considering the evidence of cytotoxicity of DMSO and ethanol on cell culture (468,469), we examined if these solvents used to dissolve the drugs had an effect on cell viability. A titration of DMSO and ethanol revealed that after 72 hours, concentrations below 1% v/v have no apparent effect on cell viability (Figure 3.25). To confirm the lack of effects of these solvents on cell viability, additional assessment was performed on ACHN cells treated with 0.1% v/v ethanol, used as solvent for Temsirolimus, and 0.1% v/v DMSO, used as solvent for the remaining drugs, for 72 hours. The concentration corresponded to the maximum volume of drug stock dilution used in the cell viability assays. An untreated control and a blank were used for each solvent as described in the materials and methods section 2.3.1. The effect of the carriers (in all cases <3%) was not significant when compared to untreated cells (Figure 3.26). Therefore, we conclude that neither solvent has a significant effect on cell viability at the highest concentrations used.

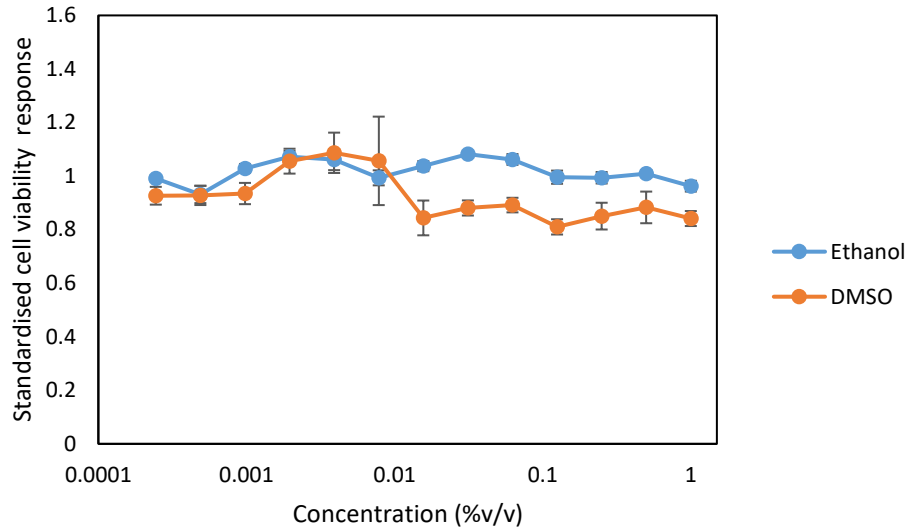


Figure 3.25. Effect of solvents on cell viability. The plot shows the standardised cell viability response of ACHN cells treated with increasing concentrations of ethanol and DMSO for 72 hours. The error bars indicate Standard Error of the Mean. The error bars indicate Standard Error of the Mean for replicates of 3 wells of a single experiment.

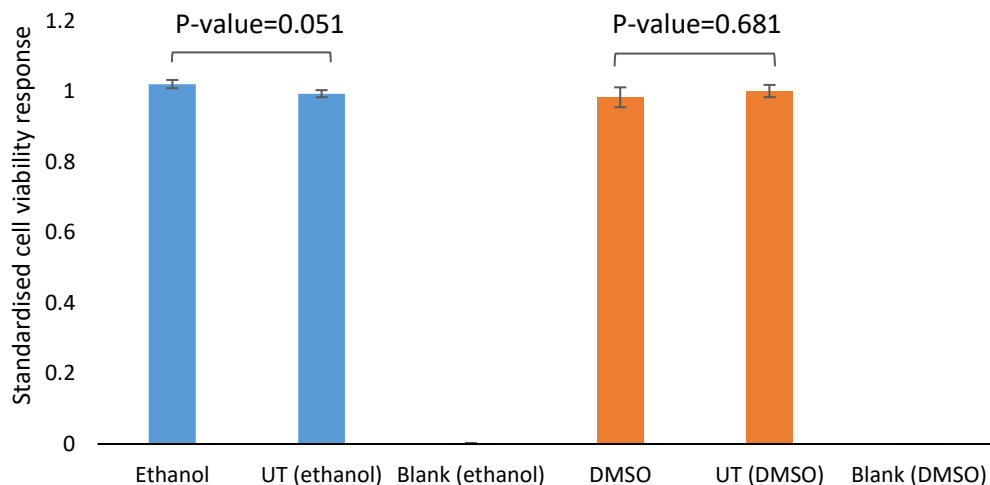


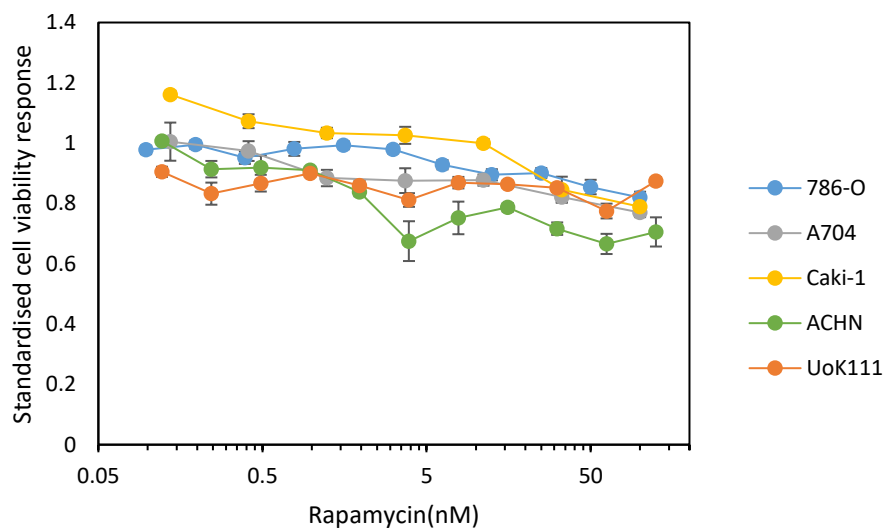
Figure 3.26. Effect of ethanol and DMSO on cell viability in comparison with untreated (UT) ACHN cells. All observations were standardised by dividing by the average of the UT readings as described in the materials and methods section 2.3.3. The error bars indicate Standard Error of the Mean for replicates of 3 wells of a single experiment.

3.1.4.2 ATP-competitive but not allosteric mTOR inhibitors reduces the viability of RCC cells in vitro

To identify any cell line with differential sensitivity to Rapamycin and Temsirolimus that would provide a better system to study effects of mTORis on nucleolar rRNA synthesis, cell viability of 785-O, A704, ACHN, Caki-1 and UoK111 cell lines in response to these drugs was assessed using the MTT assay as described in section 2.3.1. As observed

in Figure 3.27, none of the cell lines displayed a typical response curve within the range of concentrations tested. Higher concentrations of Rapamycin were not used because, as shown in section 3.1.1, the IC₅₀ of Rapamycin for inhibition of phosphorylation of S6K at Thr389 is 5.35 nM and 0.09 nM in ACHN and UoK111 cells respectively, and we reasoned that any effect observed at 100nM or higher could be attributed to other off-target effects of the drug. This criterion for not extending the concentration range in cell viability assays to higher than approximately 100-fold that of the S6K phosphorylation IC₅₀ was subsequently applied to all the allosteric inhibitors which did not show a clear dose response in the MTT assay.

A)



B)

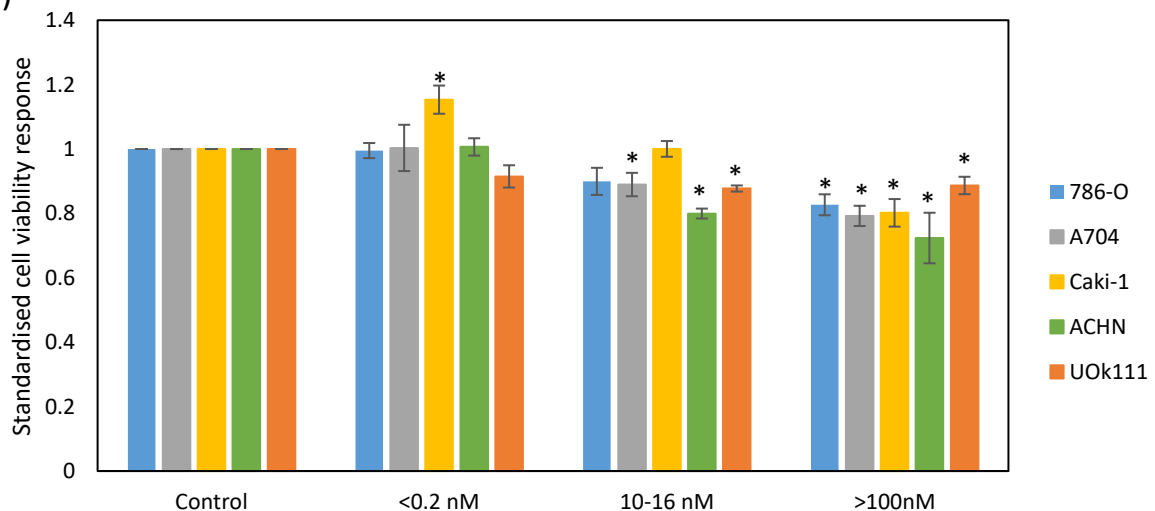


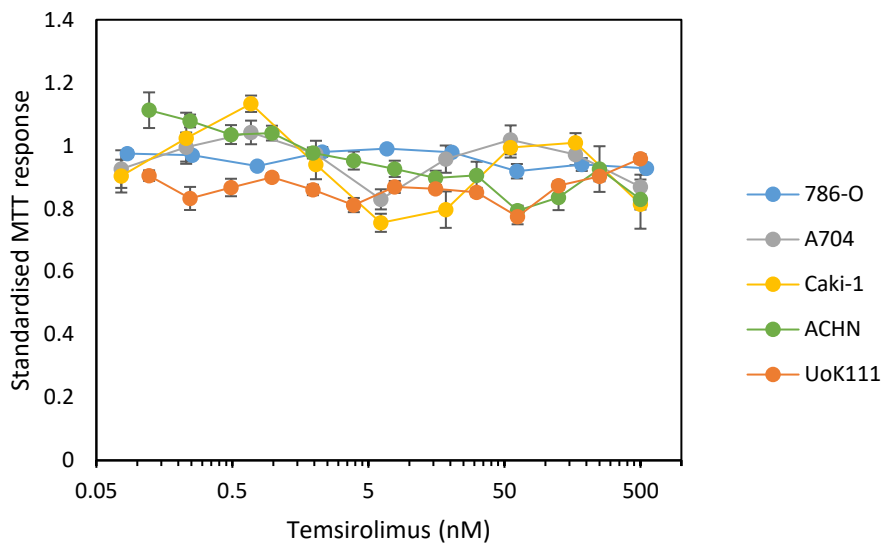
Figure 3.27. Effect of Rapamycin on cell viability of RCC cell lines. A) The plot shows the cell viability of RCC cells in response to increasing concentrations of Rapamycin, calculated as the response in MTT assay standardised by the control, as described in materials and methods, section 2.3.3. The RCC cell lines tested are 785-O (blue), A704 (grey), Caki-1 (yellow), ACHN (green), and

UoK111 (orange). The error bars indicate Standard Error of the Mean for replicates of 3 wells of a single experiment. B) The effect of low, median and high concentrations of rapamycin on the cell viability of each of the cell lines tested was compared to the control using triplicates of a single experiment. * denotes significance with p-values <0.05. Rapamycin concentrations for cell lines were as follows: 786-O=0.19 nM, 12.5 nM, 100 nM; A704=0.13 nM, 11.11 nM, 100 nM; Caki-1=0.13 nM, 11.11 nM, 100 nM; ACHN= 0.12 nM, 15.62 nM, 125 nM; UoK111= 0.12 nM, 15.62 nM, 125 nM.

It is nevertheless noticeable that in some cell lines (particularly ACHN and UoK111) the standardised MTT signal over the whole concentration range of Rapamycin used is clearly below controls (<1.0 in the standardised plots). Moreover, while an IC₅₀ cannot be calculated and no maximum effect within the concentration range tested, cell decreases with concentration in all cell lines tested (p<0.05). While this concentration-dependent reduction in cell viability does not resemble a typical dose-response curve, it is significant compared to the control (p-value<0.05) (Figure 3.27 B) and is likely caused by the drug since the data shown in Figure 3.25 make it unlikely to be a solvent effect. It should be noted that this effect on cell viability recapitulates the reduction in incorporation of 5-EU by allosteric mTOR inhibitors discussed above (section 3.1.2.3). We also note that these results differ slightly from the Genomics of Drug Sensitivity in Cancer (GDSC) database (470), where 786-O cells were reported to be more sensitive to Rapamycin than ACHN (Figure 3.27).

The same cell lines were then treated with Temsirolimus for 72 hours. With concentrations as high as 500 nM, none of the cell lines displayed a response curve within the range of concentrations tested (Figure 3.28). However, we still observed a small but significant (p<0.05 for all cell lines except A704) concentration-dependent reduction of cell viability over the concentration range tested. Interestingly, some cell lines (including UoK111) showed a response below the controls (<1.0 following standardisation) for the whole concentration range tested. As discussed above for Rapamycin, we do not consider this reduction in cell viability to be a solvent artefact.

A)



B)

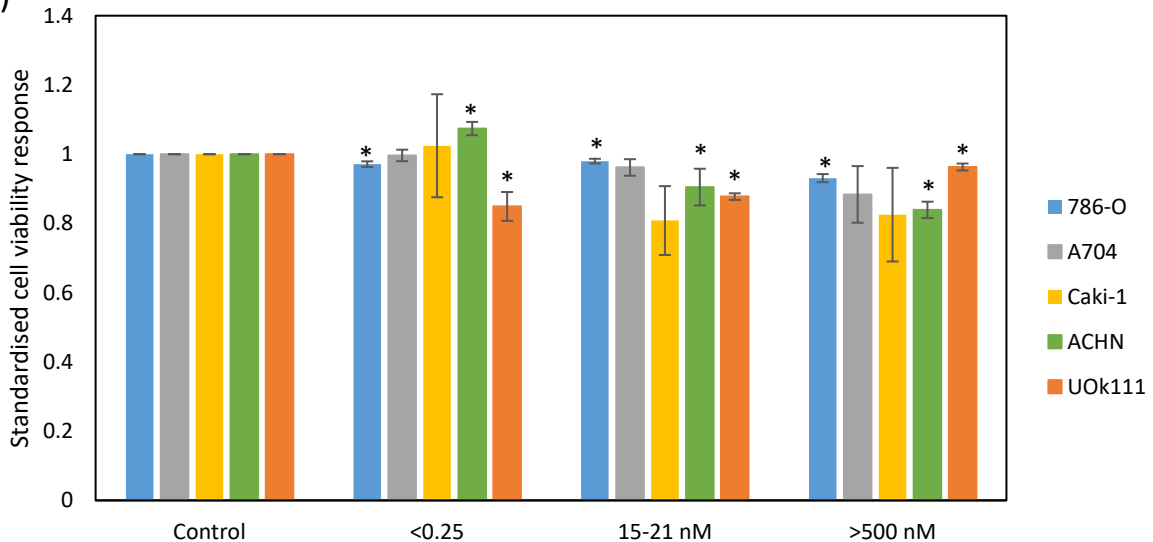
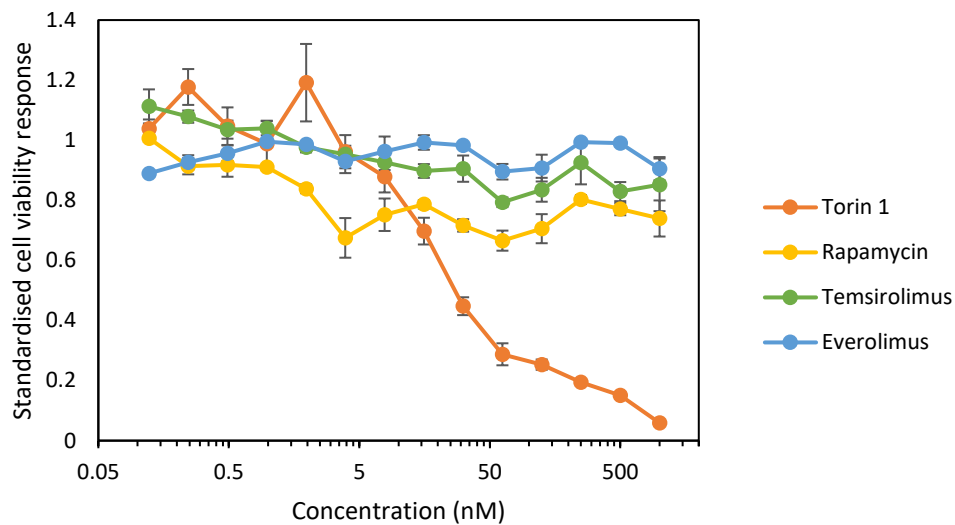


Figure 3.28. Effect of Temezirolimus on cell viability of RCC cell lines. A) The plot shows the cell viability of RCC cells in response to increasing concentrations of Temezirolimus, calculated as the response in MTT assay standardised by the control, as described in materials and methods, section 2.3.3. The RCC cell lines tested are 785-O (blue), A704 (grey), Caki-1 (yellow), ACHN (green), and UoK111 (orange). The error bars indicate Standard Error of the Mean for replicates of 3 wells of a single experiment. B) The effect of low, median and high concentrations of temezirolimus on the cell viability of each of the cell lines tested was compared to the control using triplicates of a single experiment. * denotes significance with p-values <0.05. Temezirolimus concentrations for cell lines were as follows: 786-O=0.25 nM, 20.58 nM, 555.5 nM; A704=0.22 nM, 18.52 nM, 500 nM; Caki-1=0.22 nM, 18.52 nM, 500 nM; ACHN= 0.24 nM, 15.62 nM, 500 nM; UoK111= 0.24 nM, 15.62 nM, 500 nM.

Since no differential effect was observed *in vitro* with either drug, among cell lines, we selected ACHN and UoK111 cells, which the lab was familiar with their growth characteristics and that provided an example of p53wt and p53mut. The reason for this is the role of the nucleolus as a modulator of p53 levels. However, p53wt in RCC

does not appear to have any functional activity (471). As observed in Figures 3.29 and 3.30, the viability of ACHN and UoK111 cells was inhibited by Torin 1 in a concentration-dependent manner, with an IC₅₀ of 29 nM for ACHN cells and 76.4 nM for UoK111 cells. ACHN cells treated with Rapamycin, Temsirolimus and Everolimus do not display a response curve within the range of concentrations tested for either allosteric mTOR inhibitor. However, the concentration-dependent reduction in MTT signal is clearly observable for Rapamycin and Temsirolimus, as was discussed earlier.

A)



B)

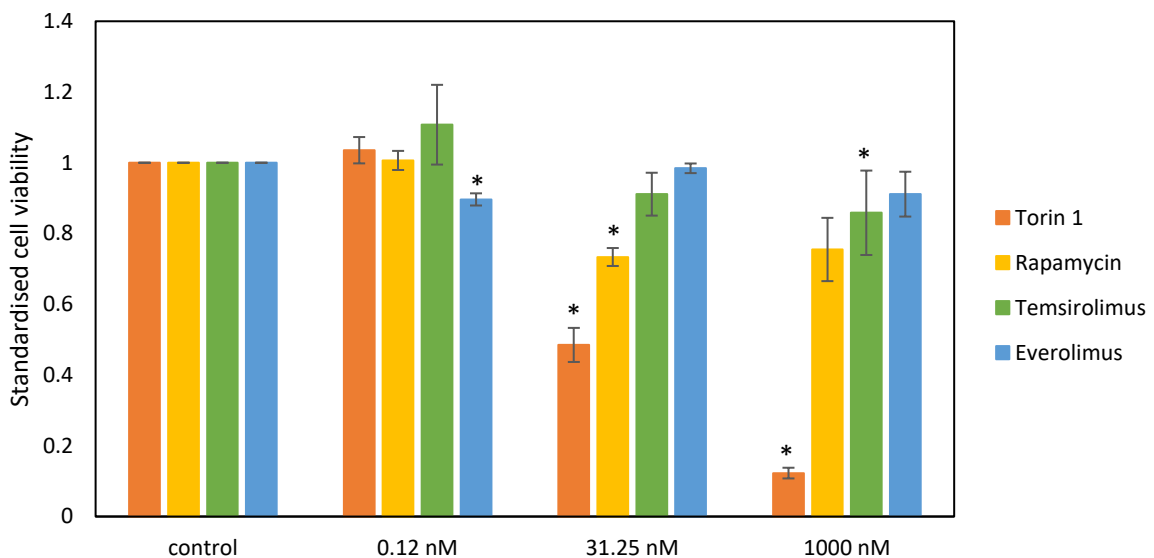
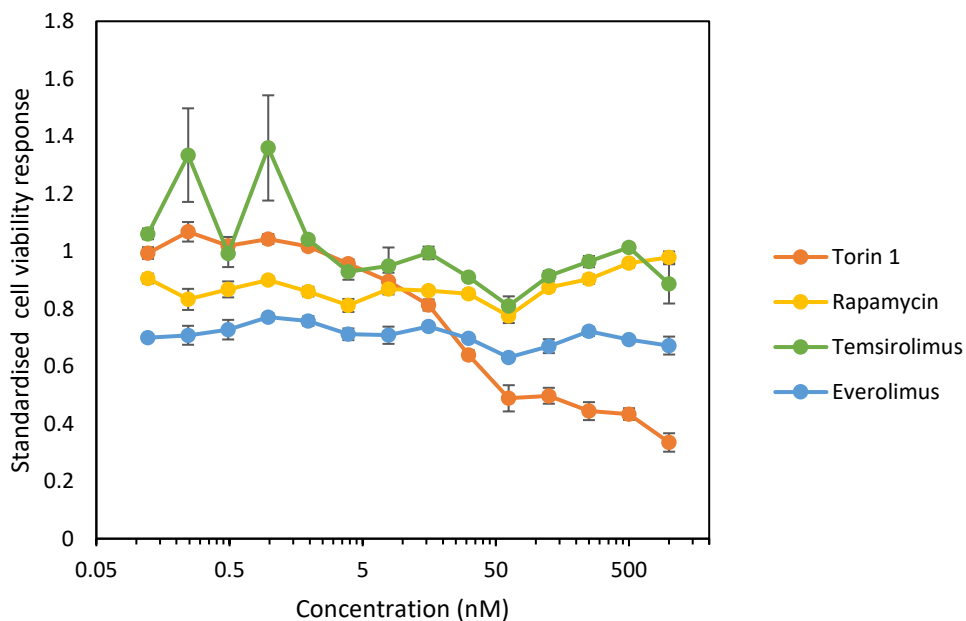


Figure 3.29. Effect of mTOR inhibitors on cell viability of ACHN cells. A) The plot shows the cell viability response of ACHN cells to increasing concentrations of Torin 1 (orange), Rapamycin (yellow), Temsirolimus (green), and Everolimus (blue), calculated as the response in MTT assay standardised by the control as described in materials and methods section 2.3.3. The error bars indicate Standard Error of the Mean for replicates of 3 wells of a single experiment. B) The effect of 0.12 nM, 31.25 nM,

and 1000 nM of different mTORis on the cell viability of ACHN cells was compared to the control using triplicates of a single experiment. * denotes significance with p-values <0.05.

Similar to ACHN cells, UoK111 cells treated with increasing concentrations of Torin 1 also show a reduction of cell viability (Figure 3.30). Even though the maximum effect is not observed within the range of concentrations tested, a clear concentration-dependent inhibition of cell viability is observed in Torin 1-treated UoK111 cells. As in the case of ACHN cells, UoK111 cells treated with the allosteric mTOR inhibitors Rapamycin and Temsirolimus show again a lower MTT signal across all the concentrations tested, although there is no apparent concentration-dependent reduction in cell viability (Figure 3.30). Although a slight reduction of viability is observed in Uok111 cells treated with Everolimus, there is not a response curve observed but rather the effect remains stable within the whole range of concentrations tested. Together, these results suggest that, at least in RCC cell lines, inhibition of both mTORC1 and mTORC2, which is achieved by ATP-competitive inhibitor Torin 1, is necessary to reduce cell viability effectively.

A)



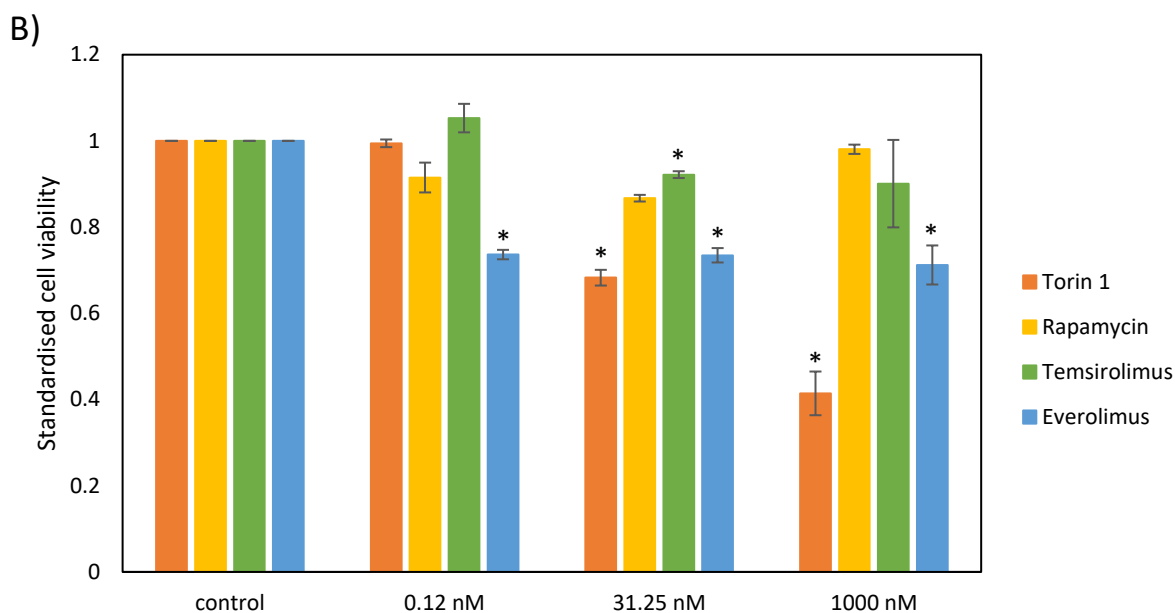
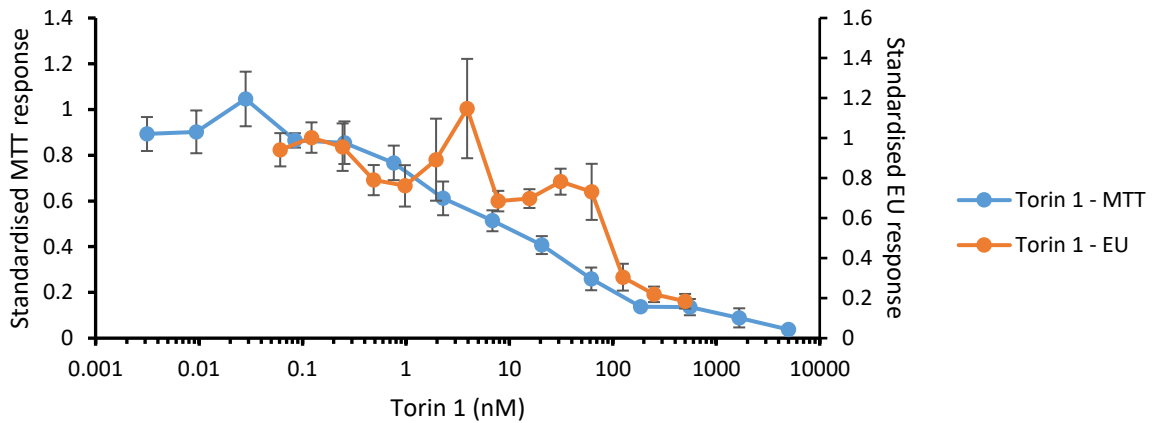


Figure 3.30. Effect of mTOR inhibitors on cell viability of UoK111 cells. The plot shows the cell viability response of UoK111 cells to increasing concentrations of Torin 1 (orange), Rapamycin (yellow), Temsirolimus (green), and Everolimus (blue), calculated as the response in MTT assay standardised by the control as described in materials and methods section 2.3.3. The error bars indicate Standard Error of the Mean for replicates of 3 wells of a single experiment. B) The effect of 0.12 nM, 31.25 nM, and 1000 nM of different mTORis on the cell viability of UoK111 cells was compared to the control using triplicates of a single experiment. * denotes significance with p-values <0.05.

Having demonstrated that Torin 1 but not the allosteric inhibitors, a) reduces rRNA synthesis of ACHN and UoK111 cells (Figures 3.13 and 3.14) and inhibits phosphorylation TIF-1A (Figures 3.17 and 3.18); and b) reduces the cell viability of ACHN and UoK111 cells (Figures 3.29 and 3.30), we speculated that nucleolar function inhibition could be a major mediator of the cell viability reduction caused by Torin 1 *in vitro*. It would have been desirable to be able to test this interesting hypothesis directly. However, this cannot be done directly since abrogation of nucleolar function in order to detect any nucleolus-independent activity of Torin 1 on cell viability would cause cell death. Instead, we explored to what extent the dose responses for rRNA synthesis and cell viability inhibition matched each other. As can be observed in Figures 3.31 A and B, both cell lines displayed curves with response regions closely matching each other. This is particularly noticeable in UoK11 cells, where the cell viability and rRNA synthesis curves overlap extensively throughout the response range. These results give strength to our hypothesis that nucleolar function inhibition is a major component of the cell viability reduction caused by Torin 1 *in vitro*.

A)



B)

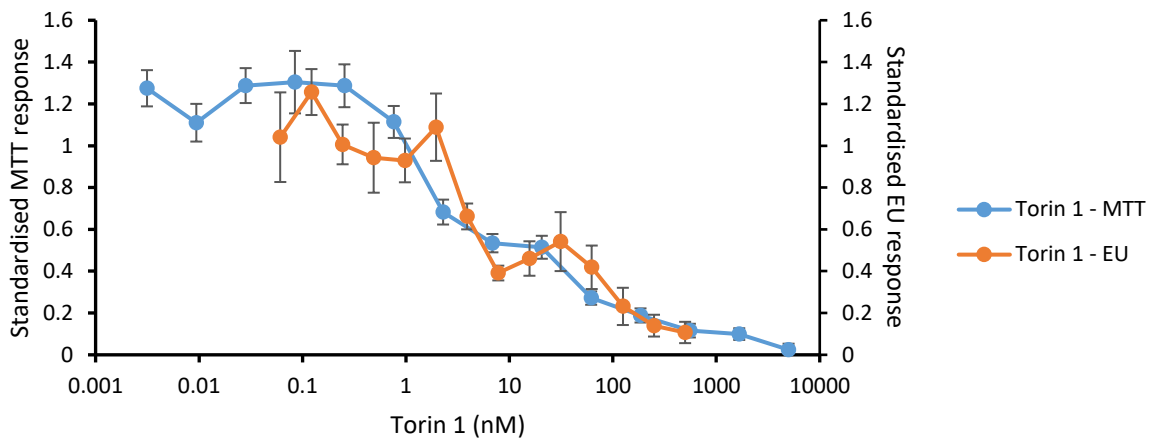


Figure 3.31. Inhibition of cell viability and rRNA mediated by Torin 1 in RCC cells. The effect of Torin 1 on cell viability (blue) was assessed on A) ACHN and B) UoK111 cells treated with Torin 1 for 72 hours. The effect of Torin 1 on rRNA synthesis (orange) was measured in A) ACHN and B) UoK111 treated with Torin 1 for 2 hours and labelling nascent rRNA for the last 30 min with 5-EU. 5-EU detection, imaging and analysis were performed as described in materials and methods section 2.5 The error bars indicate Standard Error of the Mean for replicates of 3 wells of a single experiment.

3.1.5 ActD and Torin 1 cause different cell cycle changes associated with loss of cell viability

The cell viability assay used so far does not inform us on whether any reduction in the number of viable cells is due to a reduction in the rate of proliferation or an induction of cell death. Thus, cell cycle analysis was performed using flow cytometry.

3.1.5.1 Optimization of flow cytometry assay

Prior to conducting the flow cytometry assay we optimised the detection of S-phase cells by incorporation of EdU in nascent DNA followed by detection with Click-chemistry. In order to determine the EdU-incubation time that provides the optimal incorporation of EdU to detect the cell cycle stage of the cells, cells were pulsed with EdU for 15, 30 or 60 minutes as described in section 2.4.3, followed by fixation, staining for incorporated EdU with FITC-azide (Click detection) and total DNA with 7-AAD, and flow cytometric analysis. As can be observed in the density plots on Figure 3.32, a 60-minute incubation provides a better resolution of the percentage of cells in S phase from the percentage of cells in G1 and G2, due to a higher incorporation of EdU detected with the BL-1 channel (see materials and methods section 2.4.3 for description of the channels used), while still maintaining an acceptable labelling time.

To confirm that the assay is capable of identifying cell cycle changes in ACHN and UoK111 cells, cells were treated with ActD for 72 hours, then pulsed with EdU, fixed and stained as described in the materials and methods section 2.4. The concentrations of ActD used in this assay were determined as the concentrations of ActD that achieve minimum, half-maximum, and maximum inhibitory effect in cell viability. As can be observed in Figure 3.33, ACHN cells treated with 2.5 nM ActD show a decreased percentage of cells in S-phase and an increased percentage of cells in G1 compared to control and cells treated with 0.25 nM ActD (concentration that induces minimum inhibition of cell viability), which is consistent with cell cycle arrest at 2.5nM ActD and no effect on cell cycle or cell viability at 0.25nM. A slight increase in the percentage of cells with sub-G1 DNA content is also observed in cells treated with 2.5 nM ActD reflecting cell death, which for ActD is typically apoptotic (472). A complete shutdown of S-phase occurs in ACHN cells treated with 25 nM ActD, along with significant increase of cell death compared to control and cells treated with 0.25 nM and 2.5 nM ActD. Correlation between increasing concentrations of ActD with increased cell death and decreased percentage of cells in S-phase was confirmed with Spearman's correlation coefficients of 0.8 and -0.8, respectively, although the correlation is not significant as there is not enough data. Figure 7.7 in the appendix presents the dot plots and histograms created for identification of percentage of ACHN cells in G1, S, G2 and cell death after treatment with increasing concentrations of ActD.

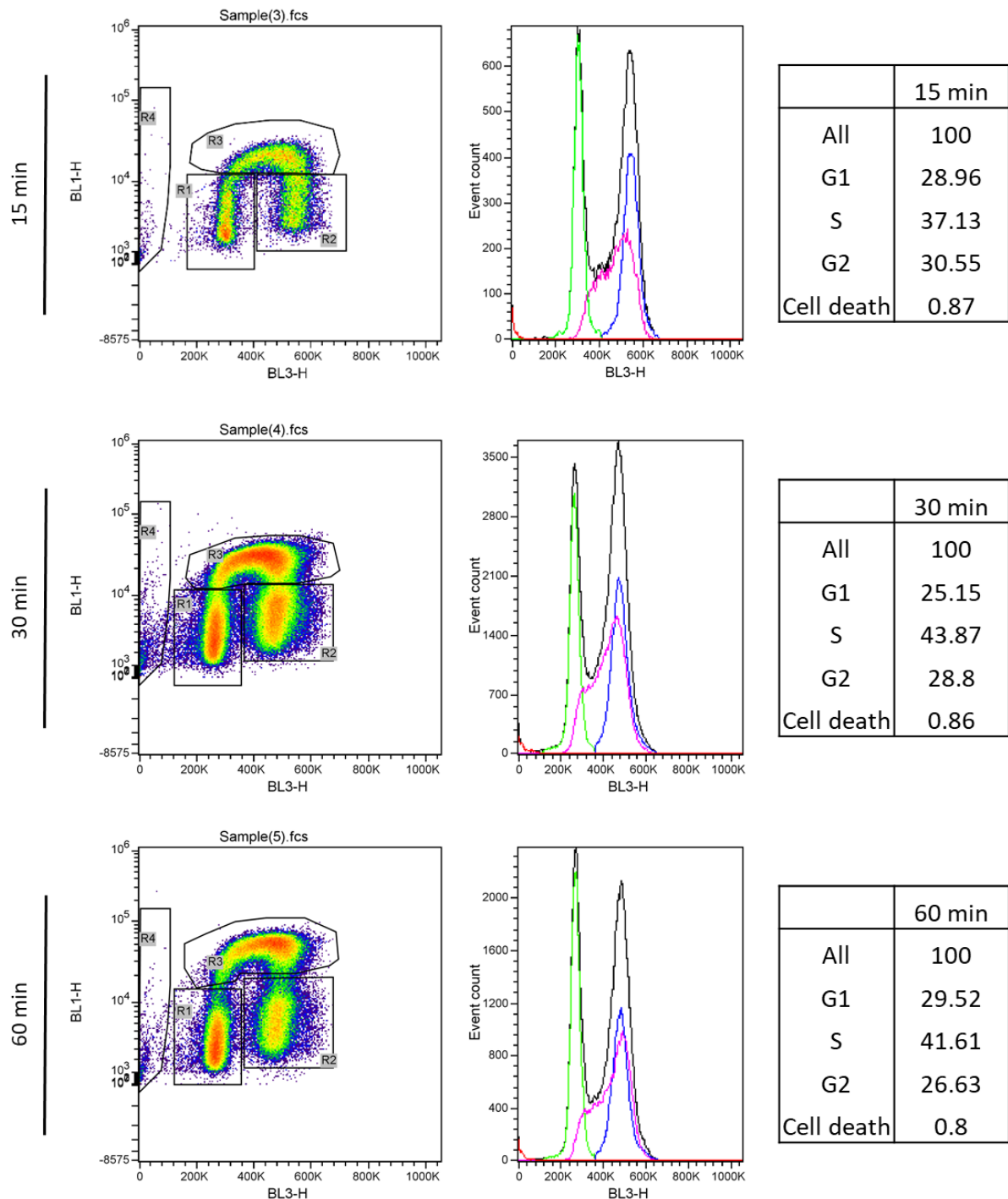


Figure 3.32. Testing of different EdU-incubation times for optimal segmentation of cell cycle stages using labelled nascent DNA with EdU and detection using Click and flow cytometry. The density dot plots illustrate gating of cell populations in G1 (R1), S (R3), G2 (R2) phases, and dead cells (R4) depending on the signal of total DNA detected by 7-AAD staining on the X-axis and the nascent DNA labelled with Click-chemistry, detected by 6-FAM staining on the Y-axis. The histogram displays an overlay of the cell populations in G1 (green), S (pink), G2 (blue), and cell death (red) identified in the density plots, in respect to the 7-AAD fluorescent intensity, which is correlated to the amount of DNA within each cell. The tables on the right present the percentage of cells in the different stages of cell cycle according to intensity of 7-AAD and 6-FAM in the density plots. Initial population was gated to reject doublets using Attune recommended peak height vs Area, as described in method and materials section 2.4.6.

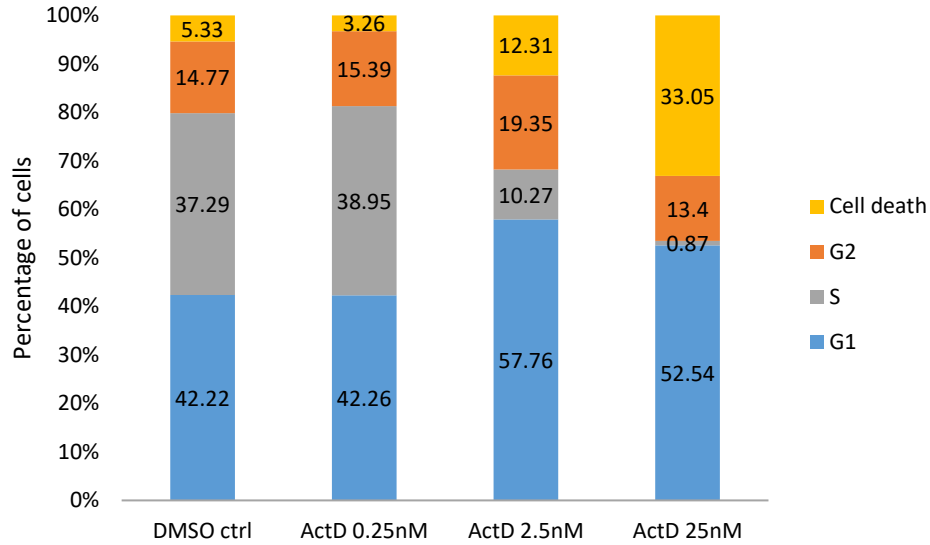


Figure 3.33. Identification of cell cycle changes in ACHN cells treated with ActD by labelling nascent DNA with EdU and detecting using Click and flow cytometry. Identification of cell populations in ACHN cells treated with increasing concentrations of ActD was performed as described in materials and methods section 2.4.6. The percentage of cells in S-phase diminishes in ACHN cells treated with increasing concentrations of ActD. The percentage of dead cells increases with increasing concentrations of ActD. The percentage of the cells distributed in the different stages of cell cycle was performed on data obtained from a single experiment.

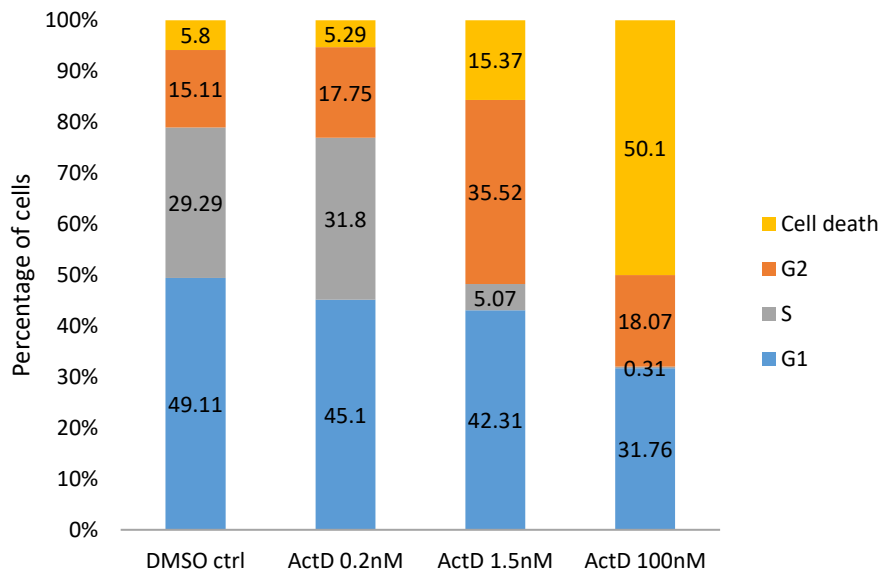


Figure 3.34 Identification of cell cycle changes in UoK111 cells treated with ActD by labelling nascent DNA with EdU and detecting using Click and flow cytometry. Identification of cell populations in UoK111 cells treated with increasing concentrations of ActD was performed as described in materials and methods section 2.4.6. The percentage of cells in S-phase diminishes in UoK111 cells treated with increasing concentrations of ActD. The percentage of dead cells increases with increasing concentrations of ActD. The percentage of dead cells increases with increasing concentrations of ActD. The percentage of the cells distributed in the different stages of cell cycle was performed on data obtained from a single experiment.

UoK111 cells treated with 1.5 nM ActD (IC₅₀ for inhibition of viability of UoK111 cells, Figure 3.34) also display arrest of cell cycle with decreased percentage of cells in S-phase and increased percentage of cells in G₂, compared to the control (Figure 3.34). The percentage of dead cells increases in this group compared to the control and treatment with 0.2 nM ActD. UoK111 treated with 100 nM display complete shutdown of S-phase and induction of cell death. As with ACHN cells, a strong correlation was established between increasing concentrations of ActD and increased sub-G₁ population with a Spearman's correlation coefficient of 0.8, while a strong negative correlation between increasing concentrations of ActD and percentage of cells in S-phase was observed, with a coefficient of -0.8, however there is not enough power to establish significance. Figure 7.8 in the appendix shows the analysis of flow cytometry data using dot plots and histograms for identification of percentage of UoK111 cells in G₁, S, G₂ and cell death after treatment with increasing concentrations of ActD.

To further demonstrate the capacity of our system to detect cell cycle changes we assessed the changes in ACHN cells in conditions of perturbation of the cell cycle completely independent from the ones we intended to test. For this purpose, ACHN cells were treated either with 10 μM etoposide, which induces arrest in the G₂ phase (473) or with 1 μM staurosporine, which is a potent inducer of apoptosis (474) for 24 hours, then pulsed with EdU, fixed and stained as described in section 2.4. As can be observed in Figure 3.35, ACHN cells treated with etoposide show the expected increase in G₂ phase cells at the expense of G₁ and S phases, While ACHN cells treated with staurosporine display a marked increase in sub-G₁ cells (cell death). Taken together, these results confirm that the technique is capable of detecting changes in all phases of the cell cycle.

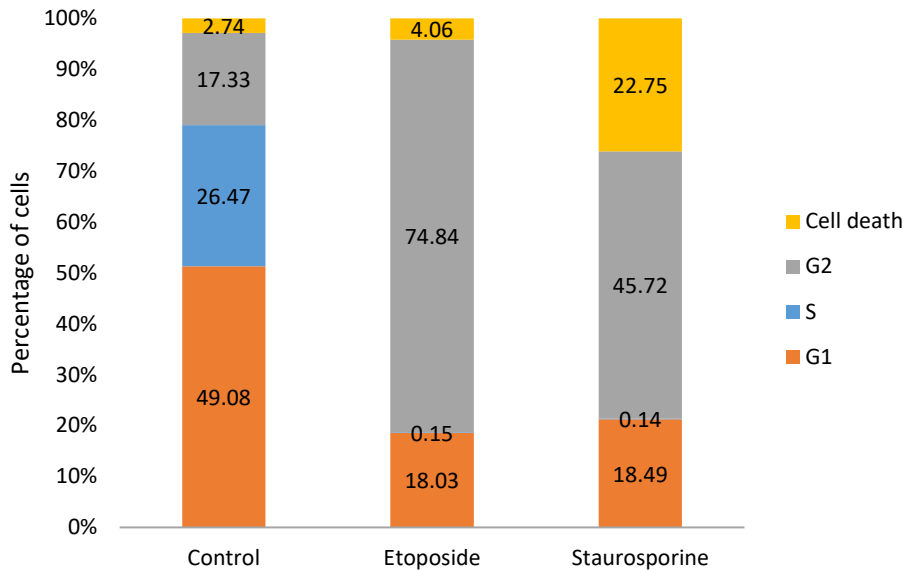


Figure 3.35. Identification of cell death and segmentation of cell populations into cell cycle stages in ACHN cultures treated with staurosporine and etoposide for 24 hours. The stacked column plot shows the different cell populations (G1, S, G2, and cell death) identified within the control, etoposide-treated and staurosporine-treated cultures by detection of EdU-labelled DNA with Click-chemistry and 7-AAD staining using flow cytometry.

3.1.5.2 Cell cycle changes induced by ActD in RCC cells

Having validated the flow cytometry technique used, we next analysed the cytostatic and cytotoxic effect of ActD on ACHN and UoK111 cells, we compared the observed percentages of S-phase cells and sub- G1 cells in independent experiments. Figure 3.36 shows the percentages of cells observed for each of those populations in ACHN and UoK111 cells treated with ActD doses that corresponded to the IC₅₀ and minimum and maximum plateau regions of the cell viability response curves (Figures 3.22 and 3.23). As can be seen in Figure 3.36 A and B, the effect of ActD doses over the maximum slope region (IC₅₀) of the viability dose response curve is more marked on the proportion of cells in S-phase, while strong induction of cell death is only observed at high doses. It is noticeable that the error bars for most of the means are relatively small for n=5, demonstrating the strong reproducibility of the flow cytometry analysis. The exceptions to this are the error bars in S-phase fraction of UoK111 cells at IC₅₀ (probably due to an underestimation of the IC₅₀ in a region of maximal dose dependence), and the fraction of dead cells in both cell lines at maximum ActD dose (probably due to cell fragility and variability in the recovery of dead cells).

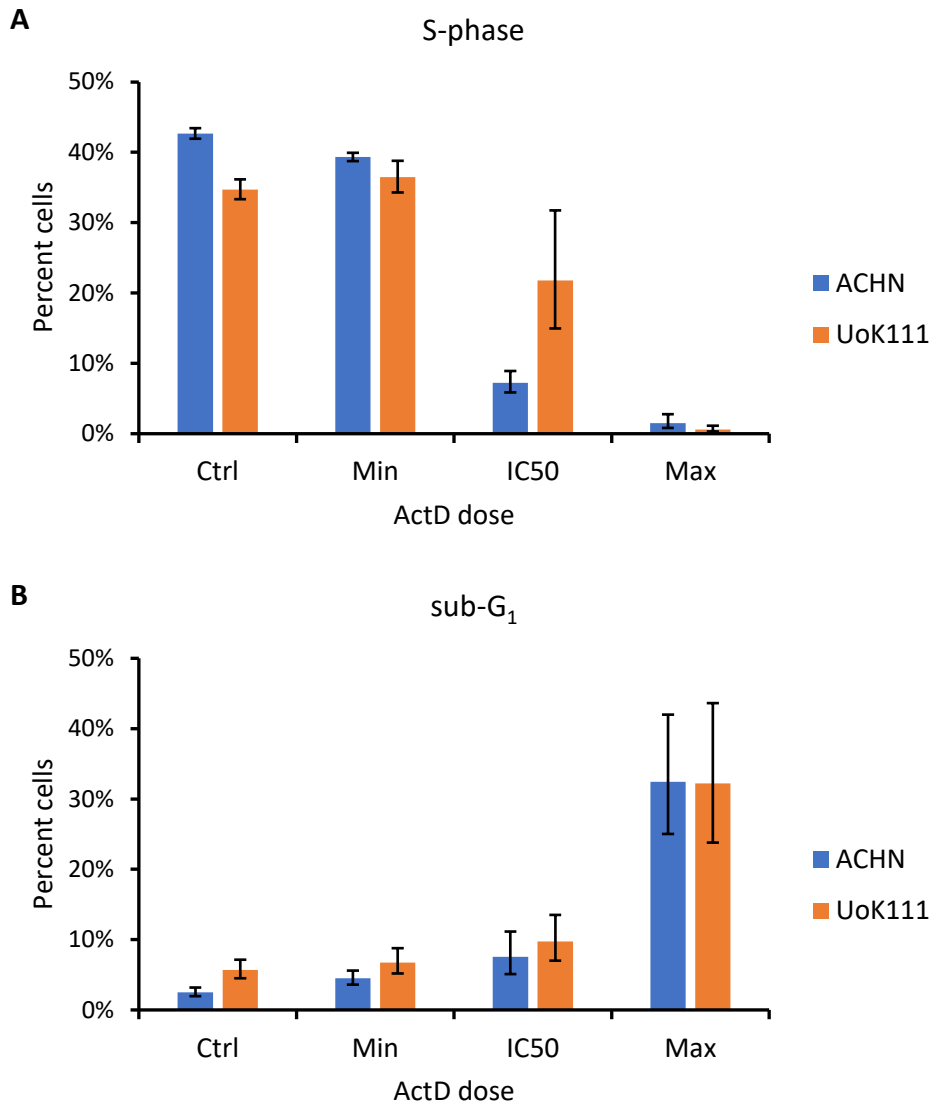


Figure 3.36 Percentage of S-phase cells (A) and sub-G₁ cells (B) detected by flow cytometry on ACHN and UoK111 cells (indicated) treated either with DMSO (Ctrl) or with different doses of ActD. The ActD doses were obtained from the cell viability dose-response curves and were as follows: ACHN cells: Min=0.25nM, IC50=2.5nM, Max=25nM; UoK111 cells: Min=0.2nM, IC50=1.5nM, Max=100nM. Bars indicate mean percentages from 5 independent experiments. The error bars indicate Standard Error of the Mean.

ANOVA appears as a reasonable approach for the multifactorial analysis of differences in percentages of a cell cycle population under different treatments; however, the statistical distributions of percentages or proportions are not symmetrical and normal, thus precluding the standard ANOVA approach. The solutions to this problem are a) “normalisation” of proportions using a logit transform, or b) using a non-parametric test such as Kruskal-Wallis. In addition, to demonstrate that the effects of ActD on S-phase and sub-G₁ fractions are concentration-dependent we applied Spearman’s correlation analysis whereby the p-value obtained indicates whether the

correlation is statistically significant and the sign of the ρ parameter indicates whether the effect increases (+) or decreases (-) with increasing ActD concentration. Table 3.2 shows the p-values obtained using each of those approaches.

Table 3.2. Multifactorial analysis of the cell cycle fractions shown in Figure 3.36 A and B. Numbers indicate the p-values calculated for the different statistical tests indicated in the text, except for Spearman's analysis, where ρ is also shown. Note that for ANOVA the Bonferroni-corrected significance level is 0.0125.

Fraction	Cell Line	Uncorrected	logit	K-W	Spearman		n
					ρ	p-value	
sub-G ₁	ACHN	0.0026	0.0002	0.0057	0.826	7.1 x10⁻⁰⁶	5
	UoK111	0.0002	0.0011	0.0099	0.752	0.0001	5
S-phase	ACHN	8.50x10⁻¹¹	6.77x10⁻⁶	0.0022	-0.84	3.41 x10⁻⁰⁶	5
	UoK111	4.25x10⁻⁵	1.26x10⁻⁶	0.0120	-0.628	0.003	5

The data shown in Table 3.2, validates the conclusions from Figure 3.36 A and B that both the S-phase and sub- G₁ fractions vary with ActD treatment in a dose-dependent manner in both cell lines studied. This data supports the conclusions from Figure 3.36 A and B mentioned above, that cell death becomes prominent only at high ActD doses (the maximum plateau region in the cell viability dose-response curve – see figures 3.22 and 3.23).

3.1.5.3 ATP-competitive mTORC1/2 inhibitors have a cytostatic effect on RCC cells

To examine the effect of mTOR inhibitors on the cell cycle, and to determine if the reduction of cell viability of ACHN and UoK111 cells treated with Torin 1 observed in section 3.1.3 is caused by a cytostatic effect driving cell cycle arrest or by promotion of cell death, the cell cycle profiles at key concentrations were analysed on ACHN and UoK111 cells treated with increasing concentrations of Torin 1. ACHN cells were treated with 0.5 nM, 15 nM and 500 nM Torin 1 for 72 hours, and processed for EdU/7AAD labelling and flow cytometric analysis as described in section 2.4. Analysis of flow cytometry data is shown in the appendix section 7.4.

As observed in Figure 3.37 A), 0.5 nM Torin 1, a concentration within the region with no effect on cell viability (see Figure 3.29), has no apparent effect on the cell cycle of ACHN cells, with comparable percentages of cells in G1, S, G2 and cell death to those obtained in the untreated control. The percentage of cells in S-phase is slightly reduced in a concentration dependent manner in concentrations between 0.5-100 nM. However, complete shutdown of S-phase is achieved in ACHN treated with 500 nM Torin 1.

Similarly, Figure 3.37 B) shows that treatment of UoK111 cells with increasing concentrations of Torin 1 taken from Figure 3.30, reduce the percentage of cells in S-phase in a concentration-dependent manner. Together, these results suggest that Torin 1 has a cytostatic effect on ACHN and UoK111 cells, promoting cell cycle arrest.

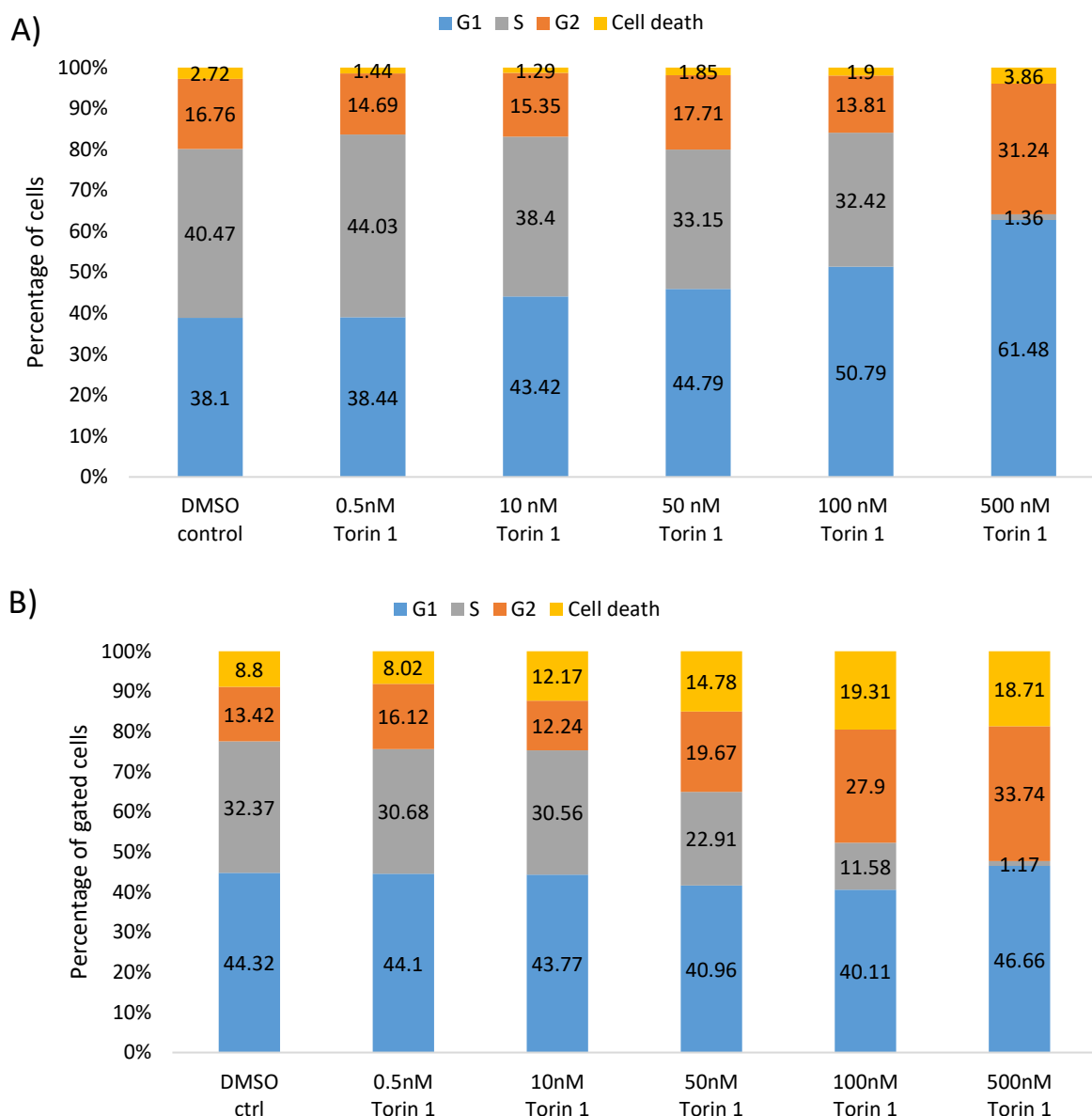


Figure 3.37. Effect of increased concentrations of Torin 1 on the cell cycle of A) ACHN and B) UoK111 cells. The stacked column plot displays the percentage of cells identified as populations in G1, S, G2, and cell death detecting EdU-labelled DNA with Click-chemistry and 7-AAD staining using flow cytometry. The percentage of dead cells increases with increasing concentrations of ActD. The percentage of the cells distributed in the different stages of cell cycle was performed on data obtained from a single experiment.

An analysis similar to the one shown for ActD in Figure 3.36 was also performed on flow cytometry data for Torin 1-treated cells and is shown in Figure 3.38 A and B. The doses for each experiment were determined from an accompanying cell viability dose-response study and fell in the concentration ranges indicated in the figure legend.

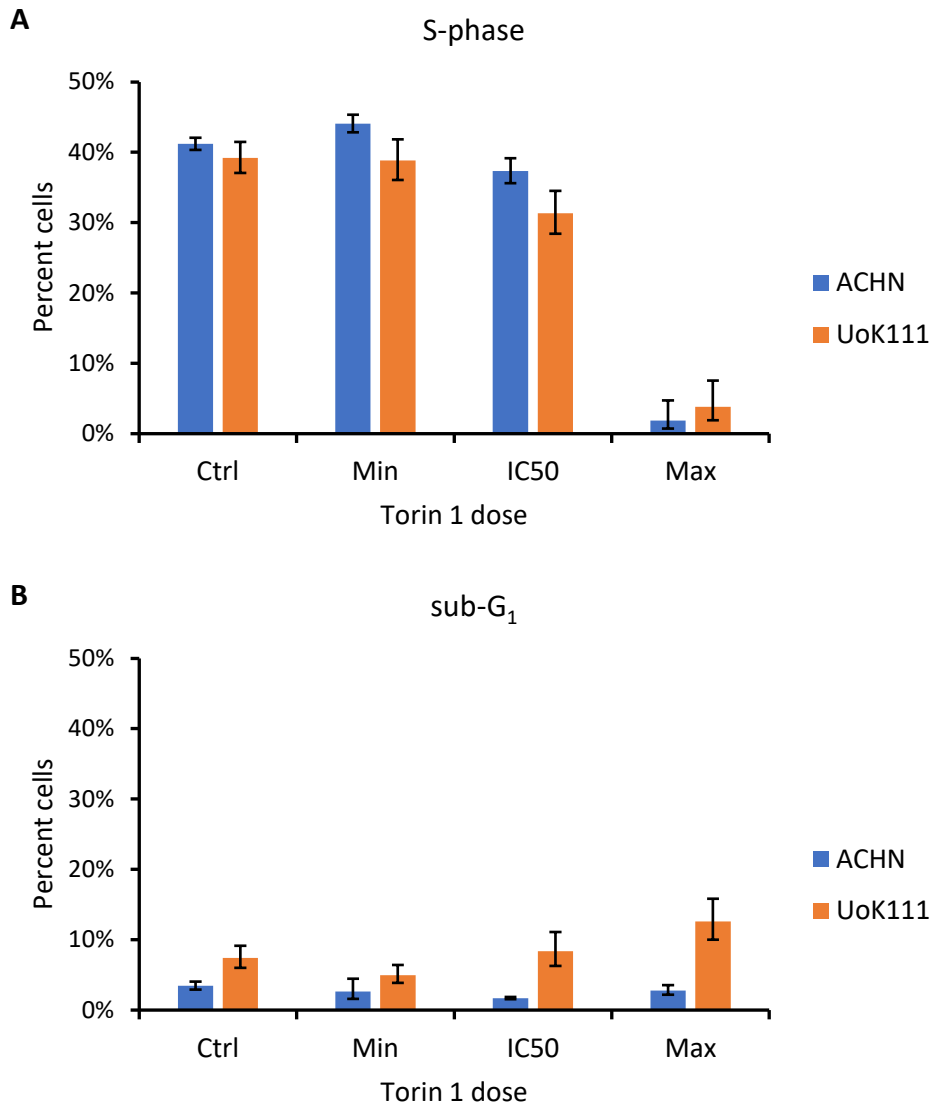


Figure 3.38. Percentage of S-phase cells (A) and sub-G₁ cells (B) detected by flow cytometry on ACHN and UoK111 cells (indicated) treated either with DMSO (Ctrl) or with different doses of Torin 1. The Torin 1 doses were obtained from the cell viability dose-response curves and were as follows: Min=doses below 5nM, IC50=10-50nM, Max=100nM or larger. Bars indicate mean percentages from 3-4 independent experiments. Error bars indicated SEM. The scale of the vertical axis in B was set to match the one used for ActD treatment (Figure 3.36).

The multifactorial statistical analyses (Table 3.3) indicate that there is a dose effect of on the fraction of S-phase cells, as seen in Figure 3.38. There is no statistically significant effect of Torin 1 on cell death, but this part of the analysis may be slightly underpowered; nevertheless, the fraction of sub-G₁ cells observed in Figure 3.38 B is similar for all treatments and untreated control such that even reaching statistical significance the biological relevance would be minimal.

Table 3.3. Multifactorial analysis of the cell cycle fractions shown in Figure 3.38 A and B. Numbers indicate the p-values calculated for the different statistical tests indicated in the text except for Spearman's analysis, where ρ is also shown. Significant p-values are indicated in bold Note that for ANOVA the Bonferroni-corrected significance level is 0.0125.

Fraction	Cell Line	Uncorrected	logit	K-W	Spearman		n
					ρ	p-value	
sub-G ₁	ACHN	0.4346	0.3409	0.2370	0.0089	0.976	3
	UoK111	0.1557	0.1441	0.1690	0.358	0.209	4
S-phase	ACHN	2.93x10⁻⁷	0.0006	0.0249	-0.751	0.002	3
	UoK111	4.38x10⁻⁵	0.0023	0.0189	-0.86	8x10⁻⁵	4

To assess if allosteric inhibitors can promote cell cycle arrest in RCC cell lines, ACHN and UoK111 were treated with different concentrations of rapamycin, temsirolimus and everolimus for 72 hours and the DNA was labelled using Click-chemistry as described in the methods section 2.4. Figure 3.39 illustrates the effects of Rapamycin, Temsirolimus and Everolimus on the cell cycle of ACHN cells and the entire analysis of the flow cytometry data is available in the appendix Figures 7.11, 7.12, and 7.13, respectively. As can be observed, the percentage of cells in S-phase is reduced slightly upon treatment with rapamycin. Nevertheless, reduction of the percentage of cells in S phase does not appear to be driven by higher concentrations of the drug since the Spearman's correlation is not statistically significant (p-value= 0.2). The percentage of cell death remains below 3% even 500 nM, and the Spearman's correlation among higher concentration of Rapamycin and increased percentage of cell death is not statistically significant (p-value=0.6). These results indicate that rapamycin does not induce cell cycle arrest nor cell death in ACHN cells, and are consistent with the observations made in section 3.1.4.2, where it was shown that rapamycin does not affect cell viability of ACHN cells (see Figure 3.29). Rapamycin treatment does not affect the cell cycle of UoK111 cells either. As illustrated in Figure 3.40 and in the appendix Figure 7.14, the percentage of cells in S-phase is only reduced by 8% at the highest concentration of Rapamycin tested (500 nM) compared to the control. In addition, decrease of the percentage of cells in S phase does not correlate with increasing concentrations of Rapamycin used in this assay (p-value=0.6). The percentage of cell death is increases by 1.36%, 1.22% and 2.33% in

Uok111 cells treated with 15 nM, 50 nM, and 500 nM, respectively, with no correlation (p-value=0.6), suggesting that rapamycin does not associate with a cytostatic nor a cytotoxic effect in UoK111 cells. These results are consistent with absence of effects of rapamycin on cell viability of UoK111 cells, presented on section 3.1.4.2 (see Figure 3.30).

Figure 3.39 and appendix Figure 7.12 demonstrate that Temsirolimus does not affect significantly the cell cycle of ACHN cells, with a reduction of the percentage of cells in S-phase from 43.82% in the control to 40.52%, 40.42%, and 38.17% in cells treated with 15 nM, 50 nM and 500 nM Temsirolimus, respectively. Although Spearman correlation between increased concentration of Temsirolimus and reduction of the percentage of cells in S-phase is statistically significant with a p-value of 2.22×10^{-16} , the percentage of cells in S-phase is only reduced by 5.65% at the highest concentration tested (500 nM) compared to the control, which renders the alteration observed in the cell cycle as not relevant for the purposes of this study. Additionally, a minor change in the percentage of cell death is observed, from 1.77% to 3.24% in ACHN cells treated with 500 nM Temsirolimus, but the correlation between the concentration of this drug and the slight increase of cell death is not significant (p-value=0.2). These results are consistent with the lack of effect of Temsirolimus in viability of ACHN cells observed in section 3.1.4.2 (see Figure 3.29).

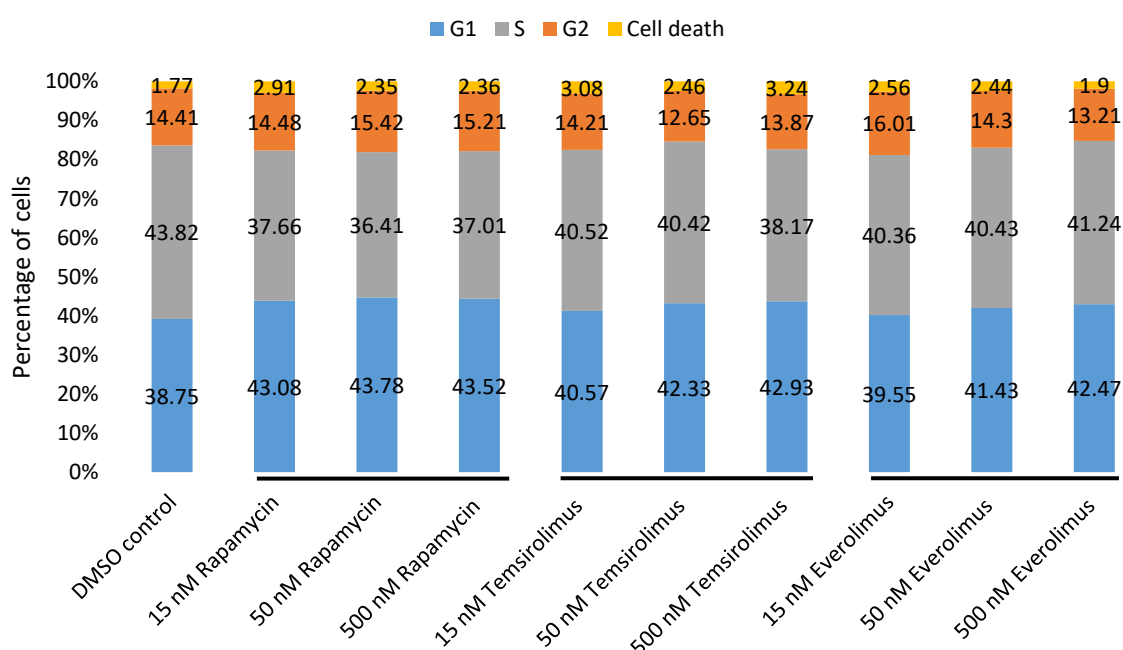


Figure 3.39. Effect of increased concentrations of allosteric mTORis on the cell cycle of ACHN cells. The stacked column plot displays the percentage of cells identified as populations in G1, S, G2,

and cell death by detecting EdU-labelled DNA with Click-chemistry and 7-AAD staining using flow cytometry. The percentage of dead cells increases with increasing concentrations of ActD. The percentage of the cells distributed in the different stages of cell cycle was performed on data obtained from a single experiment.

As illustrated in Figure 3.40 and appendix Figure 7.15, UoK111 cells treated with Temsirolimus present a slight decrease in the percentage of cells in S-phase compared to the control, shifting from 41.50% to 39.95%, 37.18%, and 34.08% when treated with 15 nM, 50 nM and 500 nM, respectively. The variation in the percentage of S-phase cells correlates with the increased concentrations of Temsirolimus ($p=2.22 \times 10^{-16}$), however, the percentage of cells in S-phase after treatment with 500 nM only decreases by 7.4%. The percentage of cell death also displays a minor increase of almost 4% in cells treated with 500 nM Temsirolimus compared to the control, but the correlation of cell death and the concentration of Temsirolimus is not significant ($p\text{-value}=0.2$). Overall, Temsirolimus does not appear to have a cytostatic effect in UoK111 cells, which is consistent with the effects on cell viability of UoK111 treated with Temsirolimus observed in the section 3.1.4.2 (see Figure 3.30).

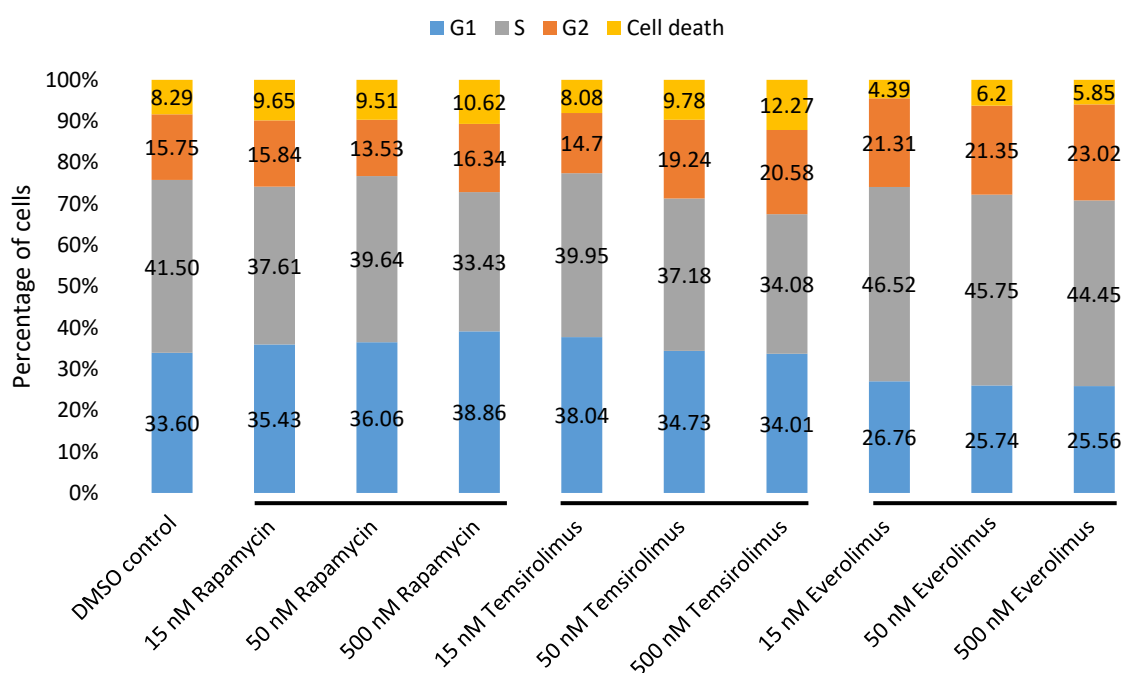
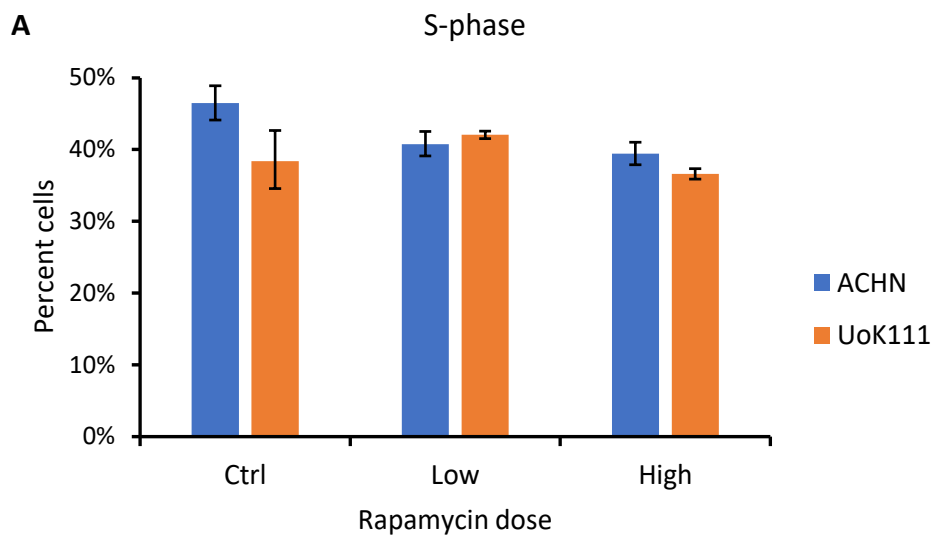


Figure 3.40. Effect of increased concentrations of allosteric mTORis on the cell cycle of UoK111 cells. The stacked column plot displays the percentage of cells identified as populations in G1, S, G2, and cell death by detecting EdU-labelled DNA with Click-chemistry and 7-AAD staining using flow cytometry. The percentage of dead cells increases with increasing concentrations of ActD. The percentage of the cells distributed in the different stages of cell cycle was performed on data obtained from a single experiment.

Lastly, results of ACHN and UoK111 cells treated with Everolimus are displayed in Figures 3.39 and 3.40, and the appendix Figures 7.13 and 7.16, respectively. As observed in said Figures, Everolimus had no effect on the cell cycle of either ACHN or UoK111 cells, nor did it induce cell death, which is consistent with the lack of effect of Everolimus on viability of ACHN and UoK111 cells described in section 3.1.4.2 (see Figures 3.29 and 3.30).

Since Rapamycin is a good representation of allosteric mTOR inhibitors and appears to show some small degree of activity on the viability of RCC cells (Figure 3.27) we analysed the flow cytometric profiles of RCC cells treated with Rapamycin in a manner similar to the cases of ActD and Torin 1 treatments (Figures 3.36 and 3.38) Figure 3.41 A and B show the percentages of cells in the S-phase and sub-G1 populations. Since there was no clear dose-response curve observed for cell viability (see Section 3.1.4.2), Figures 3.41 A and B were constructed by grouping Rapamycin doses into low ($\leq 100\text{nM}$) and high ($>100\text{nM}$) concentrations. As can be seen in Figure 3.41 and confirmed by statistical analyses in Table 3.4, there is no significant effect of Rapamycin at any of the concentrations studied.



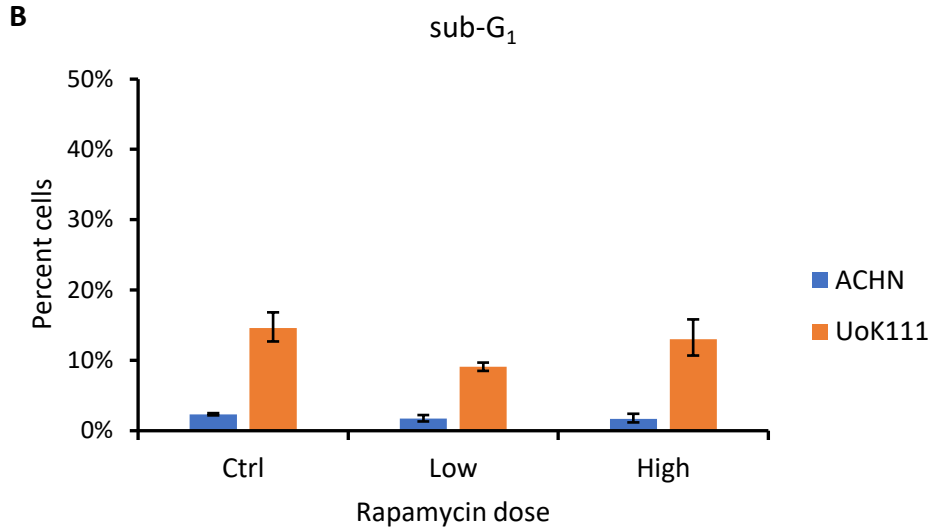


Figure 3.41. Percentage of S-phase cells (A) and sub-G₁ cells (B) detected by flow cytometry on ACHN and UoK111 cells (indicated) treated either with DMSO (Ctrl) or with different doses of Rapamycin. The Rapamycin doses were obtained from the cell viability dose-response curves and were as follows: Low=doses below 50, High=500nM. Bars indicate mean percentages from 2 independent experiments. Error bars indicated SEM. The scale of the vertical axis in B was set to match the one used for ActD treatment (Figure 3.36).

Table 3.4. Multifactorial analysis of the cell cycle fractions shown in Figure 3.41 A and B. Numbers indicate the p-values calculated for the different statistical tests indicated in the text, except for Spearman's analysis, where ρ is also shown. Significant p-values are indicated in bold. Note that for ANOVA the Bonferroni-corrected significance level is 0.017.

Fraction	Cell Line	Uncorrected	logit	K-W	Spearman		n
					ρ	p-value	
sub-G ₁	ACHN	0.773	0.721	0.795	-0.158	0.709	2
	UoK111	0.129	0.104	0.095	-0.109	0.816	2
S-phase	ACHN	0.149	0.152	0.223	-0.727	0.041	2
	UoK111	0.231	0.233	0.331	-0.073	0.877	2

Together, these results suggest that the ATP-competitive mTOR inhibitor Torin 1 can act as a cytostatic drug that can also induce cell death in certain cell lines, while allosteric inhibitors that only target mTORC1 do not promote cell cycle arrest nor cell death.

3.1.6 Conclusion

This chapter aimed to establish a model system with which to test the hypothesis that modulation of nucleolar activity by targeting signalling pathways would sensitise the cells to the cytostatic/cytotoxic effect of the NFI ActD. Our data show that Torin 1 fulfils the requirement for the model system since it is a) demonstrably active at inhibiting phosphorylation of mTOR downstream targets (S6K and TIF-IA); b) capable of inhibiting rRNA synthesis as demonstrated by decreased 5-EU incorporation and c) capable of reducing cell viability. Moreover, the similarity of IC50s for those effects further supports the notion that they are related.

Our results also suggest that the effect of mTORis on cell viability might be dependent on inhibition of nucleolar function. This will be discussed further in the general conclusions.

In conclusion, these results demonstrate that the Torin 1/ActD is a suitable model system to test our hypothesis.

3.2 Sensitising RCC cells to nucleolar function inhibitors

As discussed in section 1.5, the main hypothesis of this thesis is that cancer cells can be sensitised to chemotherapy directed against the nucleolus by using targeted therapies against selected metabolic pathways. In section 3.1, we demonstrated that an ATP-competitive mTOR inhibitor, Torin 1, was capable of: 1) inhibiting the phosphorylation of two key regulators of nucleolar activity; 2) inhibiting rRNA synthesis; 3) reducing cell viability. Furthermore, the fact that the mTOR allosteric inhibitors tested had a minimal effect on both inhibition of rRNA synthesis and reduction of cell viability supported the notion that the two effects might be related in the cytostatic/cytotoxic action of mTOR inhibitors *in vitro*. Thus, we concluded that Torin 1 offers a suitable model with which to test our hypothesis and that the allosteric mTOR inhibitors studied (Rapamycin, Temsirolimus and Everolimus) would constitute an optimal negative control.

3.2.1 ATP-competitive inhibition of mTOR enhances the inhibition of rRNA synthesis by ActD

We needed to determine two crucial points of our model. First, whether ActD and an ATP-dependent mTOR inhibitor would each maintain its rRNA synthesis inhibitory activity in the presence of the other drug; second, whether the inhibitory actions of both drugs would add.

For this section of the work, the effect of drug combinations on rRNA synthesis, we changed the ATP-competitive mTOR inhibitor from Torin 1 to AZD8055 (404) for two reasons. First, while we had expected Torin 1 to enter clinical trials, this did not happen; instead, AZD8055 has completed four Phase I trials (see <https://clinicaltrials.gov/>) which makes it a more realistic therapeutic agent than Torin 1. Second, while we had successfully performed cell viability experiments using the ActD/Torin 1 combination, when we started the 5-EU incorporation studies for drug combinations we encountered problems with a new batch of Torin 1 (likely to be due to drug solubility) which produced unreliable results with IC₅₀s several fold higher than those observed earlier (see Figures 3.13 and 3.14). Interestingly, AZD8055 is an ATP-competitive inhibitor of mTOR that inhibits phosphorylation of mTORC1 downstream targets S6K and 4EBP1, as well as mTORC2-dependent phosphorylation of Akt. Inhibition of the kinase activity of both mTOR complexes is key to prevent the over-activation of Akt that results from

feedback loop signalling upon rapamycin-induced inhibition of mTORC1. AZD8055 has been observed to inhibit proliferation and cell cycle progression in vitro and to achieve significantly better tumour growth inhibition than rapamycin in vivo (404,475,476). Various phase 1 studies have proved AZD8055 to be safe and tolerable for patients with advanced solid tumours and lymphoma with a maximum tolerated dose of 90 mg twice a day (406,407,477). Thus, we continued with the work for this section using the ATP-competitive mTOR inhibitor AZD8055.

To study rRNA synthesis in the presence of drug combinations, we first established the rRNA synthesis inhibition dose-response curves for each drug separately (not shown). With this information, we identified a concentration of AZD8055 alone that would produce an intermediate inhibitory effect (50 nM) and constructed the drug combination assay shown in Figures 3.42 A and B, which comprised a range of concentrations of the individual drugs plus a combination of varying ActD with constant AZD8055 at 50 nM. Figure 3.42 A and B show that, as predicted, the ATP-competitive mTOR inhibitor produced a Hill-like dose-response curve of 5-EU incorporation in both cell lines, confirming that it can cause rRNA synthesis inhibition as observed with Torin 1 (Figures 3.13 and 3.14). When combined with AZD8055, the cellular response to the lower concentrations of ActD was capped to a maximum 5-EU incorporation equal to that of 50 nM AZD8055 alone (grey line in Figure 3.42 A and B), indicating that AZD8055 maintained its activity for the whole combination range. At higher ActD doses, 5-EU incorporation progressively diminished (grey line in Figure 3.42 A and B), indicating that ActD retained its inhibitory capacity in the mixture. From these results, we conclude that in a mixture of ActD and AZD8055 both drugs contribute to the inhibition of rRNA synthesis. Furthermore, these results give strength to our prediction that ATP-competitive mTOR inhibitors would inhibit rRNA synthesis.

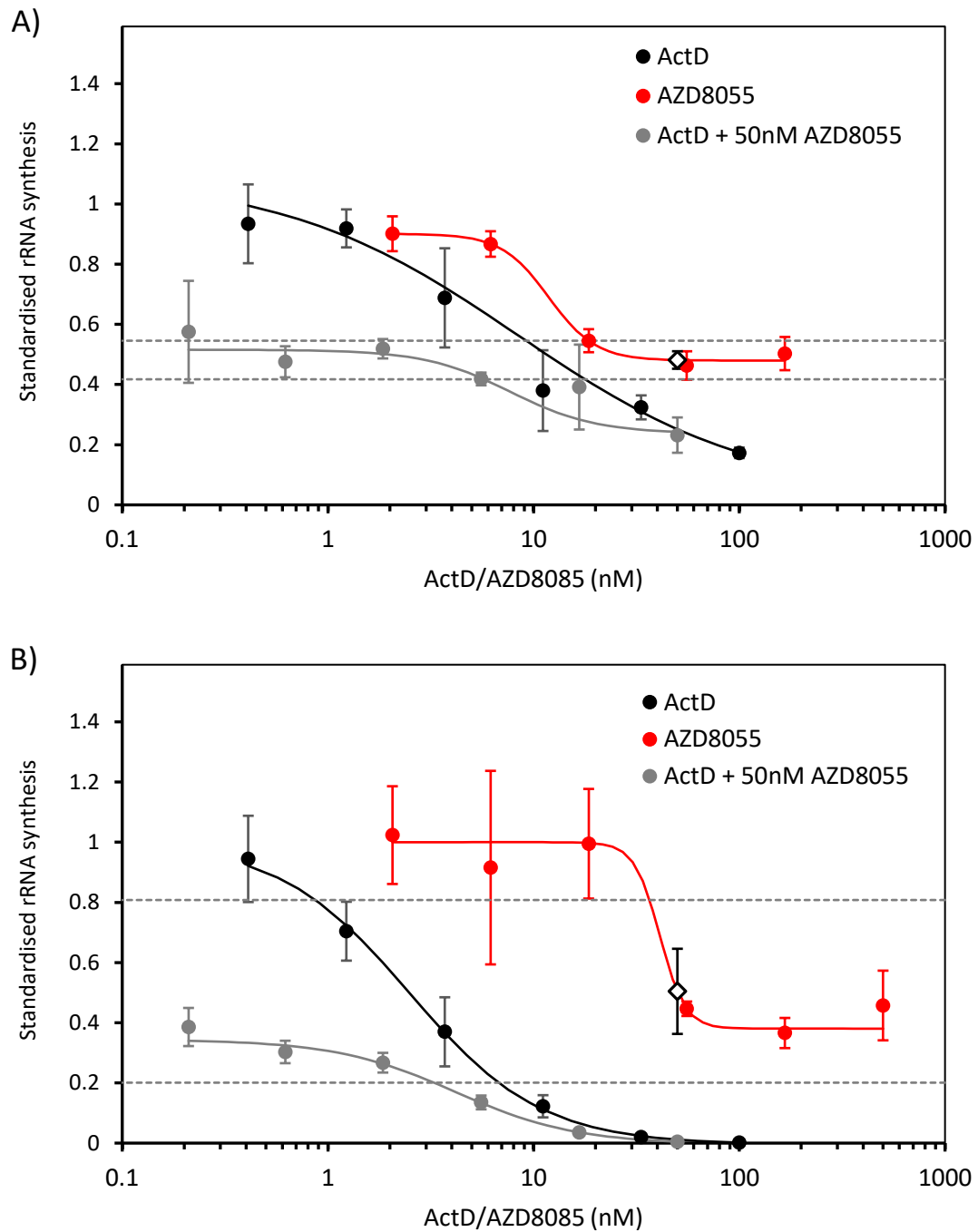


Figure 3.42. rRNA synthesis dose-response curves for ActD and AZD8055 alone and in combination. A) ACHN cells and B) UoK111 cells were treated for 2 hours with the indicated doses of ActD alone (black line), AZD8055 alone (red line) or variable doses of ActD in the presence of a constant dose of 50nM AZD8055 (grey line), then labelled with 5-EU followed by fixation and Click detection as described in section 2.5. The white rhombus indicates the estimated response of AZD8055 alone at 50nM. The dashed grey lines indicate the prediction interval of 95% confidence for the effect of 50 nM AZD8055. The error bars indicate Standard Error of the Mean for replicates of 3 wells (50-300 cells imaged per well) of a single experiment.

3.2.2 ATP-competitive inhibition of mTOR enhances the suppression of cell viability induced by ActD

Having established that ActD and AZD8055 both cooperate to inhibit rRNA synthesis, we then studied whether the two drugs would similarly cooperate to suppress cell viability, as predicted by our model. To achieve this, we followed a strategy identical to that of the previous section (3.2.1) this time applied to an MTT assay.

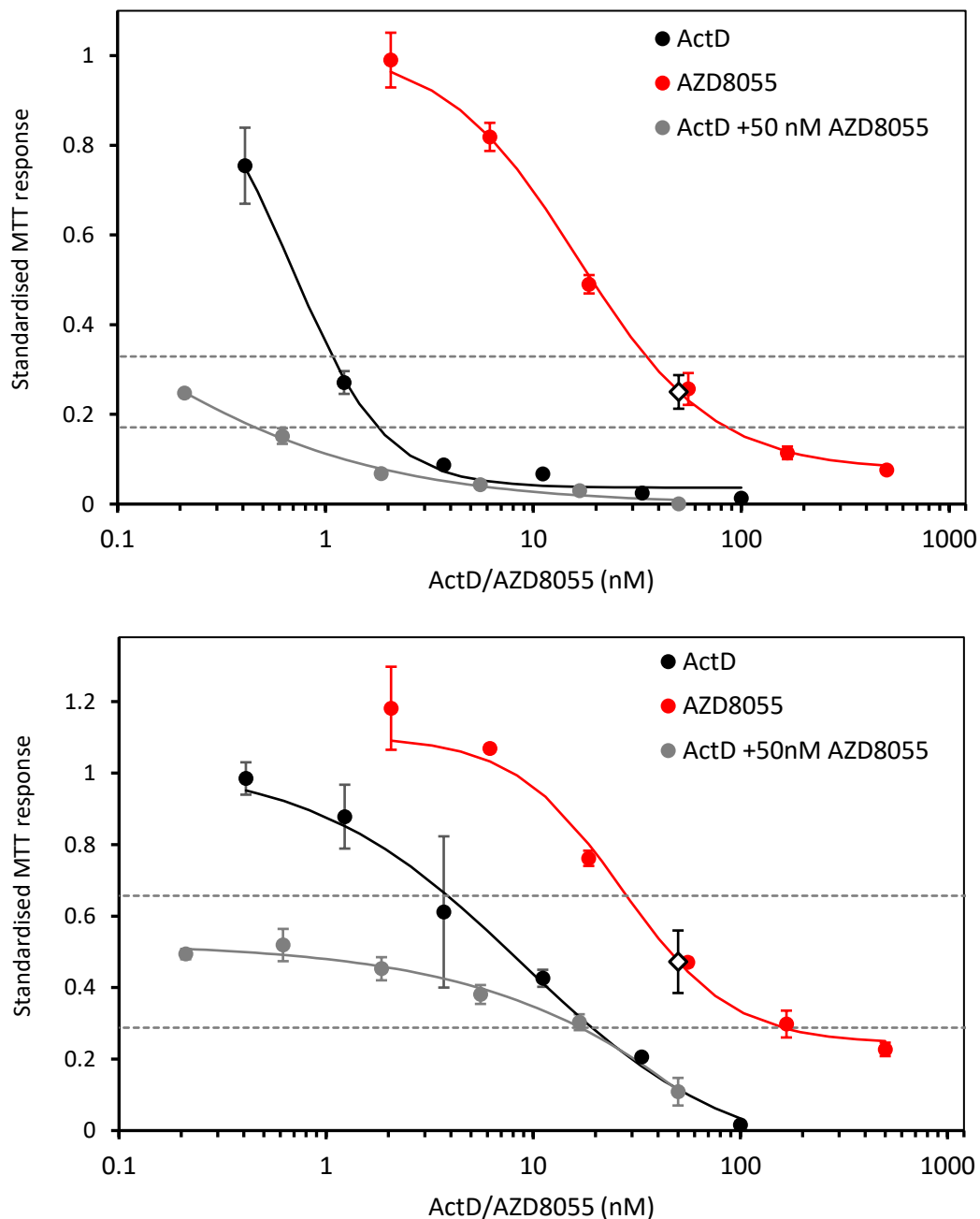


Figure 3.43. Cell viability dose-response curves for ActD and AZD8055 alone and in combination. A) ACHN cells and B) UoK111 cells were treated for 72 hours with the indicated concentration of ActD alone (black line), AZD8055 alone (red line) or variable concentration of ActD in the presence of a constant concentration of 50nM AZD8055 (grey line), then incubated with MTT and developed as described in section 2.3.1. The white rhombus indicates the estimated response of AZD8055 alone at

50nM. The dashed grey lines indicate the prediction interval of 95% confidence for the effect of 50 nM AZD8055. The error bars indicate Standard Error of the Mean for replicates of 3 wells of a single experiment.

We constructed the drug combination assay shown in Figures 3.43 A and B, comprising a range of concentrations of the individual drugs plus a combination of varying ActD with constant AZD8055 at 50 nM. Figure 3.43 A and B show that AZD8055 suppresses cell viability in both cell lines. When combined with AZD8055, the cellular response to the lower concentrations of ActD was capped to a maximum cell viability equal to that of 50 nM AZD8055 alone (grey line in Figure 3.43 A and B), indicating that AZD8055 maintained its activity for the whole combination range. At higher ActD concentrations cell viability progressively diminished (grey line in Figure 3.43 A and B), indicating that ActD retained its inhibitory capacity in the mixture. From these results, we conclude that in a mixture of ActD and AZD8055 both drugs contribute to the suppression of cell viability. This is therefore an observation that strongly supports our working hypothesis.

As stated above, we had also performed drug combination studies on the effects of ActD and Torin 1 on cell viability. The strategy that we followed was identical to that used for AZD8055, with a range of ActD concentrations in a mixture with a constant concentration of Torin 1 of 50 nM.

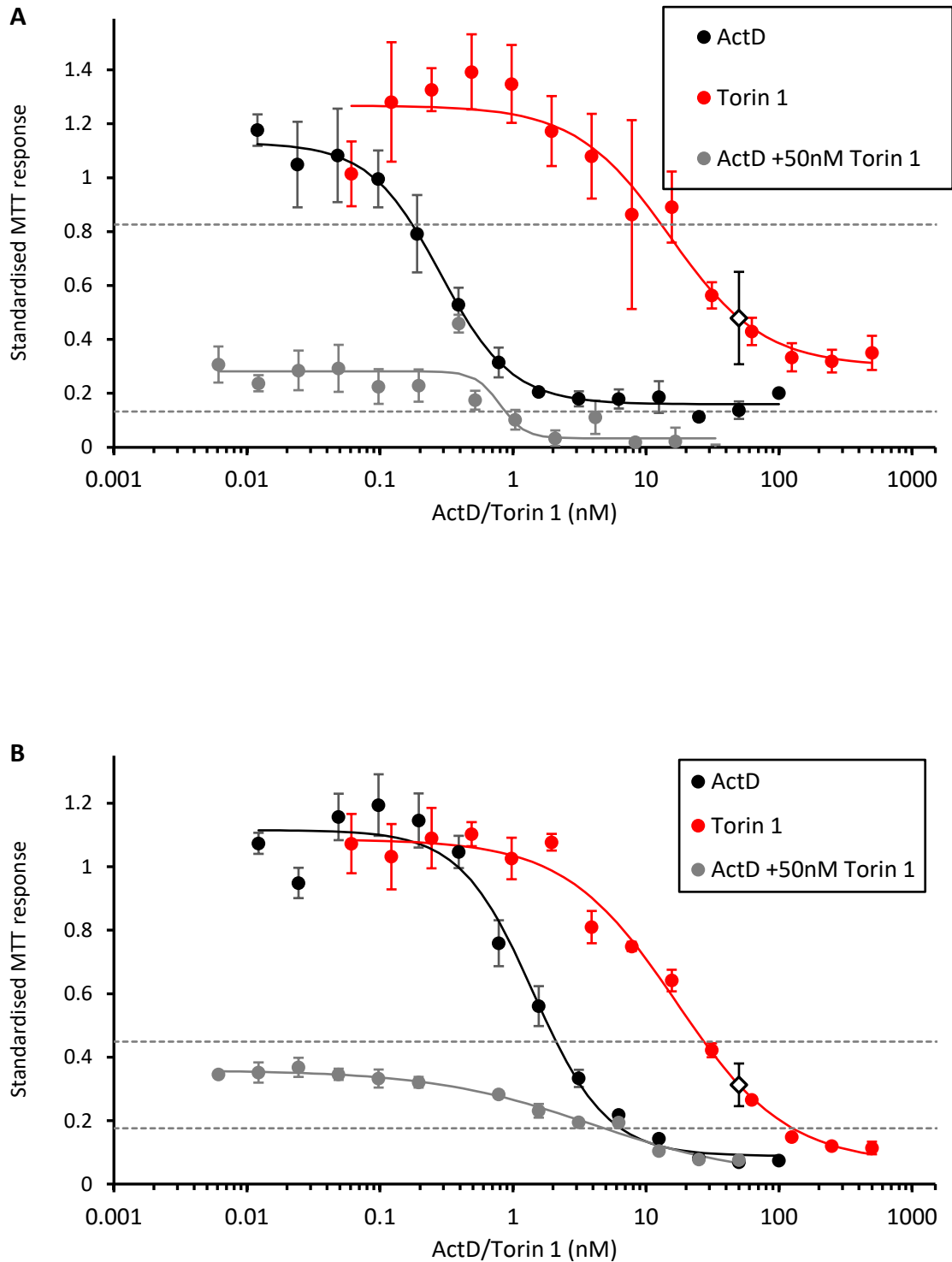


Figure 3.44. Cell viability dose-response curves for ActD and Torin 1 alone and in combination. **A)** ACHN cells and **B)** UoK111 cells were treated for 72 hours with the indicated concentrations of ActD alone (black line), Torin 1 alone (red line) or variable concentrations of ActD in the presence of a constant concentration of 50nM Torin 1 (grey line), then incubated with MTT and developed as described in section 2.3.1. The white rhombus indicates the estimated response of Torin 1 alone at 50nM. The dashed grey lines indicate the prediction interval of 95% confidence for the effect of 50 nM Torin 1. The error bars indicate Standard Error of the Mean for replicates of 3 wells of a single experiment.

Figure 3.44 A and B shows that Torin 1 suppresses cell viability in ACHN and UoK111 cells. Similar to AZD8055, combination of low concentrations of ActD with Torin 1 reduced cell viability to a comparable effect than that achieved by 50 nM Torin 1 alone, (grey line in Figure 3.44 A and B), indicating that the activity of Torin 1 was maintained throughout the combination range. Viability of ACHN and UoK111 cells was gradually reduced at higher concentration of ActD (grey line in Figure 3.44 A and B), indicating that the inhibitory effect of ActD was retained in the combinations with Torin 1. From these results we conclude that in a mixture of ActD and Torin 1 both drugs contribute to the suppression of cell viability. This observed behaviour of another ATP-competitive mTOR inhibitor further supports our working hypothesis.

3.2.3 Effect additivity analysis of the mixture of drugs in the suppression of cell viability

As stated above, the results presented in Figures 3.43 and 3.44 indicate that both drugs retain inhibitory activity on cell viability in the presence of each other. Therefore, we wanted to confirm that the effects of both drugs are at least additive, that is, that there is no antagonism that the analyses of Figures 3.43 and 3.44 might miss. Furthermore, we wanted to extend our analyses to a range of concentrations for both drugs simultaneously, not just ActD. To achieve this, we applied the isobolographic analysis method, based on the drug additivity model of Loewe, which is mechanism-independent (447,478) and we considered to be the most appropriate method for our purposes.

The most commonly used approaches for the assessment of drug additivity are Bliss score and Loewe additivity (isobolograms) (for a comparison see (447,451,479)). The Bliss model assumes that the targets of two drugs are independent and that the probability of a combination of such drugs achieving an effect on a cell is the multiplicative probability calculated for the statistically independent target eliminations (479). However, in the Bliss model a combination of a drug with itself may appear as synergistic or antagonistic (it violates the principle of sham combination – see explanation in (447)). Loewe additivity, on the other hand, assumes that the two drug concentrations are equivalent if they produce the same effect, and that the total effect of the combination is the addition of the effects contributed by each drug (447). Thus, due to both the self-interaction issues presented by Bliss additivity, and the fact that Loewe additivity assumes identical targets (in our case, rRNA synthesis inhibition);

thus, the Loewe isobolograms was chosen to analyse the drug interactions tested in this investigation. However, while Bliss score, a “response additivity” method (447), only requires comparison of effects at a given concentration, Loewe isobologram, a “dose additivity” method (447), depends on estimation of the single drug concentrations that would give the same effect as observed in the combination. Specifically, the calculation of the most common drug combination measure obtained from isobolograms, the Combination Index (CI, or α , also called Interaction Index (447,478) requires, for a given effect level, the determination of the doses of the individual drugs that would achieve that effect, as well as the determination of the drug concentrations in the mixture that achieve the effect:

$$\alpha = \frac{A_{Mix}}{A_{Indiv}} + \frac{B_{Mix}}{B_{Indiv}}$$

Where A_{Indiv} and B_{Indiv} are the doses at which each drug A and B would separately achieve the effect, and A_{Mix} and B_{Mix} are the concentrations of the drugs in a mix that reach that effect (note that CI/ α may vary for different effect levels/concentrations). Therefore, the method requires full determination of the response curve parameters (which is assumed to follow the Hill equation - (446)).

According to the drug dose equivalence principle on which an isobologram is constructed (447), if we determine the concentrations A_0 and B_0 of the individual drugs that produce a certain effect (typically 50%, in which case A_0 and B_0 are called IC50s), all mixing proportions of those drugs at those concentrations (that is, all combinations of $p A_0 + (1-p) B_0$, with $0 \leq p \leq 1$) will produce the same level of effect. The resulting predicted curve of same effect is illustrated in Figure 3.45 A for a 50% effect (IC50).

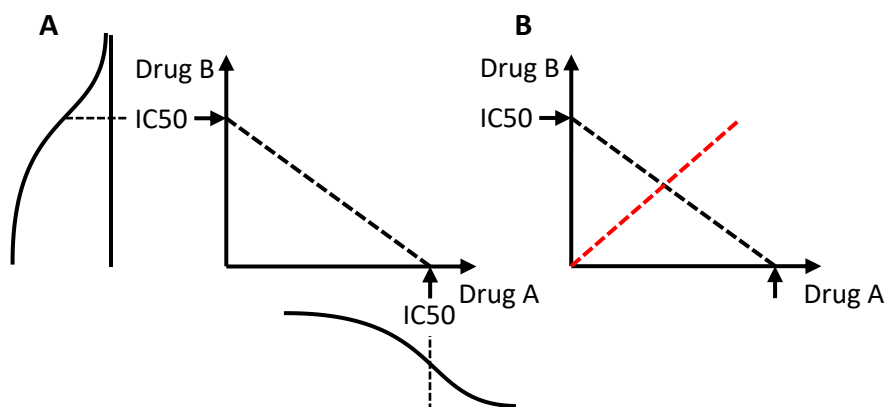
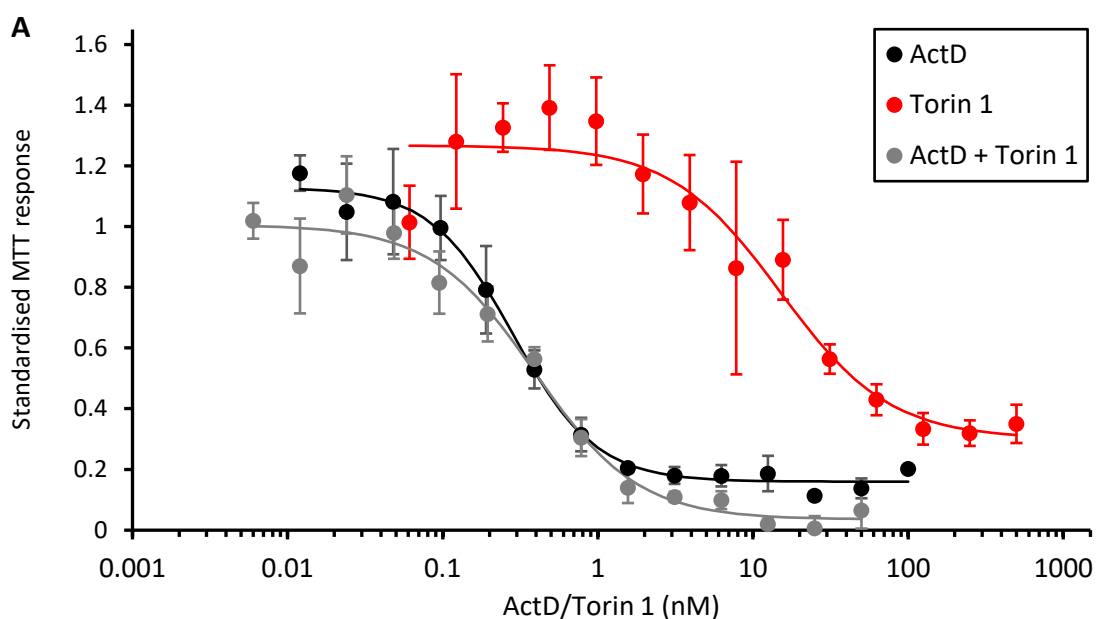


Figure 3.45. Isobologram construction scheme used in this work. A) Scheme of a basic isobologram. The dashed line indicates the pairs of concentrations of drugs A and B predicted to produce the same effect (50% in this case) when combined. From the dose response curves determined for each drug, isobolograms for any desired effect can be constructed. B) Combination response for constant A/B ratio mixing.

Once an isobologram is constructed, any pair of combined concentrations can be tested (A_{Mix} and B_{Mix} in the equation above). Here we test drugs mixed at a constant ratio (Figure 3.45 B) as it allows for the fitting of a dose response curve from which any effect level can later be extracted.

Figure 3.46 A and B show the cell viability dose response curves for ActD, Torin 1, and a mixture of ActD and Torin 1 at constant ratio of concentrations for ACHN and UoK111 cells, respectively. Figure 3.46 C and D show the isobolograms constructed from the data of Figure 3.46 A and B, respectively (see legend for details). Figure 3.46 E and F shows the Combination Indices calculated for the concentration pairs indicated in C and D, respectively. The 95% confidence intervals for the Combination Indices that span the value 1.0 indicate that at such concentrations the level of cell viability suppression caused by a combination of ActD and Torin 1 is compatible with an effect additivity model. These results confirm that both drugs maintain their activity in the presence of each other and that these activities combine to produce an added effect.



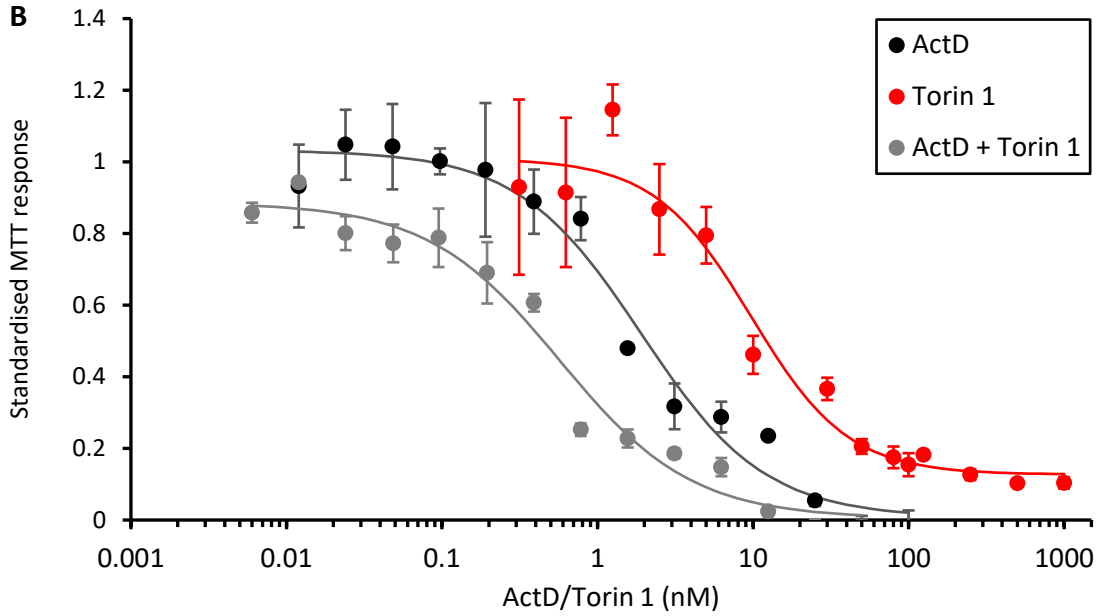
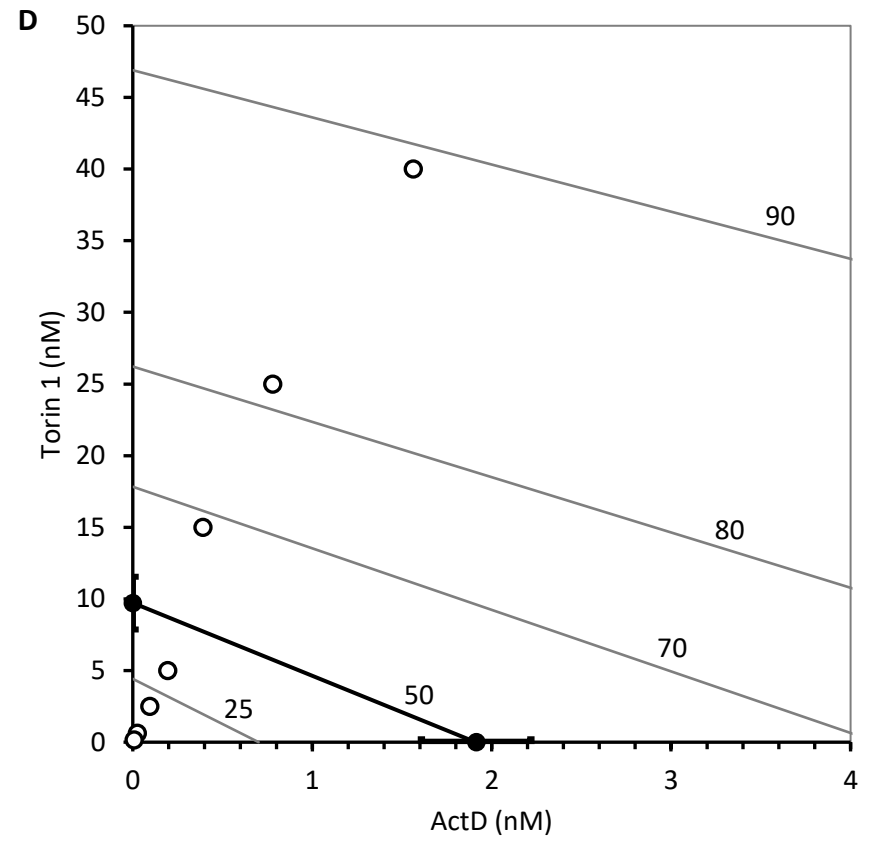
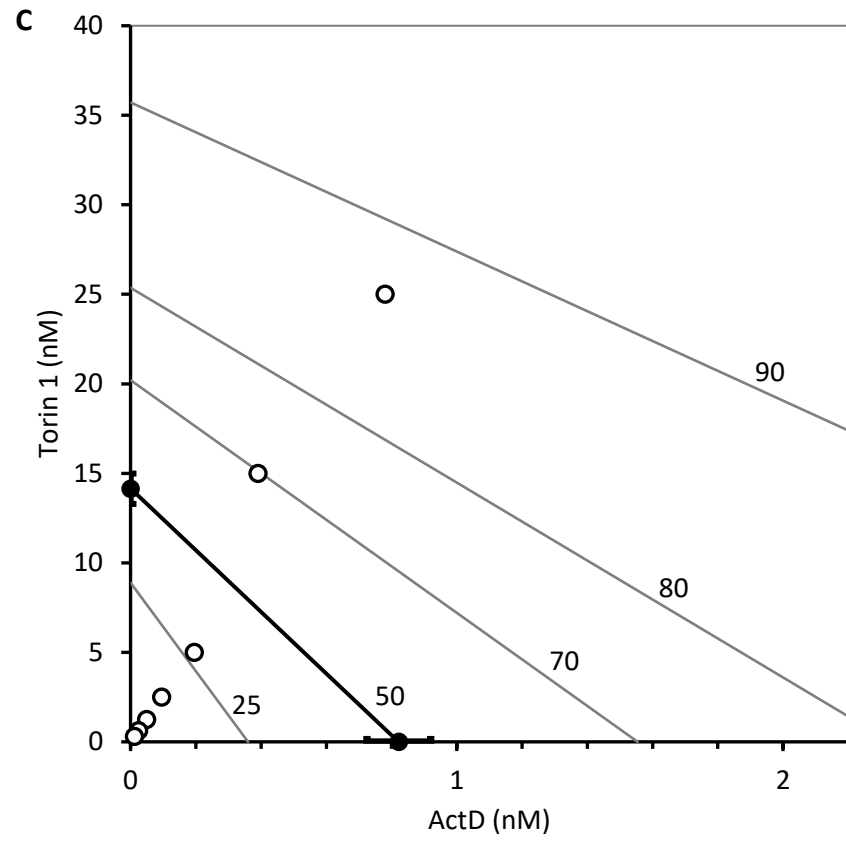
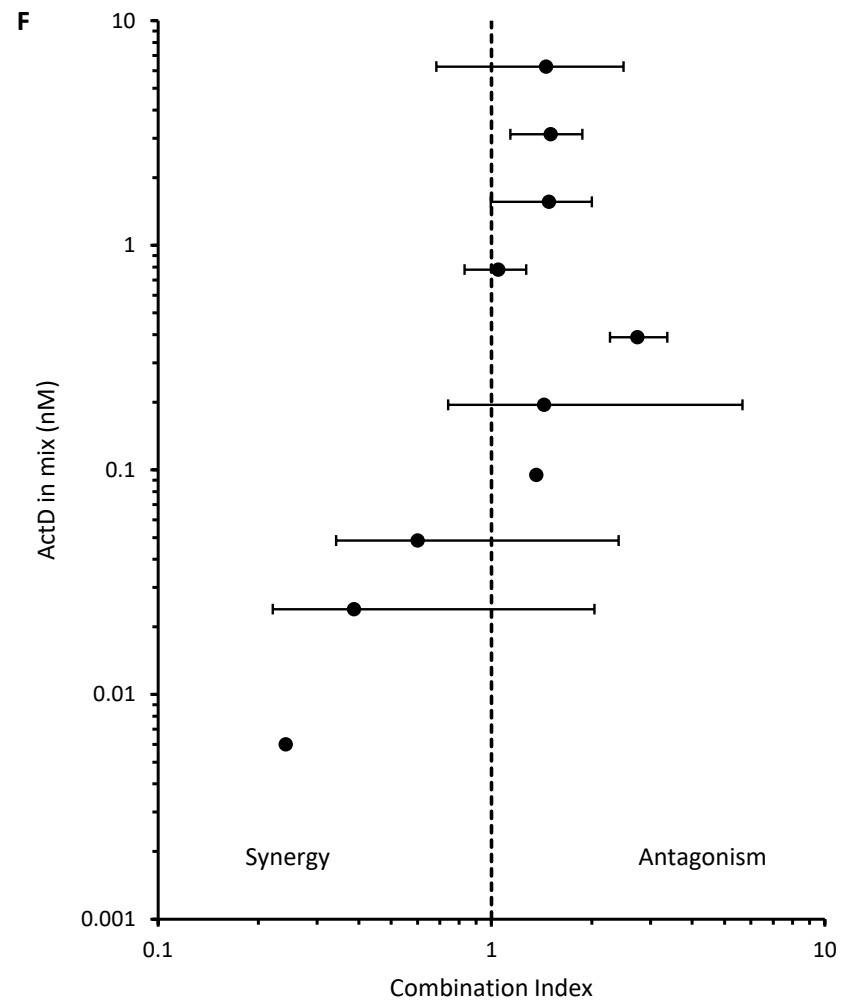
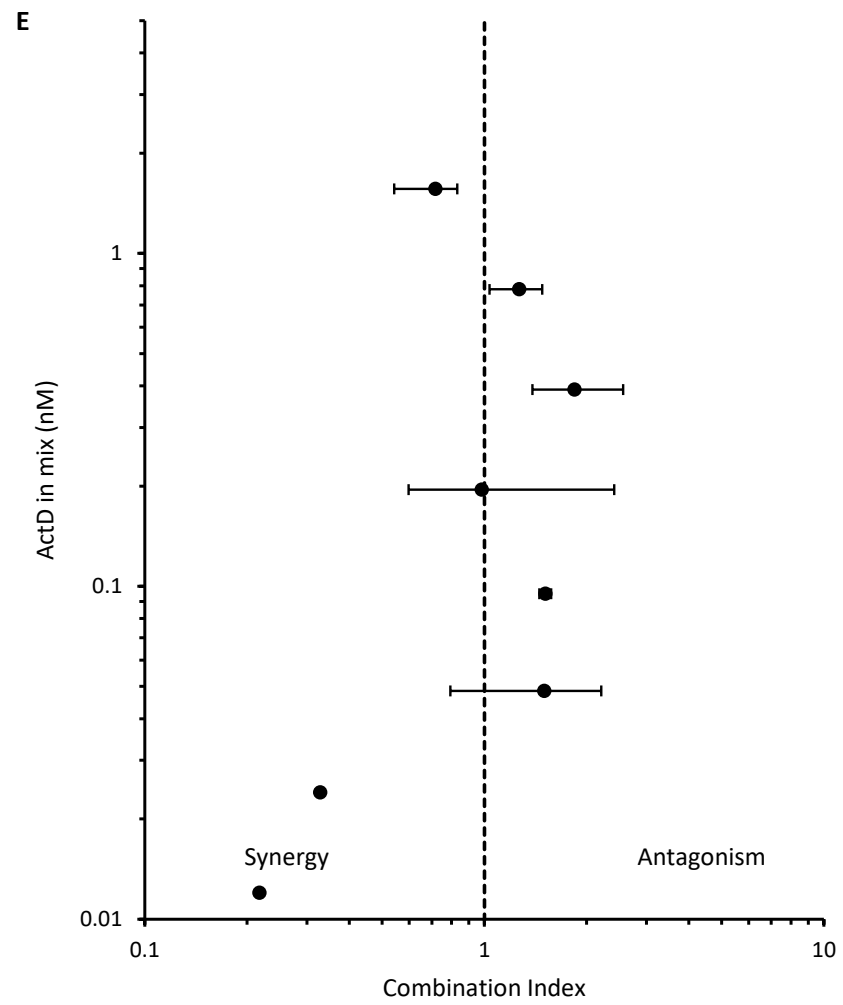


Figure 3.46. Isobolographic analysis of the cell viability response of a combination of ActD and Torin 1 mixed at constant concentration ratio. **A:** Curves for ACHN cells, **B:** curves for UoK111 cells, depicting the standardised MTT response for ActD alone (black), Torin 1 alone (red) and a mixture of ActD and Torin 1 at constant ration(grey). Cell treatments and times were performed as in Figure 3.44. The error bars indicate Standard Error of the Mean for replicates of 3 of a single experiment. **C** and **D:** isobolograms constructed for ACHN and UoK111 cells, respectively, constructed for effect levels of 25%, 50% (thicker line), 70%, 80% and 90%, with the IC₅₀ and its standard error indicated for each drug; the circles indicate the concentration pairs at which the drug combinations were tested. **E** and **F:** Plot for ACHN and UoK111 cells, respectively, indicating the Combination Indices measured for the various drug combination pairs tested. Only the ActD concentration is indicated on the vertical axis. Bars indicate the 95% confidence interval for the Combination Index of each pair.





3.2.4 Rapamycin also enhances the rRNA synthesis and cell viability suppression activity of ActD

We next tested Rapamycin in combination with ActD as we were intrigued by the fact that it displayed an unaccountable ability to suppress both rRNA synthesis and cell viability. While this activity did not cause a significant suppression of either phenotype and did not produce a Hill-like saturation response curve, it was nevertheless consistently observed across all experiments and cell lines.

Therefore, we first determined whether the addition of Rapamycin would have any effect on the capacity of ActD to inhibit rRNA synthesis. We performed this analysis with UoK111 cells only because in our experiments it was the cell line that more consistently and strongly showed an effect of Rapamycin on 5-EU incorporation.

Figure 3.47 shows an rRNA synthesis response analysis performed identically to that of Figure 3.42, although the constant Rapamycin concentration was increased to 100 nM in order to obtain a good response. It is clear from the Figure 3.47 that Rapamycin contributes to the inhibitory activity of ActD and that both drugs are simultaneously active in the mixture to suppress rRNA synthesis.

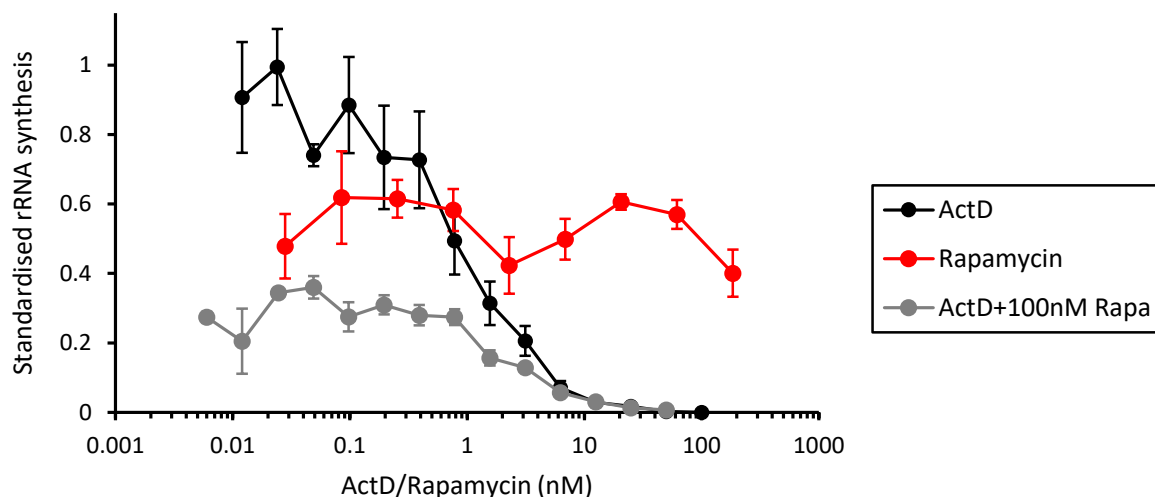


Figure 3.47. rRNA synthesis response curves for ActD and Rapamycin alone and in combination. UoK111 cells were treated for 2 hours with the indicated concentrations of ActD alone (black line), Rapamycin alone (red line) or variable concentrations of ActD in the presence of a constant concentration of 100 nM Rapamycin (grey line), then labelled with 5-EU followed by fixation and Click detection as described in section 2.5. The error bars indicate Standard Error of the Mean for replicates of 3 wells (50-300 cells imaged per well) of a single experiment.

Next we studied the behaviour of the mixture of Rapamycin and ActD with respect to suppression of cell viability. Figure 3.48 A and B show the response curves for ACHN and UoK111 cells, respectively. Again, it can be seen that in both cell lines Rapamycin contributes to the inhibitory activity of ActD and that both drugs are simultaneously active in the mixture to suppress cell viability.

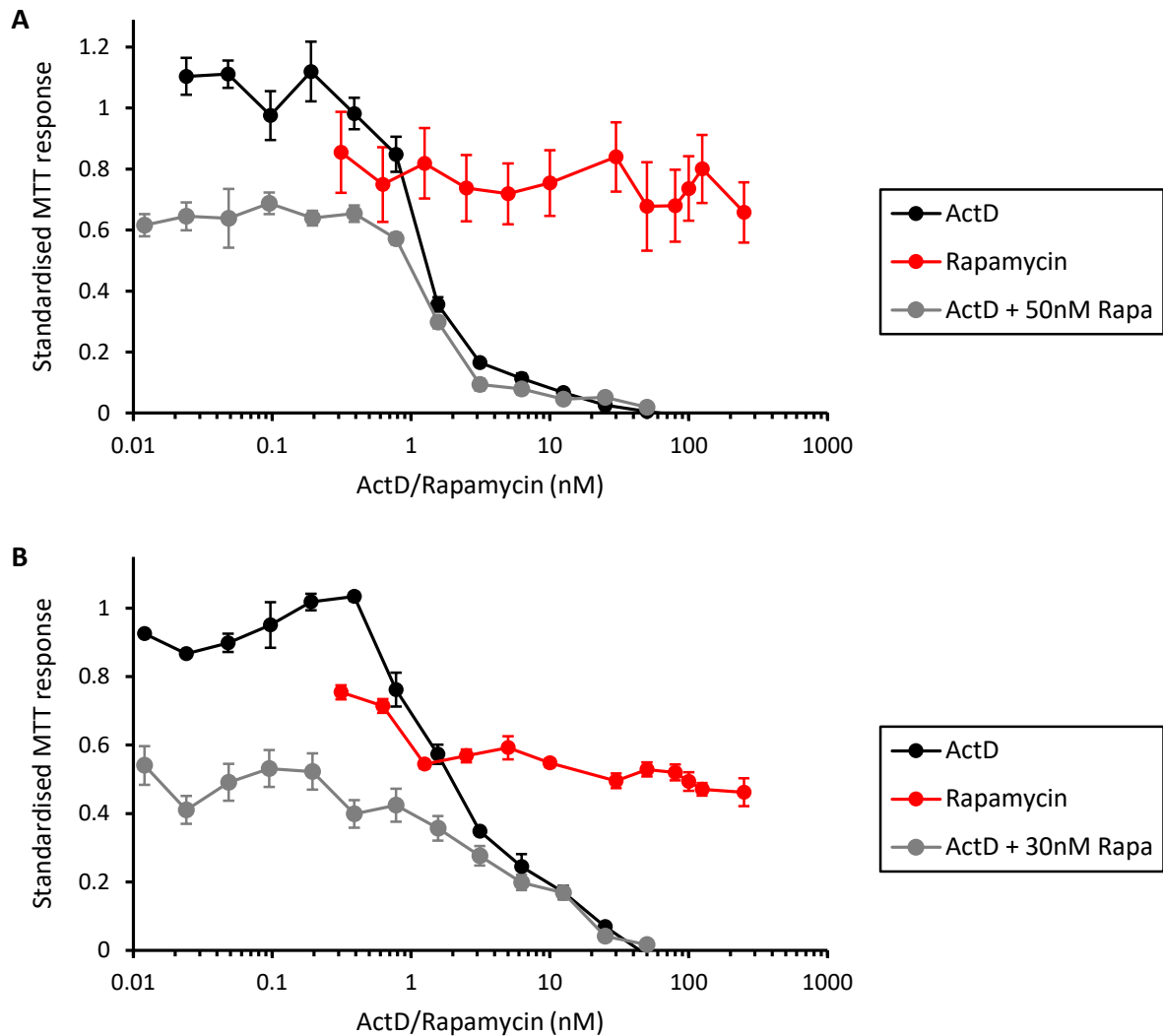


Figure 3.48. Cell viability dose-response curves for ActD and Rapamycin alone and in combination. A) ACHN cells and B) UoK111 cells were treated for 72 hours with the indicated concentrations of ActD alone (black line), Rapamycin alone (red line) or variable concentration of ActD in the presence of a constant concentration of 50nM Rapamycin (A, grey line) or 30nM Rapamycin (B, grey line), then incubated with MTT and developed as described in section 2.3.1. The error bars indicate Standard Error of the Mean for replicates of 3 wells of a single experiment.

From these results we speculate that Rapamycin, and possibly other allosteric inhibitors as well, exerts a limited amount of inhibition of rRNA synthesis which is not normally strong enough to cause a dramatic change in cell viability. However, when

Rapamycin is mixed with a NFI, this inhibitory effect adds to elicit a more dramatic phenotypic change. This possibility is further considered in the Discussion section.

It is important to note that the Loewe additive method (also Bliss score) applies to any dose dependent phenotype, provided it can be quantitated. Therefore, here we shall apply this same mechanism independent analysis to inhibition of both cell viability (MTT response) and rRNA synthesis (5-EU incorporation). However, time-dependent changes in cell viability can be due to cell cycle arrest or to cell death (cytostatic or cytotoxic effects), but isobolograms cannot detect any changes in the mechanism of cell viability reduction that might occur when drugs are combined, only total cell viability. Therefore, transitions from cytostatic to cytotoxic responses will be studied by cell cycle analysis as well.

3.2.5 Cytostatic and cytotoxic components of the inhibition of cell viability with drug combinations

The drug combination analyses that we utilised above measure changes in cell viability (standardised MTT assay response) in response to varying concentrations of the drugs studied. However, this analysis does not resolve whether those changes in the numbers of viable cells are due to cell cycle arrest or to cell death. As we showed in section 3.1.5.2, the reduction in cell viability caused by treatment with Torin 1 appears to be mediated mainly by cell cycle arrest (reduction of the proportion of cells in S-phase) with very limited cytotoxicity. ActD, on the other hand, was both cytostatic and cytotoxic, with the effects prominent at lower and higher concentrations, respectively (see section 3.1.5.1 and see below). Therefore, we also needed to determine which effect dominated the cell viability response when drugs were combined. In particular, we wanted to determine whether the cytotoxic effect of ActD might be boosted by the presence of Torin 1, something suggested as possible by the stronger maximum inhibitory effects observed in the drug combinations compared with the individual drugs (see particularly Figure 3.44 A).

To study the cytostatic and cytotoxic components of the cellular response to the drug combinations, again we resorted to cell cycle analysis (see section 2.4). Figure 3.49 shows the proportions of cell cycle phases observed in ACHN (3.49 A) and UoK111 cells (3.49 B) treated with ActD and Torin 1 either alone or in combination, using drug concentrations that represent regions of maximum slope (near the IC₅₀) and of

maximum effect. As can be seen for both cell lines (Figure 3.49 A, B), near the IC50 ActD causes a strong reduction in the proportion of S-phase cells with a moderate increase in the sub-G1 fraction, which indicates cell death (presumed here to be apoptosis based on the behaviour of ActD (472), but not experimentally confirmed). At high concentrations there is a virtual disappearance of S-phase cells and a prominent cytotoxic response. Torin 1, on the other hand, induces practically no cell death at any concentration but induces a concentration-dependent decrease of the S-phase population in both cell lines (Figure 3.49 A, B). In both cell lines, the combinations of drugs at the concentrations of maximum effects cause an increase in the sub-G1 fraction (Figure 3.49 A, B). The Bliss approach statistically independent target elimination by both agents (447) is valid here, and applied to the data of Figure 3.49 A, B, results in Scores of 1.44 and 1.00 for ACHN and UoK111 cells, respectively, suggesting that the combination is additive, if not synergistic for cell death. Nevertheless, it should be noted that, unlike the Loewe additivity model, if one of the drugs of the combination has no activity at all, the Bliss model would still produce a score of 1.0.

It is interesting to notice that, as our studies show (see for example Figures 3.31 A and B), drug treatments that cause prominent cell death always coincide with a massive shutdown of rRNA synthesis (~90%), while sub-maximal rRNA synthesis inhibition correlates with a cytostatic effect. This correlation suggests a possible explanation for the additive effect on cell death by a drug (Torin 1) which in our system appears only to be cytostatic: the rRNA synthesis inhibition caused by Torin 1, while by itself not strong enough to cause cell death, in combination with a sub-maximal dose of ActD might drive cells to abrogate enough nucleolar function to mediate cell death. This possibility is further explored in the Discussion section.

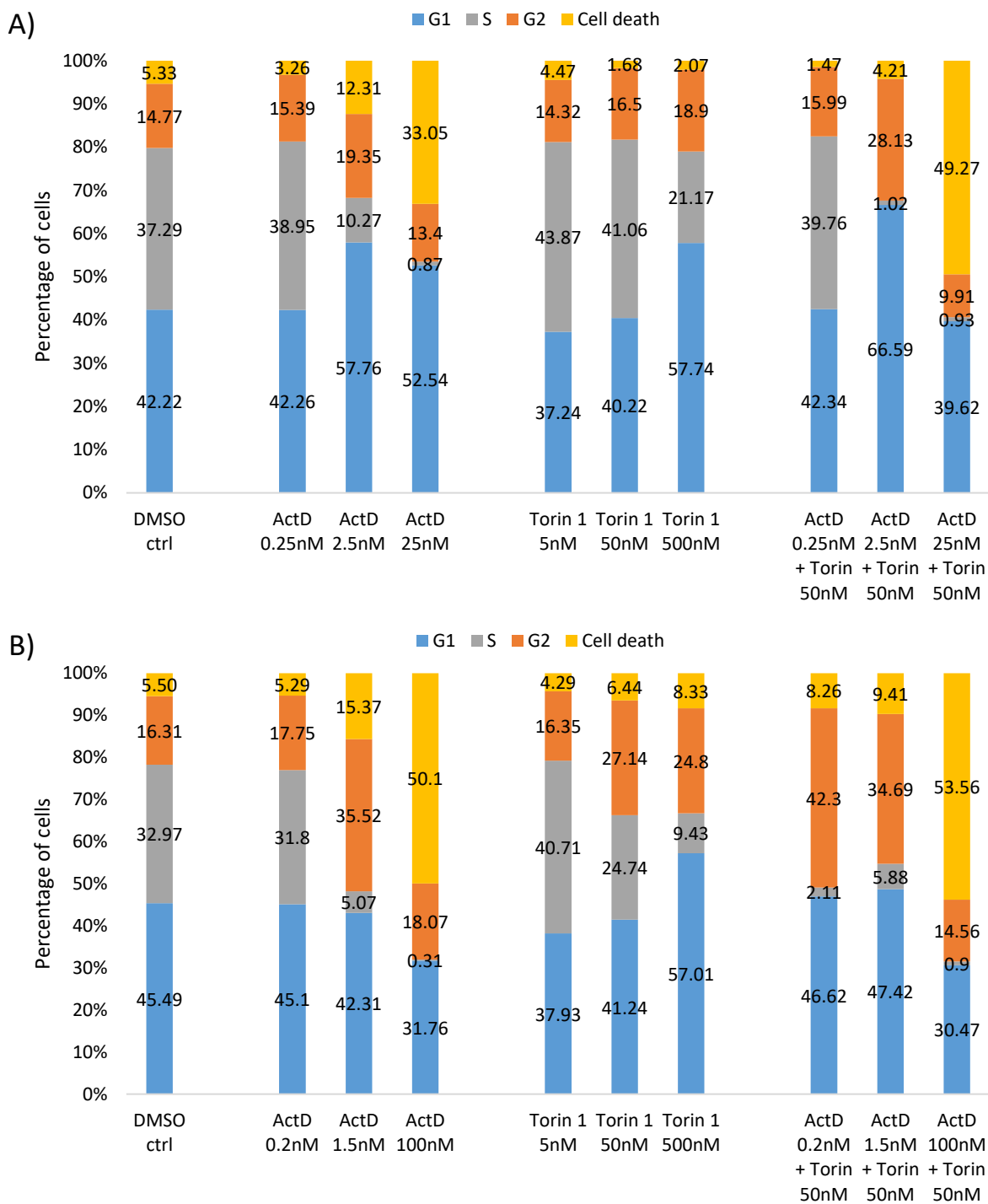


Figure 3.49. Effect of ActD and Torin 1 combinations on the cell cycle of RCC cells. A) ACHN and B) UoK111 cells treated with ActD and Torin 1 alone and in combination for 72 hours, followed by labelling of DNA with click chemistry, staining with 7-AAD, and flow cytometry analysis, as described in sections 2.4.5 and 2.4.6. A) The combination of 2.5 nM ActD with 50 nM Torin 1 significantly reduces the percentage of ACHN cells in S phase compared to the single drugs, while the combination of 25 nM ActD and 50 nM Torin 1 increases the percentage of cell death compared to the single drugs. B) The combination of 0.2 nM ActD with 50 nM Torin 1 significantly reduces the percentage of cells in S phase compared to the single drugs. The combination of 100 nM ActD and 50 nM Torin 1 increases the percentage of cell death compared to the single drugs. The percentage of the cells distributed in the different stages of cell cycle was performed on data obtained from a single experiment. Torin=Torin 1

Similarly, to determine if the reduction in viability of ACHN and UoK111 cells treated with combinations of ActD and AZD8055 observed in section 3.2.2 (Figure 3.43) is due to cell cycle arrest or to cell death we implemented cell cycle analysis using flow cytometry (see section 2.4). Figure 3.50 A) shows that in ACHN cells treated with increasing concentrations of ActD, the S-phase cell populations decrease dramatically, from 39.87% in cells treated with 0.25 nM to 4.39% when increasing the concentration by ten-fold, and to 0.43% when increasing ActD concentration by 100-fold. These cells also present increased percentages of cell death that change from 2.81% in ACHN treated with 0.25 nM ActD, to 4.56% and further 23.7% when treated with 2.5 nM and 25 nM, respectively. The effect of increased concentrations of AZD8055 in ACHN cells is less prominent than that of ActD, but decreased percentage of cells in S-phase is observed, diminishing from 48.8% to 41.81% and 35.78% when treated with 5 nM, 50 nM and 500 nM, respectively. There was no increase in the percent of cell death observed in ACHN cells treated with any AZD8055 concentration. Importantly, the combinations of 2.5 nM and 25 nM ActD with 50 nM AZD8055 show decreased populations of cells in S-phase compared to those observed with the single drugs. Additionally, the cells treated with 25 nM ActD and 50 nM AZD8055 display increased cell death (38.75%) compared to those observed in ACHN cells treated with 25 nM ActD alone (23.7%). These results are consistent with the effects observed for these combinations on viability of ACHN cells, presented in section 3.2.2.

Figure 3.50 B shows that UoK111 cells treated with increased concentrations of ActD display reduced populations of cells in S-phase that change from 34.52% when treated with 0.2 nM to 21.28% and 1.05%, when increasing the ActD concentration to 1.5 nM and 100 nM, respectively. Increased concentration of AZD8055 resulted in a 4.46% increase of cell death, and 11.16% decrease in the population in S-phase, comparing UoK111 cells treated with 500 nM versus 5 nM AZD8066. The combinations of ActD with 50 nM AZD8055 resulted in reduced percentages of cells in S-phase compared to treatment with ActD alone. The combination of 100 nM ActD with 50 nM AZD8055 also increased the percentage of cell death.

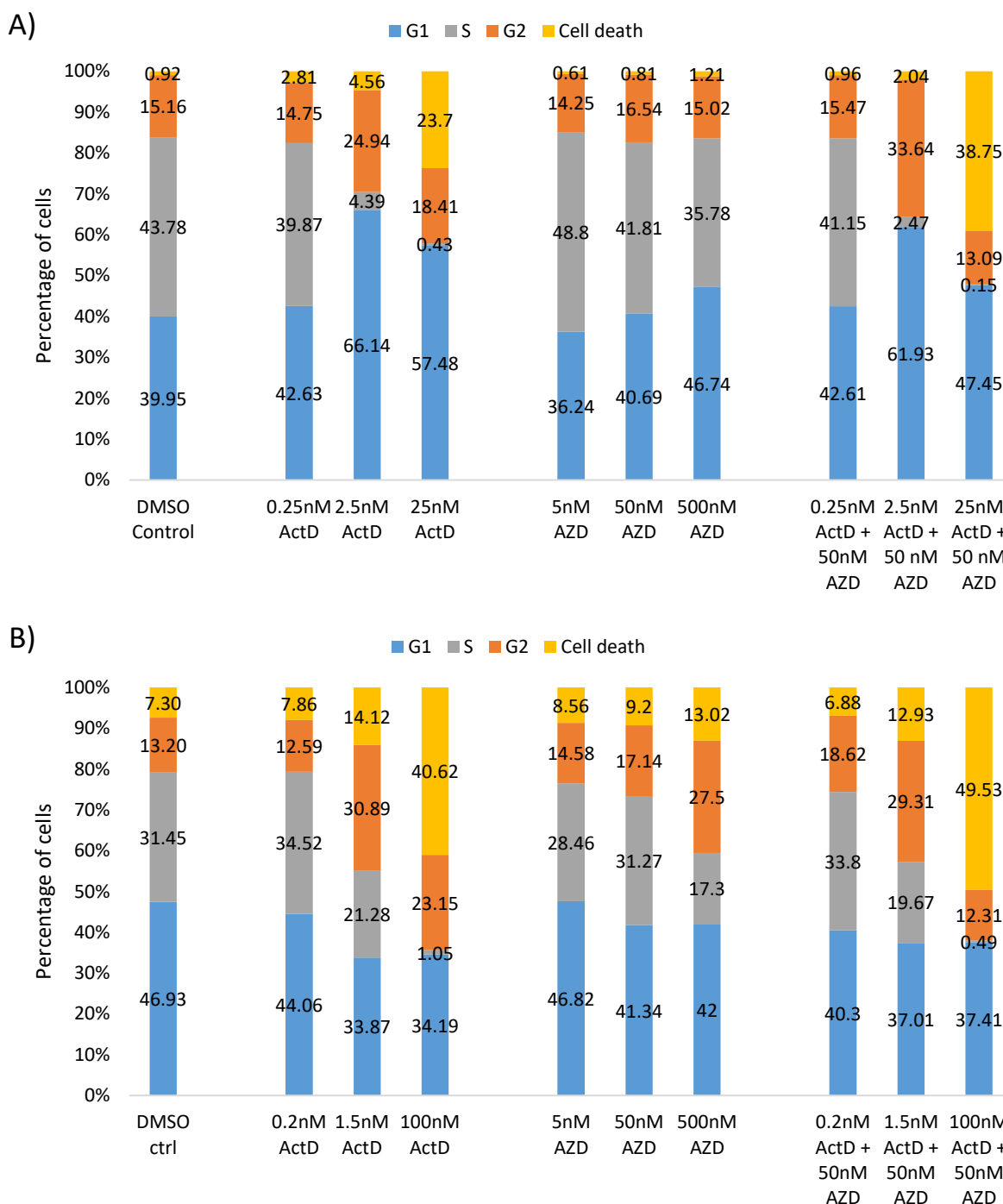


Figure 3.50. Effect of ActD and AZD8055 combinations on the cell cycle of RCC cells. A) ACHN and B) UoK111 cells treated with ActD and AZD8055 alone and in combination for 72 hours, followed by labelling of DNA with click chemistry, staining with 7-AAD, and flow cytometry analysis, as described in sections 2.4.5 and 2.4.6. A) The combination of 2.5 nM ActD with 50 nM AZD8055 significantly reduces the percentage of cells gated in S phase compared to the single drugs, while the combination of 25 nM ActD and 50 nM AZD8055 decreases the percentage of S-phase cells and increases the percentage apoptotic cells compared to the single drugs. B) The combination of 100 nM ActD and 50 nM AZD8055 decreases the percentage of S-phase cells and increases the percentage apoptotic cells compared to the single drugs. The percentage of the cells distributed in the different stages of cell cycle was performed on data obtained from a single experiment.

To further explore if the effects of the combinations of ActD and Rapamycin on viability of ACHN and UoK111 cells observed in section 3.2.4 (Figure 3.48) is due to cell cycle arrest or to cell death, we implemented cell cycle analysis using flow cytometry (see section 2.4).

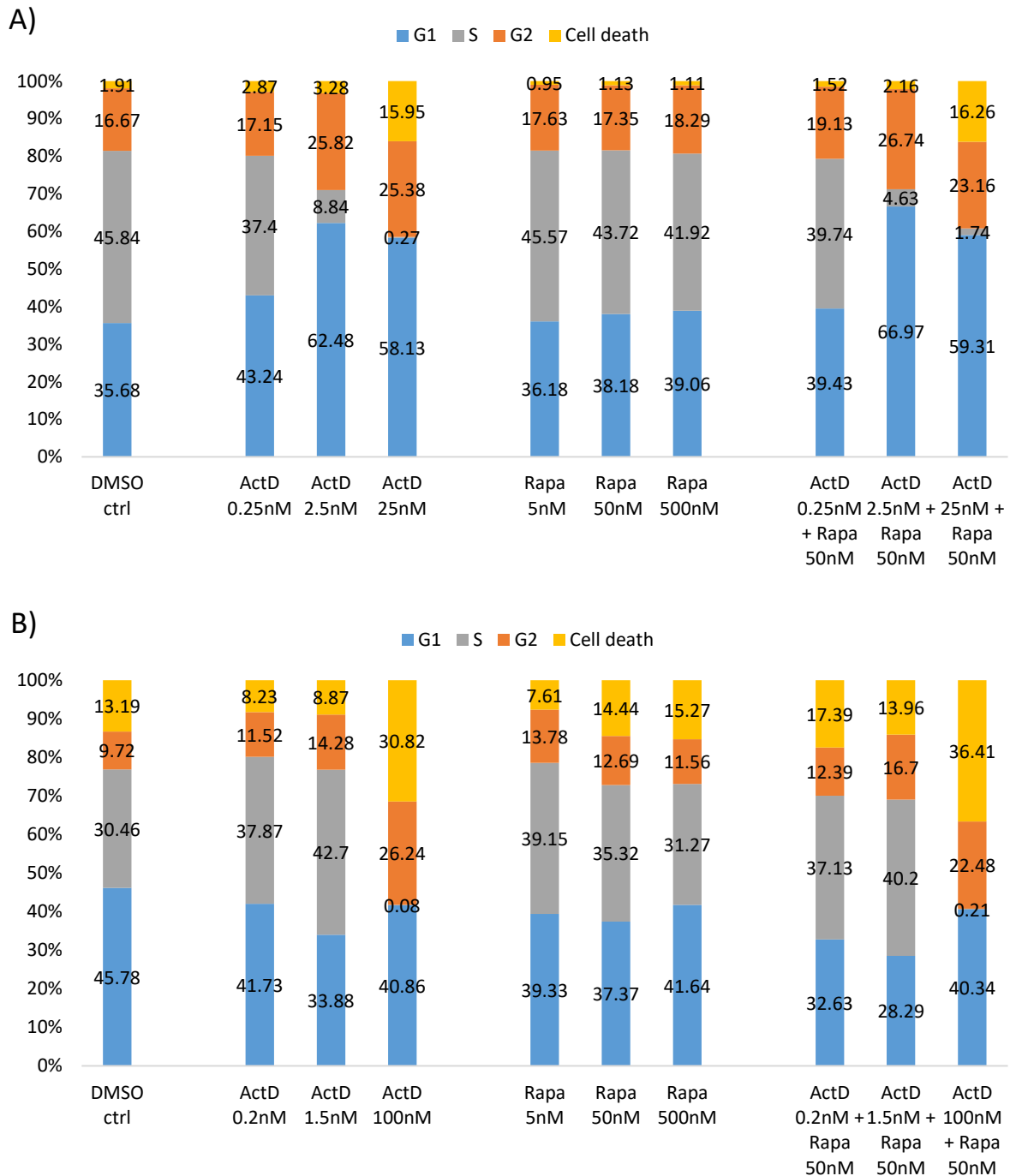


Figure 3.51. Effect of ActD and Rapamycin combinations on the cell cycle of RCC cells. A) ACHN and B) UoK111 cells treated with ActD and Rapamycin alone and in combination for 72 hours, followed by labelling of DNA with click chemistry, staining with 7-AAD, and flow cytometry analysis, as described in sections 2.4.5 and 2.4.6. A) The combination of 2.5 nM ActD with 50 nM Rapamycin further reduces the percentage of cells in S phase compared to 2.5 nM ActD alone, while the combination of 25 nM

ActD and 50 nM Rapamycin slightly increases the percentage cell death compared to the single drugs. B) The combination of 50 nM Rapamycin and ActD at 0.2 nM, 1.5 nM and 100 nM increase the percentage of cell death compared to the single drugs. The percentage of the cells distributed in the different stages of cell cycle was performed on data obtained from a single experiment. Rapa=Rapamycin.

Figure 3.51 A) shows reduction of the percentage of cells in S-phase and increased cell death in ACHN cells treated with increasing concentrations of ActD, as it has consistently being shown, while Rapamycin treatment did not elicit any changes in the cell cycle. The combination of ActD 2.5 nM with Rapamycin 50 nM displays slight reduction of the percentage of cells in S-phase compared to ActD alone. In Figure 3.51 B), UoK111 cells treated with increasing concentrations of ActD display reduced percentage of cells in S-phase and increased cell death. Treatment with Rapamycin showed a slight increase of cell death and reduction of the percentage of cells in S-phase. Combination of ActD 100 nM with Rapamycin 50 nM increased the percentage of cell death compared to ActD 100 nM alone.

Together, these results suggest that the combination of competitive mTOR inhibitors with ActD increase the cytostatic/cytotoxic effect of ActD alone, by reducing the percentage of cells in S-phase and promoting cell death at higher concentrations.

3.2.6 Conclusion

In this chapter, we aimed to test the hypothesis that modulation of nucleolar activity by targeting signalling pathways would sensitise the cells to the cytostatic/cytotoxic effect of the NFI ActD. The data presented shows that when used in combination, competitive inhibitors of the mTOR pathway maintain their inhibitory effect on the synthesis of rRNA and cell viability and it suggests that their additive interaction contributes to enhance the cytostatic/cytotoxic effects of ActD.

Our data shows that even when the allosteric inhibitor Rapamycin display limited inhibition of rRNA synthesis and cell viability at the concentrations tested, it contributes to the inhibitory activity of ActD when used in combination. This can be observed in figure 3.48, where ACHN and UoK111 cells treated with low concentrations of ActD in combination with rapamycin display decreased cell viability compared to cells treated with ActD alone.

In conclusion, these results demonstrate that in the combination of the NFI ActD with mTOR inhibitors, the inhibitory effect of both drugs on the synthesis of rRNA and cell viability is maintained, and suggests that the cytostatic/cytotoxic activity of ActD might be elicited.

4. Discussion

As outlined in section 1.5, the primary aims of this thesis were to assess if mTOR inhibitors effectively modulate nucleolar function in RCC cell lines, and if they can be used to sensitise cancer cells to the effects of nucleolar function inhibitors. The rationale behind these research aims included first the relevance of kidney cancer being among the ten types of cancer with highest incidence in the UK, and for which mortality rates have increased over 70% since the early 1970s (1). Of particular interest for this research is the fact that RCC accounts for 85% of kidney cancers and that survival to this type of cancer is deeply associated with the stage at diagnosis, where only a 12% 5-year survival rate is observed in patients diagnosed with metastatic RCC (2). As discussed in section 1.2, patients with metastatic cancer are often treated with systemic therapies and this is also the case for patients with advanced RCC, for whom treatment has changed drastically over the last 20 years with the development of new treatments such as mTOR inhibitors (480). Nevertheless, toxicity of these drugs, consequence of limited therapeutic index, remains a relevant issue as side effects severely affect the quality of life of the patients and their ability to continue the administration of the treatment (3–5). This, in addition to the expensive and time-consuming processes involved in the development of new drugs, underline the need to optimise the efficacy of the existing drugs for the treatment of patients with advanced RCC. The approach to address the latter proposed in the present thesis, relies in a strategy to sensitise RCC cells to the effects of nucleolar function inhibitors, particularly given the fact that changes in the morphology of the nucleoli are associated with high aggressiveness and poor prognosis of RCC patients (6), and the role that dysregulated nucleolar activity plays on increased proliferation of cancer cells (7). Additionally, identification of cellular pathways that modulate the nucleolar function for which targeted therapy exist, as is the case for the mTOR pathway (8,9), propels mTOR inhibitors as potential candidates for target-sensitised chemotherapy, especially when mTOR inhibitors are amongst the standard treatments for metastatic RCC. The proposed therapeutic strategy presented here will be the focus of discussion in this section.

Data presented in section 3.1 begins to address the aims of this thesis by assessing the effect of two types of mTOR inhibitors, allosteric and ATP-competitive inhibitors,

on the activity of mTOR using Western Blot to identify changes in the phosphorylation of two mTORC1 substrates, S6K and 4EBP1, which are the best known and most widely used markers of mTOR activity. The results shown in this section revealed that both types of mTOR inhibitors abrogate the phosphorylation of S6K at Thr389 in ACHN and UoK111 cells at low nanomolar concentrations. Additionally, the Western Blots of ACHN and UoK111 cells treated with mTOR inhibitors probing for 4EBP1 show that at concentrations around 1-2 nM there is a transition from an α -rich to β -rich pattern that is consistent with the concentrations at which inhibition of S6K phosphorylation at S389 is observed. A heightened intensity in the β and γ bands is observed in both cell lines treated with any mTOR inhibitor studied at concentrations 10 nM, 20 nM and 200 nM, which indicate, as expected (481,482), that the mTOR inhibitors tested effectively affect mTORC1 activity. While the use of an antibody against phosphorylated 4EBP1 at Thr37/46 was assessed here, 4EBP1 is actually known to have at least 7 phosphorylation sites out of which 5 are known to be phosphorylated by mTOR (455). For this reason, it was decided to use an antibody against total 4EBP1, and rely on the analysis of the different bands, which represent conformational variations of 4EBP1 that results from distinct phosphorylation pattern. Therefore, these data serve to inform the phenotypic studies to follow and draw attention to possibly different behaviours between allosteric and ATP-competitive inhibitors.

Increased signal of 4EBP1 β - and γ -forms in ACHN and UoK111 following treatment with allosteric and ATP-competitive mTOR inhibitors might indicate changes in the phosphorylation status of 4EBP1 and/or increased expression of 4EBP1. Interestingly, hyper-phosphorylation and over-expression of 4EBP1 have been widely reported across different types of cancer, including ccRCC, and these markers are associated with worsening prognosis of cancer patients (483–485). It has been observed that activation of ERK and p38 decrease expression of 4EBP1 (486). Considering that ERK and p38 are mitogen-activated protein kinases, an inhibitory off-target effect of mTORis on these kinases could be causing increased expression of 4EBP1. Furthermore, HIF-1 α has been reported to contribute to 4EBP1 expression (487), while HIF-1 α transcription has been shown to be promoted by mTORC1 activity and repressed following rapamycin treatment (488). Thus, reduced transcription of HIF-1 α following inhibition of mTORC1 activity in ACHN and UoK111 treated with mTORis

could account for the increased signal of 4EBP1 β - and γ -forms observed in figures 3.5 and 3.7. The increased signal of 4EBP1 bands following treatment with mTORis could also be the outcome of prevention of 4EBP1 degradation. Although phosphorylation is an important mechanism for protein ubiquitination and subsequent degradation, in proteins that require multi-site phosphorylation such as 4EBP1, which has at least 7 phosphorylation sites, it can contribute to the stabilisation of short-lived protein (485). Therefore, changes in the phosphorylation of 4EBP1 after treatment mTORis might not be sufficient for ubiquitination and degradation of 4EBP1.

The microplate-based analysis of rRNA synthesis used through this thesis to assess the effects of the drugs on the nucleolar function, consists on detection of nascent RNA labelled with 5-EU using Click chemistry, for which pulse labelling recommended time is between 30 to 60 minutes (489). Having compared the signal of 5-EU-labelled rRNA in cells that were pulsed with 5-EU for 30, 45 and 60 minutes, we concluded that 60 minute-pulse were required for optimum detection of newly synthesized rRNA (see Figure 3.10). Subsequently, the treatment time with ActD and mTOR inhibitors was determined taking into consideration that treatment with low concentrations of ActD has been shown to significantly inhibit the synthesis of rRNA after only 30 minutes (490). Ideally, treatment length is required to be longer than the pulse so that and that 5-EU-labelled rRNA provides a brief picture of the rDNA transcription status after treatment (491). The length of the drug treatment preceding the 5-EU pulse labelling was determined to be 2 hours, ensuring that the pulse would last a third of the treatment, while remaining short enough to visualise the effects of ActD on rRNA synthesis before other effects on the cell functions that might affect the results take place.

Detection of 5-EU-labelled rRNA using Click chemistry after treatment with a range of concentrations of ActD (0.1-100 nM) provided a full dose-response curve for both cell lines, ACHN and UoK111 cells. It is noticeable that the IC₅₀s for rRNA synthesis inhibition by ActD are consistently similar across cell lines. In addition to the dose response data shown in Figure 3.11 for ACHN and UoK111 cells showing remarkably similar IC₅₀s, in our lab we have also observed such similarity with other human cell lines and even murine embryo fibroblasts (Rogoysky, Moreno-Laporta et al., manuscript in preparation). The same is not true for the IC₅₀s for the inhibition of cell

viability, where other factors play a role, particularly the p53 status of cells (Rogoysky, Moreno-Laporta *et al.*, manuscript in preparation). This similarity in IC50s for rRNA synthesis inhibition by ActD across cell lines may not be surprising. A simple model of chemical equilibrium for a target (T) and a ligand (L) shows that the ratio of ligand bound to the target to free ligand is $\frac{[LT]}{[L]} = [T]k_{Aff}$. Given the fact that the target in this case is rDNA, its high conservation across species (Gerbi, 1986) would imply almost identical k_{Aff} , while the consistent number of nucleolar organising regions (NORs) per diploid genome ensures a similar $[T]$ across cell lines. Thus, it would be reasonable to expect that a measured activity of ActD could be extrapolatable to other systems.

Detection of labelled rRNA with 5-EU in ACHN and UoK111 cells treated with mTOR inhibitors revealed that only Torin 1 but none of the allosteric mTOR inhibitors (Rapamycin, Temsirolimus and Everolimus) inhibits rRNA synthesis in a concentration-dependent manner within the concentration range tested. In contrast to our findings, decreased rDNA transcription following treatment with rapamycin has been previously reported in lymphosarcoma cells (492). However, these results were observed after an incubation period of 24 hours whereas our results were observed after only 2-hour treatment. This is relevant because prolonged treatment with rapamycin has been reported to inhibit mTORC2 activity along with mTORC1 (392,493), hence reduced rDNA transcription could be caused by the effect of the allosteric inhibitor on both mTOR complexes, which we were able to observe after only 2-hour treatment with the ATP-competitive inhibitor Torin 1.

Importantly, we observed that treatment with Torin 1 not only decreased 5-EU incorporation, but also significantly reduced nucleolar area compared to the allosteric inhibitors. Increased size of nucleoli is associated with amplified ribosomal biogenesis and higher protein turnover, which are frequently found in cancer (195), whereas reduction of nucleolar size is associated to inhibition of rDNA transcription and nucleolar disruption. Accordingly, our results show that the ATP-competitive inhibitor Torin 1, decreases 5-EU incorporation, reduces nucleolar area, and inhibits the phosphorylation of TIF-IA at S649, which is required for TIF-IA activity and initiation of rDNA transcription. Thus, our results suggest that inhibition of TIF-IA phosphorylation by Torin 1 might affect nucleolar function and morphology by repressing rDNA

transcription. Interestingly, small nucleoli have been associated with longevity and recently the use of mTOR inhibitors to treat age-related pathologies as well as to extend lifespan has been the focus of research (494–496). Our findings showing the effect of the ATP-competitive inhibitor of mTOR Torin 1 on the phosphorylation of TIF-IA and reduction of nucleolar size could provide another mechanism underlying the involvement of mTOR and nucleolar function on the regulation of aging.

Although treatment with allosteric mTORis did not reduced rDNA transcription in a concentration-dependent manner, cells treated with allosteric mTOR inhibitors display a slightly reduced incorporation of 5-EU when compared to the control, for which we do not have a full explanation. The Cy3 signal is reduced by 10-40% with respect to controls and this reduction appears variable over experiments. Interestingly, Valentina Iadevaia and colleagues reported partial inhibition of rDNA transcription following treatment with 5 nM rapamycin for 90 minutes, and observed that higher concentrations of rapamycin inhibited synthesis of RNA to a similar extent than that achieved at 5 nM (9). We speculate that this small reduction may be due to an mTOR target protein, or a phosphorylation site within a protein that we fail to detect in Western blot (8,208,497). It may also be due to a change in subcellular localisation of a small fraction of an mTOR target (498). If only a small fraction of a target is involved, then it is reasonable to assume that any effect observed would be small and that would preclude detection of a shoulder typical of a Hill-type of dose response curve.

Having observed consistent inhibition of the phosphorylation of S6K, along with increased presence of β and γ forms of 4EBP1 in cells treated with in cells treated with both types of mTOR inhibitors, the differential effect of these drugs on the synthesis of rRNA suggested alternate effect on the mTOR activity. It is well documented that while allosteric inhibitors only affect the activity of mTORC1, ATP-competitive inhibitors abrogate the activity of both mTOR complexes (499). However, modulation of the nucleolar function by the mTOR pathway has been attributed to the activation of RNA Pol I transcription factor TIF-IA by the mTORC1 substrate S6K (186), which would not explain the differential effect observed on rRNA synthesis. Given that, Torin 1 is a kinase inhibitor which are known to produce off-target effects (500), study of alternative targets of Torin 1 that might explain the differential effect of Torin 1 on the synthesis of rRNA using siRNA was considered. Nevertheless, said studies would

require incubation of cells without some mTOR components for at least 24 hours that might cause even larger, indirect, off-target effects which would make the interpretation of such results even more difficult. Considering the aforementioned reasons, in section 3.1.3 we focused on TIF-IA and examined whether Torin 1 and the allosteric inhibitors differently affected phosphorylation of this transcription factor at concentrations in the range of the S6K and 4EBP1 phosphorylation inhibition ranges, which are assumed to be on-target. Western Blot analyses presented in section 3.1.3 showed that indeed, phosphorylation of TIF-IA at S649 was inhibited in cells treated with Torin 1 with IC50s of 0.13 nM and 1.08 nM for ACHN and UoK111 cells respectively, while none of the allosteric inhibitors affected TIF-IA phosphorylation. Importantly, TIF-IA activity is regulated through multi-site phosphorylation, and while S199 has been observed to be dependent on mTORC1 activity and inhibited by rapamycin (186), of S633 and S649 are phosphorylated by ERK and ribosomal S6 kinase (RSK), respectively (184). Importantly, RSK is also activated through phosphorylation by ERK, PDK1, and RSK itself (501). Interestingly, mTORC2 substrate AKT negatively regulates the activation of ERK by phosphorylating inhibitory sites in the Raf N-terminus (502). This could explain why ATP-competitive inhibitor Torin 1, but not the allosteric inhibitors, inhibits phosphorylation of TIF-IA at S649 and reduces rDNA transcription. In order to further demonstrate whether inhibition of mTORC2 by the ATP-competitive inhibitor is causing inhibition of TIF-IA phosphorylation and rDNA synthesis, knockdown of mTORC2 using RICTOR siRNA could be performed. The effect of Rictor siRNA on TIF-IA phosphorylation and rDNA transcription could be then compared to the effects of treatment with Torin 1 and Akt siRNA to establish if it is Torin 1-mediated inhibition of mTORC2 activity what is actually causing decreased rDNA transcription through inhibition of TIF-IA S649 phosphorylation.

This finding was relevant to identify Torin 1 as a modulator of nucleolar function and a potential candidate to test the primary hypothesis of this thesis. Since investigating the precise mechanism by which ATP-competitive but not allosteric mTOR inhibitors modulate rRNA synthesis was not the aim of the present thesis, we did not performed additional studies. Nevertheless, we recognise that further studies, including analysis of the phosphorylation of mTORC1 and mTORC2 substrates on cells treated with

allosteric and ATP-competitive mTOR inhibitors using mass-spectrometry would be required for a better understanding of how the different type of drugs affect the activity of both mTOR complexes and their interaction with their respective substrates. An example of such study was performed by Christine Mayer and colleagues, who demonstrated that Rapamycin impairs initiation of rDNA transcription by inhibiting the activity of TIF-IA, and identified that mTOR signalling-dependent phosphorylation of TIF-IA at S44 is required for TIF-IA activation (186).

Finding that Torin 1, but not allosteric inhibitors, modulate the synthesis of rRNA in RCC cells, and that the differential effect on nucleolar function is mirrored by the phosphorylation of TIF-IA proposed Torin 1 to be the system to test whether cells can be sensitised to the action of a nucleolar function inhibitor through mTOR-mediated modulation of the nucleolar activity. We then investigated if the mTOR inhibitors have an effect on cell viability of RCC cell lines, and if so, whether the effect is consistent with the nucleolar modulation previously observed. Results from the cell viability assays presented on section 3.1.4 indicate that RCC cells treated with allosteric inhibitors do not display a typical response curve within the range of concentrations tested. We limited the concentration range of the mTOR inhibitors considering that the phosphorylation of S6K on T389 is the best-known marker for mTOR activity, and that effects observed at concentrations higher than 100-fold the IC₅₀ for inhibition of the phosphorylation of S6K could be off-target effects. The lack of effect of allosteric mTOR inhibitors Rapamycin, Temsirolimus and Everolimus observed on viability *in vitro* was unexpected considering that sensitivity of these drugs has been reported in the Genomics of Drug Sensitivity in Cancer database (cancerrxgene.org) (503), and that the drugs work with RCC patients. The major discrepancies observed among our findings and the cancerrxgene.org database were the reported IC₅₀s for inhibition of cell viability of ACHN and 786-O cells treated with rapamycin of 0.0489 μ M and 0.0368 μ M, respectively, in contrast to the lack of effect observed in our assays. While the maximum screening concentration of Rapamycin used by the Cancer Genome Project at the Wellcome Sanger Institute was 0.1 μ M, which is within the concentration range that we used, experimental conditions varied, including the type of assay used to measure cell viability, which in their case Promega CellTiter-Glo, whereas we used MTT assay. Additionally, Rapamycin IC₅₀s for inhibition of cell viability reported for

A704 and Caki-1 are 0.1866 μM and 0.3544 μM . However, these values are higher than the maximum screening concentration of Rapamycin that we used 0.125 μM . The IC50s of Temsirolimus for inhibition of cell viability of ACHN, A704, Caki-1 and 786-O were all above 4.2 μM , which is almost 10-fold the maximum screening concentration of Temsirolimus that we used 0.5 μM .

As for the therapeutic effect observed by Temsirolimus and Everolimus in RCC patients, it is important to note that mTOR inhibitors target various hallmarks of cancer apart from preventing dysregulation of the mTOR pathway that lead to oncogenic capacity for self-sufficiency in growth signals and insensitivity to growth-inhibitory signals (see introduction section 1.4.3). mTOR inhibitors also display anti-angiogenic properties by reducing endothelial cell proliferation, survival and migration, decreasing vascular endothelial growth factor (VEGF) production, and inducing polarization of tumour-associated macrophages to an anti-angiogenic phenotype (504). Additionally, the mTOR pathway influences immunity within the tumour microenvironment through modulation of the responses of immune cells including T-cells, macrophages and B-cells (505). Thus, it is likely that the clinical response to mTOR inhibitors Temsirolimus and Everolimus is a consequence of the interaction of the drugs with the tumour microenvironment and other signalling pathways associated with different hallmarks of cancer.

Subsequent analyses of the effect of mTOR inhibitors on cell viability revealed that only the competitive inhibitor Torin 1 reduced viability of ACHN and UoK111 cells in a concentration-dependent manner, and that reduction of cell viability was achieved at a similar concentration range than that observed to decrease rRNA synthesis. This raises the question of whether it is reasonable to assume that the observed correlation between inhibition of rRNA synthesis and cell viability reduction is actually causal. Considering the well-established role of nucleolar disruption in the induction of tumour cell death (see and references therein)(141,506), it is quite possible that inhibition of nucleolar function is an important part of the mechanism of action of these drugs.

While MTT assay showed us that ActD and Torin 1 inhibit cell viability of ACHN and UoK111, this assay does not provide information regarding the cellular outcome(s) mediating said inhibition of cell viability. To understand whether inhibition of cell

viability by these drugs was caused by cell cycle arrest or induction of cell death we performed cell cycle analysis using flow cytometry. Cells treated with ActD displayed concentration-dependent decreased percentage of S-phase cells and increased cell death, which in the case of ActD is presumably apoptosis (472). Interestingly, at concentrations closer to the IC₅₀ for inhibition of cell viability, a marked reduction of cells in S-phase is observed, while at higher concentrations (closer to that where maximum inhibition of cell viability is observed) S-phase is completely shut down and the percentage of apoptotic cells increases significantly. Considering that the calculated IC₅₀s of ActD for inhibition of cell viability (approx. 0.8 nM and 1.9 nM for ACHN and UoK111 cells respectively) and the IC₅₀ for inhibition of rRNA synthesis (approx. 1.25 nM and 1.26 nM for ACHN and UoK111 cells respectively) are similar, it can be suggested that partial inhibition of rRNA synthesis at concentrations around the IC₅₀, elicits the cytostatic effect of ActD mediated by reduction of cells in S-phase, whereas extensive inhibition of rRNA synthesis (still achieved at low-doses) prompts its cytotoxic effect promoting apoptosis. If this supposition were true, one could then argue that low concentrations of ActD (around the IC₅₀) could turn the effect of ActD from cytostatic to cytotoxic when combined with a nucleolar modulator, such as the mTOR inhibitors like Torin 1 that can inhibit rRNA synthesis while displaying only a cytostatic effect (see Figure 4.1 below).

Having proved that the ATP-competitive mTOR inhibitor Torin 1 is an adequate system to test the working hypothesis of this thesis, we proceeded to assess the effect of the combination on rRNA synthesis. As mentioned before (see section 3.2.1), we changed the ATP-competitive inhibitor used in combination with ActD to the ATP-competitive mTOR inhibitor AZD8055 when investigating the effect of the drug combination on the synthesis of rRNA. Similarly to Torin 1, this drug inhibits mTOR kinase, repressing the activity of both mTOR complexes (404), and it displayed concentration-dependent inhibition of rRNA synthesis and cell viability when used alone. Detection of 5-EU-labelled rRNA with Click chemistry in ACHN and UoK111 cells treated with ActD and AZD8055, as single drugs and in combination, revealed that, when combined both drugs maintained their individual inhibitory effects on rRNA, while they both contribute to the inhibition of rRNA. These results are encouraging and suggest there the combination is additive (507).

We followed to examine whether the effect of the combination of ATP-competitive inhibitor with the nucleolar function inhibitor ActD on cell viability of ACHN and UoK111 cells would be consistent with the inhibitory effect they displayed on rRNA synthesis. Results from the MTT assay from ACHN and UoK111 treated with ActD and AZD8055, alone and in combination shows that as single drugs, ActD and AZD8055 inhibit cell viability and that when combined, each drug maintains their individual effect, contributing to inhibition of cell viability. Similar results were obtained for ActD and Torin 1, highlighting that our hypothesis is not exclusive for Torin 1, but that it can apply to other ATP-competitive mTOR inhibitors – and even other kinase inhibitors – as long as they modulate the nucleolar function. Evaluation of the drug interaction between ActD and Torin 1 using isobolograms confirms that in the combination, the drugs retain their individual inhibitory effects on cell viability, contributing to an added effect (447,478).

Flow cytometry analysis of ACHN and UoK111 cells treated with ActD and an ATP-competitive inhibitor alone and in combination were undertaken in order to determine the nature of the cellular effects responsible for the loss of cell viability in the different treatment conditions. As observed in Figure 3.50, treating cells with a concentration of ActD close to the IC₅₀ of inhibition of rRNA synthesis with 50 nM AZD8055 (a concentration that inhibits rRNA synthesis), reduces the percentage of cells in S-phase compared to the single drugs. Alternatively, cells treated with a combination of a concentration of ActD close to the maximum inhibitory effect with 50 nM AZD8055 display an increase in the percentage of cell death.

The fact that at high concentrations the cellular response tends to switch from proliferation arrest to cell death means that assessing overall cell viability by MTT may not be quantitatively reliable at those concentrations. Isobolograms were constructed on the basis of quantitating an overall cell viability response. However, the underlying cellular change that causes the change in MTT response appears to change along the dose-response curve, from proliferation arrest to cell death. The calculation of an isobologram depends on using the dose-response curves of the individual drugs to predict what dose would produce an effect equivalent to the one reached by the mix. Given the qualitative changes observed, the isobolographic calculation may not be strictly valid at high concentrations.

Hence, at high concentrations we find the data from Figures 3.43 and 3.44 to be more reliable. It is important to note, from the earlier comment, that in the cases of Figures 3.43 and 3.44 the isobolographic calculation cannot be performed: since the isobolographic calculation depends on estimating the concentrations of the individual drugs require to reach a certain effect level observed in the mix, if both individual drugs cannot reach such an effect level (as in Figures 3.43 and 3.44), then the isobologram is not defined (i.e. calculable) at such concentrations.

In fact, when cell viability curves for ActD are constructed with a large number of concentrations points in the high slope region, it can be observed that the curves are actually bimodal (bimodality is apparent in Figures 3.22 and 3.23), with one response correlating mainly with cell cycle arrest and the other with cell death (see Figures 3.33 and 3.34). The response of rRNA synthesis inhibition by ActD, on the other hand does not seem to show more than one mode. This different behaviour of the rRNA synthesis and cell viability responses is described in Figure 4.1.

Torin 1 and AZD80555, on the other hand, never reach high levels of rRNA synthesis inhibition, and we speculate that this is the reason why they usually do not cause a significant increase in cell death *in vitro*. As discussed, they do not push cells into the cell death region within the concentrations tested in the scheme of Figure 4.1. In summary, to draw our conclusions on the behaviour of the drug combinations at high concentrations we rely on the cell viability plots of Figures 3.43 and 3.44 and the cell cycle analysis of Figures 3.49 and 3.50.

In conclusion, we propose that drugs that inhibit pathways that regulate nucleolar function may be combined with drugs that target nucleolar function to achieve a cytotoxic effect at lower concentration of both drugs. As depicted in the scheme shown below (Figure 4.1), the targeted therapy drug serves to contribute to drive rRNA synthesis down to allow a NFI to reach a cytotoxic level of rRNA synthesis shutdown. It is not yet fully understood how nucleolar disruption can be translated into cell death. Our group has established a link between nucleolar stress and p53 activation (141,506), but this mechanism would not operate in tumour cells harbouring TP53 mutations. However, recently Thoms and Stark have proposed a mechanism by which nucleolar stress translates into a NF- κ B response (168). Regardless of the mechanism,

we propose that nucleolar function is determinant of the cellular fate, which can progress from full replicative capacity with no or weak inhibition to cell cycle arrest and cell death at strong inhibition. This mechanism is depicted in the scheme of Figure 4.1. The targeted therapeutic thus serves to sensitise the nucleoli and does not have to be (and generally is not) cytotoxic: the final cytotoxic effect is achieved by the degree of rRNA synthesis shutdown (Figure 4.1).

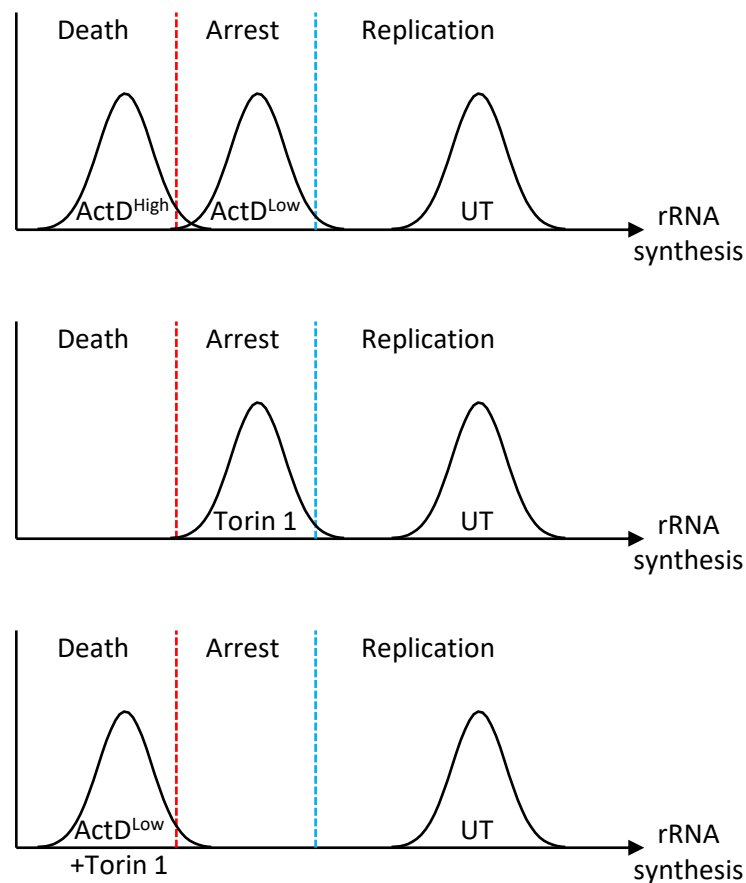


Figure 4.1. Model for sensitised nucleolar chemotherapy. The scheme depicts cell populations with varying degrees of rRNA synthesis inhibition, which for untreated (UT) cells corresponds to no inhibition, and their proliferative status.

We consider that this proposed mechanism offers the means for the rational design of potentially useful anti-cancer therapies that take advantage of the high specificity of targeted therapies and of the cytotoxicity of chemotherapy.

5. Conclusions

The present work identifies a novel feature of nucleolar targeting-based chemotherapy, in that it can be sensitised by targeted therapeutic agents. To our knowledge, the more common DNA damage-based forms of chemotherapy are difficult to sensitise in order to increase the therapeutic index. Often, this is achieved by combinations of two or more chemotherapeutic agents, but these combinations can be limited by the fact that a cell cycle arresting chemotherapeutic agent might prevent the activity of another agent that arrests the cell cycle at a different stage. This phenomenon is called cell cycle mediated resistance (CCMR) (111). Separate research in our laboratory has shown that NFIs offer a therapeutic opportunity in this respect. Since nucleoli are active at all stages of the cell cycle, except mitosis (508,509), so are NFIs effective at all stages and we have observed that combinations of DNA-based chemotherapeutics with ActD can overcome CCMR (Rogoysky, Moreno-Laporta *et al.*, manuscript in preparation). Another strategy for the sensitisation of cancer cells to DNA-based chemotherapeutics that has been explored is “cyclotherapy”, which depends on the tumour cells harbouring mutated or otherwise inactivated TP53 (472). Cyclotherapy exploits the fact that normal cells express functional p53 and, in principle, could undergo cell cycle arrest by an appropriate agent, which would render them less sensitive than tumour cells to an anti-proliferative agent. This approach to increasing the therapeutic index of an agent is therefore based on diminishing the sensitivity of normal cells, rather than increasing that of tumour cells (472).

In the present work we show that nucleoli can be sensitised to the action of a nucleolus- (or rRNA synthesis-) specific agent by compounds that specifically target a signalling pathway that modulates nucleolar activity. The consequence of this sensitisation is that a NFI can then be applied at a lower dose to achieve the same therapeutic effect. Thus, the approach combines the target specificity of biochemical pathway inhibitors with the cytotoxicity of a chemotherapeutic agent. This approach, which can be called “target-sensitised chemotherapy”, opens a number of opportunities to explore. While we resorted to mTOR as the most likely candidate for proof of concept, other signalling pathways that modulate the metabolic activity of cancer cells can and should be explored. Emerging NFIs as well as established chemotherapeutic drugs that might comprise nucleolar disruption as part of their

mechanism of action are also candidates. Finally, other nucleolar processes apart from rRNA synthesis, such as rRNA processing, that we can currently target (231,510) should also be explored for combinatorial potential. However, one important advantage of the drug combination strategy presented here is that it can be implemented with existing oncology drugs, and can therefore be readily subjected to pre-clinical studies and, if successful, easily translated from bench to bedside.

6. Future Work

A number of possible research lines emerge from the validation of our hypothesis that the nucleolus can be sensitised by targeted therapies to the action of nucleolar function inhibiting chemotherapeutic agents.

In terms of the sensitising targeted therapy, mTOR appears to be the best choice at present, since we know that it is a major controller of cell metabolism, including nucleolar function. Importantly, mTOR targeting is a currently used cancer therapeutic strategy, which would make a successful combination easily translatable to pre-clinical and clinical trials. However, the Western blot approach that we have followed here, while sufficient for proof of concept that we sought, leaves a number of questions unanswered regarding the exact identity and cellular location of the signalling events involved. It would therefore be interesting to apply mass spectrometry of phosphorylated proteins to resolve the cause of the difference between the actions of allosteric and ATP-competitive mTOR inhibitors, and also to identify any phosphorylation events that might form the basis for the activity of Rapamycin in combination with ActD. This information might not be required to plan pre-clinical studies, but it might help to stratify tumours that would present higher or lower sensitivity to an anti-nucleolar drug combination.

In terms of other potentially useful targeting drugs, it would be interesting to explore other signalling pathways such as EGFR, ERK, MAPK, etc., which are currently clinically exploited. As mentioned in the previous section, other NFIs, particularly those targeting nucleolar functions different from 48S rRNA synthesis, should also be explored.


For a better understanding of the role of nucleoli as stress sensors, investigation of nucleolar morphological changes and nucleolar protein translocation to explore if there is any process associated with the stages of cell proliferation, arrest and cell death. This would shed light on the mechanism by which nucleolar function inhibition translates to cell stress.

Finally, we believe that the data presented here outlines the opportunity of applying the combination of ActD and AZD8055 to a pre-clinical murine system. One advantage of the mechanism of action that we propose here is that it can be validated *in vivo*

because 5-EU incorporation to label RNA synthesis can also be performed on whole animals. This means that all aspects of the model studied here *in vitro* (rRNA synthesis, phosphorylation, cell proliferation and death) could in principle be studied *in vivo* as well. Thus, a transition to an *in vivo* system need not be limited to studying tumour reduction only but could include assessment of the validity of the proposed underlying mechanism as well.

7. Appendix

7.1 Certificates of cell line authenticity for RCC cells

 UNIVERSITY OF LIVERPOOL Institute of Translational Medicine	Cell Line Authentication Facility Academic lead: Dr Lakis Liloglou WH Duncan Building, W. Derby Str, L7 8TX Tel 0151 7949121 Email: T.Liloglou@liv.ac.uk
---	--

Certificate of cell line authenticity

Customer	Carlos Rubbi
Organisation	UOL
Tested Cell line	ACHN
Authentication method	GenePrint® 10, Promega Corporation
Database(s) used for comparison	DSMZ
Authentication undertaken by	AJB
Date	17/04/2019

	Alleles		Match
	Reference	Sample	
TH01	8	8	✓
D21S11	30	30	✓
D5S818	12	12	✓
D13S317	12	12	✓
D7S820	9	11	✓
D16S539	12	13	✓
CSF1PO	11	11	✓
AMEL	X	X	✓
vWA	16	17	✓
TPOX	8	11	✓

Comments (optional): 100% as cell line on Cellosaurus and DSMZ sites.

Operator

Andy Birss
 Research Technician

Academic Lead



Dr Lakis Liloglou
 Senior Lecturer

Certificate of cell line authenticity

Customer	Carlos Rubbi
Organisation	UOL
Tested Cell line	UOK111
Authentication method	GenePrint® 10, Promega Corporation
Database(s) used for comparison	DSMZ
Authentication undertaken by	AJB
Date	17/04/2019

	Alleles		Match
	9	9.3	
TH01	9	9.3	✓
D21S11	30.2	31.2	Not used
D5S818	12	13	✓
D13S317	11	12	✓
D7S820	10	12	✓
D16S539	10	12	X
CSF1PO	10	12	✓
AMEL	X	X	✓
vWA	16	16	X
TPOX	8	8	✓

Comments (optional): 86% on DSMZ site as CCL-110 Detroit 551.


Operator

Andy Birss
Research Technician

Academic Lead



Dr Lakis Liloglou
Senior Lecturer

 UNIVERSITY OF LIVERPOOL Institute of Translational Medicine	Cell Line Authentication Facility Academic lead: Dr Lakis Liloglou WH Duncan Building, W. Derby Str, L7 8TX Tel 0151 7949121 Email: T.Liloglou@liv.ac.uk
---	--

Certificate of cell line authenticity

Customer	Lucia Moreno Laporta
Organisation	UoL
Tested Cell line	Caki-1
Authentication method	GenePrint® 10, Promega Corporation
Database(s) used for comparison	Cellosaurus / DSMZ / ATCC
Authentication undertaken by	SDH
Date	08/01/2020

	Alleles		Match
TH01	6	8	✓
D21S11	/	/	/
D5S818	15	16	X
D13S317	11	12	✓
D7S820	8	12	✓
D16S539	12	12	✓
CSF1PO	8	10	X / ✓
AMEL	X	X	✓
vWA	15	17	✓
TPOX	8	11	✓

Comments (optional): 80% match as Caki-1 on Cellosaurus, DSMZ, and ATCC sites.

https://web.expasy.org/cellosaurus/CVCL_0234

Operator




Steven Hoang
Research Technician

Academic Lead



Dr Lakis Liloglou
Senior Lecturer

 UNIVERSITY OF LIVERPOOL Institute of Translational Medicine	Cell Line Authentication Facility Academic lead: Dr Lakis Liloglou WH Duncan Building, W. Derby Str, L7 8TX Tel 0151 7949121 Email: T.Liloglou@liv.ac.uk
---	--

Certificate of cell line authenticity

Customer	Lucia Moreno Laporta
Organisation	UoL
Tested Cell line	A704
Authentication method	GenePrint® 10, Promega Corporation
Database(s) used for comparison	Cellosaurus / ATCC / DSMZ
Authentication undertaken by	SDH
Date	08/01/2020

	Alleles		Match
TH01	7	9	✓
D21S11	28	32	✓
D5S818	15	15	X
D13S317	8	8	✓
D7S820	10	10	✓
D16S539	12	13	✓
CSF1PO	7	8	✓
AMEL	X	Y	✓
vWA	14	18	✓
TPOX	11	11	✓

Comments (optional): 89% match as A704 on Cellosaurus, DSMZ and ATCC sites.

https://web.expasy.org/cellosaurus/CVCL_1065

Operator




Steven Hoang
Research Technician

Academic Lead



Dr Lakis Liloglou
Senior Lecturer

 UNIVERSITY OF LIVERPOOL Institute of Translational Medicine	Cell Line Authentication Facility Academic lead: Dr Lakis Liloglou WH Duncan Building, W. Derby Str, L7 8TX Tel 0151 7949121 Email: T.Liloglou@liv.ac.uk
---	--

Certificate of cell line authenticity

Customer	Lucia Moreno Laporta
Organisation	UoL
Tested Cell line	786-O
Authentication method	GenePrint® 10, Promega Corporation
Database(s) used for comparison	Cellosaurus / DSMZ / ATCC
Authentication undertaken by	SDH
Date	08/01/2020

	Alleles		Match
TH01	6	9.3	✓
D21S11	29	30	✓
D5S818	15	16	✗
D13S317	8	8	✓
D7S820	11	12	✓
D16S539	12	12	✓
CSF1PO	10	10	✓
AMEL	X	Y	✓
vWA	15	17	✓
TPOX	8	11	✓

Comments (optional): 89% match as 786-O on Cellosaurus, DSMZ and ATCC sites.

Operator



Steven Hoang
Research Technician

Academic Lead



Dr Lakis Liloglou
Senior Lecturer

7.2 Analysis protocol for 5-ethynyl uridine-labelled nucleolar images

Analyses were implemented in CellProfiler (436) and SQLiteStudio v3.3.3 (<https://sqlitestudio.pl/>) running SQLite version 3.35.4.

Table 7.1 Segmentation of nuclear images

Input	One- or more-channel images of nuclei (DAPI). Image metadata CSV file (plate location, treatment, cell line, etc.)
Output	Binary masks of nuclei. The filling number of the mask corresponds to the object number.
Step	Purpose
Metadata extraction	Metadata is extracted from folder and file names and CSV files and images are matched to metadata.
DoG filter	A Difference of Gaussian bandpass filter both reduces image noise and low frequency intensity variations across the field of view.
Nuclei segmentation	DAPI images are segmented with a Minimum Cross-Entropy method to produce raw nuclear masks
Object filtering	Nuclear masks are filtered by size and form factor to eliminate poorly resolved nuclei.
Saving	Binary masks of nuclei are exported.

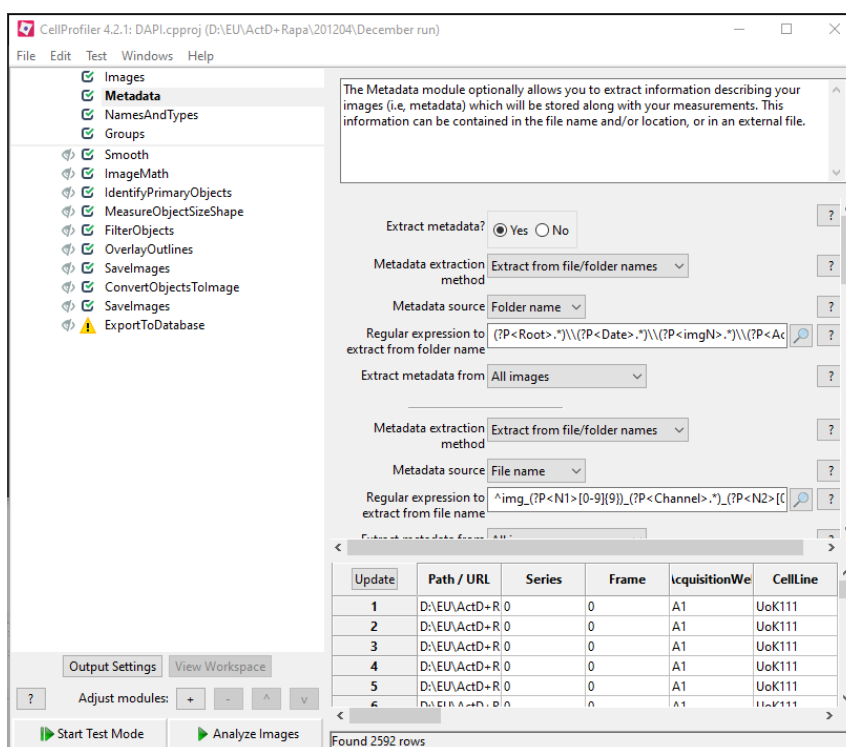


Figure 7.1. Screenshot of CellProfiler window taken while performing segmentation of nuclear images.

Table 7.2 Analysis of nucleolar images

Input	Two-channel images of nucleoli (Cy3) and nuclei (DAPI). Nuclear masks. Image metadata CSV file (plate location, treatment, cell line, etc.)
Output	Images of nuclear and nucleolar contours. Shading reference image. Background reference image. SQLite database of quantitated data linked to original images, contours and metadata as well as parent-child relationships between nuclei and nucleoli.
Step	Purpose
Metadata extraction	Metadata is extracted from folder and file names and CSV files and images are matched to metadata.
Feature enhancing	A Top Hat transform of a diameter similar to that of a typical nucleolus is applied in order to contrast the images of nucleoli.
Nucleoli segmentation	Transformed images are segmented with a Robust Background method to produce nucleolar masks.
Object filtering	Nucleolar masks are filtered by size to eliminate small size artefacts.
Expansion of masks	Nucleolar masks are expanded by 5 pixels to create masks of the surrounding nucleoplasm.
Intensity measurement	Intensities of nucleoli and surrounding nucleoplasm are quantitated.
Filtering	Only nucleolar regions with mean intensities at least 25% higher than that of the surrounding nucleoplasm are retained.
Parent-child matching	Filtered nucleoli (child) are linked to their enclosing nuclei (parent).
Intensity measurement	Final intensity measurements are made on nucleoli and nuclei.
Saving	Binary masks of nuclei are exported.
Exporting	A SQLite database is created containing quantitated data, image metadata, links to original images, contours and metadata as well as parent-child relationships between nuclei and nucleoli.

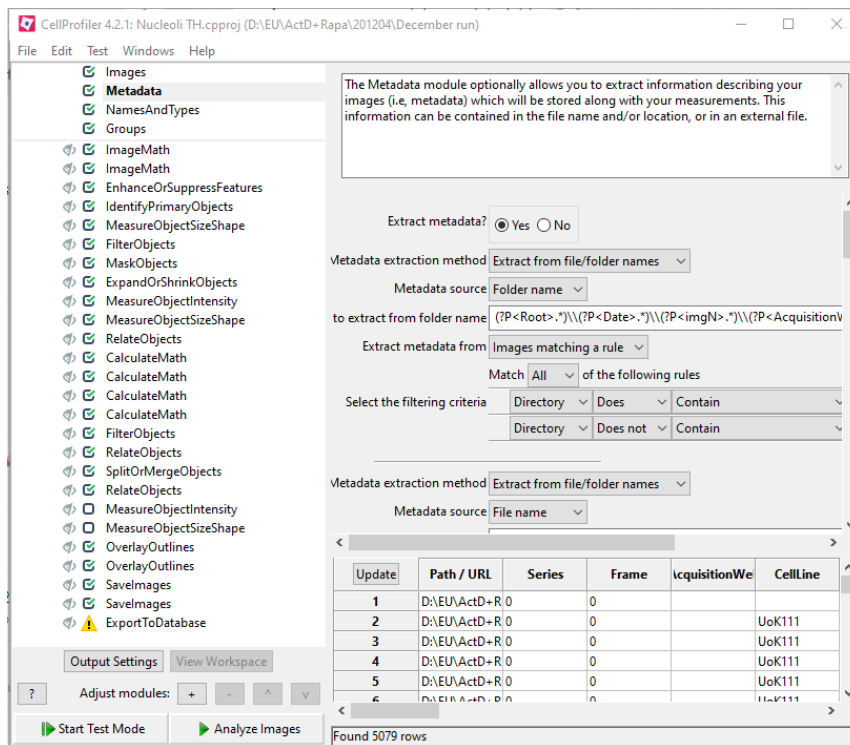


Figure 7.2. Screenshot of CellProfiler window taken while performing analysis of nucleolar images.

Data extraction and calculations

Data was extracted from the SQLite databases using scripts run in SQLiteStudio.

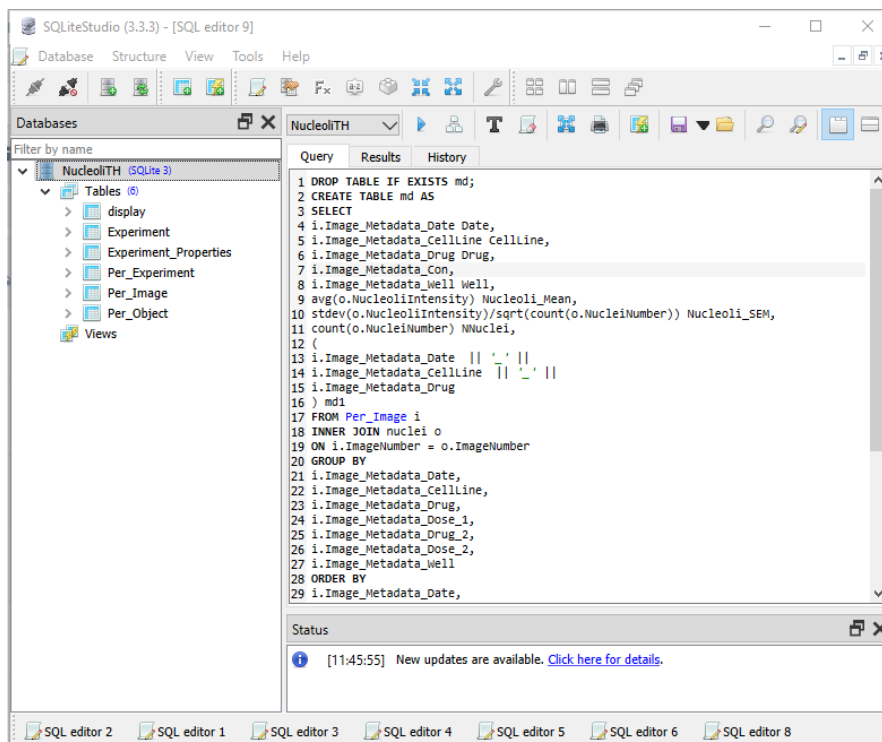


Figure 7.3. Screenshot of SQLiteStudio window taken while performing data extraction.

These scripts grouped multi-well plate wells by treatment and performed calculations of means and standard errors of the means (SEM).

7.3 Comparison of the percentage of cells gated on the different phases of cell cycle calculated using EdU incorporation vs. histogram deconvolution with 7-AAD staining

ACHN cells were treated with 0.01% v/v DMSO (vehicle control) as described in the section 1.4.5 of the methods. Data obtained from the flow cytometer was analysed as described on section 1.4.6 and four gates representing G1, S, G2 phases and cell death were created the density plot shown below (Figure 7.4).

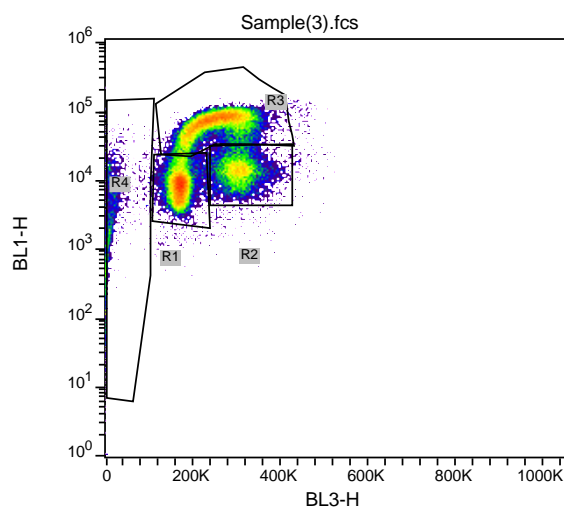


Figure 7.4. Density plot of ACHN cells stained with 7-AAD and 6-FAM. R1=G1; R2=G2; R3=S; R4=cell death

The resulting populations were plotted as overlays on a histogram showing 7-AAD staining only (Figure 7.5).

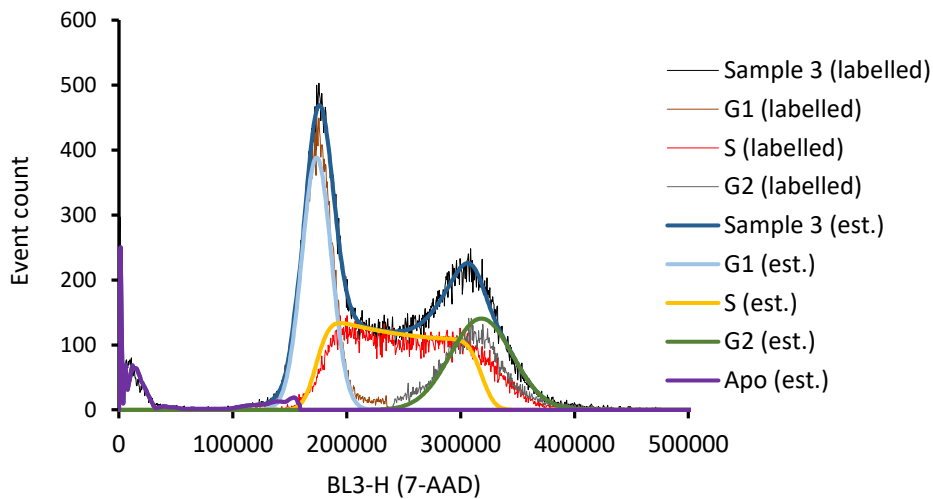


Figure 7.5. Histogram showing a comparison of 6-FAM-staining and deconvolution of 7-AAD-staining data for estimation of the percentage of cells in the different phases of cell cycle. The data tagged as “labelled” show the populations of cells in phases G1, G2, S and apoptosis in the density plot above. The data tagged as “est.” show the populations of cells in phases G1, G2, S and cell death, which is assumed to be apoptosis, estimated by histogram deconvolution of 7-AAD-stained cells.

A comparison of both methods shows that estimation of the percentage of cells in each of the phases of cell cycle is similar (Table 7.3.; Figures 7.5 and 7.6).

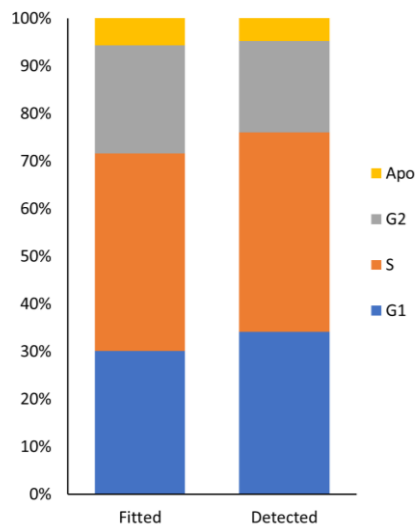


Figure 7.6. Comparison of the estimation of cell cycle population distribution by labelling with 6-FAM and 7-AAD and by data deconvolution of 7-AAD-stained cells.

	G1	S	G2	Apo
Fitted	30.11	41.45	22.79	5.65
Detected	33.88	41.76	19.07	4.76

Table 7.3. Estimated distribution of cells through the cell cycle by labelling with 6-FAM and 7-AAD and by data deconvolution of 7-AAD-stained cells.

7.4 Flow cytometry analysis of the effects of mTORis on the cell cycle

This section of the annex includes the analysis of flow cytometry data through density dot plots and overlaid histograms to determine the percentage of ACHN and UoK111 cell populations on G1, S, G2 and cell death after 72-hour treatment with mTOR inhibitors.

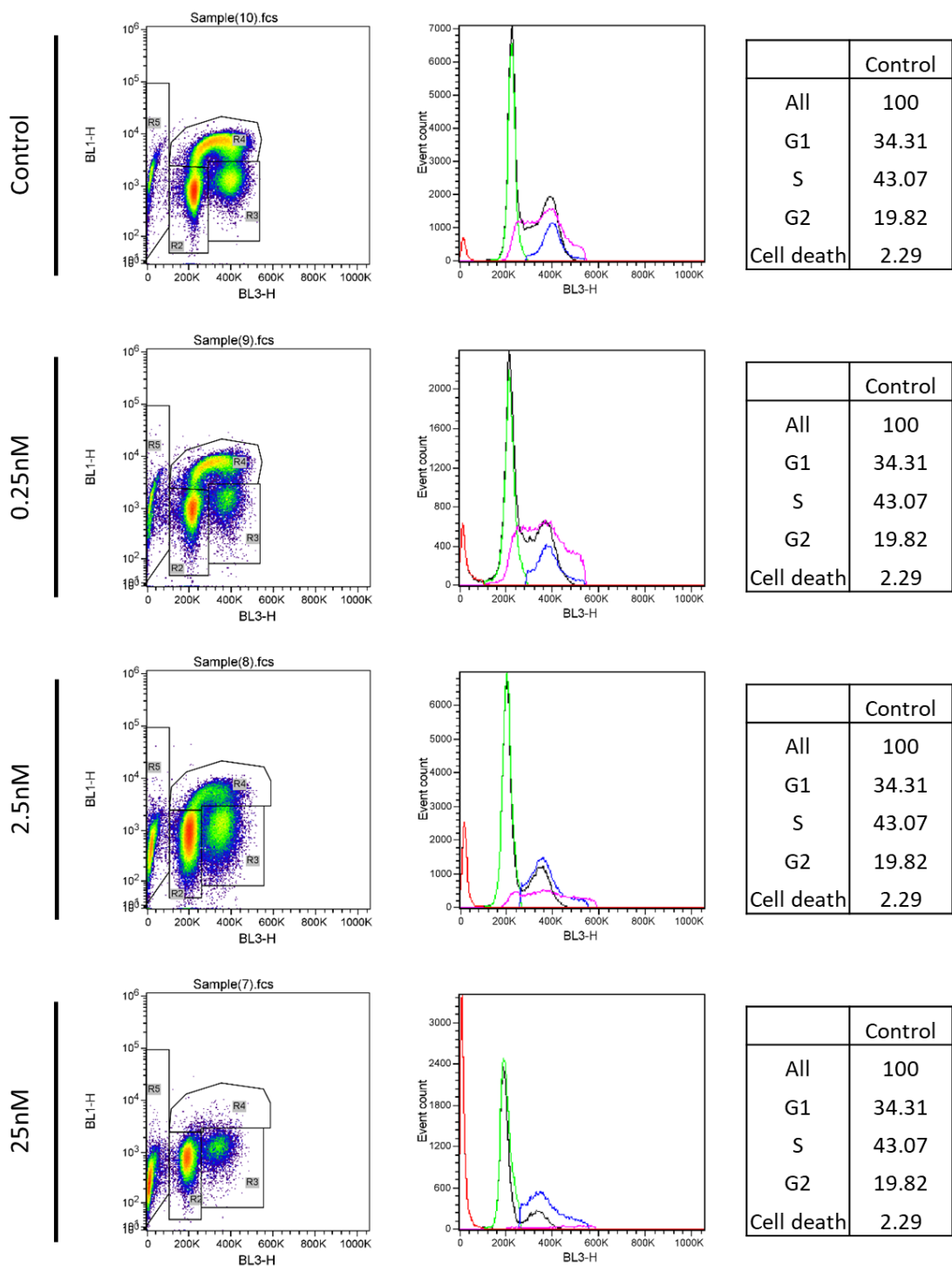


Figure 7.7. Analysis of cell cycle of ACHN cells treated with ActD using click chemistry-labelled DNA detected with flow cytometry. The density dot plots illustrate the identification of cell populations in G1 (R1), S (R3), G2 (R2) phases, and dead cells (R4) depending on the signal of total DNA detected by 7-AAD staining on the X-axis and the nascent DNA labelled with click chemistry, detected by 6-FAM staining on the Y-axis. The histogram displays an overlay of the cell populations in G1 (green), S (pink), G2 (blue), and cell death (red) gated in the density plots, in respect to the 7-AAD fluorescent intensity, which is correlated to the amount of DNA within each cell. The tables on the right present the percentage of cells in the different stages of cell cycle according to intensity of 7-AAD and 6-FAM in the density plots. Initial population was gated to reject doublets using Attune recommended peak height vs Area, as described in method and materials section 2.4.6.

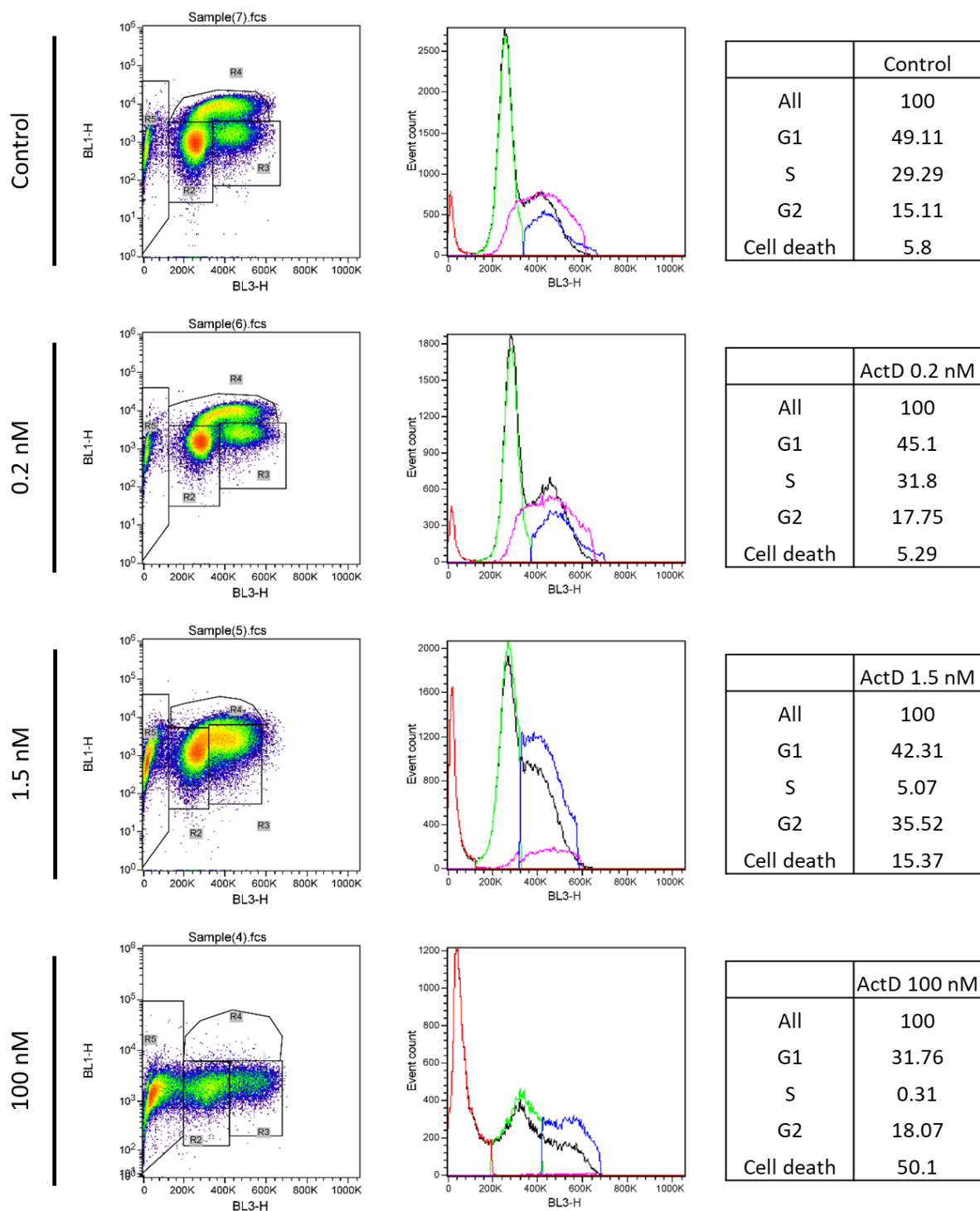


Figure 7.8. Analysis of cell cycle of UoK111 cells treated with ActD using click chemistry-labelled DNA detected with flow cytometry. The density dot plots illustrate the identification of cell populations in G1 (R1), S (R3), G2 (R2) phases, and dead cells (R4) depending on the signal of total DNA detected by 7-AAD staining on the X-axis and the nascent DNA labelled with click chemistry, detected by 6-FAM staining on the Y-axis. The histogram displays an overlay of the cell populations in G1 (green), S (pink), G2 (blue), and cell death (red) gated in the density plots, in respect to the 7-AAD fluorescent intensity, which is correlated to the amount of DNA within each cell. The tables on the right present the percentage of cells in the different stages of cell cycle according to intensity of 7-AAD and 6-FAM in the density plots. Initial population was gated to reject doublets using Attune recommended peak height vs Area, as described in method and materials section 2.4.6.

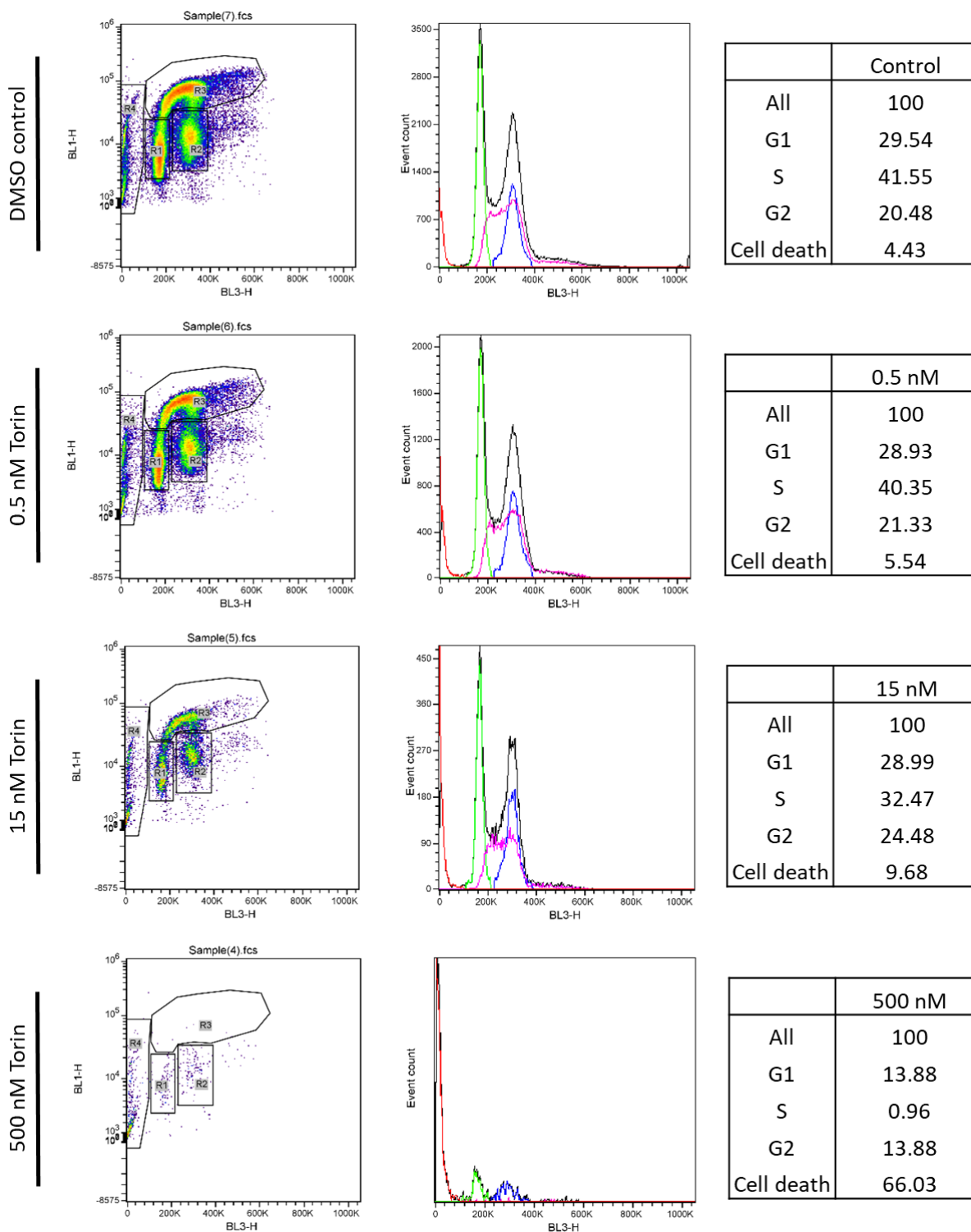


Figure 7.9. Analysis of cell cycle of ACHN cells treated with Torin 1 using click chemistry-labelled DNA detected with flow cytometry. The dot plots on the left side show the selection performed for doublet discrimination. The density dot plots illustrate the identification of the cell populations in the different stages of cell cycle. The histograms display an overlay of the cell populations in G1 (green), S (pink), G2 (blue), and apoptosis (red) gated in the density plots, in respect to the 7-AAD fluorescent intensity (black), which is correlated to the amount of DNA within each cell. The tables on the right present the percentage of cells in the different stages of cell cycle according to intensity of 7-AAD and 6-FAM in the density plots.

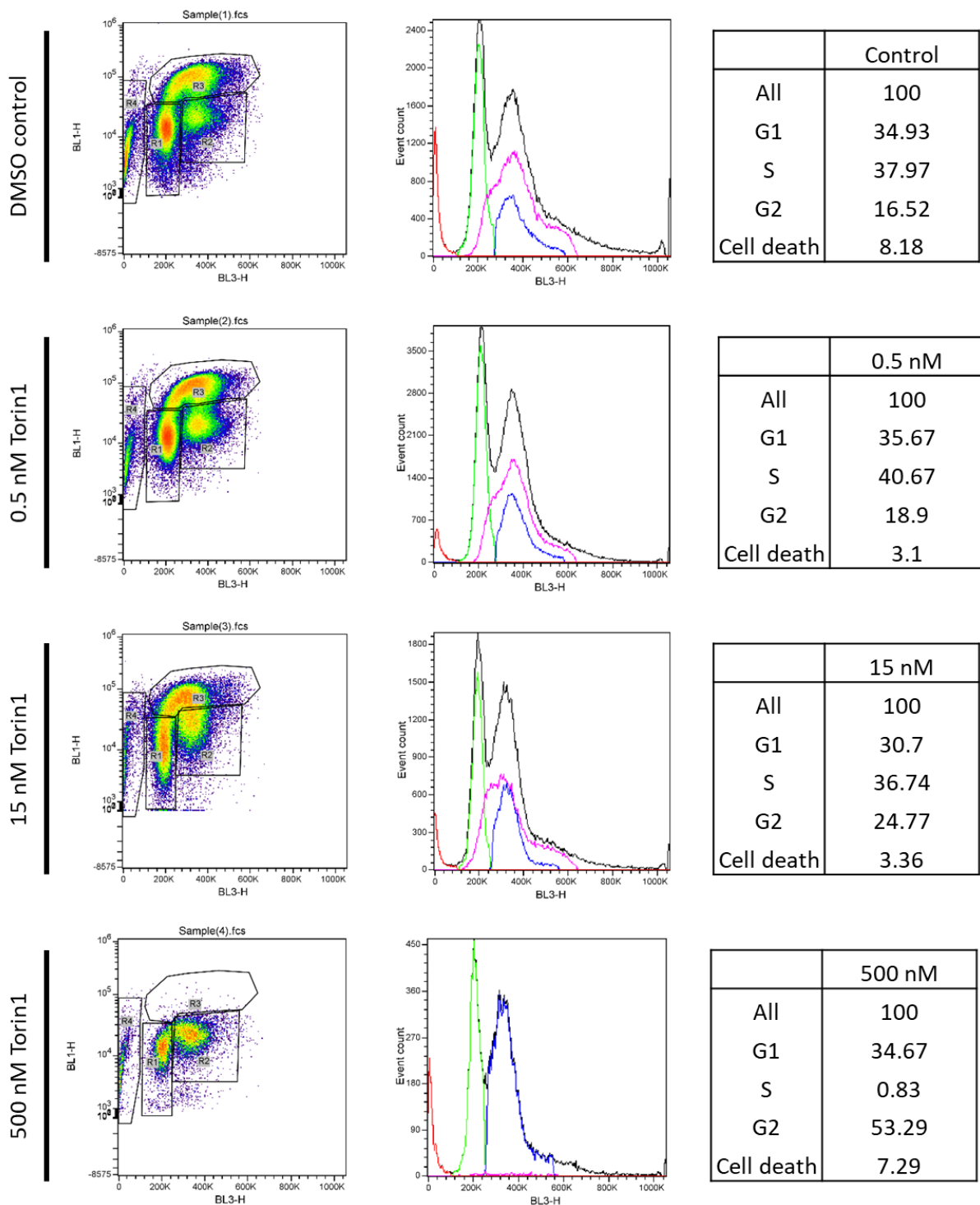


Figure 7.10. Analysis of cell cycle of UoK111 cells treated with Torin 1 using click chemistry-labelled DNA detected with flow cytometry. The dot plots on the left side show the selection performed for doublet discrimination. The density dot plots illustrate the identification of the cell populations in the different stages of cell cycle. The histograms display an overlay of the cell populations in G1 (green), S (pink), G2 (blue), and apoptosis (red) gated in the density plots, in respect to the 7-AAD fluorescent intensity (black), which is correlated to the amount of DNA within each cell. The tables on the right present the percentage of cells in the different stages of cell cycle according to intensity of 7-AAD and 6-FAM in the density plots.

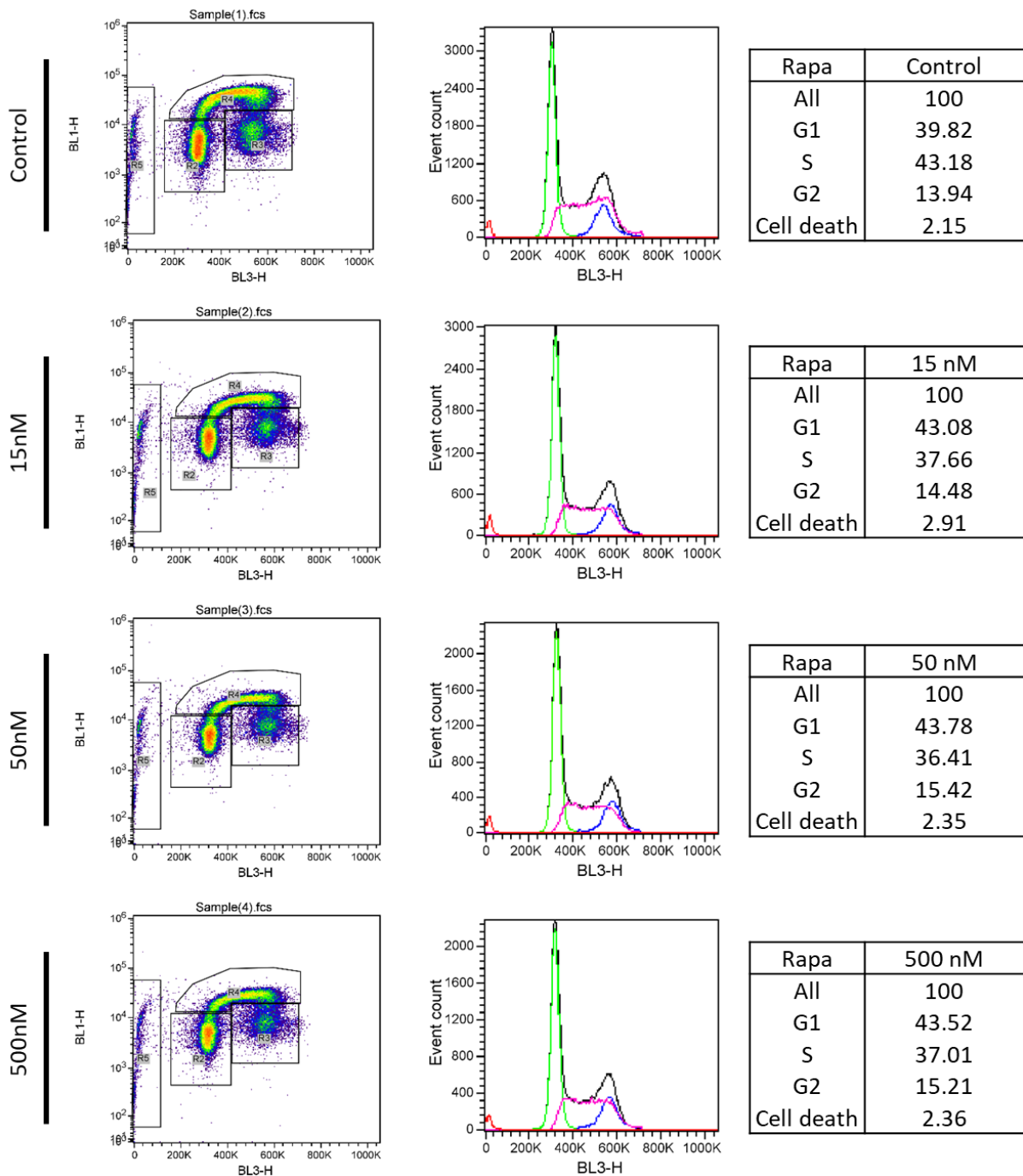


Figure 7.11. Analysis of cell cycle of ACHN cells treated with Rapamycin using click chemistry-labelled DNA detected with flow cytometry. The dot plots on the left side show the selection performed for doublet discrimination. The density dot plots illustrate the identification of the cell populations in the different stages of cell cycle. The histograms display an overlay of the cell populations in G1 (green), S (pink), G2 (blue), and apoptosis (red) gated in the density plots, in respect to the 7-AAD fluorescent intensity (black), which is correlated to the amount of DNA within each cell. The tables on the right present the percentage of cells in the different stages of cell cycle according to intensity of 7-AAD and 6-FAM in the density plots.

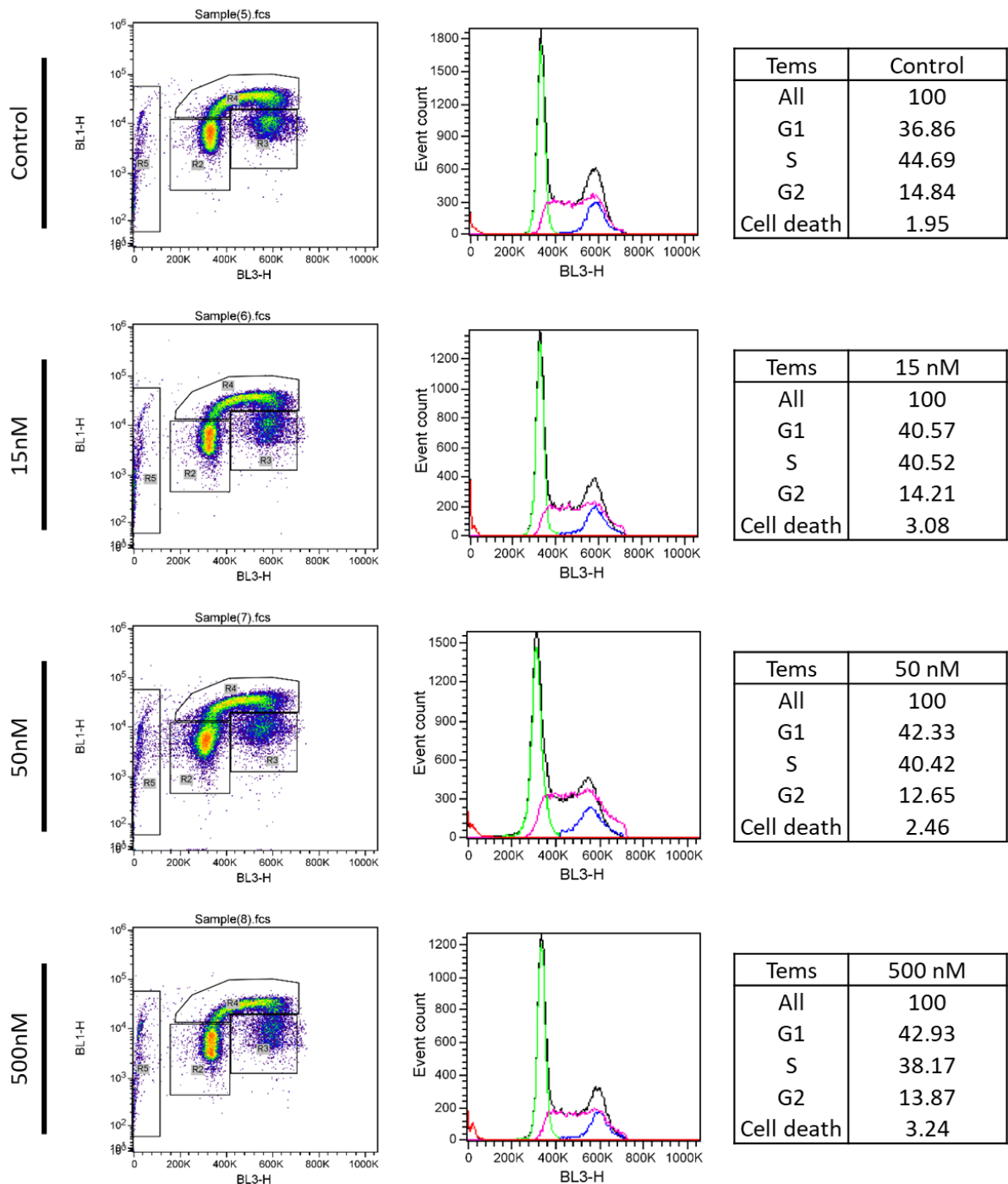


Figure 7.12. Analysis of cell cycle of ACHN cells treated with Temozolomide using click chemistry-labelled DNA detected with flow cytometry. The dot plots on the left side show the selection performed for doublet discrimination. The density dot plots illustrate the identification of the cell populations in the different stages of cell cycle. The histograms display an overlay of the cell populations in G1 (green), S (pink), G2 (blue), and apoptosis (red) gated in the density plots, in respect to the 7-AAD fluorescent intensity (black), which is correlated to the amount of DNA within each cell. The tables on the right present the percentage of cells in the different stages of cell cycle according to intensity of 7-AAD and 6-FAM in the density plots.

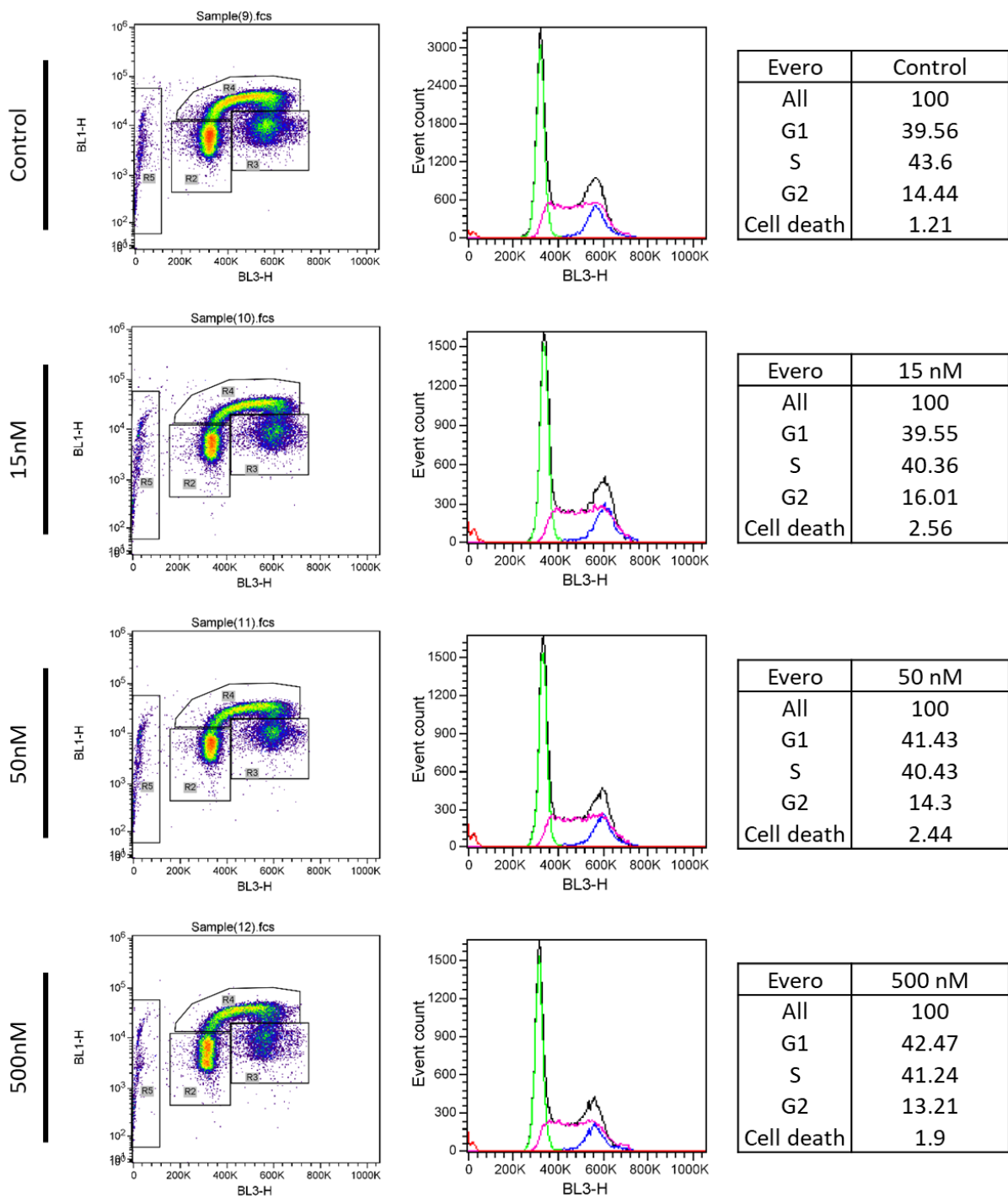


Figure 7.13. Analysis of cell cycle of ACHN cells treated with Everolimus using click chemistry-labelled DNA detected with flow cytometry. The dot plots on the left side show the selection performed for doublet discrimination. The density dot plots illustrate the identification of the cell populations in the different stages of cell cycle. The histograms display an overlay of the cell populations in G1 (green), S (pink), G2 (blue), and apoptosis (red) gated in the density plots, in respect to the 7-AAD fluorescent intensity (black), which is correlated to the amount of DNA within each cell. The tables on the right present the percentage of cells in the different stages of cell cycle according to intensity of 7-AAD and 6-FAM in the density plots.

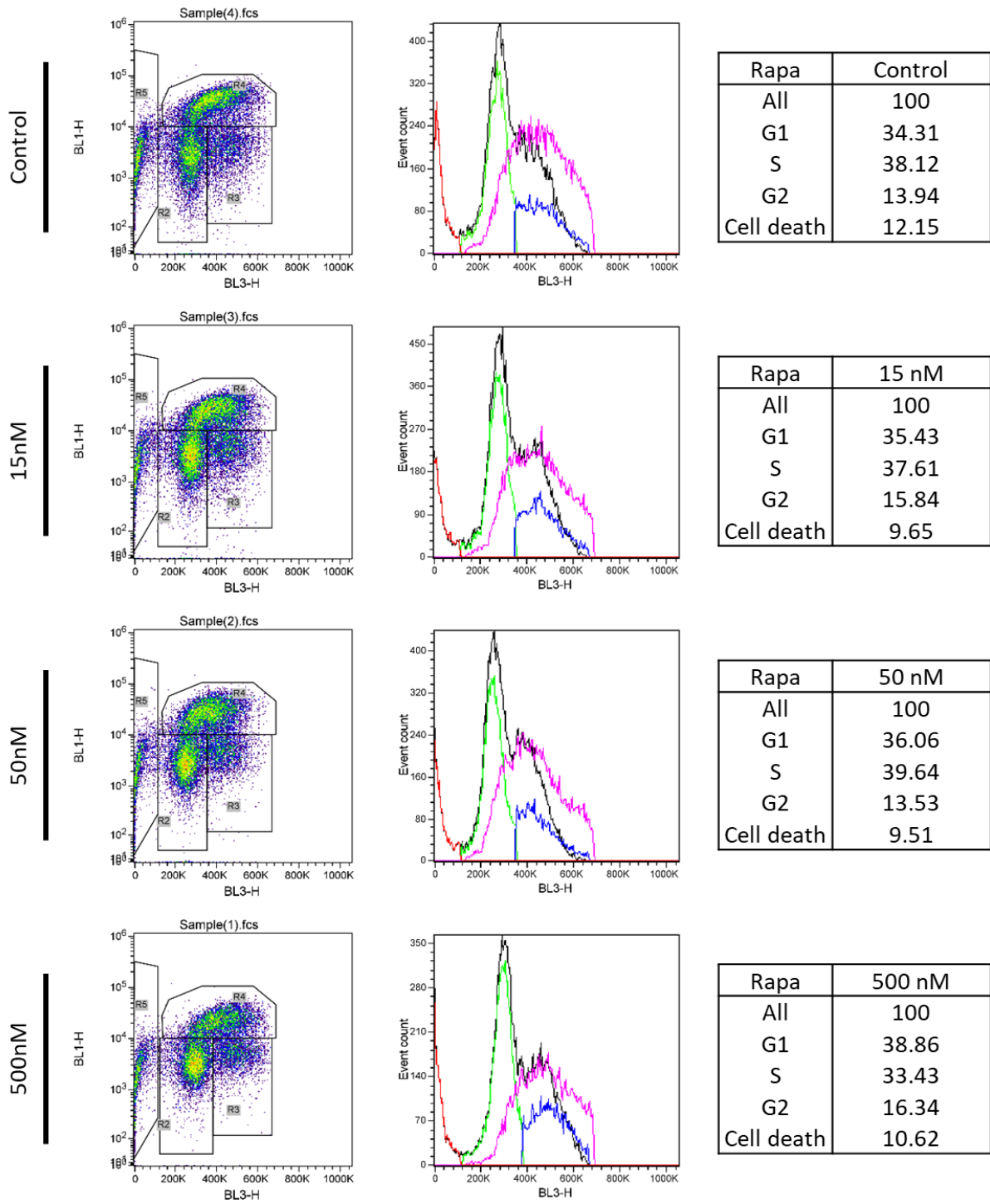


Figure 7.14. Analysis of cell cycle of UoK111 cells treated with Rapamycin using click chemistry-labelled DNA detected with flow cytometry. The dot plots on the left side show the selection performed for doublet discrimination. The density dot plots illustrate the identification of the cell populations in the different stages of cell cycle. The histograms display an overlay of the cell populations in G1 (green), S (pink), G2 (blue), and apoptosis (red) gated in the density plots, in respect to the 7-AAD fluorescent intensity (black), which is correlated to the amount of DNA within each cell. The tables on the right present the percentage of cells in the different stages of cell cycle according to intensity of 7-AAD and 6-FAM in the density plots.

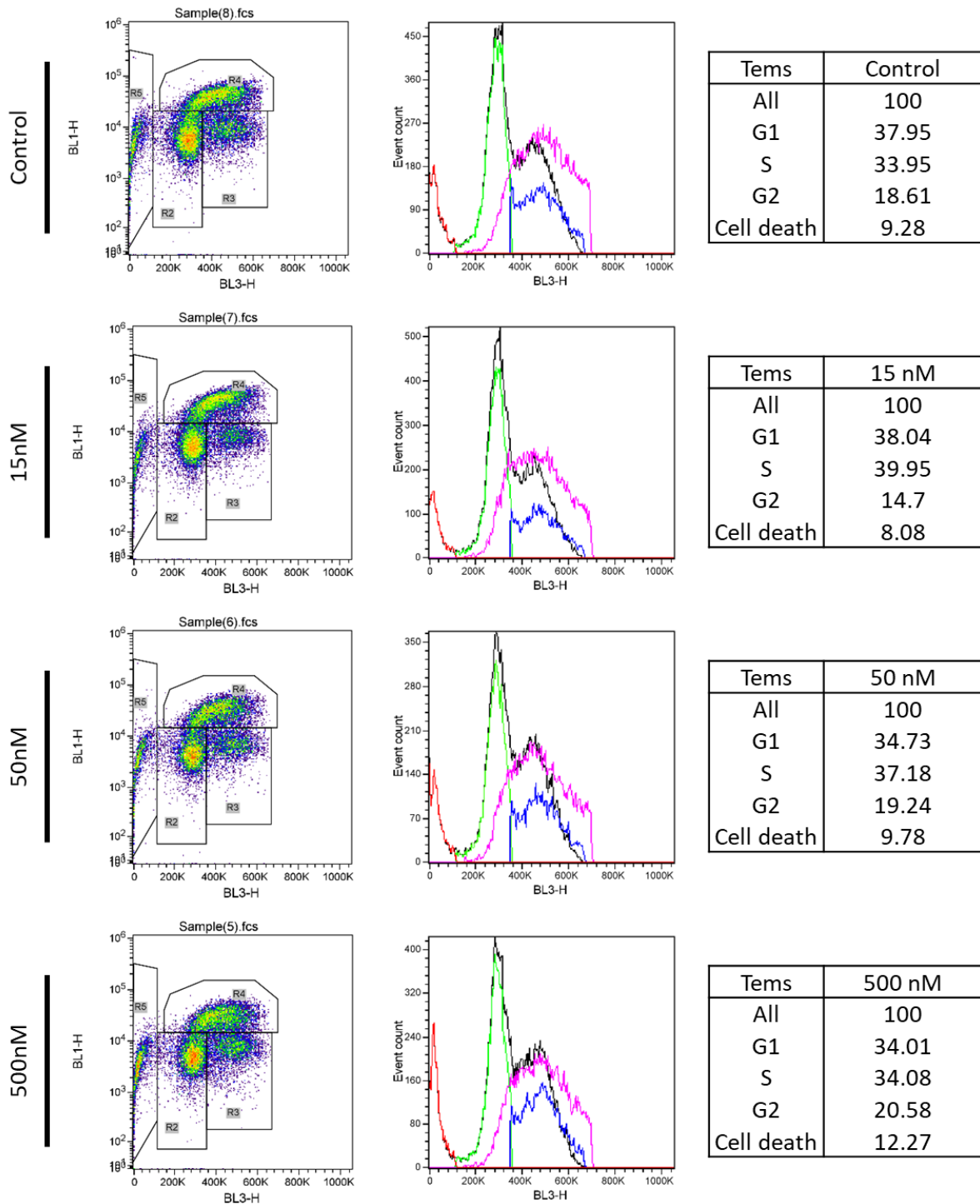


Figure 7.15. Analysis of cell cycle of UoK111 cells treated with Temozolomide using click chemistry-labelled DNA detected with flow cytometry. The dot plots on the left side show the selection performed for doublet discrimination. The density dot plots illustrate the identification of the cell populations in the different stages of cell cycle. The histograms display an overlay of the cell populations in G1 (green), S (pink), G2 (blue), and apoptosis (red) gated in the density plots, in respect to the 7-AAD fluorescent intensity (black), which is correlated to the amount of DNA within each cell. The tables on the right present the percentage of cells in the different stages of cell cycle according to intensity of 7-AAD and 6-FAM in the density plots.

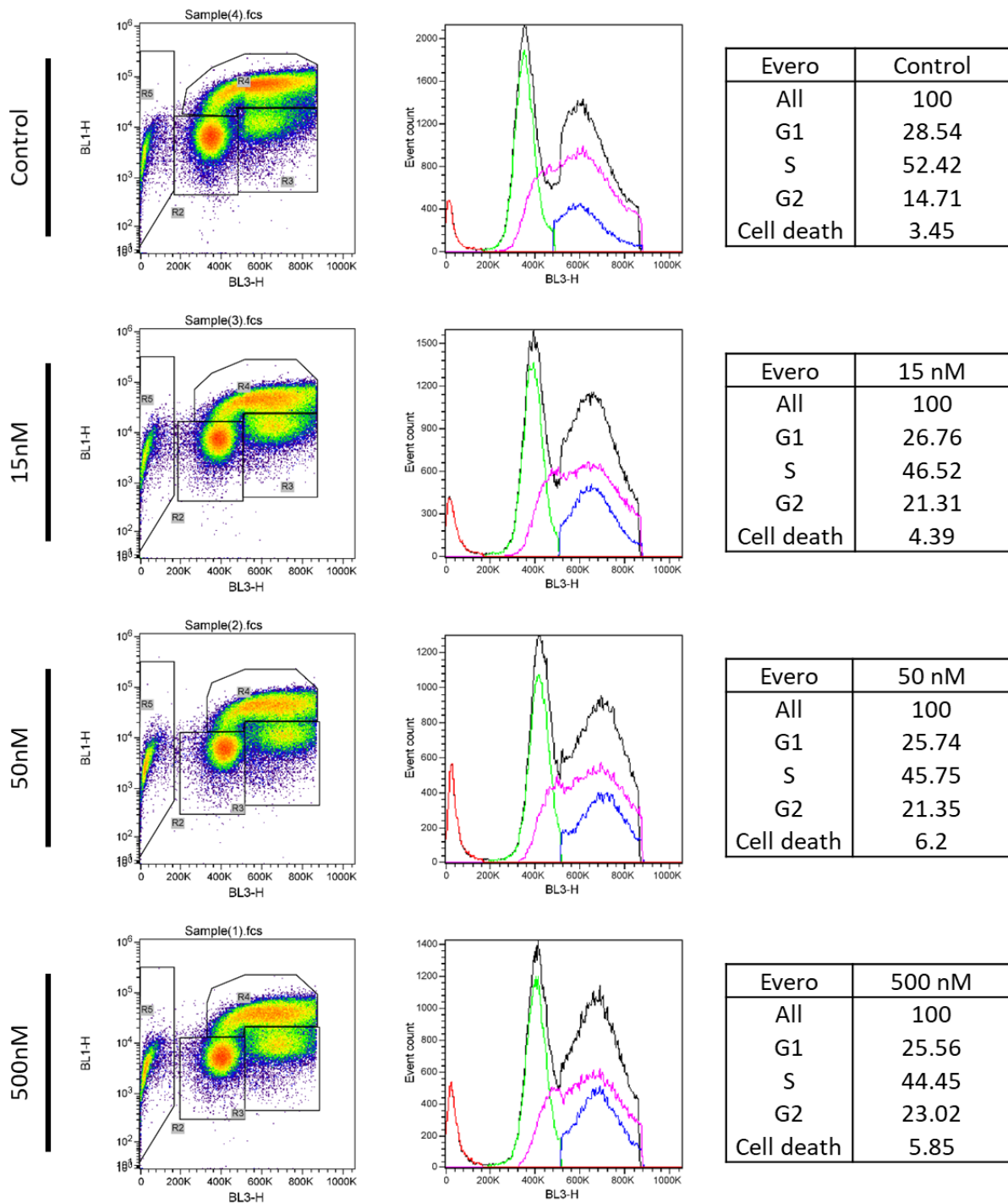


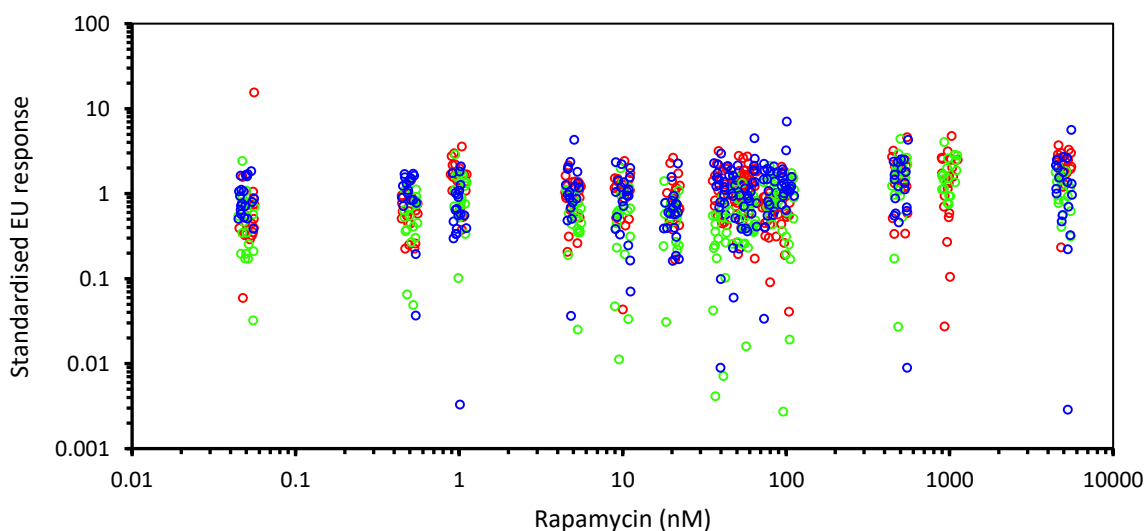
Figure 7.16. Analysis of cell cycle of UoK111 cells treated with Everolimus using click chemistry-labelled DNA detected with flow cytometry. The dot plots on the left side show the selection performed for doublet discrimination. The density dot plots illustrate the identification of the cell populations in the different stages of cell cycle. The histograms display an overlay of the cell populations in G1 (green), S (pink), G2 (blue), and apoptosis (red) gated in the density plots, in respect to the 7-AAD fluorescent intensity (black), which is correlated to the amount of DNA within each cell. The tables on the right present the percentage of cells in the different stages of cell cycle according to intensity of 7-AAD and 6-FAM in the density plots.

7.5 Analysis of 5-ethynyl uridine-labelled nucleolar images

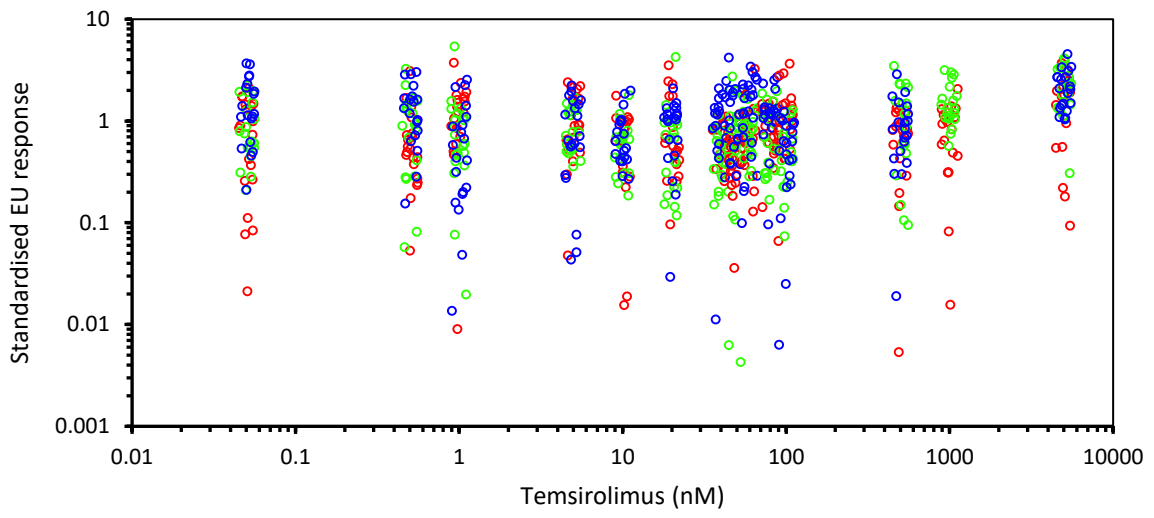
The data presented in Figures 3.12 and 3.13 (see section 3.1.2.3) was analysed in more detail to explore the single-cell distributions of nucleolar area, total 5-EU incorporation signal, and 5-EU incorporation per unit area. The resulting cell populations were plotted by individual well in order to visualise well-to-well variations and are shown in Figures 7.17, 7.18 and 7.19. Each point in the plots corresponds to the totality of the nucleoli of a single cell nucleus. Since the readings from each well comprised between 100 and 400 nuclei, to be able to visualise the distributions only 20 cells from each well are plotted.

In agreement with the summary descriptors (Mean \pm SEM) plotted in Figures 3.12 and 3.13, only the competitive mTOR inhibitor Torin 1 and ActD show an effect. The responses to Torin 1 and to ActD comprise both a reduction in nucleolar size and a reduction in mean 5-EU signal intensity (5-EU incorporation rate per nucleolus), with the resulting overall reduction of 5-EU incorporation per nucleus being due to both changes. Only 20 randomly selected nuclei from each well were compared; ACHN and UoK111 cells are shown in A and B panels, respectively, for the mTOR inhibitors and the drugs to which each plot correspond are indicated in the horizontal axes. The responses to ActD are shown in panels C and D for ACHN and UoK111 cells, respectively. The images also illustrate the presence of both intra- and inter-well variance, which led us to calculate the standard error of the mean using a two-stage nested design approach (450).

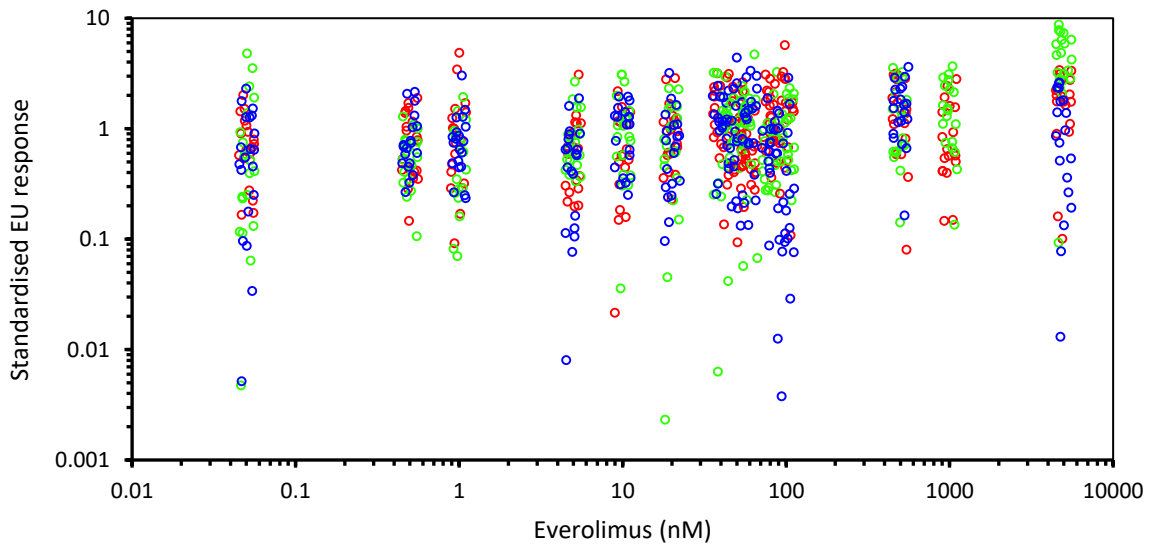
A)



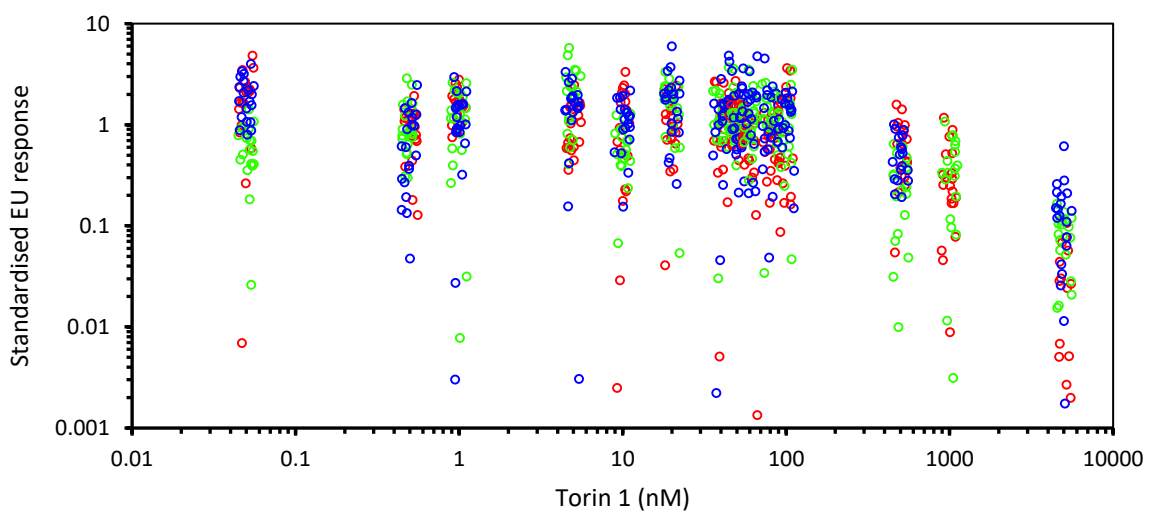
B)



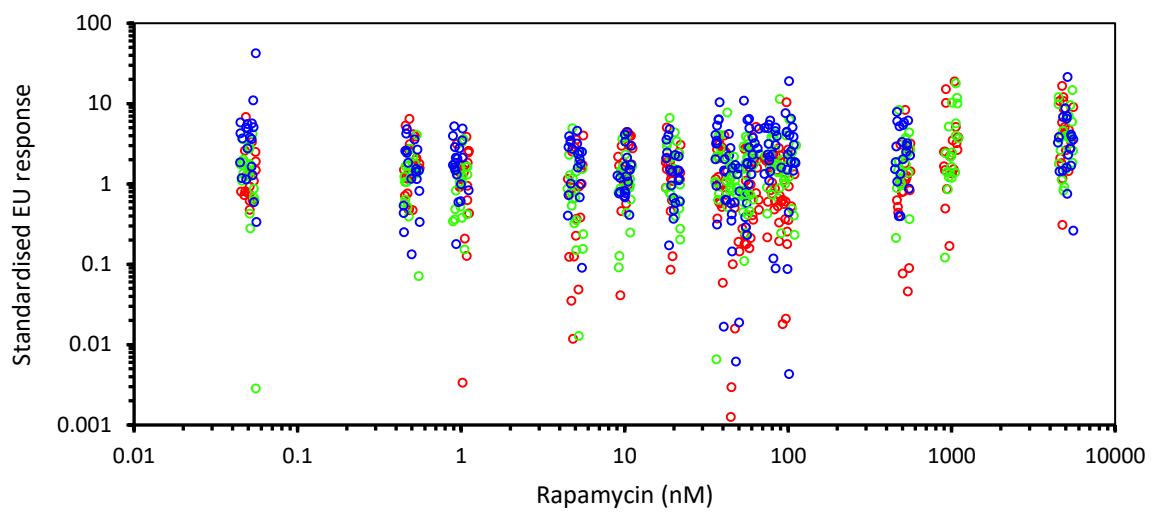
C)



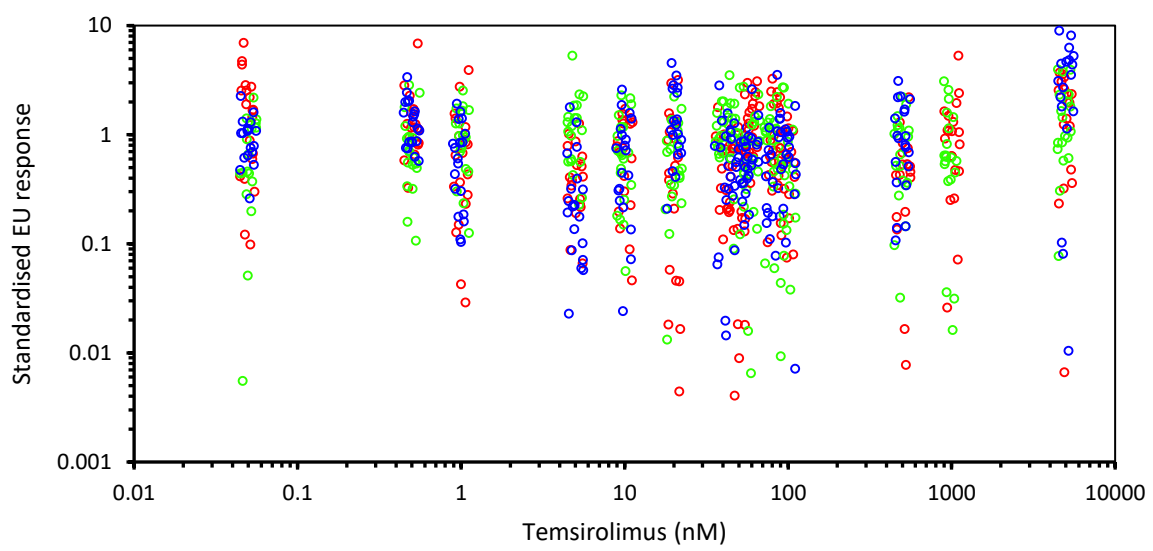
D)



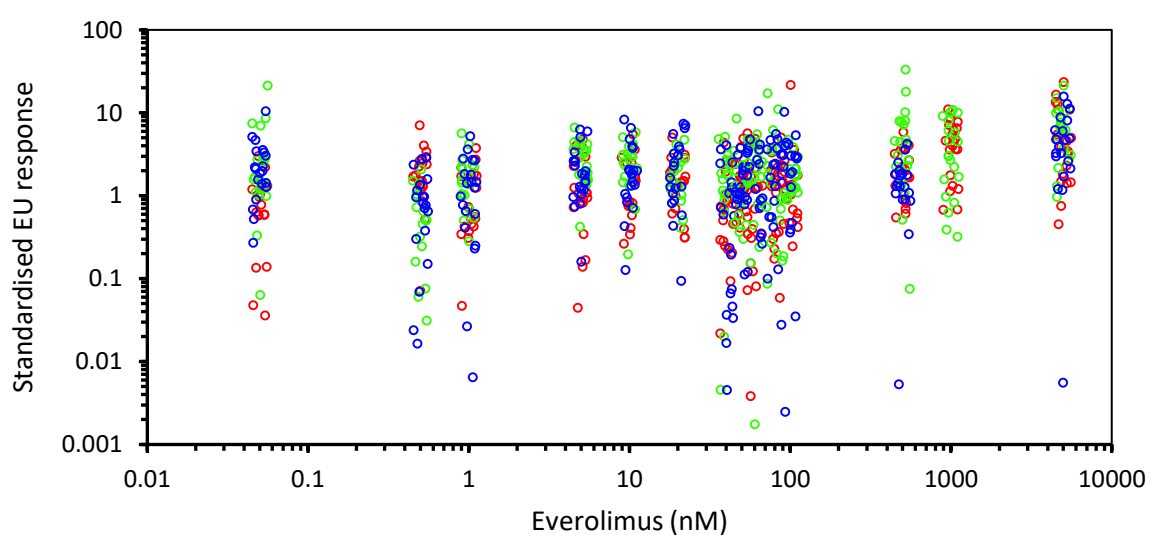
E)



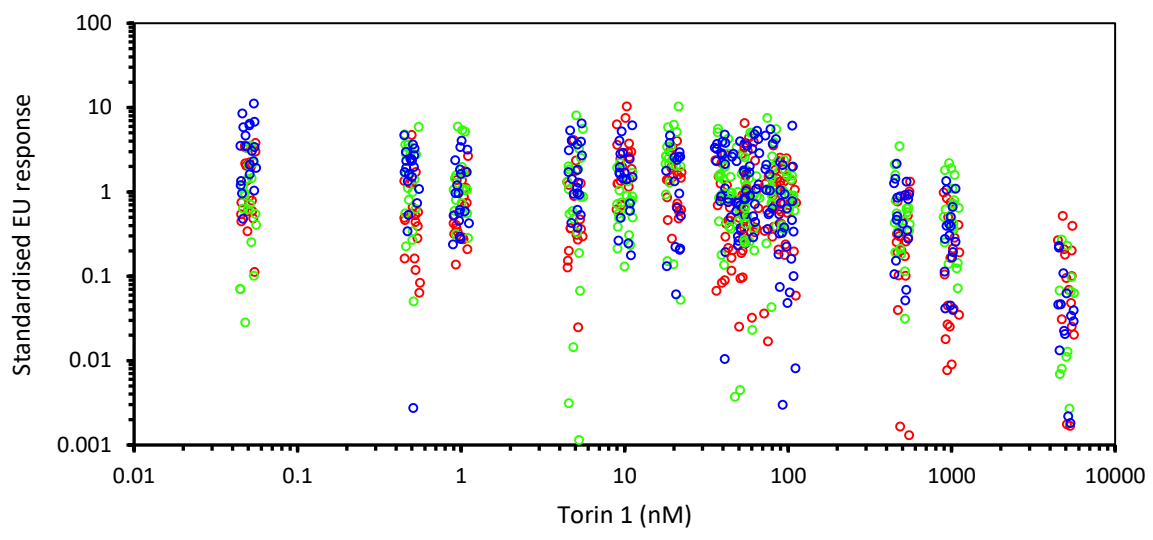
F)



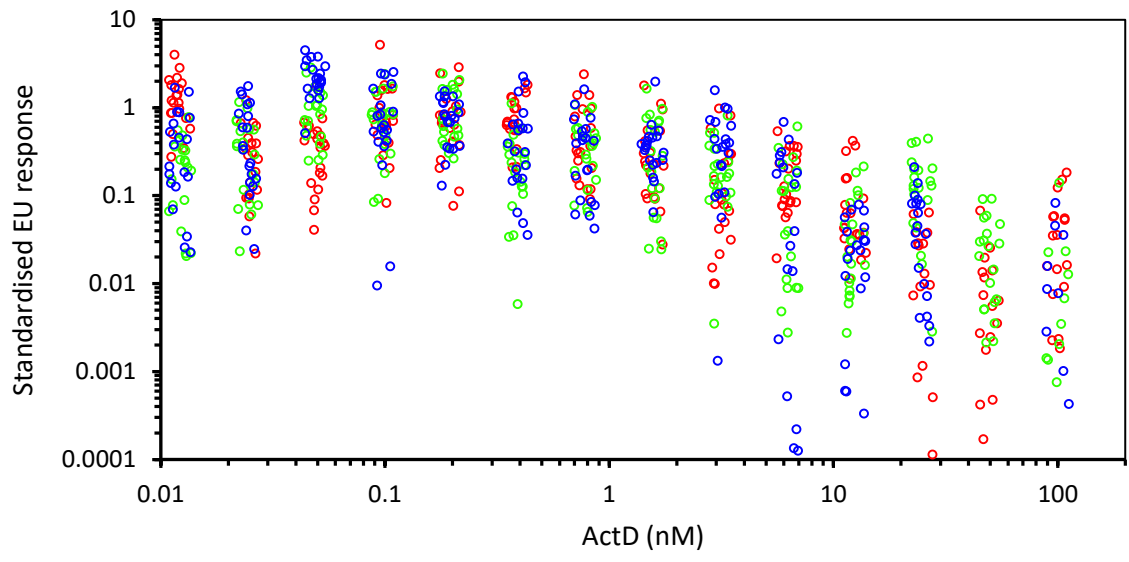
G)



H)



I)



J)

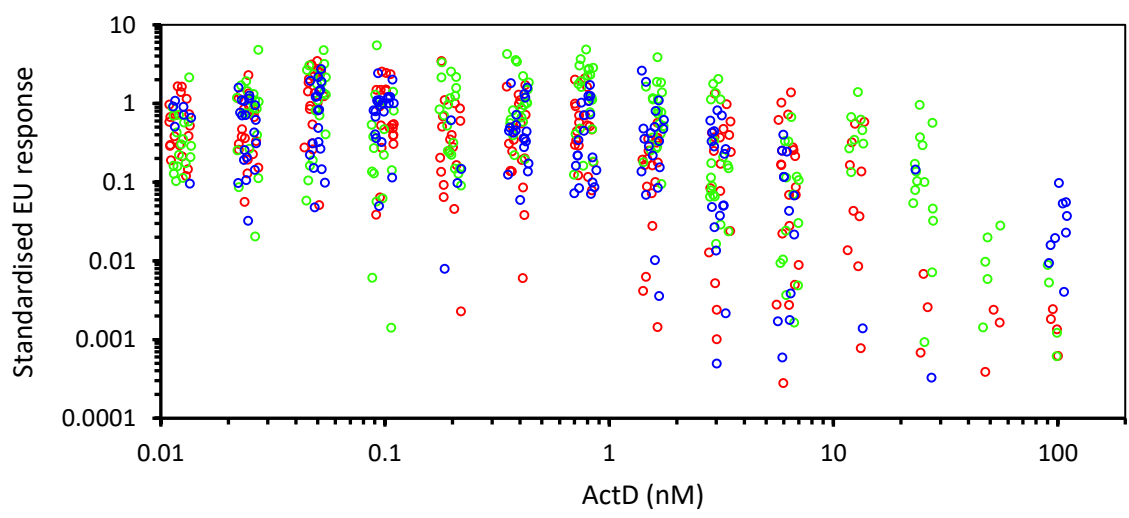
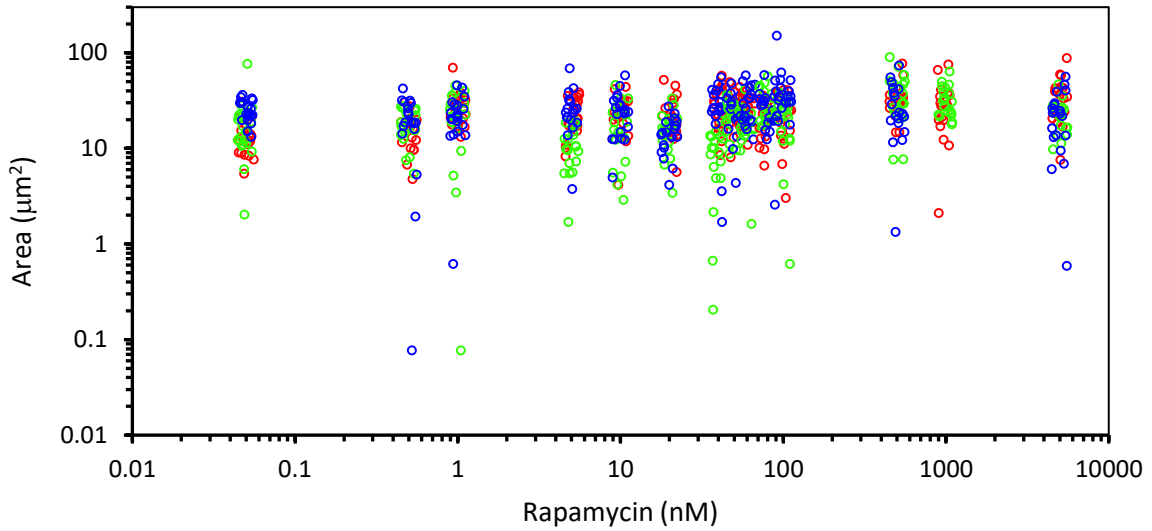
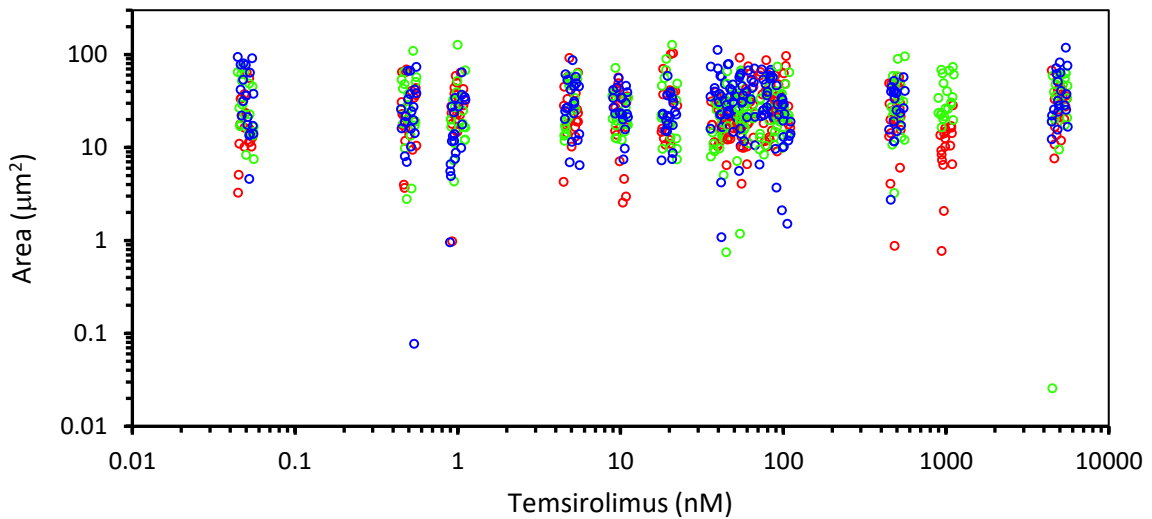


Figure 7.17. 5-EU incorporation vs. drug dose. A, B, C, D) ACHN and E, F, G, H) UoK111 cells were treated with increasing concentrations of mTORis for 2 hours and then processed and analysed as described in section 2.5. The dots represent the standardised 5-EU incorporation per nuclei, where 20 nuclei were randomly selected from each well and compared (each well labelled with a different colour). I) ACHN and J) UoK111 cells were treated with increasing concentrations of ActD for 2 hours and treated as above.

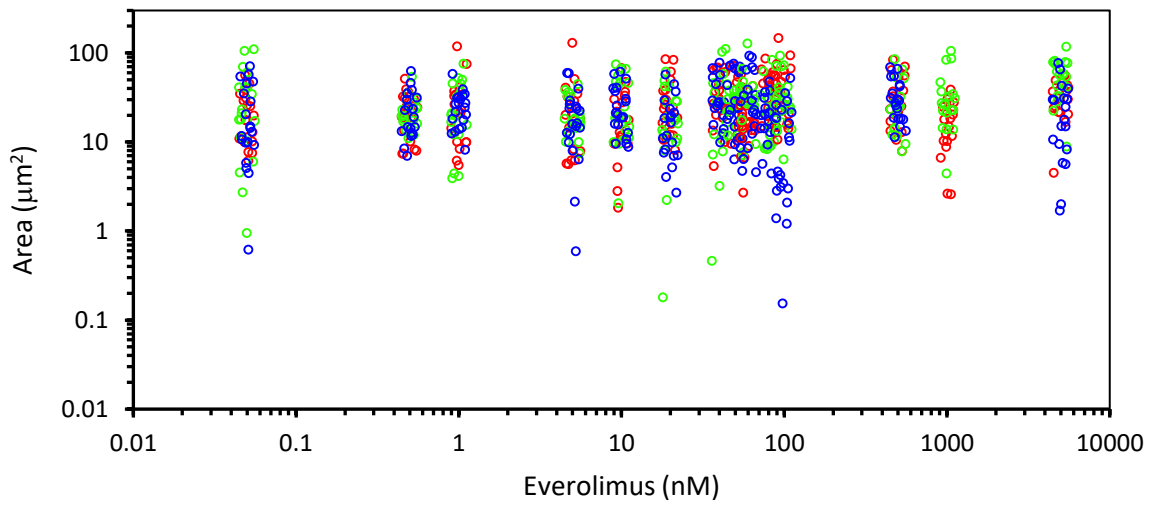
A)



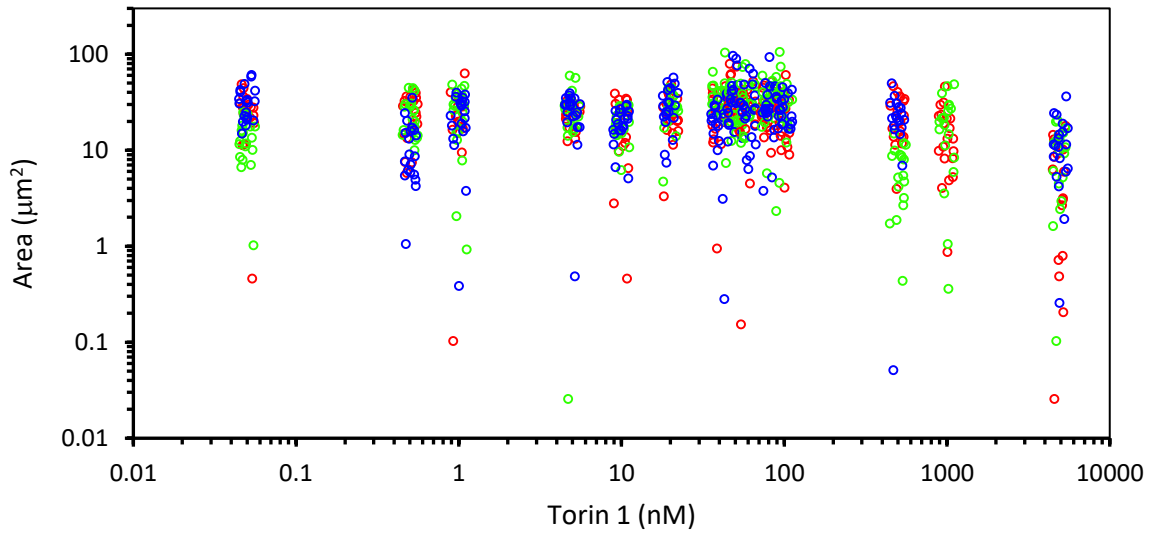
B)



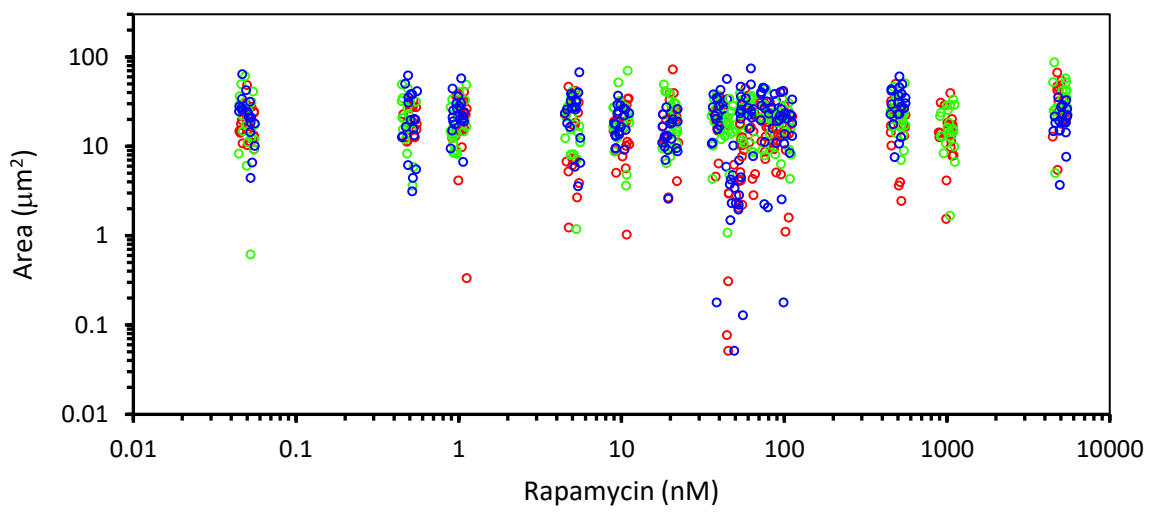
C)



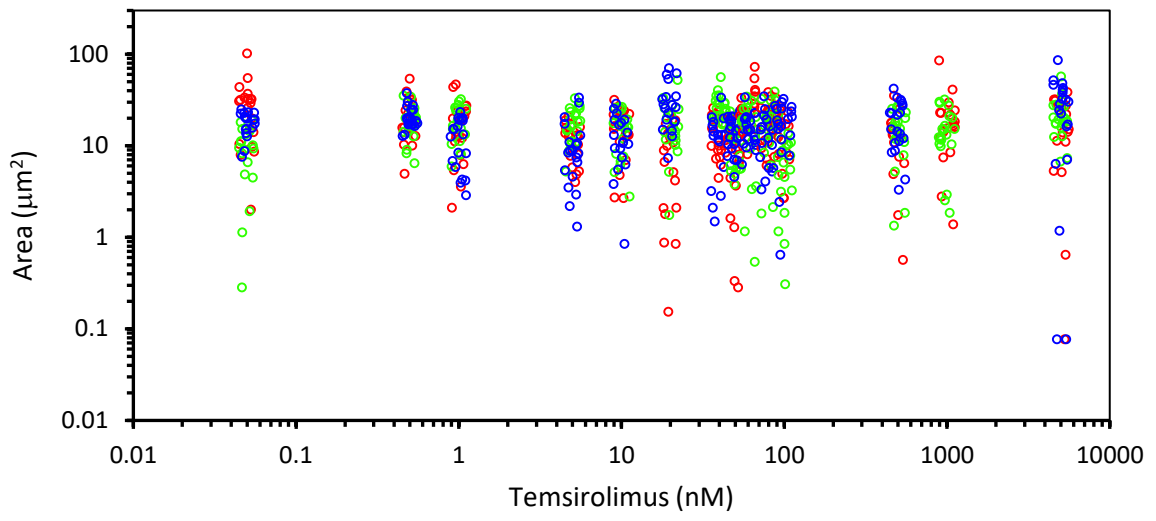
D)



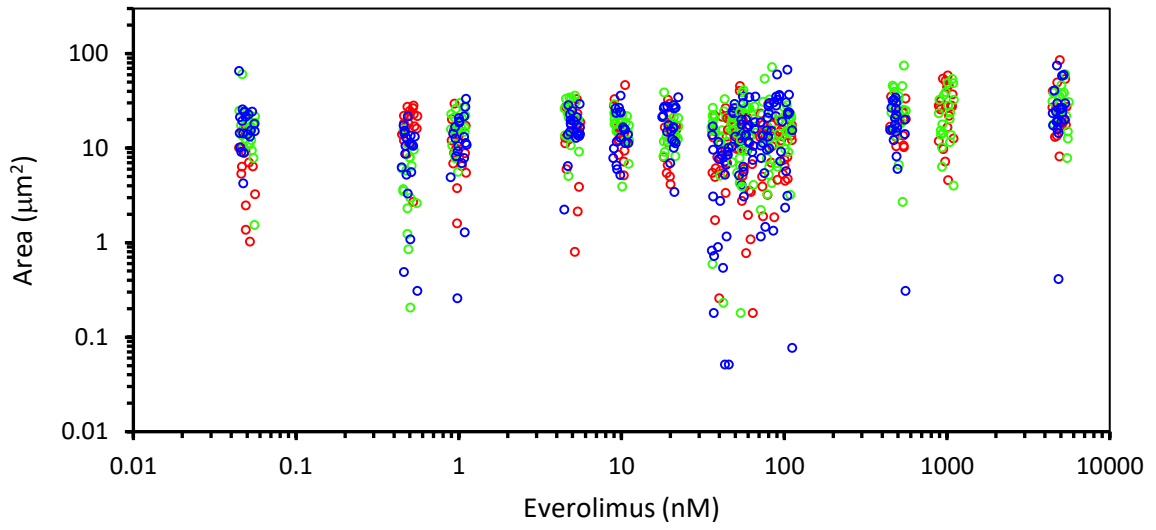
E)



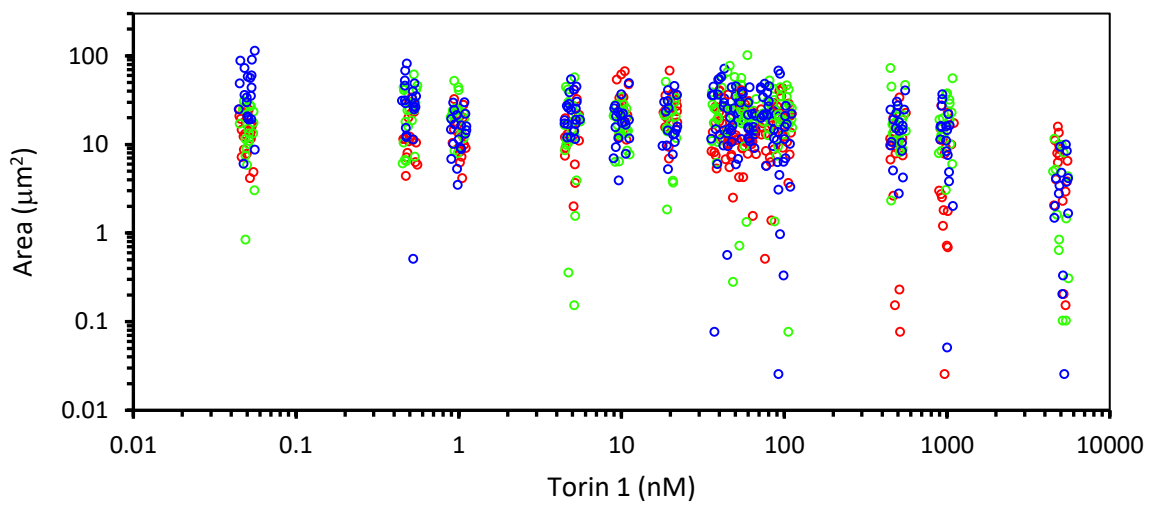
F)



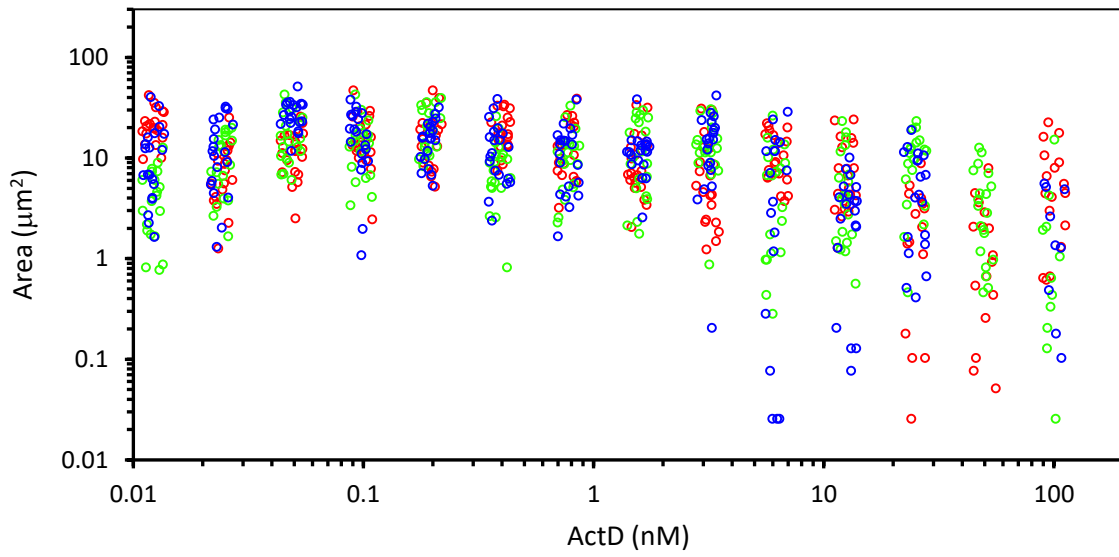
G)



H)



I)



J)

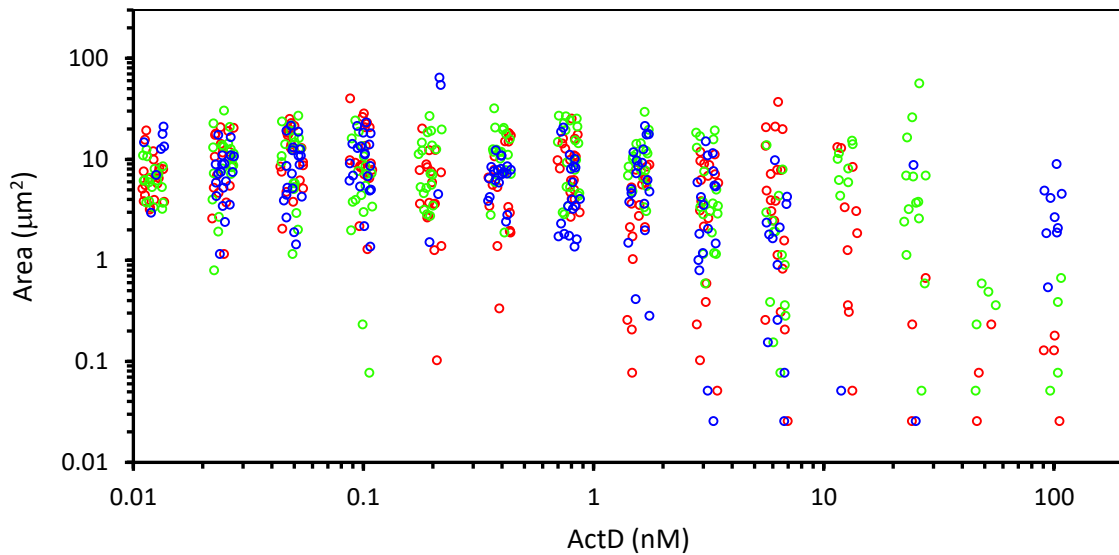
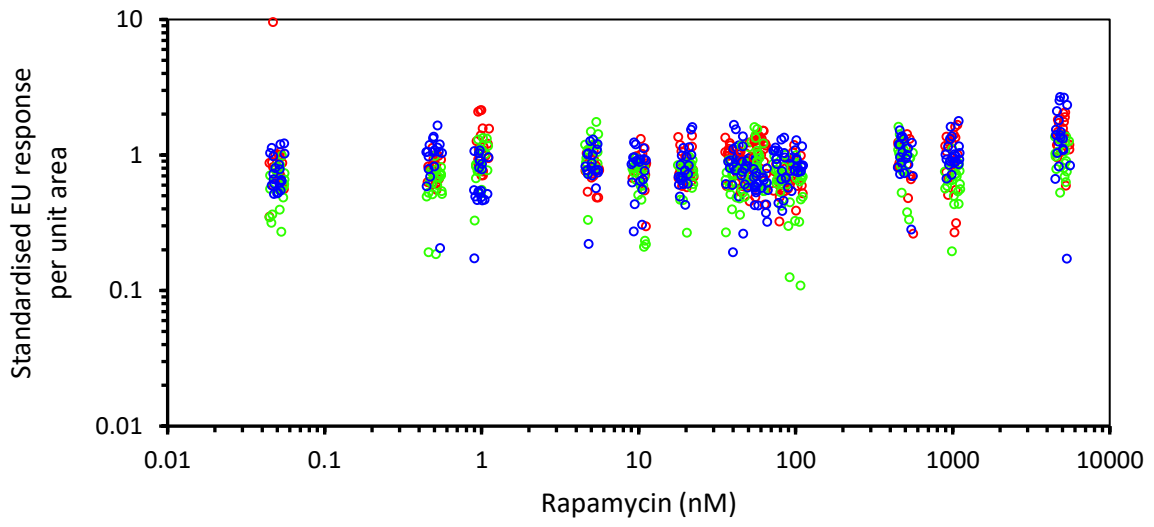
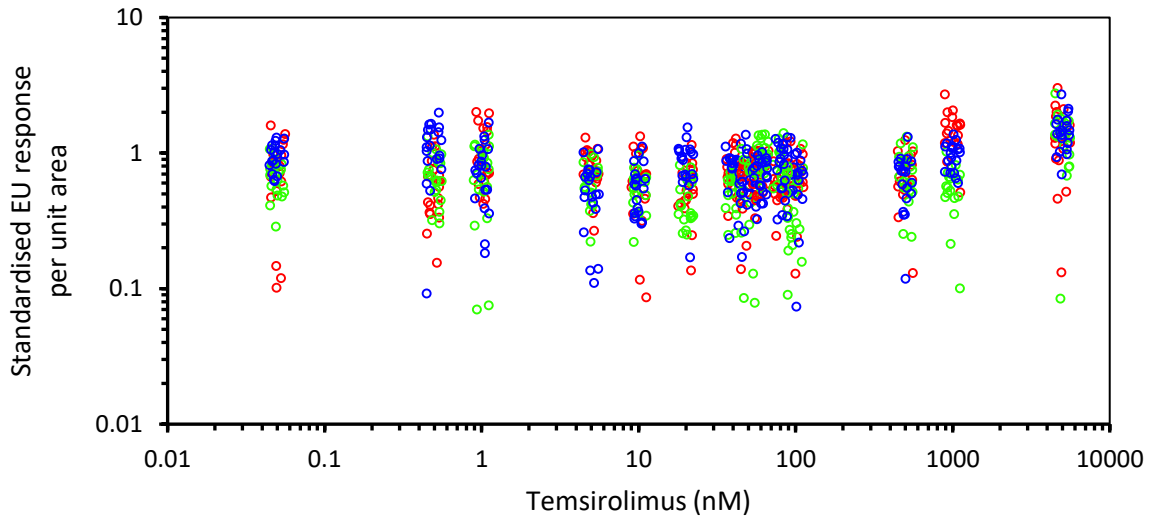


Figure 7.18. Nucleolar area vs. drug dose. A, B, C, D) ACHN and E, F, G, H) UoK111 cells were treated with increasing concentrations of mTORis for 2 hours and then treated as described in section 2.5. The dots represent the nucleolar area from 20 randomly selected nuclei from each well (each well labelled with a different colour). I) ACHN and J) UoK111 cells were treated with increasing concentrations of ActD for 2 hours and treated as above.

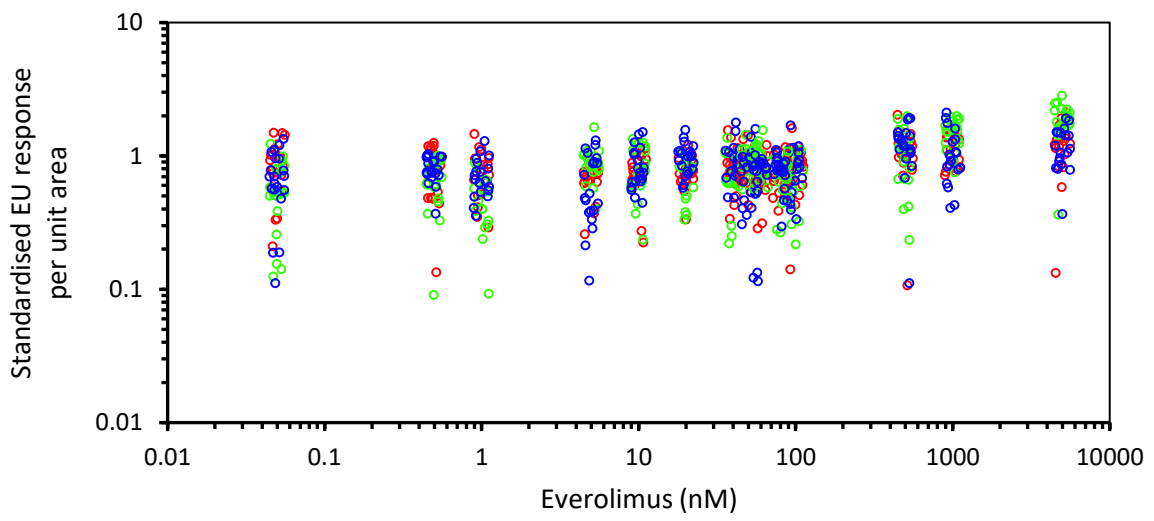
A)



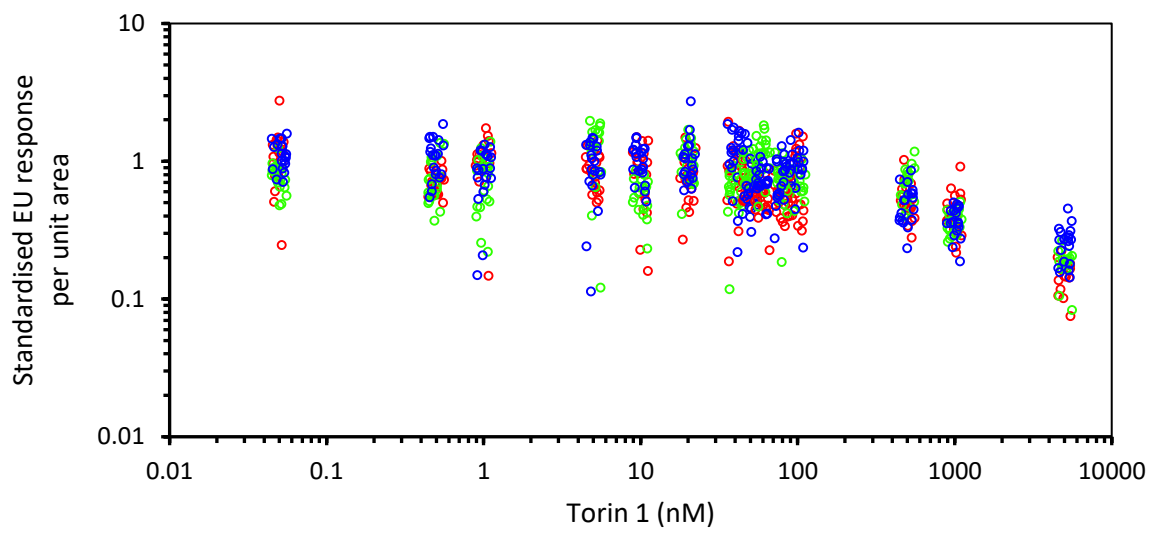
B)



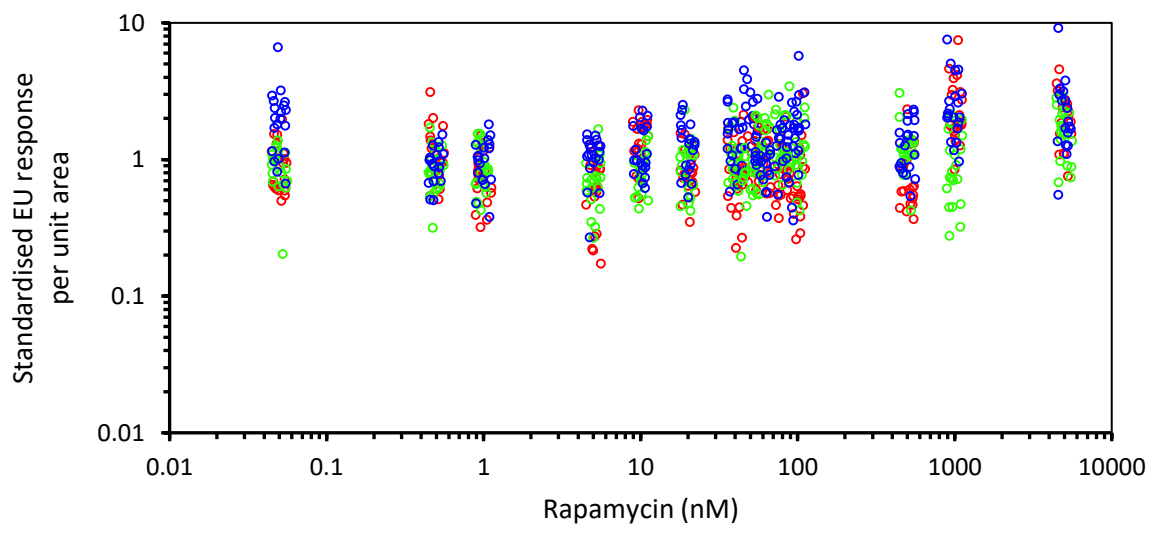
C)



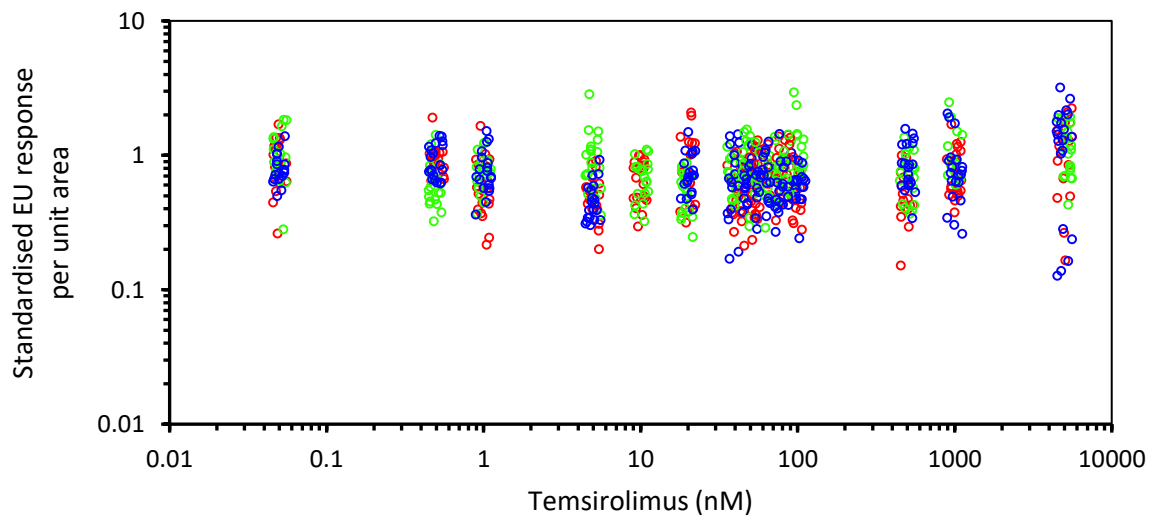
D)



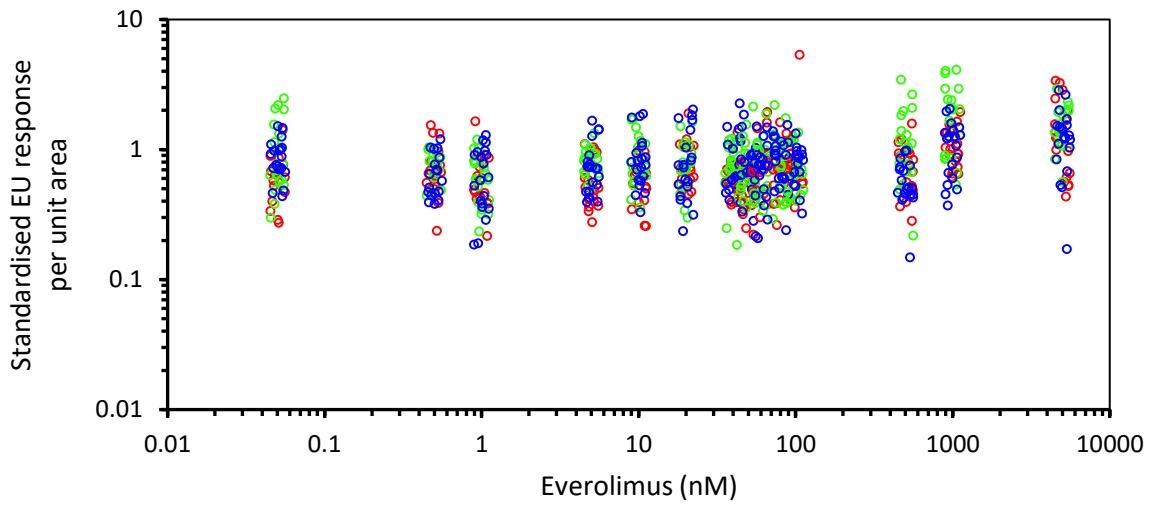
E)



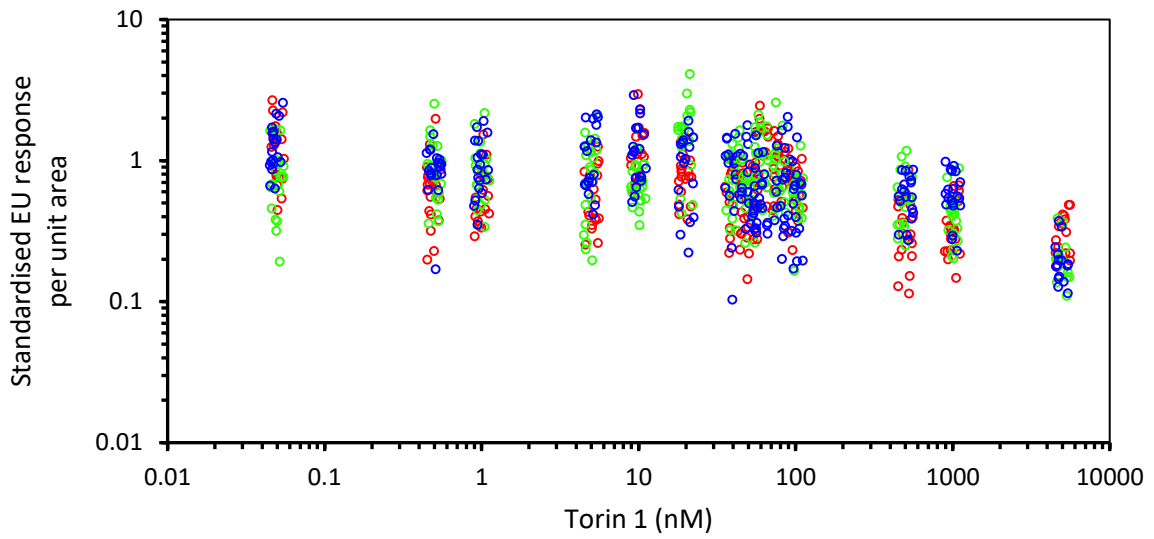
F)



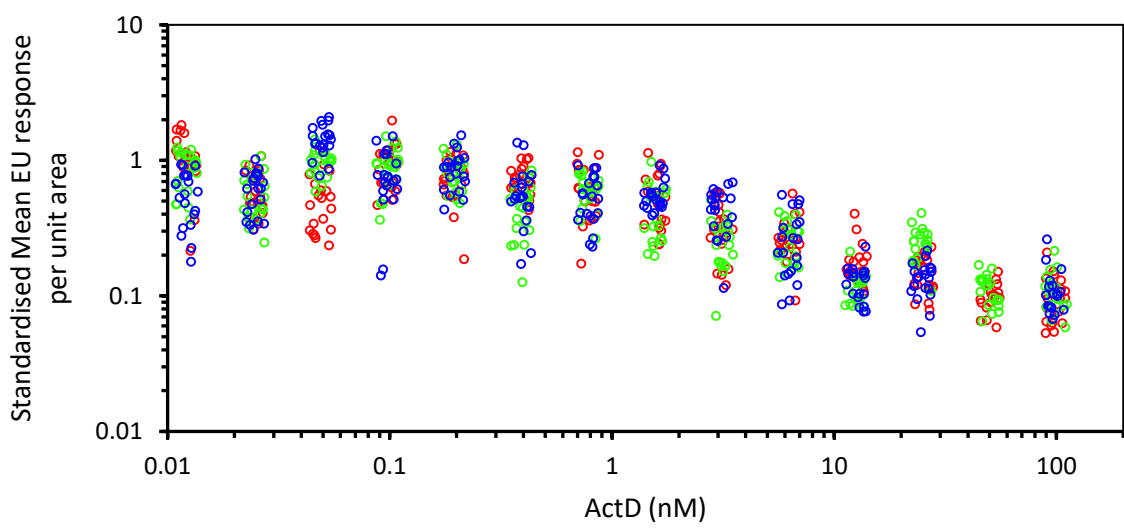
G)



H)



I)



J)

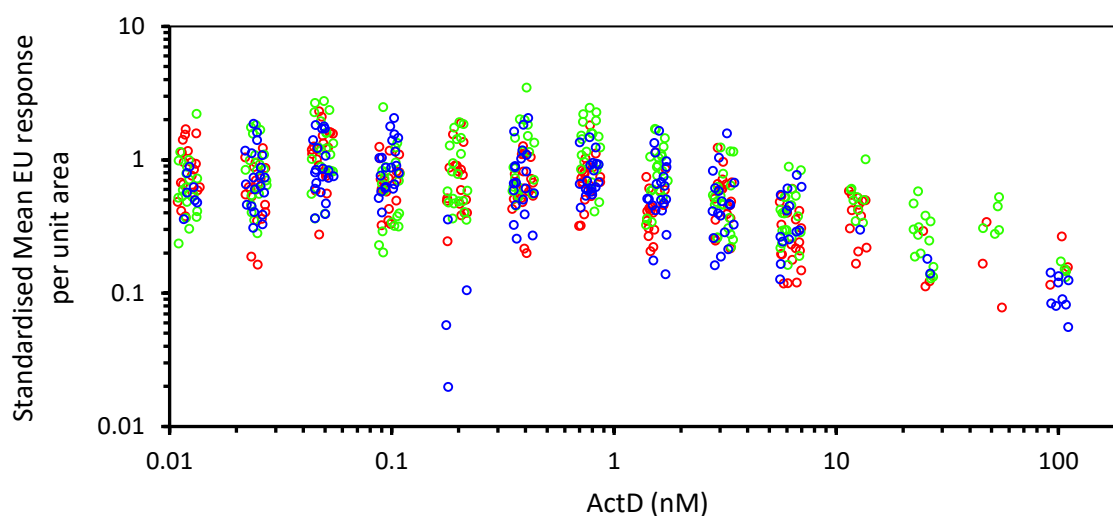


Figure 7.19. 5-EU incorporation per unit area vs. drug dose. A, B, C, D) ACHN and E, F, G, H) UoK111 cells were treated with increasing concentrations of mTORis for 2 hours and then treated as described in section 2.5. The dots represent the nucleolar area from 20 randomly selected nuclei from each well (each well labelled with a different colour). I) ACHN and J) UoK111 cells were treated with increasing concentrations of ActD for 2 hours and treated as above.

Figure 7.20 shows the full data distribution and statistical analyses for the response to a typical treatment of interest (ACHN cells treated with 100nM Torin 1) showing the individual nuclei for individual wells (each well labelled with a different colour, as in Figures 7.17, 7.18 and 7.19). The mean values per well and their SEMs are indicated with the corresponding well colour. The overall (grand) mean for the treatment is indicated in black. The plots clearly reveal that there are two sources of variation in the 5-EU incorporation response: cell-to-cell (within a well) and well-to-well (within a treatment). To deal with these two sources of error, the SEM for the overall mean (black point and error bars) was calculated using a two-stage nested design (fixed effect) as indicated above (450), see also (449) for a graphical explanation of multi-level replication). The grey point and error bars show the overall mean and SEM for the treatment without considering within well variation. The difference between this SEM and the two-stage SEM is very small due to the large sample size (n) within each well; nevertheless, the two-stage nested analysis was used throughout both for analytical accuracy and to cope with possible instances of low cell numbers per well.

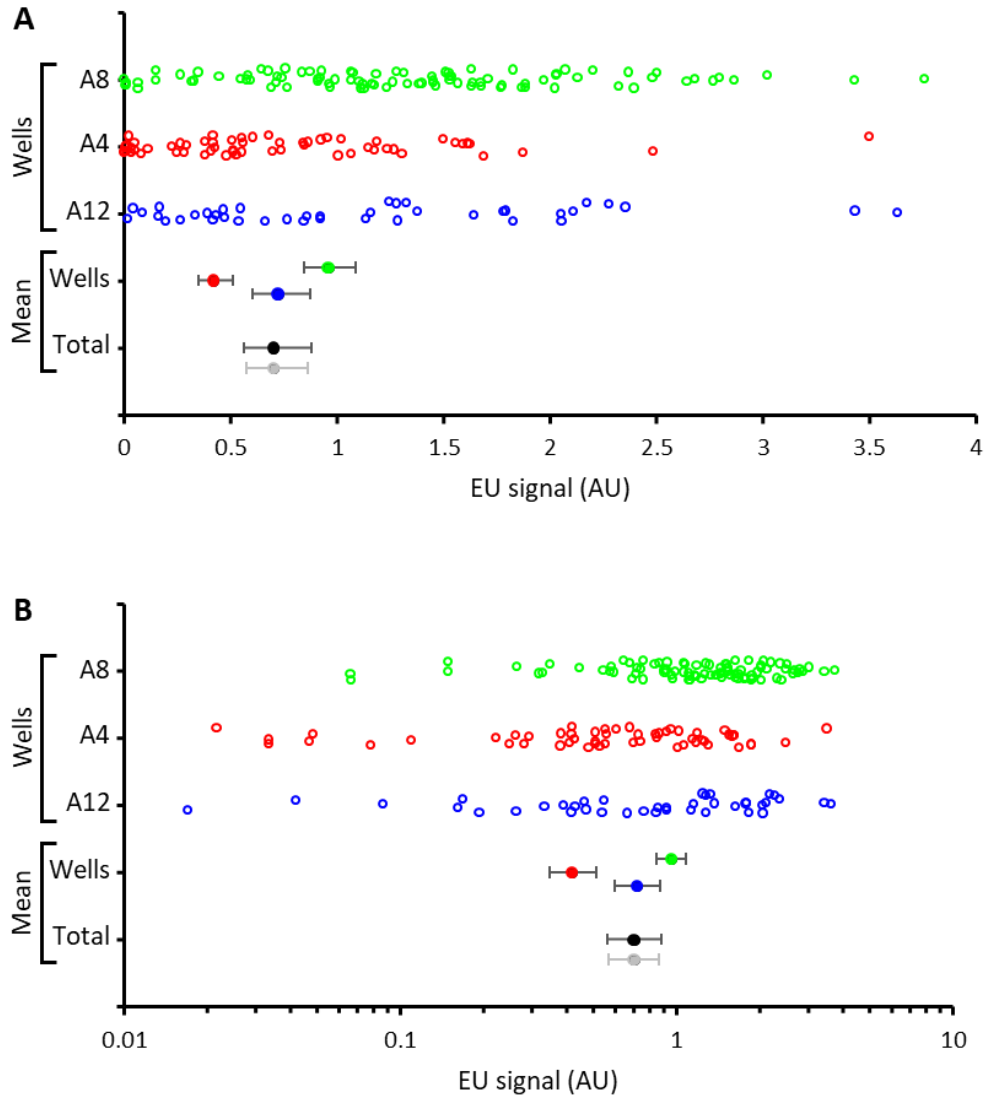


Figure 7.20. Data distribution for the response to a typical treatment of interest. ACHN cells were treated with 100nM Torin 1 for 2 hours and then processed as described in section 2.5. Total 5-EU signal is plotted linearly (A) and logarithmically (B) for individual wells and the averages per well and per treatment are indicated. The dots represent individual nuclei from each individual well (each well labelled with a different colour). The mean values per well and their SEMs are indicated with the corresponding well colour. The overall (grand) mean for the treatment is indicated in black. The grey point and error bars show the overall mean and SEM for the treatment without considering within well variation.

8. References

1. Cancer Research UK. Kidney cancer mortality statistics [Internet]. Cancer Research UK. 2022 [cited 2022 Dec 29]. Available from: <https://www.cancerresearchuk.org/health-professional/cancer-statistics/statistics-by-cancer-type/kidney-cancer/mortality>
2. Padala SA, Barsouk A, Thandra KC, Saginala K, Mohammed A, Vakiti A, et al. Epidemiology of Renal Cell Carcinoma. *World J Oncol* [Internet]. 2020/05/14. 2020 Jun;11(3):79–87. Available from: <https://pubmed.ncbi.nlm.nih.gov/32494314>
3. Hutson TE, Figlin RA, Kuhn JG, Motzer RJ. Targeted Therapies for Metastatic Renal Cell Carcinoma: An Overview of Toxicity and Dosing Strategies. *Oncologist* [Internet]. 2008 Oct 1;13(10):1084–96. Available from: <https://doi.org/10.1634/theoncologist.2008-0120>
4. Schmidinger M, Danesi R. Management of Adverse Events Associated with Cabozantinib Therapy in Renal Cell Carcinoma. *Oncologist*. 2018 Mar;23(3):306–15.
5. Kollmannsberger C, Soulieres D, Wong R, Scalera A, Gaspo R, Bjarnason G. Sunitinib therapy for metastatic renal cell carcinoma: recommendations for management of side effects. *Can Urol Assoc J = J l'Association des Urol du Canada*. 2007 Jun;1(2 Suppl):S41-54.
6. Popławski P, Bogusławska J, Hanusek K, Piekiełko-Witkowska A. Nucleolar Proteins and Non-Coding RNAs: Roles in Renal Cancer. Vol. 22, *International Journal of Molecular Sciences*. 2021.
7. Stępiński D. The nucleolus, an ally, and an enemy of cancer cells. *Histochem Cell Biol* [Internet]. 08/13. 2018;150(6):607–29. Available from: <internal-pdf://178.92.210.88/Stepinski, D. 2018. The nucleolus, an ally, an.pdf>
8. Hannan KM, Brandenburger Y, Jenkins A, Sharkey K, Cavanaugh A, Rothblum L, et al. mTOR-Dependent Regulation of Ribosomal Gene Transcription Requires S6K1 and Is Mediated by Phosphorylation of the Carboxy-Terminal Activation Domain of the Nucleolar Transcription Factor UBF†. *Mol Cell Biol* [Internet]. 2003;23(23):8862–77. Available from: <internal-pdf://92.101.110.169/Hannan, K. 2003. mTOR-Dependent Regulation of.pdf>
9. Iadevaia V, Zhang Z, Jan E, Proud CG. mTOR signaling regulates the processing of pre-rRNA in human cells. *Nucleic Acids Res* [Internet]. 2012;40(6):2527–39. Available from: <internal-pdf://173.82.222.192/mTOR signaling regulates the processing of pre.pdf>
10. Hajdu SI. A note from history: landmarks in history of cancer, part 1. *Cancer*. 2011 Mar;117(5):1097–102.
11. Bray F, Laversanne M, Weiderpass E, Soerjomataram I. The ever-increasing importance of cancer as a leading cause of premature death worldwide. *Cancer* [Internet]. 2021 Aug 15;127(16):3029–30. Available from: <https://doi.org/10.1002/cncr.33587>
12. Sung H, Ferlay J, Siegel RL, Laversanne M, Soerjomataram I, Jemal A, et al. Global Cancer Statistics 2020: GLOBOCAN Estimates of Incidence and Mortality Worldwide for 36 Cancers in 185 Countries. *CA Cancer J Clin* [Internet]. 2021 May 1;71(3):209–49. Available from: <https://doi.org/10.3322/caac.21660>
13. CancerData. Staging data in England [Internet]. 2021 [cited 2022 Jan 11]. Available from: https://www.cancerdata.nhs.uk/stage_at_diagnosis
14. Orsolich I, Jurada D, Pullen N, Oren M, Eliopoulos AG, Volarevic S. Review: The relationship

- between the nucleolus and cancer: Current evidence and emerging paradigms. *Semin Cancer Biol* [Internet]. 2016;37–38:36–50. Available from: [internal-pdf://146.16.86.34/Orsolich, I. 2015. The relationship between the.pdf](https://doi.org/10.1038/s12298-015-0146-1)
15. Cancer Research UK. Cancer incidence statistics [Internet]. [cited 2022 Jan 10]. Available from: <https://www.cancerresearchuk.org/health-professional/cancer-statistics/incidence#heading-Zero>
 16. Cancer Research UK. Cancer mortality statistics [Internet]. [cited 2022 Jan 10]. Available from: <https://www.cancerresearchuk.org/health-professional/cancer-statistics/mortality#heading-Zero>
 17. Ahmad AS, Ormiston-Smith N, Sasieni PD. Trends in the lifetime risk of developing cancer in Great Britain: comparison of risk for those born from 1930 to 1960. *Br J Cancer* [Internet]. 2015;112(5):943–7. Available from: <https://doi.org/10.1038/bjc.2014.606>
 18. Martincorena I, Campbell PJ. Somatic mutation in cancer and normal cells. *Science* (80-) [Internet]. 2015 Sep 25;349(6255):1483–9. Available from: <https://doi.org/10.1126/science.aab4082>
 19. Pecorino L. Oncogenes and tumor suppressor genes. In: *Molecular biology of cancer Mechanisms, Targets, and Therapeutics*. Third. Oxford: Oxford University Press; 2012. p. 7–9.
 20. Lambert P. Oncogenic Viruses. In: Schaechter MBT-E of M (Third E, editor. Oxford: Academic Press; 2009. p. 421–9. Available from: <https://www.sciencedirect.com/science/article/pii/B9780123739445003084>
 21. Pierotti M, Sozzi G, Croce C. Mechanisms of oncogene activation. In: Kufe D, Pollock R, Weichselbaum R, editors. *Holland-Frei Cancer Medicine* [Internet]. 6th ed. BC Decker; 2003. Available from: <https://www.ncbi.nlm.nih.gov/books/NBK12538/>
 22. Levitt NC, Hickson ID. Caretaker tumour suppressor genes that defend genome integrity. *Trends Mol Med* [Internet]. 2002;8(4):179–86. Available from: <https://www.sciencedirect.com/science/article/pii/S1471491402022980>
 23. Chatterjee N, Walker GC. Mechanisms of DNA damage, repair, and mutagenesis. *Environ Mol Mutagen* [Internet]. 2017/05/09. 2017 Jun;58(5):235–63. Available from: <https://pubmed.ncbi.nlm.nih.gov/28485537>
 24. Elmore S. Apoptosis: a review of programmed cell death. *Toxicol Pathol* [Internet]. 2007 Jun;35(4):495–516. Available from: <https://pubmed.ncbi.nlm.nih.gov/17562483>
 25. Giacinti C, Giordano A. RB and cell cycle progression. *Oncogene* [Internet]. 2006;25(38):5220–7. Available from: <https://doi.org/10.1038/sj.onc.1209615>
 26. Thériault BL, Dimaras H, Gallie BL, Corson TW. The genomic landscape of retinoblastoma: a review. *Clin Experiment Ophthalmol* [Internet]. 2014 Jan 1;42(1):33–52. Available from: <https://doi.org/10.1111/ceo.12132>
 27. Boyd MT, Vlatkovic N. p53: a molecular marker for the detection of cancer. *Expert Opin Med Diagn* [Internet]. 2008 Sep 1;2(9):1013–24. Available from: <https://doi.org/10.1517/17530059.2.9.1013>
 28. Croce CM. Oncogenes and Cancer. *N Engl J Med* [Internet]. 2008 Jan 31;358(5):502–11. Available from: <https://doi.org/10.1056/NEJMra072367>
 29. Hanahan D, Weinberg RA. The Hallmarks of Cancer. *Cell* [Internet]. 2000 Jan 7;100(1):57–70.

Available from: [https://doi.org/10.1016/S0092-8674\(00\)81683-9](https://doi.org/10.1016/S0092-8674(00)81683-9)

30. Hanahan D, Weinberg RA. Hallmarks of cancer: The next generation. *Cell*. 2011 Mar 4;144(5):646–74.
31. Hanahan D. Hallmarks of Cancer: New Dimensions. *Cancer Discov* [Internet]. 2022 Jan 1;12(1):31 LP – 46. Available from: <http://cancerdiscovery.aacrjournals.org/content/12/1/31.abstract>
32. Guertin DA, Sabatini DM. Chapter 12 - Cell Growth. In: Mendelsohn J, Howley PM, Israel MA, Gray JW, Thompson CBBT-TMB of C (Third E, editors. Philadelphia: W.B. Saunders; 2008. p. 169–75. Available from: <https://www.sciencedirect.com/science/article/pii/B9781416037033100123>
33. Yuan H-X, Xiong Y, Guan K-L. Nutrient sensing, metabolism, and cell growth control. *Mol Cell* [Internet]. 2013 Feb 7;49(3):379–87. Available from: <https://pubmed.ncbi.nlm.nih.gov/23395268>
34. Kaldis P. Quo Vadis Cell Growth and Division? [Internet]. Vol. 4, *Frontiers in Cell and Developmental Biology*. 2016. Available from: <https://www.frontiersin.org/article/10.3389/fcell.2016.00095>
35. Das-Bradoo S, Bielinsky A. DNA Replication and Checkpoint Control in S Phase. *Nat Educ*. 2010;3(9):50.
36. Takeda DY, Dutta A. DNA replication and progression through S phase. *Oncogene*. 2005;24(17):2827–43.
37. Chow AY. Cell Cycle Control by Oncogenes and Tumor Suppressors: Driving the Transformation of Normal Cells into Cancerous Cells. *Nat Educ*. 2010;3(9):7.
38. Ramirez de Molina A, Rodriguez-Gonzalez A, Lacal Carlos J. Targeting new anticancer drugs within signalling pathways regulated by the Ras GTPase superfamily (Review). *Int J Oncol* [Internet]. 2001;19(1):5–17. Available from: <https://doi.org/10.3892/ijo.19.1.5>
39. Prior IA, Hood FE, Hartley JL. The Frequency of Ras Mutations in Cancer. *Cancer Res*. 2020 Jul;80(14):2969–74.
40. Abreu Velez AM, Howard MS. Tumor-suppressor Genes, Cell Cycle Regulatory Checkpoints, and the Skin. *N Am J Med Sci* [Internet]. 2015 May;7(5):176–88. Available from: <https://pubmed.ncbi.nlm.nih.gov/26110128>
41. Senturk E, Manfredi JJ. p53 and cell cycle effects after DNA damage. In: *p53 Protocols*. Springer; 2013. p. 49–61.
42. Znaor A, Lortet-Tieulent J, Laversanne M, Jemal A, Bray F. International Variations and Trends in Renal Cell Carcinoma Incidence and Mortality. *Eur Urol* [Internet]. 2015;67(3):519–30. Available from: <https://www.sciencedirect.com/science/article/pii/S0302283814010100>
43. Smittenaar CR, Petersen KA, Stewart K, Moitt N. Cancer incidence and mortality projections in the UK until 2035. *Br J Cancer* [Internet]. 2016;115(9):1147–55. Available from: <https://doi.org/10.1038/bjc.2016.304>
44. Nabi S, Kessler ER, Bernard B, Flaig TW, Lam ET. Renal cell carcinoma: a review of biology and pathophysiology. *F1000Research* [Internet]. 2018 Mar 12;7:307. Available from: <https://pubmed.ncbi.nlm.nih.gov/29568504>

45. Howlader N, Noone A, Krapcho M, Miller D, Brest A, Yu M, et al. SEER Cancer Statistics Review, 1975-2016, National Cancer Institute. [Internet]. Bethesda, MD; 2019. Available from: https://seer.cancer.gov/csr/1975_2016/
46. Cohen HT, McGovern FJ. Renal-Cell Carcinoma. *N Engl J Med* [Internet]. 2005 Dec 8;353(23):2477–90. Available from: <https://doi.org/10.1056/NEJMra043172>
47. Washecka R, Hanna M. Malignant renal tumors intuberos sclerosis. *Urology* [Internet]. 1991;37(4):340–3. Available from: <https://www.sciencedirect.com/science/article/pii/0090429591802615>
48. Pavlovich CP, Schmidt LS. Searching for the hereditary causes of renal-cell carcinoma. *Nat Rev Cancer* [Internet]. 2004;4(5):381–93. Available from: <https://doi.org/10.1038/nrc1364>
49. Hsieh JJ, Purdue MP, Signoretti S, Swanton C, Albiges L, Schmidinger M, et al. Renal cell carcinoma. *Nat Rev Dis Prim* [Internet]. 2017;3(1):17009. Available from: <https://doi.org/10.1038/nrdp.2017.9>
50. Eble JN, Sauter G, Epstein JI, Sesterhenn IA. Pathology and genetics of tumours of the urinary system and male genital organs: World Health Organization classification of tumours. *Int Agency Res Cancer*. 2004;
51. Haase VH. The VHL tumor suppressor: master regulator of HIF. *Curr Pharm Des* [Internet]. 2009;15(33):3895–903. Available from: <https://pubmed.ncbi.nlm.nih.gov/19671042>
52. Dengler VL, Galbraith M, Espinosa JM. Transcriptional regulation by hypoxia inducible factors. *Crit Rev Biochem Mol Biol* [Internet]. 2013/10/07. 2014;49(1):1–15. Available from: <https://pubmed.ncbi.nlm.nih.gov/24099156>
53. Allory Y, Ouazana D, Boucher E, Thiounn N, Vieillefond A. Papillary renal cell carcinoma. *Virchows Arch* [Internet]. 2003;442(4):336–42. Available from: <https://doi.org/10.1007/s00428-003-0787-1>
54. Yang XJ, Tan M-H, Kim HL, Ditlev JA, Betten MW, Png CE, et al. A Molecular Classification of Papillary Renal Cell Carcinoma. *Cancer Res* [Internet]. 2005 Jul 1;65(13):5628 LP – 5637. Available from: <http://cancerres.aacrjournals.org/content/65/13/5628.abstract>
55. Linehan WM. Comprehensive Molecular Characterization of Papillary Renal-Cell Carcinoma. *N Engl J Med* [Internet]. 2015 Nov 4;374(2):135–45. Available from: <https://doi.org/10.1056/NEJMoa1505917>
56. Cindolo L, de la Taille A, Schips L, Zigeuner RE, Ficarra V, Tostain J, et al. Chromophobe renal cell carcinoma: Comprehensive analysis of 104 cases from multicenter European database. *Urology* [Internet]. 2005;65(4):681–6. Available from: <https://www.sciencedirect.com/science/article/pii/S009042950401341X>
57. Casuscelli J, Becerra MF, Seier K, Manley BJ, Benfante N, Redzematovic A, et al. Chromophobe Renal Cell Carcinoma: Results From a Large Single-Institution Series. *Clin Genitourin Cancer* [Internet]. 2019;17(5):373-379.e4. Available from: <https://www.sciencedirect.com/science/article/pii/S1558767319302009>
58. Garje R, Elhag D, Yasin HA, Acharya L, Vaena D, Dahmouh L. Comprehensive review of chromophobe renal cell carcinoma. *Crit Rev Oncol Hematol* [Internet]. 2021;160:103287. Available from: <https://www.sciencedirect.com/science/article/pii/S1040842821000755>
59. Davis CF, Ricketts CJ, Wang M, Yang L, Cherniack AD, Shen H, et al. The Somatic Genomic

- Landscape of Chromophobe Renal Cell Carcinoma. *Cancer Cell* [Internet]. 2014;26(3):319–30. Available from: <https://www.sciencedirect.com/science/article/pii/S1535610814003043>
60. Colvin MO. Alkylating Agents. In: *Encyclopedia of Cancer*. 2nd ed. Academic Press; 2002. p. 35–42.
 61. Singh RK, Kumar S, Prasad DN, Bhardwaj TR. Therapeutic journey of nitrogen mustard as alkylating anticancer agents: Historic to future perspectives. Vol. 151, *European Journal of Medicinal Chemistry*. Elsevier Masson SAS; 2018. p. 401–33.
 62. D’Andrea AD. DNA Repair Pathways and Human Cancer . In: *The Molecular Basis of Cancer* . 4th ed. 2015. p. 47–66.
 63. Germanas J, Pandya AG. Alkylating agents. *Dermatol Ther*. 2002 Dec 1;15(4):317–24.
 64. Berman HM, Young PR. INTERCALATING DRUGS WITH NUCLEIC ACIDS. *Annu Rev Biophys Bioeng* [Internet]. 1981 [cited 2020 Apr 23];10:87–114. Available from: www.annualreviews.org
 65. Bhagavan NV, Ha C-E. Structure and Properties of DNA. In: *Essentials of Medical Biochemistry* [Internet]. Elsevier; 2011 [cited 2020 Apr 23]. p. 275–86. Available from: <https://linkinghub.elsevier.com/retrieve/pii/B9780120954612000217>
 66. Liang X, Wu Q, Luan S, Yin Z, He C, Yin L, et al. A comprehensive review of topoisomerase inhibitors as anticancer agents in the past decade. *Eur J Med Chem*. 2019 Jun 1;171:129–68.
 67. Willey CD, Bonner JA. Interaction of Chemotherapy and Radiation. In: *Clinical Radiation Oncology: Third Edition*. Elsevier Inc.; 2012. p. 65–82.
 68. Povirk LF. DNA damage and mutagenesis by radiomimetic DNA-cleaving agents: Bleomycin, neocarzinostatin and other enediynes. *Mutat Res - Fundam Mol Mech Mutagen*. 1996 Aug 17;355(1–2):71–89.
 69. Burger RM. Cleavage of nucleic acids by bleomycin. *Chem Rev*. 1998 May;98(3):1153–69.
 70. Stubbe J, Kozarich JW. Mechanisms of Bleomycin-Induced DNA Degradation. *Chem Rev*. 1987 Aug 1;87(5):1107–36.
 71. Kang ZJ, Liu YF, Xu LZ, Long ZJ, Huang D, Yang Y, et al. The philadelphia chromosome in leukemogenesis. *Chin J Cancer*. 2016 May 27;35(1).
 72. Damjanov I. Neoplasia. In: *Pathology Secrets*. Elsevier Inc.; 2009. p. 76–97.
 73. FDA USF and DA. Gleevec ® [Internet]. 2006 [cited 2020 Apr 21]. Available from: https://www.accessdata.fda.gov/drugsatfda_docs/label/2006/021588s009lbl.pdf
 74. An X, Tiwari AK, Sun Y, Ding PR, Ashby CR, Chen ZS. BCR-ABL tyrosine kinase inhibitors in the treatment of Philadelphia chromosome positive chronic myeloid leukemia: A review [Internet]. Vol. 34, *Leukemia Research*. 2010 [cited 2020 Apr 21]. p. 1255–68. Available from: <http://www.ncbi.nlm.nih.gov/pubmed/20537386>
 75. Pecorino L. Growth factor signalling and oncogenes. In: *Molecular biology of cancer Mechanisms, Targets, and Therapeutics*. 3rd ed. Oxford University Press; 2012. p. 77–102.
 76. Dean L. Trastuzumab (Herceptin) Therapy and ERBB2 (HER2) Genotype [Internet]. *Medical Genetics Summaries*. National Center for Biotechnology Information (US); 2012 [cited 2020 Apr 22]. Available from: <http://www.ncbi.nlm.nih.gov/pubmed/28520362>

77. Sen B, Johnson FM. Regulation of Src Family Kinases in Human Cancers. *J Signal Transduct* [Internet]. 2011 Apr 4 [cited 2020 Apr 22]; Available from: <https://www.ncbi.nlm.nih.gov/pmc/articles/PMC3135246/>
78. Zhang S, Yu D. Targeting Src family kinases in anti-cancer therapies: Turning promise into triumph. *Trends Pharmacol Sci*. 2012 Mar;33(3):122–8.
79. García-Echeverría C. Allosteric and ATP-competitive kinase inhibitors of mTOR for cancer treatment. *Bioorg Med Chem Lett* [Internet]. 2010;20(15):4308–12. Available from: <http://www.sciencedirect.com/science/article/pii/S0960894X10007523>
80. Zanardi E, Verzoni E, Grassi P, Necchi A, Giannatempo P, Raggi D, et al. Clinical experience with temsirolimus in the treatment of advanced renal cell carcinoma. Vol. 7, *Therapeutic Advances in Urology*. SAGE Publications; 2015. p. 152–61.
81. Royce ME, Osman D. Everolimus in the treatment of metastatic breast cancer. *Breast Cancer Basic Clin Res*. 2015 Sep 6;9:73–9.
82. Durrant DE, Morrison DK. Targeting the Raf kinases in human cancer: The Raf dimer dilemma. Vol. 118, *British Journal of Cancer*. Nature Publishing Group; 2018. p. 3–8.
83. Vaughan C, Pearsall I, Yeudall A, Deb SP, Deb S. p53: Its mutations and their impact on transcription. In: *Mutant p53 and MDM2 in Cancer*. Springer New York; 2014. p. 71–90.
84. Oliner JD, Saiki AY, Caenepeel S. The role of MDM2 amplification and overexpression in tumorigenesis. *Cold Spring Harb Perspect Med*. 2016 Jun 1;6(6).
85. Liu J, Zhang C, Hu W, Feng Z. Tumor suppressor p53 and metabolism. - PubMed - NCBI. *J Mol Cell Biol* [Internet]. 2019 Apr 1 [cited 2020 Apr 22];11(4):284–92. Available from: <https://www.ncbi.nlm.nih.gov/pubmed/30500901>
86. Drakos E, Singh RR, Rassidakis GZ, Schlette E, Li J, Claret FX, et al. Activation of the p53 pathway by the MDM2 inhibitor nutlin-3a overcomes BCL2 overexpression in a preclinical model of diffuse large B-cell lymphoma associated with t(14;18)(q32;q21). *Leukemia*. 2011 May 11;25(5):856–67.
87. Crane EK, Kwan SY, Izaguirre DI, Tsang YTM, Mullany LK, Zu Z, et al. Nutlin-3a: A potential therapeutic opportunity for TP53 wild-type ovarian carcinomas. *PLoS One*. 2015 Aug 6;10(8).
88. Polański R, Noon AP, Blaydes J, Phillips A, Rubbi CP, Parsons K, et al. Senescence induction in renal carcinoma cells by Nutlin-3: A potential therapeutic strategy based on MDM2 antagonism. *Cancer Lett*. 2014 Oct 28;353(2):211–9.
89. Vassilev LT, Vu BT, Graves B, Carvajal D, Podlaski F, Filipovic Z, et al. In Vivo Activation of the p53 Pathway by Small-Molecule Antagonists of MDM2. *Science* (80-). 2004 Feb 6;303(5659):844–8.
90. Tonini T, Rossi F, Claudio PP. Molecular basis of angiogenesis and cancer. *Oncogene*. 2003 Oct 3;22(43):6549–56.
91. Pecorino L. Metastasis. In: *Molecular biology of cancer Mechanisms, Targets, and Therapeutics*. 3rd ed. Oxford University Press; 2012. p. 197–224.
92. El-Kenawi AE, El-Remessy AB. Angiogenesis inhibitors in cancer therapy: Mechanistic perspective on classification and treatment rationales. *Br J Pharmacol*. 2013 Oct;170(4):712–29.

93. Shingarev R, Jaimes EA. Renal cell carcinoma: new insights and challenges for a clinician scientist. *Am J Physiol Physiol* [Internet]. 2017 Apr 5;313(2):F145–54. Available from: <https://doi.org/10.1152/ajprenal.00480.2016>
94. Petejova N, Martinek A. Renal cell carcinoma: Review of etiology, pathophysiology and risk factors. *Biomed Pap Med Fac Palacky Univ Olomouc*. 2016;160(2).
95. Unwin RD, Craven RA, Harnden P, Hanrahan S, Totty N, Knowles M, et al. Proteomic changes in renal cancer and co-ordinate demonstration of both the glycolytic and mitochondrial aspects of the Warburg effect. *Proteomics* [Internet]. 2003 Aug 1;3(8):1620–32. Available from: <https://doi.org/10.1002/pmic.200300464>
96. Choi WSW, Boland J, Lin J. Hypoxia-Inducible Factor-2 α as a Novel Target in Renal Cell Carcinoma. *J kidney cancer VHL* [Internet]. 2021 Apr 7;8(2):1–7. Available from: <https://pubmed.ncbi.nlm.nih.gov/33868900>
97. Haas NB, Nathanson KL. Hereditary Kidney Cancer Syndromes. *Adv Chronic Kidney Dis* [Internet]. 2014;21(1):81–90. Available from: <https://www.sciencedirect.com/science/article/pii/S1548559513001444>
98. Faes S, Demartines N, Dormond O. Mechanistic Target of Rapamycin Inhibitors in Renal Cell Carcinoma: Potential, Limitations, and Perspectives [Internet]. Vol. 9, *Frontiers in Cell and Developmental Biology*. 2021. Available from: <https://www.frontiersin.org/article/10.3389/fcell.2021.636037>
99. Hua H, Kong Q, Zhang H, Wang J, Luo T, Jiang Y. Targeting mTOR for cancer therapy. *J Hematol Oncol* [Internet]. 2019 Jul 5 [cited 2020 Mar 19];12(1):71. Available from: <https://doi.org/10.1186/s13045-019-0754-1>
100. Deleuze A, Saout J, Dugay F, Peyronnet B, Mathieu R, Verhoest G, et al. Immunotherapy in Renal Cell Carcinoma: The Future Is Now. *Int J Mol Sci* [Internet]. 2020 Apr 5;21(7):2532. Available from: <https://pubmed.ncbi.nlm.nih.gov/32260578>
101. Groenendijk FH, Bernardis R. Drug resistance to targeted therapies: Déjà vu all over again. *Mol Oncol*. 2014 Sep 21;8(6):1067–83.
102. Lim ZF, Ma PC. Emerging insights of tumor heterogeneity and drug resistance mechanisms in lung cancer targeted therapy. *J Hematol Oncol*. 2019 Dec 9;12(1):1–18.
103. Neel DS, Bivona TG. Resistance is futile: overcoming resistance to targeted therapies in lung adenocarcinoma. *npj Precis Oncol*. 2017 Dec 20;1(1):1–6.
104. Facchinetti F, Proto C, Minari R, Garassino M, Tiseo M. Mechanisms of resistance to target therapies in non-small cell lung cancer. In: Mandalà M, Romano E, editors. *Handbook of Experimental Pharmacology*. Springer New York LLC; 2018. p. 63–89.
105. Engelman JA, Zejnullahu K, Mitsudomi T, Song Y, Hyland C, Joon OP, et al. MET amplification leads to gefitinib resistance in lung cancer by activating ERBB3 signaling. *Science* (80-). 2007 May 18;316(5827):1039–43.
106. Piloto O, Wright M, Brown P, Kim KT, Levis M, Small D. Prolonged exposure to FLT3 inhibitors leads to resistance via activation of parallel signaling pathways. *Blood*. 2007 Feb 15;109(4):1643–52.
107. Bentires-Alj M, Barbu V, Fillet M, Chariot A, Relic B, Jacobs N, et al. NF- κ B transcription factor induces drug resistance through MDR1 expression in cancer cells. *Oncogene*. 2003 Jan

- 9;22(1):90–7.
108. Godwin P, Baird AM, Heavey S, Barr MP, O’Byrne KJ, Gately K. Targeting nuclear factor-kappa B to overcome resistance to chemotherapy. *Front Oncol*. 2013 May 16;3(120).
 109. Freireich EJ, Karon M, Frei III E. Quadruple combination therapy (VAMP) for acute lymphocytic leukemia of childhood. In: *Proc Am Assoc Cancer Res*. 1964. p. 20.
 110. Chua KN, Kong LR, Sim WJ, Ng HC, Ong WR, Thiery JP, et al. Combinatorial treatment using targeted MEK and SRC inhibitors synergistically abrogates tumor cell growth and induces mesenchymal-epithelial transition in non-small-cell lung carcinoma. *Oncotarget*. 2015;6(30):29991–30005.
 111. Shah MA, Schwartz GK. Cell Cycle-mediated Drug Resistance. An Emerg Concept *Cancer Ther* [Internet]. 2001;7(8):2168–81. Available from: internal-pdf://6.193.93.144/Shah, M. 2001. Cell cycle-mediated drug resist.pdf
 112. Gieling RG, Parker CA, De Costa LA, Robertson N, Harris AL, Stratford IJ, et al. Inhibition of carbonic anhydrase activity modifies the toxicity of doxorubicin and melphalan in tumour cells in vitro. *J Enzyme Inhib Med Chem*. 2012 Nov 19;28(2):360–9.
 113. Blagosklonny M V. Overcoming limitations of natural anticancer drugs by combining with artificial agents. *Trends Pharmacol Sci*. 2005 Feb 1;26(2):77–81.
 114. Blagosklonny M V, Darzynkiewicz Z. Cyclotherapy: Protection of Normal Cells and Unshielding of Cancer Cells. *Cell Cycle* [Internet]. 2002 [cited 2020 Apr 13];1(6):375–82. Available from: <https://www.tandfonline.com/action/journalInformation?journalCode=kccy20>
 115. Mokhtari RB, Homayouni TS, Baluch N, Morgatskaya E, Kumar S, Das B, et al. Combination therapy in combating cancer. *Oncotarget*. 2017 Jun 6;8(23):38022–43.
 116. Osakwe O, Rizvi SAA. Introduction. In: *Social Aspects of Drug Discovery, Development and Commercialization* [Internet]. Elsevier; 2016 [cited 2020 May 7]. p. xvii–xxx. Available from: <https://linkinghub.elsevier.com/retrieve/pii/B978012802220700017X>
 117. Li J, Kim SG, Blenis J. Rapamycin: one drug, many effects. *Cell Metab* [Internet]. 02/06. 2014;19(3):373–9. Available from: <https://www.ncbi.nlm.nih.gov/pubmed/24508508>
<https://www.ncbi.nlm.nih.gov/pmc/PMC3972801/>
 118. Tonkens R. An overview of the drug development process. *Physician Exec*. 2005;31(3):48–52.
 119. Zhang Z, Zhou L, Xie N, Nice EC, Zhang T, Cui Y, et al. Overcoming cancer therapeutic bottleneck by drug repurposing. *Signal Transduct Target Ther* [Internet]. 2020;5(1):113. Available from: <https://doi.org/10.1038/s41392-020-00213-8>
 120. Carnero A. High throughput screening in drug discovery. *Clin Transl Oncol Off Publ Fed Spanish Oncol Soc Natl Cancer Inst Mex*. 2006 Jul;8(7):482–90.
 121. Kaitin KI. Deconstructing the drug development process: the new face of innovation. *Clin Pharmacol Ther*. 2010 Mar;87(3):356–61.
 122. Rawlins MD. Cutting the cost of drug development? *Nat Rev Drug Discov*. 2004 Apr;3(4):360–4.
 123. Kola I. The State of Innovation in Drug Development. *Clin Pharmacol Ther* [Internet]. 2008 Feb 1;83(2):227–30. Available from: <https://doi.org/10.1038/sj.clpt.6100479>

124. Schein CH. Repurposing approved drugs for cancer therapy. *Br Med Bull*. 2021;137(1):13–27.
125. Sun W, Sanderson PE, Zheng W. Drug combination therapy increases successful drug repositioning. *Drug Discov Today*. 2016;21(7):1189–95.
126. Knight ZA, Lin H, Shokat KM. Targeting the cancer kinome through polypharmacology. *Nat Rev Cancer* [Internet]. 2010 Feb;10(2):130–7. Available from: <https://pubmed.ncbi.nlm.nih.gov/20094047>
127. Zsákai L, Sipos A, Dobos J, Erős D, Szántai-Kis C, Bánhegyi P, et al. Targeted drug combination therapy design based on driver genes. *Oncotarget* [Internet]. 2019 Sep 3;10(51):5255–66. Available from: <https://pubmed.ncbi.nlm.nih.gov/31523388>
128. Grummt I. The nucleolus - Guardian of cellular homeostasis and genome integrity. Vol. 122, *Chromosoma*. 2013. p. 487–97.
129. McLennan A, Bates A, Turner P, White M. RNA Pol I genes: the ribosomal repeat. In: *Molecular Biology*. 4th ed. Garland Science, Taylor & Francis Group; 2013. p. 126–9.
130. Copenhagen GP, Putnam CD, Denton ML, Pikaard CS. The RNA polymerase I transcription factor UBF is a sequence-tolerant HMG-box protein that can recognize structured nucleic acids. *Nucleic Acids Res* [Internet]. 1994 Jul 11;22(13):2651–7. Available from: <https://doi.org/10.1093/nar/22.13.2651>
131. Pilsl M, Crucifix C, Papai G, Krupp F, Steinbauer R, Griesenbeck J, et al. Structure of the initiation-competent RNA polymerase I and its implication for transcription. *Nat Commun* [Internet]. 2016 Jul 15;7:12126. Available from: <https://pubmed.ncbi.nlm.nih.gov/27418187>
132. Engel C, Plitzko J, Cramer P. RNA polymerase I-Rrn3 complex at 4.8 Å resolution. *Nat Commun* [Internet]. 2016 Jul 15;7:12129. Available from: <https://pubmed.ncbi.nlm.nih.gov/27418309>
133. Schnapp A, Pfeleiderer C, Rosenbauer H, Grummt I. A growth-dependent transcription initiation factor (TIF-IA) interacting with RNA polymerase I regulates mouse ribosomal RNA synthesis. *EMBO J* [Internet]. 1990 Sep 1 [cited 2020 Mar 31];9(9):2857–63. Available from: <http://doi.wiley.com/10.1002/j.1460-2075.1990.tb07475.x>
134. Nelson, David L., Cox MM. RNA Processing. In: *Principios de Bioquímica*, Lehninger. 5th ed. W.H. Freeman; 2008. p. 1033–49.
135. McLennan A, Bates A, Turner P, White M. rRNA processing and ribosomes. In: *Molecular Biology*. 4th ed. Garland Science, Taylor & Francis Group; 2013. p. 154–9.
136. Woods SJ, Hannan KM, Pearson RB, Hannan RD. The nucleolus as a fundamental regulator of the p53 response and a new target for cancer therapy. Vol. 1849, *Biochimica et Biophysica Acta - Gene Regulatory Mechanisms*. Elsevier; 2015. p. 821–9.
137. Farley K, Surovtseva Y, Merkel J, Baserga S. Determinants of Mammalian Nucleolar Architecture. *Chromosoma*. 2015 Feb 12;124.
138. Nissan TA, Bassler J, Petfalski E, Tollervey D, Hurt E. 60S pre-ribosome formation viewed from assembly in the nucleolus until export to the cytoplasm. *EMBO J*. 2002 Oct;21(20):5539–47.
139. Granneman S, Baserga SJ. Ribosome biogenesis: of knobs and RNA processing. *Exp Cell Res* [Internet]. 2004;296(1):43–50. Available from: <https://www.sciencedirect.com/science/article/pii/S0014482704001284>
140. Khatter H, Myasnikov AG, Natchiar SK, Klaholz BP. Structure of the human 80S ribosome.

- Nature [Internet]. 2015 [cited 2020 Apr 1];520(7549):640–5. Available from: <https://eds-b-ebscohost-com.liverpool.idm.oclc.org/eds/pdfviewer/pdfviewer?vid=2&sid=c45577f8-ee70-42ce-a072-ac0e1cd25fda%40pdc-v-sessmgr02>
141. Rubbi CP, Milner J. Disruption of the nucleolus mediates stabilization of p53 in response to DNA damage and other stresses. *EMBO J* [Internet]. 2003;22(22):6068–77. Available from: <internal-pdf://69.116.21.41/Rubbi, C. 2003 EMBO Journal. Disruption of the.pdf>
 142. Yoneda M, Nakagawa T, Hattori N, Ito T. The nucleolus from a liquid droplet perspective. *J Biochem* [Internet]. 2021 Aug 1;170(2):153–62. Available from: <https://doi.org/10.1093/jb/mvab090>
 143. Lafontaine DLJ, Riback JA, Bascetin R, Brangwynne CP. The nucleolus as a multiphase liquid condensate. *Nat Rev Mol Cell Biol* [Internet]. 2021;22(3):165–82. Available from: <https://doi.org/10.1038/s41580-020-0272-6>
 144. Pollard KM, Hultman P. Chapter 38 - Fibrillarin Autoantibodies. In: Shoenfeld Y, Meroni PL, Gershwin MEBT-A (Third E, editors. San Diego: Elsevier; 2014. p. 319–25. Available from: <https://www.sciencedirect.com/science/article/pii/B9780444563781000381>
 145. Yang K, Yang J, Yi J. Nucleolar Stress: hallmarks, sensing mechanism and diseases. *Cell Stress* [Internet]. 2018;2(6):125–40. Available from: <http://www.cell-stress.com/wp-content/uploads/2018/05/2018A-Yang-Cell-Stress.pdf>
 146. Maggi LBJ, Kuchenruether M, Dadey DYA, Schwoppe RM, Grisendi S, Townsend RR, et al. Nucleophosmin serves as a rate-limiting nuclear export chaperone for the Mammalian ribosome. *Mol Cell Biol*. 2008 Dec;28(23):7050–65.
 147. Feric M, Vaidya N, Harmon TS, Mitrea DM, Zhu L, Richardson TM, et al. Coexisting Liquid Phases Underlie Nucleolar Subcompartments. *Cell* [Internet]. 2016;165(7):1686–97. Available from: <https://www.sciencedirect.com/science/article/pii/S0092867416304925>
 148. Hernandez-Verdun D. Assembly and disassembly of the nucleolus during the cell cycle. *Nucleus*. 2011;2(3):189–94.
 149. Trinkle-Mulcahy L, Lamond AI. Mitotic phosphatases: no longer silent partners. *Curr Opin Cell Biol*. 2006 Dec;18(6):623–31.
 150. Boulon S, Westman BJ, Hutten S, Boisvert F-M, Lamond AI. The Nucleolus under Stress. *Mol Cell* [Internet]. 2010 Oct 22 [cited 2020 Apr 9];40(2):216–27. Available from: <https://www.sciencedirect.com/science/article/pii/S1097276510007525?pes=vor#!>
 151. Shav-Tal Y, Blechman J, Darzacq X, Montagna C, Dye BT, Patton JG, et al. Dynamic sorting of nuclear components into distinct nucleolar caps during transcriptional inhibition. *Mol Biol Cell*. 2005 May;16(5):2395–413.
 152. Montanaro L, Treré D, Derenzini M. Nucleolus, Ribosomes, and Cancer. *Am J Pathol* [Internet]. 2008;173(2):301–10. Available from: <http://www.sciencedirect.com/science/article/pii/S0002944010616070>
 153. Weeks SE, Metge BJ, Samant RS. The nucleolus: a central response hub for the stressors that drive cancer progression. Vol. 76, *Cellular and Molecular Life Sciences*. 2019.
 154. Derenzini M, Montanaro L, Trerè D. Ribosome biogenesis and cancer. *Acta Histochem* [Internet]. 2017;119(3):190–7. Available from: <http://www.sciencedirect.com/science/article/pii/S0065128117300119>

155. Lu KL, Nelson JO, Watase GJ, Warsinger-Pepe N, Yamashita YM. Transgenerational dynamics of rDNA copy number in *Drosophila* male germline stem cells. *Elife*. 2018 Feb;7.
156. Sinclair DA, Mills K, Guarente L. Accelerated Aging and Nucleolar Fragmentation in Yeast *sgs1* Mutants. *Science* (80-) [Internet]. 1997 Aug 29;277(5330):1313–6. Available from: <https://doi.org/10.1126/science.277.5330.1313>
157. Parlato R, Liss B. How Parkinson's disease meets nucleolar stress. *Biochim Biophys Acta - Mol Basis Dis* [Internet]. 2014;1842(6):791–7. Available from: <https://www.sciencedirect.com/science/article/pii/S0925443914000039>
158. Parlato R, Kreiner G. Nucleolar activity in neurodegenerative diseases: a missing piece of the puzzle? *J Mol Med* [Internet]. 2013;91(5):541–7. Available from: <https://doi.org/10.1007/s00109-012-0981-1>
159. Rieker C, Engblom D, Kreiner G, Domanskyi A, Schober A, Stotz S, et al. Nucleolar Disruption in Dopaminergic Neurons Leads to Oxidative Damage and Parkinsonism through Repression of Mammalian Target of Rapamycin Signaling. *J Neurosci* [Internet]. 2011;31(2):453. Available from: <http://www.jneurosci.org/content/31/2/453.abstract>
160. Bywater MJ, Poortinga G, Sanij E, Hein N, Peck A, Cullinane C, et al. Inhibition of RNA Polymerase I as a Therapeutic Strategy to Promote Cancer-Specific Activation of p53. *Cancer Cell*. 2012 Jul 10;22(1):51–65.
161. Andersen JS, Lyon CE, Fox AH, Leung AKL, Lam YW, Steen H, et al. Directed proteomic analysis of the human nucleolus. *Curr Biol*. 2002 Jan 8;12(1):1–11.
162. Scherl A, Couté Y, Déon C, Callé A, Kindbeiter K, Sanchez J-CC, et al. Functional Proteomic Analysis of Human Nucleolus. *Mol Biol Cell* [Internet]. 2002 Nov 1 [cited 2020 Apr 2];13(11):4100–9. Available from: <https://doi.org/10.1091/mbc.e02-05-0271>
163. Hannan RD, Drygin D, Pearson RB. Targeting RNA polymerase I transcription and the nucleolus for cancer therapy. *Expert Opin Ther Targets* [Internet]. 2013;17(8):873–8. Available from: <internal-pdf://118.164.170.183/Hannan R. 2013. Targeting RNA Pol I transcript.pdf>
164. Audas TE, Jacob MD, Lee S. Immobilization of proteins in the nucleolus by ribosomal intergenic spacer noncoding RNA. *Mol Cell*. 2012/01/31. 2012;45(2):147–57.
165. Sen Gupta A, Joshi G, Pawar S, Sengupta K. Nucleolin modulates compartmentalization and dynamics of histone 2B-ECFP in the nucleolus. *Nucleus* [Internet]. 06/26. 2018;9(1):350–67. Available from: <https://www.ncbi.nlm.nih.gov/pubmed/29943658>
<https://www.ncbi.nlm.nih.gov/pmc/PMC6165600/>
166. Quin JE, Devlin JR, Cameron D, Hannan KM, Pearson RB, Hannan RD. Targeting the nucleolus for cancer intervention. Vol. 1842, *Biochimica et Biophysica Acta - Molecular Basis of Disease*. Elsevier; 2014. p. 802–16.
167. Mayer C, Grummt I. Cellular Stress and Nucleolar Function. *Cell Cycle* [Internet]. 2005;4(8):1036–8. Available from: <internal-pdf://0980866782/Christine Mayer. 2005. Cellular Stress and Nucl.pdf>
168. Thoms HC, Stark LA. The NF- κ B Nucleolar Stress Response Pathway. *Biomedicines*. 2021 Aug;9(9).
169. Mayer C, Bierhoff H, Grummt I. The nucleolus as a stress sensor: JNK2 inactivates the

- transcription factor TIF-IA and down-regulates rRNA synthesis. *Genes Dev.* 2005 Apr 15;19(8):933–41.
170. Hoppe S, Bierhoff H, Cado I, Weber A, Tiebe M, Grummt I, et al. AMP-activated protein kinase adapts rRNA synthesis to cellular energy supply. *Proc Natl Acad Sci U S A.* 2009 Oct 20;106(42):17781–6.
 171. Zhang Y, Xiong Y, Yarbrough WG. ARF promotes MDM2 degradation and stabilizes p53: ARF-INK4a locus deletion impairs both the Rb and p53 tumor suppression pathways. *Cell.* 1998 Mar 20;92(6):725–34.
 172. Olson MOJ. Sensing Cellular Stress: Another New Function for the Nucleolus? *Sci STKE* [Internet]. 2004;2004(224):pe10–pe10. Available from: internal-pdf://188.41.37.17/OlsonSTKE.pdf
 173. Kang J, Brajanovski N, Chan KT, Xuan J, Pearson RB, Sanij E. Ribosomal proteins and human diseases: molecular mechanisms and targeted therapy. *Signal Transduct Target Ther* [Internet]. 2021;6(1):323. Available from: <https://doi.org/10.1038/s41392-021-00728-8>
 174. Zhang Y, Lu H. Signaling to p53: Ribosomal Proteins Find Their Way. *Cancer Cell* [Internet]. 2009 Nov 3;16(5):369–77. Available from: <https://doi.org/10.1016/j.ccr.2009.09.024>
 175. Fumagalli S, Di Cara A, Neb-Gulati A, Natt F, Schwemberger S, Hall J, et al. Absence of nucleolar disruption after impairment of 40S ribosome biogenesis reveals an rpL11-translationdependent mechanism of p53 induction. *Nat Cell Biol.* 2009;11(4):501–8.
 176. Takagi M, Absalon MJ, McLure KG, Kastan MB. Regulation of p53 translation and induction after DNA damage by ribosomal protein L26 and nucleolin. *Cell.* 2005 Oct 7;123(1):49–63.
 177. Chen J, Kastan MB. 5′–3′-UTR interactions regulate p53 mRNA translation and provide a target for modulating p53 induction after DNA damage. *Genes Dev.* 2010;24(19):2146–56.
 178. Grandori C, Gomez-Roman N, Felton-Edkins ZA, Ngouenet C, Galloway DA, Eisenman RN, et al. c-Myc binds to human ribosomal DNA and stimulates transcription of rRNA genes by RNA polymerase I. *Nat Cell Biol.* 2005 Mar 20;7(3):311–8.
 179. Arabi A, Wu S, Ridderstråle K, Bierhoff H, Shiue C, Fatyol K, et al. c-Myc associates with ribosomal DNA and activates RNA polymerase I transcription. *Nat Cell Biol.* 2005 Mar;7(3):303–10.
 180. Dai M-S, Arnold H, Sun X-X, Sears R, Lu H. Inhibition of c-Myc activity by ribosomal protein L11. *EMBO J* [Internet]. 2007 Jul 25 [cited 2020 Apr 9];26(14):3332–45. Available from: <http://emboj.embopress.org/cgi/doi/10.1038/sj.emboj.7601776>
 181. Donati G, Montanaro L, Derenzini M. Ribosome biogenesis and control of cell proliferation: p53 is not alone. Vol. 72, *Cancer Research*. American Association for Cancer Research; 2012. p. 1602–7.
 182. Li J, Yu L, Zhang H, Wu J, Yuan J, Li X, et al. Down-regulation of pescadillo inhibits proliferation and tumorigenicity of breast cancer cells. *Cancer Sci* [Internet]. 2009 Dec 1;100(12):2255–60. Available from: <https://doi.org/10.1111/j.1349-7006.2009.01325.x>
 183. Donati G, Brighenti E, Vici M, Mazzini G, Treré D, Montanaro L, et al. Selective inhibition of rRNA transcription downregulates E2F-1: A new p53-independent mechanism linking cell growth to cell proliferation. *J Cell Sci.* 2011 Sep 1;124(17):3017–28.
 184. Zhao J, Yuan X, Frödin M, Grummt I. ERK-Dependent Phosphorylation of the Transcription

- Initiation Factor TIF-IA Is Required for RNA Polymerase I Transcription and Cell Growth. *Mol Cell* [Internet]. 2003 Feb 1 [cited 2020 Jan 14];11(2):405–13. Available from: <https://www.sciencedirect.com/science/article/pii/S1097276503000364>
185. Grummt I. Life on a planet of its own: regulation of RNA polymerase I transcription in the nucleolus. *Genes Dev* [Internet]. 2003 Jul 15 [cited 2020 Apr 1];17(14):1691–702. Available from: <internal-pdf://1.209.119.209/Genes Dev.-2003-Grummt-1691-702.pdf>
 186. Mayer C, Zhao J, Yuan X, Grummt I. mTOR-dependent activation of the transcription factor TIF-IA links rRNA synthesis to nutrient availability. *Genes Dev* [Internet]. 2004;18(4):423–34. Available from: <internal-pdf://184.191.221.9/Mayer, C. 2004. mTOR-dependent activation of t.pdf>
 187. Zhang C, Comai L, Johnson DL. PTEN Represses RNA Polymerase I Transcription by Disrupting the SL1 Complex. *Mol Cell Biol*. 2005 Aug 15;25(16):6899–911.
 188. Voit R, Schnapp A, Kuhn A, Rosenbauer H, Hirschmann P, Stunnenberg HG, et al. The nucleolar transcription factor mUBF is phosphorylated by casein kinase II in the C-terminal hyperacidic tail which is essential for transactivation. *EMBO J* [Internet]. 1992 Jun 1 [cited 2020 May 13];11(6):2211–8. Available from: <http://doi.wiley.com/10.1002/j.1460-2075.1992.tb05280.x>
 189. Voit R, Kuhn A, Sander EE, Grummt I. Activation of mammalian ribosomal gene transcription requires phosphorylation of the nucleolar transcription factor UBF | *Nucleic Acids Research* | Oxford Academic. *Nucleic Acids Res* [Internet]. 1995 Jul 25 [cited 2020 May 13];23(14):2593–9. Available from: <https://academic.oup.com/nar/article-abstract/23/14/2593/1016873>
 190. Heix J, Vente A, Voit R, Budde A, Michaelidis TM, Grummt I. Mitotic silencing of human rRNA synthesis: inactivation of the promoter selectivity factor SL1 by cdc2/cyclin B-mediated phosphorylation. *EMBO J*. 1998 Dec 15;17(24):7373–81.
 191. Voit R, Grummt I. Phosphorylation of UBF at serine 388 is required for interaction with RNA polymerase I and activation of rDNA transcription. *Proc Natl Acad Sci U S A* [Internet]. 11/06. 2001;98(24):13631–6. Available from: <https://www.ncbi.nlm.nih.gov/pubmed/11698641>
<https://www.ncbi.nlm.nih.gov/pmc/articles/PMC61092/>
 192. Klein J, Grummt I. Cell cycle-dependent regulation of RNA polymerase I transcription: The nucleolar transcription factor UBF is inactive in mitosis and early G1. *Proc Natl Acad Sci* [Internet]. 1999;96(11):6096. Available from: <http://www.pnas.org/content/96/11/6096.abstract>
 193. Voit R, Hoffmann M, Grummt I. Phosphorylation by G1-specific cdk–cyclin complexes activates the nucleolar transcription factor UBF | *The EMBO Journal*. *EMBO J* [Internet]. 1999 [cited 2020 May 13];18(7):1891–9. Available from: <https://www.embopress.org/doi/pdf/10.1093/emboj/18.7.1891>
 194. Angelier N, Tramier M, Louvet E, Coppey-Moisan M, Savino TM, De Mey JR, et al. Tracking the interactions of rRNA processing proteins during nucleolar assembly in living cells. *Mol Biol Cell* [Internet]. 2005/04/06. 2005 Jun;16(6):2862–71. Available from: <https://pubmed.ncbi.nlm.nih.gov/15814843>
 195. Derenzini M, Trerè D, Pession A, Montanaro L, Sirri V, Ochs RL. Nucleolar function and size in cancer cells. *Am J Pathol* [Internet]. 1998 May;152(5):1291–7. Available from: <https://pubmed.ncbi.nlm.nih.gov/9588897>

196. Hein N, Hannan KM, George AJ, Sanij E, Hannan RD. The nucleolus: an emerging target for cancer therapy. *Trends Mol Med* [Internet]. 2013;19(11):643–54. Available from: <http://www.sciencedirect.com/science/article/pii/S1471491413001263>
197. Treré D, Ceccarelli C, Montanaro L, Tosti E, Derenzini M. Nucleolar size and activity are related to pRb and p53 status in human breast cancer. *J Histochem Cytochem* [Internet]. 2004 Dec [cited 2020 Apr 2];52(12):1601–7. Available from: <http://www.ncbi.nlm.nih.gov/pubmed/15557214>
198. Tsoi H, Lam KC, Dong Y, Zhang X, Lee CK, Zhang J, et al. Pre-45s rRNA promotes colon cancer and is associated with poor survival of CRC patients. *Oncogene*. 2017 Nov 2;36(44):6109–18.
199. Ibaragi S, Yoshioka N, Kishikawa H, Hu JK, Sadow PM, Li M, et al. Angiogenin-stimulated rRNA transcription is essential for initiation and survival of AKT-induced prostate intraepithelial neoplasia. *Mol Cancer Res*. 2009 Mar 1;7(3):415–24.
200. Jastrzebski K, Hannan KM, Tchoubrieva EB, Hannan RD, Pearson RB. Coordinate regulation of ribosome biogenesis and function by the ribosomal protein S6 kinase, a key mediator of mTOR function. Vol. 25, *Growth Factors*. 2007. p. 209–26.
201. Gaviraghi, Vivori, Tonon. How Cancer Exploits Ribosomal RNA Biogenesis: A Journey beyond the Boundaries of rRNA Transcription. *Cells*. 2019 Sep 17;8(9):1098.
202. Brown IN, Lafita-Navarro MC, Conacci-Sorrell M. Regulation of Nucleolar Activity by MYC. *Cells*. 2022;11(3):574.
203. Poortinga G, Hannan KM, Snelling H, Walkley CR, Jenkins A, Sharkey K, et al. MAD1 and c-MYC regulate UBF and rDNA transcription during granulocyte differentiation. *EMBO J* [Internet]. 2004 Aug 18 [cited 2020 May 19];23(16):3325–35. Available from: <http://emboj.embopress.org/cgi/doi/10.1038/sj.emboj.7600335>
204. Poortinga G, Wall M, Sanij E, Siwicki K, Ellul J, Brown D, et al. c-MYC coordinately regulates ribosomal gene chromatin remodeling and Pol I availability during granulocyte differentiation. *Nucleic Acids Res* [Internet]. 2011 [cited 2020 May 19];39(8):3267–81. Available from: <https://academic.oup.com/nar/article-abstract/39/8/3267/2411233>
205. Guo QM, Malek RL, Kim S, Chiao C, He M, Ruffy M, et al. Identification of c-Myc responsive genes using rat cDNA microarray. *Cancer Res*. 2000 Nov 1;60(21):5922–8.
206. Gomez-Roman N, Grandori C, Eisenman RN, White RJ. Direct activation of RNA polymerase III transcription by c-Myc. *Nature*. 2003 Jan 16;421(6920):290–4.
207. Schlosser I, Ho M, Lzel È, Mu M, Rnseer È, Burtscher H, et al. A role for c-Myc in the regulation of ribosomal RNA processing. *Nucleic Acids Res* [Internet]. 2003 [cited 2020 May 19];31(21):6148–56. Available from: <https://academic.oup.com/nar/article-abstract/31/21/6148/1042319>
208. Gentilella A, Kozma SC, Thomas G. A liaison between mTOR signaling, ribosome biogenesis and cancer. *Biochim Biophys Acta - Gene Regul Mech* [Internet]. 2015;1849(7):812–20. Available from: <https://www.sciencedirect.com/science/article/pii/S187493991500053X>
209. Stefanovsky V, Langlois F, Gagnon-Kugler T, Rothblum LI, Moss T. Growth Factor Signaling Regulates Elongation of RNA Polymerase I Transcription in Mammals via UBF Phosphorylation and r-Chromatin Remodeling. *Mol Cell* [Internet]. 2006;21(5):629–39. Available from: <http://www.sciencedirect.com/science/article/pii/S1097276506000451>

210. Stefanovsky VY, Pelletier G, Hannan R, Gagnon-Kugler T, Rothblum LI, Moss T. An immediate response of ribosomal transcription to growth factor stimulation in mammals is mediated by ERK phosphorylation of UBF. *Mol Cell*. 2001 Nov 21;8(5):1063–73.
211. Gaviraghi M, Vivori C, Tonon G. How Cancer Exploits Ribosomal RNA Biogenesis: A Journey beyond the Boundaries of rRNA Transcription. *Cells*. 2019;8(9).
212. Penzo M, Montanaro L, Treré D, Derenzini M. The Ribosome Biogenesis—Cancer Connection. *Cells* [Internet]. 2019 Jan 15 [cited 2020 Apr 2];8(1):55. Available from: <http://www.ncbi.nlm.nih.gov/pubmed/30650663>
213. Ko A, Han SY, Song J. Regulatory Network of ARF in Cancer Development. *Mol Cells*. 2018 May;41(5):381–9.
214. Lessard F, Morin F, Ivanchuk S, Langlois F, Stefanovsky V, Rutka J, et al. The ARF Tumor Suppressor Controls Ribosome Biogenesis by Regulating the RNA Polymerase I Transcription Factor TTF-I. *Mol Cell* [Internet]. 2010;38(4):539–50. Available from: <https://www.sciencedirect.com/science/article/pii/S1097276510003205>
215. Mitra S, Lee J-S, Cantrell M, Van Den Berg CL. c-Jun N-terminal Kinase 2 (JNK2) Enhances Cell Migration through Epidermal Growth Factor Substrate 8 (EPS8) * . *J Biol Chem* [Internet]. 2011 Apr 29;286(17):15287–97. Available from: <https://doi.org/10.1074/jbc.M109.094441>
216. Pan C-W, Liu H, Zhao Y, Qian C, Wang L, Qi J. JNK2 downregulation promotes tumorigenesis and chemoresistance by decreasing p53 stability in bladder cancer. *Oncotarget*. 2016 Jun;7(23):35119–31.
217. Jin R, Zhou W. TIF-IA: An oncogenic target of pre-ribosomal RNA synthesis. *Biochim Biophys Acta - Rev Cancer* [Internet]. 09/15. 2016;1866(2):189–96. Available from: <https://www.ncbi.nlm.nih.gov/pubmed/27641688>
<https://www.ncbi.nlm.nih.gov/pmc/articles/PMC5138081/>
218. Li W, Saud SM, Young MR, Chen G, Hua B. Targeting AMPK for cancer prevention and treatment. *Oncotarget*. 2015 Apr;6(10):7365–78.
219. B. PT, I. PK, Jackie R, M. ZJCB. Casein Kinase 2 Associates with Initiation-Competent RNA Polymerase I and Has Multiple Roles in Ribosomal DNA Transcription. *Mol Cell Biol* [Internet]. 2006 Aug 15;26(16):5957–68. Available from: <https://doi.org/10.1128/MCB.00673-06>
220. Loyer P, Trembley JH, Katona R, Kidd VJ, Lahti JM. Role of CDK/cyclin complexes in transcription and RNA splicing. Vol. 17, *Cellular Signalling*. 2005. p. 1033–51.
221. Cavanaugh AH, Hempel WM, Taylor LJ, Rogalsky V, Todorov G, Rothblum LI. Activity of RNA polymerase I transcription factor UBF blocked by Rb gene product. *Nature*. 1995;374(6518):177–80.
222. Hannan KM, Hannan RD, Smith SD, Jefferson LS, Lun M, Rothblum LI. Rb and p130 regulate RNA polymerase I transcription: Rb disrupts the interaction between UBF and SL-1. *Oncogene*. 2000 Oct 12;19(43):4988–99.
223. Busch H, Smetana K. *The nucleolus* by Harris Busch and Karel Smetana. New York: Academic Press; 1970.
224. Drygin D, Rice WG, Grummt I. The RNA Polymerase I Transcription Machinery: An Emerging Target for the Treatment of Cancer. *Annu Rev Pharmacol Toxicol* [Internet]. 2010;50(1):131–56. Available from: <internal-pdf://0346344880/annurev.pharmtox.010909.105844.pdf>

225. Chan PK, Chan FY. A study of correlation between NPM-translocation and apoptosis in cells induced by daunomycin. *Biochem Pharmacol.* 1999 Jun 1;57(11):1265–73.
226. Chan PK, Qi Y, Amley J, Koller CA. Quantitation of the nucleophosmin/B23-translocation using imaging analysis. *Cancer Lett.* 1996 Feb 27;100(1–2):191–7.
227. Drygin D, Lin A, Bliesath J, Ho CB, O'Brien SE, Proffitt C, et al. Targeting RNA Polymerase I with an Oral Small Molecule CX-5461 Inhibits Ribosomal RNA Synthesis and Solid Tumor Growth [Internet]. Vol. 71. 2011. p. 1418–30. Available from: <https://liverpool.idm.oclc.org/login?url=https://search.ebscohost.com/login.aspx?direct=true&db=edswsc&AN=000287352600024&site=eds-live&scope=site>
228. Drygin D, Siddiqui-Jain A, O'Brien S, Schwaebe M, Lin A, Bliesath J, et al. Anticancer activity of CX-3543: A direct inhibitor of rRNA biogenesis. *Cancer Res.* 2009 Oct 1;69(19):7653–61.
229. Peltonen K, Colis L, Liu H, Trivedi R, Moubarek MS, Moore HM, et al. A Targeting Modality for Destruction of RNA Polymerase I that Possesses Anticancer Activity. *Cancer Cell* [Internet]. 2014;25(1):77–90. Available from: <internal-pdf://85.199.33.229/Peltonen, K. 2013. A targeting modality for de.pdf>
230. Perry RP, Kelley DE. Inhibition of RNA synthesis by actinomycin D: Characteristic dose-response of different RNA species. *J Cell Physiol.* 1970;76(2):127–39.
231. Burger K, Mühl B, Harasim T, Rohrmoser M, Malamoussi A, Orban M, et al. Chemotherapeutic Drugs Inhibit Ribosome Biogenesis at Various Levels. *J Biol Chem* [Internet]. 2010;285(16):12416–25. Available from: <internal-pdf://255.180.72.76/Burger K. 2010. Chemotherapeutic drugs inhibit.pdf>
232. Pan M, Wright WC, Chapple RH, Zubair A, Sandhu M, Batchelder JE, et al. The chemotherapeutic CX-5461 primarily targets TOP2B and exhibits selective activity in high-risk neuroblastoma. *Nat Commun* [Internet]. 2021;12(1):6468. Available from: <https://doi.org/10.1038/s41467-021-26640-x>
233. Bruno PM, Lu M, Dennis KA, Inam H, Moore CJ, Shee J, et al. The primary mechanism of cytotoxicity of the chemotherapeutic agent CX-5461 is topoisomerase II poisoning. *Proc Natl Acad Sci* [Internet]. 2020 Feb 25;117(8):4053–60. Available from: <https://doi.org/10.1073/pnas.1921649117>
234. Avendaño C, Menéndez JC. Chapter 7 - Other Anticancer Drugs Targeting DNA and DNA-Associated Enzymes. In: Avendaño C, Menéndez JC BT- MC of AD (Second E, editors. Boston: Elsevier; 2015. p. 273–323. Available from: <https://www.sciencedirect.com/science/article/pii/B9780444626493000077>
235. Singh SB, Genilloud O, Peláez F. 2.05 - Terrestrial Microorganisms – Filamentous Bacteria. In: Liu H-W (Ben), Mander LBT-CNPII, editors. Oxford: Elsevier; 2010. p. 109–40. Available from: <https://www.sciencedirect.com/science/article/pii/B9780080453828000368>
236. Sobell HM. Actinomycin and DNA transcription. *Proc Natl Acad Sci* [Internet]. 1985 Aug 1;82(16):5328–31. Available from: <https://doi.org/10.1073/pnas.82.16.5328>
237. Kwok KK, Vincent EC, Gibson JN. 36 - Antineoplastic Drugs. In: Dowd FJ, Johnson BS, Mariotti AJBT-P and T for D (Seventh E, editors. Mosby; 2017. p. 530–62. Available from: <https://www.sciencedirect.com/science/article/pii/B9780323393072000369>
238. Fen LX, Laiman X, Qi Z, Jean-Philippe C, Marco P, Gerhard N, et al. Actinomycin D enhances killing of cancer cells by immunotoxin RG7787 through activation of the extrinsic pathway of

- apoptosis. *Proc Natl Acad Sci* [Internet]. 2016 Sep 20;113(38):10666–71. Available from: <https://doi.org/10.1073/pnas.1611481113>
239. Avendaño C, Menéndez JC. Chapter 7 - DNA Intercalators and Topoisomerase Inhibitors. In: Avendaño C, Menéndez JC, editors. *Medicinal Chemistry of Anticancer Drugs* [Internet]. Amsterdam: Elsevier; 2008. p. 199–228. Available from: <http://www.sciencedirect.com/science/article/pii/B978044452824700007X>
 240. Aronson JK. Dactinomycin. In: Aronson JK, editor. *Meyler's Side Effects of Drugs* [Internet]. 16th ed. Oxford: Elsevier; 2016. p. 816. Available from: <https://www.sciencedirect.com/science/article/pii/B9780444537171005825>
 241. Peters GJ, Backus HHJ, Freemantle S, van Triest B, Codacci-Pisanelli G, van der Wilt CL, et al. Induction of thymidylate synthase as a 5-fluorouracil resistance mechanism. *Biochim Biophys Acta - Mol Basis Dis* [Internet]. 2002;1587(2):194–205. Available from: <https://www.sciencedirect.com/science/article/pii/S0925443902000820>
 242. Pritchard DM, Watson AJM, Potten CS, Jackman AL, Hickman JA. Inhibition by uridine but not thymidine of p53-dependent intestinal apoptosis initiated by 5-fluorouracil: Evidence for the involvement of RNA perturbation. *Proc Natl Acad Sci* [Internet]. 1997 Mar 4;94(5):1795–9. Available from: <https://doi.org/10.1073/pnas.94.5.1795>
 243. Ghoshal K, Jacob ST. An alternative molecular mechanism of action of 5-fluorouracil, a potent anticancer drug. Vol. 53, *Biochemical Pharmacology*. *Biochem Pharmacol*; 1997. p. 1569–75.
 244. Ohndorf U-M, Rould MA, He Q, Pabo CO, Lippard SJ. Basis for recognition of cisplatin-modified DNA by high-mobility-group proteins. *Nature* [Internet]. 1999;399(6737):708–12. Available from: <https://doi.org/10.1038/21460>
 245. Johnson SW, Perez RP, Godwin AK, Yeung AT, Handel LM, Ozols RF, et al. Role of platinum-DNA adduct formation and removal in cisplatin resistance in human ovarian cancer cell lines. *Biochem Pharmacol*. 1994 Feb;47(4):689–97.
 246. Huang JC, Zamble DB, Reardon JT, Lippard SJ, Sancar A. HMG-domain proteins specifically inhibit the repair of the major DNA adduct of the anticancer drug cisplatin by human excision nuclease. *Proc Natl Acad Sci U S A*. 1994 Oct;91(22):10394–8.
 247. Billings PC, Engelsberg BN, Hughes EN. Proteins binding to cisplatin-damaged DNA in human cell lines. *Cancer Invest*. 1994;12(6):597–604.
 248. Jordan P, Carmo-Fonseca M. Cisplatin inhibits synthesis of ribosomal RNA in vivo. *Nucleic Acids Res*. 1998;26(12):2831–6.
 249. Zhai X, Beckmann H, Jantzen HM, Essigmann JM. Cisplatin-DNA adducts inhibit ribosomal RNA synthesis by hijacking the transcription factor human upstream binding factor. *Biochemistry*. 1998 Nov 17;37(46):16307–15.
 250. Treiber DK, Zhai X, Jantzen HM, Essigmann JM. Cisplatin-DNA adducts are molecular decoys for the ribosomal RNA transcription factor hUBF (human upstream binding factor). *Proc Natl Acad Sci U S A*. 1994 Jun;91(12):5672–6.
 251. Brabec V, Kasparkova J. Modifications of DNA by platinum complexes. Relation to resistance of tumors to platinum antitumor drugs. *Drug Resist Updat Rev Comment Antimicrob Anticancer Chemother*. 2005 Jun;8(3):131–46.
 252. Marini V, Christofis P, Novakova O, Kasparkova J, Farrell N, Brabec V. Conformation, protein

- recognition and repair of DNA interstrand and intrastrand cross-links of antitumor trans-[PtCl₂(NH₃)(thiazole)]. *Nucleic Acids Res.* 2005;33(18):5819–28.
253. McKeage MJ, Hsu T, Screnci D, Haddad G, Baguley BC. Nucleolar damage correlates with neurotoxicity induced by different platinum drugs. *Br J Cancer [Internet]*. 2001;85(8):1219–25. Available from: <https://doi.org/10.1054/bjoc.2001.2024>
 254. Pizzolato JF, Saltz LB. The camptothecins. *Lancet (London, England)*. 2003 Jun;361(9376):2235–42.
 255. Weisenberger D, Scheer U, Benavente R. The DNA topoisomerase I inhibitor camptothecin blocks postmitotic reformation of nucleoli in mammalian cells. *Eur J Cell Biol.* 1993 Jun;61(1):189–92.
 256. Suja JA, Gébrane-Younès J, Géraud G, Hernandez-Verdun D. Relative distribution of rDNA and proteins of the RNA polymerase I transcription machinery at chromosomal NORs. *Chromosoma [Internet]*. 1997;105(7):459–69. Available from: <https://doi.org/10.1007/BF02510483>
 257. Christensen MO, Krokowski RM, Barthelmes HU, Hock R, Boege F, Mielke C. Distinct Effects of Topoisomerase I and RNA Polymerase I Inhibitors Suggest a Dual Mechanism of Nucleolar/Nucleoplasmic Partitioning of Topoisomerase I *. *J Biol Chem [Internet]*. 2004 May 21;279(21):21873–82. Available from: <https://doi.org/10.1074/jbc.M400498200>
 258. Chan PK. Characterization and cellular localization of nucleophosmin/B23 in HeLa cells treated with selected cytotoxic agents (studies of B23-translocation mechanism). *Exp Cell Res.* 1992 Nov;203(1):174–81.
 259. Andrade MA, Bork P. HEAT repeats in the Huntington's disease protein. *Nat Genet [Internet]*. 1995;11(2):115–6. Available from: <https://doi.org/10.1038/ng1095-115>
 260. Bosotti R, Isacchi A, Sonnhammer ELL. FAT: a novel domain in PIK-related kinases. *Trends Biochem Sci [Internet]*. 2000;25(5):225–7. Available from: <https://www.sciencedirect.com/science/article/pii/S0968000400015632>
 261. Banaszynski LA, Liu CW, Wandless TJ. Characterization of the FKBP-Rapamycin-FRB Ternary Complex. *J Am Chem Soc [Internet]*. 2005 Apr 1;127(13):4715–21. Available from: <https://doi.org/10.1021/ja043277y>
 262. Schapira M, Tyers M, Torrent M, Arrowsmith CH. WD40 repeat domain proteins: a novel target class? *Nat Rev Drug Discov [Internet]*. 2017;16(11):773–86. Available from: <https://doi.org/10.1038/nrd.2017.179>
 263. Lee H-J, Zheng JJ. PDZ domains and their binding partners: structure, specificity, and modification. *Cell Commun Signal.* 2010 May;8:8.
 264. Smith GCM, Jackson SP. The PIKK family of protein kinases. In: *Handbook of Cell Signaling*, 2/e. Elsevier Inc.; 2010. p. 575–80.
 265. Yang Q, Guan KL. Expanding mTOR signaling. Vol. 17, *Cell Research*. Nature Publishing Group; 2007. p. 666–81.
 266. Schmelzle T, Hall MN. TOR, a central controller of cell growth. Vol. 103, *Cell*. Cell Press; 2000. p. 253–62.
 267. Yip CK, Murata K, Walz T, Sabatini DM, Kang SA. Structure of the Human mTOR Complex I and Its Implications for Rapamycin Inhibition. *Mol Cell.* 2010 Jun 11;38(5):768–74.

268. Aylett CHS, Sauer E, Imseng S, Boehringer D, Hall MN, Ban N, et al. Architecture of human mTOR complex 1. *Science* (80-) [Internet]. 2016;351(6268):48–52. Available from: [internal-pdf://209.232.42.251/Architecture of human mTOR 1. Science 01 Jan.pdf](https://doi.org/10.1126/science.1251111)
269. Yasemin S, R. PT, D. SY, A. LR, C. TC, Liron B-P, et al. The Rag GTPases Bind Raptor and Mediate Amino Acid Signaling to mTORC1. *Science* (80-) [Internet]. 2008 Jun 13;320(5882):1496–501. Available from: <https://doi.org/10.1126/science.1157535>
270. Sancak Y, Thoreen CC, Peterson TR, Lindquist RA, Kang SA, Spooner E, et al. PRAS40 Is an Insulin-Regulated Inhibitor of the mTORC1 Protein Kinase. *Mol Cell*. 2007 Mar 23;25(6):903–15.
271. Fonseca BD, Smith EM, Lee VHY, MacKintosh C, Proud CG. PRAS40 is a target for mammalian target of rapamycin complex 1 and is required for signaling downstream of this complex. *J Biol Chem*. 2007 Aug 24;282(34):24514–24.
272. Wiza C, Nascimento EBM, Ouwens DM. Role of PRAS40 in Akt and mTOR signaling in health and disease. Vol. 302, *American Journal of Physiology - Endocrinology and Metabolism*. Am J Physiol Endocrinol Metab; 2012.
273. Peterson TR, Laplante M, Thoreen CC, Sancak Y, Kang SA, Kuehl WM, et al. DEPTOR Is an mTOR Inhibitor Frequently Overexpressed in Multiple Myeloma Cells and Required for Their Survival. *Cell*. 2009 May 29;137(5):873–86.
274. Gao D, Inuzuka H, Tan MKM, Fukushima H, Locasale JW, Liu P, et al. mTOR drives its own activation via SCF β TrCP-dependent degradation of the mTOR inhibitor DEPTOR. *Mol Cell*. 2011 Oct 21;44(2):290–303.
275. Sengupta S, Peterson TR, Sabatini DM. Regulation of the mTOR Complex 1 Pathway by Nutrients, Growth Factors, and Stress. Vol. 40, *Molecular Cell*. 2010. p. 310–22.
276. Kist R, Timmers LFSM, Caceres RA. Understanding the role of mTOR-mLst8 binding through coarse-grained simulation approaches. *Mol Simul* [Internet]. 2021 Sep 22;47(14):1198–207. Available from: <https://doi.org/10.1080/08927022.2021.1962525>
277. Dibble CC, Elis W, Menon S, Qin W, Klekota J, Asara JM, et al. TBC1D7 Is a Third Subunit of the TSC1-TSC2 Complex Upstream of mTORC1. *Mol Cell* [Internet]. 2012;47(4):535–46. Available from: <https://www.sciencedirect.com/science/article/pii/S1097276512005047>
278. Huang J, Manning BD. The TSC1–TSC2 complex: a molecular switchboard controlling cell growth. *Biochem J* [Internet]. 2008 May 14;412(2):179–90. Available from: <https://doi.org/10.1042/BJ20080281>
279. Potter CJ, Pedraza LG, Xu T. Akt regulates growth by directly phosphorylating Tsc2. *Nat Cell Biol*. 2002 Sep;4(9):658–65.
280. Dan HC, Sun M, Yang L, Feldman RI, Sui X-M, Ou CC, et al. Phosphatidylinositol 3-kinase/Akt pathway regulates tuberous sclerosis tumor suppressor complex by phosphorylation of tuberlin. *J Biol Chem*. 2002 Sep;277(38):35364–70.
281. Lv D, Guo L, Zhang T, Huang L. PRAS40 signaling in tumor. *Oncotarget* [Internet]. 2017 Apr 20;8(40):69076–85. Available from: <https://pubmed.ncbi.nlm.nih.gov/28978182>
282. P. RP, A. BB, Rana A, P. GS, John B. Tumor-promoting phorbol esters and activated Ras inactivate the tuberous sclerosis tumor suppressor complex via p90 ribosomal S6 kinase. *Proc Natl Acad Sci* [Internet]. 2004 Sep 14;101(37):13489–94. Available from:

<https://doi.org/10.1073/pnas.0405659101>

283. Ma L, Chen Z, Erdjument-Bromage H, Tempst P, Pandolfi PP. Phosphorylation and functional inactivation of TSC2 by Erk: Implications for tuberous sclerosis and cancer pathogenesis. *Cell*. 2005 Apr 22;121(2):179–93.
284. Carriere A, Romeo Y, Acosta-Jaquez HA, Moreau J, Bonneil E, Thibault P, et al. ERK1/2 phosphorylate Raptor to promote Ras-dependent activation of mTOR complex 1 (mTORC1). *J Biol Chem*. 2011 Jan;286(1):567–77.
285. Carrière A, Cargnello M, Julien L-A, Gao H, Bonneil E, Thibault P, et al. Oncogenic MAPK signaling stimulates mTORC1 activity by promoting RSK-mediated raptor phosphorylation. *Curr Biol*. 2008 Sep;18(17):1269–77.
286. Inoki K, Zhu T, Guan K-L. TSC2 mediates cellular energy response to control cell growth and survival. *Cell*. 2003 Nov;115(5):577–90.
287. Buller CL, Loberg RD, Fan M-H, Zhu Q, Park JL, Vesely E, et al. A GSK-3/TSC2/mTOR pathway regulates glucose uptake and GLUT1 glucose transporter expression. *Am J Physiol Cell Physiol*. 2008 Sep;295(3):C836-43.
288. Inoki K, Ouyang H, Zhu T, Lindvall C, Wang Y, Zhang X, et al. TSC2 integrates Wnt and energy signals via a coordinated phosphorylation by AMPK and GSK3 to regulate cell growth. *Cell*. 2006 Sep;126(5):955–68.
289. DeYoung MP, Horak P, Sofer A, Sgroi D, Ellisen LW. Hypoxia regulates TSC1/2-mTOR signaling and tumor suppression through REDD1-mediated 14-3-3 shuttling. *Genes Dev*. 2008 Jan;22(2):239–51.
290. Lee D-F, Kuo H-P, Chen C-T, Hsu J-M, Chou C-K, Wei Y, et al. IKK beta suppression of TSC1 links inflammation and tumor angiogenesis via the mTOR pathway. *Cell*. 2007 Aug;130(3):440–55.
291. Feng Z, Hu W, de Stanchina E, Teresky AK, Jin S, Lowe S, et al. The Regulation of AMPK β 1, TSC2, and PTEN Expression by p53: Stress, Cell and Tissue Specificity, and the Role of These Gene Products in Modulating the IGF-1-AKT-mTOR Pathways. *Cancer Res [Internet]*. 2007 Apr 4;67(7):3043–53. Available from: <https://doi.org/10.1158/0008-5472.CAN-06-4149>
292. Feng Z, Zhang H, Levine AJ, Jin S. The coordinate regulation of the p53 and mTOR pathways in cells. *Proc Natl Acad Sci U S A*. 2005 Jun 7;102(23):8204–9.
293. Plescher M, Teleman AA, Demetriades C. TSC2 mediates hyperosmotic stress-induced inactivation of mTORC1. *Sci Rep*. 2015 Sep;5:13828.
294. Demetriades C, Plescher M, Teleman AA. Lysosomal recruitment of TSC2 is a universal response to cellular stress. *Nat Commun*. 2016 Feb;7:10662.
295. Kim E, Goraksha-Hicks P, Li L, Neufeld TP, Guan KL. Regulation of TORC1 by Rag GTPases in nutrient response. *Nat Cell Biol*. 2008;10(8):935–45.
296. Sancak Y, Peterson TR, Shaul YD, Lindquist RA, Thoreen CC, Bar-Peled L, et al. The rag GTPases bind raptor and mediate amino acid signaling to mTORC1. *Science (80-)*. 2008 Jun 13;320(5882):1496–501.
297. Sancak Y, Bar-Peled L, Zoncu R, Markhard AL, Nada S, Sabatini DM. Ragulator-rag complex targets mTORC1 to the lysosomal surface and is necessary for its activation by amino acids. *Cell*. 2010 Apr 16;141(2):290–303.

298. Kuang S, M. SD. Ragulator and SLC38A9 activate the Rag GTPases through noncanonical GEF mechanisms. *Proc Natl Acad Sci [Internet]*. 2018 Sep 18;115(38):9545–50. Available from: <https://doi.org/10.1073/pnas.1811727115>
299. Shuyu W, Zhi-Yang T, L. WR, Kuang S, A. WG, E. PM, et al. Lysosomal amino acid transporter SLC38A9 signals arginine sufficiency to mTORC1. *Science (80-) [Internet]*. 2015 Jan 9;347(6218):188–94. Available from: <https://doi.org/10.1126/science.1257132>
300. Rebsamen M, Pochini L, Stasyk T, de Araújo MEG, Galluccio M, Kandasamy RK, et al. SLC38A9 is a component of the lysosomal amino acid sensing machinery that controls mTORC1. *Nature*. 2015 Mar;519(7544):477–81.
301. Saxton RA, Sabatini DM. mTOR Signaling in Growth, Metabolism, and Disease. *Cell [Internet]*. 2017;168(6):960–76. Available from: <internal-pdf://205.86.46.196/mTOR-Signaling-in-Growth-Metabolism-and-Diseas.pdf>
302. Bar-Peled L, Chantranupong L, Cherniack AD, Chen WW, Ottina KA, Grabiner BC, et al. A Tumor suppressor complex with GAP activity for the Rag GTPases that signal amino acid sufficiency to mTORC1. *Science [Internet]*. 2013 May 31;340(6136):1100–6. Available from: <https://pubmed.ncbi.nlm.nih.gov/23723238>
303. Kim JS, Ro S-H, Kim M, Park H-W, Semple IA, Park H, et al. Sestrin2 inhibits mTORC1 through modulation of GATOR complexes. *Sci Rep [Internet]*. 2015;5(1):9502. Available from: <https://doi.org/10.1038/srep09502>
304. Parmigiani A, Nourbakhsh A, Ding B, Wang W, Kim YC, Akopiants K, et al. Sestrins Inhibit mTORC1 Kinase Activation through the GATOR Complex. *Cell Rep [Internet]*. 2014 Nov 20;9(4):1281–91. Available from: <https://doi.org/10.1016/j.celrep.2014.10.019>
305. Gai Z, Wang Q, Yang C, Wang L, Deng W, Wu G. Structural mechanism for the arginine sensing and regulation of CASTOR1 in the mTORC1 signaling pathway. *Cell Discov [Internet]*. 2016;2(1):16051. Available from: <https://doi.org/10.1038/celldisc.2016.51>
306. Chantranupong L, Scaria SM, Saxton RA, Gygi MP, Shen K, Wyant GA, et al. The CASTOR Proteins Are Arginine Sensors for the mTORC1 Pathway. *Cell [Internet]*. 2016;165(1):153–64. Available from: <https://www.sciencedirect.com/science/article/pii/S0092867416301374>
307. Laplante M, Sabatini DM. An emerging role of mTOR in lipid biosynthesis. *Curr Biol*. 2009;19(22):R1046–52.
308. Nojima H, Tokunaga C, Eguchi S, Oshiro N, Hidayat S, Yoshino K, et al. The mammalian target of rapamycin (mTOR) partner, raptor, binds the mTOR substrates p70 S6 kinase and 4E-BP1 through their TOR signaling (TOS) motif. *J Biol Chem*. 2003;278(18):15461–4.
309. Arif A, Jia J, Willard B, Li X, Fox PL. Multisite Phosphorylation of S6K1 Directs a Kinase Phospho-code that Determines Substrate Selection. *Mol Cell [Internet]*. 2019/01/08. 2019;73(3):446-457.e6. Available from: <internal-pdf://165.25.56.32/1-s2.0-S1097276518309870-main.pdf>
310. Ma XM, Blenis J. Molecular mechanisms of mTOR-mediated translational control. *Nat Rev Mol Cell Biol*. 2009 May;10(5):307–18.
311. Dufner A, Thomas G. Ribosomal S6 Kinase Signaling and the Control of Translation. *Exp Cell Res [Internet]*. 1999;253(1):100–9. Available from: <https://www.sciencedirect.com/science/article/pii/S0014482799946839>

312. Shah OJ, Anthony JC, Kimball SR, Jefferson LS. 4E-BP1 and S6K1: translational integration sites for nutritional and hormonal information in muscle. *Am J Physiol Metab* [Internet]. 2000 Oct 1;279(4):E715–29. Available from: <https://doi.org/10.1152/ajpendo.2000.279.4.E715>
313. Cockman E, Anderson P, Ivanov P. TOP mRNPs: Molecular Mechanisms and Principles of Regulation. *Biomolecules*. 2020 Jun;10(7).
314. Dorrello NV, Peschiaroli A, Guardavaccaro D, Colburn NH, Sherman NE, Pagano M. S6K1- and betaTRCP-mediated degradation of PDCD4 promotes protein translation and cell growth. *Science*. 2006 Oct;314(5798):467–71.
315. Richardson CJ, Bröenstrup M, Fingar DC, Jülich K, Ballif BA, Gygi S, et al. SKAR Is a Specific Target of S6 Kinase 1 in Cell Growth Control. *Curr Biol* [Internet]. 2004;14(17):1540–9. Available from: <https://www.sciencedirect.com/science/article/pii/S0960982204006530>
316. Ma XM, Yoon S-O, Richardson CJ, Jülich K, Blenis J. SKAR Links Pre-mRNA Splicing to mTOR/S6K1-Mediated Enhanced Translation Efficiency of Spliced mRNAs. *Cell* [Internet]. 2008;133(2):303–13. Available from: <https://www.sciencedirect.com/science/article/pii/S0092867408002821>
317. Zhang J, Gao Z, Yin J, Quon MJ, Ye J. S6K Directly Phosphorylates IRS-1 on Ser-270 to Promote Insulin Resistance in Response to TNF- α ; Signaling through IKK2 *. *J Biol Chem* [Internet]. 2008 Dec 19;283(51):35375–82. Available from: <https://doi.org/10.1074/jbc.M806480200>
318. Gingras AC, Raught B, Sonenberg N. Regulation of translation initiation by FRAP/mTOR. *Genes Dev*. 2001 Apr;15(7):807–26.
319. Böhm R, Imseng S, Jakob RP, Hall MN, Maier T, Hiller S. The dynamic mechanism of 4E-BP1 recognition and phosphorylation by mTORC1. *Mol Cell*. 2021;81(11):2403–16.
320. Mayer C, Grummt I. Ribosome biogenesis and cell growth: mTOR coordinates transcription by all three classes of nuclear RNA polymerases. *Oncogene* [Internet]. 2006;25(48):6384–91. Available from: [internal-pdf://0185222509/Oncogene \(2006\) 25, 6384–6391.pdf](internal-pdf://0185222509/Oncogene (2006) 25, 6384–6391.pdf)
321. Tsang CK, Liu H, Zheng XFS. mTOR binds to the promoters of RNA polymerase I- and III-transcribed genes. *Cell Cycle* [Internet]. 2010/03/07. 2010 Mar 1;9(5):953–7. Available from: <https://pubmed.ncbi.nlm.nih.gov/20038818>
322. Lin CH, Platt MD, Ficarro SB, Hoofnagle MH, Shabanowitz J, Comai L, et al. Mass spectrometric identification of phosphorylation sites of rRNA transcription factor upstream binding factor. *Am J Physiol Physiol* [Internet]. 2007 May 1;292(5):C1617–24. Available from: <https://doi.org/10.1152/ajpcell.00176.2006>
323. Harris TE, Finck BN. Dual function lipin proteins and glycerolipid metabolism. *Trends Endocrinol Metab* [Internet]. 2011/04/04. 2011 Jun;22(6):226–33. Available from: <https://pubmed.ncbi.nlm.nih.gov/21470873>
324. Lamming DW, Sabatini DM. A Central role for mTOR in lipid homeostasis. *Cell Metab*. 2013 Oct;18(4):465–9.
325. Le Bacquer O, Petroulakis E, Paglialunga S, Poulin F, Richard D, Cianflone K, et al. Elevated sensitivity to diet-induced obesity and insulin resistance in mice lacking 4E-BP1 and 4E-BP2. *J Clin Invest* [Internet]. 2007 Feb 1;117(2):387–96. Available from: <https://doi.org/10.1172/JCI29528>

326. Malley CO, Pidgeon GP. The mTOR pathway in obesity driven gastrointestinal cancers: Potential targets and clinical trials. *BBA Clin.* 2016 Jun;5:29–40.
327. Dunlop EA, Tee AR. mTOR and autophagy: A dynamic relationship governed by nutrients and energy. *Semin Cell Dev Biol* [Internet]. 2014;36:121–9. Available from: <https://www.sciencedirect.com/science/article/pii/S1084952114002420>
328. Liu GY, Sabatini DM. mTOR at the nexus of nutrition, growth, ageing and disease. *Nat Rev Mol Cell Biol.* 2020 Apr;21(4):183–203.
329. Kim J, Kundu M, Viollet B, Guan KL. AMPK and mTOR regulate autophagy through direct phosphorylation of Ulk1. *Nat Cell Biol.* 2011/01/25. 2011;13(2):132–41.
330. Dunlop EA, Hunt DK, Acosta-Jaquez HA, Fingar DC, Tee AR. ULK1 inhibits mTORC1 signaling, promotes multisite Raptor phosphorylation and hinders substrate binding. *Autophagy.* 2011;7(7):737–47.
331. Yuan H-X, Russell RC, Guan K-L. Regulation of PIK3C3/VPS34 complexes by MTOR in nutrient stress-induced autophagy. *Autophagy* [Internet]. 2013 Dec 5;9(12):1983–95. Available from: <https://doi.org/10.4161/auto.26058>
332. Chen C, Liu Y, Liu R, Ikenoue T, Guan K-L, Liu Y, et al. TSC-mTOR maintains quiescence and function of hematopoietic stem cells by repressing mitochondrial biogenesis and reactive oxygen species. *J Exp Med* [Internet]. 2008/09/22. 2008 Sep 29;205(10):2397–408. Available from: <https://pubmed.ncbi.nlm.nih.gov/18809716>
333. Cunningham JT, Rodgers JT, Arlow DH, Vazquez F, Mootha VK, Puigserver P. mTOR controls mitochondrial oxidative function through a YY1–PGC-1 α transcriptional complex. *Nature* [Internet]. 2007;450(7170):736–40. Available from: <https://doi.org/10.1038/nature06322>
334. Hwang Y, Kim LC, Song W, Edwards DN, Cook RS, Chen J. Disruption of the Scaffolding Function of mLST8 Selectively Inhibits mTORC2 Assembly and Function and Suppresses mTORC2-Dependent Tumor Growth In Vivo. *Cancer Res.* 2019 Jul;79(13):3178–84.
335. Kocalis HE, Hagan SL, George L, Turney MK, Siuta MA, Laryea GN, et al. Rictor/mTORC2 facilitates central regulation of energy and glucose homeostasis. *Mol Metab* [Internet]. 2014;3(4):394–407. Available from: <https://www.sciencedirect.com/science/article/pii/S2212877814000192>
336. Jacinto E, Facchinetti V, Liu D, Soto N, Wei S, Jung SY, et al. SIN1/MIP1 maintains rictor-mTOR complex integrity and regulates Akt phosphorylation and substrate specificity. *Cell.* 2006 Oct;127(1):125–37.
337. Yang Q, Inoki K, Ikenoue T, Guan K-L. Identification of Sin1 as an essential TORC2 component required for complex formation and kinase activity. *Genes Dev.* 2006;20(20):2820–32.
338. Pearce LR, Huang X, Boudeau J, Pawłowski R, Wullschleger S, Deak M, et al. Identification of Protor as a novel Rictor-binding component of mTOR complex-2. *Biochem J.* 2007 Aug;405(3):513–22.
339. Pearce LR, Sommer EM, Sakamoto K, Wullschleger S, Alessi DR. Protor-1 is required for efficient mTORC2-mediated activation of SGK1 in the kidney. *Biochem J.* 2011 May;436(1):169–79.
340. Scaiola A, Mangia F, Imseng S, Boehringer D, Berneiser K, Shimobayashi M, et al. The 3.2-Å resolution structure of human mTORC2. *Sci Adv.* 2020 Nov;6(45).

341. Schroder WA, Buck M, Cloonan N, Hancock JF, Suhrbier A, Sculley T, et al. Human Sin1 contains Ras-binding and pleckstrin homology domains and suppresses Ras signalling. *Cell Signal* [Internet]. 2007;19(6):1279–89. Available from: <https://www.sciencedirect.com/science/article/pii/S0898656807000241>
342. Kataoka S, Furuita K, Hattori Y, Kobayashi N, Ikegami T, Shiozaki K, et al. ¹H, ¹⁵N and ¹³C resonance assignments of the conserved region in the middle domain of *S. pombe* Sin1 protein. *Biomol NMR Assign* [Internet]. 2015;9(1):89–92. Available from: <https://doi.org/10.1007/s12104-014-9550-6>
343. Wälchli M, Berneiser K, Mangia F, Imseng S, Craigie L-M, Stutfeld E, et al. Regulation of human mTOR complexes by DEPTOR. Frost A, Dötsch V, Frost A, Zoncu R, editors. *Elife* [Internet]. 2021;10:e70871. Available from: <https://doi.org/10.7554/eLife.70871>
344. Liu P, Gan W, Chin YR, Ogura K, Guo J, Zhang J, et al. PtdIns(3,4,5)P₃-Dependent Activation of the mTORC2 Kinase Complex. *Cancer Discov* [Internet]. 2015 Nov 1;5(11):1194–209. Available from: <https://doi.org/10.1158/2159-8290.CD-15-0460>
345. Yuan H-X, Guan K-L. The SIN1-PH domain connects mTORC2 to PI3K. *Cancer Discov*. 2015;5(11):1127–9.
346. Liu P, Guo J, Gan W, Wei W. Dual phosphorylation of Sin1 at T86 and T398 negatively regulates mTORC2 complex integrity and activity. *Protein Cell*. 2014 Mar;5(3):171–7.
347. Liu P, Wang Z, Wei W. Phosphorylation of Akt at the C-terminal tail triggers Akt activation. *Cell Cycle*. 2014;13(14):2162–4.
348. Calnan DR, Brunet A. The FoxO code. *Oncogene* [Internet]. 2008;27(16):2276–88. Available from: <https://doi.org/10.1038/onc.2008.21>
349. Lin J, Song T, Li C, Mao W. GSK-3 β in DNA repair, apoptosis, and resistance of chemotherapy, radiotherapy of cancer. *Biochim Biophys Acta - Mol Cell Res* [Internet]. 2020;1867(5):118659. Available from: <https://www.sciencedirect.com/science/article/pii/S0167488920300173>
350. Duda P, Akula SM, Abrams SL, Steelman LS, Martelli AM, Cocco L, et al. Targeting GSK3 and Associated Signaling Pathways Involved in Cancer. Vol. 9, *Cells*. 2020.
351. Domoto T, Uehara M, Bolidong D, Minamoto T. Glycogen Synthase Kinase 3 β in Cancer Biology and Treatment. Vol. 9, *Cells*. 2020.
352. Wang H, Shao X, He Q, Wang C, Xia L, Yue D, et al. Quantitative Proteomics Implicates Rictor/mTORC2 in Cell Adhesion. *J Proteome Res*. 2018 Oct;17(10):3360–9.
353. García-Martínez JM, Alessi DR. mTOR complex 2 (mTORC2) controls hydrophobic motif phosphorylation and activation of serum- and glucocorticoid-induced protein kinase 1 (SGK1). *Biochem J*. 2008 Dec;416(3):375–85.
354. Liu Y, Ao X, Ding W, Ponnusamy M, Wu W, Hao X, et al. Critical role of FOXO3a in carcinogenesis. *Mol Cancer* [Internet]. 2018;17(1):104. Available from: <https://doi.org/10.1186/s12943-018-0856-3>
355. Nasir O, Wang K, Föller M, Gu S, Bhandaru M, Ackermann TF, et al. Relative resistance of SGK1 knockout mice against chemical carcinogenesis. *IUBMB Life*. 2009 Jul;61(7):768–76.
356. Stefanetti RJ, Voisin S, Russell A, Lamon S. Recent advances in understanding the role of FOXO3. *F1000Research* [Internet]. 2018 Aug 31;7:F1000 Faculty Rev-1372. Available from: <https://pubmed.ncbi.nlm.nih.gov/30228872>

357. Feng Z, Liu L, Zhang C, Zheng T, Wang J, Lin M, et al. Chronic restraint stress attenuates p53 function and promotes tumorigenesis. *Proc Natl Acad Sci U S A*. 2012 May;109(18):7013–8.
358. Sang Y, Kong P, Zhang S, Zhang L, Cao Y, Duan X, et al. SGK1 in Human Cancer: Emerging Roles and Mechanisms [Internet]. Vol. 10, *Frontiers in Oncology*. 2021. Available from: <https://www.frontiersin.org/article/10.3389/fonc.2020.608722>
359. Newton AC. Protein kinase C: perfectly balanced. *Crit Rev Biochem Mol Biol* [Internet]. 2018 Mar 4;53(2):208–30. Available from: <https://doi.org/10.1080/10409238.2018.1442408>
360. Sarbassov DD, Ali SM, Kim D-H, Guertin DA, Latek RR, Erdjument-Bromage H, et al. Rictor, a novel binding partner of mTOR, defines a rapamycin-insensitive and raptor-independent pathway that regulates the cytoskeleton. *Curr Biol*. 2004 Jul;14(14):1296–302.
361. Dazert E, Hall MN. mTOR signaling in disease. *Curr Opin Cell Biol* [Internet]. 2011;23(6):744–55. Available from: <https://www.sciencedirect.com/science/article/pii/S0955067411001116>
362. Chatterjee P, Seal S, Mukherjee S, Kundu R, Bhuyan M, Barua NC, et al. A carbazole alkaloid deactivates mTOR through the suppression of rictor and that induces apoptosis in lung cancer cells. *Mol Cell Biochem*. 2015 Jul;405(1–2):149–58.
363. Cheng XF, Liu Q, Zhang XF, Zhao HD, Wang W, Chu AJ. Expression of mTOR and its inhibitory effect on cell proliferation and apoptosis of breast cancer cells. Vol. 29, *Journal of biological regulators and homeostatic agents*. Italy; 2015. p. 869–73.
364. Chen X, Cheng H, Pan T, Liu Y, Su Y, Ren C, et al. mTOR regulate EMT through RhoA and Rac1 pathway in prostate cancer. *Mol Carcinog*. 2015 Oct;54(10):1086–95.
365. Liko D, Hall MN. mTOR in health and in sickness. *J Mol Med (Berl)*. 2015 Oct;93(10):1061–73.
366. Fujii T, Yajima R, Tatsuki H, Oosone K, Kuwano H. Anticancer effect of rapamycin on MCF-7 via downregulation of VEGF expression. *In Vitro Cell Dev Biol Anim*. 2016 Jan;52(1):45–8.
367. Mamane Y, Petroulakis E, LeBacquer O, Sonenberg N. mTOR, translation initiation and cancer. *Oncogene* [Internet]. 2006;25(48):6416–22. Available from: <https://doi.org/10.1038/sj.onc.1209888>
368. Laplante M, Sabatini DM. mTOR Signaling in Growth Control and Disease. *Cell* [Internet]. 2012;149(2):274–93. Available from: <http://www.sciencedirect.com/science/article/pii/S0092867412003510>
369. Hsieh AC, Ruggero D. Targeting Eukaryotic Translation Initiation Factor 4E (eIF4E) in Cancer. *Clin Cancer Res* [Internet]. 2010 Oct 13;16(20):4914–20. Available from: <https://doi.org/10.1158/1078-0432.CCR-10-0433>
370. Sharma A, Boise LH, Shanmugam M. Cancer Metabolism and the Evasion of Apoptotic Cell Death. *Cancers (Basel)*. 2019 Aug;11(8).
371. Düvel K, Yecies JL, Menon S, Raman P, Lipovsky AI, Souza AL, et al. Activation of a metabolic gene regulatory network downstream of mTOR complex 1. *Mol Cell*. 2010 Jul;39(2):171–83.
372. Sato T, Nakashima A, Guo L, Coffman K, Tamanoi F. Single amino-acid changes that confer constitutive activation of mTOR are discovered in human cancer. *Oncogene* [Internet]. 2010;29(18):2746–52. Available from: <https://doi.org/10.1038/onc.2010.28>
373. Grabiner BC, Nardi V, Birsoy K, Possemato R, Shen K, Sinha S, et al. A Diverse Array of Cancer-Associated MTOR Mutations Are Hyperactivating and Can Predict Rapamycin Sensitivity.

- Cancer Discov [Internet]. 2014 May 1;4(5):554–63. Available from: <https://doi.org/10.1158/2159-8290.CD-13-0929>
374. Chen X, Xiong X, Cui D, Yang F, Wei D, Li H, et al. DEPTOR is an in vivo tumor suppressor that inhibits prostate tumorigenesis via the inactivation of mTORC1/2 signals. *Oncogene* [Internet]. 2020;39(7):1557–71. Available from: <https://doi.org/10.1038/s41388-019-1085-y>
 375. Wang Z, Zhong J, Inuzuka H, Gao D, Shaik S, Sarkar FH, et al. An evolving role for DEPTOR in tumor development and progression. *Neoplasia*. 2012;14(5):368–75.
 376. Gong L, Shu J, Chen X, Pan H, Chen G, Bi Y, et al. DEPTOR inhibits lung tumorigenesis by inactivating the EGFR-mTOR signals. *Cancer Lett* [Internet]. 2021;519:263–76. Available from: <https://www.sciencedirect.com/science/article/pii/S0304383521003566>
 377. Tian T, Li X, Zhang J. mTOR signaling in cancer and mtor inhibitors in solid tumor targeting therapy. Vol. 20, *International Journal of Molecular Sciences*. 2019.
 378. Masri J, Bernath A, Martin J, Jo OD, Vartanian R, Funk A, et al. mTORC2 Activity Is Elevated in Gliomas and Promotes Growth and Cell Motility via Overexpression of Rictor. *Cancer Res* [Internet]. 2007 Dec 18;67(24):11712–20. Available from: <https://doi.org/10.1158/0008-5472.CAN-07-2223>
 379. Morrison Joly M, Hicks DJ, Jones B, Sanchez V, Estrada MV, Young C, et al. Rictor/mTORC2 Drives Progression and Therapeutic Resistance of HER2-Amplified Breast Cancers. *Cancer Res* [Internet]. 2016 Aug 14;76(16):4752–64. Available from: <https://doi.org/10.1158/0008-5472.CAN-15-3393>
 380. Wang L, Qi J, Yu J, Chen H, Zou Z, Lin X, et al. Overexpression of Rictor protein in colorectal cancer is correlated with tumor progression and prognosis. *Oncol Lett* [Internet]. 2017;14(5):6198–202. Available from: <https://doi.org/10.3892/ol.2017.6936>
 381. Jiang N, Dai Q, Su X, Fu J, Feng X, Peng J. Role of PI3K/AKT pathway in cancer: the framework of malignant behavior. *Mol Biol Rep* [Internet]. 2020;47(6):4587–629. Available from: <https://doi.org/10.1007/s11033-020-05435-1>
 382. Fan C, Zhao C, Wang F, Li S, Wang J. Significance of PTEN Mutation in Cellular Process, Prognosis, and Drug Selection in Clear Cell Renal Cell Carcinoma. *Front Oncol* [Internet]. 2019 May 8;9:357. Available from: <https://pubmed.ncbi.nlm.nih.gov/31139560>
 383. Roldan-Romero JM, Beuselinck B, Santos M, Rodriguez-Moreno JF, Lanillos J, Calsina B, et al. PTEN expression and mutations in TSC1, TSC2 and MTOR are associated with response to rapalogs in patients with renal cell carcinoma. *Int J Cancer* [Internet]. 2020 Mar 1;146(5):1435–44. Available from: <https://doi.org/10.1002/ijc.32579>
 384. Alqahtani A, Ayesh HSK, Halawani H. PIK3CA Gene Mutations in Solid Malignancies: Association with Clinicopathological Parameters and Prognosis. Vol. 12, *Cancers* . 2020.
 385. Liang S-Q, Bühner ED, Berezowska S, Marti TM, Xu D, Froment L, et al. mTOR mediates a mechanism of resistance to chemotherapy and defines a rational combination strategy to treat KRAS-mutant lung cancer. *Oncogene* [Internet]. 2019;38(5):622–36. Available from: <https://doi.org/10.1038/s41388-018-0479-6>
 386. Faber AC, Coffee EM, Costa C, Dastur A, Ebi H, Hata AN, et al. mTOR inhibition specifically sensitizes colorectal cancers with KRAS or BRAF mutations to BCL-2/BCL-XL inhibition by suppressing MCL-1. *Cancer Discov*. 2014 Jan;4(1):42–52.

387. Johnston LJ, Brown J, Shizuru JA, Stockerl-Goldstein KE, Stuart MJ, Blume KG, et al. Rapamycin (sirolimus) for treatment of chronic graft-versus-host disease. *Biol blood marrow Transplant J Am Soc Blood Marrow Transplant*. 2005 Jan;11(1):47–55.
388. Saunders RN, Metcalfe MS, Nicholson ML. Rapamycin in transplantation: A review of the evidence. *Kidney Int [Internet]*. 2001 Jan 1;59(1):3–16. Available from: <https://doi.org/10.1046/j.1523-1755.2001.00460.x>
389. Vilella-Bach M, Nuzzi P, Fang Y, Chen J. The FKBP12-Rapamycin-binding Domain Is Required for FKBP12-Rapamycin-associated Protein Kinase Activity and G₁ Progression *. *J Biol Chem [Internet]*. 1999 Feb 12;274(7):4266–72. Available from: <https://doi.org/10.1074/jbc.274.7.4266>
390. Choi J, Chen J, Schreiber SL, Clardy J. Structure of the FKBP12-rapamycin complex interacting with the binding domain of human FRAP. *Science*. 1996 Jul;273(5272):239–42.
391. Yang H, Rudge DG, Koos JD, Vaidialingam B, Yang HJ, Pavletich NP. mTOR kinase structure, mechanism and regulation. *Nature [Internet]*. 2013;497:217. Available from: <https://doi.org/10.1038/nature12122>
392. Sarbassov DD, Ali SM, Sengupta S, Sheen J-H, Hsu PP, Bagley AF, et al. Prolonged rapamycin treatment inhibits mTORC2 assembly and Akt/PKB. *Mol Cell*. 2006 Apr;22(2):159–68.
393. Zheng Y, Jiang Y. mTOR Inhibitors at a Glance. *Mol Cell Pharmacol [Internet]*. 2015;7(2):15–20. Available from: <https://www.ncbi.nlm.nih.gov/pubmed/27134695>
<https://www.ncbi.nlm.nih.gov/pmc/PMC4849280/>
394. Formisano L, Napolitano F, Rosa R, D'Amato V, Servetto A, Marciano R, et al. Mechanisms of resistance to mTOR inhibitors. *Crit Rev Oncol Hematol [Internet]*. 2020;147:102886. Available from: <https://www.sciencedirect.com/science/article/pii/S104084282030024X>
395. Kwitkowski VE, Prowell TM, Ibrahim A, Farrell AT, Justice R, Mitchell SS, et al. FDA approval summary: temsirolimus as treatment for advanced renal cell carcinoma. *Oncologist*. 2010;15(4):428–35.
396. FDA USF and DA. TORISEL Kit (temsirolimus) label [Internet]. 2011. Available from: https://www.accessdata.fda.gov/drugsatfda_docs/label/2011/022088s002s004s005s007s010s012lbl.pdf
397. FDA USF and DA. AFINITOR® (everolimus) label [Internet]. 2016. Available from: https://www.accessdata.fda.gov/drugsatfda_docs/label/2016/022334s036lbl.pdf
398. Verheijen RB, Atrafi F, Schellens JHM, Beijnen JH, Huitema ADR, Mathijssen RHJ, et al. Pharmacokinetic Optimization of Everolimus Dosing in Oncology: A Randomized Crossover Trial. *Clin Pharmacokinet*. 2018 May;57(5):637–44.
399. Harrington LS, Findlay GM, Gray A, Tolkacheva T, Wigfield S, Rebholz H, et al. The TSC1-2 tumor suppressor controls insulin–PI3K signaling via regulation of IRS proteins. *J Cell Biol*. 2004;166(2):213–23.
400. Treins C, Warne PH, Magnuson MA, Pende M, Downward J. Rictor is a novel target of p70 S6 kinase-1. *Oncogene*. 2010 Feb;29(7):1003–16.
401. Y. CA, Sang-Oh Y, Gyun KS, P. RP, John B. Rapamycin differentially inhibits S6Ks and 4E-BP1 to mediate cell-type-specific repression of mRNA translation. *Proc Natl Acad Sci [Internet]*. 2008 Nov 11;105(45):17414–9. Available from: <https://doi.org/10.1073/pnas.0809136105>

402. Thoreen CC, Kang SA, Chang JW, Liu Q, Zhang J, Gao Y, et al. An ATP-competitive mammalian target of rapamycin inhibitor reveals rapamycin-resistant functions of mTORC1. *J Biol Chem* [Internet]. 2009 Mar 20 [cited 2020 Mar 19];284(12):8023–32. Available from: <http://www.ncbi.nlm.nih.gov/pubmed/19150980>
403. Kauffman EC, Lang M, Rais-Bahrami S, Gupta GN, Wei D, Yang Y, et al. Preclinical efficacy of dual mTORC1/2 inhibitor AZD8055 in renal cell carcinoma harboring a TFE3 gene fusion. *BMC Cancer* [Internet]. 2019 Sep 13 [cited 2020 Jun 19];19(1):917. Available from: <https://bmccancer.biomedcentral.com/articles/10.1186/s12885-019-6096-0>
404. Chresta CM, Davies BR, Hickson I, Harding T, Cosulich S, Critchlow SE, et al. AZD8055 is a potent, selective, and orally bioavailable ATP-competitive mammalian target of rapamycin kinase inhibitor with in vitro and in vivo antitumor activity. *Cancer Res*. 2010 Jan;70(1):288–98.
405. Jordan NJ, Dutkowski CM, Barrow D, Mottram HJ, Hutcheson IR, Nicholson RI, et al. Impact of dual mTORC1/2 mTOR kinase inhibitor AZD8055 on acquired endocrine resistance in breast cancer in vitro. *Breast Cancer Res* [Internet]. 2014;16(1):R12–R12. Available from: [internal-pdf://207.233.221.171/Breast Cancer Research 2014. Jordan et al..pdf](internal-pdf://207.233.221.171/Breast%20Cancer%20Research%202014.%20Jordan%20et%20al..pdf)
406. Asahina H, Nokihara H, Yamamoto N, Yamada Y, Tamura Y, Honda K, et al. Safety and tolerability of AZD8055 in Japanese patients with advanced solid tumors; a dose-finding phase I study. *Invest New Drugs* [Internet]. 2013;31(3):677–84. Available from: <https://doi.org/10.1007/s10637-012-9860-4>
407. Naing A, Aghajanian C, Raymond E, Olmos D, Schwartz G, Oelmann E, et al. Safety, tolerability, pharmacokinetics and pharmacodynamics of AZD8055 in advanced solid tumours and lymphoma. *Br J Cancer* [Internet]. 2012;107(7):1093–9. Available from: <https://doi.org/10.1038/bjc.2012.368>
408. Mirabelli P, Coppola L, Salvatore M. Cancer Cell Lines Are Useful Model Systems for Medical Research. Vol. 11, *Cancers*. 2019.
409. Weinstein JN. Cell lines battle cancer. *Nature* [Internet]. 2012;483(7391):544–5. Available from: <https://doi.org/10.1038/483544a>
410. Brodaczevska KK, Szczylik C, Fiedorowicz M, Porta C, Czarnecka AM. Choosing the right cell line for renal cell cancer research. *Mol Cancer* [Internet]. 2016 Dec 19 [cited 2020 May 28];15(1):83. Available from: <https://doi.org/10.1186/s12943-016-0565-8>
411. Anglard P, Trahan E, Liu S, Latif F, Merino MJ, Lerman MI, et al. Molecular and Cellular Characterization of Human Renal Cell Carcinoma Cell Lines. *Cancer Res* [Internet]. 1992;52(2):348. Available from: <http://cancerres.aacrjournals.org/content/52/2/348.abstract>
412. Sinha R, Winer AG, Chevinsky M, Jakubowski C, Chen Y-BB, Dong Y, et al. Analysis of renal cancer cell lines from two major resources enables genomics-guided cell line selection. *Nat Commun* [Internet]. 2017 May 10 [cited 2020 Mar 10];8(1):15165. Available from: <https://www.ncbi.nlm.nih.gov/pubmed/28489074>
<https://www.ncbi.nlm.nih.gov/pmc/articles/PMC5436135/>
413. Williams RD, Elliott AY, Stein N, Fraley EE. In vitro cultivation of human renal cell cancer. I. Establishment of cells in culture. *In Vitro* [Internet]. 1976 Sep [cited 2020 Mar 10];12(9):623–7. Available from: <http://www.ncbi.nlm.nih.gov/pubmed/1010528>
414. Giard DJ et al. In vitro cultivation of human tumors: Establishment of cell lines derived from

- a series of solid tumors. *J Natl Cancer Inst.* 1973;51(5):1417–23.
415. Lee PY, Costumbrado J, Hsu C-Y, Kim YH. Agarose gel electrophoresis for the separation of DNA fragments. *J Vis Exp.* 2012 Apr;(62).
416. Buehring GC, Eby EA, Eby MJ. Cell line cross-contamination: how aware are Mammalian cell culturists of the problem and how to monitor it? *In Vitro Cell Dev Biol Anim.* 2004;40(7):211–5.
417. Reid Y Riss T, et al. SD. Authentication of Human Cell Lines by STR DNA Profiling Analysis. . In: Sittampalam GS Brimacombe K, et al GA, editor. *Assay Guidance Manual* [Internet] [Internet]. 2013. Available from: <https://www.ncbi.nlm.nih.gov/books/NBK144066/>
418. Gilbert DF, Friedrich O. *Cell viability assays.* Springer; 2017.
419. Riss TL, Moravec RA, Niles AL, Duellman S, Benink HA, Worzella TJ, et al. *Cell viability assays.* *Assay Guid Man* [Internet]. 2016;
420. Zembruski NCL, Stache V, Haefeli WE, Weiss J. 7-Aminoactinomycin D for apoptosis staining in flow cytometry. *Anal Biochem.* 2012 Oct;429(1):79–81.
421. Buck SB, Bradford J, Gee KR, Agnew BJ, Clarke ST, Salic A. Detection of S-phase cell cycle progression using 5-ethynyl-2'-deoxyuridine incorporation with click chemistry, an alternative to using 5-bromo-2'-deoxyuridine antibodies. *Biotechniques* [Internet]. 2008 Dec 5;44(7):927–9. Available from: <https://doi.org/10.2144/000112812>
422. Darzynkiewicz Z, Pozarowski P, Gloria J. Chapter 34 - Cell Cycle Analysis by Flow and Laser-Scanning Cytometry. In: Celis JE, TCB (Third E, editor. Burlington: Academic Press; 2006. p. 279–89. Available from: <https://www.sciencedirect.com/science/article/pii/B9780121647308500356>
423. Alfonso B-F, Al-Rubeai M. 1.42 - Flow Cytometry. In: Moo-Young MBT-CB (Second E, editor. Burlington: Academic Press; 2011. p. 559–78. Available from: <https://www.sciencedirect.com/science/article/pii/B9780080885049000659>
424. Hein CD, Liu X-M, Wang D. Click chemistry, a powerful tool for pharmaceutical sciences. *Pharm Res.* 2008 Oct;25(10):2216–30.
425. Amblard F, Cho JH, Schinazi RF. Cu(I)-Catalyzed Huisgen Azide–Alkyne 1,3-Dipolar Cycloaddition Reaction in Nucleoside, Nucleotide, and Oligonucleotide Chemistry. *Chem Rev* [Internet]. 2009 Sep 9;109(9):4207–20. Available from: <https://doi.org/10.1021/cr9001462>
426. Breugst M, Reissig H-U. The Huisgen Reaction: Milestones of the 1,3-Dipolar Cycloaddition. *Angew Chemie Int Ed* [Internet]. 2020 Jul 20;59(30):12293–307. Available from: <https://doi.org/10.1002/anie.202003115>
427. Rostovtsev V V, Green LG, Fokin V V, Sharpless KB. A Stepwise Huisgen Cycloaddition Process: Copper(I)-Catalyzed Regioselective “Ligation” of Azides and Terminal Alkynes. *Angew Chemie Int Ed* [Internet]. 2002 Jul 15;41(14):2596–9. Available from: [https://doi.org/10.1002/1521-3773\(20020715\)41:14%3C2596::AID-ANIE2596%3E3.0.CO](https://doi.org/10.1002/1521-3773(20020715)41:14%3C2596::AID-ANIE2596%3E3.0.CO)
428. Kacprzak K, Skiera I, Piasecka M, Paryzek Z. Alkaloids and Isoprenoids Modification by Copper(I)-Catalyzed Huisgen 1,3-Dipolar Cycloaddition (Click Chemistry): Toward New Functions and Molecular Architectures. *Chem Rev* [Internet]. 2016 May 25;116(10):5689–743. Available from: <https://doi.org/10.1021/acs.chemrev.5b00302>
429. Pozarowski P, Darzynkiewicz Z. Analysis of cell cycle by flow cytometry. *Methods Mol Biol.*

- 2004;281:301–11.
430. Jao CY, Salic A. Exploring RNA transcription and turnover in vivo by using click chemistry. *Proc Natl Acad Sci U S A* [Internet]. 10/07. 2008;105(41):15779–84. Available from: <https://www.ncbi.nlm.nih.gov/pubmed/18840688>
<https://www.ncbi.nlm.nih.gov/pmc/PMC2572917/>
 431. Sleiman RJ, Stewart BW. Early Caspase Activation in Leukemic Cells Subject to Etoposide-induced G2-M Arrest: Evidence of Commitment to Apoptosis Rather Than Mitotic Cell Death1. *Clin Cancer Res*. 2000 Sep 1;6(9):3756–65.
 432. Godard T, Deslandes E, Lebailly P, Vigreux C, Poulain L, Sichel F, et al. Comet assay and DNA flow cytometry analysis of staurosporine-induced apoptosis. *Cytometry* [Internet]. 1999 Jun 1;36(2):117–22. Available from: [https://doi.org/10.1002/\(SICI\)1097-0320\(19990601\)36:2%3C117::AID-CYTO5%3E3.0.CO](https://doi.org/10.1002/(SICI)1097-0320(19990601)36:2%3C117::AID-CYTO5%3E3.0.CO)
 433. Raulf A, Spahn CK, Zessin PJM, Finan K, Bernhardt S, Heckel A, et al. Click chemistry facilitates direct labelling and super-resolution imaging of nucleic acids and proteins. *RSC Adv* [Internet]. 2014;4(57):30462–6. Available from: <http://dx.doi.org/10.1039/C4RA01027B>
 434. Klöcker N, Weissenboeck FP, Rentmeister A. Covalent labeling of nucleic acids. *Chem Soc Rev* [Internet]. 2020;49(23):8749–73. Available from: <http://dx.doi.org/10.1039/D0CS00600A>
 435. Akbalik G, Langebeck-Jensen K, Tushev G, Sambandan S, Rinne J, Epstein I, et al. Visualization of newly synthesized neuronal RNA in vitro and in vivo using click-chemistry. *RNA Biol*. 2017 Jan;14(1):20–8.
 436. Carpenter AE, Jones TR, Lamprecht MR, Clarke C, Kang IH, Friman O, et al. CellProfiler: Image analysis software for identifying and quantifying cell phenotypes. *Genome Biol*. 2006 Oct 31;7(10).
 437. Rasband WS. ImageJ [Internet]. U. S. National Institutes of Health, Bethesda, Maryland, USA. [cited 2020 Apr 8]. Available from: <https://imagej.nih.gov/ij/>
 438. Hipp R, et. al. SQLite (Version 3.2.1) [Internet]. SQLite Development Team.; 2015 [cited 2020 Apr 8]. Available from: <https://www.sqlite.org/download.html>
 439. Olds W, Li J. siRNA knockdown validation 101: Incorporating negative controls in antibody research. *F1000Research* [Internet]. 2016 Mar 9;5:308. Available from: <https://pubmed.ncbi.nlm.nih.gov/26998240>
 440. Han H. RNA Interference to Knock Down Gene Expression. *Methods Mol Biol* [Internet]. 2018;1706:293–302. Available from: <https://pubmed.ncbi.nlm.nih.gov/29423805>
 441. Dana H, Chalbatani GM, Mahmoodzadeh H, Karimloo R, Rezaiean O, Moradzadeh A, et al. Molecular Mechanisms and Biological Functions of siRNA. *Int J Biomed Sci* [Internet]. 2017 Jun;13(2):48–57. Available from: <https://pubmed.ncbi.nlm.nih.gov/28824341>
 442. Renart J, Reiser J, Stark GR. Transfer of proteins from gels to diazobenzoyloxymethyl-paper and detection with antisera: a method for studying antibody specificity and antigen structure. *Proc Natl Acad Sci U S A*. 1979 Jul;76(7):3116–20.
 443. Towbin H, Staehelin T, Gordon J. Electrophoretic transfer of proteins from polyacrylamide gels to nitrocellulose sheets: procedure and some applications. *Proc Natl Acad Sci U S A*. 1979 Sep;76(9):4350–4.
 444. Moritz CP. 40 years Western blotting: A scientific birthday toast. *J Proteomics* [Internet].

- 2020;212:103575. Available from:
<https://www.sciencedirect.com/science/article/pii/S1874391919303471>
445. Harlow E, Lane D. Antibodies: a laboratory manual. [Internet]. 1988. Available from:
<https://liverpool.idm.oclc.org/login?url=https://search.ebscohost.com/login.aspx?direct=true&db=cat00003a&AN=lvp.b1566490&site=eds-live&scope=site>
446. Goutelle S, Maurin M, Rougier F, Barbaut X, Bourguignon L, Ducher M, et al. The Hill equation: a review of its capabilities in pharmacological modelling. *Fundam Clin Pharmacol* [Internet]. 2008 Dec 1;22(6):633–48. Available from: <https://doi.org/10.1111/j.1472-8206.2008.00633.x>
447. Geary N. Understanding synergy. *Am J Physiol Metab* [Internet]. 2012 Jul 11;304(3):E237–53. Available from: <https://doi.org/10.1152/ajpendo.00308.2012>
448. Tallarida RJ. An Overview of Drug Combination Analysis with Isobolograms. *J Pharmacol Exp Ther* [Internet]. 2006 Oct;319(1):1–7. Available from: [internal-pdf://224.7.204.22/Tallarida, R. 2006. An overview of Drug combin.pdf](internal-pdf://224.7.204.22/Tallarida,%20R.2006.An%20overview%20of%20Drug%20combin.pdf)
449. Blainey P, Krzywinski M, Altman N. Replication. *Nat Methods* [Internet]. 2014;11(9):879–80. Available from: <https://doi.org/10.1038/nmeth.3091>
450. Montgomery DC. Design and analysis of experiments. 8th ed. John Wiley & Sons; 2013. 604 p.
451. Demidenko E, Miller TW. Statistical determination of synergy based on Bliss definition of drugs independence. *PLoS One* [Internet]. 2019 Nov 25;14(11):e0224137. Available from: <https://doi.org/10.1371/journal.pone.0224137>
452. Guertin DA, Sabatini DM. Defining the Role of mTOR in Cancer. *Cancer Cell* [Internet]. 2007;12(1):9–22. Available from:
<http://www.sciencedirect.com/science/article/pii/S1535610807001511>
453. Richard DJ, Verheijen JC, Zask A. Recent advances in the development of selective, ATP-competitive inhibitors of mTOR. Vol. 13, *Current Opinion in Drug Discovery and Development*. Thomson Scientific Ltd.; 2010. p. 428–40.
454. Bass JJ, Wilkinson DJ, Rankin D, Phillips BE, Szewczyk NJ, Smith K, et al. An overview of technical considerations for Western blotting applications to physiological research. *Scand J Med Sci Sports* [Internet]. 2017 Jan 1;27(1):4–25. Available from:
<https://doi.org/10.1111/sms.12702>
455. Gingras AC, Raught B, Gygi SP, Niedzwiecka A, Miron M, Burley SK, et al. Hierarchical phosphorylation of the translation inhibitor 4E-BP1. *Genes Dev*. 2001 Nov;15(21):2852–64.
456. Livingstone M, Bidinosti M. Rapamycin-insensitive mTORC1 activity controls eIF4E:4E-BP1 binding. *F1000Research*. 2012;1:4.
457. Ayuso MI, Hernández-Jiménez M, Martín ME, Salinas M, Alcázar A. New Hierarchical Phosphorylation Pathway of the Translational Repressor eIF4E-binding Protein 1 (4E-BP1) in Ischemia-Reperfusion Stress *. *J Biol Chem* [Internet]. 2010 Nov 5;285(45):34355–63. Available from: <https://doi.org/10.1074/jbc.M110.135103>
458. Sheval E V, Polzikov MA, Olson MOJ, Zatssepina O V. A higher concentration of an antigen within the nucleolus may prevent its proper recognition by specific antibodies. *Eur J Histochem* [Internet]. 2009 Jun 29;49(2 SE-Original Papers):117–24. Available from:
<https://www.ejh.it/index.php/ejh/article/view/935>

459. Khadzhilov AA. The nucleolus and ribosome biogenesis [by] A.A. Hadjiolov. Wien: Springer; 1985. (CELL BIOLOGY MONOGRAPHS 12).
460. UNUMA T, SENDA R, MURAMATSU M. Mechanism of Nucleolar Segregation—Differences in Effects of Actinomycin D and Cycloheximide on Nucleoli of Rat Liver Cells—. *J Electron Microsc (Tokyo)* [Internet]. 1973 Jan 1;22(2):205–16. Available from: <https://doi.org/10.1093/oxfordjournals.jmicro.a049877>
461. Mitrea DM, Cika JA, Stanley CB, Nourse A, Onuchic PL, Banerjee PR, et al. Self-interaction of NPM1 modulates multiple mechanisms of liquid–liquid phase separation. *Nat Commun* [Internet]. 2018;9(1):842. Available from: <https://doi.org/10.1038/s41467-018-03255-3>
462. Dash S, Lamb MC, Lange JJ, McKinney MC, Tsuchiya D, Guo F, et al. rRNA transcription is integral to liquid-liquid phase separation and maintenance of nucleolar structure. *bioRxiv* [Internet]. 2022 Jan 1;2022.11.14.516489. Available from: <http://biorxiv.org/content/early/2022/11/15/2022.11.14.516489.abstract>
463. AAT Bioquest. Quest Graph™ IC50 Calculator [Internet]. AAT Bioquest Inc.; 2022. Available from: <https://www.aatbio.com/tools/ic50-calculator>
464. Riss TL, Moravec RA, Niles AL, Duellman S, Benink HA, Worzella TJ, et al. *Cell Viability Assays*. In: Markossian S, Grossman A, Brimacombe K, Arkin M, Auld D, Austin C, et al., editors. Bethesda (MD); 2004.
465. Mansoury M, Hamed M, Karmustaji R, Al Hannan F, Safrany ST. The edge effect: A global problem. The trouble with culturing cells in 96-well plates. *Biochem Biophys reports*. 2021 Jul;26:100987.
466. Rogoyski, Moreno-Laporta L. Manuscript in preparation. 2022;
467. Choong ML, Yang H, Lee MA, Lane DP. Specific activation of the p53 pathway by low dose actinomycin D: A new route to p53 based cyclotherapy. *Cell Cycle* [Internet]. 2009 Sep 1;8(17):2810–8. Available from: <https://doi.org/10.4161/cc.8.17.9503>
468. Tapani E, Taavitsainen M, Lindros K, Vehmas T, Lehtonen E. Toxicity of ethanol in low concentrations. Experimental evaluation in cell culture. *Acta Radiol*. 1996 Nov;37(6):923–6.
469. Verheijen M, Lienhard M, Schrooders Y, Clayton O, Nudischer R, Boerno S, et al. DMSO induces drastic changes in human cellular processes and epigenetic landscape in vitro. *Sci Rep* [Internet]. 2019;9(1):4641. Available from: <https://doi.org/10.1038/s41598-019-40660-0>
470. Yang W, Soares J, Greninger P, Edelman EJ, Lightfoot H, Forbes S, et al. Genomics of Drug Sensitivity in Cancer (GDSC): a resource for therapeutic biomarker discovery in cancer cells. *Nucleic Acids Res* [Internet]. 2012 Nov 22;41(D1):D955–61. Available from: <https://doi.org/10.1093/nar/gks1111>
471. Ahmed-Ebbyary A. Developing novel therapeutic strategies for targeting the p53 pathway in renal cell carcinoma. University of Liverpool.; 2014.
472. Choong ML, Yang H, Lee MA, Lane DP. Specific activation of the p53 pathway by low dose actinomycin D: A new route to p53 based cyclotherapy. *Cell Cycle*. 2009 Sep 1;8(17):2810–8.
473. Schonn I, Hennesen J, Dartsch DC. Cellular responses to etoposide: cell death despite cell cycle arrest and repair of DNA damage. *Apoptosis* [Internet]. 2010;15(2):162–72. Available from: <https://doi.org/10.1007/s10495-009-0440-9>
474. Belmokhtar CA, Hillion J, Ségal-Bendirdjian E. Staurosporine induces apoptosis through both

- caspase-dependent and caspase-independent mechanisms. *Oncogene* [Internet]. 2001;20(26):3354–62. Available from: <https://doi.org/10.1038/sj.onc.1204436>
475. Kauffman EC, Lang M, Rais-Bahrami S, Gupta GN, Wei D, Yang Y, et al. Preclinical efficacy of dual mTORC1/2 inhibitor AZD8055 in renal cell carcinoma harboring a TFE3 gene fusion. *BMC Cancer* [Internet]. 2019;19(1):917. Available from: <https://doi.org/10.1186/s12885-019-6096-0>
 476. Willems L, Chapuis N, Puissant A, Maciel TT, Green AS, Jacque N, et al. The dual mTORC1 and mTORC2 inhibitor AZD8055 has anti-tumor activity in acute myeloid leukemia. *Leukemia*. 2012 Jun;26(6):1195–202.
 477. Banerji U, Aghajanian C, Raymond E, Kurzrock R, Blanco-Codesido M, Oelmann E, et al. First results from a phase I trial of AZD8055, a dual mTORC1 and mTORC2 inhibitor. *J Clin Oncol* [Internet]. 2011 May 20;29(15_suppl):3096. Available from: https://doi.org/10.1200/jco.2011.29.15_suppl.3096
 478. Tallarida RJ. *Drug Synergism and Dose-Effect Data Analysis* [Internet]. 1st editio. New York: Chapman and Hall/CRC; 2000. 264 p. Available from: <https://www.taylorfrancis.com/books/9781420036107>
 479. Lehár J, Krueger AS, Avery W, Heilbut AM, Johansen LM, Price ER, et al. Synergistic drug combinations tend to improve therapeutically relevant selectivity. *Nat Biotechnol* [Internet]. 2009;27(7):659–66. Available from: <https://doi.org/10.1038/nbt.1549>
 480. Grimm M-O, Wolff I, Zastrow S, Fröhner M, Wirth M. Advances in renal cell carcinoma treatment. *Ther Adv Urol*. 2010 Feb;2(1):11–7.
 481. Terada N, Lucas JJ, Szepesi A, Franklin RA, Takase K, Gelfand EW. Rapamycin inhibits the phosphorylation of p70 S6 kinase in IL-2 and mitogen-activated human T cells. *Biochem Biophys Res Commun*. 1992 Aug;186(3):1315–21.
 482. Hara K, Yonezawa K, Kozlowski MT, Sugimoto T, Andrabi K, Weng Q-P, et al. Regulation of eIF-4E BP1 Phosphorylation by mTOR *. *J Biol Chem* [Internet]. 1997 Oct 17;272(42):26457–63. Available from: <https://doi.org/10.1074/jbc.272.42.26457>
 483. Hsu H-S, Lin M-H, Jang Y-H, Kuo T-T, Liu C-C, Cheng T-H. The 4E-BP1/eIF4E ratio is a determinant for rapamycin response in esophageal cancer cells. *J Thorac Cardiovasc Surg* [Internet]. 2015;149(1):378–85. Available from: <https://www.sciencedirect.com/science/article/pii/S0022522314013117>
 484. Karlsson E, Pérez-Tenorio G, Amin R, Bostner J, Skoog L, Fornander T, et al. The mTOR effectors 4EBP1 and S6K2 are frequently coexpressed, and associated with a poor prognosis and endocrine resistance in breast cancer: a retrospective study including patients from the randomised Stockholm tamoxifen trials. *Breast Cancer Res* [Internet]. 2013;15(5):R96. Available from: <https://doi.org/10.1186/bcr3557>
 485. Qin X, Jiang B, Zhang Y. 4E-BP1, a multifactor regulated multifunctional protein. *Cell Cycle* [Internet]. 2016;15(6):781–6. Available from: <https://www.ncbi.nlm.nih.gov/pubmed/26901143>
<https://www.ncbi.nlm.nih.gov/pmc/articles/PMC4845917/>
 486. Rolli-Derkinderen M, Machavoine F, Baraban JM, Grolleau A, Beretta L, Dy M. ERK and p38 Inhibit the Expression of 4E-BP1 Repressor of Translation through Induction of Egr-1 *. *J Biol Chem* [Internet]. 2003 May 23;278(21):18859–67. Available from:

<https://doi.org/10.1074/jbc.M211696200>

487. Azar R, Lasfargues C, Bousquet C, Pyronnet S. Contribution of HIF-1 α in 4E-BP1 Gene Expression. *Mol Cancer Res* [Internet]. 2013 Jan 1;11(1):54–61. Available from: <https://doi.org/10.1158/1541-7786.MCR-12-0095>
488. Dodd KM, Yang J, Shen MH, Sampson JR, Tee AR. mTORC1 drives HIF-1 α and VEGF-A signalling via multiple mechanisms involving 4E-BP1, S6K1 and STAT3. *Oncogene*. 2015 Apr;34(17):2239–50.
489. Tani H, Akimitsu N. Genome-wide technology for determining RNA stability in mammalian cells. *RNA Biol* [Internet]. 2012 Oct 1;9(10):1233–8. Available from: <https://doi.org/10.4161/rna.22036>
490. Hofgärtner FJ, Krone W, Jain K. Correlated inhibition of ribosomal RNA synthesis and silver staining by actinomycin D. *Hum Genet*. 1979 Apr;47(3):329–33.
491. Hou T, Rinderknecht CH, Hadjinicolaou A V, Busch R, Mellins E. Pulse-chase analysis for studies of MHC class II biosynthesis, maturation, and peptide loading. *Methods Mol Biol*. 2013;960:411–32.
492. Mahajan PB. Modulation of transcription of rRNA genes by rapamycin. *Int J Immunopharmacol* [Internet]. 1994;16(9):711–21. Available from: <https://www.sciencedirect.com/science/article/pii/0192056194900914>
493. Lamming DW, Ye L, Katajisto P, Goncalves MD, Saitoh M, Stevens DM, et al. Rapamycin-Induced Insulin Resistance Is Mediated by mTORC2 Loss and Uncoupled from Longevity. *Science (80-)* [Internet]. 2012 Mar 30;335(6076):1638–43. Available from: <https://doi.org/10.1126/science.1215135>
494. Buchwalter A, Hetzer MW. Nucleolar expansion and elevated protein translation in premature aging. *Nat Commun* [Internet]. 2017;8(1):328. Available from: <https://doi.org/10.1038/s41467-017-00322-z>
495. Mannick JB, Lamming DW. Targeting the biology of aging with mTOR inhibitors. *Nat Aging* [Internet]. 2023;3(6):642–60. Available from: <https://doi.org/10.1038/s43587-023-00416-y>
496. Tiku V, Jain C, Raz Y, Nakamura S, Heestand B, Liu W, et al. Small nucleoli are a cellular hallmark of longevity. *Nat Commun* [Internet]. 2017;8(1):16083. Available from: <https://doi.org/10.1038/ncomms16083>
497. Giguère V. Canonical signaling and nuclear activity of mTOR—a teamwork effort to regulate metabolism and cell growth. *FEBS J* [Internet]. 2018 May 1;285(9):1572–88. Available from: <https://doi.org/10.1111/febs.14384>
498. Carroll B. Spatial regulation of mTORC1 signalling: Beyond the Rag GTPases. *Semin Cell Dev Biol* [Internet]. 2020;107:103–11. Available from: <https://www.sciencedirect.com/science/article/pii/S1084952119301363>
499. Liu Q, Kang SA, Thoreen CC, Hur W, Wang J, Chang JW, et al. Development of ATP-Competitive mTOR Inhibitors BT - mTOR: Methods and Protocols. In: Weichhart T, editor. Totowa, NJ: Humana Press; 2012. p. 447–60. Available from: https://doi.org/10.1007/978-1-61779-430-8_29
500. Wynn ML, Ventura AC, Sepulchre JA, García HJ, Merajver SD. Kinase inhibitors can produce off-target effects and activate linked pathways by retroactivity. *BMC Syst Biol*. 2011

- Oct;5:156.
501. Woo MS, Ohta Y, Rabinovitz I, Stossel TP, Blenis J. Ribosomal S6 kinase (RSK) regulates phosphorylation of filamin A on an important regulatory site. *Mol Cell Biol*. 2004 Apr;24(7):3025–35.
 502. Mendoza MC, Er EE, Blenis J. The Ras-ERK and PI3K-mTOR pathways: cross-talk and compensation. *Trends Biochem Sci*. 2011 Jun;36(6):320–8.
 503. Yang W, Soares J, Greninger P, Edelman EJ, Lightfoot H, Forbes S, et al. Genomics of Drug Sensitivity in Cancer (GDSC): a resource for therapeutic biomarker discovery in cancer cells. *Nucleic Acids Res [Internet]*. 2013 Jan 1;41(D1):D955–61. Available from: <https://doi.org/10.1093/nar/gks1111>
 504. Faes S, Santoro T, Demartines N, Dormond O. Evolving Significance and Future Relevance of Anti-Angiogenic Activity of mTOR Inhibitors in Cancer Therapy. *Cancers (Basel)*. 2017 Nov;9(11).
 505. Kim LC, Cook RS, Chen J. mTORC1 and mTORC2 in cancer and the tumor microenvironment. *Oncogene [Internet]*. 2017;36(16):2191–201. Available from: <https://doi.org/10.1038/onc.2016.363>
 506. Boyd MT, Vlatković N, Rubbi CP. The nucleolus directly regulates p53 export and degradation. *J Cell Biol [Internet]*. 2011 Sep 5;194(5):689–703. Available from: <https://doi.org/10.1083/jcb.201105143>
 507. Tallarida RJ. Drug synergism: its detection and applications. *J Pharmacol Exp Ther*. 2001/08/16. 2001;298(3):865–72.
 508. Hernandez-Verdun D. Nucleolus: from structure to dynamics. *Histochem Cell Biol*. 2006 Jan;125(1–2):127–37.
 509. Voit R, Grummt I. The RNA Polymerase I Transcription Machinery BT - The Nucleolus. In: Olson MOJ, editor. *New York, NY: Springer New York; 2011*. p. 107–34. Available from: https://doi.org/10.1007/978-1-4614-0514-6_6
 510. Grimm T, Hölzel M, Rohrmoser M, Harasim T, Malamoussi A, Gruber-Eber A, et al. Dominant-negative Pes1 mutants inhibit ribosomal RNA processing and cell proliferation via incorporation into the PeBoW-complex. *Nucleic Acids Res [Internet]*. 2006 May 1;34(10):3030–43. Available from: <https://doi.org/10.1093/nar/gkl378>